12 December 2008 | $10

Science

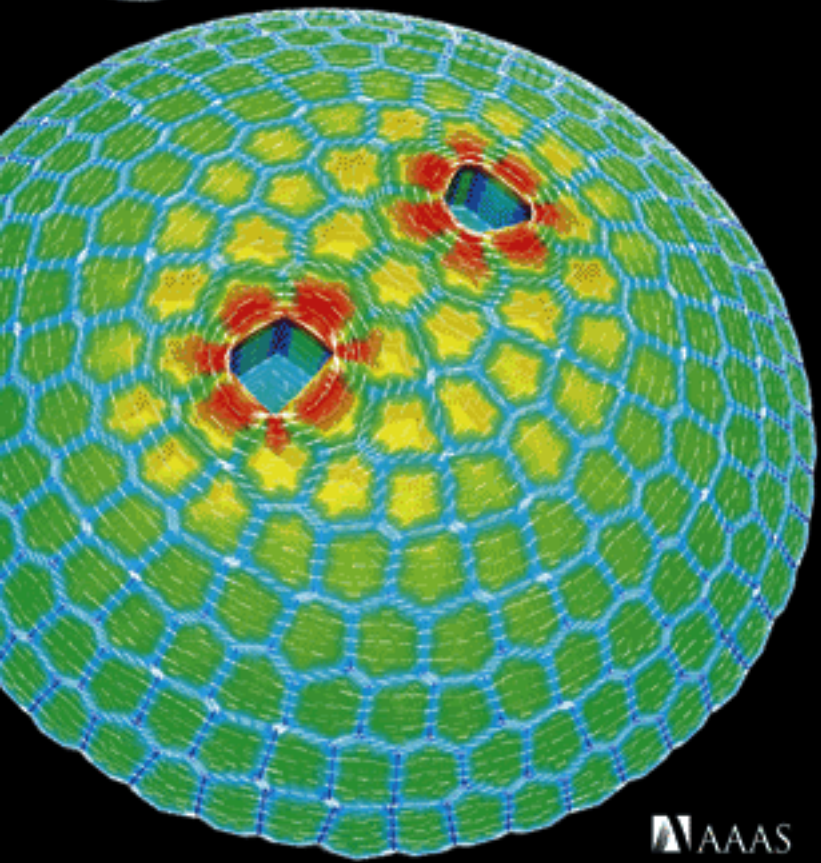

AAAS

Volume 322, Issue 5908

COVER

Finite element method simulation of an *Arabidopsis* shoot apical meristem where two cells have been laser-ablated. The color map indicates the von Mises stress (a measure of distortional stress); the white lines mark the directions of maximal principal stress, which are circumferential around the ablated cells, in agreement with experimentally determined microtubule orientations. See page 1650.

Image: Pawel Krupinski/Lund University

DEPARTMENTS

EDITORIAL

NEWS OF THE WEEK

NEWS FOCUS

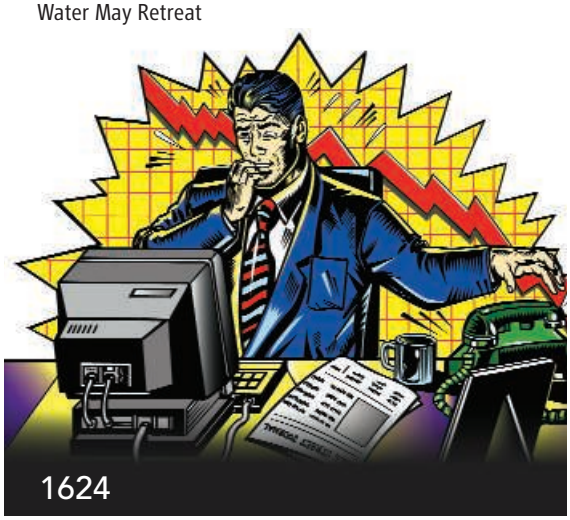
1624

LETTERS

BOOKS *ET AL.*

POLICY FORUM

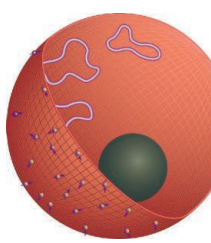
1639

PERSPECTIVES

CONTENTS continued >>

Published by AAAS

SCIENCE EXPRESS

www.sciencexpress.org

PHYSICS

Quantum Criticality in the Electrical Resistivity of $La_{2-x}Sr_xCuO_4$

R. A. Cooper et al.

High magnetic fields can strip away the superconducting regime of a cuprate superconductor, revealing the presence of an enigmatic quantum critical point.

10.1126/science.1165015

CHEMISTRY

Femtosecond XANES Study of the Light-Induced Spin Crossover Dynamics in an Iron(II) Complex

Ch. Bressler et al.

X-ray absorption spectroscopy resolves the dynamics of spin-state interconversions, which take place in less than a picosecond, in a well-studied class of iron compounds.

10.1126/science.1165733

MOLECULAR BIOLOGY

Chromatin-Associated Periodicity in Genetic Variation Downstream of Transcriptional Start Sites

S. Sasaki et al.

The periodic wrapping of DNA around nucleosomes in chromatin determines a periodic variation in mutation type and frequency around transcription start sites in a fish.

10.1126/science.1163183

DEVELOPMENTAL BIOLOGY

The Sphingolipid Transporter Spns2 Functions in Migration of Zebrafish Myocardial Precursors

A. Kawahara et al.

Normal heart development in zebrafish requires the function of a lipid transporter in a membrane surrounding the yolk, a tissue outside of the embryo proper.

10.1126/science.1167449

GENETICS

A Single Gene Causes Both Male Sterility and Segregation Distortion in *Drosophila* Hybrids

N. Phadnis and H. A. Orr

A *Drosophila* gene that causes sterility in the offspring of two species and may be important for speciation causes increased transmission of itself to progeny.

10.1126/science.1163934

GENETICS

A Mouse Speciation Gene Encodes a Meiotic Histone H3 Methyltransferase

O. Mihola et al.

A gene responsible for sterility in the offspring of two mouse species, and therefore important in speciation, regulates gene expression via methylation in chromatin.

10.1126/science.1163601

TECHNICAL COMMENT ABSTRACTS

GENETICS

BREVIA

ECOLOGY

RESEARCH ARTICLES

PLANT SCIENCE

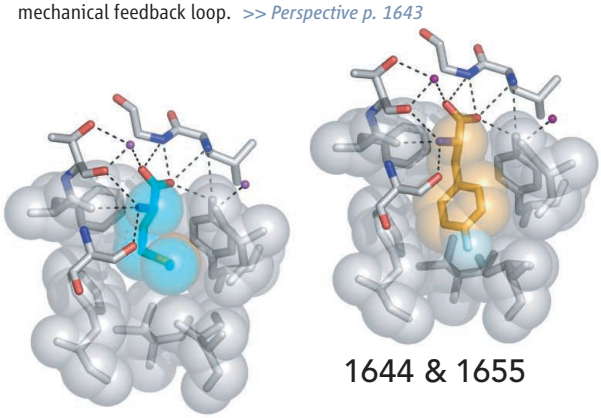

1644 & 1655

RESEARCH ARTICLES *CONTINUED...*

BIOCHEMISTRY

REPORTS

CHEMISTRY

CHEMISTRY

CHEMISTRY

CLIMATE CHANGE

CONTENTS continued >>

REPORTS *CONTINUED...*

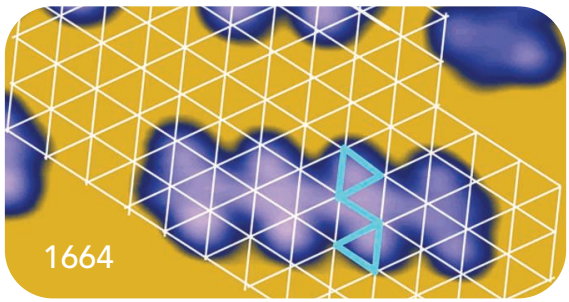

AAAS
ADVANCING SCIENCE, SERVING SOCIETY

SCIENCE (ISSN 0036-8075) is published weekly on Friday, except the last week in December, by the American Association for the Advancement of Science, 1200 New York Avenue, NW, Washington, DC 20005. Periodicals Mail postage (publication No. 484460) paid at Washington, DC, and additional mailing offices. Copyright © 2008 by the American Association for the Advancement of Science. The title SCIENCE is a registered trademark of the AAAS. Domestic individual membership and subscription (51 issues): $144 ($74 allocated to subscription). Domestic institutional subscription (51 issues): $770; Foreign postage extra: Mexico, Caribbean (surface mail) $55; other countries (air assist delivery) $85. First class, airmail, student, and emeritus rates on request. Canadian rates with GST available upon request, GST #1254 88122. Publications Mail Agreement Number 1069624. SCIENCE is printed on 30 percent post-consumer recycled paper. **Printed in the U.S.A.**

Change of address: Allow 4 weeks, giving old and new addresses and 8-digit account number. **Postmaster:** Send change of address to AAAS, P.O. Box 96178, Washington, DC 20090–6178. **Single-copy sales:** $10.00 current issue, $15.00 back issue prepaid includes surface postage; bulk rates on request. **Authorization to photocopy** material for internal or personal use under circumstances not falling within the fair use provisions of the Copyright Act is granted by AAAS to libraries and other users registered with the Copyright Clearance Center (CCC) Transactional Reporting Service, provided that $20.00 per article is paid directly to CCC, 222 Rosewood Drive, Danvers, MA 01923. *Science* is indexed in the *Reader's Guide to Periodical Literature* and in several specialized indexes.

Printed on 30% post-consumer recycled paper.

CONTENTS continued **>>**

This dog has had enough.

SCIENCE**NOW**

www.sciencenow.org

HIGHLIGHTS FROM OUR DAILY NEWS COVERAGE

Dogs Have a Nose for Inequity
Pooches get pouty over unfair treatment.

Shaken Volcanoes Blow Their Tops
Major earthquakes can set off far-flung eruptions.

The Dark Side of Tiger Conservation
Attacks on humans rise in Nepal's recovering forests.

What are you doing next summer?

SCIENCE **CAREERS**

www.sciencecareers.org/career_development

FREE CAREER RESOURCES FOR SCIENTISTS

Special Feature: Summer Internships for Undergraduates
R. N. Austin
A summer internship is a good way to get started in scientific research.

Making Your Summer Research Internship a Good One
E. Pain
Knowing what to expect and how to contribute will make your summer research experience more valuable.

Internships Offer Undergrads Full-Time Research Immersion
L. Laursen
Research internships offer undergrads experience, exposure to new fields, and networking opportunities.

Summer Internships: Resources
Science *Careers Staff*
Looking for something scientific to do next summer?

The developing plant.

SCIENCE **SIGNALING**

www.sciencesignaling.org

THE SIGNAL TRANSDUCTION KNOWLEDGE ENVIRONMENT

EDITORIAL GUIDE: Focus Issue—Organ Development from Beginning to End
A. M. VanHook
Cell signaling events play a key role in the induction, regulation, and maintenance of organ development.

RESEARCH ARTICLE: Analysis of Metagene Portraits Reveals Distinct Transitions During Kidney Organogenesis
I. Tsigelny, V. Kouznetsova, D. E. Sweeney, W. Wu, K. T. Bush, S. K. Nigam
Grouping microarray expression data into metagenes, followed by organization of these gene clusters into self-organizing maps, reveals distinct stages of kidney organogenesis.

REVIEW: De Novo Organ Formation from Differentiated Cells—Root Nodule Organogenesis
M. Crespi and F. Frugier
Root nodule organogenesis in legumes is initiated by bacterial signals and directed by plant signaling pathways.

PERSPECTIVE: Intercellular Peptide Signals Regulate Plant Meristematic Cell Fate Decisions
J. E. Gray, S. Casson, L. Hunt
By controlling stem cell fate, secreted peptides control the formation of many plant cell types.

SCIENCE**PODCAST**

www.sciencemag.org/multimedia/podcast

FREE WEEKLY SHOW

Download the 12 December *Science* Podcast to hear about the compromised welfare of zoo elephants, reconciling financial models with human behavior, and more.

CREDITS: (*SCIENCE NOW*) FRIEDERIKE RANGE; (*SCIENCE SIGNALING*) JUPITER IMAGES; (*SCIENCE CAREERS*) AGRICULTURAL RESEARCH SERVICE/USDA

Separate individual or institutional subscriptions to these products may be required for full-text access.

<< Contagious Rule-Breaking

When people see that others clearly disobey a social norm, it will increase the observers' readiness to disobey this particular norm as well (thinking "Everyone else does it, so why shouldn't I?"). But will the fact that other people disobey a particular norm make it more likely that an observer will disobey different social norms, even laws? **Keizer *et al.*** (p. 1681, published online 20 November) performed six natural field experiments in Groningen, Netherlands, in which observers had to choose to obey or disobey different social norms after observing visual disorder (such as littering or graffiti), or hearing fireworks go off when prohibited. The willingness to disobey social rules was, indeed, observed to increase when there were signs of social disorder around, and the presence of graffiti more than doubled the number of people littering and stealing.

Transporter Mechanics

Secondary transporters catalyze the movement of substrates across cellular membranes by coupling substrate passage to ion gradients. Recently described structures have provided insight into how transport occurs through alternate opening and closing of inward and outward facing cavities. Now, **Singh *et al.*** (p. 1655; see the Perspective by **Diallinas**) present extensive structural and functional studies on LeuT, a model for the pharmacologically important class of neurotransmitter:sodium symporters. Incoming amino acids transiently bind to gating residues that are only accessible in the open-to-out conformation. The amino acid then moves to the primary binding site, allowing formation of the occluded state with substrates, but sterically preventing its formation in the case of larger competitive inhibitors like tryptophan. The occluded state then isomerizes to an open-to-in conformation to allow release of substrate to the cytoplasm.

Assemble, Inject, React, Reform

Self-assembly of molecules on surfaces often occurs through weak interactions, and the reactivity of the constituent molecules usually remains unchanged. **Maksymovych *et al.*** (p. 1664) report an unusual example of altered reactivity for dimethyldisulfide (CH_3SSCH_3) molecules that self-assemble into long chains on single-crystal gold surfaces (up to 15 molecules long). When the tip of a scanning tunneling microscope injects an electron into one end of the chain, not only does the S-S bond in the molecule on the end of the chain break, but the reaction propagates down the chain. The end fragments remain isolated, and the interior fragments reassemble with new partners back into CH_3SSCH_3 molecules. Theoretical calculations indicate the barrier to this chain reaction is very low, which helps to explain how it competes successfully against energy relaxation processes.

Cancer Epigenetics 101

Proteins that methylate histones play a key role in regulating gene expression through a so-called "epigenetic" mechanism that involves alterations in chromatin structure rather than sequence changes in DNA. The histone methyltransferase EZH2 (enhancer of zeste homolog 2) is overexpressed in a subset of human cancers, especially in cancers that have metastasized. **Varambally *et al.*** (p. 1695, published online 13 November) now show that expression of EZH2 is normally inhibited by a specific microRNA, miR-101. This regulatory mechanism appears to be disrupted during prostate cancer progression when tumors lose miR-101 by genomic deletion. By virtue of its regulation of EZH2, miR-101 may thus exert control over epigenetic pathways active in cancer cells.

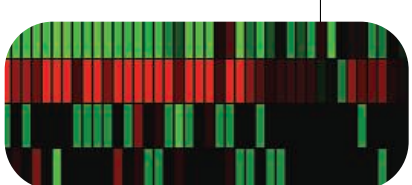

CREDITS (TOP TO BOTTOM): KEES KEIZER; VARAMBALLY *ET AL.*

Dynamic Calcium

Permanent burial of calcium carbonate in marine sediments is the major, long-term sink of atmospheric CO_2 that balances volcanic CO_2 emissions and keeps the concentration of CO_2 in the atmosphere mostly within a well-defined but variable range. **Griffith *et al.*** (p. 1671) present data on the isotopic composition of Ca in seawater, showing that it varied considerably over the past 28 million years. Major changes occurred in the concentration of Ca in seawater, with the largest excursion corresponding to a climate transition marked both by carbon and oxygen isotopes, which underscores the links between climate and marine geochemical cycles.

Sumatran Earthquake

The huge moment magnitude (M_w) 9.2 earthquake that struck Sumatra in December 2004, producing a devastating tsunami, ruptured the western end of a major plate boundary. Two subsequent earthquakes ruptured progressively eastward sections, including a M_w 8.4 earthquake in September 2004. The area to the east last ruptured in two great earthquakes in 1797 and 1833. Quakes are associated with local uplift of several meters, which expose shallow corals. **Sieh *et al.*** (p. 1674) have accurately dated bands in these corals to reconstruct the quake history. Major quakes occurred in the 1300s and again, about 200 years later. With the known quakes, this record implies that major quakes in this region appear in a series of events about 200 years apart.

Continued on page 1607

Published by AAAS

Continued from page 1605

Cytoskeleton and Substrate Stiffness

Substrate stiffness is sensed by cells and affects motility, morphology, and cell fate. Linking molecules between filamentous (F)-actin and the extracellular substrate are thought to act as "clutches" that transmit traction forces and slow F-actin retrograde flow. **Chan and Odde** (p. 1687; see the Perspective by **Aratyn-Schaus and Gardel**) now consider the effect of substrate stiffness by modeling both the clutch molecules and the substrate as Hookean springs. The model suggests that substrate stiffness-dependent changes in clutch dynamics result in higher retrograde flow rates with lower traction forces on stiff substrates, and lower retrograde flow rates on soft substrates. As predicted, in embryonic chick forebrain neurons, a switch in F-actin dynamics was observed at an elastic modulus of about 1 kilopascal.

Threading a Molecular Needle

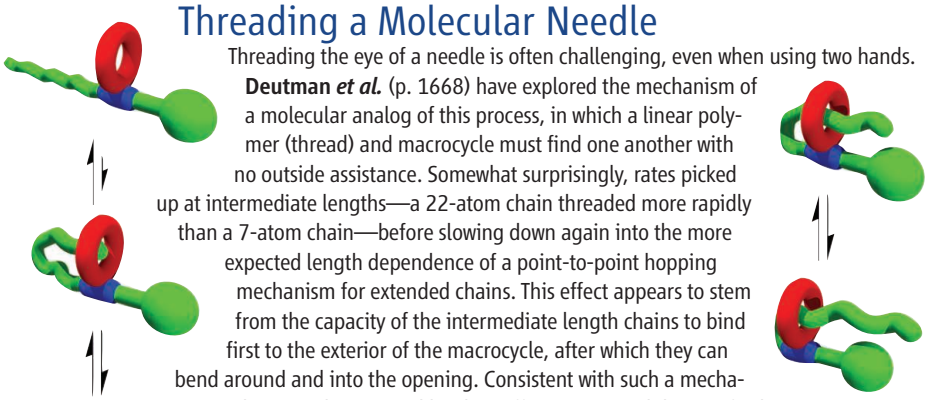

Threading the eye of a needle is often challenging, even when using two hands. **Deutman *et al.*** (p. 1668) have explored the mechanism of a molecular analog of this process, in which a linear polymer (thread) and macrocycle must find one another with no outside assistance. Somewhat surprisingly, rates picked up at intermediate lengths—a 22-atom chain threaded more rapidly than a 7-atom chain—before slowing down again into the more expected length dependence of a point-to-point hopping mechanism for extended chains. This effect appears to stem from the capacity of the intermediate length chains to bind first to the exterior of the macrocycle, after which they can bend around and into the opening. Consistent with such a mechanism, enhancing this external binding affinity increased the rate further.

CREDIT: DEUTMAN *ET AL.*

Genes, Triglycerides, and Heart Health

High blood levels of triglycerides, a major form of dietary fat, have been linked to human heart disease. To identify genes that contribute to interindividual differences in the body's handling of dietary triglycerides, **Pollin *et al.*** (p. 1702) performed a genome-wide association study of volunteers from the Lancaster Amish population whose blood triglyceride levels had been measured before and after consumption of a milkshake. Individuals with the lowest levels of blood triglycerides were found to be heterozygous carriers of a null mutation in the gene encoding an inhibitor of triglyceride hydrolysis, called apolipoprotein C–III (apoC-III). These individuals, who produce half the normal amount of apoC-III, also had a favorable cholesterol profile and coronary calcification score, suggesting that they are less likely to develop cardiovascular disease.

Invariant Chain Migration Control

The spatiotemporal regulation of the immune response remains largely unknown. Now **Faure-André *et al.*** (p. 1705; see the Perspective by **Lukacs-Kornek and Turley**) show that the invariant chain, a key regulator of antigen processing and presentation by MHC class II molecules, also controls the intrinsic migratory capacity of dendritic cells. In a study of the behavior of dendritic cells taken from mouse models on microfabricated surfaces using time-lapse imaging, the invariant chain caused dendritic cells to enter a discontinuous migration mode that alternated between low- and high-motility phases. This regulation of dendritic cell migration by the invariant chain results from its association with the actin-based motor protein, Myosin II. This use of common regulators for antigen processing and cell motility may provide dendritic cells with a way to coordinate the two functions in time and space.

Corralling the Cajal

The eukaryotic cell nucleus does not contain membrane bound organelles, nevertheless the nucleoplasm is not a homogeneous medium. The nucleoplasm is compartmentalized into a range of highly dynamic structures, including many small foci, which serve to localize intranuclear functions. How are such structures generated and maintained? **Kaiser *et al.*** (p. 1713, published online 23 October) analyzed the assembly of the Cajal body, which is involved in the biogenesis and recycling of small nuclear ribonucleoproteins. Individual Cajal body proteins and RNAs were tethered to chromatin and used as "baits" for other Cajal body components. All were able to nucleate the de novo formation of authentic Cajal bodies, with similar kinetics. Thus, assembly of this nuclear body does not occur in a linear, hierarchical manner.

Published by AAAS

Alan I. Leshner is the chief executive officer of the American Association for the Advancement of Science and executive publisher of *Science*.

Reduce Administrative Burden

THE ADMINISTRATIVE BURDEN ON PRACTICING SCIENTISTS HAS GROWN TREMENDOUSLY OVER the past decades and is limiting their ability to get important scientific work done. As the United States prepares for a new president to take office, there is an opportunity to take a fresh look at many of the government policies and regulations that concern the conduct of science. How might we find ways to reduce the administrative burden while still ensuring accountability to science funders, appropriate safeguards for human subjects, and broader societal protection from real dangers that can accompany some scientific research?

A 2007 survey by the U.S. Federal Demonstration Partnership (*A Profile of Federal-Grant Administrative Burden Among Federal Demonstration Partnership Faculty*) found that 84% of faculty in the United States believe that the administrative burden associated with federally funded grants has increased significantly in recent years. Most notably, the study indicates that of the total time that faculty devote to research, 42% is spent on pre- and post-award administrative activities. Some activities respond to university or host institution policies, whereas others respond to an array of governmental rules that are poorly integrated. The most time-consuming research-related activities include too-frequent submissions of progress reports, navigation of the complex and disparate rules for project revenue management, and institutional review board protocol development and revisions. The need to respond to new post-9/11 security concepts such as "dual-use research" or "sensitive but unclassified science" has also added substantially to the workload.

Virtually all of the issues underlying the governmental and institutional rules merit serious attention. Ensuring animal welfare and human subject protections are vitally important. Scientific fraud of any kind is intolerable. Conflicts of interest are inappropriate in any setting. Some science can be misused, and we owe society appropriate safeguards. Citizens deserve assurance that the scientific community is attending to these issues, and they are entitled to full accountability for the use of their investments in science.

However, as the U.S. National Academy of Sciences' 2007 report *Science and Security in a Post-9/11 World* pointed out very clearly, we also need to prevent overreaction. We must maintain the openness that has so productively characterized the science and technology enterprise in the United States. We also need to be certain that our approaches to scientific regulation are as cost-effective as possible. A Council on Governmental Relations study (*Report of the Working Group on the Cost of Doing Business*, 2003) reported that for each of 25 surveyed U.S. institutions, the cost of compliance activities had increased some $3 million per year over 5 years.

An ideal goal would be for every science-related rule or regulation to be rationalized and streamlined. As a group, they should be integrated as much as possible so as to reduce unnecessary duplication. New versions should address the lack of uniformity across agencies. Because the policies are variously the responsibilities of federal and state governments and of research-conducting institutions, this streamlining will require a joint effort of all sectors. The federal National Science and Technology Council, representing the leaders of the U.S. government's science-supporting agencies, created a Research Business Models Subcommittee in 2003 to work on this problem. Their findings and efforts have not yet been felt extensively in the field, but this subcommittee might be an ideal convener for this broad rules review.

Whoever takes the lead in reducing administrative burden might consider a somewhat unorthodox approach to reviewing and revising existing regulations. Rather than starting with the evaluation of each existing policy one at a time, it might ultimately be better to start anew from an integrated list of all the issues that must be addressed, and then take an entirely fresh look at what rules and regulations should be applied. Although this might trigger fears of "re-inventing the wheel," it also might prove the point of another old adage: "Never underestimate the value of 'square one.'"

– Alan I. Leshner

10.1126/science.1168345

CREDITS: (TOP) COLELLA PHOTOGRAPHY; (RIGHT) HENRIK SORENSEN/GETTY IMAGES

Published by AAAS

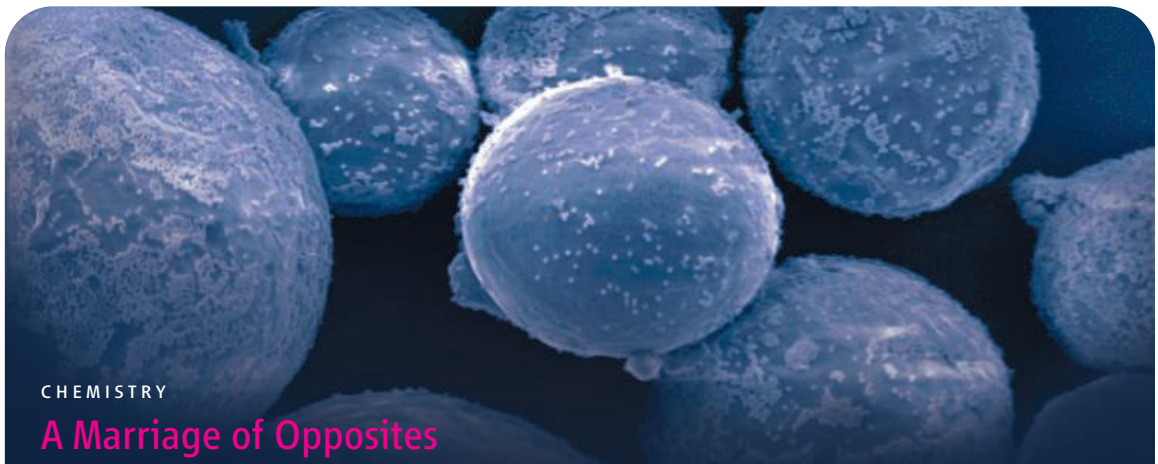

CHEMISTRY

A Marriage of Opposites

Janus particles are colloidal particles whose two hemispheres have different properties, such as optical or magnetic behavior, polarity, or the ability to attract or repel water. Berger *et al.* combined two polymerization reactions to create Janus particles with distinct acid/base reactivity. Multiple silica particles 800 nm in diameter were appended to a solid wax core, after which the exposed portions were functionalized with an acrylate polymer by surface-initiated atom-transfer radical polymerization. Once released from the wax, the previously masked hemispheres were linked to pre-formed chains of poly(2-vinylpyridine). The particles were then hydrolyzed to convert the acrylate esters to acids. The distinct basicities of the two polymers led to varying charge accumulation and consequent aggregation behavior in response to pH changes. The authors envision extending this approach for use in emulsion stabilization or for control of molecular transport at the interface between two immiscible liquids. — MSL

Macromolecules 10.1021/ma802089h (2008).

PLANT SCIENCE

Mapping Out Diversity

In plants, microtubules in the cell cortex help align cellulose fibrils in the cell wall, which in turn shape tissue structure. Microtubules are constantly in flux: growing at one end, disintegrating at the other end, and bundling together with neighbors. Microtubule-associated proteins (MAPs), specifically the MAP65 family, add some control to this otherwise fluid and self-assembling skeleton. Although animals have 1 or 2 MAP65 homologs, *Arabidopsis* has 9, and rice has 11. Smertenko *et al.* have analyzed this abundance and find that the genes fall into five families. Both rice and *Arabidopsis*, representing the ancient evolutionary divergence between monocots and dicots, have representatives of each of the five families. The MAP65 isoforms show different localizations within the cell and variable expression during development or through the cell cycle. Some are ubiquitously expressed, and others are unique to a particular tissue type, such as pollen. Some are preferentially expressed during G_1 and others during G_2. The domain responsible for this diversity among the MAP65 proteins seems to harbor the similarly diverse phosphorylation sites. — PJH

Plant Cell **20**, 10.1105/tpc.108.063362 (2008).

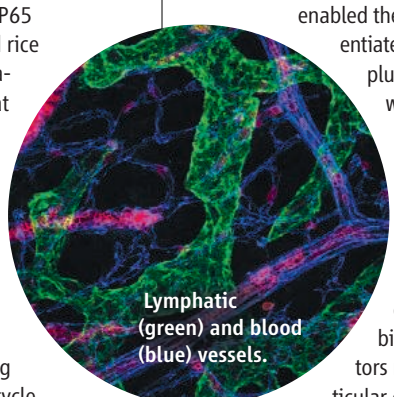

Lymphatic (green) and blood (blue) vessels.

DEVELOPMENT

Turning On and Staying On

During metazoan development, cells generally progress inexorably to a terminally differentiated fate. However, recent in vitro manipulations have enabled the conversion of one differentiated cell type either to a pluripotent state (as occurs with somatic cell nuclear transfer and induced pluripotent cells) or to another differentiated cell type (for example, reprogramming of mature B cells into T cells). Although quite a bit is known about the factors necessary to specify particular cell types, relatively little is known about the factors required to maintain the terminally differentiated phenotype. For specification of lymphatic endothelial cells (LECs), *Prox1* expression is crucial, and Johnson *et al.* extend this finding to show an additional role of *Prox1* in maintaining the lymphatic fate. Down-regulation of mouse *Prox1* results in mispatterned lymphatic vessels that fill with blood; LECs are effectively reprogrammed into blood endothelial cells (BECs). Hence, *Prox1* acts as a binary switch participating in the known roles of suppressing BEC fate and promoting LEC fate; furthermore, sustained *Prox1* expression is necessary to maintain the lymphatic cell phenotype. — BAP

Genes Dev. **22**, 10.1101/gad.1727208 (2008).

PSYCHOLOGY

Reading from Left to Right

Categorical perception is a robust phenomenon and can be illustrated by the more rapid discrimination of two colors separated by a fixed chromatic distance when the colors fall on opposite sides of a category boundary, such as blue/green, than when they both lie within a single category. Both adults and infants exhibit this capacity, and Franklin *et al.* have investigated the influence of hemispheric lateralization and of language in a pair of studies. First, by presenting the colors in the left or right visual field (LVF or RVF), they show that adults react more quickly to RVF stimuli and hence that categorical perception of color is lateralized (in a relative, though not absolute,

CREDITS (TOP TO BOTTOM): BERGER *ET AL.*, *MACROMOLECULES* 10.1021/MA802089H (2008); JOHNSON *ET AL.*, *GENES DEV.* **22**, 10.1101/GAD.1727208 (2008)

Published by AAAS

sense) to the left hemisphere, to which the RVF projects. Consistent with a left-hemispheric predominance of language skills, a verbal interference task blocked categorical perception in adults, whereas a visual interference task did not. Prelinguistic infants, on the other hand, displayed a right-hemispheric (LVF) superiority in the categorical perception of colors. Second, they recruited a group of toddlers 2 to 5 years of age and assessed their comprehension of the words blue and green. When tested on the same paired colors, the reaction times of these toddlers did not vary as a function of semantic knowledge, but those that had mastered the words demonstrated a hemispheric lateralization that was adult-like; that is, categorical perception for RVF stimuli. Toddlers who were still learning about blue and green retained the LVF pattern of categorical perception. — GJC

Proc. Natl. Acad. Sci. U.S.A. **105**, 3221; 18221 (2008).

PSYCHOLOGY

A Walk in the Woods

Spending time in the outdoors is commonly regarded as a wholesome approach to coping with the cacophony of contemporary developed societies. But does immersion in a natural environment lead to more than simply a sense of feeling refreshed—that is, might the metaphorical recharging of one's batteries be real? Berman *et al.* find that the less obtrusive sensory stimuli provided by a walk through an arboretum enabled people to perform better on a standard working memory task (backward digit span), in comparison to the stimuli of a stroll through a downtown landscape. Subsequent testing revealed a specific effect of scenic as opposed to urban settings on the executive portions (versus the alerting or orienting components) of an attentional network task, suggesting that a brief hiatus from focused application of attention allows for the replenishment and renewal of cognitive control centers. — GJC

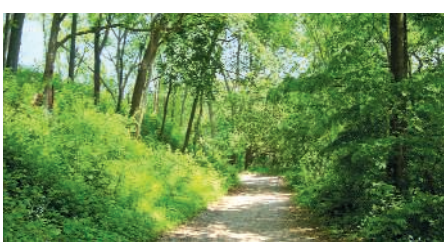

CREDIT: COURTNEY BEHNKE

Psychol. Sci. **19**, 1207 (2008).

CHEMISTRY

Weighing Down Pyridine

A common technique for unraveling the mechanism of complex organic reactions is to substitute the hydrogen atoms on different carbon centers with heavier deuterium isotopes. The mass shift can influence reaction rates through changes in the molecule's vibrational structure, thereby revealing key sites of reactivity. In general, though, isotopic substitution tends not to perturb the overall outcome of chemical or physical transformations. Crawford *et al.* uncover an intriguing exception, in which deuteration of the five carbons in pyridine leads to a distinct crystalline arrangement at low temperature. Through a careful series of x-ray and neutron diffraction studies on single-crystal and powder samples, the authors established that below 215 K, the deuterated isotopologue crystallizes in a layered phase along the (110) planes; above this temperature, the solid rearranges to align along the (100) planes, as observed across the whole temperature range for protio pyridine. Although such isotopic polymorphism has previously been observed in a number of polyatomic salts, the behavior is rare in neutral organics. — JSY

Angew. Chem. Int. Ed. **47**, 10.1002/anie.200803589 (2008).

CELL BIOLOGY

Hidden Change

Biological systems are buffered against variation by proteins termed phenotypic capacitors, of which heat shock protein 90 (Hsp90) is the founding member. This protein chaperone reveals diverse phenotypic variation when its level falls, exposing previously silenced genotypes. Given that species advancement requires genetic diversity and phenotypic change, phenotypic capacitors have been suggested to support evolution; the reduction of Hsp90, which occurs under stressful conditions, would release phenotypes that can be acted on by natural selection to drive evolution. Whether other cellular proteins harbor capacitor function is unclear. Levy and Siegel used high-throughput morphological phenotyping and found that more than 5% of yeast genes act as capacitors by buffering environmental variation and suppressing phenotypic diversity. These capacitors were found to control cellular processes, such as cell cycle regulation and stress responses. Beyond a role in natural selection, phenotypic capacitors may also support the evolution of cancer cells, which are notoriously resilient to many environmental stresses and exhibit widespread genetic instability. Hsp90 is thought to buffer these tumorigenic properties and promote survival, and Hsp90 inhibitors may have potential as cancer chemotherapeutics. — HP*

PLoS Biol. **6**, e264 (2008).

*Helen Pickersgill is a locum editor in *Science*'s editorial department.

Wrap yourself in something groundbreaking this year

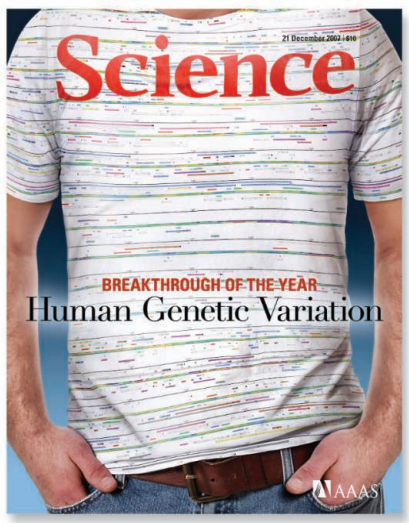

Our *Science* Gene Sequence T-shirt—get yours today!

By popular demand! Created to celebrate our Breakthrough of the Year for 2007, this T-shirt is designed from an annotated gene sequence map of human chromosome 1.

Since the shirt appeared on the cover of *Science*, we've been flooded with requests. Now it's yours for just $22.50 plus tax (where applicable), and shipping & handling. Photos of the actual shirt are available at the website below.

To order:
www.aaas.org/go/geneshirt

Science
AAAS

www.sciencemag.org

Science

1200 New York Avenue, NW
Washington, DC 20005
Editorial: 202-326-6550, FAX 202-289-7562
News: 202-326-6581, FAX 202-371-9227
Bateman House, 82-88 Hills Road
Cambridge, UK CB2 1LQ
+44 (0) 1223 326500, FAX +44 (0) 1223 326501

Subscription Services For change of address, missing issues, new orders and renewals, and payment questions: 866-434-AAAS (2227) or 202-326-6417, FAX 202-842-1065. Mailing addresses: AAAS, P.O. Box 96178, Washington, DC 20090-6178 or AAAS Member Services, 1200 New York Avenue, NW, Washington, DC 20005

Institutional Site Licenses please call 202-326-6755 for any questions or information

Reprints: Author Inquiries 800-635-7181
Commercial Inquiries 803-359-4578

Permissions 202-326-7074, FAX 202-682-0816

Member Benefits AAAS/Barnes&Noble.com bookstore www.aaas.org/bn; AAAS Online Store www.apisource.com/aaas/ code MKB6; AAAS Travels: Betchart Expeditions 800-252-4910; Apple Store www.apple/eppstore/aaas; Bank of America MasterCard 1-800-833-6262 priority code FAA3YU; Cold Spring Harbor Laboratory Press Publications www.cshlpress.com/affiliates/aaas.htm; GEICO Auto Insurance www.geico.com/landingpage/go51.htm?logo=17624; Hertz 800-654-2200 CDP#343457; Office Depot https://bsd.officedepot.com/portalLogin.do; Seabury & Smith Life Insurance 800-424-9883; Subaru VIP Program 202-326-6417; VIP Moving Services www.vipmayflower.com/domestic/index.html; Other Benefits: AAAS Member Services 202-326-6417 or www.aaasmember.org.

science_editors@aaas.org	(for general editorial queries)
science_letters@aaas.org	(for queries about letters)
science_reviews@aaas.org	(for returning manuscript reviews)
science_bookrevs@aaas.org	(for book review queries)

Published by the American Association for the Advancement of Science (AAAS), *Science* serves its readers as a forum for the presentation and discussion of important issues related to the advancement of science, including the presentation of minority or conflicting points of view, rather than by publishing only material on which a consensus has been reached. Accordingly, all articles published in *Science*—including editorials, news and comment, and book reviews—are signed and reflect the individual views of the authors and not official points of view adopted by AAAS or the institutions with which the authors are affiliated.

AAAS was founded in 1848 and incorporated in 1874. Its mission is to advance science, engineering, and innovation throughout the world for the benefit of all people. The goals of the association are to: enhance communication among scientists, engineers, and the public; promote and defend the integrity of science and its use; strengthen support for the science and technology enterprise; provide a voice for science on societal issues; promote the responsible use of science in public policy; strengthen and diversify the science and technology workforce; foster education in science and technology for everyone; increase public engagement with science and technology; and advance international cooperation in science.

Information for Authors
See pages 634 and 635 of the 1 February 2008 issue or access www.sciencemag.org/about/authors

EDITOR-IN-CHIEF **Bruce Alberts**
EXECUTIVE EDITOR **Monica M. Bradford**
DEPUTY EDITORS **R. Brooks Hanson, Barbara R. Jasny, Katrina L. Kelner**
NEWS EDITOR **Colin Norman**

Editorial supervisory senior editor Phillip D. Szuromi; **senior editor/perspectives** Lisa D. Chong; **senior editors** Gilbert J. Chin, Pamela J. Hines, Paula A. Kiberstis (Boston), Marc S. Lavine (Toronto), Beverly A. Purnell, L. Bryan Ray, Guy Riddihough, H. Jesse Smith, Valda Vinson; **associate editors** Kristen L. Mueller, Jake S. Yeston, Laura M. Zahn; **online editor** Stewart Wills; **associate online editors** Robert Frederick, Tara S. Marathe; **web content developer** Martyn Green; **book review editor** Sherman J. Suter; **associate letters editor** Jennifer Sills; **editorial manager** Cara Tate; **senior copy editors** Jeffrey E. Cook, Cynthia Howe, Harry Jach, Barbara P. Ordway, Trista Wagoner; **copy editors** Chris Filiatreau, Lauren Kmec; **editorial coordinators** Carolyn Kyle, Beverly Shields; **publications assistants** Ramatoulaye Diop, Joi S. Granger, Jeffrey Hearn, Lisa Johnson, Scott Miller, Jerry Richardson, Jennifer A. Seibert, Brian White, Anita Wynn; **editorial assistants** Carlos L. Durham, Emily Guise, Patricia M. Moore; **executive assistant** Sylvia S. Kihara; **administrative support** Maryrose Madrid

News deputy news editors Robert Coontz, Eliot Marshall, Jeffrey Mervis, Leslie Roberts; **contributing editors** Elizabeth Culotta, Polly Shulman; **news writers** Yudhijit Bhattacharjee, Adrian Cho, Jennifer Couzin, David Grimm, Constance Holden, Jocelyn Kaiser, Richard A. Kerr, Eli Kintisch, Andrew Lawler (New England), Greg Miller, Elizabeth Pennisi, Robert F. Service (Pacific NW), Erik Stokstad; **intern** Rachel Zelkowitz; **contributing correspondents** Jon Cohen (San Diego, CA), Daniel Ferber, Ann Gibbons, Robert Koenig, Mitch Leslie, Charles C. Mann, Virginia Morell, Evelyn Strauss, Gary Taubes; **copy editors** Linda B. Felaco, Melvin Gatling, Melissa Raimondi; **administrative support** Scherraine Mack, Fannie Groom; **bureaus** New England: 207-549-7755, San Diego, CA: 760-942-3252, FAX 760-942-4979, Pacific Northwest: 503-963-1940

Production director James Landry; **senior manager** Wendy K. Shank; **assistant manager** Rebecca Doshi; **senior specialists** Steve Forrester, Chris Redwood; **specialist** Anthony Rosen; **Preflight director** David M. Tompkins; **manager** Marcus Spiegler

Art director Yael Kats; **associate art director** Laura Creveling; **illustrators** Chris Bickel, Katharine Sutliff; **senior art associates** Holly Bishop, Preston Huey, Nayomi Kevitiyagala; **art associate** Jessica Newfield; **photo editor** Leslie Blizard

***Science* International**

Europe (science@science-int.co.uk) **editorial: international managing editor** Andrew M. Sugden; **senior editor/perspectives** Julia Fahrenkamp-Uppenbrink; **senior editors** Caroline Ash, Stella M. Hurtley, Ian S. Osborne, Peter Stern; **associate editor** Maria Cruz; **editorial support** Deborah Dennison, Rachel Roberts, Alice Whaley; **administrative support** John Cannell, Janet Clements; **news: europe news editor** John Travis; **deputy news editor** Daniel Clery; **contributing correspondents** Michael Balter (Paris), John Bohannon (Vienna), Martin Enserink (Amsterdam and Paris), Gretchen Vogel (Berlin); **intern** Sara Coelho

Asia Japan Office: Asca Corporation, Eiko Ishioka, Fusako Tamura, 1-8-13, Hirano-cho, Chuo-ku, Osaka-shi, Osaka, 541-0046 Japan; +81 (0) 6 6202 6272, FAX +81 (0) 6 6202 6271; asca@os.gulf.or.jp; **asia news editor** Richard Stone (Beijing: rstone@aaas.org); **contributing correspondents** Dennis Normile (Japan: +81 (0) 3 3391 0630, FAX +81 (0) 3 5936 3531; dnormile@gol.com); Hao Xin (China: +86 (0) 10 6307 4439 or 6307 3676, FAX +86 (0) 10 6307 4358; cindyhao@gmail.com); Pallava Bagla (South Asia: +91 (0) 11 2271 2896; pbagla@vsnl.com)

EXECUTIVE PUBLISHER **Alan I. Leshner**
PUBLISHER **Beth Rosner**

Fulfillment Systems and Operations (membership@aaas.org); **director** Waylon Butler; **senior systems analyst** Jonny Blaker; **customer service supervisor** Pat Butler; **specialists** Latoya Casteel, LaVonda Crawford, Vicki Linton, April Marshall; **data entry supervisor** Cynthia Johnson; **specialists** Eintou Bowden, Tarrika Hill, William Jones

Business Operations and Administration director Deborah Rivera-Wienhold; **assistant director, business operations** Randy Yi; **manager, business analysis** Michael LoBue; **manager, business operations** Jessica Tierney; **financial analysts** Priti Pamnani, Celeste Troxler; **rights and permissions: administrator** Emilie David; **associate** Elizabeth Sandler; **marketing director** Ian King; **marketing manager** Allison Pritchard; **marketing associates** Aimee Aponte, Alison Chandler, Mary Ellen Crowley, Julianne Wielga, Wendy Wise; **international marketing manager** Wendy Sturley; **marketing executive** Jennifer Reeves; **marketing/member services executive** Linda Rusk; **director, site licensing** Tom Ryan; **director, corporate relations** Eileen Bernadette Moran; **publisher relations, eresources specialist** Kiki Forsythe; **senior publisher relations specialist** Catherine Holland; **publisher relations, east coast** Phillip Smith; **publisher relations, west coast** Philip Tsolakidis; **fulfillment supervisor** Iquo Edim; **fulfillment coordinator** Laura Clemens; **electronic media: manager** Lizabeth Harman; **project manager** Trista Snyder; **assistant manager** Lisa Stanford; **senior production specialists** Christopher Coleman, Walter Jones; **production specialists** Nichele Johnston, Kimberly Oster

Advertising director, worldwide ad sales Bill Moran

Product (science_advertising@aaas.org); **midwest/west coast/w. canada** Rick Bongiovanni: 330-405-7080, FAX 330-405-7081; **east coast/e. canada** Laurie Faraday: 508-747-9395, FAX 617-507-8189; **uk/europe/asia** Roger Goncalves: TEL/FAX +41 43 234 1358; **japan** Mashy Yoshikawa: +81 (0) 3 3235 5961, FAX +81 (0) 3 3235 5852; **senior traffic associate** Deiandra Simms

Commercial Editor Sean Sanders: 202-326-6430

Project Director, Outreach Brianna Blaser

Classified (advertise@sciencecareers.org); **inside sales manager: midwest/canada** Daryl Anderson: 202-326-6543; **inside sales representative** Karen Foote: 202-326-6740; **key account manager** Joribah Able; **northeast** Alexis Fleming: 202-326-6578; **southeast** Tina Burks: 202-326-6577; **west** Nicholas Hintibidze: 202-326-6533; **sales coordinators** Rohan Edmonson, Shirley Young; **international: sales manager** Tracy Holmes: +44 (0) 1223 326525, FAX +44 (0) 1223 326532; **sales** Susanne Kharraz, Dan Pennington, Alex Palmer; **sales assistant** Louise Moore; **japan** Mashy Yoshikawa: +81 (0) 3 3235 5961, FAX +81 (0) 3 3235 5852; **advertising production operations manager** Deborah Tompkins; **senior production specialist/graphic designer** Amy Hardcastle; **senior production specialist** Robert Buck; **senior traffic associate** Christine Hall; **publications assistant** Mary Lagnaoui

AAAS Board of Directors retiring president, chair David Baltimore; **president** James J. McCarthy; **president-elect** Peter C. Agre; **treasurer** David E. Shaw; **chief executive officer** Alan I. Leshner; **board** Lynn W. Enquist, Susan M. Fitzpatrick, Alice Gast, Linda P. B. Katehi, Nancy Knowlton, Cherry A. Murray, Thomas D. Pollard, Thomas A. Woolsey

AAAS
ADVANCING SCIENCE, SERVING SOCIETY

SENIOR EDITORIAL BOARD

John I. Brauman, *Chair, Stanford Univ.*
Richard Losick, *Harvard Univ.*
Robert May, *Univ. of Oxford*
Marcia McNutt, *Monterey Bay Aquarium Research Inst.*
Linda Partridge, *Univ. College London*
Vera C. Rubin, *Carnegie Institution*
Christopher R. Somerville, *Univ. of California, Berkeley*

BOARD OF REVIEWING EDITORS

Joanna Aizenberg, *Harvard Univ.*
R. McNeill Alexander, *Leeds Univ.*
David Altshuler, *Broad Institute*
Arturo Alvarez-Buylla, *Univ. of California, San Francisco*
Richard Amasino, *Univ. of Wisconsin, Madison*
Angelika Amon, *MIT*
Meinrat O. Andreae, *Max Planck Inst., Mainz*
Kristi S. Anseth, *Univ. of Colorado*
John A. Bargh, *Yale Univ.*
Cornelia I. Bargmann, *Rockefeller Univ.*
Ben Barres, *Stanford Medical School*
Marisa Bartolomei, *Univ. of Penn. School of Med.*
Ray H. Baughman, *Univ. of Texas, Dallas*
Stephen J. Benkovic, *Penn State Univ.*
Michael J. Bevan, *Univ. of Washington*
Ton Bisseling, *Wageningen Univ.*
Mina Bissell, *Lawrence Berkeley National Lab*
Peer Bork, *EMBL*
Dianna Bowles, *Univ. of York*
Robert W. Boyd, *Univ. of Rochester*
Paul M. Brakefield, *Leiden Univ.*
Dennis Bray, *Univ. of Cambridge*
Stephen Buratowski, *Harvard Medical School*
Joseph A. Burns, *Cornell Univ.*
William P. Butz, *Population Reference Bureau*
Peter Carmeliet, *Univ. of Leuven, VIB*
Gerbrand Ceder, *MIT*
Mildred Cho, *Stanford Univ.*
David Clapham, *Children's Hospital, Boston*
David Clary, *Oxford University*
J. M. Claverie, *CNRS, Marseille*
Jonathan D. Cohen, *Princeton Univ.*
Stephen M. Cohen, *Temasek Life Sciences Lab, Singapore*
Robert H. Crabtree, *Yale Univ.*
F. Fleming Crim, *Univ. of Wisconsin*
William Cumberland, *Univ. of California, Los Angeles*
George Q. Daley, *Children's Hospital, Boston*
Jeff L. Dangl, *Univ. of North Carolina*
Stanislas Dehaene, *Collège de France*
Edward DeLong, *MIT*
Emmanouil T. Dermitzakis, *Wellcome Trust Sanger Inst.*
Robert Desimone, *MIT*
Dennis Discher, *Univ. of Pennsylvania*
Scott C. Doney, *Woods Hole Oceanographic Inst.*
Peter J. Donovan, *Univ. of California, Irvine*
W. Ford Doolittle, *Dalhousie Univ.*
Jennifer A. Doudna, *Univ. of California, Berkeley*
Julian Downward, *Cancer Research UK*
Denis Duboule, *Univ. of Geneva/EPFL Lausanne*
Christopher Dye, *WHO*
Richard Ellis, *Cal Tech*
Gerhard Ertl, *Fritz-Haber-Institut, Berlin*
Douglas H. Erwin, *Smithsonian Institution*
Mark Estelle, *Indiana Univ.*
Barry Everitt, *Univ. of Cambridge*
Paul G. Falkowski, *Rutgers Univ.*
Ernst Fehr, *Univ. of Zurich*
Tom Fenchel, *Univ. of Copenhagen*
Alain Fischer, *INSERM*
Scott E. Fraser, *Cal Tech*
Chris D. Frith, *Univ. College London*
Wulfram Gerstner, *EPFL Lausanne*
Charles Godfray, *Univ. of Oxford*
Diane Griffin, *Johns Hopkins Bloomberg School of Public Health*
Christian Haass, *Ludwig Maximilians Univ.*
Niels Hansen, *Technical Univ. of Denmark*
Dennis L. Hartmann, *Univ. of Washington*
Chris Hawkesworth, *Univ. of Bristol*
Martin Heimann, *Max Planck Inst., Jena*
James A. Hendler, *Rensselaer Polytechnic Inst.*
Ray Hilborn, *Univ. of Washington*
Ove Hoegh-Guldberg, *Univ. of Queensland*
Ronald R. Hoy, *Cornell Univ.*
Olli Ikkala, *Helsinki Univ. of Technology*
Meyer B. Jackson, *Univ. of Wisconsin Med. School*
Stephen Jackson, *Univ. of Cambridge*
Steven Jacobsen, *Univ. of California, Los Angeles*
Peter Jonas, *Universität Freiburg*
Barbara B. Kahn, *Harvard Medical School*
Daniel Kahne, *Harvard Univ.*
Gerard Karsenty, *Columbia Univ. College of P&S*
Bernhard Keimer, *Max Planck Inst., Stuttgart*
Elizabeth A. Kellog, *Univ. of Missouri, St. Louis*
Alan B. Krueger, *Princeton Univ.*
Lee Kump, *Penn State Univ.*
Mitchell A. Lazar, *Univ. of Pennsylvania*
Virginia Lee, *Univ. of Pennsylvania*
Norman L. Letvin, *Beth Israel Deaconess Medical Center*
Olle Lindvall, *Univ. Hospital, Lund*
John Lis, *Cornell Univ.*
Richard Losick, *Harvard Univ.*
Ke Lu, *Chinese Acad. of Sciences*
Andrew P. MacKenzie, *Univ. of St Andrews*
Raul Madariaga, *École Normale Supérieure, Paris*
Anne Magurran, *Univ. of St Andrews*
Virginia Miller, *Washington Univ.*
Yasushi Miyashita, *Univ. of Tokyo*
Richard Morris, *Univ. of Edinburgh*
Edvard Moser, *Norwegian Univ. of Science and Technology*
Naoto Nagaosa, *Univ. of Tokyo*
James Nelson, *Stanford Univ. School of Med.*
Timothy W. Nilsen, *Case Western Reserve Univ.*
Roeland Nolte, *Univ. of Nijmegen*
Helga Nowotny, *European Research Advisory Board*
Eric N. Olson, *Univ. of Texas, SW*
Erin O'Shea, *Harvard Univ.*
Elinor Ostrom, *Indiana Univ.*
Jonathan T. Overpeck, *Univ. of Arizona*
John Pendry, *Imperial College*
Philippe Poulin, *CNRS*
Mary Power, *Univ. of California, Berkeley*
Molly Przeworski, *Univ. of Chicago*
David J. Read, *Univ. of Sheffield*
Les Real, *Emory Univ.*
Colin Renfrew, *Univ. of Cambridge*
Trevor Robbins, *Univ. of Cambridge*
Barbara A. Romanowicz, *Univ. of California, Berkeley*
Edward M. Rubin, *Lawrence Berkeley National Lab*
Jürgen Sandkühler, *Medical Univ. of Vienna*
David S. Schimel, *National Center for Atmospheric Research*
David W. Schindler, *Univ. of Alberta*
Georg Schulz, *Albert-Ludwigs-Universität*
Paul Schulze-Lefert, *Max Planck Inst., Cologne*
Christine Seidman, *Harvard Medical School*
Terrence J. Sejnowski, *The Salk Institute*
David Sibley, *Washington Univ.*
Montgomery Slatkin, *Univ. of California, Berkeley*
George Somero, *Stanford Univ.*
Joan Steitz, *Yale Univ.*
Elsbeth Stern, *ETH Zürich*
Jerome Strauss, *Virginia Commonwealth Univ.*
Glenn Telling, *Univ. of Kentucky*
Marc Tessier-Lavigne, *Genentech*
Jurg Tschopp, *Univ. of Lausanne*
Michiel van der Klis, *Astronomical Inst. of Amsterdam*
Derek van der Kooy, *Univ. of Toronto*
Bert Vogelstein, *Johns Hopkins Univ.*
Ulrich H. von Andrian, *Harvard Medical School*
Bruce D. Walker, *Harvard Medical School*
Christopher A. Walsh, *Harvard Medical School*
Graham Warren, *Yale Univ. School of Med.*
Colin Watts, *Univ. of Dundee*
Detlef Weigel, *Max Planck Inst., Tübingen*
Jonathan Weissman, *Univ. of California, San Francisco*
Ellen D. Williams, *Univ. of Maryland*
Ian A. Wilson, *The Scripps Res. Inst.*
Jerry Workman, *Stowers Inst. for Medical Research*
John R. Yates III, *The Scripps Res. Inst.*
Jan Zaanen, *Leiden Univ.*
Martin Zatz, *NIMH, NIH*
Huda Zoghbi, *Baylor College of Medicine*
Maria Zuber, *MIT*

BOOK REVIEW BOARD

John Aldrich, *Duke Univ.*
David Bloom, *Harvard Univ.*
Angela Creager, *Princeton Univ.*
Richard Shweder, *Univ. of Chicago*
Ed Wasserman, *DuPont*
Lewis Wolpert, *Univ. College London*

WHAT'S SMALL, GREEN, AND INTELLIGENT?

Meet the Pivo 2, Nissan's compact electric concept car, designed for urban travel with a 360° rotating cabin and wheels that allow the car to scoot sideways for parking. It's one of the stars of the new exhibit "Japan Car: Designs for the Crowded Globe" at London's Science Museum, spotlighting "mobile cells"—small cars fueled by low-polluting electricity or hydrogen and equipped with intelligent driver interfaces.

Other examples include Toyota's iREAL, a sitting version of a Segway that looks like a futuristic wheelchair, with sensors that alert a driver to obstacles down the road, and Mitsubishi's electrical iMiEV, planned for release next year, that can go 160 kilometers on an overnight charge.

Key features of these vehicles are their brains. Pivo 2 has a talking "robotic agent" that offers traffic updates and route information and has voice-recognition capability to answer a driver's questions. The agent is personified by a swiveling head mounted beside the instrument panel that nods and shakes to keep the driver in a "positive frame of mind." "It infers the driver's mood through conversation and facial-monitoring technology," Nissan says. But can you make it shut up? Nissan doesn't say.

CREDITS (TOP TO BOTTOM): NISSAN; CHRISTIE'S; SUN MEDIA CORP.; DTU

Feathered and Tarred

The expensive process of getting oil from Canada's vast tar sands is not only dirtying the air and water but also threatening millions of migratory birds, according to a report by three environmental groups.

Mining the sticky sand under the boreal forest in northern Alberta and refining it into crude oil doesn't just destroy bird habitat. As many as 100,000 birds are contaminated by oil or drown each year in tailing ponds, the report says.

The 14 million hectares that contain oil sands are used by 22 million to 170 million birds each summer for breeding and nesting. Ornithologist Jeff Wells of the Boreal Songbird Initiative, a U.S. conservation group in Seattle, Washington, and co-authors estimate that over the next 3 to 5 decades, as many as 166 million birds from 290 species might be lost, representing, at worst, a 50% decline in the population. "We wanted to provide an honest assessment of the potential risks of continuing with this development," Wells says. The report, *Danger in the Nursery*, calls for a halt to new mining until the impact on birds can be lessened. So far, the industry shows no signs of changing course.

Earthly Magnetism

Lost in the South Atlantic Ocean, 1750 kilometers from the nearest coastline, Tristan da Cunha is the world's most remote island. But it made waves in some research circles last month, when Danish scientists cut the ribbon on a new geomagnetic observatory station there.

The island lies within the South Atlantic Anomaly, an elliptical area roughly 560 km across where Earth's magnetic fields are weakest—less than 30 μT, about half the intensity of its strongest regions. The anomaly is "one of the biggest gaps in our current network of ground stations," says Jürgen Matzka, a researcher at the Danish Meteorological Institute in Copenhagen. The $385,000 observatory will collect readings every 3 seconds to detect the constant, minute variations in the magnetic field and send the data back to Copenhagen. The new information will help researchers understand how areas of weak geomagnetic force develop and grow, says geophysicist Peter Olson of Johns Hopkins University in Baltimore, Maryland. But major changes in magnetic forces within Earth's core can take years to penetrate the mantle, so "what payoff there will be, will be down the road," Olson says.

Fit for a Queen?

They are listed as "neo-Assyrian gold earrings circa 8th-7th centuries BC," and Christie's planned to auction them off this week for upward of $50,000.

But the Iraqi government claims the jewelry almost certainly came from the ancient tombs of Assyrian queens discovered in 1990 at Nimrud in northern Iraq. The jewelry was stored in Baghdad's Central Bank until 2003, when it was moved from flooded underground vaults to the Iraq Museum. Elizabeth Stone, a Mesopotamian archaeologist at Stony Brook University in New York, says British officials alerted archaeologists after spotting the artifacts for sale.

Christie's says the earrings were taken out of Iraq in 1969, long before the Nimrud excavations. But Donny George Youkhanna, the former head of Iraq archaeology now at Stony Brook, insists they are from Nimrud. Stone also says "they look identical" to the Nimrud earrings. The Iraqi government last week reportedly requested that Christie's halt the sale and return the earrings. They were taken off the block on 4 December; no word yet on their fate.

Published by AAAS


Solomon with Academy Vice President Jean Salençon.

Three Q's

U.S. atmospheric scientist **Susan Solomon** has won this year's Grande Médaille from the Institute of France's Academy of Sciences for her contributions to both ozone chemistry and climate. In the 1980s, Solomon—a senior scientist with the U.S. National Oceanic and Atmospheric Administration in Boulder, Colorado—helped link the growing ozone hole to pollutant chlorofluorocarbons. CFCs are also potent greenhouse gases, and the loss of stratospheric ozone can alter climate. So more recently, she co-chaired the science working group of the Nobel Prize–winning Intergovernmental Panel on Climate Change (IPCC).

Q: What prompted your career shift?
I realized how important chemistry can be in climate. The [1987] Montreal Protocol [controlling CFC emissions] did more to benefit climate than the [1992] Kyoto Protocol has. Montreal is five to six times Kyoto.

Q: Why would an atmospheric chemist spend years leading a climate assessment?
A moment of madness, I suppose. But all these things have to be looked at together, and I learned a terrific amount about climate.

Q: Any benefits to IPCC from having its first woman working group co-chair?
A woman's perspective is at times a little different, and different is good.

MOVERS

NEW UNAIDS HEAD. The United Nations has chosen an economist instead of a medical scientist to lead its efforts to slow the spread of HIV and help infected people. Michel Sidibé, originally from Mali, will take the helm in January at the Joint United Nations Programme on HIV/AIDS (UNAIDS). Sidibé, who has worked at UNAIDS since 2001 and currently is deputy executive director of programmes, replaces Belgian epidemiologist Peter Piot, who will leave the job at the end of the year (*Science*, 31 October, p. 657).

Sidibé expects his background to serve him well given the current global financial crisis. "We have to pay more attention to accelerated implementation with a need for results and more accountability," he says. "One of the first things we need to do is reduce the cost of doing business. The unit cost is not sustainable; let us be honest." Sidibé, who speaks several African languages, says he hopes to use his knowledge of the region "to create a pressure for producing results."

INSIDE GOVERNMENT

NEW BOSS AT NIEHS. Linda Birnbaum, a longtime government toxicologist, has been named director of the $730 million National Institute of Environmental Health Sciences (NIEHS) in Research Triangle Park, North Carolina. Birnbaum succeeds David Schwartz, who left in February amid ethics concerns (*Science*, 22 February, p. 1021).

Birnbaum, who takes over next month, is an expert on the health effects of dioxin and other hormonelike pollutants. She has spent nearly 29 years in government, first at NIEHS and more recently at the Environmental Protection Agency's research lab near NIEHS. Some researchers are worried that Birnbaum might be less supportive of investigator-initiated research than of studies to support regulations. On the other hand, her research has bridged both because "it's been very focused on [biological] mechanisms," says toxicologist David Eaton of the University of Washington, Seattle, who says Birnbaum "is well-prepared to lead NIEHS." Birnbaum says any concerns about a decline in blue-sky basic research are "unfounded" and adds that "it's still going to be extremely important."

Birnbaum sees "a lot of opportunities for improvement" at the institute. For example, she wants to look more closely at whether the trace levels of pollutants in most Americans are harmful.

Celebrities >>

CROSSING THE POND. Stephen Hawking is at the head of what officials at the Perimeter Institute for Theoretical Physics hope will be a parade of 40 prominent scientists coming to the 7-year-old center in Waterloo, Canada.

Hawking is retiring next year from the University of Cambridge in the U.K. after reaching the school's mandatory retirement age of 67. Starting in July, he will spend 6 weeks a year as a "distinguished research chair" at the Perimeter Institute. "It was really easy to persuade him" to accept the appointment, says Neil Turok, executive director of the institute, because Perimeter focuses on quantum theory and the physics of spacetime, Hawking's precise field of interest.

In addition to naming the 40 distinguished research chairs, officials also hope to double Perimeter's 10-person faculty and contingent of 65 postdocs and graduate students over the next 5 years. The institute is funded in part by business tycoon Mike Lazaridis, whose company makes BlackBerry electronic devices, and Canada's national and regional governments. Turok says Perimeter will be able to support the expansion with existing funds.

Got a tip for this page? E-mail people@aaas.org

CREDITS (TOP TO BOTTOM): B. EYMANN/ACADEMIE DES SCIENCES; NIEHS; UNAIDS; RANDALL BENTON/MCT/LANDOV

The LHC's worrisome problem
1620

Biodefense goes to Kansas
1620

NASA

Delays in Mars Mission Will Ripple Across Space Science

Faced with mounting technical glitches, last week NASA decided to delay its Mars Science Laboratory (MSL) for at least 2 years. That means the spacecraft will not get off the ground before fall 2011. The new date is a major disappointment for researchers eager to learn whether Mars ever supported microbial life. But what worries them even more is the price that other planetary missions may have to pay to free up the additional $400 million that a delayed MSL will cost NASA.

The troubles surrounding the sophisticated lab, twice as long and three times as heavy as the rovers that have explored Mars since 2004, are part of a growing crisis that President-elect Barack Obama will inherit in January. NASA's science program needs more money for a host of planned spacecraft. But so do the agency's efforts to complete the space station, retire the space shuttle, and build a new launcher to send humans to the moon. Obama pledged during his campaign to back a new generation of science missions as well as the new launcher, which would add billions to NASA's current $18 billion annual budget.

Speaking to reporters on 4 December, grim-faced NASA managers blamed problems with the lab's small but complex motors, called actuators, that control many of its critical moving parts. If they don't function properly, said NASA Mars Exploration Director Doug McCuistion, the massive lander could turn into "a metric ton of junk." He says completing tests and keeping the MSL team together will cost $400 million over several years, bringing the total price tag to as much as $2.3 billion. The lab was already 15% over budget before the latest estimate.

The extra money, says NASA science chief Edward Weiler, will come from other projects involving Mars and possibly other planets. The queue contains three spacecraft to be launched in 2011—a small atmospheric probe to Mars, a robot to survey Jupiter, and a mission to chart the moon's interior. A 2016 Mars mission that has not been fleshed out will cost $800 million to $1.4 billion. And next month, NASA is expected to select a $3 billion spacecraft to study a moon of either Jupiter or Saturn that would be launched by 2020. "There will be impacts," says Weiler. "We probably will have to delay a major planetary mission."

That's not what planetary scientists want to hear. "It's all bad news," says Fran Bagenal, a planetary scientist at the University of Colorado, Boulder. "There is no silver lining." But Weiler does see an upside in combining forces with the European Space Agency (ESA) on a common plan for Mars exploration. "We could probably do a heck of a lot better missions if we do it together," he said. "It's a no-brainer."

David Southwood, ESA's director of science, is reluctant to discuss NASA's possible contributions to ESA's ExoMars mission, proposed for 2016, before joint technical discussions are held early next year. He says that "some things are at the heart of the European investment," noting that ESA wants to test its mettle at landing on Mars and roving across its surface. But providing an orbiter to aid communication with Earth or instruments for the lander are areas in which NASA might be able to help, he adds. Cooperation would also be vital for any sample-return mission. This collaboration "is lifting a curtain on the future," Southwood says.

The causes of MSL's overruns are controversial. Weiler's predecessor, S. Alan Stern, wrote recently in *The New York Times* that his boss, Administrator Michael Griffin, feared retribution from the U.S. Congress if he canceled the mission, and that NASA managers have failed to control MSL and other space science overruns. The delay is both "disheartening" and "predictable," he told *Science* last week, adding that further MSL overruns are likely to surface.

But some scientists point the finger at Stern for planning to divert funds from the Mars program before he resigned from the agency 8 months ago. "If Stern hadn't mucked around, the Mars program would have been able to handle" the overruns, says John Mustard, a planetary scientist at Brown University who also chairs a Mars advisory committee. Stern dismissed such charges as "scapegoating."

Much ire has also been directed at the Jet Propulsion Laboratory in Pasadena, California, which is handling the MSL mission. Its director, Charles Elachi, admitted at the press conference that "we have not been good at doing cost estimates." But he says the lab is proud of its record of three successful Mars landings in the past 5 years.

Space scientists agree that NASA and the science community must rein in costs to avoid a data-dry future. Bagenal says that the "MSL debacle" cannot be allowed to happen again, lest planned missions never get off the ground. "We have to put more attention on careful costing," she says.

In the meantime, Griffin promises to find "the least damaging way" out of the mess by talking with Congress, the White House, and the scientific community. "This is math we will be doing in public," he says. "We just don't have the answers."

–ANDREW LAWLER

With reporting by Daniel Clery.

CREDIT: JPL/NASA

Extra protection. A 2-year delay in the Mars Science Laboratory mission gives NASA time to test all its components, including the "clamshell" to buffer the landing.

Irrationality and financial modeling
1624

Ferrying oceanographic research
1627

OBAMA TRANSITION

A Fresh Start for Embryonic Stem Cells

U.S. researchers are eagerly anticipating the moment that President-elect Barack Obama takes office and sweeps away the Bush Administration's restrictions on federal funding for research with human embryonic stem (ES) cells. Scientists at the U.S. National Institutes of Health (NIH) are making no secret of their glee. "I think everybody here is incredibly excited about the new Administration," says Story Landis, director of the National Institute of Neurological Disorders and Stroke and chair of the NIH Stem Cell Task Force.

Landis predicts that despite the static NIH budget, more federal money will be going into basic research on human ES cells—funded at $42 million this year. Grants will be highly competitive, she says, because "there are incredibly promising things to do." Since President George W. Bush's directive of 9 August 2001, federally funded researchers have been limited to 21 human ES cell lines that were derived before that date. But as soon as Obama says the word, as he has repeatedly promised to do, they will be able to use hundreds of lines derived since.

Picking up where the Clinton Administration left off in 2000, NIH will be drafting new guidelines on matters such as informed consent by donors of embryos from which cell lines were derived. Just how many of the more recently derived lines will qualify under the guidelines—and how the guidelines will be implemented—is yet to be determined. Nonetheless, Harvard University researcher Kevin Eggan predicts that "there will be a massive switch in the lines that people use."

Gone will be onerous requirements to keep federally funded ES cell research separate from privately funded research using nonapproved lines, which for some investigators has entailed the construction and outfitting of separate labs. It's been "a pain in the behind even for someone [like me] with plenty of private cash," says Eggan. "This was a crazy artifact of the Bush policy that is antithetical to everything that good science is supposed to be about," says Sean Morrison of the University of Michigan, Ann Arbor.

Now, says Columbia University motor neuron disease researcher Christopher Henderson, "we will be able to design projects in the most efficient way possible using the most appropriate lines," doing away with duplication in both research and equipment.

"As president, I will lift the current administration's ban on federal funding of research on embryonic stem cell lines created after August 9, 2001 through executive order."

—BARACK OBAMA, SCIENCE DEBATE 2008

For example, says Landis, federally funded researchers will now have access to ES cells from embryos that carry the genes for Huntington's disease, donated from fertility clinics after preimplantation genetic diagnosis. They will be able to test ES-like induced pluripotent stem cells generated from the skin cells of Huntington's patients by comparing them with ES cells, the "gold standard." And they'll be able to test new drugs on neurons grown from ES cell lines.

Money problems aside, research still won't proceed unfettered. The government will not be funding the derivation of new ES cell lines or the practice of research cloning, known as somatic cell nuclear transfer (SCNT). Both are out of bounds because language imposing a federal ban on embryo research, known as the Dickey-Wicker Amendment, has been attached to NIH appropriations bills since 1995.

Congress is expected to ratify Obama's new policy by passing legislation again that Bush vetoed twice. But no one is currently expecting lawmakers to attack Dickey-Wicker, and although scientists want to be able to use SCNT, they say the field can advance without it. For the near future, says Morrison, "my sense is that the field will be more focused on adult cell reprogramming"—that is, finding new ways to turn a patient's own skin cells directly into liver cells, for example, rather than using an egg to reprogram them.

Zach Hall, former president of the California Institute for Regenerative Medicine (CIRM) in San Francisco, thinks the upcoming federal policy change will have a "multiplier" effect on state projects that were started largely to circumvent the Bush restrictions. These initiatives may provide more leeway than federal guidelines, allowing researchers to generate new lines and possibly try SCNT. As for California, CIRM mastermind Robert Klein says the agency is in good shape, at least through mid-2009, despite the state's $28 billion budget deficit.

A new Obama policy relaxing controls on ES cells should help foster more realistic attitudes about the promise of stem cell therapies, says Amy Comstock Rick, president of the Coalition for the Advancement of Medical Research in Washington, D.C. At a recent meeting, she said, "There's been a shift in understanding" on the part of people in the patient community—they are less inclined to blame all obstacles on the restrictions imposed by Bush and recognize that in any case "the field has an awfully long way to go."

–CONSTANCE HOLDEN

CREDIT: JIN LEE/BLOOMBERG NEWS/LANDOV

Published by AAAS

PARTICLE PHYSICS

Sotto Voce, LHC Repair Plan Points To Weaknesses in Original Design

Officials at CERN, the European particle physics lab near Geneva, Switzerland, issued a four-page report last week tersely describing how they plan to get the 27-kilometer-long Large Hadron Collider (LHC), the world's biggest particle smasher, working again after its 19 September breakdown. Although the report doesn't mention errors in design, the list of fixes does point to flaws, including one that some physicists say cannot be completely eliminated. "There are some questions about the design, and they are fixing some of them and some of them cannot be fixed," says Peter Limon, an accelerator physicist at Fermi National Accelerator Laboratory in Batavia, Illinois.

The breakdown occurred just 9 days after researchers first circulated protons through the $5.5 billion LHC. The collider comprises more than 1600 electromagnets linked like sausages to form a ring. Researchers were raising the current past 9000 amps in a string of 209 magnets when an electrical connection between two of them melted. This burned a hole in the pipe that surrounds the superconducting niobium titanium wire and keeps it bathed in frigid liquid helium. Boiling helium flooded the magnets' casings, creating a pressure wave that pushed around some of the 35-metric-ton magnets and propelled soot and debris down the pristine beam pipe through which the protons speed.

CERN workers have begun to remove 53 damaged magnets from the LHC's tunnel. They will rebuild 39 and clean the rest. The LHC will not collide particles until July at the earliest, officials now say.

The pressure built up in the magnet casings because only every fourth one had an emergency relief valve and those were too small to release the errant helium into the LHC tunnel quickly enough. To correct that shortcoming, workers will install a larger valve on every casing, the report says.

It will be trickier to ensure that an electrical connection does not melt again. The faulty connection lay in a straight-shot return line called a "bus bar." After current winds its way through every magnet in a string, the bus bar carries it back through the magnet casings to the power supply. Between casings, the bar has a solder splice like the one that melted. Although the LHC has a system to detect when individual magnets overheat and lose their superconductivity, the bus bar is protected by a relatively insensitive system that looks for a voltage increase—a sign of heating—across the full length of the bar. That's a design flaw, says Thomas Roser, an accelerator physicist at Brookhaven National Laboratory in Upton, New York.

To better detect overheating, CERN will install equipment to individually monitor the voltages across each connection. They will also monitor the temperature of the surrounding liquid helium. Still, it takes 100 seconds to shunt current out of a magnet string. That time is too long to keep a very hot connection from melting, but the machinery cannot feasibly be changed to shorten it. So the ▶

BIOSECURITY

How Kansas Nabbed the New Bio- and Agro-Defense Lab

If you build it, they will come. The maxim seems to have worked for Kansas State University (KSU) in Manhattan, which the U.S. Department of Homeland Security (DHS) selected last week as its preferred site for a $450 million facility to replace the aging Plum Island Animal Disease Center off Long Island, New York. What made the university stand out from the competition, KSU and federal officials say, was a recently completed $54 million biocontainment lab on campus for animal research, funded by the state, as well as the lack of any vigorous local opposition to work involving dangerous animal pathogens.

DHS announced in 2006 that it would replace the Plum Island center, a biosecurity level 3 (BSL-3) lab where researchers have been studying livestock diseases such as foot-and-mouth disease and anthrax for 5 decades, with a BSL-4 National Bio- and Agro-Defense Facility (NBAF) to be located on Plum Island or somewhere on the mainland. Although some environmental groups opposed the decision, DHS argued that the new facility was needed to study emerging animal diseases such as African swine fever—which can only be handled in a BSL-4 lab—and that building it would cost less than upgrading the existing lab at Plum Island.

Advocate. Kansas Senator Pat Roberts spearheaded the state's aggressive lobbying, which included building this BSL-3 lab on the KSU campus.

CREDIT: KANSAS STATE UNIVERSITY

A total of 29 institutions submitted proposals to host the facility. DHS short-listed six of them, including Plum Island, in July 2007. Last week, DHS published a final Environmental Impact Statement for all six candidates, recommending KSU as its top choice and placing the University of Texas, San Antonio, and Georgia State University in Athens in second and third place, respectively. Governors of two of the losing states, Texas and Mississippi, have indicated that they may challenge the decision during the 30-day comment period before the selection becomes final. But federal officials say the choice is unlikely to be reversed.

"Kansas by far had more strengths than any of the other sites," says Jamie Johnson, director of national labs at DHS. The new Biosecurity Research Institute (BRI) on campus means there is already considerable research expertise in livestock diseases there, he says. "They also had strong community acceptance, and they offered a solid package to help offset the cost of building the facility."

KSU has offered 15 hectares of land for the project, and the Kansas legislature has granted permission to the state to spend up to $105 million to bring roads and other infra-

Published by AAAS

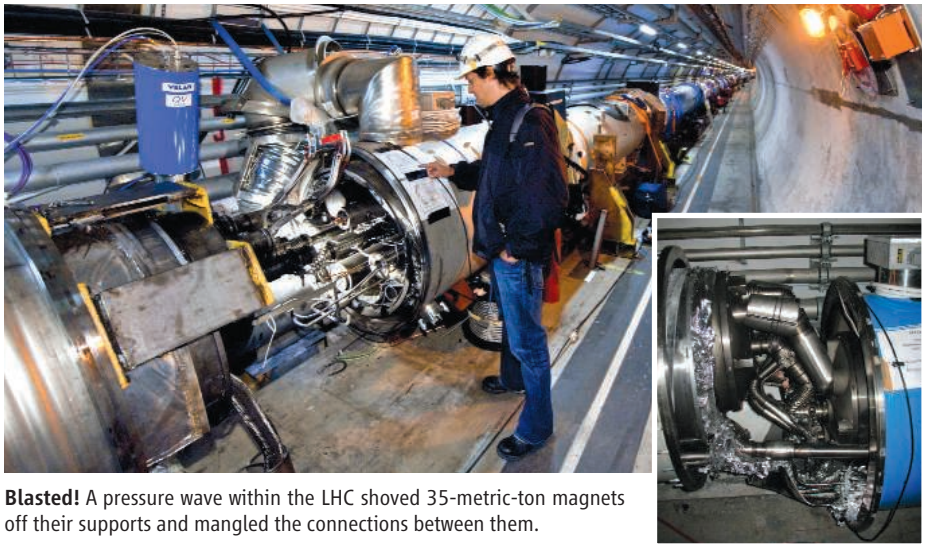

Blasted! A pressure wave within the LHC shoved 35-metric-ton magnets off their supports and mangled the connections between them.

only "fix" is to spot a warm splice before it gets too hot. "It absolutely must not be allowed to happen again," says CERN's Lyn Evans, who leads the LHC project. "It's a machine on the edge, and all effort must go into learning the warning signs" of trouble.

Physicists hope that the 20 nations that fund CERN will be patient while they work out the kinks. As *Science* went to press, delegates to the CERN Council were meeting at the lab. "I expect the council will understand that this is a difficult machine and that we will have a few hiccups," Evans says. Patience may wane if the LHC suffers another setback, however. "If they have another one, then it's going to get more serious," Limon says. "The council is going to say, 'What's going on here?' " So relief valves won't reduce the pressure on CERN physicists next summer.

–ADRIAN CHO

CREDITS: CERN

structure to the site. State officials expect NBAF to bring 1500 construction jobs, boost the state's veterinary and animal-care industry, and add a net $3.5 billion to the state economy.

For more than a decade, political leaders, scientists, and businesses in Kansas have been trying to make their state the leading venue for research on food safety and animal diseases. Efforts began in 1998 when Kansas Senator Pat Roberts (R), then chair of the U.S. Senate's Emerging Threats Subcommittee, invited KSU researchers to testify on the potential risks and consequences of bioterrorism on livestock and agriculture. "Nobody at the time was talking about the terrorist threat within the agricultural community," says Jerry Jaax, a former U.S. Army veterinarian who is KSU's associate vice provost for research compliance.

At Roberts's urging, KSU leaders came up with a proposal to build a research facility to study diseases that could devastate Kansas's cattle-based economy. After failing to get funding from the U.S. Department of Agriculture, the university approached the state legislature, which appropriated funding in 2002. The facility was completed in 2007 and is now being set up for experiments.

Ron Trewyn, vice president for research, says the bipartisan political support behind BRI paved the way for the state's proposal to DHS. The university had already invested a lot of effort to reassure ranchers and business owners that the BSL-3 facility did not pose a hazard to the surrounding community. Jaax, who did much of the outreach, said the university also emphasized "the importance of this research to the economic security of Kansas—how much Kansas would lose if there were a major bioterrorism event."

It was a "well-organized, extremely well-funded consortium of proponents," says Tom Manney, a retired KSU biophysics professor who led a local campaign to stop the facility from coming to Manhattan. Although he says he knows "a lot of ranchers who are very upset about doing foot-and-mouth research in the middle of this area," Manney said he had difficulty rallying opposition to the project.

If the choice is finalized, DHS officials say they expect to have the facility running by 2015 and staff it with 350 employees, half of them scientists. Some researchers will likely be hired locally, DHS officials say. Until NBAF is ready for operation, Trewyn says, the federal government is welcome to "take over" BRI to start some transition projects.

–YUDHIJIT BHATTACHARJEE

With reporting by Jocelyn Kaiser.

Scientific Integrity at Issue

A new high-profile group is launching the first major nonpartisan effort to study how the U.S. government ought to use scientific information to make decisions. "We will be looking at what policymakers can do that is legitimate and what is beyond the pale," says David Goldston, an organizer for the 13-member panel and former staff director for the U.S. House of Representatives Science and Technology Committee. He says the group is not trying to "to dissect what the Bush Administration has done right or wrong." Instead, it will examine federal advisory boards, conflict-of-interest policies, and what role scientists should play in decisions by regulatory agencies such as the Environmental Protection Agency. The panel includes former Bush Administration officials, former House Science Chair Sherwood Boehlert (R–NY), and the president of the left-leaning Union of Concerned Scientists, which has criticized the Bush Administration for alleged political meddling in federal science. The group hopes to release its report in June. **–ELI KINTISCH**

Obama at Sea

Ocean scientists are hoping a friendly meeting with President-elect Barack Obama's transition team last week will bode well for ocean research. The 90-minute sitdown included representatives from environmental and scientific groups and transition officials including Sally Yozell, a former official with the National Oceanic and Atmospheric Administration (NOAA). Bob Gagosian of the nonprofit Consortium for Ocean Leadership in Washington, D.C., says he's buoyed by the new Administration's focus on ocean issues—"You could hear a pin drop"—and its choice of New Mexico Governor Bill Richardson to head the Department of Commerce, where NOAA is housed. "He knows how to manage science," Gagosian said of the former secretary of energy. **–ELI KINTISCH**

Inside *Science*Insider

The new policy blog on *Science*'s Web site continues to attract thousands of new readers. Written by the magazine's staff from Beijing to Washington, D.C., *Science*Insider provides breaking news and analysis from the world of science and the people who shape it. Entries this week included news on Barack Obama's interest in quarks, an analysis of efforts to curb conflicts of interest at the U.S. National Institutes of Health, and new twists in the fight between government reformers and scientist-protesters in France. Check it out at blogs.sciencemag.org/scienceinsider.

Published by AAAS

NATIONAL INSTITUTES OF HEALTH

Researchers Could Face More Scrutiny of Outside Income

Faced with an escalating controversy about researchers who allegedly broke rules on reporting income from drug companies, U.S. National Institutes of Health officials outlined plans last week to tighten federal conflict-of-interest regulations for NIH grantees within the next 6 to 12 months. The news came the same week that several research institutions said they intend to make industry payments to their faculty members public.

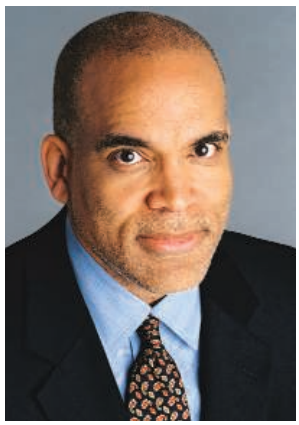

Decider. Acting NIH chief Raynard Kington gets the first crack at fixing the conflicts-of-interest furor.

NIH standards have been under intense public scrutiny since last summer, when Senator Chuck Grassley (R–IA) claimed that three prominent Harvard University psychiatrists with NIH grants had failed to report millions of dollars in outside income to their institutions (*Science*, 27 June, p 1708). Until now, NIH has said little about these and half a dozen similar cases that Grassley has identified. Last week at a meeting of the NIH director's advisory committee, however, the agency disclosed that it has been investigating 20 individuals over the past year, some identified in press reports and in Grassley's probe and others identified by NIH. According to Sally Rockey, acting director of the NIH office of extramural research, in 13 of the cases no rules were broken, and six are still being investigated. One "serious" case led to the suspension of a $9.3 million grant to Emory University (*Science*, 24 October, p. 513).

Although current federal conflict-of-interest regulations are "likely being followed in the majority of cases," said NIH acting director Raynard Kington, NIH and officials at the Department of Health and Human Services (HHS) are now considering a revision. NIH and HHS have prepared a draft notice soliciting public input through a series of questions. It asks: Should researchers be required to report all income, not just income exceeding $10,000 per year? Should NIH review the nature of conflicts, including details that are now reviewed only by institutions? Should NIH require a policy for institutional conflicts of interest? Last week, HHS submitted the notice to the White House Office of Management and Budget. It must act within 90 days; a period of 60 days for public comment follows.

Grassley is proposing his own solution: new legislation that would require drug and device companies to post all payments to physicians in a national public database. Anticipating this action, the Cleveland Clinic in Ohio announced on 3 December that it is posting information in its physician directory about outside income over $5000 a year and royalty and equity interests for bench scientists and clinical researchers. This step is a first for a major academic research center, the clinic says. Guy Chisolm, a professor of cell biology and director of the clinic's new conflict-of-interest program, explains that the Cleveland Clinic is listing names but holding off on posting the payment amounts until it can discuss with drug companies and Grassley's staff how they will distinguish among different types of payments, such as those for travel expenses and consulting fees. "I don't want our faculty in jeopardy" of having to explain discrepancies, Chisolm says.

The University of Pennsylvania plans to post similar information in the spring, says Arthur H. Rubenstein, dean of the medical school. Duke University in Durham, North Carolina, where an affiliated institute that performs industry-sponsored clinical trials already posts complete disclosure forms for 21 faculty members, is considering doing the same, says Ross McKinney Jr., a professor of pediatric infectious diseases at Duke. Chisolm says Johns Hopkins University and Stanford University are also "interested in the concept."

–JOCELYN KAISER AND LILA GUTERMAN

Lila Guterman is a science writer in Washington, D.C.

MALARIA

Vaccine Comes Another Step Closer

NEW ORLEANS, LOUISIANA—The most advanced candidate vaccine for malaria has cleared another major hurdle and is now ready for its last and biggest test: a phase III trial of 12,000 to 16,000 children at 11 locations in seven African countries. Two new studies published this week by *The New England Journal of Medicine*—and presented, to considerable excitement, at a meeting* here on Monday—confirm that the vaccine works and is safe, and, perhaps most important, they show it can be given along with a series of other vaccines that many babies in the developing world receive shortly after birth.

The vaccine, called RTS,S, is far from perfect: It appears to prevent roughly half of all clinical episodes of malaria at best. But researchers believe that's good enough to help make a major dent in the disease, especially when applied in tandem with other tools, such as long-lasting insecticide-impregnated bed nets and a new generation of drugs called ACTs. And they're encouraged by the fact that trial outcomes so far have been consistent. After a "long history of sob stories" in malaria vaccine development, "this seems like a solid vaccine, study after study," says Christopher Plowe of the University of Maryland School of Medicine's Center for Vaccine Development in Baltimore.

RTS,S, designed in the late 1980s by an ancestor company of GlaxoSmithKline (GSK) in Rixensart, Belgium, aims to prevent the parasite *Plasmodium falciparum* from infecting and surviving in human liver cells. It consists of a fragment of a protein from the parasite's outer surface, fused with a hepatitis B virus protein that helps trigger a more vigorous immune response. Since 2001, the vaccine has been developed in a partnership between GSK and the PATH Malaria Vaccine Initiative, with financial backing from the Bill and Melinda Gates Foundation.

Previously, a study among children aged 1 to 4 in Mozambique showed that the vaccine, coupled with a GSK-developed immune booster or "adjuvant" named AS02, prevented 30% of malaria cases in the first 6 months after the shots were given, and perhaps as many as 58% of severe cases (*Science*, 22 October 2004, p. 587). Another study published last year showed that it protected infants—its intended target audience—as well.

Researchers hope to keep administration of the malaria vaccine simple and cheap by making it part of the Expanded Program on ▶

*57th Annual Meeting of the American Society of Tropical Medicine and Hygiene.

CREDIT: NIH

Published by AAAS

SCIENCE POLICY

Biosummit Seeks to Draw Obama's Attention to the Life Sciences

How do you make a pitch for spending more money on basic science at a time when the whole world seems to be going broke? That question faces a group of scientists who met last week in Washington, D.C., at a "Biosummit," part of a new campaign to focus public attention on the importance of the life sciences. It's not clear whether the meeting and two planned follow-up reports will ask for an explicit increase in public spending. But one organizer—biologist Keith Yamamoto of the University of California, San Francisco—says he expects the project will give "very explicit" proposals for improving science education and grant mechanisms. The idea, he said, is to focus on "broad issues that will have a very big impact," such as removing barriers between fields. The first step, he said, will be to deliver an overview "white paper" to the Obama Administration by February.

Speakers at the 3 December Biosummit, organized by the U.S. National Academies, included two former directors of the U.S. National Institutes of Health (NIH), Elias Zerhouni and Harold Varmus; the president of the Howard Hughes Medical Institute, Thomas Cech; Massachusetts Institute of Technology (MIT) President Susan Hockfield; and others. Their comments went to a 17-member panel chaired by MIT biologist Phillip Sharp and E. I. du Pont de Nemours Vice President Thomas M. Connelly Jr., who will oversee the project and deliver a full report with recommendations in August. For the academies, that's "warp speed," says project officer Ann Reid.

The project began to take shape about a year ago, says Yamamoto, who chairs the Academies Board on Life Sciences. In a way, he concedes, it was a reaction to an earlier pitch for science, a report from the academies in 2005 called *Rising Above the Gathering Storm*. Many credit that document with galvanizing support in Congress for the physical sciences (*Science*, 9 May, p. 728). But *Gathering Storm* said little about bioscience. Yamamoto notes that "it sectored out the physical sciences and engineering away from life sciences." This was understandable, he adds, because NIH had just come off a 5-year doubling of its budget. But NIH's budget is now stagnant.

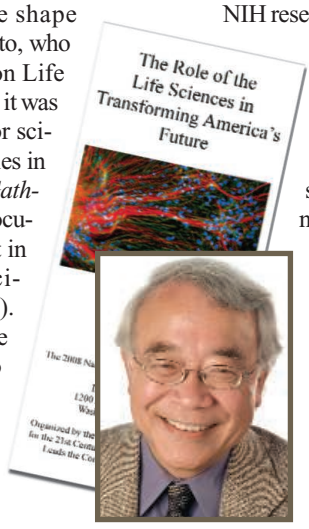

Brainstorming. Keith Yamamoto helped orchestrate a review of what's needed in basic research.

The Board on Life Sciences recruited two sponsors—NIH and the U.S. National Science Foundation—to finance the anticipated $500,000 cost of the Biosummit project. Yamamoto says he hopes the new "gathering storm for biology" will help open up the life sciences to other disciplines such as physics, engineering, and mathematics. Setting priorities will be more important than seeking "lots of new dollars," he says.

In his talk, Zerhouni stressed the need to "create venture space" where scientists can take risks. The peer-review system, although good at stopping weak science, he said, is "not very good" at identifying new ideas. He disparaged the "herd mentality" reflected in much NIH research and gave a short list of what he'd like to see, including more methods to analyze dynamic biology "in a standardized and reproducible fashion." In an interview, Varmus spoke of the need for inclusiveness and the importance of avoiding a "tit for tat" competition among fields.

One person who says he wouldn't hesitate to ask for a hefty increase in bioscience funding is the chief author of the original *Gathering Storm* report, former aerospace executive Norman Augustine. "The life sciences need to be given additional resources," he says. Legislators would be "proud" to invest in science, education, and "fixing the long-term problems" of the economy rather than bailing out failed companies. And the cost would be small in comparison to what's being spent on financial rescues, he says: "You wouldn't even have to replot the charts."

–ELIOT MARSHALL

Immunization (EPI), a series of shots against diphtheria, tetanus, polio, and *Haemophilus influenzae B* given shortly after birth. To test whether that can be done safely, the researchers gave RTS,S with AS02 along with the EPI vaccines to 340 Tanzanian babies at 8, 12, and 16 weeks after birth. The new shot did not reduce antibodies against the other vaccines, they found, and reduced the incidence of malaria during the first 6 months after vaccination by more than half.

A shot at prevention. Salim Abdulla, a lead author on one of the vaccine studies, examines a Tanzanian child with malaria.

The second new study tested whether it's safe to give RTS,S with a slightly different adjuvant called AS01, which GSK believes to be more potent. Carried out in 894 children aged 5 to 17 months in Tanzania and Kenya, the study found that the combination was safe and led to a 53% reduction of clinical malaria in the 8 months following vaccination. Based on those findings and another study in Ghana, also presented here, the partnership has picked AS01 as the adjuvant for its phase III trial. That study, still awaiting approval in some of the participating countries, will start within 3 months, says GSK researcher Joe Cohen, a co-inventor of RTS,S.

"These are rigorous studies. I'm impressed," says Blaise Genton, a malaria researcher at the Ifakara Health Research & Development Centre in Tanzania, who was not involved in the trials. Several worries remain, however. One is that rather than preventing serious malaria, the vaccine may simply be delaying it by a number of years. But even if RTS,S should fail its final exam, researchers take heart from the fact that more possible replacements than ever are behind it in the development pipeline.

–MARTIN ENSERINK

CREDITS (TOP TO BOTTOM): THE NATIONAL ACADEMIES; PHOTO COURTESY OF UCSF; JOHN-MICHAEL MAAS/DARBY COMMUNICATIONS

Published by AAAS

Crazy Money

Humans aren't rational, as the recent economic crisis shows. So why should financial theories assume that they are?

NEW YORK CITY—Falling housing prices, crashing stock markets, contracting credit: Even the experts seem bewildered by the current economic crisis. Quantitative analysts (quants)—the whiz-kid financial engineers whose algorithms have dominated Wall Street trading in recent years—have watched those algorithms fail. Former Federal Reserve Chair Alan Greenspan acknowledged in October that there was "a flaw in the model that I perceived … defines how the world works." U.S. Treasury Secretary Henry Paulson flip-flops about the most effective way to spend an increasingly inadequate-seeming $700 billion of taxpayer money.

Online
sciencemag.org
Podcast interview with the author of this article.

How could the experts be at such a loss? "One of the biggest factors in the current crisis is human behavior," says Andrew Lo, a financial economist at MIT Sloan School of Management in Cambridge, Massachusetts. However, the classical theory of finance simply does not address human psychology. It looks more like a physical science than a social science—relying on the premises that markets are "efficient," immediately reflecting new information, and investors are "rational," always acting in their self-interest. Although industry and regulators don't adopt classical finance theory wholesale, its assumptions underlie many of their choices.

Most of the time, classical finance theory works very well—and there's the rub. Lo compares it to Newtonian gravitation. During normal circumstances, people are generally rational, and the theory describes observed reality quite well. But in extreme circumstances—such as the past months for our economy—people panic, and the theory fails. Is a grander, general relativity–like theory of finance in reach? Lo says it is. Others, such as Jeffrey Wurgler, a financial economist at New York University's (NYU's) Stern School of Business, say the effort would be more like searching for a financial "string theory, which is unbelievably more complicated"—and possibly futile.

What went wrong

Most accounts of the current financial crisis begin earlier this decade, when, inspired by the booming real estate market, mortgage lenders started giving loans to just about anyone who asked for one. Those loans got bundled and repackaged many times into risk-obscuring financial instruments, such as the now-infamous collateralized debt obligations (CDOs).

Through the unregulated "shadow banking system," these instruments ended up in the portfolios of nearly every bank and financial firm around the world. Because of the lack of regulation, members of this shadow system habitually borrowed dozens of times their own worth in cash—a debt that would be perilous if their bets didn't pan out.

And that's what happened when the real estate market, and thus the CDOs, turned sour. The losses surged through the world economy. Many firms—and, in some cases, their associated commercial banks—couldn't stay above water. Not knowing who would fail next, banks stopped lending, leading to further failures. To raise money, investors were forced to sell perfectly good stocks, causing stock prices to fall. "It's a very complicated system that's malfunctioning," says Yale University economist Robert Shiller.

Blame has fallen on quants for various aspects of the crisis. First, mathematical models were increasingly used to determine

CREDIT: IMAGES.COM/CORBIS

whether someone deserved a loan, bypassing individual judgments. "In the end, there was very little sound credit judgment going into making these credit calls," says Bjorn Flesaker, a senior quant at Bloomberg in New York. Then, quant models were used to rate the riskiness of financial instruments, including the CDOs. "We never necessarily viewed the rating agencies as having the greatest rocket scientists around," says Flesaker, yet investors accepted those ratings, taking on more risk than even they realized. Finally, Value at Risk models claimed to tell trading departments of Wall Street companies the maximum loss they could expect to see on any day and therefore how much money they needed on hand to avoid total collapse. These models were "the wink-and-a-nod of Wall Street," says financial engineer Lee Maclin of NYU. Risk managers should have known to use common sense, but, in some cases, Maclin says, "the models were used to justify a bigger appetite for risk."

Despite their errors, Flesaker says he is "not in the 'blame the quants' camp," and he's not alone. Shiller says that, like many of the elements that economists and the media have focused on, the quant models are simply "proximate causes." Ultimately, experts must examine human behavior to find out why the crisis happened. Why did so many people take on mortgages that they would not be able to pay? Why did the best minds of Wall Street ignore warnings about a housing bubble? "The bottom-line question that economists, I think, still are struggling with is: 'Did anybody know that the risks were so great and, if so, why did they continue investing?' " says Lo. "I don't think they have an answer for that."

The madness of crowds

For more than 2 decades, researchers in behavioral finance have sought out the signatures of human irrationality in markets. "Behavioral finance is an intellectual revolution that tries to give a broader perspective from multiple social sciences," including psychology and sociology, says Shiller, a founder of the field.

For example, says economist José Scheinkman of Princeton University, classical finance theory's model of speculative bubbles, such as the dot-com bubble of the late '90s and the recent housing bubble, does not match real-life observations. Classical finance contends that rational investors will always have the best possible portfolio, so they will not buy or sell unless they have extra money to invest or need to cash in their investments. However, researchers have observed that people buy and sell much more often than that during a bubble—with the rate of transactions becoming increasingly manic the bigger the bubble gets.

Lacking a good classical model for stock-market bubbles, Scheinkman, whose work is primarily classical, turned to a concept in behavioral finance. Psychologists have found that people often overestimate the precision of their knowledge. Scheinkman and his Princeton colleague Wei Xiong guessed that overconfident investors would trust their own opinions about the price of an asset, so they would consider others' opinions, if different, a little "crazy," says Scheinkman. Looking to make money off others' crazy opinions, investors would be willing to pay more than they think an asset is actually worth because they believe that they will be able to sell it in the future to an overeager buyer. This process would inflate prices and cause a trading frenzy. Incorporating investor overconfidence into a theoretical model published in 2003 in the *Journal of Political Economy*, Scheinkman and Xiong were able to recreate more accurately the hyperactive trading in bubbles.

As Wurgler sees it, the time of most extreme irrationality was the housing bubble of the past several years, not the crash of the past few months. "The crash is the healthy return to normalcy," he says.

"Financial crises may be an unavoidable aspect of modern capitalism, a consequence of the interactions between hard-wired human behavior and the unfettered ability to innovate, compete, and evolve."
—ANDREW LO

Evolving a theory

Although behavioral theory has succeeded at challenging classical theory—and has spawned several bestsellers, including this year's *Nudge*—some complain that it is only a series of critiques, not an alternative framework for understanding how markets work. "I would argue it takes a theory to beat a theory," says Lo.

Lo started his career developing quantitative models in line with classical finance theory, he says, but when he compared the models' predictions with stock-market data, "the models I developed ended up being rejected by the data pretty soundly." So for the past several years, he has been working on a new theory that combines insights from evolutionary biology and neuroscience, called the Adaptive Market Hypothesis (AMH), in contrast to the Efficient Market Hypothesis. Instead of seeing market participants as computers, which can always calculate the best way to achieve their goals, the AMH sees them as "species," which evolve strategies to compete for limited profits through trial and error. Overconfidence, he explains, is an adaptation. Overconfident investors who bet big and win get noticed; underconfident investors never even get in the game. He has found that quantitative models, based on the AMH's principles and equations from evolutionary biology, can replicate similar behavioral concepts.

Unlike investors in classical finance theory, Lo's species behave differently based on what part of their brains they are using. When things go well and people make money, as they did for the past decade, the experience stimulates investors' reward circuitry. This causes them to seek more profits and ignore possible risk, leading, for example, to a bubble. When things take a turn for the worse, panic overrides rational decision-making, leading to a crash. Only when the market is steady does the rational brain take over. Lo is starting to use functional magnetic resonance imaging and other tools of neuroscience to quantify these behaviors and incorporate them into his models. He also needs more real-world data on the way different funds invest money—data that are now secret or that no one bothers to collect.

Although Lo's idiosyncratic approach lies outside of the behavioral and classical theories, he says it reconciles them. "If you were an efficient-markets type, I think you'd be hard-pressed to explain what happened over the last few weeks. And if you were an irrational finance person, you'd be hard-pressed to explain what happened over the previous 10 years. So I think that the only way to reconcile the two is to acknowledge that both are different aspects of the exact same truth."

Keeping it real

Others say that the very message of behavioral finance is that a comprehensive theory is unrealistic, not only in practice but also in principle. "Economists deeply admire

Published by AAAS

the physical sciences and wish we could be like that," says Shiller. But, he says, "there's a human element that can get lost" when researchers emphasize quantitative methods instead of, say, historical ones. "I don't want to slavishly copy what is superficially scientific."

Nonetheless, behavioral researchers are eager to prove that their ideas mirror nature by using quantitative methods to link them directly to real-life data, NYU's Wurgler says. Stock pricing lends itself to such studies, because valuing a stock involves conjecture—which is subject to psychological factors—and a lot of stock-market data have recently become available to academic researchers.

In a 2007 paper in the *Journal of Economic Perspectives*, Wurgler and co-author Malcolm Baker, a financial economist at Harvard Business School, looked for signatures of investor sentiment—irrational optimism or pessimism—in stock-market data since the 1960s. They hypothesized that certain stocks would be more subject to sentiment than others: broadly speaking, stocks for which the true value is difficult to determine. For example, a young, promising company would fit the bill. "The combination of no earnings history and a highly uncertain future allows investors to defend valuations ranging from much too low to much too high," they write.

Behave! Jeffrey Wurgler (*left*) and Andrew Lo (*right*) incorporate irrational behavior into models of financial markets.

Comparing the stock-market data with their measure of investor sentiment, they found what they had expected. In optimistic times, difficult-to-value stocks were wildly popular and therefore made much more money than average. In pessimistic times, they were wildly unpopular and therefore made much less money than average. On the other hand, easy-to-value stocks, which are considered safer, were more popular in pessimistic times than optimistic ones, but their prices stayed much closer to average. This helps explain past bubbles in certain types of stocks—say, dot-com stocks in the 1990s—and is also useful for making predictions for the future, Wurgler says.

Mathematician Gunduz Caginalp of the University of Pittsburgh in Pennsylvania unifies theoretical modeling, laboratory experiments, and statistical studies of real-world market data. He and his colleagues, including Nobel Prize–winning economist Vernon Smith of George Mason University in Fairfax, Virginia, wanted to know how increased cash in the stock market would affect a bubble. In classical finance theory, more cash would make no difference, Caginalp says. "The fact that you have extra money, why should that push up prices?" he asks. "But that's exactly what we saw." In a 2001 paper in the *Journal of Psychology and Financial Markets*, Caginalp and his colleagues had volunteers trade for real money in an experimental market. They found that adding $1 per share to the market pushed up the price of shares by about $1. The result fit their predictions in an earlier theoretical modeling paper. Later, they also saw the effect in an analysis of New York Stock Exchange data. Caginalp draws the connection with the recent housing bubble: Loosened mortgage lending policies poured money into the housing market. "There's really no place for that money to go except to fuel various bubbles," he says.

Using behavioral finance, researchers will get better at explaining specific phenomena such as bubbles, says Wurgler. But, he argues, human psychology is so complex that a unifying theory is not within reach. "We'll putter along with an increasingly complex and diverse set of models," he says.

Putting it into practice

New theoretical models from academics may not affect Wall Street quants all that much. Quant models can be loosely divided into two types, says Flesaker: "trying to forecast future states of the world and trying to forecast the behavior of a particular financial instrument given the state of the world." The algorithms that help make decisions on when to buy and sell assets fall into the latter category, and they have held up reasonably well, he says. They work by exploiting tiny insights that others don't yet have, so anything published in the academic literature will be useless almost immediately.

The quant models that failed catastrophically—ratings models, Value at Risk models—are all in the former category, says Flesaker. But even these can be "pretty useful, if local, approximations to a much more complex reality," says Lo. A new theoretical framework could help quants better understand where their models are likely to be wrong. That could prevent managers from putting too much trust in their models, a factor in the failure of many companies. "The true skill of the practitioner is to know the ins and outs of the models," says financial engineer Petter Kolm of NYU. Practical decisions "can't just be based on some numbers that a model spits out."

On the other hand, new models could be very useful on the regulatory side. Last month, Lo testified at the U.S. Congress House Committee on Oversight and Government Reform's hearing on hedge funds. If markets are adaptive, he argued, then regulation should also be adaptive. For example, instead of making a rule about a particular new financial instrument, regulators could make a rule that applies to any new financial instrument that becomes "too big to fail." In that way, innovation would not get ahead of regulation, as it did in the shadow banking system.

Unfortunately, although new models—small or grand—may help experts understand bubbles and crashes better, behavioral finance predicts that they will never be able to prevent the behaviors that cause them. "Financial crises may be an unavoidable aspect of modern capitalism, a consequence of the interactions between hard-wired human behavior and the unfettered ability to innovate, compete, and evolve," Lo told the committee. In other words, says Caginalp, "human nature being what it is," when it comes to money, people will always be just a little bit crazy.

–CHELSEA WALD

Chelsea Wald is a freelance writer in New York City.

CREDITS (LEFT TO RIGHT): COURTESY OF NYU; MIT SLOAN SCHOOL OF MANAGEMENT

Published by AAAS

OCEANOGRAPHY

FerryBoxes Begin To Make Waves

European researchers have enlisted a fleet of ferries to inexpensively gather valuable data about the region's waters

Regular customer. With 32 daily crossings, this Dutch ferry makes regular, detailed measurements of a tidal inlet.

White and navy livery glinting in the late afternoon sun, engines quietly thundering, the passenger ferry *Pride of Bilbao* steams purposefully into dock, on the final leg of a 2-day voyage that started on the northern coast of Spain. Her passage has taken her past pods of dolphins playing in the Bay of Biscay, across the ship-filled English Channel, and into Portsmouth Harbour on the south coast of Britain. Once moored, her ramp swings down to disgorge her cargo of cars, trucks, and chattering passengers. Dressed in fluorescent yellow jackets and ear defenders are marine scientists David Hydes and Mark Hartman, squeezing their way against the melee. They've come to get their data.

The pair heads toward the hot, noisy engine room in the belly of *Pride*'s 37,500-ton hull. There, tapped into a pipe that brings seawater into the ship to cool its refrigerator spaces and air conditioning is a metal box, about the size of a domestic washing machine. Inside is an array of sensors that sample the water as it flows through the box, sending measurements directly back to the team's Web site. But the satellite link can't handle all the data, which are collected once per second, so Hydes retrieves a memory card containing the rest of the readings. He and Hartman then carefully clean and check the device's individual sensors. It's a ritual the two, both based at the National Oceanography Centre, Southampton (NOCS), United Kingdom, perform once every 9 days, after the *Pride of Bilbao* has made three round trips to Spain.

The machine they're servicing is a "FerryBox," and it is an attempt to solve a problem plaguing oceanographers the world over: how to get enough data to understand our planet's oceans, without breaking the bank. FerryBoxes consist of suites of sensors that measure water variables such as temperature, salinity, carbon dioxide, and oxygen content, as well as biological features such as the amount of chlorophyll a, a molecule that betrays the activity of photosynthesizing plankton in the surface waters of the sea. More than 30 FerryBoxes now quietly chug between ports in Europe, with similar systems at work in the waters of countries including Japan, South Korea, Australia, and the United States. At a meeting in Southampton at the end of September on research uses of FerryBoxes, scientists also presented plans to establish a program in the waters around Africa.

On board. FerryBox advocate David Hydes works with a ship-based sensor of CO_2 in water.

The idea of using a "ship of opportunity" (SOOP) for science has been around for centuries, of course. Marine researchers of yore would hand cruise liner captains a bucket and a thermometer before waving them on their way. (And some modern researchers are retroactively prying data out of ancient ships—see sidebar on page 1629.) Modern-day SOOPs are rather more sophisticated in the way they make measurements. In particular, says Hydes, vessels equipped with FerryBoxes or their relatives represent a new generation of SOOPs that has moved from making just basic hydrographical measurements to encompassing chemistry and biology.

Ferries are cost-effective and reliable SOOPs, operating under a range of weather conditions that may restrict smaller vessels, says Hans Paerl of the University of North Carolina, Chapel Hill. Paerl heads a research team running the first ferry-box-type project in the United States, FerryMon, which began in 2000 in North Carolina's Pamlico Sound. What's more, the regular nature of ferry crossings lets sensors pick up on short-term phenomena that would otherwise be missed. FerryBox data can also be used to calibrate remote-sensing data. "The quality of the data is just as good [as], if not better than, existing water-monitoring programs," says Paerl.

By providing repeated observations of dynamic waters, these relatively low-cost sensor systems are tackling scientific puzzles such as the source of an odd freshwater layer in the English Channel and how currents flow in the Mediterranean Sea. FerryBoxes, say their fans, could also help address one of the biggest issues in oceanography: how the seas are

CREDITS (TOP TO BOTTOM): JAN BOON (NIOZ); DAVID HYDES

Published by AAAS

doing at absorbing all the carbon dioxide humans have been pumping into the atmosphere, and how this may change in the future.

Smooth waters

Between the world's dedicated research vessels, oceanographic buoys, and remote-sensing satellites, scientists would seem to have the ocean well-covered. And they do—up to a point. But to really understand how Earth's oceans and marine ecosystems behave, researchers need widespread, detailed, regular monitoring sustained over the long term. If oceanographers were to use research vessels for all the operational monitoring that they want, however, the costs would be astronomical. Running just one U.K. research ship, for example, costs between £10,000 and £15,000 (U.S.$17,000 to $26,000) per day.

That is why in the 1990s European researchers started eyeing the 800 or so ferries that ply the region's waters. The FerryBox in the bowels of the *Pride of Bilbao*, for example, cost about £35,000 to set up and has minimal ongoing costs, says Hydes. "It's getting the regular data you can't get in any other way," he says.

Indeed, one Dutch FerryBox-equipped ship operating in the Wadden Sea between Den Helder and the island of Texel makes two crossings per hour, 16 hours per day, 320 days per year. This has allowed Herman Ridderinkhof and his team at NIOZ Royal Netherlands Institute for Sea Research on Texel to build up a detailed picture of how sediments are transported in the Marsdiep tidal inlet, a key issue for the coastal ecosystem there. At the conference, Ridderinkhof showed a video made from FerryBox data that depicted how sand waves propagate across the estuary floor. "The longer you measure, the more interesting these kinds of things become," he says.

In the early 1990s, scientists at the Finnish Institute of Marine Research, in partnership with other institutes and companies in Finland and Estonia, pioneered the use of water-monitoring devices on ferries that sailed the Gulf of Finland and the Baltic Sea. Data from these ships were combined with measurements from other sources, such as satellite imaging and buoy recordings, to monitor the development of the harmful algal blooms that plague the area. The success of the project, called Alg@Line, prompted 10 other research groups to put together a proposal that won E.U. funding to develop the FerryBox technology and infrastructure. In that project, which ran from 2002 to 2005, eight ferry lines successfully collected data.

The 30 or so European lines now in operation are allowing oceanographers to study marine processes in a way that would not have been possible otherwise. For example, researchers had long noted that the western part of the English Channel often developed a puzzling freshwater layer during the summer, which varied in size from year to year. Conventional sampling methods failed to explain why, but the regular FerryBox measurements from the *Pride of Bilbao* revealed the appearance of fresh water off the coast of Ushant in western Brittany during March and April each year. French researchers, meanwhile, had reported that freshwater runoff from the Loire and Gironde areas appeared in the Bay of Biscay during winter. Boris Kelly-Gerreyn, a marine biogeochemist at NOCS, and his colleagues put those clues together and in 2006 concluded that Loire and Gironde freshwater was being blown all the way up into the Channel. The extent to which the fresh water spread into the channel depended on the state of the tides and the direction of the prevailing wind.

Understanding the origin of the freshwater layer could be key to predicting algal blooms harmful to fisheries and tourism, because that water may spur algal growth. The team utilizing the *Pride of Bilbao* found that the largest algal bloom ever recorded in the channel, which happened in 2003, also coincided with the greatest freshwater intrusion detected by the FerryBox.

Marine science. The routes of some of the data-gathering ferries, such as the *Pride of Bilbao* (*above*), that crisscross European waters.

Tackling CO_2

As scientists consider how they can expand the use of FerryBoxes, the Mediterranean Sea is an inviting target. The Mediterranean is surprisingly underexplored, Isabelle Taupier-Letage, an oceanographer based in Toulon at the French Research Institute for Exploitation of the Sea, said at the Southampton conference. She proposed that a network of FerryBox-like lines could help fill in data gaps, such as salinity measurements, and also resolve confusion about the direction of the prevailing path of the surface current in the southern part of the eastern basin. After the water from the Atlantic enters at Gibraltar, it forms currents that tend to flow eastward along the southern coastlines. In both basins, these currents generate large clockwise eddies (~100-km diameter), which propagate across the basin, transiently altering the direction of water flow. "If you don't sample these eddies correctly, you get the wrong picture," says Taupier-Letage. "You have to monitor at the basin scale."

Another potential target is the U.S. coast. There are currently only three ferry-box projects operating in the United States, although two more are in the works. In general, it's getting easier for scientists to set up ferry-based sensors. Manufacturers are now making off-the-shelf systems to save researchers the time and trouble of building them themselves. "We have a firm belief that the market is developing," says Justin Dunning, sales manager at Chelsea Technologies, a U.K. marine sensors company that sponsored the Southampton conference.

The technology is also improving, Dunning says. One goal is to reduce fouling—the growth of marine organisms such as algae on equipment—and the need for regular servicing by a trained technician. "You are never going to have a completely standalone vessel that you can just leave for a year," says Dunning. But the technology to increase the length of time between servicing and data-collection visits, including some self-cleaning ability, is developing, he says.

FerryBoxes are also tackling new problems. For example, they are starting to play an important role in monitoring the ability of the world's oceans to absorb the carbon dioxide emitted as a result of human activi-

CREDIT: ADAPTED FROM MAP PROVIDED BY DAVID HYDES; (IMAGE) UKPAOLO/WIKIMEDIA COMMONS

Published by AAAS

Logbooks Record Weather's History

"What better data could a patient meteorological philosopher desire?" Francis Beaufort, inventor of the famous wind force scale that bears his name, wrote that in 1809 in reference to the British Royal Navy's logbooks, in which captains made detailed daily recordings of sea and weather conditions as they plied the waters of the globe.

Dennis Wheeler, a geographer at the University of Sunderland in the U.K., is following Beaufort's example: He is using old maritime logbooks to reconstruct a record of the weather stretching back to the 17th century. Wheeler got interested in the scientific potential of these historical logbooks while researching the weather conditions of great maritime battles. "It just occurred to me that these logbooks had a great deal of weather data in them," he says.

Weather report. *HMS Experiment*'s logbook.

In 2000, Wheeler teamed up with colleagues in England, Spain, and the Netherlands to produce the world's first daily climatological record for the period 1750 to 1850 by studying logbooks from different European countries. Given that traditional meteorological records date back only 150 years, says Wheeler, the hope is that the logbook work will bring improved understanding of the current climate and how to model its future trends.

Captains of naval and merchant ships used to record observations, including wind force and direction and general weather, as many as three times a day. Because navy ships sailed in fleets, Wheeler and his colleagues confirmed the consistency and reliability of such data by comparing logbooks of ships sailing together on the same day. They've compiled the information into a repository called the Climatological Database for the World's Oceans (CLIWOC).

In 2006, Wheeler and his team reported that the Royal Navy logbook data showed that during the 1680s and 1690s, the waters off Britain experienced much stormier summers than normal. Whereas such a trend today might be attributed to global warming, Europe was experiencing a "Little Ice Age" at the time. Such findings illustrate how a long-term historical record could help distinguish between natural variability and humanmade climate change, says Wheeler.

The logbook data are a useful addition to historical climate records, agrees Rob Allan, a climate scientist at the Met Office Hadley Centre in Exeter, U.K. Allan heads an international project, known as Atmospheric Circulation Reconstructions over the Earth, that aims to build up a long historical data set of global marine and terrestrial instrumental weather observations. These observations can help computer models produce "hindcasts" of past weather, to gain a better understanding of how the weather affects the environment, ecosystems, and society, as well using them to test the accuracy of the models. "We can check whether computer models and our reconstructions of past weather agree on what has happened and thus improve our confidence in computer-model simulations of future climate," says Allan.

CLIWOC, completed in 2003, contains 273,269 observations gleaned from 1624 logbooks. Wheeler and his colleagues in Europe and the United States are now working on an international project to digitize selected subgroups from the tens of thousands of logbooks that remain to be studied, including those of the English East India Company and the U.S. Navy. Given that there are more than 120,000 pre-instrumental logbooks out there, it's likely to make patient meteorological philosophers of them all. "There's still an awful lot to be done," says Wheeler. **–C.A.**

ties. The oceans are an important "sink" for the greenhouse gas—they have managed to absorb about half of all our CO_2 emissions so far—but no one can be sure whether this check against global warming will continue. And even if it does, will the oceans' rising acidity increasingly damage marine ecosystems? "We need in situ data like never before," says Nick Hardman-Mountford, acting director for the Centre for observation of Air-Sea Interactions & fluXes at the Plymouth Marine Laboratory in the U.K. Consequently, he and his colleagues, in collaboration with the engineering company Dartcom, have developed a system that senses the amount of the carbon dioxide in surface waters, a measurement known as the partial pressure of CO_2 (pCO_2), for FerryBox use.

The overall sparseness of pCO_2 data is a huge stumbling block, notes Ute Schuster, an oceanographer at the University of East Anglia in Norwich, U.K. "Up until now, the E.U. has funded [pCO_2 studies] in short-term projects, but much work needs to be done to persuade both the E.U. and national funding bodies that long-term sustained monitoring of pCO_2 is vital and can be done very cost effectively working with commercial ships," she says.

Ferry and merchant shipping companies seem happy to help. After reading about successful pCO_2 measurements on research vessels in a NOCS newsletter, an executive from a subsidiary of Swire Shipping, a merchant shipping company that operates mainly in Asia-Pacific, contacted Hydes to ask whether similar measurements could be made from their ships. The Swire Group Charitable Trust then funded Hydes to install a sensor system on its *Pacific Celebes*, a ship that has since circumnavigated the globe, collecting data on pCO_2 and other variables. The company has pledged more funding to continue the work. It has even provided money for a Ph.D. studentship linking the work at NOCS with marine scientists at Xiamen University in China.

World traveler. The *Pacific Celebes* circles the globe collecting CO_2 data.

FerryBox scientists would love to see the day when their sensors are routinely built into new ships. Some are even more ambitious. Thanks to good relations with the TESO ferry company running the Marsdiep route, Ridderinkhof managed to persuade executives to design their latest ship with a dedicated lab and a moon pool, an opening in the hull from which sensors can be lowered into the water. "We asked them if they wanted to make a hole in their brand-new ferry and they said, 'Yes,'" he quips. Hydes would like to see more of this sort of partnership. "There are a lot of ships out there," he says. "We want to spread the message." **–CLAIRE AINSWORTH**

Claire Ainsworth is a freelance writer in Southampton, U.K.

CREDITS (TOP TO BOTTOM): DENNIS WHEELER; DAVID HYDES

Published by AAAS

ECOLOGY

When Juniper and Woody Plants Invade, Water May Retreat

Dense plants are taking over grasslands in many areas; researchers in the U.S. Southwest are studying how they tap into water supplies—and how to keep them in check

AUSTIN—The day is hot and humid, as Robert Jackson descends into the mouth of Powell Cave and down a ladder that drops into the limestone bedrock of the Edwards Plateau about 240 kilometers west of Austin. He follows an ancient streambed through several large caverns and a few tight crawl spaces, until he arrives at a point about 18 meters below the surface, where a crystal-clear stream bubbles out of the rock.

Several thick tree roots burst out from the limestone, reach down, and suck moisture from the water. Some of them have been wired with electronic probes. Applying pulses of heat, Jackson and his lab can gauge water flow by how fast that heat dissipates. Jackson, a biologist at Duke University in Durham, North Carolina, is investigating how roots transfer water from this depth up to the surface. "A single taproot can provide a third or more of the tree's water during a drought," says Jackson.

His study aims to determine what enables juniper to survive in these arid environments and how much ground water they are using. Funded by the U.S. National Science Foundation, the U.S. Department of Agriculture, and the Andrew W. Mellon Foundation, this research indicates that wildlife and water management would benefit from fewer of these trees.

Woody shrubs and trees like juniper have in recent decades replaced arid and semiarid grasslands and savannas throughout much of the western United States, from the Great Plains to the Gulf Coast. "Encroachment of woody plants limits the amount of forage available to livestock, alters the natural landscape for native wildlife, impedes the flow of water available at the surface, and creates conditions for more catastrophic fires," Jackson says.

With global warming predictions calling for increased droughts, expansion could continue. And it's not just a U.S. problem: The shrubs and trees are proliferating in grasslands and savannas in South America, Africa, and Australia.

Depleted streams

The effect of expanding woodlands on water flow can be dramatic. Kathleen Farley of San Diego State University in California and Jackson reviewed data sets from efforts to establish new forests in Africa, New Zealand, Australia, and Europe and found that increased tree and shrub growth typically resulted in the loss of one-third to three-quarters of stream flow. "In areas where natural runoff is less than 10% of mean annual precipitation, afforestation can result in complete loss of runoff," says Farley. As a consequence, some say, afforestation efforts that have been proposed as carbon offsets need close scrutiny.

The same types of growth appear to be draining water from the Swiss-cheese structure of the limestone bedrock, known as karst, on the Edwards Plateau. Such systems cover one-fifth of Texas and 7% to 10% of the globe's land surface. This area in Texas gets about 63.5 centimeters of rain a year, yet there are few aboveground streams. Jackson's research shows that the drinking habits of these trees may be partly responsible.

One hundred and fifty years ago, this area was comprised of grasslands and savanna where oak trees dotted the landscape. They were more frequently swept by wildfires, one of several factors that kept woody plants at bay. "There is likely no single driver" of the change to denser growth, says Steve Archer, a professor at the School of Natural Resources at the University of Arizona, Tucson. Fire suppression, overgrazing, droughts, and climate change have all played a part in helping woody plants succeed, he says.

Juniper is the dominant woody invader throughout much of the Great Plains and the West, but mesquite plays a role in the southern Great Plains and the Southwest, creosote in the Southwest, and Chinese tallow in the Gulf Coast Prairies. Juniper and mesquite have invaded the plateau, forming dense monocultures in which birds and wildlife don't do well. Black-capped vireos and golden-cheeked warblers, two Texas birds that are both endangered, are among those that require a mixed-forest habitat to thrive.

Large mammals are affected as well. The bighorn sheep of New Mexico, already endangered, are increasingly threatened by attack from mountain lions, which are moving into wooded mountaintops that were bald in the past. According to Eric Rominger, a bighorn sheep biologist at the New Mexico

CREDIT: TIMOTHY HEARSUM/CORBIS

Published by AAAS

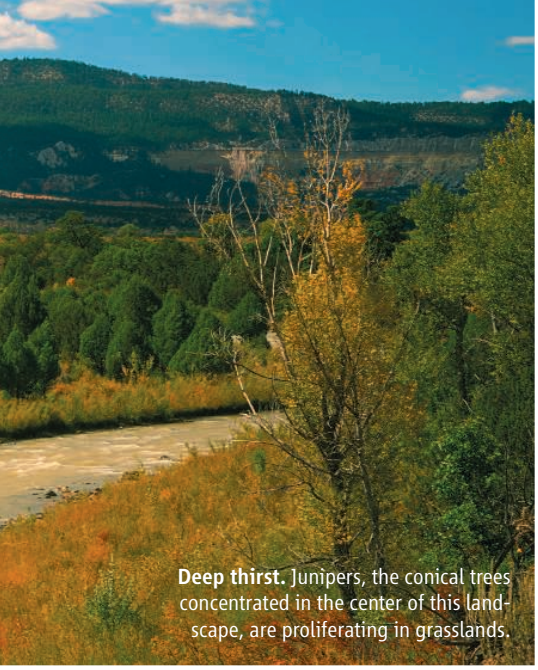

Deep thirst. Junipers, the conical trees concentrated in the center of this landscape, are proliferating in grasslands.

Department of Game and Fish in Santa Fe, "Mountain lions are ambush predators, and they need cover to launch their attacks." The emboldened predators are also taking a toll on ranchers' livestock, mainly young cattle.

Thickets

One goal of Jackson's study is to learn how these trees survive drought. Finding water is only half the battle. All woody plants have to lift that water aboveground, which they do by creating an evaporative flow. The leaves are speckled with pores that open to absorb carbon dioxide (CO_2). The leaves of a juniper are needlelike, or awl-shaped. When the pores open, they release moisture, setting up a powerful vacuum through short, interconnected passages called tracheids that draw moisture from the tree's root system in the same way one might pull soda through a straw. "When a tree doesn't have enough water to conduct this process, it doesn't die of thirst but of starvation"—because the intake of CO_2 drops, and "it can't fix carbon to make food," says Jackson.

Tim Bleby, a research associate at the University of Western Australia in Perth, who worked with Jackson, studied root water uptake in juniper and found that water is delivered from one part of the tree to another to equalize water distribution. This gives such plants, which have multilevel root systems, a distinct advantage over shallow-rooted grasses. "When the surface is dry, they use deep roots; when it rains, they switch over to shallow roots."

The water-uptake mechanisms of juniper aren't fundamentally different from those of other woody plants, just more efficient. Cynthia Wilson, a former Ph.D. student in Jackson's lab, sampled junipers all over the West and then studied them for anatomy, wood density, hydraulic conductivity, and resistance to cavitation, or the formation of bubbles that interrupt the flow of water through the tracheids. Cavitation resistance is a marker for drought resistance. Wilson took branches from different junipers and spun them in a centrifuge, mimicking conditions under which the branches would cavitate and no longer transport water. According to Wilson, "Juniper are among the most cavitation-resistant tree species ever studied."

These attributes, coupled with fire suppression and overgrazing, have given woody plants like juniper an advantage in the West. Archer refers to the result as "thicketization." Says Archer: "When we introduced grazing in the West in the late 1800s, fine-grass fuels were removed, and that greatly reduced fire frequency. Woody plants then had wider windows of opportunity to establish and become large enough to resist the effects of future fires."

Pushing back

Ranchers and land managers have been fighting woody encroachment for years using everything from chemicals to goats. The straightforward approach—deploying chain saws and bulldozers—can be effective.

For example, New Mexico has hired crews to cut piñon pine and juniper on sheep habitat, part of a management process including relocation and predator control that may soon see this animal downlisted. But Archer warns against trying to stop the woody invasion with a "wall-to-wall clearing of brush." It's critical, he says, to take account of plants' "historical distribution and abundance."

Some groups have developed clever ways to use brush control to restore historical grasslands. Jackson cites the example of J. David Bamberger, a co-founder of the Church's Fried Chicken franchise. Bamberger has been clearing juniper thickets on his land since 1969 and replanting them with grass. According to Colleen Gardner, executive director of the Bamberger Ranch Preserve in Johnson City, Texas, the ranch has established a native mix of grasses that includes 80 species and has restored 27 ponds and lakes.

Biologist Marsha May of Texas Parks and Wildlife conducts tri-annual Audubon bird counts on the ranch and notes that the counts have grown from 48 to 205 species. She and other state biologists have located breeding pairs of black-capped vireos and golden-cheeked warblers on the property.

Texas A&M University scientists conducted research on shrub control and water yield that addresses different vegetation types and geographic zones on the Edwards Plateau. The Edwards Aquifer Authority, in conjunction with the Natural Resources Conservation Service, is using the study as a basis to provide cash assistance to ranchers and land managers to help clear mesquite and juniper thickets from their lands. Ranchers can get as much as 70% of their expenses back. Texas Parks and Wildlife has a program to assist landowners with what they call "brush sculpting," a careful method to return a property to historical purposes.

If successful, the effort should help increase water flow as far away as San Antonio and Austin. Says Jackson: "It's not the typical case where you're faced with environmental and economic tradeoffs. Brush clearing here has advantages for water availability, forage production, and native wildlife. We are reaping multiple benefits."

–MICHAEL TENNESEN

Tapping in. Biologist Robert Jackson wires up tree roots in Texas's Edwards Plateau to monitor their water uptake.

CREDIT: © MICHAEL TENNESEN

Michael Tennesen, a writer in Lomita Pines, California, was a media fellow at the Nicholas School of the Environment and Earth Sciences at Duke University.

Published by AAAS

Vaccines are not the cause
1635

String theory meets a solid state
1639

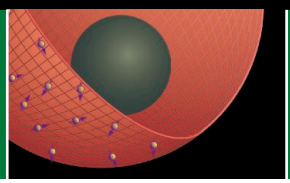

LETTERS

edited by Jennifer Sills

Testing the Limits of "Concrete" and "Generic"

HERE ARE TWO WAYS TO INTRODUCE THE MATHEMATICAL GROUP OF ORDER THREE: (I) SAY that it is the set of 0, 1, and 2, together with the operation of "addition modulo 3." (ii) Say that it is made of three elements a, b, and c, together with an explicitly defined operation.

J. A. Kaminski *et al*. ("The advantage of abstract examples in learning math," Education Forum, 25 April, p. 454) labeled as "concrete" the examples based on the first definition and labeled as "generic" the ones based on the second.

In Kaminski *et al*.'s study, students' transfer of knowledge was tested by an assessment that followed the second, "generic" definition, regardless of the definition the students were introduced to during their training. It is thus not surprising that students performed better if they first practiced using the "generic" examples than they did if they trained on the "concrete" ones. Because the transfer test was more similar to one training condition, it would be unwise to generalize the results to the advantages of abstract examples in other situations, as suggested by the Education Forum's title.

JEAN-CHRISTOPHE MOURRAT

Department of Mathematics, Université de Provence, Marseille, France. E-mail: mourrat@cmi.univ-mrs.fr

"Concrete" Examples a Fraction Too Abstract

AFTER EXAMINING THE SUPPORTING ONLINE Material for the Education Forum by J. A. Kaminski *et al*., "The advantage of abstract examples in learning math" (25 April, p. 454), I doubt that abstract examples are better. Rather, the study shows that the effectiveness of teaching examples depends less on whether they are "generic" or "concrete" (a somewhat confused distinction) and more on the examples' affordances that lead students to (or distract from) the learning goal.

In the study, students must learn the abstract mathematical concept of mod 3. Teaching such a concept requires appropriate modeling. The study's "generic" examples (circles, diamonds, and flag shapes) and the assessment examples both serve this purpose well. Each set of examples uses three distinct symbols, which help students master the specific, limited concept. A set of shapes does not lead to confusion because it does not introduce numerosity, which is irrelevant to mod 3. By contrast, the three "concrete" examples seem geared to teaching the broader, generalized concept that includes mod 4, mod 5, and so on. These examples (such as measuring cups 1/3, 2/3, or 3/3 full) easily generalize to higher integer orders by increasing the number of symbol states (e.g., by dividing the cups into fourths, fifths, and so on, instead of thirds), but invite confusion when introducing the study's limited concept. This interferes with the lesson. Arguably, the intuitive appeal to numerosity in these "concrete" examples (invoking specific fractions) makes them more, rather than less, abstract than the "generic" example (using only shapes and no numbers).

The symbols used in the assessment, although showing hints of numerical associations, do not obviously invoke numerosity. Moreover, the assessment is almost identical to the "generic" example. It is no wonder that students who learned using the "generic" example performed better on the assessment than those who learned using the "concrete" example(s). The numerical—even abstract—nature of the "concrete" examples distracted students instead of helping them.

The study clearly demonstrates the possibility of constructing confusing "concrete" examples of a particular concept, but we cannot infer that "generic" examples are always superior to "concrete" examples. Whether a confusing example is "concrete" or "generic" is beside the point.

LOUIS J. CUTRONA JR.

Teleonetics Ltd., 625 North Monroe Street, Ridgewood, NJ 07450, USA. E-mail: ljc@teleonetics.com

Concrete Examples Must Jibe with Experience

IN THEIR EDUCATION FORUM "THE ADVANtage of abstract examples in learning math" (25 April, p. 454), J. A. Kaminski *et al*. investigated several ways to teach the mathematical concept of mod 3, in which all numbers are simplified to their remainder when divided by 3. (For example, 3 divided by 3 has a remainder of 0, 4 divided by 3 has a remainder of 1, and 5 divided by 3 has a remainder of 2. In mod 3, the numbers 3, 4, and 5 are equal to their remainders: 0, 1, and 2, respectively.) To teach this concept to students, Kaminski *et al.* represented the three possible mod 3 values with abstract examples (such as a circle, diamond, and flag shape) and with concrete examples (such as three cups of water in a measuring cup). On the basis of student performance on post-tests, Kaminski *et al*. concluded that using abstract examples was the more effective teaching strategy. I disagree. I believe that the vocabulary and examples

CREDIT: JUPITER IMAGES

Published by AAAS

Challenges in food safety 1641

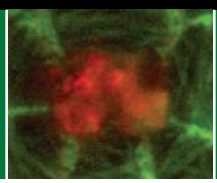

Force and form 1643

used in the experiment conflicted with students' prior knowledge, and it was this confusion and not the concrete example strategy that led to the reported results.

In theory, concrete examples (such as measuring cups of water) activate knowledge stored in memory (such as baking a cake), and this connection facilitates learning and problem solving (*1*). However, concrete examples are counterproductive if they are inconsistent with prior knowledge. This is the case for the measuring cup example in Kaminski *et al*.'s experiment. For example, Rule 2 states that combining 1/3 cups with 2/3 cups produces a filled cup and refers to the filled cup as the "left over." This use of the phrase "left over" is inconsistent with its use in everyday language. Whereas the concrete strategy had the potential to help the students understand the new concept, these misleading labels most likely led to confusion instead.

STEPHEN K. REED

CRMSE, San Diego State University, San Diego, CA 92120, USA. E-mail: sreed@sunstroke.sdsu.edu

Reference

1. S. K. Reed, A. C. Evans, *J. Exp. Psychol. Gen*. **116**, 106 (1987).

Response

MOURRAT RAISED THE POSSIBILITY THAT THE examples used in our Education Forum are mathematically different across conditions and that these differences led to differences in performance on the assessment (transfer task). We argue that the mathematics underlying the generic and concrete examples was identical and that both sets of examples met the definition of a commutative group of order three (*1*). This concept can be accurately instantiated through numbers, shapes, or scenarios such as filling measuring cups or the children's game. Therefore, there is every reason to believe that the differences between the examples we used are not mathematical, but cognitive.

Cutrona and Mourrat further suggest that the difficulty transferring knowledge from the concrete examples stems from possible numerical aspects of the concrete examples that were absent from the transfer task. Because the concept of a mathematical group can be instantiated in an unlimited number of ways, only a subset of which involve numbers (as modular arithmetic), we argue that numerical characteristics are extraneous and as such are part of concreteness. Therefore, it is possible this numerical information could hinder transfer to non-numerical domains. We have foreseen this possibility and have already conducted research to investigate transfer from a numerical domain. Our (unpublished) results do not contradict our findings reported in the Education Forum.

Reed proposes that participants failed to transfer from the concrete examples because these examples are inconsistent with prior knowledge. We disagree and believe that the rules and the storyline of the concrete examples are consistent with prior knowledge (see Supporting Online Material for the Education Forum). More important, if the concrete examples were inconsistent with prior knowledge, then why did they result in fast and efficient initial learning (*2*)?

We do not deny that transfer can occur when students learn using concrete examples. Rather, we have asked whether learning multiple concrete examples is the most efficient route to promoting transfer. Our data clearly suggest that it is not. Generic examples that are neither realistic nor grounded in prior knowledge resulted in significant transfer, while concrete examples did not.

JENNIFER A. KAMINSKI,[1]* VLADIMIR M. SLOUTSKY,[1,2] ANDREW F. HECKLER[3]

[1]Center for Cognitive Science, The Ohio State University, Columbus, OH 43210, USA. [2]Department of Psychology, The Ohio State University, Columbus, OH 43210, USA. [3]Department of Physics, The Ohio State University, Columbus, OH 43210, USA.

Letters to the Editor

Letters (~300 words) discuss material published in *Science* in the previous 3 months or issues of general interest. They can be submitted through the Web (www.submit2science.org) or by regular mail (1200 New York Ave., NW, Washington, DC 20005, USA). Letters are not acknowledged upon receipt, nor are authors generally consulted before publication. Whether published in full or in part, letters are subject to editing for clarity and space.

*To whom correspondence should be addressed. E-mail: kaminski.16@osu.edu

References

1. I. N. Herstein, *Topics in Algebra* (Xerox, 1975).
2. J. A. Kaminski, V. M. Sloutsky, A. F. Heckler, in *Proceedings of the 27th Annual Conference of the Cognitive Science Society*, B. Bara, L. Barsalou, M. Bucciarelli, Eds., Stresa, Italy, 21 to 23 July 2005 (Lawrence Erlbaum, Mahwah, NJ, 2005), pp. 1090–1095.

Gene Regulation in Evolution: A History

AN OTHERWISE INTERESTING AND INFORmative News Focus story by E. Pennisi, "Deciphering the genetics of evolution" (8 August, p. 760), was marred by a flawed recounting of the key scientists responsible for advancing the importance of gene regulation in evolutionary change. In particular, the statement "Early suggestions that gene regulation could be important to evolution came in the 1970s. …" is incorrect.

As early as the 1940s, developmental geneticists such as C. H. Waddington and Richard Goldschmidt began to explore the possible involvement of gene regulation in evolution (*1*). Then, in 1969, Roy J. Britten and Eric H. Davidson published a detailed and highly influential paper in *Science* (*2*), "Gene regulation for higher cells: A theory," which clearly and explicitly argued for the importance of gene regulation in evolution. For example, on p. 356 of this paper, Britten and Davidson concluded, "At higher grades of organization, evolution might indeed be considered principally in terms of changes in the [gene] regulatory systems."

Britten and Davidson's theory of gene regulation was inspired in large part by Britten's groundbreaking work in the 1960s on DNA reassociation kinetics, which led him to discover that repetitive sequences are ubiquitous in eukaryotic genomes. Some of these repetitive sequences were later shown to influence gene regulation, and they often consist of transposons and transposon remnants that are able to cause changes in gene regulation. Because of these developments, some feel that Britten should have shared the 1983 Nobel Prize in Physiology or Medicine with Barbara McClintock for the discovery of mobile genetic elements.

JOHN W. GRULA

Carnegie Observatories, 813 Santa Barbara Street, Pasadena, CA 91101, USA. E-mail: jgrula@ociw.edu

References

1. D. J. Depew, B. H. Weber, *Darwinism Evolving: Systems Dynamics and the Genealogy of Natural Selection* (MIT Press, Cambridge, MA, 1995), pp. 414–416.
2. R. J. Britten, E. H. Davidson, *Science* **165**, 349 (1969).

Published by AAAS

CORRECTIONS AND CLARIFICATIONS

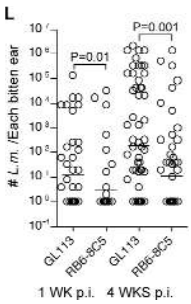

Reports: "In vivo imaging reveals an essential role for neutrophils in leishmaniasis transmitted by sand flies" by N. C. Peters *et al*. (15 August, p. 970). In Fig. 4L, some data points were inadvertently omitted during production. The corrected panel is shown here (left). The interpretation of the data is unchanged.

Reports: "Hidden neotropical diversity: Greater than the sum of its parts" by M. A. Condon *et al*. (16 May, p. 928). The first sentence of the main text was erroneous and should be replaced with the following two sentences: "Insects are extraordinarily diverse, with estimates ranging in number from 3 million to 30 million species (*1*). Recent studies focus specifically on the diversity of tropical herbivorous insects (*2*, *3*) and suggest that the diversity of herbivorous insects is a function of plant diversity (*2*), but the degree to which specialization shapes that function is contentious (*3*)." This correction supersedes the correction published in the 5 September issue.

Reports: "Pairing without superfluidity: The ground state of an imbalanced Fermi mixture" by C. H. Schunck *et al*. (11 May 2007, p. 867). Following previous work, we interpreted a spectral gap observed in the radio-frequency (rf) spectrum of a strongly imbalanced Fermi mixture as evidence for fermion pairs that do not form a condensate even at very low temperature. This conclusion was based on the assumption that unitarity-limited interactions in both initial and final states cancel out. However, recent experiments by the same group [*Phys. Rev. Lett*. **101**, 140403 (2008); *Nature* **454**, 739 (2008)] have shown that the observed spectra were strongly affected by final-state interactions. Using a new superfluid system where these interactions were weak and rf tomography to obtain local spectra without inhomogeneous broadening, the following conclusions were reached: (i) Similar to previous observations with strong final-state interactions, the minority spectrum does not show any signature of the superfluid phase transition and features similar interaction shifts in the superfluid and normal phases. (ii) In contrast, a comparison with the majority spectrum reveals that identical pairing peaks are present in both spectra only in the superfluid phase, and that the two peaks lose overlap in the normal region. (iii) This suggests that the spectral gap in the minority spectrum of the highly imbalanced normal phase should be interpreted as a signature of polaronic binding instead of evidence for pairs. (iv) The previous identification of the spectral gap with a pairing gap or a superfluid gap is incorrect. However, we have now observed locally the presence of both a pairing peak and a quasiparticle peak in the majority spectrum. The splitting between these peaks is directly related to the superfluid pairing gap.

TECHNICAL COMMENT ABSTRACTS

COMMENT ON "An Association Between the Kinship and Fertility of Human Couples"

Rodrigo Labouriau and António Amorim

Helgason *et al*. (Reports, 8 February 2008, p. 813) reported a positive association between kinship and fertility in the Icelandic population. We point out that the data further suggest that fertility initially increases with kinship and then decays. This is supported by another large study on the Danish population suggesting a superposition of effects of inbreeding and outbreeding depression on human fertility.

Full text at www.sciencemag.org/cgi/content/full/322/5908/1634b

RESPONSE TO COMMENT ON "An Association Between the Kinship and Fertility of Human Couples"

Agnar Helgason, Snæbjörn Pálsson, Daníel F. Guðbjartsson, Þórður Kristjánsson, Kári Stefánsson

Analyses of 137,844 Icelandic couples born between 1800 and 1965 reveals a monotonic drop in fertility with increasing marital radius (distance between the birthplaces of spouses). Marital radius was moderately correlated with kinship between spouses. This correlation was strongest during the peak of urbanization (1875 to 1925) but very weak after 1950. These results raise doubts about the use of marital radius as a proxy for kinship in contemporary human populations.

Full text at www.sciencemag.org/cgi/content/full/322/5908/1634c

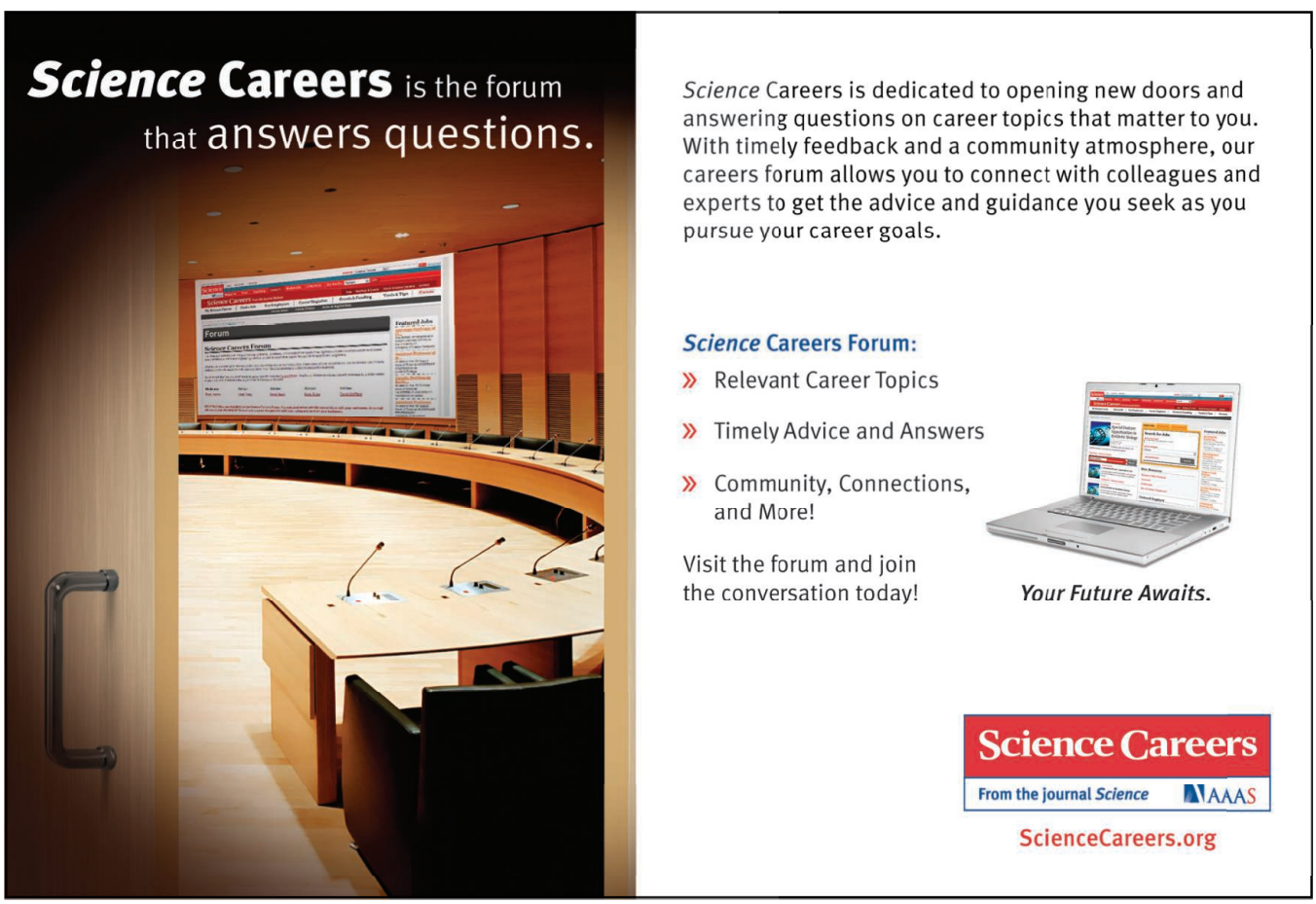

Published by AAAS

Comment on "An Association Between the Kinship and Fertility of Human Couples"

Rodrigo Labouriau[1]* and António Amorim[2]

Helgason *et al*. (Reports, 8 February 2008, p. 813) reported a positive association between kinship and fertility in the Icelandic population. We point out that the data further suggest that fertility initially increases with kinship and then decays. This is supported by another large study on the Danish population suggesting a superposition of effects of inbreeding and outbreeding depression on human fertility.

Helgason *et al*. (*1*) reported a positive association between kinship and human fertility based on comprehensive registers containing long historical series of the Icelandic population. Their results, interpreted as a manifestation of outbreeding depression, are in line with other similar findings in nonhuman populations (*2*–*4*). In parallel, we presented a positive association between fertility and marital radius (the distance between mates' birthplaces), based on a large Danish cohort (all women born in Denmark in 1954) (*5*). As a consequence of the classic Malécot theory on spatial genetic structure of populations (*5*–*9*), which states that the kinship is a decreasing function of marital radius, the results in (*5*) suggest a negative association between consanguinity and human fertility. Although the results of (*1*) and (*5*) appear to contradict each other, we argue that a closer look at both data sets reveals that this is not the case. Both studies corroborate the hypothesis that the superposed contrary forces of inbreeding and outbreeding depression have an effect on human fertility. The coincidence of the conclusions of these two independent large-scale studies suggests that this is a general phenomenon in human populations.

Although we do not cast doubt on the existence of a positive association between kinship and fertility as presented in (*1*), we remark that the relation between the mean number of children and kinship is not the same in the different periods reported. Examination of figure S2 in (*1*) reveals that the curve representing the number of children as a function of the kinship coefficient is not monotonic in the periods 1900 to 1924, 1925 to 1949, and 1950 to 1965, although the general curve obtained on the basis of all the periods together [figure 1A in (*1*)] does indeed seem to be monotonic. Here, the most striking example is the period 1950 to 1965, in which the mean number of children successively increases from the kinship interval with the lowest range (0 to 0.030518×10^{-3}) up to the interval 7.8125×10^{-3} to 31.25×10^{-3} (the reported positive association), but then the mean drops drastically for couples with kinship larger than 31.25×10^{-3}. Indeed, the mean number of children of couples with kinship larger than 31.25×10^{-3} is smaller than all the other reported means in this period and definitively much smaller than the mean for the interval 7.8125×10^{-3} to 31.25×10^{-3} (the 95% confidence interval for this interval does not include the mean for kinships larger than 31.25×10^{-3}). This is compatible with the hypothesis of a combination of effects of outbreeding and inbreeding depression on human fertility.

The Danish study (*5*) was based on the cohort of all women born in Denmark in 1954 who were alive and living in Denmark in 1969, totaling 42,165 women. This cohort was followed up to the end of 1999. The number of children born to each mother between the ages of 15 and 45 years old was determined and is referred to as fertility. The mean marital radius (MR) associated with each mother in the cohort was estimated using the distance between the centroids of the parish where she was born and the parishes where the partners with which she had children were born. The Spearman correlation between MR and fertility in the cohort was 0.38 ($P < 0.0001$), indicating a positive association. This was interpreted as evidence of the negative effects of inbreeding depression on fertility. A closer look at these data reveals, however, that the curve relating fertility and MR increases rapidly for low values of MR and tends to decrease for higher values of MR, with a maximum around 75 km (Fig. 1). Indeed, the Spearman correlation between fertility and MR is 0.083 ($P < 0.0001$) for the observations with MR smaller than 75 km and is –0.049 ($P < 0.0001$) for the observations with MR larger than 75 km. These results are also compatible with the hypothesized effect of a combination of inbreeding and outbreeding depression on human fertility.

Both studies attempt to control the possibility of spurious associations due to effects of socioeconomic factors, although using different arguments. The argument in (*1*) relies on the assertion that the Icelandic population is "one of the most socioeconomically and culturally homogeneous societies in the world," while our argument in (*5*) is based on conditional analyses given key socioeconomic indicators available for each mother in the cohort.

Here, we present an additional conditional analysis using the Danish data, including the following key socioeconomic indicators: education, family income, urbanicity, mother's age at first birth, and six variables representing proximity to kin [maternal radius, i.e., distance between mother's and child's birthplace; paternal radius; and presence of each grandparent in the child's birth parish or neighboring parish [see supporting online material (SOM)]. The distribution of information among these socioeconomic factors, together with MR and fertility, was characterized using graphical models (*5*, *10*–*12*) (see also SOM text) (fig. S1). The most relevant feature of this representation is that the conditional correlations between MR and fertility, given the socioeconomic indicators above, are 0.086 and –0.048 ($P < 0.0001$) for MR values smaller and larger than 75 km, respectively. According to the theory of graphical models (*5*, *10*, *11*), this implies that MR carries information on fertility that is not already contained in the other variables. Therefore, the associations found in the unconditional analyses are not a mere artifact due to effects of the socioeconomic factors mentioned above.

Both (*1*) and (*5*) suggest that human fertility often increases with kinship until a maximum and then decays as the kinship increases further. The pictures obtained resemble simulations performed in (*13*) under general genetic scenarios

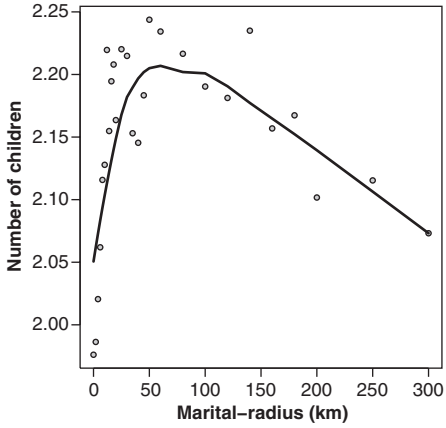

Fig. 1. Mean number of children for different intervals of marital radius observed in the Danish cohort of all women born in 1954 (and a Lowess nonparametric regression curve adjusted to the points with weights proportional to the number of observations of each interval).

[1]Department of Genetics and Biotechnology, Faculty of Agricultural Sciences, Aarhus University, DK-8830 Tjele, Denmark. [2]Faculty of Sciences and Institute of Molecular Pathology and Immunology (IPATIMUP), University of Porto, Portugal, Rua Roberto Frias, 4200-465 Porto, Portugal.

*To whom correspondence should be addressed. E-mail: rodrigo.labouriau@agrsci.dk

where inbreeding and outbreeding depression act simultaneously. Although the results discussed here are expected from the theory of inbreeding and outbreeding depression (*2*–*4*, *13*), they are hard to document in human populations. Reliable, sufficiently large human data sets, as in the two studies discussed here, are uncommon. Moreover, it is difficult to eliminate the possibility of spurious associations due to effects of socioeconomic factors unequivocally. A future challenge will be to discern which of the many possible mechanisms underlying inbreeding and outbreeding depression are in play.

References and Notes

1. A. Helgason, S. Pálsson, D. F. Guðbjartsson, Þ. Kristjánsson, K. Stefánsson, *Science* **319**, 813 (2008).
2. S. Edmands, *Mol. Ecol.* **16**, 463 (2007).
3. J. M. Grindeland, *J. Evol. Biol.* **21**, 716 (2008).
4. M. Lynch, *Evolution* **45**, 622 (1991).
5. R. Labouriau, A. Amorim, *Genetics* **178**, 601 (2008).
6. G. Malécot, *Les modèles stochastiques en genètique de population*, Publ. Inst. Statist. Univ. Paris **8** (fasc. 3), 173 (1959).
7. M. Kimura, G. H. Weiss, *Genetics* **49**, 561 (1964).
8. N. E. Morton, *Annu. Rev. Genet.* **3**, 53 (1969).
9. N. E. Morton, *Ann. Hum. Genet.* **40**, 361 (1977).
10. J. Whittaker, *Graphical Models in Applied Multivariate Statistics* (Wiley, Chichester, UK, 1990).
11. R. Labouriau, *Applying Graphical Models in Plant Genetics*, in *Quantitative Genetics and Breeding Methods: the Way Ahead*, A. Gallais, C. Dillmann, I. Goldringer [Institut National de la Recherche Agronomique (INRA), Paris, 2001], pp. 99–105.
12. L. S. Lauritzen, in *Complex Stochastic Systems,* O. E. Barndorff-Nielsen, D. R. Cox, C. Klüppelberg, Eds. (Chapman & Hall, New York, 1999).
13. M. H. Schierup, F. B. Christiansen, *Heredity* **77**, 461 (1996).

14. The work with the Danish cohort was partially done during a stay of R.L. at the National Centre for Register-based Research (NCRR) at the Aarhus University. The NCRR is supported by the Danish National Research Foundation. IPATIMUP, where A.A. works, is partially supported by the Fundação para a Ciência e Tecnologia and Programa Operational Ciência e Inovação 2010.

Supporting Online Material

www.sciencemag.org/cgi/content/full/322/5908/1634b/DC1
SOM Text
Fig. S1
References

16 June 2008; accepted 14 November 2008
10.1126/science.1161907

Response to Comments on "An Association Between the Kinship and Fertility of Human Couples"

Agnar Helgason,[1,2]* Snæbjörn Pálsson,[1,3] Daníel F. Guðbjartsson,[1] Þórður Kristjánsson,[1] Kári Stefánsson[1,4]

Analyses of 137,844 Icelandic couples born between 1800 and 1965 reveal a monotonic drop in fertility with increasing marital radius (distance between the birthplaces of spouses). Marital radius was moderately correlated with kinship between spouses. This correlation was strongest during the peak of urbanization (1875 to 1925) but very weak after 1950. These results raise doubts about the use of marital radius as a proxy for kinship in contemporary human populations.

Helgason *et al*. (*1*) reported a significant positive association between the kinship, fertility, and reproductive success of 160,811 human couples in Iceland born between 1800 and 1965. Kinship was estimated directly using genealogies up to a depth of 10 generations back from each couple; fertility was defined as the number of children born to each couple, and reproductive success was measured as the number of grandchildren (and the number of children who reproduced). We retain this terminology in the present text. Overall, a monotonic positive relationship was observed between kinship and fertility (with a maximum for couples related at the level of second cousins or closer), while the relationship between kinship and reproductive success followed an n-shaped curve (with a maximum for couples related between the level of third and fourth cousins). Although Icelanders experienced a radical socioeconomic transformation between 1800 and 1965, from a poor rural agricultural population to a rich urban industrialized population (*2*), the same general relationship between kinship, fertility, and reproductive success was observed throughout.

Based on an examination of figure S2 from our initial study (*1*), Labouriau and Amorim (*3*) rightly point out that the relationship between kinship and fertility for subintervals 1900 to 1924, 1925 to 1949, and 1950 to 1965 is not perfectly monotonic, where couples related at the level of second cousins or closer have slightly less fertility than those related at the level of second to third cousins (although this difference is only statistically significant for the subinterval 1950 to 1965; $P = 0.017$). However, their interpretation that this is indicative of inbreeding depression on human fertility is overly simplistic. Thus, in figure S2 (*1*), there is no evidence of an inbreeding depression for the earlier subintervals of 1800 to 1824, 1825 to 1849, and 1875 to 1899. Instead, there is a perfectly monotonic relationship between kinship and fertility, with significantly greater fertility of couples related at the level of second cousins or closer than those related at the level of second to third cousins for subinterval 1800 to 1824 ($P = 0.028$). Notably, the relative decrease in the fertility of the most closely related couples over time was accompanied by a drastic reduction in the overall percentage of such couples, from 5.81% in 1800 to 1824 to 0.016% in 1950 to 1965. Unlike unions between more distantly related couples, spouses related at the level of second cousins or closer are usually well aware of their genealogical relationship, as are others in their social environment. As such unions are subject to greater stigma in the largely urban and highly educated population of contemporary Iceland than in the rural preindustrial society of the 19th century, it seems more likely that the change in the relative fertility of the most related couples from 1800 to 1965 is attributable to social rather than biological factors.

After a reanalysis of their previous study (*4*), Labouriau and Amorim (*3*) further argue that their updated finding of an n-shaped curve describing the association between marital radius (the geographical distance between the birthplaces of spouses) and fertility among couples formed by all 42,165 Danish women born in 1954 is compatible with the results of our study. Further analyses of our data show that this conclusion is mistaken. First, their conclusion rests on an assumption that marital radius and the kinship coefficient are comparable measures of genealogical relationship. To evaluate this assumption, we obtained information about the birthplaces of both spouses for 137,844 couples in the 22 counties of Iceland. Defining marital radius as the geographical distance between the centroids of counties, we calculated the Spearman rank correlation (ρ) between marital radius and kinship, standardizing both variables within 5-year intervals using the approach described in (*1*) to eliminate the confounding effect of temporal change. An overall correlation of $\rho = -0.298$ ($N = 137{,}433$, $P < 1^{-6}$) indicates that marital radius is informative about the genealogical relationship between couples, but only moderately so. Nevertheless, as would be predicted from our original results, a monotonic drop in fertility with increasing marital radius is observed (Fig. 1A). Contrary to the results presented by Labouriau and Amorim (*3*) for the Danish cohort, couples from the same county (with a marital radius of 0) have the greatest fertility in Iceland.

If it were assumed that marital radius is a relatively strong correlate of kinship in the Danish cohort, the discrepancy between our results and those of Labouriau and Amorim (*3*) could reflect a real and major difference between the two populations in the relationship between kinship and fertility. However, there is reason to suspect that marital radius is not a strong correlate of kinship for the Danish couples analyzed by Labouriau and Amorim. In Iceland, the negative correlation between marital radius and kinship shows substantial change over time (Fig. 1B). A key factor underlying these temporal differences is the large-scale migration associated with the development of urban areas in Iceland, which commenced around 1870 to 1890 (i.e., involving couples born after 1830) and reached its climax between 1920 and 1950 (couples born from 1880 to 1930) (*5*). For couples born from 1800 to 1825, who met their spouses in a rural preindustrial society, $\rho = -0.116$. However, as the rate and distance of migration into urban areas increased, so did the correlation between marital radius and kinship, which reached maximum strength for couples born between 1875 and 1925 ($\rho = -0.46$). As the rate of urbanization diminished, the negative correlation weakened to its value of –0.128 for the most recent cohort of couples (1950 to 1965), most of whom were born and met their spouses in the same urban areas. Figure 1C shows a breakdown of the relationship between fertility and marital radius in Iceland by subinterval. A comparison with figure S2 in (*1*), showing the same temporal breakdown for the relationship between kinship and fertility, demonstrates that when the correlation between marital radius and kinship is weak, the pattern of association of these variables to fertility can be quite different.

Because the process of urbanization occurred in Denmark at roughly the same time as in Iceland, it follows that a relatively weak negative correlation between marital radius and kinship would be expected for the Danish couples examined by Labouriau and Amorim (*3*), whose females were all born in 1954. If our prediction is correct, then little can be inferred about the relationship between kinship and fertility from

[1]deCODE Genetics, Sturlugata 8, 101 Reykjavik, Iceland. [2]Department of Anthropology, University of Iceland, 101 Reykjavik, Iceland [3]Department of Biology, University of Iceland, 101 Reykjavik, Iceland [4]Faculty of Medicine, University of Iceland, 101 Reykjavik, Iceland.

*To whom correspondence should be addressed. E-mail: agnar@decode.is

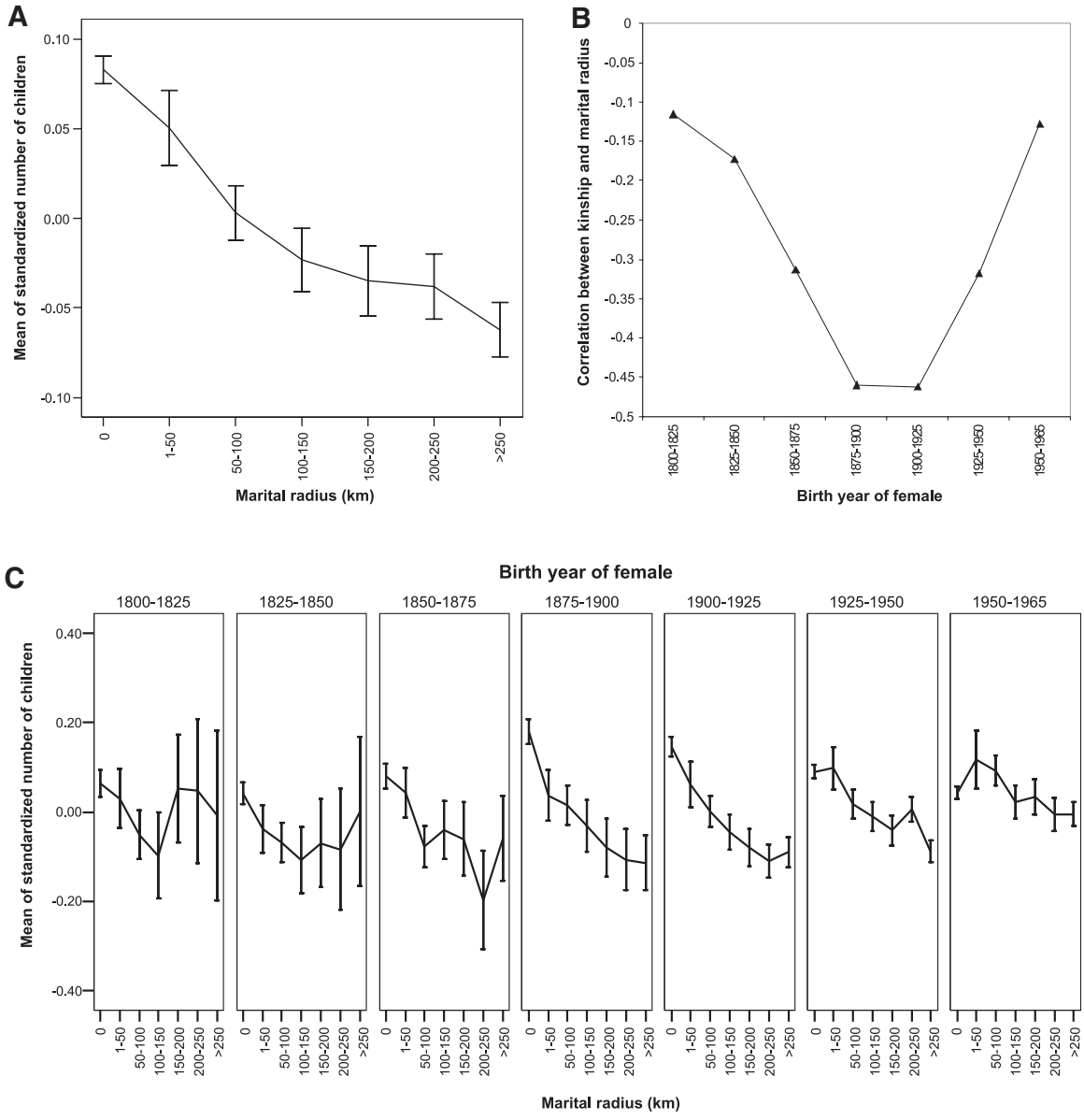

Fig. 1. The relationship between fertility and marital radius and between marital radius and kinship among Icelandic couples. (**A**) shows the mean and 95% confidence intervals of the standardized number of children per couple as a function of seven intervals of marital radius. (**B**) shows the Spearman rank correlation between standardized values of kinship and marital radius for seven successive cohorts of couples born between 1800 and 1965. (**C**) shows the mean and 95% confidence intervals of the standardized number of children per couple as a function of seven intervals of marital radius for each of the seven different cohorts of couples.

the relationship between marital radius and fertility for these Danish couples.

References

1. A. Helgason, S. Pálsson, D. F. Guðbjartsson, Þ. Kristjánsson, K. Stefánsson, *Science* **319**, 813 (2008).
2. G. A. Gunnlaugsson, *Saga og samfélag: Þættir úr félagssögu 19. og 20. aldar* (Sagnfræðistofnun Háskóla Íslands, Reykjavik, 1997).
3. R. Labouriau, A. Amorim, *Science* **322**, 1634 (2008); www.sciencemag.org/cgi/content/full/322/5908/1634b.
4. R. Labouriau, A. Amorim, *Genetics* **178**, 601 (2008).
5. G. Jónsson, M. S. Magnússon, *Hagskinna: Icelandic Historical Statistics* (Hagstofa Íslands, Reykjavík, 1997).

18 July 2008; accepted 14 November 2008
10.1126/science.1162109

MEDICINE

Yes We Can! Choose Science in Autism

Catherine Lord

The most reliable diagnosis in child psychiatry, autism nonetheless remains a mystery in many ways. It has no specific biological marker, a circumstance that likely contributes to its attractiveness to advocates and zealots, as Paul Offit describes in his forceful *Autism's False Prophets*. Persons with autism spectrum disorders (ASDs) range from nonverbal individuals with severe intellectual disabilities to highly intelligent, articulate people who struggle with social expectations. This heterogeneity invites confusion. Improvements in children with the mildest ASDs are sometimes treated as "cures," as if they were transformations of the most difficult cases, whereas in fact trajectories tend to be quite predictable within levels of severity.

Offit (a vaccine researcher and pediatrician at the Children's Hospital of Philadelphia and the University of Pennsylvania School of Medicine) takes up the story in 1998, with the now-infamous paper by Andrew Wakefield and colleagues that proposed links between measles-mumps-rubella (MMR) vaccine and autism (*1*). He offers an easy-to-read medical thriller about the consequences of greed, hubris, and intellectual sloppiness. His account weaves together cogent comments about the dangers of teleconferences in health care decision-making and accounts of scientific-legal debates about silicone breast implants and facilitated communication in ASD. Sometimes tongue-in-cheek (chapter titles include "Mercury Rising" and "Mercury Falling"), the book vividly portrays the escalation of enthusiasm for vaccination-related hypotheses:

> So dramatic was the evidence against vaccines that a major well-respected production company was going to make a movie about it. Everything was coming together. Everything made sense.

This is a tale of heroes (parents and scientists willing to stand up to threats and accusations) and some unquestionable villains. It is also the story of lesser culprits who may not profit but who cause harm by their inconsistent application of scientific standards to their own and others' work. [A recent column (*2*) by Bernadette Healy, a former head of the U.S. National Institutes of Health, exemplifies this problem.] Sometimes Offit's comments about particular individuals seemed a bit unfair. In contrast, the financial conflicts of interest of some scientists and advocates and the failure of others to take on these conflicts are much more disturbing.

Autism's False Prophets
Bad Science, Risky Medicine, and the Search for a Cure

by Paul A. Offit

Columbia University Press, New York, 2008.
322 pp. $24.95, £14.95.
ISBN 9780231146364.

Surprisingly, Offit does not discuss the fact that human decision-making is often not rational, especially when it involves evaluating relative risks and weighing anecdotal versus empirical evidence. Anyone forced to sign a consent form acknowledging that death could be the consequence of routine dental work realizes that someone somewhere is calculating the risk of ordinary procedures. With the present ease of access to unfiltered scientific and pseudoscientific data, questions of how to help parents evaluate information about risk and make rational medical choices must go beyond consent forms.

Three types of justification have been used to argue that vaccinations (either MMR or those that contain thimerosal) cause autism: specific hypotheses about effects of mercury and the measles virus on brain function, the increasing prevalence of ASDs, and the occurrence of regression in autism. Offit carefully discusses data discounting the first two justifications but spends little time on the role of regression in explaining many parents' beliefs about vaccinations. Yet this is another area where science can contribute.

Some children who will develop autism show nonspecific abnormalities (such as motor, sleeping, or eating difficulties) early in life, but autism-specific deficits in use of eye contact, facial expressions, and simple social interactions become apparent in ASD in the second year of life (*3*). Some argue that there is a clear, specific regressive subtype of ASD. However, if most children with autism manifest ordinary socially directed behaviors at 6 months and do not show these same behaviors at 24 months, then almost all children with ASD experience a regression in social-communication skills. There are children with marked regressions and children with subtle losses. Strikingly, there is no evidence that any aspect of regression in ASD is associated with timing of vaccination or exposure to thimerosal. The loss of social-communication skills is a "red flag" for ASD and must be accounted for in explanations of the development of autistic symptoms. But rather than a "clear regressive phenotype" there is a range of patterns, none of which has been shown to be related to vaccinations (*4*).

What next? Offit's call for the application of scientific principles to these questions has

CREDIT: JANINE WIEDEL PHOTOLIBRARY/ALAMY

Antivaccinationists. Demonstrators convinced of a link between MMR vaccine and autism demonstrate in London.

The reviewer is at the University of Michigan Autism and Communication Disorders Center, Ann Arbor, MI 48109 and The New York University Child Center, 145 32nd Street, 5th Floor, New York, NY 10016, USA. E-mail: celord@umich.edu

Published by AAAS

already emboldened members of the media. (YouTube offers a recent striking conversation between the Today Show's Matt Lauer and a tenacious Nancy Snyderman, the show's medical analyst.) Perhaps now we can use this momentum, as Offit fiercely argues, to shift the energy and resources from the autism-vaccination debate to the need for more research about causes and the development of effective treatments and support for individuals with ASDs and their families.

References and Notes

1. A. J. Wakefield *et al.*, *Lancet* **351**, 637 (1998); retractions followed (*5*).
2. B. Healy, *U.S. News World Rep.* (10 April 2008).
3. S. E. Bryson *et al.*, *J. Austism Dev. Disord.* **37**, 12 (2007).
4. J. Richler *et al.*, *J. Austism Dev. Disord.* **30**, 36 (2006).
5. S. H. Murch *et al.*, *Lancet* **363**, 750 (2004).

10.1126/science.1167173

NEUROSCIENCE

The Emerging Nature of Nurture

Mriganka Sur

Our minds prefer to deal in dichotomies. We like to see the world as black or white, if only to sharpen issues that demand a decision. The opposite ways in which we frame the world are the stuff of pop psychology as well as of deep dialectics. Thus, Joan Stiles starts *The Fundamentals of Brain Development* by explaining how developmental psychologists have viewed cognitive development as shaped by either nature or nurture. As the subtitle, *Integrating Nature and Nurture*, indicates, she aims to bridge this divide. At the outset, she courageously asserts that an understanding of brain development is critical for her project—courageously, because she is a cognitive scientist (at the University of California, San Diego), not an expert in developmental neuroscience. She ends up taking readers through a surprisingly detailed exposition of brain development and constructing a scholarly synthesis that will inform not only developmental psychology but even all of neuroscience and cognitive science.

Halfway through the book, I was wondering whom it was written for. The preface suggests the book is intended for students of cognitive development, and indeed they will find it highly informative. But the heart of the book is really an extended review of the recent literature on brain development. Stiles starts with the gastrulation and neurulation stages of embryogenesis and continues through the formation of the neural tube; patterning of the neural axis; production, migration, and differentiation of neurons; formation of cortical connections; and shaping of cortical circuits by experience and electrical activity. Stiles precedes this material with a description of the gene—what it is and is not and how our ideas about gene regulation and expression are evolving rapidly. Indeed, still-newer findings (on epigenetics and RNA regulation, for example) render even more complex the nature of the gene and even richer the ways in which extrinsic influences shape gene function. The author weaves her description of brain development as a process of progressive commitment of neural elements into a masterful synthesis of innateness, inheritance, development, and plasticity. I learned a great deal from the book, and I suspect other practicing neuroscientists will, too.

The Fundamentals of Brain Development
Integrating Nature and Nurture
by Joan Stiles
Harvard University Press, Cambridge, MA, 2008. 433 pp. $49.95 , £32.95, €37.50. ISBN 9780674026742.

Stiles correctly points out that among developmental neuroscientists the debate between nature and nurture has become outmoded. We now know that there is no such thing as a gene that acts in isolation and that every gene needs an environment—whether the environment is the presence of molecules made by other genes, signals generated internally within the developing nervous system, or electrical activity transduced from the external world. Thus, the discussion within the field has moved from nature versus nurture to the integration of nature and nurture and even beyond, to the nature of nurture—which kinds of environmental influences can affect gene expression at specific time points of development.

The nature of such environmental influences is a focus of much current research. At the earliest stages of brain development, the mere presence of certain molecules or signals may be sufficient: permissive influences likely suffice to shape gene and protein expression and thus influence brain development. Later on, the influence of the environment may be instructive, so that the specific pattern of signals or of electrical activity shapes brain networks and function.

This is where I suspect the divide that Stiles tries to bridge will likely persist. Nativists will argue that that the real issue is not whether an environment is required for brain development but what exactly is required. Indeed, we need to resolve the specific role of learning in development. When and under what conditions is the exact timing of spikes (as postulated by "spike timing dependent plasticity") used by the developing brain? Perhaps the earliest stages of brain development simply require the presence of external signals, and only later, as the neural machinery develops, is the pattern or structure of external information important.

Another dilemma arises from the nature of biological investigation itself. The search for mechanisms of brain development has been illuminated by selective manipulations that alter development. But the changes imposed by such a manipulation may not recapitulate the process of normal development. In the visual cortex, for example, it now appears that the pattern of projections from the two eyes is set up by the targeted early ingrowth of axons from the visual thalamus. Manipulating development by altering activity in one eye alters the pattern of projections, such that the deprived eye occupies less territory while the nondeprived eye occupies more. This plasticity, however, is a response of the system to altering the balance of activity, not a process that is necessarily used during development to settle cortical territories. Thus, the processes of plasticity, although available during development, may not be identical to the processes of development per se.

At places, the book is not an easy read. It abounds in sentences such as: "Interestingly, the introduction of Fgf8 into posterior regions where it is not normally expressed creates anomalously placed regions that express anterior identity." This is the language of developmental neurobiologists. But it is a mark of the level of engagement that Stiles brings and the way she leads readers into the material that we find such conclusions arising naturally in a discussion of cortical patterning (the way in which the developing cerebral cortex gets divided into its constituent areas).

The dichotomies of biology—nature and nurture, constancy and variation, limits and potential—while useful as artifice, are in fact inseparable from one another. As Stiles's comprehensive overview reminds us, nowhere is this more evident than in human brain development. Fundamentally derived through natural selection, the genes of brain development are impressively environment- and experience-dependent.

10.1126/science.1162117

The reviewer is at the Department of Brain and Cognitive Sciences, Massachusetts Institute of Technology, Cambridge, MA 02139, USA. E-mail: msur@mit.edu

Published by AAAS

SCIENCE AND RELIGION

Bracing for Islamic Creationism

To avoid a vast rejection of evolution in the Muslim world, scientists can present the theory as the bedrock of biology and can stress its practical applications.

Salman Hameed

Early in 2007, biologists and anthropologists at universities across the United States received an unsolicited gift of an 850-page, colored *Atlas of Creation*, produced by a Muslim creationist, Adnan Oktar, who goes by the pen name of Harun Yahya (*Science*, 16 February 2007, p. 925). The atlas was a timely notice that, although the last couple of decades have seen an increasing confrontation over the teaching of evolution in the United States, the next major battle over evolution is likely to take place in the Muslim world (i.e., predominantly Islamic countries, as well as in countries where there are large Muslim populations). Relatively poor education standards, in combination with frequent misinformation about evolutionary ideas, make the Muslim world a fertile ground for rejection of the theory. In addition, there already exists a growing and highly influential Islamic creationist movement (*1*).

Biological evolution is still a relatively new concept for a majority of Muslims, and a serious debate over its religious compatibility has not yet taken place. It is likely that public opinion on this issue will be shaped in the next decade or so because of rising education levels in the Muslim world and the increasing importance of biological sciences.

Views of Evolution from Scholars

Just as there is no monolithic Islam, there is no "official" opinion on evolution. There are indeed verses in the Koran that talk about the creation of the universe and of the living beings on Earth, but specific details are often not laid out. For example, the Koranic narrative of creation includes a 6-day account of creation. The length of each day, however, is not clearly specified. One day has been defined as "a thousand years of what you count" (32:5) or as "a day the measure of which is fifty thousand years" (70:4). The resulting ambiguity leaves open the possibility of a very old Earth. Indeed, young-Earth creationism is wholly absent in the Muslim world, and a universe billions of years old is commonly accepted. On biological evolution, Islamic scholars and popular writers hold a wide range of opinions that represent a broad spectrum of culture and politics, from secular Turkey to the conservative monarchy of Saudi Arabia and the Muslim diasporas in Europe and in the United States.

Opposition to evolution is often not centered on any particular verse from the Koran, but rather on the social and cultural threat that the theory poses for Muslims. Adnan Oktar borrows his "science" heavily from the Institute for Creation Research and, more recently, from the Intelligent Design movement in the United States (*2*). His organization, based in Turkey, has produced anti-evolution documentaries, hundreds of pamphlets, and books and has made them available for download, free of cost, from his Web site (harunyahya.com). Because the idea of an ancient Earth is not controversial among Muslims, he is comfortable presenting biological creationism in a universe billions of years old. Instead, the focus of his opposition is on the social and cultural threat posed by evolution in the form of materialism and atheism.

Some prominent Islamic scholars teaching in Western institutions also reject evolution. For example, Seyyed Hossein Nasr, a professor of Islamic studies at George Washington University, does not consider evolutionary theory to be more than an ideology: "The theory of evolution is the peg of the tent of modernism. If it were to fall down, the whole tent would fall on top of the head of modernism. And therefore it is kept as an ideology and not as a scientific theory which has been proven" (*3*). A similar view is found in the works of Muzaffar Iqbal, a biochemist by training, who is the editor of the Canadian journal *Islam & Science: Journal of Islamic Perspectives on Science.* In a recent editorial, he wrote that the logical implication of evolution is "nothing but the destruction of the sanctity of species." Rejecting evolution, he concludes, "Not only does each species preserve its characteristics, but it also receives Divine command … and acts accordingly, the Koran tells us. The ant and the honeybee have always been the ant and the honeybee and will always remain so" (*4*).

There are many others, however, who accept various interpretations of evolution.

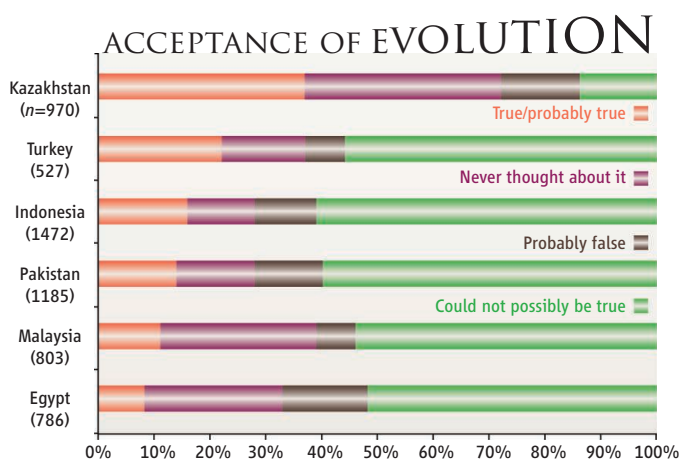

Acceptance of evolution in six Muslim countries. The data were gathered from 1996 and 2003, as part of a study of religious patterns in Muslim countries (*8*). The number of participants for each country is given in parentheses.

Often, this acceptance is justified in the context of the Koran or by crediting the theory to medieval Muslim philosophers. For example, the South Asian philosopher and poet, Mohammad Iqbal, while accepting evolution reluctantly, credited 9th century philosopher, Al-Jahiz for the idea of evolution and Ibn-Maskwaih, in the 11th century, as the "first Muslim thinker to give a clear and in many respects a thoroughly modern theory of the origin of man" (*5*). Indeed, a few medieval Muslim philosophers elaborated on the theories of common descent known at the time, but none postulated any process similar to natural selection.

Human evolution, however, is usually excluded from this scheme. Some, though, have come up with creative ways to reconcile Islam with evidence for early hominid species. For example, Maurice Bucaille, famous in the Islamic world for his book

School of Cognitive Science and School of Natural Science, Hampshire College, Amherst, MA 01002, USA. E-mail: shameed@hampshire.edu

Published by AAAS

claiming that many of the modern scientific discoveries were already mentioned in the Koran, accepts animal evolution up to early hominid species and then posits a separate hominid evolution leading to modern humans (*6*). These evolutionary ideas are a far cry from the theory of evolution as accepted by biologists all over the world.

There are also many Muslim academic biologists and medical doctors that accept evolution in ways that are similar to religious scientists in the West. Although limited in numbers, this educated class represents an influential minority for policy decisions.

Opinions of the General Population

We do not know much about general views about science in Muslim countries, let alone on the specific question of evolution. A recent survey of public acceptance of evolution in 34 countries did include one Muslim country, Turkey (*7*). The study found that about 25% of adults in Turkey agree with the statement, "Human beings, as we know them, developed from earlier species of animals," well below the United States (at 40%). The result is all the more worrisome, because Turkey is one of the most educated and secular of Muslim countries.

A recent sociological study analyzing religious patterns in Muslim countries (Indonesia, Pakistan, Egypt, Malaysia, Turkey, and Kazakhstan) included a question about evolution as an example of an idea that challenges a "fundamental religious belief widely held by Muslims" (*8*). The respondents were asked: "Do you agree or disagree with Darwin's theory of evolution?" Only 16% of Indonesians, 14% of Pakistanis, 8% of Egyptians, 11% of Malaysians, and 22% of Turks agree that Darwin's theory is probably or most certainly true (see chart, page 1637). The former Soviet republic of Kazakhstan, already showing differences in religious patterns with other countries in the study, had the highest fraction that accepted evolutionary theory. In fact, only 28% of Kazakhs thought that evolution is false, a fraction much lower than that of the U.S. adult population (~40%) (*7*).

These results paint a depressing picture. However, the question regarding evolution relies heavily on the definition of evolution as understood by individual respondents. This is especially a problem when many, perhaps most, in the Muslim world confuse evolution with atheism and consider it inherently against religion.

Teaching of Evolution

Although the survey results may point to a dire situation, the reality on the ground is more complicated. Evolutionary biology is included in the high-school curricula of many Muslim countries. In fact, science foundations of 14 Muslim countries, including Pakistan, Iran, Turkey, Indonesia, and Egypt, recently signed a statement by the Interacademy Panel (IAP, a global network of science academies), in support of the teaching of evolution, including human evolution (*9*). In general, however, biology (as is true for all other subjects) is often taught in a highly religious environment. For example, in Pakistan, where there is no separation of state and religion, the goal of the national biology curriculum for grades 9 to 12 is to "enable the students to appreciate that Allah … is the Creator and Sustainer of the universe" (*10*), and the textbooks include the relevant Koranic verses on the origin and creation of life. Biology textbooks in Pakistan contain a chapter on evolution, and evolutionary theory is presented as a fact of science. Nevertheless, the epigraph for the evolution chapter in the 12th-grade biology textbook is the Koranic verse, "And He is Who had produced you from a single being" (6:98). Apart from this epigraph, there are no religious references about creation or evolution in the remaining chapter or in suggested questions at the end (*11*). Although evolutionary theory is presented as a fact, the IAP statement notwithstanding, human evolution is missing from these textbooks. The follow-up chapters to evolution, instead, emphasize the practical aspects of biology such as health, environment, and biotechnology.

Asghar and Alters recently interviewed 18 science schoolteachers in Pakistani schools located in Karachi and Lahore and found that all favored using religious explanations about the creation of life, but most presented both scientific and religious perspectives while teaching biological evolution (*10*). Most (14 out of 18) accepted, or at least held as possible, the evolution of organisms; but at the same time, 15 out of 18 rejected human evolution. All agreed that there is no contradiction between Islam and science.

These contradictory attitudes were also reflected in a recent study of 25 Muslim university students from Turkey and Morocco studying in various disciplines in Holland (*12*). Although most accepted microevolution, almost all rejected macroevolution and connected the idea to atheistic aspirations and to the impossibility of chance and mutations leading to complex species. However, none expressed antiscience attitudes or foresaw any significant tension between Islam and science (*12*).

Communicating Evolution

The message about evolution in the Islamic world needs to be framed in a way that emphasizes practical applications and show that it is the bedrock of modern biology—thereby capitalizing on the existing proscience attitude (*13*). The national academies of Muslim countries will need to tailor the specifics of the message according to the political and cultural realities of their respective countries. Religion in the Muslim world plays a much larger role in the social and cultural landscape, and thus, our discussions with the general public need to take that into account. As scientists, we should present, without compromise, the best available science. Evolutionary ideas about human origins may face serious obstacles, but a peaceful religious accommodation is also possible. However, efforts that link evolution with atheism will cut short the dialogue, and a vast majority of Muslims will reject evolution.

A general respect for science affords scientists a high prestige in the Islamic world. Research scientists, especially biologists, should take advantage of this and write for Muslim audiences in the form of newspaper and magazine articles. At the present time, Harun Yahya is the loudest voice in the debate over evolution in the Islamic world. At this critical juncture, we cannot afford to leave the initiative with Muslim Creationists.

References

1. R. L. Numbers, *The Creationists: From Scientific Creationism to Intelligent Design* (Harvard Univ. Press, Cambridge, MA, 2006).
2. T. Edis, *An Illusion of Harmony: Science & Religion in Islam* (Prometheus Books, Amherst, NY, 2007).
3. S. H. Nasr, *Islam Sci.* **4**(2), 181 (2006).
4. M. Iqbal, *Islam Sci.* **4**(2), 89 (2006).
5. M. Iqbal, *The Reconstruction of Religious Thought* (Lahore Printing Press, Lahore, India, 1930).
6. M. Bucaille, *What Is the Origin of Man?* (Al-Falah Islamic Books, Lahore, 1989).
7. J. D. Miller, E. C. Scott, S. Okamoto, *Science* **313**, 765 (2006).
8. R. Hassan, *Muslim World* **97**, 437 (2007).
9. IAP statement on the teaching of evolution (2006), www.interacademies.net/?id=6159.
10. A. Asghar, B. Alters, *Proceedings, National Association for Research in Science Teaching (NARST) Conference*, New Orleans, LA, 15 to 18 April 2007.
11. Punjab Textbook Board, *Biology 12* (Lahore, Pakistan, 2003), p. 222.
12. D. Koning, *ISIM Rev.* **18**, 48 (2006).
13. M. C. Nisbet, C. Mooney, *Science* **316**, 56 (2007).

10.1126/science.1163672

Published by AAAS

PHYSICS

Stringing Together a Solid State

Formulations of string theory may describe some complex electronic interactions in condensed matter systems.

Sean Hartnoll

String theory was first formulated in the early 1970s with the objective of explaining aspects of the strong interactions of particle physics. The strings were literally strings of energy that bound together a quark and an antiquark to form subatomic particles called mesons. This original string theory, however, was ultimately unsuccessful and it was only consistent in 10 dimensions of spacetime. String theory was then reincarnated as a unifying theory of quantum gravity, with breakthroughs in the mid-1980s ushering this grander version into the mainstream. A recent turn of events is leading a growing fraction of string theory research back to studying specific laboratory systems, including those of condensed matter physics.

This shift has been possible due to recent developments in the mathematical construct known as the holographic correspondence. Also known as the anti–de Sitter/conformal field theory correspondence (or AdS/CFT for short) (*1*), it relates Einstein's general theory of relativity to quantum mechanics. It asserts that string theory in 10 or 11 dimensions may be equivalent to a distinct theory in the four space-time dimensions in which we live. This correspondence is called holographic by analogy to a hologram, in which a three-dimensional image is stored on a two-dimensional surface. Through the holographic correspondence, the many dimensions of string theory are encoded in a lower-dimensional theory that appears not to have anything to do with strings at all. Instead, this lower-dimensional theory shares many features with exotic theories that describe electrons in materials at so-called quantum critical points (*2*) (see the figure).

Quantum critical systems and the holographically repacked string theory share the feature of scale invariance, whereby the system responds in the same way at whatever energy scale or distance scale it is probed. An example of quantum criticality arises in the superconducting-to-insulator transition seen in thin films at zero temperature as the thickness of the film is varied (*3*). Precisely at the quantum critical point, the film is neither superconducting nor perfectly insulating but instead has a universal finite resistivity. The scale invariance of quantum critical systems makes them difficult to study using the traditional tool kit of condensed matter physics. This is because the electrons are strongly correlated and cannot be treated as individual particles weakly interacting with each other. Furthermore, the absence of a preferred scale means that approximations for low-energy or high-energy processes cannot be made. Because quantum critical behavior has been observed in many systems and is believed to play a role in important processes such as high-temperature superconductivity (*4*), it is therefore necessary to overcome these difficulties.

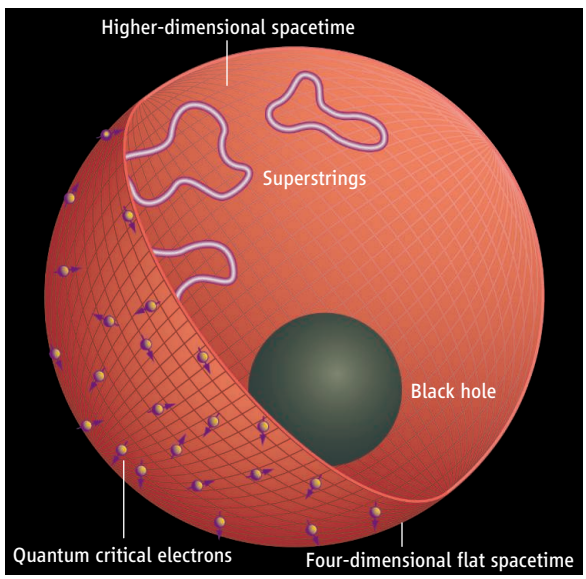

A dual description. The holographic correspondence relates string theory in a high number of space-time dimensions to a quantum critical theory in a lower number of dimensions. The quantum critical theory may be thought of as living on the boundary of the higher-dimensional string theory spacetime.

The immediate consequence of the holographic correspondence is that there is a different description, a "dual" description, of the condensed matter system in terms of higher-dimensional string theory. Certain questions actually turn out to be easier to address using the dual method. One reason is that scale invariance is built into the string theory description from the start. Another is that, whereas the original system was highly quantum mechanical, the dual description can be purely classical.

Several recent works have used string theory techniques to attack condensed matter problems involving quantum critical transport (*5*, *6*). From a theoretical description of the flow of electric and heat currents in systems that are close to quantum criticality, it was possible to predict a "hydrodynamic cyclotron resonance" for a charged quantum critical system in the presence of an external magnetic field (*6*, *7*). This resonance has certain characteristic features—for instance, its width is related to the universal conductivity at the critical point—and may be observable in future measurements on graphene (*8*).

String theory methods have begun to be applied to a range of condensed matter phenomena. Two clusters of activity have been around "holographic superconductors" (*9*, *10*) and "nonrelativistic quantum critical points" (*11*–*13*). The string theoretic description of these phenomena involve objects that have intrigued general relativists for decades: "hairy black holes," in which the black hole event horizon is not featureless, in the former, and "gravitational plane waves," the gravitational analog of electromagnetic radiation, in the latter.

A dual description of superconductivity is of interest because there are technologically and theoretically important systems that become superconducting at low temperature and where the pairing mechanism binding electrons together is known not to be the established microscopic theory of superconductivity (BCS theory). The holographic correspondence provides an inherently strongly coupled model of the onset of superconductivity, involving quantum critical fluctuations rather than phonons, which is computationally tractable. Encouragingly, the values of certain characteristic quantities, in particular, the zero-temperature energy gap over the critical temperature, are found to be consistent with those observed in high-temperature superconductors (*14*).

Nonrelativistic quantum critical points have a scale invariance in which time and space scale differently. An instance of such a critical point is believed to be relevant for the so-called "BEC to BCS crossover" in ultracold atoms, in which a qualitative change in a

Department of Physics, Harvard University, Cambridge, MA 02138, USA. E-mail: hartnoll@physics.harvard.edu

CREDIT: P. HUEY/SCIENCE

Published by AAAS

gas of atoms is induced by tuning the strength of the interactions between the atoms (*15*). In one regime the atoms form bound states while in the other they interact only weakly. One ongoing objective for string theoretic approaches to this problem is to compute transport coefficients, such as the conductivity and shear viscosity. These involve time dependent processes and so are difficult to obtain by other methods, such as modeling the system numerically with a computer.

In parallel to these recent developments, string theory also continues to probe fundamental physics: from the constituents of black holes to the possible existence of a multiverse. There is no tension between the "fundamental" and "applied" faces of string theory. Rather, the holographic correspondence offers a novel conceptual unification of physics that in fact works toward erasing this distinction. There is a certain intellectual exhilaration in formulating problems that involve both electrons in a metal and black holes, as well as a growing acknowledgement that such juxtaposition is a fertile ground for further progress.

References

1. G. Taubes, *Science* **285**, 512 (1999).
2. S. Sachdev, *Nat. Phys.* **4**, 173 (2008).
3. A. M. Goldman, N. Markovic, *Phys. Today* **51**, 39 (1998).
4. S. Sachdev, *Rev. Mod. Phys*. **75**, 913 (2003).
5. C. P. Herzog, P. Kovtun, S. Sachdev, D. T. Son, *Phys. Rev. D* **75**, 085020 (2007).
6. S. A. Hartnoll, P. K. Kovtun, M. Muller, S. Sachdev, *Phys. Rev. B* **76**, 144502 (2007).
7. S. A. Hartnoll, C. P. Herzog, *Phys. Rev. D* **76**, 106012 (2007).
8. M. Mueller, L. Fritz, S. Sachdev, J. Schmalian, http://arxiv.org/abs/0810.3657.
9. S. S. Gubser, http://arXiv.org/abs/0801.2977.
10. S. A. Hartnoll, C. P. Herzog, G. T. Horowitz, *Phys. Rev. Lett.* **101**, 031601 (2008).
11. K. Balasubramanian, J. McGreevy, *Phys. Rev. Lett.* **101**, 061601 (2008).
12. D. T. Son, *Phys. Rev. D* **78**, 046003 (2008).
13. S. Kachru, X. Liu, M. Mulligan, http://arXiv.org/abs/0808.1725.
14. K. K. Gomes *et al.*, *Nature* **447**, 569 (2007).
15. I. Bloch, *Science* **319**, 1202 (2008).

10.1126/science.1166668

IMMUNOLOGY

Chaperone Puts the Brakes On

A molecule controls both antigen processing and cell motility, ensuring that dendritic cells efficiently activate T cells to initiate protective immunity.

Veronika Lukacs-Kornek and Shannon J. Turley

Dendritic cells function primarily as immune sentinels. In the periphery, they actively scan surrounding interstitial spaces for pathogenic invaders and internalize (through a process called endocytosis) foreign antigens present in the extracellular milieu (*1*). In secondary lymphoid tissues, dendritic cells shift their attention to presenting previously internalized antigen as peptides to T cells, thus alerting the immune system to an impending threat. To carry out the latter function of activating T cells, dendritic cells must migrate from peripheral nonlymphoid tissues to draining lymph nodes, where the likelihood of meeting a rare antigen-specific T cell is highest (*2*). During this migration, dendritic cells degrade internalized antigen into peptide fragments that are then loaded onto major histocompatibility complex (MHC class II) molecules for display at the cell surface. On page 1705 of this issue, Faure-André *et al.* report their unexpected finding that dendritic cell motility is linked to the invariant chain (Ii), a key molecule in antigen processing (*3*).

MHC class II molecules are highly expressed in dendritic cells and B cells of the immune system (*4*). MHC class II is synthesized as a heterodimer in the endoplasmic reticulum, where it associates with the non-MHC molecule, Ii. Ii, which is a type II membrane protein, spans the length of the heterodimer, but a 14 amino acid domain known as the class II–associated invariant chain peptide (CLIP) extends to fill the peptide binding groove of the MHC class II molecule. A dileucine targeting motif in the cytoplasmic tail of Ii guides newly synthesized MHCII-Ii complexes through the Golgi apparatus and to antigen-rich endolysosomal vesicles (*4*, *5*).

Removal of Ii from an MHC class II molecule is a tightly regulated, stepwise process involving multiple lysosomal proteases (*4*, *6*). A key step is its cleavage by the lysosomal cysteine protease cathepsin S, which liberates MHC class II molecules from retention in endolysosomal compartments. Ablation of cathepsin S activity either from genetic deficiency or by treatment with a specific compound (LHVS) prevents Ii degradation, thereby trapping newly synthesized MHC class II molecules in endolysosomal compart-

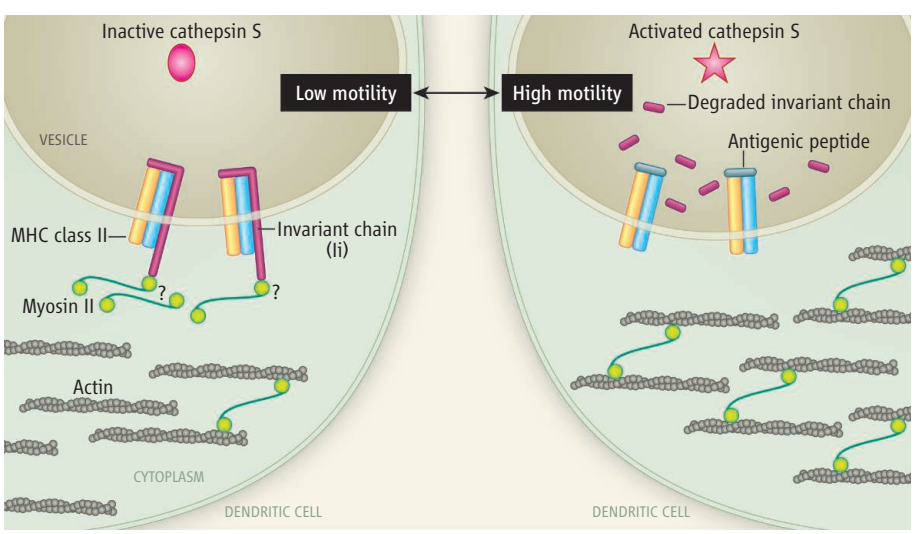

Slow it down. In dendritic cells, MHC class II–Ii complexes localize to endolysosomal compartments laden with foreign antigens that have been internalized. Myosin II motors associate with these complexes when the amount of intact Ii is high. Direct or indirect association of myosin II with Ii imposes low cell motility in migrating dendritic cells. Activated proteases (including cathepsin S) cleave Ii, thereby releasing MHC class II and myosin II from endolysosomes. Myosin II is then free to interact with the actin cytoskeleton, resulting in high cell motility. The fluctuation between high and low motility may enable dendritic cells to coordinate vesicular transport and antigen presentation with cellular locomotion.

Department of Cancer Immunology and AIDS, Dana Farber Cancer Institute, Boston, MA 02115, USA. E-mail: shannon_turley@dfci.harvard.edu

Published by AAAS

ments. Even after cleavage by cathepsin S, peptide loading onto an MHC class II molecule cannot occur until the CLIP domain of Ii is displaced from the peptide binding groove. This protective function of Ii is critical for preventing self-peptides from binding to MHC class II molecules in the endoplasmic reticulum or Golgi. Replacement of CLIP with a high-affinity antigenic peptide is facilitated at low pH by a membrane protein, HLA-DM (*4*, *7*). Once released from Ii and loaded with antigenic peptide, MHC class II molecules are transported to the plasma membrane. Thus, Ii serves as a chaperone to guide MHC class II molecules to antigen processing, endolysosomal compartments and also to protect the peptide binding groove.

Faure-André *et al.* discovered that Ii not only is fundamentally important in the antigen-processing pathway, but also can function in the same context as a regulator of dendritic cell locomotion (see the figure). Recently, it was reported that myosin II, a motor protein that binds filamentous actin and controls cellular contractility, is required for dendritic cells to navigate narrow spaces that are characteristic of parenchymal tissues (*8*). Taking this report into account and their own recent finding that myosin II interacts with MHC class II–Ii complexes through the cytoplasmic tail of Ii in B cells (*9*, *10*), Faure-André *et al.* asked whether dendritic cell motility might be influenced by Ii. The authors determined that Ii-deficient dendritic cells in mice migrated more efficiently from skin to lymph nodes compared with their wild-type counterparts. Likewise, an increase in the amount of Ii present in endolysosomes (which occurs in the absence of cathepsin-S), impaired the migratory capacity of dendritic cells. Using real-time imaging to measure the velocity of cell migration in fabricated microchannels, the authors noted that dendritic cells normally oscillate between high and low motility phases. In dendritic cells lacking Ii, however, the switch to low motility phases occurred less frequently, resulting in an overall higher velocity.

A pressing question is whether MHC class II–Ii complexes interact with myosin II or with other actin-binding partners, to tether cytoskeletal regulators to antigen-processing compartments in the endocytic pathway of dendritic cells. Faure-André *et al.* found that inhibiting myosin II activity with the compound blebbistatin dampened dendritic cell migration. They further found that an increase in Ii in endolysosomes of cathepsin-S-deficient dendritic cells augmented the association of myosin II motors with antigen-processing compartments. The accumulation of Ii in endolysosomes also reduced the amount of activated (phosphorylated) motor protein present in the cell. A short burst in Ii synthesis was sufficient to enhance the association of Ii with myosin II and, in turn, to negatively impact dendritic cell motility. These results suggest that cleavage of Ii by cathepsin S restores high motility in dendritic cells by freeing myosin II from endolysosomal association, thereby renewing the actin-binding potential of this key motor protein. Whether myosin II and MHC class II–Ii complexes interact directly or indirectly through an accessory protein remains to be determined.

Migration involves protrusions at the front of a cell and retraction at the trailing end. It is the contraction of the actin network by myosin II that propels the cell body forward. To generate the necessary internal force to move the cell forward, it has long been thought that myosin II activity must be rigidly anchored to the extracellular matrix through an association with the cell adhesion molecules integrins (*11*). A recent study by Lammermann *et al.* demonstrates that in migrating dendritic cells, the force generated by the actin-network and myosin II contractility occurs independently of functional integrins (*8*). Coupled with the discovery by Faure-André *et al.* that Ii regulates locomotion in dendritic cells, there is cause to wonder whether the mechanisms underlying migration of dendritic cells and other MHC class II–expressing leukocytes are dissimilar from most other migratory cell types.

References

1. R. M. Steinman, H. Hemmi, *Curr. Top. Microbiol. Immunol.* **311**, 17 (2006).
2. G. J. Randolph, J. Ochando, S. Partida-Sanchez, *Annu. Rev. Immunol.* **26**, 293 (2008).
3. G. Faure-André *et al.*, *Science* **322**, 1705 (2008).
4. E. S. Trombetta, I. Mellman, *Annu. Rev. Immunol.* **23**, 975 (2005).
5. G. van Niel, R. Wubbolts, W. Stoorvogel, *Curr. Opin. Cell Biol.* **20**, 437 (2008).
6. N. Rocha, J. Neefjes, *EMBO J.* **27**, 1 (2008).
7. J. Vyas *et al.*, *Nat. Rev. Immunol.* **8**, 607 (2008).
8. T. Lammermann *et al.*, *Nature* **453**, 51 (2008).
9. F. Vascotto *et al.*, *Curr. Opin. Immunol.* **19**, 93 (2007).
10. F. Vascotto *et al.*, *J. Cell Biol.* **176**, 1007 (2007).
11. G. Giannone *et al.*, *Cell* **128**, 561 (2007).

10.1126/science.1168103

EPIDEMIOLOGY

Why Can't We Test Our Way to Absolute Food Safety?

Shaun Kennedy

Efforts to ensure food safety must take into account long supply chains and unanticipated threats.

Public attention to recent foodborne illness outbreaks raises an obvious question: Why aren't contaminants found before they sicken consumers? Several recent examples—including *Salmonella enterica* serovar Saintpaul in produce, *Escherchia coli* O157:H7 in ground beef, *Listeria monocytogenes* in ready-to-eat meat, and melamine in infant formula—have led elected officials and consumer groups to call on the food industry and regulatory agencies to prevent contaminated foods from reaching the kitchen or restaurant. The problem is that no amount of testing can ensure that every food item is free from accidental or intentional contamination. However, protection strategies can be developed that combine low-cost detection methods with steps that mitigate hazardous outcomes.

Methods for detecting food contamination face several hurdles. Ideally, they should be specific—correctly identifying the contaminant—and sensitive, confirming the lack of contamination. Methods should be fast (giving results in minutes or hours), require minimal sample preparation before analysis, and be low in cost. However, these goals are often conflicting. The ability of detection strategies to mitigate harm to public health is further challenged by unanticipated combinations of foods and contamination agents, as well as the threat of intentional contamination.

The single largest challenge is often overlooked: deciding when to test, and for what agents. Detection strategies can be categorized as "detect to prevent" (confirmation that food is not contaminated before it leaves the farm or facility); "detect to protect" (detection before food items become available for consumption); and "detect to recover/detect to regret" [limiting the scope

National Center for Food Protection and Defense, Department of Homeland Security Center of Excellence, and Veterinary Population Medicine, University of Minnesota, Saint Paul, MN 55108, USA. E-mail: kenne108@umn.edu

Published by AAAS

of an outbreak, attributing its origin, or both (*1*, *2*)]. If the goal is "detect to prevent/protect," sampling strategies that incorporate food supply-chain characteristics become paramount, but also complicated.

Testing earlier in the supply chain, near the point of primary production, might seem like the most advantageous approach. However, contamination can occur at any point along the food chain, from field to table. Testing jalapeno peppers at the farm might reduce the potential for foodborne illness through salsa made with contaminated peppers, but only if all of the peppers are tested for all potential pathogens, and no peppers are contaminated by postfarm handling. Field testing of carrots for pot pies will not help if environmental contamination in the processing plant is the real illness risk. Testing at each point of the chain is impractical both in terms of cost and, for fresh foods, time.

From field to table. Although measures can be taken to assess food along its long supply chain, they cannot necessarily ensure its purity.

In this year's *Salmonella* Saintpaul outbreak in fresh produce, intensive testing was conducted by industry, the U.S. Food and Drug Administration, and other agencies. Yet, it took months to find a produce item contaminated with the outbreak strain, because of the complexity of the fresh-produce supply chain and the uncertainty in the epidemiological investigation (both tomatoes and peppers were implicated). Even if the outbreak source had been rapidly identified as contaminated Mexican peppers, the combination of more than 500 producers in Mexico, 300 importers, and 25,000 shipments of peppers in March through June of 2008 would have presented a daunting challenge. Given the apparent low level and sporadic contamination, and because each shipment includes tens to hundreds of thousands of servings, preemptively identifying the contaminated peppers would have required a combination of detection-method sensitivity, sampling-strategy efficiency, and speed that does not yet exist (and would likely be prohibitively expensive if it did).

Melamine contamination of dairy products in China, which occurred 1 year after melamine contamination of wheat gluten, outlines the challenges associated with intentional adulteration and global supply chains. In both cases, disreputable firms took advantage of existing supply-chain practices by introducing melamine to make the protein level appear greater than it actually was (many "protein assays" are actually only assays for nitrogen). In both events, the point of contamination occurred well after harvesting. The broad use of wheat gluten resulted in the recall of more than 900 products in last year's event. The contamination of Chinese dairy products has caused tens of thousands of illnesses and recalls or trade restrictions in more than 18 countries.

For any detection strategy, financial considerations vary greatly depending on where and how frequently a contaminant-detection technology is used. For example, there are tests for quality and contamination at every stage of the dairy supply chain (see the figure), but the challenge is the selection of what to test for, how to test for a specific agent, and how frequently to test in a globally distributed food system. In the U.S. dairy system, a detection method with a cost of $5.00 per analysis would result in an annual cost of about $150,000,000 if done daily at farm level. Testing every milk tanker received at a processing plant is a somewhat more manageable number, approximately $21,000,000, but represents testing for just one contaminant. The efficiency of testing at the tanker level is why regulations require such testing for antibiotic residues. Testing every milk tanker for antibiotics does not, however, ensure that no antibiotics from normal farm animal health practices reach consumers through milk. It is an overall system verification that no individual load is above a threshold level of specific antibiotics. No detection strategy can guarantee that no contamination is present.

For food defense against intentional contamination, the lack of any known probability and the large number of potential agents make detection strategies even more problematic. If only 10 of the select agents that might be stable in milk are considered, the cost of testing each dairy tanker truck load for each pathogen increases to $210,000,000, regardless of other chemical or nontraditional threat agents that might be of concern. Chemicals and toxins are more vexing because there usually is no easy way to enrich their presence in a sample and enhance their sensitivity for detection, as can be done with bacterial enrichment (encouraging organism growth). For example, the mouse assay that is still the gold standard for botulinum neurotoxin detection (*3*) is both costly and difficult to deploy.

From an industry, and ultimately a consumer, perspective, false-positive detections are a major concern. If a detection technique has a relatively low false-positive rate of 1 per 100,000, a tanker truck of milk could potentially test "positive" every 8½ days. For intentional contamination agents where the probability of actual presence approaches zero, asking industry to assume both the direct costs and the consumer confidence impact of a suspect intentional contamination nearly every week is unreasonable.

The dichotomy between testing strategies for food-safety threat agents (low levels of contamination, sporadic occurrence, high morbidity but usually low mortality) and food-defense threat agents (high levels of contamination, intentional and unpredictable occurrence, high mortality or severe morbidity) further complicates detection and sampling strategies. For food defense, the emphasis shifts away from both traditional sensitivity and specificity to rapid identification of anything unusual present at a high enough level to cause harm to public health. This consideration suggests that, along with the false-positive considerations, rapid confirmatory tests will need to be deployed alongside any detection technology used for food defense.

There are international standards for testing food for potential contamination (*4*). These standards draw from many inputs, especially the International Commission on Microbiological Specifications for Foods (*5*, *6*), and although they can improve the effectiveness of testing strategies, there are still foodborne illness outbreaks. The existing standards do not cover intentional contamination, especially the differences between detection strategies in assessing a contamination threat.

Against this backdrop, the most rational path forward is the selective use of low-cost, highly sensitive and specific assays for food safety along with even more selective use of low-cost, less sensitive but very low false-positive rate assays for food defense. Points of detection must also be selected with a detailed understanding of the supply chain to ensure

CREDIT: PETER HOEY

Published by AAAS

that public health is protected in an economically sustainable way. Given that the "tricorder" of *Star Trek* lore is still a scientific fantasy, pathogen detection alone will not eliminate the potential for contaminated food reaching the consumer. Detection strategies must be combined with multiple prevention efforts to best protect consumers of the global food system.

References

1. R. Danzig, *Catastrophic Bioterrorism—What Is to Be Done?* (Center for Technology and National Security Policy, National Defense University, Washington, DC, 2003).
2. S. P Kennedy, F. Busta, in *Food Microbiology: Fundamentals and Frontiers*, M. Doyle, L. Beuchatt, Eds. (American Society for Microbiology, Washington, DC, ed. 3, 2007), chap. 5.
3. J. L. Ferreira, S. J. Eliasberg, P. Edmonds, M. A. Harrison, *J. Food Prot.* **67**, 203 (2004).
4. See, for example, www.codexalimentarius.net/web/standard_list.do?lang=en.
5. International Commission for the Microbiological Specifications of Foods, *Microorganisms in Foods 2: Sampling for Microbiological Analysis: Principles and Specific Applications* (Blackwell Scientific, New York, 1986).
6. International Commission for the Microbiological Specifications of Foods, *Microorganisms in Foods 7: Microbiological Testing in Food Safety Management* (Kluwer Academic, New York, 2002).

10.1126/science.1163867

DEVELOPMENTAL BIOLOGY

On Growth and Force

The physical stress on plant tissue during growth controls the precise organization of a major structural element in the plant cell.

Bela Mulder

Almost a century ago, zoologist D'Arcy Thompson wrote, "Cell and tissue, shell and bone, leaf and flower, are so many portions of matter, and it is in obedience to the laws of physics that their particles have been moved, moulded and conformed" (*1*). The current preeminence of the molecular genetic approach to biology, in which living systems are conceptualized as networks of interacting genes and proteins, may have obscured this inevitable link between physics and biology in the mind of scientists and the public alike. Nonetheless, there are clear signs that a revival is under way. Moreover, and perhaps fittingly, the clearest signs of this revival come from developmental biology, the field that Thompson so profoundly influenced. A striking example of this trend is found on page 1650 of this issue, where Hamant *et al*. (*2*) show that mechanical stress plays a key role in the development of plant organs.

In a naïve view, tissues and cells might be thought of as passive, simply responding to the forces acting on them according to their respective fixed mechanical properties (such as stiffness and plasticity). But we are becoming increasingly aware of the fact that cells not only can detect and respond to mechanical signals—that is, forces exerted on them, either locally or globally (e.g., pressure)—by changing their own state, but can directly mechanically manipulate their environment through the production of forces.

A remarkable example of how cells respond to their mechanical environment is how stem cells can be directed to differentiate into specific cell types by the stiffness of the extracellular matrix into which they are embedded. Mesenchymal stem cells cultured on a very soft synthetic matrix (mimicking brain tissue) will develop into neurons, whereas they develop into muscle cells and bone cells, respectively, in matrices of increasing stiffness (*3*). Tellingly, these developmental cues from the environment are no longer effective when a drug is introduced that inhibits the activity of a myosin-type motor protein. Motor proteins are force-generating molecules that drive the transport of materials within a cell (among other functions); myosin motors do so by interacting with the actin cytoskeleton. The result indicates that these cells are actively probing their environment by a force-feedback mechanism. But cells can also mechanically act on their environment, sometimes with major developmental consequences. For example, the left-right asymmetry of vertebrate embryos is due to an asymmetric fluid flow set up by the rotatory motion of cilia, motor protein–driven filamentous appendages of the embryonic cells themselves (*4*, *5*).

The examples above all involve animal cells, but almost half of Earth's biomass is stored in organisms that have solved a unique set of mechanical problems of their own: plants. The lack of a bony endo- or exoskeleton forced plants to adopt a different strategy to grow against the pull of gravity. They developed a fiber-laminate outer casing—the cell wall—containing long cellulose microfibrils, often deposited in ordered patterns, as the main structural element. This tensile wall allows plant cells to support a sizable internal osmotic pressure, which is the source of nonwoody cells' rigidity. How the direction of deposition of the cellulose microfibrils is controlled has been an open question for decades. Even before microtubules were first fully characterized, plant biologist Paul Green had speculated that the anisotropic growth typical of plant cells requires the presence of filamentous proteins to guide cell wall deposition (*6*). In all plant cells, microtubules—dynamic cytoskeletal proteins—form an ordered cortical array. In growing cells, this array is typically oriented transverse to the growth direction, coincident with the direction of the cellulose microfibrils in the walls of these cells. The long-standing hypothesis that cortical microtubules may guide the movement of the motile transmembrane protein complexes that synthesize the cellulose microfibrils, and thus

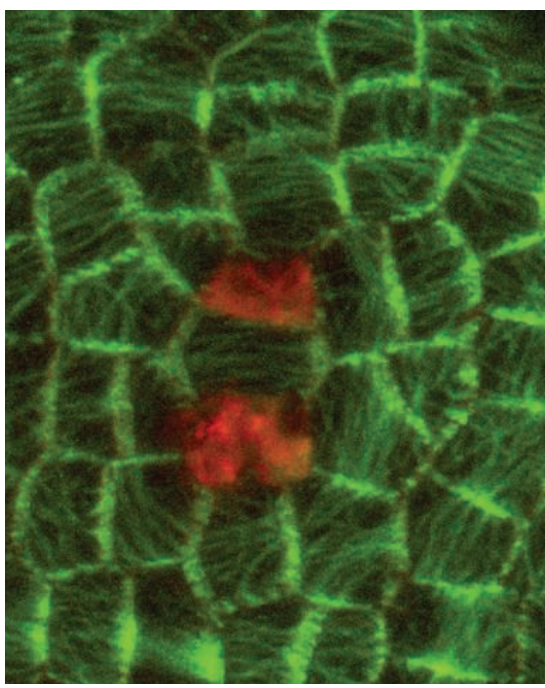

Showing stress. The shoot apical meristem of the plant *A. thaliana* is shown after two cells (red) have been ablated by laser treatment. The concentric pattern of microtubules (green) surrounding the ablated cells resembles the pattern of maximal stresses predicted by mechanical modeling and simulation of cell ablation (*2*).

CREDIT: MARCUS HEISLER

Department of Biomolecular Systems, FOM Institute for Atomic and Molecular Physics, Kruislaan 407, 1098 SJ Amsterdam, Netherlands, and Laboratory for Plant Cell Biology, Wageningen University, Arboretumlaan 4, 6703 BD Wageningen, Netherlands. E-mail: mulder@amolf.nl

Published by AAAS

dictate the direction of deposition, has recently been supported with direct observational evidence (*7*).

Although the precise relationship between cortical microtubules and cellulose-synthesizing enzymes is still far from understood (*8*), the question of what determines the pattern of microtubule orientations in growing cells is now pertinent. Hamant *et al.* show that in the developing shoot apex of the model plant *Arabidopsis thaliana*, microtubule orientation and morphogenesis are coupled in a feedback loop that involves mechanical signals that are triggered by growth of the organ itself. The authors reaffirmed the morphogenetic role of microtubules by showing that both cell shape and overall organ morphology of the shoot meristem were disturbed in response to treatment with the microtubule-depolymerizing drug oryzalin. Using fluorescently labeled microtubules, they established that the pattern of microtubule orientations correlated both spatially and temporally with the evolving morphology. Next, they implemented a simple mechanical model of the growing shoot and observed that microtubule orientations corresponded to the predicted directions of maximal stress. And by ablating specific cells in the outer layer of the meristem, they forced a stress redistribution, which the authors could compute in a more detailed mechanical model of the organ. This new stress pattern again matched the observed changes in the microtubule configurations (see the figure).

How can microtubules "read" stress in the cell wall? Here, there may be a role for the still-uncharacterized molecules that anchor the cortical microtubules to the plasma membrane and possibly also to the cell wall (*9*), potentially allowing them to act as strain gauges. Also, how generic is the tight coupling between the direction of cellulose microfibril deposition and microtubule orientation (*10*)? Cellulose microfibril orientation does not always correlate with microtubule orientation (*11*), and cellulose-synthesizing complexes can adopt ordered patterns of motion even in the absence of orientational cues provided by microtubules (*7*), implying the existence of a default mechanism (*12*).

The multidisciplinary composition of the research team of Hamant *et al.* and the tight integration of experiment and theory would have gladdened Thompson. In his 1917 masterpiece, *On Growth and Form* (*1*), Thompson eloquently argued that the methods and mathematics of the physical sciences are indispensable in the study of living nature. Indeed, physics is bound to become a closer ally of biology, now that the physical mechanisms underpinning biological phenomena are increasingly laid bare.

References

1. D. W. Thompson, *On Growth and Form* (1917); abridged edition, J. T. Bonner, Ed. (Cambridge Univ. Press, Cambridge, 1961).
2. O. Hamant *et al.*, *Science* **322**, 1650 (2008).
3. A. J. Engler, S. Shen, H. L. Swinney, D. E. Discher, *Cell* **126**, 677 (2006).
4. J. J. Essner *et al.*, *Nature* **418**, 37 (2002).
5. S. Nonaka, H. Shiratori, Y. Saijoh, H. Hamada, *Nature* **418**, 96 (2002).
6. P. B. Green, *Science* **138**, 1404 (1962).
7. A. R. Paredez, C. R. Somerville, D. W. Ehrhardt, *Science* **312**, 1491 (2006); published online 20 April 2006 (10.1126/science.1126551).
8. A. R. Paredez, S. Persson, D. W. Ehrhardt, *Plant Physiol.* **147**, 1723 (2008)
9. P. A. Vesk, M. Vesk, B. E. S. Gunning, *Protoplasma* **195**, 168 (1996).
10. A. M. C. Emons, H. Höfte, B. M. Mulder, *Trends Plant Sci.* **12**, 279 (2007).
11. T. I. Baskin, *Protoplasma* **215**, 150 (2001).
12. A. M. C. Emons, B. M. Mulder, *Proc. Natl. Acad. Sci. U.S.A.* **95**, 7215 (1998).

10.1126/science.1168512

BIOCHEMISTRY

An Almost-Complete Movie

Structural snapshots of transporter proteins reveal how they transport species across membranes.

George Diallinas

Transmembrane transport proteins are encoded by about 5 to 15% of genes in all genomes and are involved in numerous biological functions by mediating the movement of solutes and ions across membranes. Recent studies, including the report by Singh *et al.* on page 1655 of this issue (*1*), have provided new insights into the structure and function of an important group of transmembrane proteins.

Recent years have seen the publication of crystal structures of two types of such proteins: channels and transporters (*2*). Both include several (mostly 10 to 12) α-helical transmembrane domains (TMDs) connected by intracellular and extracellular loops. In channels, several TMDs construct a selective gated pore, whereas in transporters, there is no continuous pore, suggesting that the latter should have at least two alternating conformations to make them accessible to substrates either from within or from outside of cells. This structural difference is reflected in function. Channels are selective for specific ions, letting them flow rapidly (up to 10^7 ions per second) down chemical and electrostatic gradients. Transporters mediate much slower (10^2 to 10^5 molecules per second) movements of nutrients and other solutes along downhill (diffusion) or uphill (active transport) concentration gradients. The energy needed for active transport is provided either by intrinsic hydrolysis of adenosine 5′-triphosphate or by coupling with an energetically favorable flow or counterflow of ions (usually H^+ or Na^+).

Most of what we know about transporter structure comes from extensive studies of the LacY permease of *Escherichia coli*, a paradigm for the largest transporter family known as the major facilitator superfamily (MFS) (*3*–*5*). LacY and other MFS carriers (*6*) are made of two parallel symmetrical halves consisting of six TMDs each; these halves share a unique substrate binding site at their interfaces in the middle of the membrane. All three MFS structures known to date have been "caught" in crystals in their inward-facing conformation (which is accessible to substrates intracellularly) (*3*–*6*). An outward-facing MFS conformation is still hypothetical, but biochemical and biophysical data support an alternating access model, in which the conformational change needed for completion of transport catalysis occurs via a rocker-switch movement (*4*, *5*).

Several recent studies (*7*–*11*), including that of Singh *et al.* (*1*), go beyond MFS, describing the crystal structures of four bacterial transporters from other transporter families. These structures suggest an alternating access mechanism, similar to that of gated pores. These carriers belong to the families of neurotransmitter sodium symporters [NSS; glutamate transporter (GltPh) and leucine transporter (LeuT)], solute sodium symporters [SSS; sodium galactose transporter (vSGLT)], and nucleobase cation symporters [NCS1; benzyl-hydantoin transporter (Mhp1)].

Faculty of Biology, University of Athens, Panepistimioupolis 15781, Athens, Greece. E-mail: diallina@biol.uoa.gr

Published by AAAS

Surprisingly, all four transporters share a similar structure, despite belonging to three evolutionarily distinct protein families with no primary amino acid sequence similarity and different substrate specificities. The core of this structure consists of two V-shaped domains (with five TMDs each), intertwined in an antiparallel topology. A substrate binding site is located in a nearly identical position at two broken helices, one from each domain. The ion binding sites necessary for energy coupling are located close to the substrate binding site, but their position in the different transporters is more variable.

As a result of the recent structures, we now have four structurally homologous transporters caught in three conformations: "outward-facing open" [LeuT (*1*), Mhp1 (*11*)], "outward-facing occluded" [GltPh (*8*, *9*), LeuT (*1*), Mhp1 (*11*)], and "inward-facing occluded" [vSGLT (*10*)]. Due to their common topology, it has been possible to map each one through computer modeling on the three different conformations, providing insights into the mechanistic basis of transporter function. A fourth conformation, corresponding to an inward-facing open structure, can so far only be hypothesized (see the figure). This creates a sequence of snapshots that previews the protein movements associated with transport (see the figure).

In all cases, what distinguishes open from occluded states, in the outward-facing conformation, is the positioning of a few amino acid residues (in LeuT) or parts of flexible helices (in Mhp1 and GltPh) in the hydrophilic vestibule just above the substrate binding site. A similar situation has been hypothesized for the inward-facing conformations, where only the occluded structure is available (in vSGLT and Mhp1) (*10*, *11*).

In both open and occluded outward-facing conformations of LeuT and Mhp1, the other side (the intracellular gate) is closed by a considerable protein mass. Similarly, in the occluded inward-facing conformation of vSGLT, a considerable helical mass closes the extracellular gate. This implies that there are two kinds of sequential conformational changes (see the figure). The first involves specific gating amino acids or parts of helices located over and below the substrate binding site, and the second involves a more massive movement of TMDs, which leads to alternating inward- or outward-facing hydrophilic vestibules.

Singh *et al*. show that two residues of the extracellular gate can act as parts of a low-affinity, transiently occupied binding site. Once the substrate moves to the primary substrate binding site, these residues interact, closing the extracellular gate and promoting an occluded conformation state. Occlusion from the outside seems to be a prerequisite for subsequent larger conformational changes that lead to the inward-facing conformation.

What do the recent articles on gated pores tell us about the rocker-switch mechanism proposed for MFS transporters? Are the two mechanisms different? Can these models be reconciled with each other or with a Brownian ratchet model (an alternative to the rocker-switch model that has been proposed for LacY and other MFS proteins), which states that substrates slide through serial dissociation-association reactions between several "docking" sites in the transporter (*12*)?

The figure implies that the mechanistic differences among the transporters studied, including MFS, might be minimal. A rocker-switch movement is probably the mechanism used by all known transporters. Gating might have evolved to add extra specificity or to prevent leakage of substrates in the wrong direction. Genetic evidence for that has been obtained with a purine transporter (from the NAT/NCS2 family), in which the gating elements and substrate binding site synergize to determine substrate specificity (*13*). In some transporters, secondary binding sites might exist at the gates or elsewhere along the substrate translocation pathway. Substrate docking at these sites might be essential for access to the primary binding site located in the core of the transporter.

Key questions concerning transporter function remain unanswered: What is the mechanism of ion coupling? What are the specific gating elements in each transporter? How does a transporter, after substrate release, return to the outward-facing conformation? Which amino acids define transport rate, substrate specificity, or ion selectivity? Answering these questions requires knowledge of all basic conformational changes associated with the full transport cycle for any single transporter. Also needed are structures with different substrates or ligands, as described by Singh *et al*. Genetic and biochemical studies, carried out in model organisms such as bacteria and fungi, would provide an exciting complement to structural studies. Mutant versions of transporters altering the kinetics of transport, substrate specificity, or ion selectivity can be selected or rationally designed to test the structural and mechanistic models proposed. A structure by itself is not sufficient to predict function. Life after crystals is now starting.

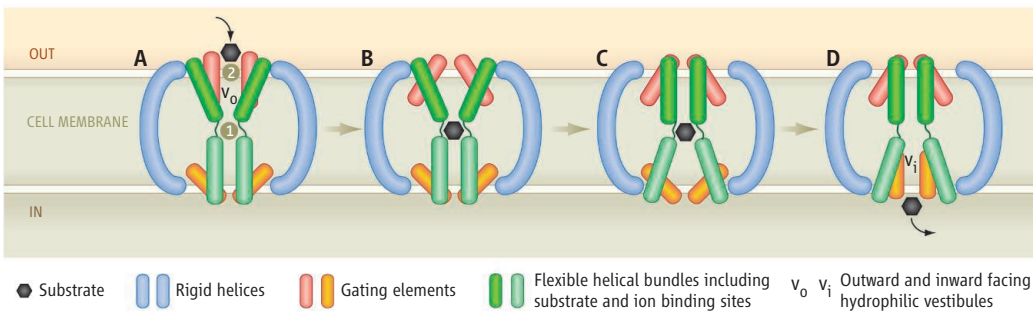

Substrate-induced structural conformations of gated rocker-switch transporters. (**A**) The outward-facing open conformation is ready to receive the substrate (black hexagon) and ion (not shown) (*1*, *11*). **1** indicates the primary substrate binding site between two broken helices, identically positioned in all gated rocker switches; **2** marks a secondary binding site found in the outward-facing open conformer of LeuT described by Singh *et al.* (*1*). (**B**) In the outward-facing occluded conformation, the substrate (and ion) is bound in the primary binding site and the external gate closes (*1*, *7*, *8*). (**C**) Closure of the external gate promotes the inward-facing occluded conformation (*10*). (**D**) The inward-facing conformation opens its gate for substrate and ion release. This conformation is hypothetical.

CREDIT: P. HUEY/*SCIENCE*

References and Notes

1. S. K. Singh, C. L. Piscitelli, A. Yamashita, E. Gouaux, *Science* **322**, 1655 (2008).
2. For a database of membrane proteins with known three-dimensional structure, see blanco.biomol.uci.edu/Membrane_Proteins_xtal.html.
3. J. Abramson *et al.*, *Science* **301**, 610 (2003).
4. L. Guan, O. Mirza, G. Verner, S. Iwata, H. R. Kaback, *Proc. Natl. Acad. Sci. U.S.A.* **104**, 15294 (2007).
5. Y. Zhou, L. Guan, J. A. Freites, H. R. Kaback, *Proc. Natl. Acad. Sci. U.S.A.* **105**, 3774 (2008).
6. Y. Huang *et al.*, *Science* **301**, 616 (2003).
7. D. Yernool, O. Boudker, Y. Jin, E. Gouaux, *Nature* **431**, 811 (2004).
8. A. Yamashita, S. K. Singh, T. Kawate, Y. Jin, E. Gouaux, *Nature* **437**, 215 (2005).
9. O. Boudker *et al.*, *Nature* **445**, 387 (2007).
10. S. Faham *et al.*, *Science* **321**, 810 (2008).
11. S. Weyand *et al.*, *Science* **322**, 709 (2008).
12. R. J. Naftalin, N. Green, P. Cunningham, *Biophys. J.* **92**, 3474 (2007).
13. I. Papageorgiou *et al.*, *J. Mol. Biol.* **382**, 1121 (2008).

10.1126/science.1168107

Published by AAAS

BIOPHYSICS

Clutch Dynamics

A mechanical model describes how actin cytoskeletal dynamics and cell adhesion control mechanosensing and force generation.

Yvonne Aratyn-Schaus[1] and Margaret L. Gardel[1,2]

Growth cone filopodia are long, rodlike protrusions that extend from the leading cell edge of a migrating neuron and scan the local environment to sense and decode signals for growth cone advance (*1*). This exploratory function involves the transmission of both chemical cues and mechanical stimuli at filopodial tips. However, our knowledge of how filopodia sense and probe external mechanical cues is extremely limited. On page 1687 of this issue, Chan and Odde show that growth cone filopodia function as mechanosensitive organelles and propose a model in which the cell's internal architecture—the actin cytoskeleton—is harnessed for mechanosensing at sites where the growth cone is adherent to the extracellular matrix (*2*).

The dynamic filamentous actin (F-actin) cytoskeleton is crucial for cell shape change and directed cell migration. A striking feature of the F-actin cytoskeleton in adherent cells is that actin filaments move from the cell periphery toward the cell center in a process called "retrograde flow." Retrograde flow is ubiquitous and has been observed across many cell types, including fibroblasts (*3*), neurons (*4*), and epithelial cells (*5*). Near the cell's leading edge, rapid retrograde flow is driven by forces generated by the polymerization of F-actin against the cell membrane. Closer to the cell center, tensile forces generated by motor proteins (myosin II) drive retrograde flow. Although filopodia are composed of long, parallel actin bundles that protrude beyond the cell's leading edge, the base of each filopodial actin bundle is embedded within the myosin II–containing actin network. Consequently, retrograde flow in filopodia is at least partially myosin II–dependent (*6*).

The role and utility of F-actin retrograde flow in regulating cell adhesion and migration has been an outstanding question for several decades. A leading hypothesis is that the assembly of transmembrane proteins into complexes could create points of adhesion between the F-actin cytoskeleton and the immobile extracellular matrix to modulate its retrograde motion; thus, these cell-substrate adhesions may act as a "molecular clutch." Immobilization of the F-actin network by the clutch to the external matrix would allow new F-actin assembly to push forward the cell membrane and thus enable cell protrusion. Indeed, an inverse correlation between cellular protrusion and F-actin retrograde flow has been observed in fast-moving cells (*7*). This immobilization of F-actin also would be a means to efficiently transmit mechanical forces generated by the actin cytoskeleton to the extracellular matrix (*8*). Such cellular "traction forces" are essential in cell migration and remodeling of extracellular matrix. However, F-actin retrograde flow is not completely abrogated in adhesion sites (*9*, *10*), and changes in retrograde flow speed regulate cellular traction force on the extracellular matrix (*11*). Thus, it is clear that the dynamics of adhesion proteins are a necessary feature of any motor-clutch model (*12*).

Chan and Odde have proposed a model of a dynamic motor clutch and find, surprisingly, that the clutch is also a mechanism by which cells can sense changes in the rigidity of their extracellular matrix. In their model, myosin II drives actin retrograde flow in a load-dependent manner, and the formation of clutch bonds that engage the F-actin to the extracellular matrix occurs at a characteristic rate. As tension builds within the extracellular matrix, tension also builds within bonds of the clutch, and bond dissociation increases exponentially until there is a failure of the clutch to engage the extracellular matrix with intracellular actin. The authors find that for soft matrices, the rate of tension buildup in the clutch is slow enough that a sufficient number of bonds remain engaged at early times of cell adhesion. At a critical time, the failure of a single bond results in catastrophic failure of all bonds. Thus, this regime is characterized by periods of adhesion formation and traction force buildup in the extracellular matrix that alternate with rapid adhesion failure and traction release (see the figure). On stiffer matrices, tension develops quickly within individual clutch bonds, and thus the failure of bonds limits the amount of traction force transmitted to the extracellular matrix at all times—a regime the authors call "frictional slippage."

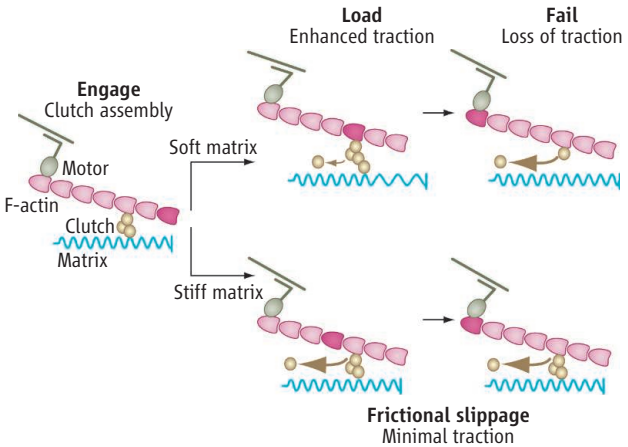

Harnessing actin for mechanosensing. Intracellular filamentous actin (F-actin) interacts with the extracellular matrix through a molecular assembly, or clutch. As the motor protein (anchored to an undefined intracellular substrate) generates tension on F-actin, tension builds in the bonds of the clutch and the extracellular matrix. On a soft matrix, the slow rate of tension buildup within clutch bonds maintains a low rate of bond dissociation (thin, brown arrow) and enhanced traction force on the extracellular matrix (stretching of the wavy line). Beyond a critical tension, the clutch bonds can no longer support the growth in tension and disengage from the extracellular matrix, resulting in loss of traction force and flux of F-actin (indicated by progression of the dark-colored chevron to the left). On a stiff matrix, rapid tension buildup in clutch bonds results in enhanced dissociation of adhesive bonds (thick, brown arrow), minimal traction force, and movement (slippage) of the F-actin at all times.

Chan and Odde observed these distinct phenotypes in filopodia of neurons plated on matrices of two different stiffnesses. On the softer matrix, traction forces increase over several seconds before they rapidly fail; enhanced traction force occurs concomitantly with decreased retrograde F-actin flow speed. On the stiffer matrix, a consistently faster retrograde flow speed and lower traction forces are measured at all times. Interestingly, Chan and Odde found that the critical stiffness (the degree of matrix compliance predicted to lead to failure of all clutch bonds) sensed by filopodia was of the same order as measured in brain tissue (*13*). Previous studies have

[1]Institute for Biophysical Dynamics, University of Chicago, Chicago, IL 60637, USA. [2]Department of Physics, University of Chicago, Chicago, IL 60637, USA. E-mail: gardel@uchicago.edu

Published by AAAS

shown that branching morphogenesis of neuronal cells is only observed when cells are cultured on soft matrices (*13*); the present work suggests that the mechanosensing function of filopodia, with preferred adhesion to soft matrices, could guide branching morphogenesis at the cellular level. This has implications for the development of neuronal tissue in vivo.

Perhaps the most striking feature of this study is the simplicity of the motor clutch. A filopodial adhesion is modeled as a single, linear spring and the molecular details of the interface where bonds form, fail, and slip are not specified. In a filopodial adhesion, the "weakest link" of cell-substrate adhesion may occur at the level of transmembrane protein binding to the extracellular matrix. For example, integrin cell adhesion molecules translocate in filopodial tips (*14*). By contrast, adhesions that form proximal to the leading cell edge, called focal adhesions, undergo tension-dependent modification to their composition and size. Intracellular "shear slippage" has been observed at the interface of focal adhesion proteins (talin and vinculin) and the actin network (*9*, *10*). This suggests that changes in the composition of focal adhesions during their assembly and growth may regulate the interface of the weakest link in this molecular clutch. Indeed, variation in the flux of the protein zyxin at focal adhesions has been observed in response to externally applied mechanical perturbations (*15*). Unexpectedly, focal adhesions generate higher traction forces and strengthen in response to stiff matrices (*16*–*18*), whereas this study finds that filopodial adhesions generate higher traction on soft matrices. Further work is required to distinguish the roles of focal adhesions and filopodial adhesions in translating mechanical stimuli to the rest of the cell.

The work of Chan and Odde is an important step in building a quantitative framework to describe how actin cytoskeletal dynamics and focal adhesions can control cellular mechanosensing and force generation. This kind of mechanical model may be able to describe a range of cellular behaviors, as suggested by a similar model describing the saltatory motion of the pathogen *Listeria monocytogenes* (*19*). Thus, understanding the general mechanisms by which tension in actin cytoskeletal networks is built and released, at mesoscopic length scales, will elucidate a biophysical understanding of mechanosensing, force generation, shape change, and migration at the cellular level.

References and Notes

1. R. W. Davenport, P. Dou, V. Rehder, S. B. Kater, *Nature* **361**, 721 (1993).
2. C. E. Chan, D. J. Odde, *Science* **322**, 1687 (2008).
3. J. A. Theriot, T. J. Mitchison, *J. Cell Biol.* **119**, 367 (1992).
4. C. H. Lin, P. Forscher, *Neuron* **14**, 763 (1995).
5. A. Ponti, M. Machacek, S. L. Gupton, C. M. Waterman-Storer, G. Danuser, *Science* **305**, 1782 (2004).
6. C. H. Lin, E. M. Espreafico, M. S. Mooseker, P. Forscher, *Biol. Bull.* **192**, 183 (1997).
7. J. A. Theriot, T. J. Mitchison, *Nature* **352**, 126 (1991).
8. T. Mitchison, M. Kirschner, *Neuron* **1**, 761 (1988).
9. C. M. Brown *et al.*, *J. Cell Sci.* **119**, 5204 (2006).
10. K. Hu, L. Ji, K. T. Applegate, G. Danuser, C. M. Waterman-Storer, *Science* **315**, 111 (2007).
11. M. Gardel *et al.*, *J. Cell Biol.* **183**, 10.1083/jcb.200810060 (2008).
12. A. Macdonald, A. R. Horwitz, D. A. Lauffenburger, *Cell Adhes. Migrat.* **2**, 25 (2008).
13. P. C. Georges *et al.*, *Biophys. J.* **90**, 3012 (2006).
14. C. G. Galbraith, K. M. Yamada, J. A. Galbraith, *Science* **315**, 992 (2007).
15. W.-H. Guo, Y.-L. Wang, *Mol. Biol. Cell* **18**, 4519 (2007).
16. D. Choquet, D. P. Felsenfeld, M. P. Sheetz, *Cell* **88**, 39 (1997).
17. D. Riveline *et al.*, *J. Cell Biol.* **153**, 1175 (2001).
18. C.-M. Lo, H.-B. Wang, M. Dembo, Y.-L. Wang, *Biophys. J.* **79**, 144 (2000).
19. F. Gerbal, P. Chaikin, Y. Rabin, J. Prost, *Biophys. J.* **79**, 2259 (2000).

20. M. L. G. acknowledges support from the Burroughs Wellcome Career Award at the Scientific Interface.

10.1126/science.1168102

BIOCHEMISTRY

Pressing Levers or Pulling Strings?

The unique stalk of the molecular motor protein dynein may serve as a smart tether rather than as a lever during motion along microtubules.

Linda A. Amos

Dynein is a molecular motor protein responsible for the movement of organelles, vesicles, and macromolecular complexes, for several steps in mitosis, and for flagellar and ciliary beating. It moves toward the minus ends of microtubules, the filamentous track used for long-distance transport in eukaryotic cytoplasm. On page 1691 of this issue, Vale and co-workers (*1*) report a crystal structure showing the stalk that protrudes from dynein's motor domain and interacts with a microtubule. The authors suggest how relative sliding between the antiparallel strands of the coiled-coil part of the stalk may change the structure of the globular domain at the tip of the stalk, enabling it to switch between strong and weak microtubule binding. They also elucidate the role of the stalk in determining the direction of movement along the microtubule and suggest a radical new model of the motility mechanism, in which the stalk is a smart tether rather than a lever for mechanical amplification.

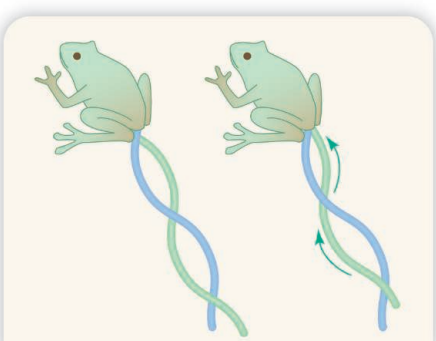

Interstrand sliding (*4*). A MTBD with a distinct polarity (shown as a frog) and an antiparallel coiled-coil stalk in two conformations; the blue and green strands are shown sliding over each other.

Dynein is a molecular machine belonging to the family of ring-shaped adenosine triphosphatases (ATPases) associated with various cellular activities (referred to as AAA+). Most AAA+ rings are assembled from six identical subunits, but a dynein monomer contains six different AAA+ domains in tandem. Only four of these domains bind ATP; the other two seem to play a purely structural role (*2*). The heavy chain also forms a tail domain and a linker before the first AAA+ domain, and a C-terminal domain after the sixth AAA+ domain. Dyneins differ from other molecular motors such as kinesins and myosins in that the domain responsible for binding to the filamentous protein track—the microtubule-binding domain (MTBD) (*3*)—is distant from the ATPase domains, being situated at the end of the stalk, a 15-nm coiled-coil rod that folds up from an insertion between the fourth and fifth AAA+ domains (see the figures).

In earlier studies (*4*) aimed at understanding the means of communication between the

MRC Laboratory of Molecular Biology, Hills Road, Cambridge CB2 0QH, UK. E-mail: laa@mrc-lmb.cam.ac.uk

CREDIT: ADAPTED BY P. HUEY/*SCIENCE*

Published by AAAS

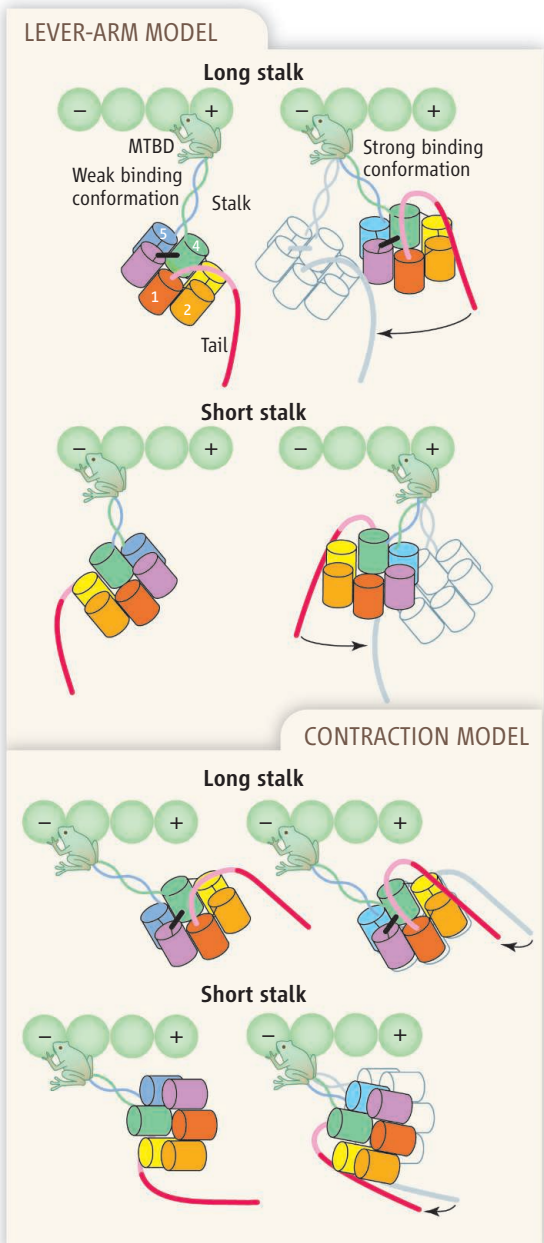

Lever-arm versus contraction models of dynein motility. A dynein monomer consists of an N-terminal tail domain (dark red) followed by a linker (pink), a ring of six AAA+ domains (red to violet), a stalk (including the MTBD) that loops out between domains 4 and 5, and an uncharacterized C-terminal domain (black); the MTBD is shown binding to tubulin subunits (pale green circles) of a microtubule. The conformations of the dynein tail and linker in the weakly and strongly binding states are based on electron microscopy images (*5*, *7*). During movement along a microtubule, each dynein motor is assumed to switch from one conformation to the other while bound to the microtubule, and to switch back again while detached. However, the order of these changes depends on the model; there are several possible variants of each of the models shown. In a lever-arm model (**top**), the stalk detaches after reaching the weakly bound state, swings toward the microtubule minus end before binding tightly, and then pushes on the microtubule while straightening again to reach the position shown in gray; the arrow shows the direction in which the tail would be moved. Upon shortening the stalk, the major part of the molecule should rotate relative to the MTBD, and the direction of movement should be reversed. Vale and co-workers did not, however, observe this effect. To account for their data, the authors propose a model in which the stalk acts as a flexible tether while the linker contracts (**bottom**). In this model, shortening the stalk does not change the direction of movement.

ATPase domains and the MTBD, Vale and co-workers expressed genetically modified proteins consisting of part of the stalk, fused onto the coiled coil of a tRNA synthetase. The work identified two optimal alignments: one that put the MTBD in a strongly binding conformation, and another that bound weakly. The authors suggested that communication along the coiled coil of a normal dynein molecule is effected by interstrand sliding (see the first figure).

The same group of researchers has now crystallized the weakly binding fusion protein. The strongly binding state did not crystallize. However, good agreement with a three-dimensional map reconstructed from electron microscope images of microtubules complexed with the tightly binding protein indicates that the conformational change in the MTBD is fairly subtle.

Typical models for dynein movement that involve some form of leverage (*2*, *5*, *6*) depend on a change in the angle between the microtubule and the stalk; the stalk acts as a fairly stiff lever arm that pushes against the microtubule (see the second figure, top panel). Electron microscopy images of isolated molecules (*5*) have shown that when the ATPase domains are filled by adenosine diphosphate (ADP) or when they are empty, the tail projects out from the ring at a point close to the stalk, but in the presence of ADP and vanadate, the tail emerges from a point ~90° from the stalk. The change in angle suggested that the stalk would push on the microtubule by swinging through a ~90° angle (*5*). However, cryo–electron microscope images of whole molecules interacting with microtubules obtained by Hirose and colleagues (*7*) have revealed that, even though the tail and linker shift relative to the ring and stalk as in isolated dynein molecules, the stalk orientation on the microtubule remains fixed. This observation seems to be inconsistent with any of the proposed lever-arm models.

Vale and co-workers have now changed the length of the coiled coil in dynein motor domains that could be tested in motility assays. Assuming that the MTBD still binds to tubulin in the same way, the rest of the molecule should be rotated, and the direction of movement was therefore expected to be reversed (see the second figure, top panel). Yet the authors found that movement was still directed toward the minus end of the microtubule.

To account for the unexpected result, the authors propose that movement toward the minus end is due to contraction of the dynein molecule; if the stalk binds at ~45° to the microtubule, movement parallel to the microtubule may be conserved even after a rotation around the stalk axis (see the second figure, bottom panel). The model is supported by the authors' electron microscopy images of microtubules decorated with stalks, which suggest that the stalks point in a suitable direction. The apparent binding angle is also consistent with the recent images of whole dynein molecules bound to microtubules (*7*), in which the stalks always point toward the microtubule minus end.

AAA+ machines seem to have related mechanisms, in which ATP hydrolysis leads to mechanical work that is achieved by pulling on protein chains. For example, hexameric ClpX, a polypeptide unfoldase, grips its substrates to unfold and translocate them (*8*). Katanin and spastin are thought to recognize the C-terminal tails of tubulin subunits and to sever microtubules by pulling the tails through the central pore of the AAA+ ring (*9*). Thus, it seems possible that contraction of the dynein molecule may be achieved by pulling some part of the linker through the ring. Future research is likely to focus on the structure and properties of the linker domain and its interactions with the AAA+ domains.

References

1. A. P. Carter *et al.*, *Science* **322**, 1691 (2008).
2. N. Numata *et al.*, *Biochem. Soc. Trans.* **36**, 131 (2008).
3. M. P. Koonce, *J. Biol. Chem.* **272**, 19714 (1997).
4. I. R. Gibbons *et al.*, *J. Biol. Chem.* **280**, 23960 (2005).
5. S. A. Burgess *et al.*, *Nature* **421**, 715 (2003).
6. N. Mizuno *et al.*, *Proc. Natl. Acad. Sci. U.S.A.* **104**, 20832 (2007).
7. H. Ueno, T. Yasunaga, C. Shingyoji, K. Hirose, *Biophysics (Japan)* **47** (suppl. 1), S155 (2007).
8. A. Martin *et al.*, *Nat. Struct. Mol. Biol.* **15**, 1147 (2008).
9. A. Roll-Mecak, R. D. Vale, *Nature* **451**, 363 (2008).

10.1126/science.1168178

CREDIT: ADAPTED BY P. HUEY/*SCIENCE*

Published by AAAS

Compromised Survivorship in Zoo Elephants

Ros Clubb,[1] Marcus Rowcliffe,[2] Phyllis Lee,[3,4] Khyne U. Mar,[2,5] Cynthia Moss,[4] Georgia J. Mason[6]*

Wild animals can experience poor welfare when held captive (*1*), an effect with ethical and practical implications. In zoos, the welfare of African elephants (*Loxodonta africana*) and Asian elephants (*Elephas maximus*) has long caused concern. Infanticide, *Herpes*, tuberculosis, lameness, infertility, and stereotypic behavior are prevalent (*2*), and zoo elephant populations are not self-sustaining without importation (*3*). We compiled data from over 4500 individuals to compare survivorship in zoos with protected populations in range countries. Data representing about half the global zoo population (1960 to 2005) came from European "studbooks" and the European Elephant Group (*4*). We focused on females as relevant to population viability ($N = 786$, both wild-caught and captive-born; 302 African and 484 Asian). African elephants in Amboseli National Park, Kenya ($N = 1089$), and Asian elephants in the Burmese logging industry (Myanma Timber Enterprise, M.T.E., $N = 2905$, wild-caught and captive-born) acted as well-provisioned reference populations [for details, see (*2*) and (*5*)].

For African elephants, median life spans (excluding premature and still births) were 16.9 years [95% confidence interval (CI) 16.4 to unknown; upper estimate for median not reached] for zoo-born females and 56.0 years (95% CI 51.5 to unknown) for Amboseli females undergoing natural mortality (35.9 years with human-induced deaths, 95% CI 33.8 to 40.3). Neither infant nor juvenile mortality differed between populations (Fig. 1A and tables S1 and S2), but adult females died earlier in zoos than in Amboseli (Fig. 1B and table S2). Zoo adult African survivorship has improved in recent years [$z = -2.75$, $P < 0.01$ (*5*)], but mortality risks in our data set's final year (2005) remained 2.8 times higher (95% CI 1.2 to 6.5) than that of Amboseli females undergoing natural mortality.

For Asian elephants, median life spans (excluding premature and still births) for captive-born females were 18.9 years in zoos (95% CI 17.7 to 34.0) and 41.7 years in the M.T.E. population (95% CI 38.2 to 44.6). Zoo infant mortality rates were high (over double those of M.T.E.): A female's first pregnancy therefore had only a 42% chance of yielding a live year-old in zoos compared with 83% in M.T.E. (table S1). Rates have not significantly improved over time (e.g., live births controlling for parity: $z = 1.19$, $P > 0.10$). For juveniles, captive-born survivorship did not significantly differ between populations, whereas wild-born survivorship was poorer in Burma (Fig. 1C and table S2) because of after-effects of capture (*5*). In adulthood, however, survivorship was lower in zoos (Fig. 1D and table S2), with no detectable improvement in recent years ($z = -1.48$, $P > 0.10$).

Within zoos, captive-born Asians have poorer adult survivorship than wild-born Asians (Fig. 1D and table S2). This is a true birth origin effect: Whereas zoo-born elephants are more likely to have been born recently and to primiparous dams, neither dam parity ($z = 0.86$, $P > 0.10$) nor recency ($z = -1.48$, $P > 0.10$) predict adult survivorship (controlling for recency makes birth origin more significant: $z = -3.52$, $P < 0.001$). Because the median importation age of wild-born females was about 3.4 years, this suggests that zoo-born Asians' elevated adult mortality risks are conferred during gestation or early infancy.

Interzoo transfers also reduced Asian survivorship (see supporting online text), an effect lasting 4 years posttransfer ($z = -2.10$, $P < 0.05$, controlling for birth origin). Additionally, survivorship tended to be poorer in Asian calves removed from mothers at young ages ($z = -1.92$, $P < 0.10$) (*5*).

Overall, bringing elephants into zoos profoundly impairs their viability. The effects of early experience, interzoo transfer, and possibly maternal loss, plus the health and reproductive problems recorded in zoo elephants [e.g., (*2*)], suggest stress and/or obesity as likely causes.

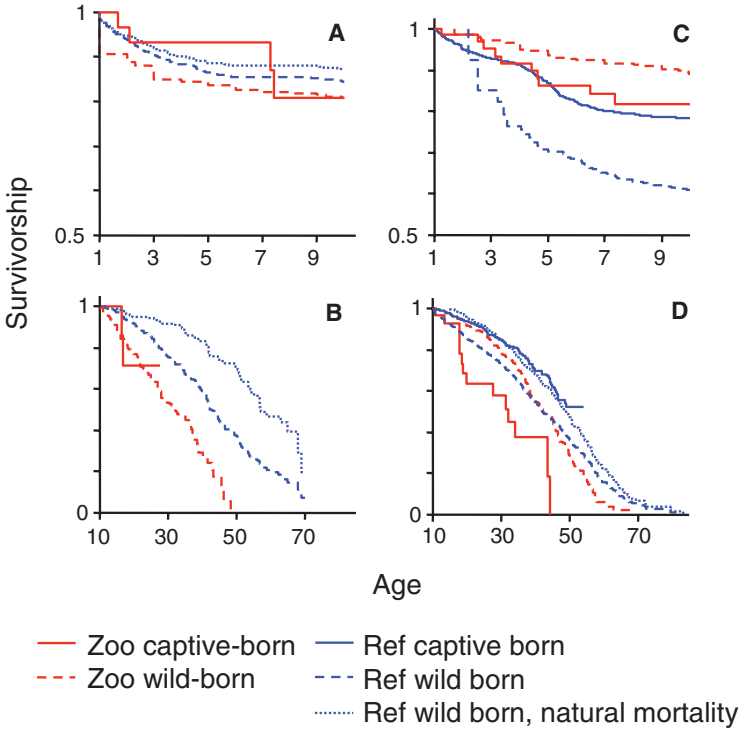

Fig. 1. Kaplan-Meier survivorship curves for female African (**A** and **B**) and Asian (**C** and **D**) elephants aged 1 to 10 [juveniles in (A) and (C)] and 10+ years [adults in (B) and (D)]. For wild-born reference (Ref, Amboseli or M.T.E.) populations, natural mortality excludes human-caused deaths; all mortality includes them (*5*). Results of statistical comparisons are given in table S2.

References and Notes

1. R. Clubb, G. Mason, *Nature* **425**, 473 (2003).
2. R. Clubb, G. Mason, *A Review of the Welfare of Zoo Elephants in Europe* (RSPCA, Horsham, UK, 2002).
3. M. Hutchins, M. Keele, *Zoo Biol.* **25**, 219 (2006).
4. European Elephant Group, "Elefanten in zoos und safariparks Europa" (European Elephant Group, Grünwald, Germany, 2002).
5. Methods and supplementary results are available as supporting material on *Science* Online.

6. G.J.M. thanks the Natural Science and Engineering Research Council for funding; R.C. and G.J.M. thank R. Ripley for statistical advice; P.L. and C.M. thank many conservation nongovernmental organizations and private donors for supporting the Amboseli Elephant Trust; K.U.M. thanks colleagues at M.T.E. for data compilation and comments. G.J.M. is a visiting professor at The Royal Veterinary College, London, UK. K.U.M. has received funding from Prospect Burma Foundation, Charles Wallace Burma Trust, Three Oaks Foundation, Whitney-Laing Foundation (Rufford Small Grants), Toyota Foundation, Fantham Memorial Research Scholarship, and University College London. K.U.M. has been a paid consultant for Woburn Safari Park, UK. G.J.M. has been a paid consultant to Disney's Animal Kingdom, USA.

Supporting Online Material

www.sciencemag.org/cgi/content/full/322/5908/1649/DC1
Materials and Methods
SOM Text
Tables S1 and S2
References

6 August 2008; accepted 22 September 2008
10.1126/science.1164298

[1]Royal Society for the Prevention of Cruelty to Animals (RSPCA), Wilberforce Way, Southwater, West Sussex, RH13 9RS, UK. [2]Institute of Zoology, Zoological Society of London, London NW1 4RY, UK. [3]Psychology Department, University of Stirling, Stirling FK9 4LA, UK. [4]Amboseli Trust for Elephants, Post Office Box 15135, Nairobi, Kenya. [5]Department of Animal and Plant Sciences, University of Sheffield, Western Bank, Sheffield S10 2TN, UK. [6]Animal Sciences Department, University of Guelph, Guelph N1G 2M7, Canada.

*To whom correspondence should be addressed. E-mail: gmason@uoguelph.ca

Developmental Patterning by Mechanical Signals in *Arabidopsis*

Olivier Hamant,[1,2]* Marcus G. Heisler,[3]* Henrik Jönsson,[4]* Pawel Krupinski,[4] Magalie Uyttewaal,[1,2] Plamen Bokov,[5,6] Francis Corson,[5] Patrik Sahlin,[4] Arezki Boudaoud,[5] Elliot M. Meyerowitz,[3]† Yves Couder,[6]† Jan Traas[1,2]†

A central question in developmental biology is whether and how mechanical forces serve as cues for cellular behavior and thereby regulate morphogenesis. We found that morphogenesis at the *Arabidopsis* shoot apex depends on the microtubule cytoskeleton, which in turn is regulated by mechanical stress. A combination of experiments and modeling shows that a feedback loop encompassing tissue morphology, stress patterns, and microtubule-mediated cellular properties is sufficient to account for the coordinated patterns of microtubule arrays observed in epidermal cells, as well as for patterns of apical morphogenesis.

The surface layers of plant tissues are under considerable tension (*1*). This results from the fact that individual cells, including those in deeper layers, are tightly bound to each other through their cellulosic walls, on which they exert turgor pressure (*2*). In addition, plant cell walls resist stress (force per unit area) differentially, depending on the direction of stress (*3*). This anisotropy is a consequence of the direction in which the rigid cellulose microfibrils are laid down during wall synthesis (*4*). Because this direction is often parallel to the cortical microtubules of the plant cell, it is thought that the microtubules might serve as tracks along which the cellulose synthase complexes travel (*5*, *6*). Green and others have proposed that cortical microtubule orientations correlate with anisotropic stresses, but the existence of such a causal link with morphogenesis has never been further investigated (*7*–*11*). We have chosen to dissect this link in shoot apical meristems, a population of stem cells that continuously generate aerial organs while undergoing complex shape transformations (*12*, *13*) (fig. S1).

Morphogenetic role of the microtubules at the shoot apex. To assess the functional importance of microtubules within the *Arabidopsis* meristem, we depolymerized the microtubules with the use of oryzalin and monitored the resulting cell morphology (*14*). In the absence of microtubules, the meristems kept growing but no cytokinesis occurred, and giant polyploid cells formed (Fig. 1A) (*14*). Despite these changes, differentiation and patterning were not drastically affected. We observed slow-growing cells in the meristem and fast-growing cells in the primordia, and phyllotaxis was not altered 46 hours after complete depolymerization of microtubules (Fig. 1B and fig. S2). Cell identity in the boundary domain between the meristem and new floral primordia did not seem to be altered, as a boundary domain reporter, *pBOUND-GFP*, was induced in this domain several days after the treatment (Fig. 1C and fig. S2).

However, depolymerization of the microtubules resulted in a distinct change in the geometry of the cells. The final structure resembled two-dimensional (2D) foams, which are purely isotropic in nature. Notably, all the walls met at angles of 120° and the curvature of the walls approached that of a soap-bubble network (Fig. 1A) (*15*, *16*). In addition, certain morphogenetic events did not occur. In particular, the crease between the meristem and primordia no longer formed (Fig. 1, B to D, and fig. S2). Hence, although microtubules may not be critical for developmental patterns such as phyllotaxis, they are required for certain morphogenetic events such as tissue folding.

In the presence of oryzalin, organ outgrowth was still observed, which suggests that plant shape is at least partially independent of microtubule-based anisotropy. Because growth patterns are thought to depend largely on the plant hormone auxin (*17*–*21*), we next used a double drug treatment where both microtubules and auxin transport were inhibited. This led to the formation of a spherical shoot tip (fig. S3A) (*14*), as might be expected if microtubule-controlled anisotropy operates in parallel with auxin-driven growth rate patterns.

Cortical microtubule orientations and dynamics are correlated with morphogenesis. To further analyze the role of microtubules in morphogenesis, we investigated microtubule dynamics in the meristem via live imaging of plants expressing green fluorescent protein (GFP) fused to the microtubule-binding domain (MBD) of microtubule-associated protein 4 MAP4 (*22*, *23*). A quantitative analysis of the cortical microtubules at the surface of more than 30 meristems revealed three aspects of microtubular arrays:

1) The microtubules at the meristem summit were highly dynamic, constantly changing their orientation at 1- to 2-hour intervals (Fig. 2, A to C, and movie S1) (*24*, *25*).

2) At the periphery and base of the meristem, orthoradial (circumferential) cortical microtubule arrays were dominant. This orientation was more apparent when organ initiation was inhibited in the presence of the auxin transport inhibitor *N*-1-naphthylphthalamic acid (NPA) and seemed to be the default orientation at the periphery in the absence of floral primordia (fig. S4).

3) As flower primordia started to grow out, a supracellular alignment of microtubules along the boundary between the meristem and the primordium appeared (Fig. 2, A and B, and fig. S4). This configuration was stably maintained over prolonged periods (up to 20 hours). Consistent with these highly ordered and stable interphase arrays, about 90% of the cells (n = 158, eight meristems) in this zone displayed preprophase bands and division planes in the same tangential orientation. Microtubules were aligned during the activation of *pFIL::dsRED-N7* (*18*), a late marker of floral primordium initiation, showing that the alignment accompanies flower outgrowth (Fig. 2D).

Microtubule orientations align along predicted principal stresses. In a multicellular setting, the field of physical forces represents a potential source of information for the cells to know their relative position (*7*, *26*–*30*). Several studies have supported the proposal that maximal stress directions orient cortical microtubules, most probably via a response to strain in the cell wall (*8*, *10*, *31*–*33*). However, these studies do not address the link with morphogenesis. In addition, it remains difficult to test the plausibility of such a hypothesis in a tissue context. We therefore used a combination of physical and mathematical approaches to address these issues.

To assess whether stresses might orient microtubules, we first calculated the expected pattern of stresses at the shoot apical meristem surface by considering the apex at the tissue scale. Our mechanical model of the meristem as a pressure vessel—a shell inflated by an inner pressure—depends on the following assumptions: (i) The tissue is elastic [(*34*, *35*) and our results], (ii) the outer wall of the epidermal layer supports the turgor pressure and acts as a limiting factor for growth (*36*, *37*), and (iii) the outer wall of the epidermal layer is under a uniform pressure from the inside (*34*). Using these properties, we calculated the directions of principal stresses in different domains of the shoot apex and found that they are parallel to the observed cortical microtubule orientations (Fig. 3, A and B).

[1]INRA, Laboratoire de Reproduction et Développement des Plantes, 46 Allée d'Italie, 69364 Lyon Cedex 07, France. [2]Université de Lyon, CNRS, ENS, 46 Allée d'Italie, 69364 Lyon Cedex 07, France. [3]Division of Biology, California Institute of Technology, Pasadena, CA 91125, USA. [4]Computational Biology and Biological Physics Group, Department of Theoretical Physics, Lund University, S-221 00 Lund, Sweden. [5]Laboratoire de Physique Statistique, Ecole Normale Supérieure, 24 rue Lhomond, 75231 Paris Cedex 05, France. [6]Matière et Systèmes Complexes, Université Paris-Diderot, 10 rue Alice Domont et Léonie Duquet, 75025 Paris Cedex 13, France.

*These authors contributed equally to this work.
†To whom correspondence should be addressed. E-mail: jan.traas@ens-lyon.fr (J.T.); meyerow@caltech.edu (E.M.M.); couder@lps.ens.fr (Y.C.)

To further investigate the correlation between predicted stresses and microtubule orientations, we designed a 3D cell- and wall-based tissue model representing the surface of the L1 layer of the shoot and incorporating the three assumptions listed above. The model includes mechanisms such as elastic wall mechanics, wall growth, cellular mechanical anisotropy (microfibrils), stress feedback, and growth and proliferation (fig. S5, A and B) (*38*). Mechanical anisotropy is introduced by defining a microtubule direction within each 2D cell where the stiffness of the wall material increases as the wall becomes more parallel to the direction of the cortical microtubules. Stress feedback is introduced by updating the microtubule directions to align along maximal stress directions, which for one cell is measured by the directional weighted average of its wall stresses. Note that strengthening of the walls (by aligning microfibrils) counteracts the main stress intensity but maintains the main stress direction.

The model faithfully reproduced the orthoradial and random microtubule alignments on synthetic templates of the stem and tip of a dome, respectively, and predicted alignment along the crease for a saddle-shaped template (fig. S6). Simulated microtubule directions in a template extracted from a confocal data set also predicted the experimentally seen boundary alignment zone as well as the more random microtubule orientations at the apex (Fig. 3C). A growth model was then introduced to examine microtubule orientations during morphogenetic events, including primordium growth and tip growth (*38*). Primordium growth was initiated by locally decreasing wall stiffness, leading to the outgrowth of a well-defined bump. As the simulated primordium formed, the model also predicted an orthoradial microtubule alignment as observed in the region between the meristem and the primordium (Fig. 3D and movie S2) as well as around the simulated primordium, thus reproducing the alignment zone between the meristem and the primordium. Growth of the meristem and stem was simulated by implementing growth at a rate that was depen-

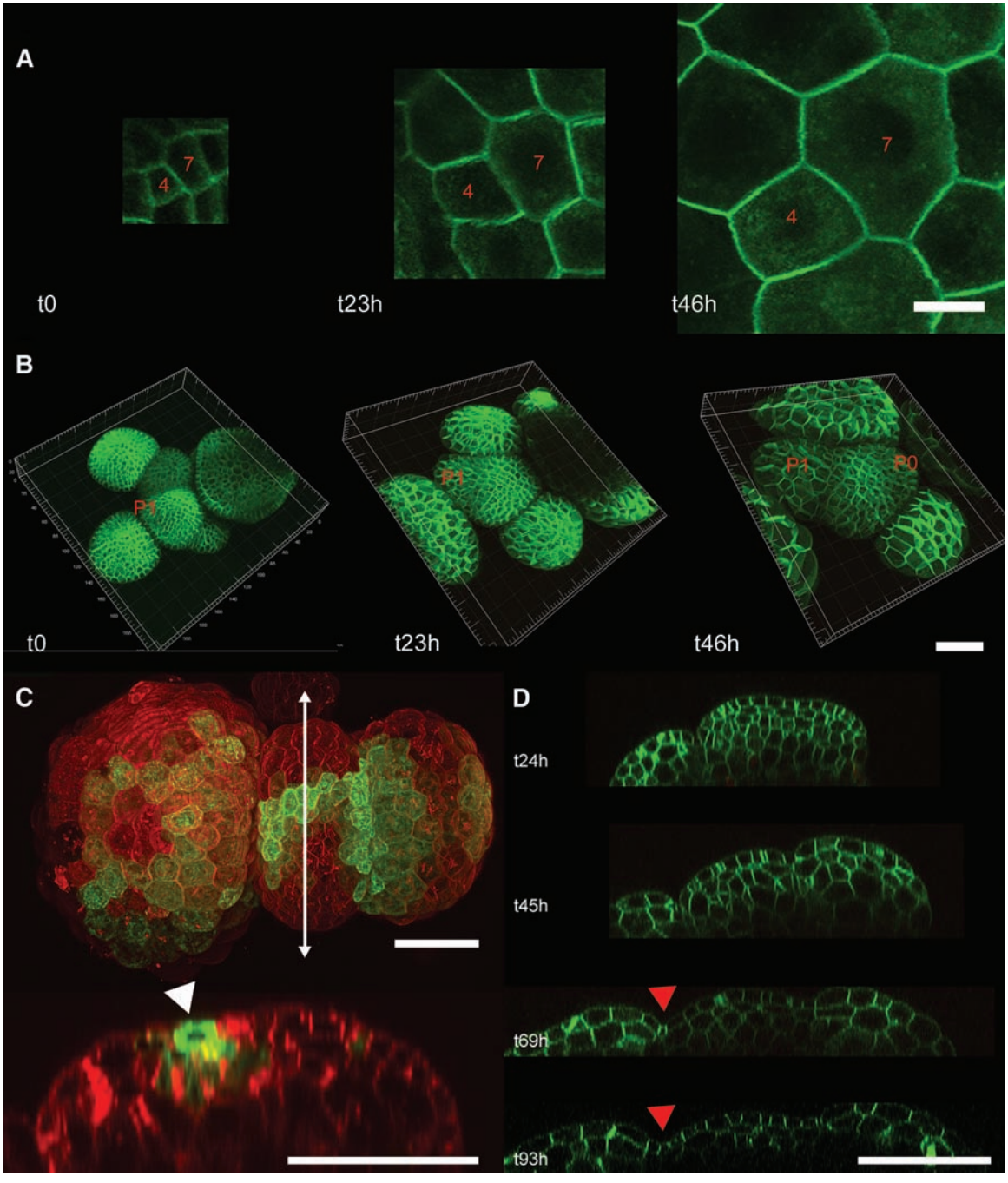

Fig. 1. Morphogenetic role of the microtubules. (**A**) Effect of oryzalin treatment on cell shape. Walls tend to meet at 120° and become convex or concave in cells with less or more than six walls, respectively, as observed in a 2D foam. Numbers of walls are in red. Scale bar, 10 μm. (**B**) Three-dimensional reconstructions of *GFP-LTI6b* meristems treated with oryzalin immediately after the treatment (t0) and 23 and 46 hours later. Note the absence of a crease at P1 and the position of P0 following the expected phyllotactic pattern. Scale bar, 50 μm. (**C**) *pBOUND-GFP* (green) expression 3 days after the first oryzalin treatment, in the absence of a crease (arrowhead), in a meristem stained with the fluorescent lipophilic dye FM4-64 (red). Scale bars, 50 μm. (**D**) Longitudinal optical sections of an existing crease being flattened over time after oryzalin treatment (red arrowhead). Scale bar, 50 μm.

dent on the distance to the apex (Fig. 3E and movie S3) (*39*). In these simulations, the microtubule orientations were unstable at the apex while the orientations on the stem stabilized in a mainly orthoradial pattern, as was observed. Finally, we tested whether the model could also predict the effects of oryzalin treatment, simulated by removing the anisotropic contribution to wall mechanics. Both a loss of the crease in the experimental template and ballooning of cells in a pin-shaped growth simulation were qualitatively predicted (fig. S3, B and C).

Cell ablation results in characteristic microtubule reorientations. The results so far suggest a scenario where the alignment of microtubules to maximal stress directions modifies the orientation of newly deposited cellulose microfibrils, thereby regulating morphogenesis. We next tested this scenario experimentally.

We began with a laser ablation approach. We reasoned that by killing cells and thereby locally eliminating turgor pressure and weakening cell walls, we could induce characteristic changes in stress and strain patterns. To obtain theoretical predictions for the resultant stress patterns due to laser ablation, we used the finite-element method (FEM) to model the L1 layer of meristem cells (*38*). The ablation is simulated as a loss of turgor as well as diminution of elastic properties of the walls of the ablated cells (fig. S5C) (*38*).

The simulation predicts rearrangement of principal stress directions during ablation. Before the removal of the cell, the principal stress patterns depend more on the geometry of each individual cell than on the relationship between cells (Fig. 4A, left). Assuming that the top wall is intact at $t = 0$ hours and gradually weakens afterward, our modeling predicted the maximal stress direction (hence the microtubule orientations) initially to be radial and then to become circumferential with respect to the wound (Fig. 4A).

We used a laser to target cells within the central zone of the meristem, where observed cortical microtubule alignments and growth patterns suggest that cell walls are largely mechanically isotropic. Time-lapse analysis of cells surrounding an ablation site showed a slight initial expansion of surrounding cells into the wound during the first 1.5 hours after laser treatment, consistent with a sudden imbalance in stresses due to loss of turgor in the dead cell or cells (Fig. 4B and movie S4). During this time, no significant microtubule reorientation was detected. However, starting at 1.5 hours and continuing to about 5.5 hours after ablation, we subsequently observed microtubule orientations to align circumferentially (Fig. 4B and movie S4). These results match the predictions of our model and are also consistent with previous reports of circumferential microtubule rearrangements in response to wounding (*40*, *41*). The absence of an initial radial alignment suggests that the initial stresses associated with radial expansion are too transient to trigger a response.

Although these results support our hypothesis, several alternative hypotheses could not be excluded at this stage. For instance, it is possible that the microtubules may be reorienting perpendicular to the observed initial cell deformations, contrary to our stress alignment proposal. However, because the realignment occurs hours after the initial radial deformation is initiated, this possibility seems less likely. Another hypothesis is that the microtubules may not be responding to mechanical stress but rather to unrelated biochemical wound signals. To test this last scenario, we first proceeded with ablations in the boundary domain. We reasoned that local diffusion of a biochemical signal in this domain and in the central zone should be roughly similar, whereas in the boundary the stress field generated by the ablation should be in competition with the strong tangential stress at the crease (fig. S7, A and B). In contrast to central zone ablations, ablations in boundary regions resulted in a lack of microtubule reorientation in neighboring cells, or a delay of reorientation lasting 7.5 hours or more in some cases. In most cases (five of six experiments), we could find at least one cell with no circumferential microtubule orientation 7.5 hours after ablation, and in two cases, no reorientations

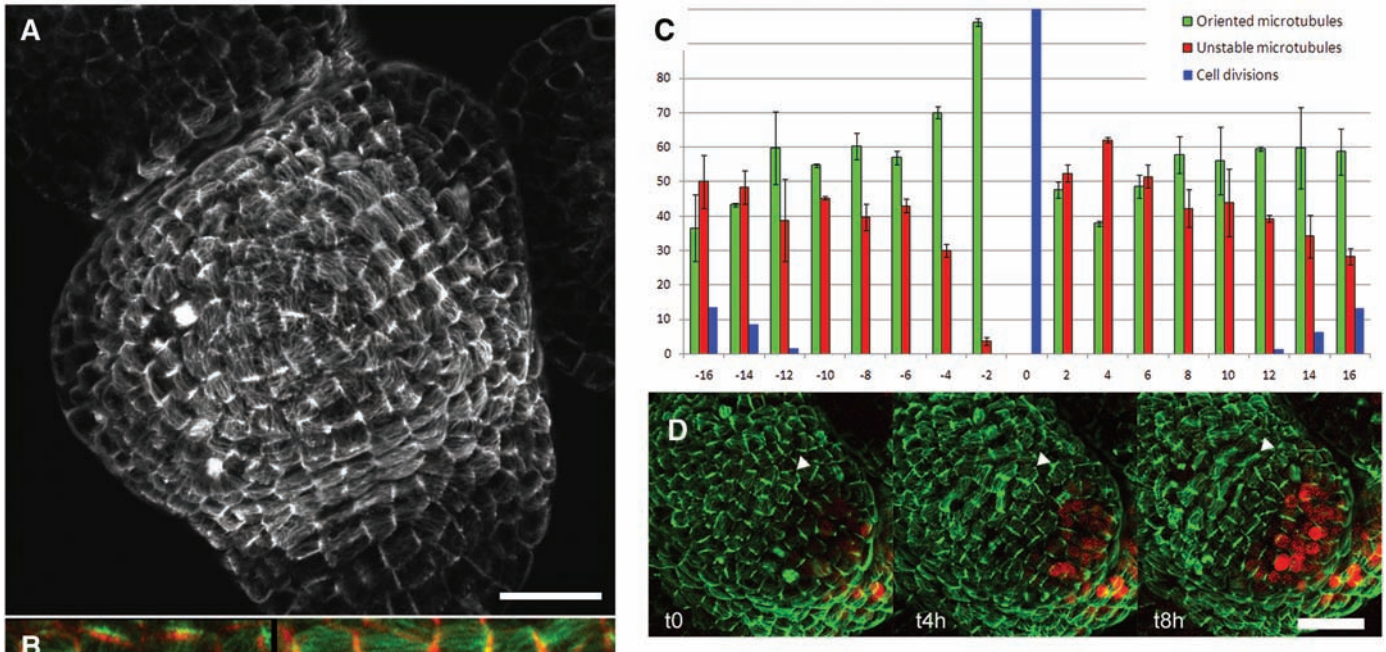

Fig. 2. Microtubule patterns in the shoot apical meristem. (**A**) *p35S::GFP-MBD* expression at the surface of a representative meristem 48 hours after NPA removal. Scale bar, 20 μm. (**B**) Close-up of the same group of cells at the periphery of the meristem, with mixed microtubule orientation before primordium initiation and a coherent supracellular microtubule alignment 20 hours later as the primordium grows out. The blue star marks the same position in both images. Scale bar, 10 μm. (**C**) Cortical microtubule behavior in each cell of the meristematic dome every 2 hours for 16 hours before and after cell division ($n = 144$ cells, compiled from five meristems). Blue, percentage of dividing cells at each time point; green, percentage of cells with one major orientation maintained between two time points; red, percentage of cells with a changing microtubule orientation greater than 30° over two time points. (**D**) *p35S::GFP-MBD* (green) and *pFIL::dsRED-N7* (red) expression in the boundary (arrowhead) of a representative meristem at three time points. Scale bar, 20 μm.

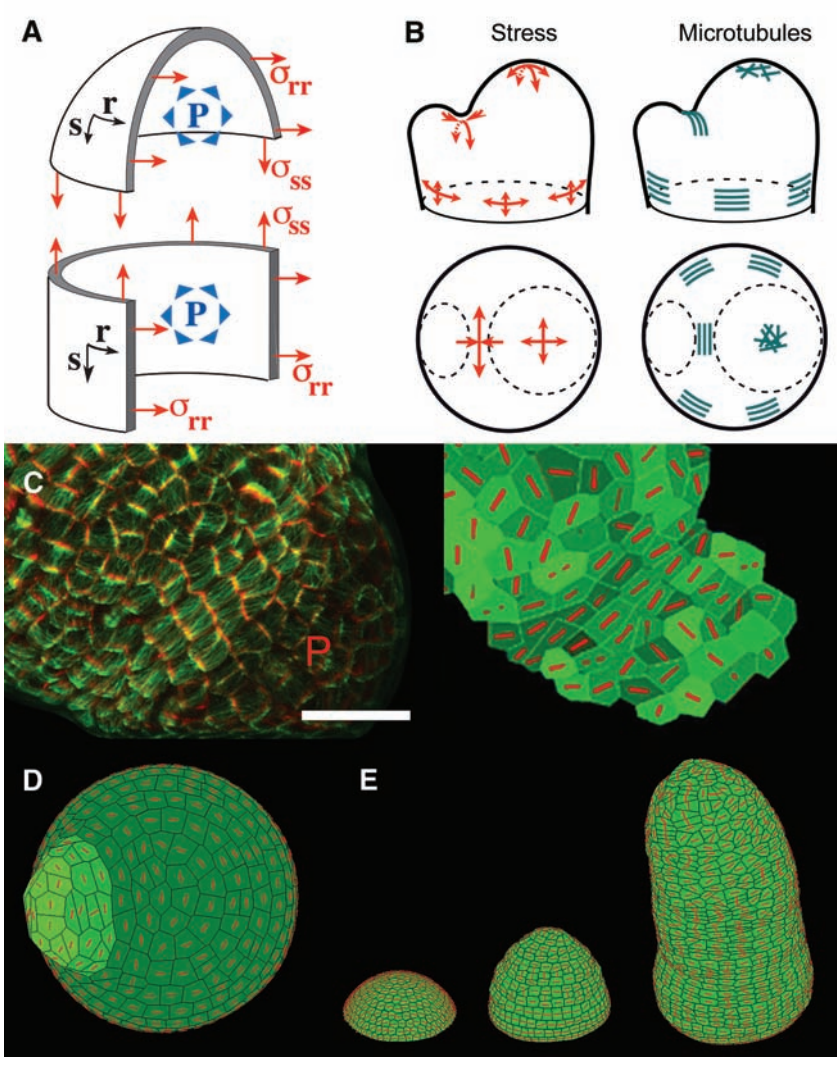

Fig. 3. Physical calculations and modeling of stress patterns in the meristem. (**A**) The meristem modeled as a pressure vessel. Each point has a coordinate in the orthoradial (*r*) and meridional (*s*) direction and is characterized by a curvature tensor (C_{ss}, C_{rr}, C_{rs}) and a stress tensor (σ_{ss}, σ_{rr}, σ_{rs}), where *R* is the radius of the cylindrical stem and of the apical dome, and *P* is pressure. (**B**) The direction of microtubules is in agreement with the highest-stress orientations. The mechanical equilibrium of the outer layer imposes $\partial_s\sigma_{ss} + \partial_r\sigma_{rs} = 0$, $\partial_s\sigma_{rs} + \partial_r\sigma_{rr} = 0$, and $C_{ss}\sigma_{ss} + C_{rr}\sigma_{rr} + 2C_{rs}\sigma_{rs} = P$, where ∂_s is the partial derivative with respect to *s*. In the following, we consider only special points (of local symmetry) for which (*r*,*s*) are principal directions and $C_{rs} = 0$, $\sigma_{rs} = 0$. If the apical dome is represented as a spherical dome of radius *R*, we obtain $\sigma_{ss} = \sigma_{rr} = PR/2$, meaning that the stress is isotropic (*44*). This is correlated with the absence of preferential direction for microtubules in the apical dome. $\sigma_N = PR/2$ serves as a reference for stress and $\delta = |\sigma_{ss} - \sigma_{rr}|/\sigma_N$ as a measure of the anisotropy of stress. We represent the flanks of the meristem as a cylinder of radius *R*. The stress is greater in the circumferential direction, $\sigma_{rr} = PR$, than along the meridian, $\sigma_{ss} = PR/2$ (*44*), so that $\delta = 1$, thus leading to a strongly anisotropic stress on the flanks of the meristem. We consider the center of the crease between a primordium and the apex as having radii of curvature *R* along the axis of the crease, *r*, and $-\rho$ in the perpendicular direction, *s*. The minus sign denotes the inverted direction of curvature with respect to the rest of the meristem. The corresponding curvatures are $C_{ss} = -1/\rho$ and $C_{rr} = 1/R$. The equations of equilibrium can be solved in the limit where ρ is small relative to *R*: $\sigma_{ss} \approx -P\rho/2$ and $\sigma_{rr} \approx PR/2$, so that $\delta \approx 1$, thus leading to a strongly anisotropic stress at the crease between a primordium and the apex. (**C**) Left: *p35S::GFP-MBD* marking cortical microtubules (green) and cell shape (red) at the surface of a meristem generating a young primordium (P). Scale bar, 20 μm. Right: Microtubule orientation (red bars) in the 2D stress-feedback model on cells extracted from the confocal data, notably reproducing the original microtubule orientations in the boundary. (**D**) Simulation of an auxin-induced primordium. The 2D stress-feedback model results in alignment of microtubules orthoradially around the growing primordium. (**E**) Tip-growing simulation with the stress-feedback model generating a growing stem. Microtubules align mainly orthoradially on the stem, which has a regular shape.

occurred in any of the surrounding cells 7.5 hours after ablation (fig. S7C). The variability of the results could reflect the different stages of boundary development or the exact position of the ablated cells. We also tried a different set of experiments in which two cells or patches of cells, in close proximity but separated, were ablated. We reasoned that diffusion of any type of biochemical signal emanating from the ablated regions would result in a relatively flat diffusion gradient in the regions between them, and therefore that the microtubule arrays in these regions should not be well defined (fig. S8, A and B). In both cases, with ablations separated by multiple cells or single cells, we found that the resulting microtubule orientations for regions between the ablation sites were well defined and clearly circumferential in nature (fig. S8C; four of four experiments). This pattern matches our theoretical predictions for stress patterns surrounding two ablation sites but did not match our prediction for response to a diffusion gradient. Although stress is the simplest explanation, more complex, non-mechanical cell-cell communication models are still possible.

Application of constraints shows a cell-autonomous microtubule response to stress. To more directly ascertain the relationship between microtubule orientations and mechanical signals, we pursued a second approach involving the direct application of force to the meristem. We designed growth chambers in which meristems could be constrained between one fixed teflon blade and one teflon blade attached to a spring (Fig. 4, C and D). Using this device, we were able to change meristem shape (Fig. 4E and figs. S9A and S10). After the release of the constraint, the meristem reverted to its original shape, showing its elastic properties, and later initiated organs (fig. S9A). We predicted a weakly anisotropic stress larger in the direction parallel to the blades (fig. S10). Consistent with these calculations, only weak anisotropic changes in the shape of individual cells were visible at the meristem summit of the constrained meristems (Fig. 4F and movie S5).

We next analyzed the behavior of the cortical microtubules in each cell before and after the constraint. This revealed that the number of cells with unstable microtubules decreased relative to observations of nonconstrained meristems (Fig. 4G, green histograms, and figs. S9B and S10). Second, an analysis of microtubule orientation in 489 individual cells from 13 compressed meristems showed that most cells reoriented their microtubules toward the axis parallel to the blades, either by stabilizing an orientation parallel to the blades after compression or by rotating their microtubules parallel to the blades (Fig. 4F, figs. S10 and S11, and movies S5 and S6). These data are consistent with our proposal that microtubules align parallel to maximal stress directions. Although the response was statistically significant under the conditions tested here, it was also a noisy response because even neighboring cells can have micro-

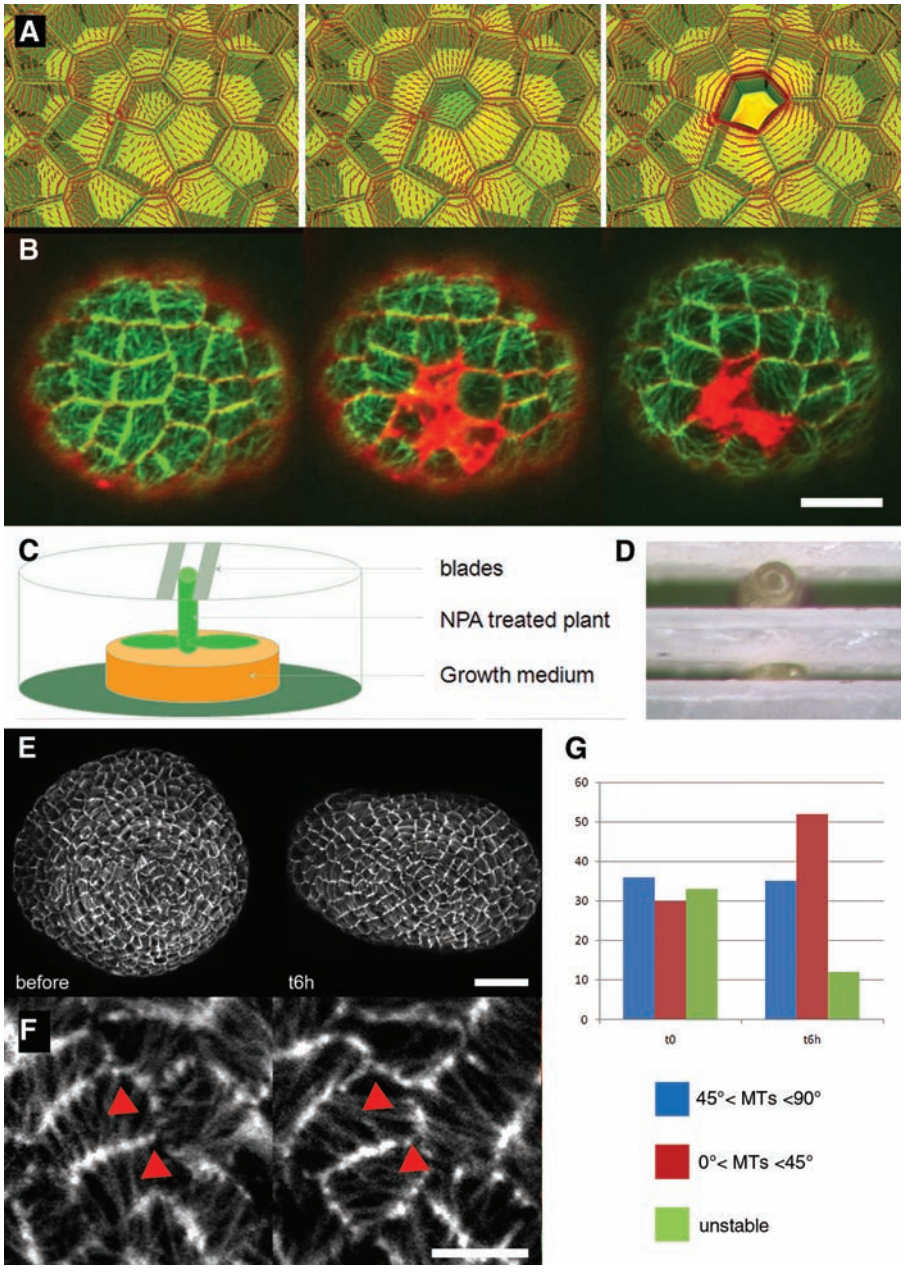

Fig. 4. Reorientation of the cortical microtubules in the presence of a mechanical stress. (**A**) Theoretical principal stress direction pattern (red lines) in outer surface of meristem tissue obtained from FEM simulation of L1 layer under uniform tension and turgor pressure, before and after ablation. Color gives relative values of maximal stress (green, low; red, high). Left: A stress pattern in a group of reference cells. Middle: Radial stresses after the drop of turgor in an ablated cell at the center. Right: Circumferential stresses after the weakening of the top wall. (**B**) *GFP-MBD* expression (green) in the L1 layer of the central zone of a meristem just before, just after, and 6 hours 30 min after ablation (FM4-64 staining in red). Scale bar, 10 μm. (**C**) Schematic drawing of the setup used to apply lateral constraints onto the meristem. (**D**) An NPA-treated plant with a naked meristem is put between two blades, and the blades are then adjusted to compress the apex. (**E**) *GFP-MBD* expression in the L1 layer of a meristem before the application of the constraint (left) and 6 hours (right) after the application of the constraint. Scale bar, 20 μm. (**F**) Close-up showing the microtubule reorientations before and after the application of the constraint. Arrowheads mark cells where microtubules have reoriented parallel to the blades. Scale bar, 5 μm. (**G**) Six hours after the application of the constraint, the number of cells with unclear microtubule orientation (green) is decreasing while the number of cells with microtubules having an angle greater than 45° (blue) remains relatively stable and the number of cells with microtubules having an angle less than 45° with the blades (red) is increasing; t0 corresponds to 0 hours after compression. This tendency to alignment matches the predicted weak anisotropy of stress (see fig. S10).

tubules with radically different orientations (Fig. 4F and movie S5). We propose that this variability reflects the cell-autonomous nature of the response and that this follows from the likely different mechanical configurations of different plant cells.

Concluding remarks. We have described a link between mechanical forces and development in plants. Recent work has also revealed such a relation in animals. In particular, the phenomenon of wound-induced actin alignment in epithelial sheets closely parallels the alignment of plant microtubules around a wound, with both responses presumably functioning to reduce or heal tissue damage (*42*). Unlike animals, however, plant tissues seem to react to oriented forces by conferring anisotropic properties to their extracellular matrix. As a result, plant tissues seem to react to mechanical forces as solids, whereas animal tissues react as fluids. From a physical perspective, this points to a basic difference between the two kingdoms.

On the basis of our results, we propose that two fundamental regulatory circuits control plant morphogenesis at the shoot apex. First, a microtubule-dependent, cell-autonomous mechanism mechanically reinforces cells against maximal tension directions along the meristem surface, most likely via the regulation of load-bearing cellulose fiber deposition and by the addition of new walls generated by oriented mitosis in these directions. This mechanism is required for specific morphogenetic events such as tissue folding and the maintenance of a cylindrical stem. However, in contrast to previous proposals (*36*, *43*), this stress-dependent control of morphogenesis at the meristem can be uncoupled from the control of differential expansion rates, because the rapid outgrowth of organs at particular locations continues despite microtubule depolymerization. This second process involves the creation of differential auxin concentrations through polar transport and possibly synthesis (*17*–*21*). We therefore propose that auxin-dependent patterning operates at least partially independently of, and in parallel to, the microtubule-controlled anisotropy. Our experimental results and models show that these two mechanisms are sufficient to explain all observed complex shape changes at the meristem.

References and Notes

1. W. S. Peters, A. D. Tomos, *Ann. Bot.* **77**, 657 (1996).
2. P. Schopfer, *Am. J. Bot.* **93**, 1415 (2006).
3. E. S. Castle, *J. Cell. Comp. Physiol.* **10**, 113 (1937).
4. D. J. Cosgrove, *Plant Physiol. Biochem.* **38**, 109 (2000).
5. G. O. Wasteneys, M. E. Galway, *Annu. Rev. Plant Biol.* **54**, 691 (2003).
6. A. R. Paredez, C. R. Somerville, D. W. Ehrhardt, *Science* **312**, 1491 (2006); published online 20 April 2006 (10.1126/science.1126551).
7. P. B. Green, A. King, *Aust. J. Biol. Sci.* **19**, 421 (1966).
8. R. E. Williamson, *Aust. J. Plant Physiol.* **17**, 601 (1990).
9. A. L. Cleary, A. R. Hardham, *Plant Cell Physiol.* **34**, 1003 (1993).
10. C. L. Wymer, S. A. Wymer, D. J. Cosgrove, R. J. Cyr, *Plant Physiol.* **110**, 425 (1996).
11. K. Fischer, P. Schopfer, *Plant J.* **15**, 119 (1998).
12. J. Traas, J. H. Doonan, *Int. Rev. Cytol.* **208**, 161 (2001).
13. D. Kwiatkowska, J. Dumais, *J. Exp. Bot.* **54**, 1585 (2003).
14. O. Grandjean *et al.*, *Plant Cell* **16**, 74 (2004).

15. C. W. J. Beenakker, *Phys. Rev. Lett.* **57**, 2454 (1986).
16. J. A. Glazier, S. P. Gross, J. Stavans, *Phys. Rev. A* **36**, 306 (1987).
17. D. Reinhardt *et al*., *Nature* **426**, 255 (2003).
18. M. G. Heisler *et al*., *Curr. Biol.* **15**, 1899 (2005).
19. P. B. de Reuille *et al*., *Proc. Natl. Acad. Sci. U.S.A.* **103**, 1627 (2006).
20. H. Jönsson, M. G. Heisler, B. E. Shapiro, E. M. Meyerowitz, E. Mjolsness, *Proc. Natl. Acad. Sci. U.S.A.* **103**, 1633 (2006).
21. R. S. Smith *et al*., *Proc. Natl. Acad. Sci. U.S.A.* **103**, 1301 (2006).
22. S. Sakaguchi, T. Hogetsu, N. Hara, *Bot. Mag. (Tokyo)* **101**, 497 (1988).
23. J. M. Selker, *Protoplasma* **158**, 95 (1990).
24. Z. Hejnowicz, *Protoplasma* **225**, 243 (2005).
25. J. Chan, G. Calder, S. Fox, C. Lloyd, *Nat. Cell Biol.* **9**, 171 (2007).
26. P. M. Lintilhac, in *Positional Controls in Plant Development*, P. W. Barlow, D. J. Carr, Eds. (Cambridge Univ. Press, Cambridge, 1984), pp. 83–105.
27. J. Dumais, C. R. Steele, *J. Plant Growth Regul.* **19**, 7 (2000).
28. E. Farge, *Curr. Biol.* **13**, 1365 (2003).
29. L. Hufnagel, A. A. Teleman, H. Rouault, S. M. Cohen, B. I. Shraiman, *Proc. Natl. Acad. Sci. U.S.A.* **104**, 3835 (2007).
30. T. Lecuit, P. F. Lenne, *Nat. Rev. Mol. Cell Biol.* **8**, 633 (2007).
31. J. M. Hush, R. L. Overall, *Cell Biol. Int. Rep.* **15**, 551 (1991).
32. R. E. Williamson, *Int. Rev. Cytol.* **129**, 135 (1991).
33. R. J. Cyr, *Annu. Rev. Cell Biol.* **10**, 153 (1994).
34. Z. Hejnowicz, in *Pattern Formation in Biology, Vision and Dynamics*, A. Carbone, M. Gromov, P. Prusinkiewicz, Eds. (World Scientific, Singapore, 2000), pp. 240–251.
35. C. Wei, P. M. Lintilhac, J. J. Tanguay, *Plant Physiol.* **126**, 1129 (2001).
36. J. M. Selker, G. L. Steucek, P. B. Green, *Dev. Biol.* **153**, 29 (1992).
37. S. Savaldi-Goldstein, J. Chory, *Curr. Opin. Plant Biol.* **11**, 42 (2008).
38. See supporting material on *Science* Online.
39. J. Dumais, S. L. Shaw, C. R. Steele, S. R. Long, P. M. Ray, *Int. J. Dev. Biol.* **50**, 209 (2006).
40. J. M. Hush, C. R. Hawes, R. L. Overall, *J. Cell Sci.* **96**, 47 (1990).
41. K. C. Goodbody, C. Lloyd, *Protoplasma* **157**, 92 (1990).
42. P. Martin, J. Lewis, *Nature* **360**, 179 (1992).
43. L. F. Hernandez, P. B. Green, *Plant Cell* **5**, 1725 (1993).
44. W. Flugge, *Stresses in Shells* (Springer-Verlag, New York, ed. 2, 1973).
45. We thank A. Roeder for critical reading of the manuscript, and P. Barbier de Reuille and IFR128 Platim for help with imaging. Supported by the International Human Frontier Science Program Organization, by U.S. Department of Energy grant FG02-88ER13873 (E.M.M.), by the Balzan Foundation (E.M.M.), and by the Swedish Research Council (H.J.).

Supporting Online Material

www.sciencemag.org/cgi/content/full/322/5908/1650/DC1
Materials and Methods
SOM Text
Figs. S1 to S11
Movies S1 to S6
References

8 September 2008; accepted 14 November 2008
10.1126/science.1165594

A Competitive Inhibitor Traps LeuT in an Open-to-Out Conformation

Satinder K. Singh,[1] Chayne L. Piscitelli,[1,3] Atsuko Yamashita,[4]* Eric Gouaux[1,2]

Secondary transporters are workhorses of cellular membranes, catalyzing the movement of small molecules and ions across the bilayer and coupling substrate passage to ion gradients. However, the conformational changes that accompany substrate transport, the mechanism by which a substrate moves through the transporter, and principles of competitive inhibition remain unclear. We used crystallographic and functional studies on the leucine transporter (LeuT), a model for neurotransmitter sodium symporters, to show that various amino acid substrates induce the same occluded conformational state and that a competitive inhibitor, tryptophan (Trp), traps LeuT in an open-to-out conformation. In the Trp complex, the extracellular gate residues arginine 30 and aspartic acid 404 define a second weak binding site for substrates or inhibitors as they permeate from the extracellular solution to the primary substrate site, which demonstrates how residues that participate in gating also mediate permeation.

Secondary active transporters are ubiquitous integral membrane proteins that couple the potential energy stored in preexisting ion gradients to the concentrative uptake of polar and charged molecules across the lipid bilayer of the cell (*1*–*3*). Members of the solute carrier 6 (SLC6) family of sodium-coupled transporters, also known as neurotransmitter sodium symporters, make up one of the most widely investigated and pharmacologically important classes (*4*, *5*). SLC6 proteins play a central role in diverse physiological processes, ranging from the maintenance of cellular osmotic pressure (*6*) to the reuptake of small-molecule neurotransmitters in the brain (*7*). SLC6 dysfunction is implicated in numerous debilitating illnesses, such as depression (*8*), obsessive-compulsive disorder (*9*), epilepsy (*10*), autism (*11*), orthostatic intolerance (*12*), X-linked creatine-deficiency syndrome (*13*), and retinal degeneration (*14*). The transport activity of these molecular machines can be inhibited by many different compounds, including tricyclic antidepressants (TCAs) (*15*), selective serotonergic reuptake inhibitors (*15*), anticonvulsants (*16*), and cocaine (*17*).

Unraveling the molecular principles that define a substrate (a molecule that can be transported) versus a competitive inhibitor (a molecule that can displace the substrate but is not itself transported) is intimately linked to the larger goal of elucidating transport mechanism and ultimately to the development of new therapeutic agents. The leucine transporter (LeuT), a prokaryotic SLC6 member (*18*), provides an opportunity to couple functional and structural data to uncover the molecular mechanisms of transport and inhibition. Recently, a model for noncompetitive inhibition was derived from a combination of steady-state kinetics (*19*), binding, and crystallographic studies with LeuT and three TCAs (*19*, *20*). The structures of LeuT bound to the TCAs clomipramine (*19*), imipramine (*19*), or desipramine (*19*, *20*) revealed that each of these drugs binds to LeuT in the extracellular vestibule, about 11 Å above the substrate and directly above the extracellular gating residues R30 and D404 (*19*–*21*), stabilizing the occluded state in a closed conformation. Zhou *et al*. have proposed that the TCA-binding site observed in LeuT is equivalent to the primary TCA site in the serotonin transporter (SERT) and the norepinephrine transporter (NET), the therapeutic targets in humans. However, in SERT and NET, TCAs are competitive inhibitors (*22*–*24*), and their binding site probably overlaps with the substrate-binding site (*25*). Therefore, we suggest that the LeuT-TCA complexes do not provide a model for competitive inhibition of eukaryotic SLC6 transporters.

Here we show that LeuT is capable of transporting many hydrophobic amino acids and that a fundamental requirement for a molecule to be a substrate is that it must fit within the occluded substrate-binding cavity. Molecules such as tryptophan (Trp) that can bind but are too large to be accommodated within the occluded-state cavity are not substrates but instead are competitive nontransportable inhibitors. Structural analysis of the LeuT-Trp complex reveals that Trp traps LeuT in an open-to-out conformation and unveils the movements that accompany transition from the occluded to an open-to-out state. Molecular insights gleaned from our studies are especially relevant to the transporter mechanism because many other transporter families, including SLC5 (*26*), have the same fold as LeuT and probably share mechanistic principles.

Substrate screen of LeuT. To identify a competitive inhibitor of LeuT, we examined the ability of a spectrum of amino acids to displace [^{3}H]Leu binding from purified detergent-solubilized LeuT and inhibit [^{3}H]Leu transport by LeuT reconstituted into lipid vesicles (Fig.

[1]Vollum Institute, Oregon Health and Science University, 3181 Southwest Sam Jackson Park Road, Portland, OR 97239, USA. [2]Howard Hughes Medical Institute, Oregon Health and Science University, 3181 Southwest Sam Jackson Park Road, Portland, OR 97239, USA. [3]Department of Biochemistry and Molecular Biology, Oregon Health and Science University, 3181 Southwest Sam Jackson Park Road, Portland, OR 97239, USA. [4]Department of Biochemistry and Molecular Biophysics, Columbia University, New York, NY 10032, USA.

*Present address: RIKEN SPring-8 Center, 1-1-1, Kouto, Sayo, Hyogo 679-5148, Japan.

1A) (*27*). We found that multiple aliphatic and aromatic amino acids of varying size inhibited [^{3}H]Leu binding and transport. We chose Gly, Ala, Leu, Met, Tyr, and Trp (Table 1) for further functional analysis. Competition binding of [^{3}H]Leu with unlabeled amino acids (Fig. 1B, Table 1) revealed that after Leu, Met binds the most tightly, followed by Ala, Tyr, Trp, and Gly. A similar trend of affinities for LeuT was observed in direct radioligand-binding experiments with Leu (fig S1A), Ala (fig S1B), and Met (fig. S1C and Table 1).

For a compound to be a competitive inhibitor, it must not only displace the substrate but cannot itself be transported. We previously demonstrated (*18*, *19*) and have replicated in this study that Leu and Ala are substrates (fig. S2, A and B). Compared with Leu, Ala is transported with a fivefold higher turnover rate (k_{cat}) and a 27% higher catalytic efficiency [k_{cat}/K_m (K_m is the Michaelis constant)] (fig. S3, A and B, and Table 1). We show that LeuT also catalyzes the uptake of Met, Tyr, and Gly (fig. S2, C to E) with catalytic efficiencies roughly correlated to the inverse of substrate volume (fig. S3, C to E, and Table 1).

Trp is not a substrate of LeuT (fig. S4A) but rather is an inhibitor. To determine the kinetic mechanism of Trp inhibition, we performed steady-state kinetic experiments. With [^{3}H]Ala as the substrate, increasing concentrations of Trp increased the K_m of LeuT for [^{3}H]Ala without changing the maximum velocity (V_{max}) (fig. S4b and Table 1). The corresponding Eadie-Hofstee plot (fig. S4C) exhibited nonparallel lines intersecting on the *y* axis, which are hallmarks of competitive inhibition.

LeuT-substrate crystal structures reveal an occluded state. To probe the atomic basis of ligand specificity, we cocrystallized LeuT with each of the six amino acids, measured x-ray diffraction data to a high resolution, and solved the structures with molecular replacement. The readily soluble isosteric Tyr analog L-4-fluorophenylalanine (L-4-F-Phe) was used in place of Tyr because Tyr's low solubility limit precluded successful cocrystallization. All cocrystals diffracted to 1.8 to 2.3 Å resolution (table S1), and the resulting structures refined well (table S2).

The structures of LeuT in complex with each of the substrates [glycine (Gly), alanine (Ala), Leu, methionine (Met), and L-4-F-Phe] are similar, with overall root mean square deviations of α carbon atoms (Cα) ranging from 0.2 to 0.3 Å (Fig. 1C) despite the 132 Å^3 variation in substrate volume. All five structures adopt the same outward-facing occluded state as originally seen in the LeuT-Leu complex, in which access to the substrate-binding pocket from both the extracellular and cytoplasmic sides of the membrane is obstructed: Access from the extracellular side is blocked by just a few residues, and access from the intracellular side is blocked by ~25 Å of tightly packed protein (*18*, *19*) (Fig. 1, D and E). Simulated-annealing omit maps (fig. S5, A to D) confirm the position of the substrates in the occluded binding pocket located in the center of the transporter halfway across the lipid bilayer. Residues F253 and Y108 reside on

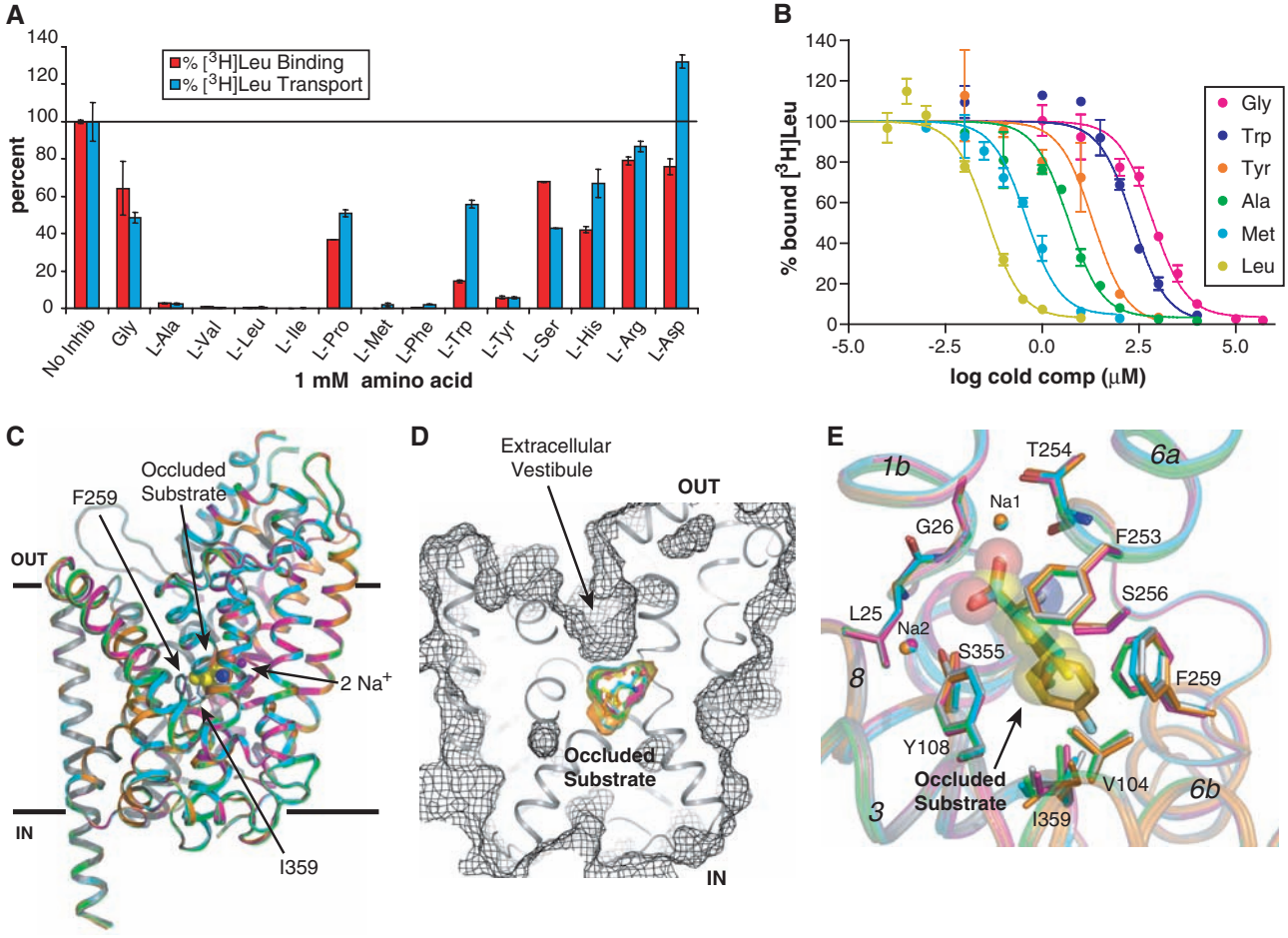

Fig. 1. LeuT substrate screen and occluded-state structures. (**A**) Inhibition of [^{3}H]Leu binding (red bars) and transport (blue bars) by L amino acids. (**B**) Displacement of [^{3}H]Leu binding by Leu (yellow), methionine (light blue), alanine (green), tyrosine (orange), Trp (dark blue), and glycine (magenta). Error bars represent SEM of triplicate (A) or duplicate (B) measurements. (**C**) Superposition of the LeuT-Leu (gray), LeuT-Ala (green), LeuT-Gly (magenta), LeuT-Met (blue), and L-4-F-Phe (orange) complexes by use of α-carbon positions. Membrane boundaries are demarcated by the two solid black lines. (**D**) Solvent-accessible surface (depicted in mesh) illustrating the occluded state of the LeuT-substrate complexes. (**E**) Close-up of the substrate-binding pocket, with substrates depicted as sticks. Atoms of the bound Leu are shown as semitransparent van der Waals spheres. Coloring is the same as in (C).

Table 1. Binding and kinetic constants. Unless otherwise noted, the errors represent the SEM from two or three independent experiments, each performed in duplicate or triplicate. n.d., not determined.

Binding and displacement constants

L-amino acid (Å^3)*	K_d (nM)†	K_i (nM)‡
Gly (65)	n.d.	322,000 ± 36,900
Ala (90)	512 ± 131	3320 ± 810
Leu (164)	20 ± 2	16 ± 1
Met (167)	69 ± 8	232 ± 21
Tyr (197)	n.d.	9040 ± 550
L-4-F-Phe	n.d.	950 ± 100
Trp (228)	n.d.	64800 ± 4670

Steady-state kinetics

L-amino acid (Å^3)*	K_m (nM)	V_{max} (pmol/min/mg)	k_{cat} (hr^{-1})	k_{cat}/K_m (nM^{-1} hr^{-1})
Gly (65)	1910 ± 30	444 ± 57	1.58 ± 0.20	0.0008
Ala (90)	583 ± 28	1730 ± 94	6.06 ± 0.30	0.0104
Leu (164)	146 ± 25	343 ± 46	1.20 ± 0.20	0.0082
Met (167)	289 ± 27	523 ± 12	1.86 ± 0.04	0.0064
Tyr (197)	2830 ± 150	209 ± 15	0.74 ± 0.05	0.0003
Trp (228)	Not transported			

Competitive inhibition of L-Ala transport by L-Trp

[Trp] μM	K_m (nM)	V_{max} (pmol/min/mg)	K_i (μM)§
0	665 ± 78	1530 ± 50	
20	1020 ± 230	1550 ± 110	24 ± 3
50	1880 ± 330	1610 ± 110	

*Volume in Å^3 of amino acid as defined in (*38*). †K_d is the dissociation constant. ‡K_i refers to inhibition of [^{3}H]Leu binding. §K_i refers to inhibition of [^{3}H]Ala transport.

"top" of the substrate, with electrostatic interactions formed by D404 and R30 layered directly above F253 and Y108. The hydroxyl of Y108 retains its two critical hydrogen bonds: one with the substrate carboxylate that helps anchor the substrate in place and the second with the amide nitrogen of L25 that stabilizes the unwound region of transmembrane 1 (TM1) and bridges TM1 with TM3 (Figs. 1E and 2, A to E).

Despite overall congruence among the structures, there are differences in comparison with the Leu complex, localized primarily to F259 and I359. For the Gly and Ala complexes, the R groups of these ligands induce a ~30° torsion of F259's phenyl ring and ~15° torsion of I359's *sec*-butyl moiety into the substrate-binding cavity, which compensates for the poor fit of the substrate to the binding pocket (Figs. 1E and 2, A and B) and is consistent with the weak affinity of LeuT for these two amino acids. The LeuT-Met and LeuT-Leu complexes superimpose within experimental error (Figs. 1E and 2, C and D), a finding in accord with their similar binding and transport parameters. Substituents larger than those of Leu or Met begin to sterically hinder binding and formation of the occluded state. The structure of the L-4-F-Phe complex exhibits the most pronounced differences: a ~180° rotation of I359's *sec*-butyl group as well as a ~0.5 Å outward shift in the

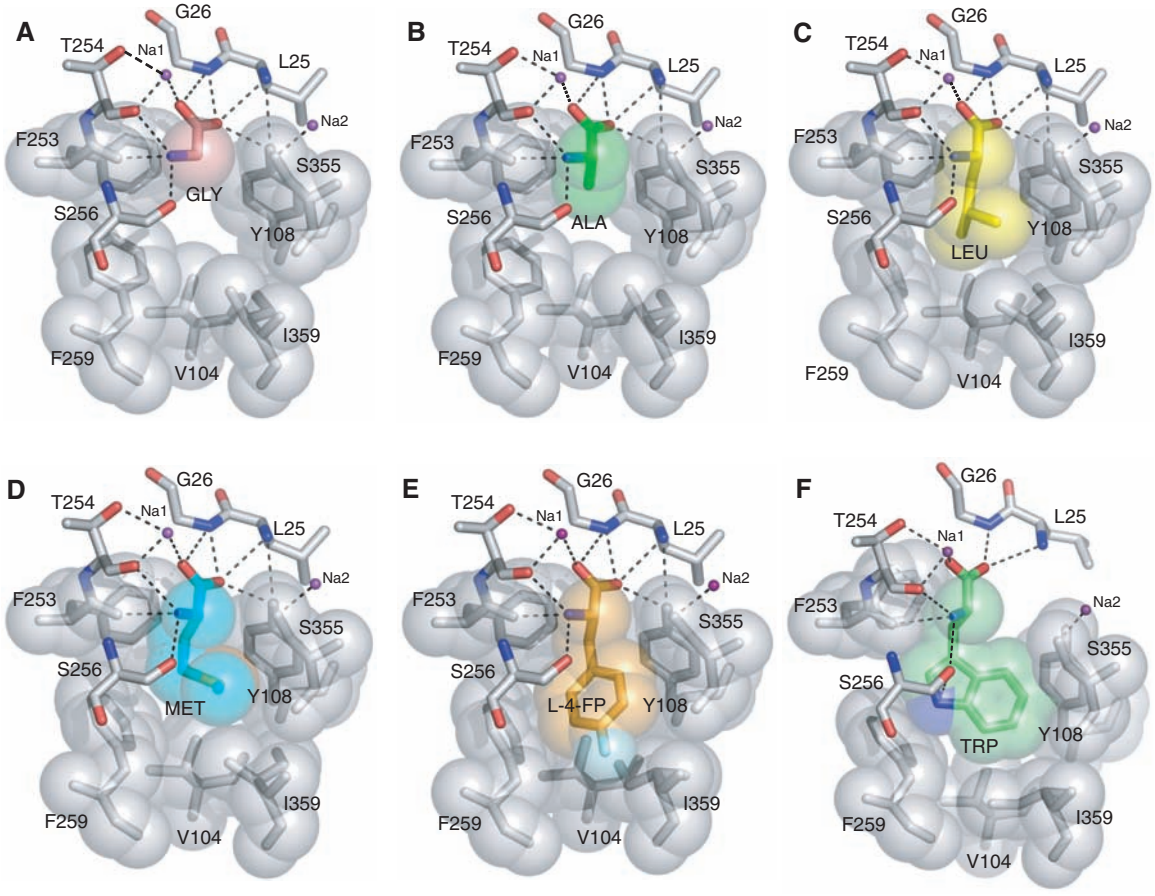

Fig. 2. Substrate-binding pocket–substrate and –inhibitor interactions. Substrate-binding pockets of the (**A**) LeuT-Gly, (**B**) LeuT-Ala, (**C**) LeuT-Leu, (**D**) LeuT-Met, (**E**) LeuT-L-4-F-Phe, and (**F**) LeuT-Trp complexes are shown. Hydrogen bonds and polar interactions are illustrated by black dotted lines.

backbone of the unwound region in TM6 (G258 to A261) (Figs. 1E and 2E). The displacement of the backbone is suggestive of a strained occluded state, perhaps one that is less likely to isomerize to the open-to-in state. Although speculative, this hypothesis is consistent with Tyr's reduced turnover rate.

The LeuT-Trp complex adopts an open-to-out conformation. What are the structural principles by which Trp acts as a competitive inhibitor of LeuT? The LeuT-Trp complex exhibits an open-to-out conformation that is characterized by a widening of the extracellular vestibule and solvent accessibility to the substrate-binding pocket (Fig. 3, A and B). Relative to the occluded state, in the LeuT-Trp complex there is a 9° outward rotation of a structural element composed of TMs 1b (residues 23 to 38), 2a (residues 40 to 54), and 6a (residues 241 to 257) about an axis oriented nearly parallel to the membrane and located near the unwound regions of TMs 1 and 6 (Fig. 3C and movie S1). To accommodate the movement of these helices, the highly conserved Gly-rich loop between TMs 1b and 2a slides under EL3 (residues 233 to 240), the latter of which also undergoes a concerted translation along its helical axis, approximately parallel to the membrane. The EL4a helix (residues 307 to 318) also undergoes an outward rotation of nearly 13° about an axis running approximately perpendicular to the plane formed by the EL4 loop (Fig. 3C and movie S1). Together, these movements widen the extracellular vestibule at the base by 3 Å, as defined by measurements between residues Y108 and F253 (Fig. 3, A, B, and E).

TM11 also undergoes a substantial displacement in the LeuT-Trp complex. Concomitant with the outward rotation of neighboring TM6a, TM11 shifts inward by ~2 Å in the region around W467, whereas the indole side chain of W467 on the interior face of the helix rotates 90° relative to its position in the occluded-state structures. The space vacated by the rotation of this indole ring and the outward movement of TM6a is partly occupied by the alkyl chain of a β-octylglucoside molecule (fig. S6).

Like substrates, the amino group of Trp^{601} forms hydrogen bonds with oxygen atoms in TMs 1b and 6a (Figs. 2F and 3D). Similar coordination exists between the carboxylate of Trp^{601} and the backbone amide nitrogens of TM1b (L25 and G26) as well as Na1 (Figs. 2F and 3D); Na2 is also present in the Trp complex and is coordinated in a similar manner as the occluded-state complexes. The indole ring is accommodated in the binding pocket and, with only minor adjustments to the side-chain geometry of I359 and a slight rotation of Y108, engages in nonpolar interactions with these residues (Fig. 3E). Furthermore, the indole-ring nitrogen of Trp^{601} is within ~3.2 Å of the phenyl-ring face of F259, forming an edge-to-face aromatic interaction (Figs. 2F and 3D).

Unlike the substrate-bound complexes, the LeuT-Trp structure reveals substantial differences that define the molecular basis of competitive inhibition. The α-amino and α-carboxyl substituents of Trp^{601} are shifted by ~2 Å relative to the corresponding positions of these atoms in the substrate-bound occluded-state complexes (Fig. 3E). Trp^{601}'s rigid indole ring acts like a strut that braces the binding pocket open, with the α-amino and carboxyl groups maintaining their conserved interactions with TMs 1 and 6 (Fig. 3D) and the distal edge of the indole ring lodged against TMs 3 and 8. This mode of binding prevents the extracellular vestibule from closing and adopting the occluded state (Fig. 3, A and B). Specifically, the hydrogen bond observed in the occluded state between the substrate and Y108 hydroxyl does not form with Trp^{601} (Figs. 2F and 3, D and E), and the extracellular gate residue F253 on TM6a is ~3.0 Å farther away from Y108, resulting in a solvent-accessible channel to the binding pocket (Fig. 3B).

Second ligand-binding site is specific to the open-to-out conformation. Electron-density maps revealed unanticipated density for a second Trp molecule (Trp^{602}) at the base of the extracellular vestibule. Trp^{602} contacts TM10, and its α-substituents form an ionic bridge between residues D404 and R30 of the extracellular gate (Fig. 4A). The amino group also makes a hydrogen bond with the side-chain hydroxyl of T409, whereas the indole nitrogen hydrogen-bonds with the carbonyl oxygen of G408, which is located in a stretch of π-helix between M403 and V412 (Fig. 4A).

We suggest that Trp^{602}, located ~4 Å above Trp^{601}, represents a low-affinity transiently occupied site for amino acids as they move from the extracellular vestibule to the substrate-binding pocket, perhaps with R30 and D404 serving to dehydrate the incoming amino acid. Although molecular dynamics studies (*28*, *29*) and binding assays (*29*) suggest that the substrate Leu can bind to a site similar to the Trp^{602} site when LeuT is in an occluded-like state, the LeuT-Trp crystal structure demonstrates that occupancy of the Trp^{602} site requires an open-to-out state, with the guanidium group of R30 and the side-chain carboxylate of D404 separated by ~7 to 8 Å. To determine if substrates can bind to the Trp^{602} site in the occluded state, we solved the crystal structure of LeuT with 30 mM Leu and did not observe any amino acid density in the extracellular vestibule (fig. S7). We also measured diffraction data on a LeuT-selenomethionine complex. Anomalous difference Fourier maps show a strong peak [25 standard deviations above the mean (σ)] in the primary binding site but no substantial peaks elsewhere (Fig. 4B).

In addition to Trp^{601} and Trp^{602}, we observed two additional Trps, 603 and 604, at the cytoplasmic and extracellular faces of LeuT, respectively (Fig. 3C). Trp^{603} is located in the cleft between EL2 and EL4, whereas Trp^{604} is situated at the cytoplasmic face of LeuT and forms a salt bridge with R11. At present, we believe these Trp molecules are not relevant to the function of LeuT, in large part because they are removed from mechanistically crucial regions of the transporter.

A model for transport and inhibition. How do inhibitors prevent substrate translocation? For LeuT we postulate that inhibition of transport occurs by preventing distinct steps of the transport cycle (Fig. 5, D and E). Here we show that a competitive inhibitor displaces the substrate and traps the transporter in an open-to-out conformation, thereby preventing progression to the occluded state (Fig. 5, A and D). The LeuT-Trp complex demonstrates how the extracellular-facing TMs 1b, 2a (residues 40 to 54), and 6a are involved in the binding of a competitive inhibitor and in the ensuing conformational changes, which shows that TMs 1b, 2a, and 6a move independently of their respective intracellular-facing counterparts, TMs 1a, 2b (residues 55 to 70), and 6b, and that the TM1, -2, -6, and -7 helix bundle does not move as a rigid body, in contrast to a recent proposal by Forrest *et al*. (*30*). The notion that TMs 1b and 6a undergo conformational changes upon substrate or inhibitor binding is further supported by chemical modification experiments on single-cysteine mutants of the γ-aminobutyric acid transporter GAT1 (*31*–*32*) and SERT (*33*).

What are the molecular principles associated with binding; that is, the formation of the occluded state? We suggest that substrates permeate from extracellular solution to the primary substrate site, located halfway across the membrane, by transiently binding to the extracellular gate residues R30 and D404. We argue that this binding event is possible only when the transporter is in the open-to-out conformation, typified by the LeuT-Trp complex. The substrate then moves to the primary binding site and the open-to-out state "collapses" to the occluded state (Fig. 5, A and B) before isomerizing to the open-to-in state and permitting the release of substrate to the cytoplasm (Fig. 5, B and C). The transporter can then cycle to the open-to-out state, perhaps through an apo-transporter occluded-like conformation. Optimal substrate binding and formation of the occluded state require complementary shape and charge and are best satisfied by Leu and Met. The apparent paradox posed by these two amino acids, which exhibit high binding affinities but low turnover rates and catalytic efficiencies, is reconciled by the notion that transport is a balance between affinities for different intermediates in the transport cycle. Accordingly, the slow turnover rates of Leu and Met are due to the fact that their occluded-state complexes are very stable and the energy barriers associated with isomerization to open-to-in (Fig. 5, B and C) or open-to-out conformations are relatively high. In contrast, the reduced affinity but higher turnover rate and catalytic efficiency of the smaller Ala are probably a reflection of the limited degree to which

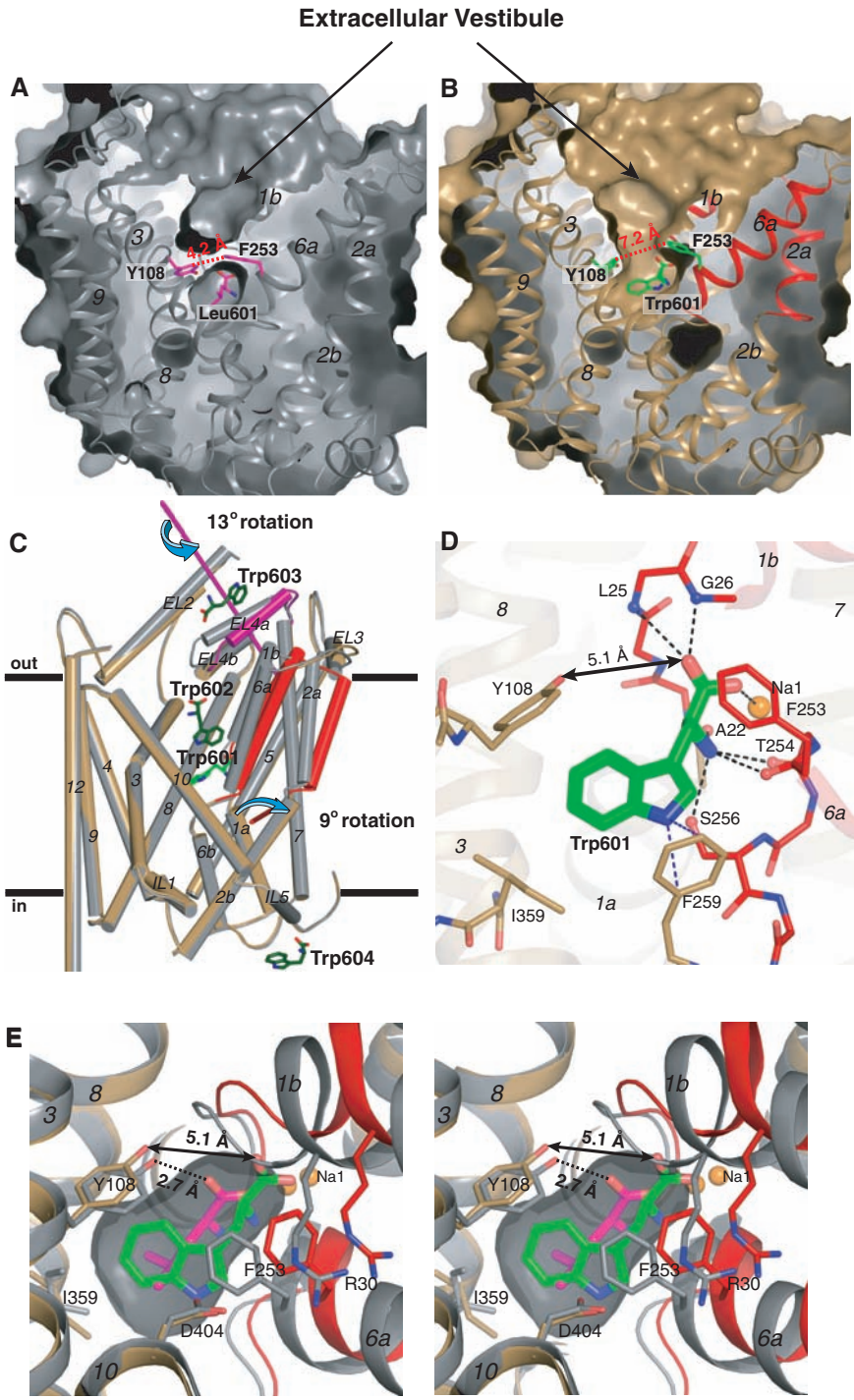

Fig. 3. Trp is a competitive inhibitor that stabilizes an open-to-outside conformation. The solvent-accessible surface of the (**A**) LeuT-Leu (gray) and (**B**) LeuT-Trp complexes (sand, red, and magenta) is shown. Leu, Trp, Y108, and F253 are depicted in both panels. Distances between Y108 (Cδ1) and F253 (Cζ) in each panel are shown. Helices involved in the domain shift (TM1b, -2a, and -6a) are colored red. (**C**) Cα superposition (depicted as cylinders) of the LeuT-Leu and LeuT-Trp complexes. Colors are the same as in (A) and (B). EL4a, an additional element involved in the domain shift, is magenta. The rotation axes of the two domains are depicted in their respective colors. The bound Trps are shown as stick models, with Trp^{601} colored bright green and the other three colored dark green. TM11 is omitted from the figure for clarity. (**D**) Close-up of the Cα superposition depicting the hydrogen-bonding network in the substrate-binding pocket of the LeuT-Trp complex. Shown is the disruption of the critical hydrogen bond between Y108 and the carboxylate of Trp, indicated by a double-headed arrow. (**E**) Overlay (in stereoview) of the Leu- and Trp-binding sites to illustrate the relative displacement of the Trp α-amino and carboxyl groups and the concomitant shift in protein and sodium positions. Leu and Trp are colored in magenta and green, respectively.

it can stabilize the occluded state as compared with how well Leu or Met can.

The distinction between a substrate and a competitive inhibitor is provided by the ability of the ligand to promote formation of the occluded state. For LeuT, this distinction is highlighted by the differences between Tyr and Trp. Because Tyr is a substrate and Trp is not, there is an apparent size "boundary" for transport between 197 and 228 $Å^3$, the volumes of Tyr and Trp, respectively. In GAT1, the existence of a size boundary between transport and inhibition has been shown, in which the addition of an aromatic moiety transforms the substrate nipecotic acid into the nontransportable competitive inhibitor SKF89976A (*34*). In the SLC5 family, this size boundary has also been demonstrated with a series of glycoside derivatives in experiments on the human glucose transporter (hSGLT1) (*34*). Whereas galactose is a substrate,

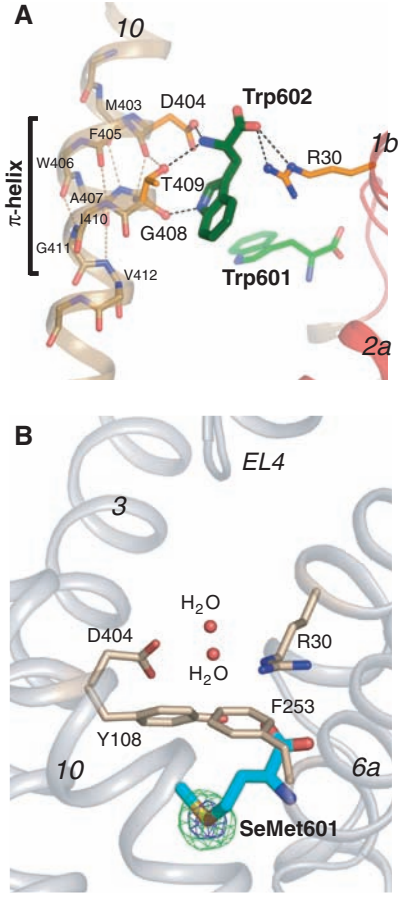

Fig. 4. A second Trp molecule is bound between R30 and D404 of the extracellular gate only in the open-to-out conformation. (**A**) Trp602 bound in the extracellular vestibule of LeuT, residing between D404 and R30, flanked by the π-helix in TM10. (**B**) Extracellular vestibule of the LeuT-SeMet complex. Anomalous-difference Fourier map (contoured at 5σ and 15σ and depicted in green and blue mesh, respectively) showing no substantial density peaks in the extracellular vestibule.

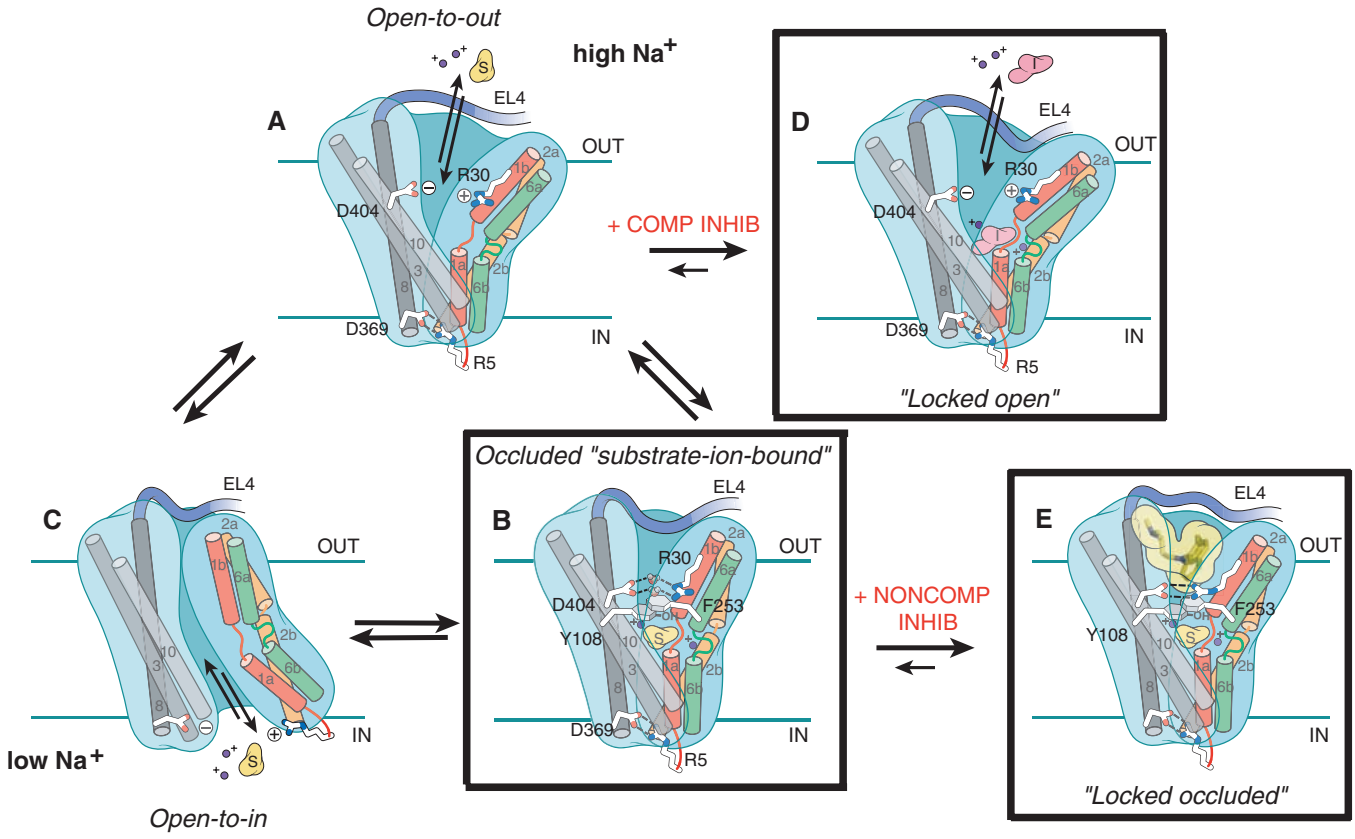

Fig. 5. Schematic of transport and inhibition in LeuT. Postulated conformational changes associated with isomerization from the open-to-out (**A**) to the outward-facing occluded state (**B**) on binding of substrate and ions, from the occluded (B) to open-to-in state (**C**) and dissociation of transported substrate and ions, and from the open-to-in (C) back to the open-to-out state (A). (**D**) Effect of the competitive inhibitor Trp on transport: stabilizing the open-to-out conformation. (**E**) Effect of the noncompetitive TCA inhibitors on transport-stabilizing the outward-facing occluded conformation. The boxed conformations represent actual crystal structures, whereas the unboxed conformations are hypothetical.

1-naphtylgalactose is a nontransportable competitive inhibitor. But the boundary between a substrate and a competitive inhibitor does not solely reside with the ligand. More generally, the definition of this boundary depends on the size, shape, and rigidity of the ligand relative to the constraints imposed by the binding pocket. Thus, amino acid substitutions in the binding pocket that alter these constraints (that is, increase volume) should also alter this boundary. An example of this second case is TnaT, a prokaryotic SLC6 Trp transporter (*35*). Comparison of the amino acids lining the substrate-binding pocket in LeuT and TnaT (*36*) reveals that a prominent difference is the substitution of the larger Phe at position 259 of LeuT with the smaller Val in TnaT. These substitutions increase the volume of the binding pocket in TnaT to permit accommodation of Trp in an occluded state. The molecular principles elaborated here are not only relevant to our understanding of LeuT and its SLC6 orthologs but are also germane to the structurally related glucose and nucleobase transporters (*26*, *37*).

References and Notes

1. S. M. Parsons, *FASEB J.* **14**, 2423 (2000).
2. M. J. Roux, S. Supplisson, *Neuron* **25**, 373 (2000).
3. N. Zerangue, M. P. Kavanaugh, *Nature* **383**, 634 (1996).
4. N. H. Chen, M. E. Reith, M. W. Quick, *Pflugers Arch.* **447**, 519 (2004).
5. B. I. Kanner, *J. Membr. Biol.* **213**, 89 (2006).
6. U. Warskulat, A. Reinen, S. Grether-Beck, J. Krutmann, D. Haussinger, *J. Invest. Dermatol.* **123**, 516 (2004).
7. J. Masson, C. Sagne, M. Hamon, S. E. Mestikawy, *Pharmacol. Rev.* **51**, 439 (1999).
8. M. K. Hahn, R. D. Blakely, *Pharmacogenomics J.* **2**, 217 (2002).
9. N. Ozaki *et al.*, *Mol. Psychiatry* **8**, 933 (2003).
10. G. B. Richerson, Y. Wu, *Adv. Exp. Med. Biol.* **548**, 76 (2004).
11. J. S. Sutcliffe *et al.*, *Am. J. Hum. Genet.* **77**, 265 (2005).
12. J. R. Shannon *et al.*, *J. Med.* **342**, 541 (2000).
13. G. S. Salomons *et al.*, *Am. J. Hum. Genet.* **68**, 1497 (2001).
14. B. Heller-Stilb *et al.*, *FASEB J.* **16**, 231 (2002).
15. E. L. Barker, R. D. Blakely, in *Psychopharmacology: the Fourth Generation of Progress*, F. E. Bloom, D. J. Kupfer, Eds. (Raven Press, New York, 2000), pp. 321–333.
16. P. Krogsgaard-Larsen, B. Frolund, K. Frydenvang, *Curr. Pharm. Des.* **6**, 1193 (2000).
17. S. G. Amara, M. S. Sonders, *Drug Alcohol Depend.* **51**, 87 (1998).
18. A. Yamashita, S. K. Singh, T. Kawate, Y. Jin, E. Gouaux, *Nature* **437**, 215 (2005).
19. S. K. Singh, A. Yamashita, E. Gouaux, *Nature* **448**, 952 (2007).
20. Z. Zhou *et al.*, *Science* **317**, 1390 (2007).
21. Single-letter abbreviations for the amino acid residues are as follows: A, Ala; C, Cys; D, Asp; E, Glu; F, Phe; G, Gly; H, His; I, Ile; K, Lys; L, Leu; M, Met; N, Asn; P, Pro; Q, Gln; R, Arg; S, Ser; T, Thr; V, Val; W, Trp; and Y, Tyr.
22. J. Talvenheimo, P. J. Nelson, G. Rudnick, *J. Biol. Chem.* **254**, 4631 (1979).
23. S. Apparsundaram, D. J. Stockdale, R. A. Henningsen, M. E. Milla, R. S. Martin, *J. Pharmacol. Exp. Ther.* **327**, 982 (2008).
24. H. K. Kimelberg, E. W. Pelton 2nd, *J. Neurochem.* **40**, 1265 (1983).
25. L. K. Henry *et al.*, *J. Biol. Chem.* **281**, 2012 (2006).
26. S. Faham *et al.*, *Science* **321**, 810 (2008).
27. Materials and methods are available as supporting material on *Science* Online.
28. L. Celik, B. Schiott, E. Tajkhorshid, *Biophys. J.* **94**, 1600 (2008).
29. L. Shi, M. Quick, Y. Zhao, H. Weinstein, J. A. Javitch, *Mol. Cell* **30**, 667 (2008).
30. L. R. Forrest *et al.*, *Proc. Natl. Acad. Sci. U.S.A.* **105**, 10338 (2008).
31. Y. Zhou, E. R. Bennett, B. I. Kanner, *J. Biol. Chem.* **279**, 13800 (2004).
32. A. Rosenberg, B. I. Kanner, *J. Biol. Chem.* **283**, 14376 (2008).
33. L. K. Henry, E. M. Adkins, Q. Han, R. D. Blakely, *J. Biol. Chem.* **278**, 37052 (2003).
34. B. A. Hirayama, A. Diez-Sampedro, E. M. Wright, *Br. J. Pharmacol.* **134**, 484 (2001).
35. A. Androutsellis-Theotokis *et al.*, *J. Biol. Chem.* **278**, 12703 (2003).
36. T. Beuming, L. Shi, J. A. Javitch, H. Weinstein, *Mol. Pharmacol.* **70**, 1630 (2006).
37. S. Weyand *et al.*, *Science* **322**, 709 (2008).
38. J. Tsai, R. Taylor, C. Chothia, M. Gerstein, *J. Mol. Biol.* **290**, 253 (1999).

39. We are grateful to the staff of National Synchrotron Light Source beamline X29A and Advanced Light Source beamlines 8.2.1 and 8.2.2 for assistance with data collection. S.K.S. was supported by an individual NIH/National Institute of Neurological Disorders and Stroke National Research Service Award postdoctoral fellowship and a NIH/National Institute of Mental Health

K99/R00 Pathway to Independence Award. C.L.P. was supported by an institutional NIH Multidisciplinary Training in Neuroendocrinology grant. A.Y. was on leave from the Laboratory for Structural Biochemistry, RIKEN Harima Institute at SPring-8, Japan. This work was supported by NIH (E.G.). E.G. is an investigator with the Howard Hughes Medical Institute. Coordinates and structure factors of the LeuT complexes have been deposited in the Protein Data Bank with the following accession codes: glycine (3F4J), alanine (3F48), 30 mM Leu (3F3E), methionine (3F3D), selenomethionine (3F4I), 4-fluorophenylalanine (3F3C) and Trp (3F3A).

Supporting Online Material
www.sciencemag.org/cgi/content/full/322/5908/1655/DC1
Materials and Methods
Figs. S1 to S7
Tables S1 and S2
Movie S1
References

3 October 2008; accepted 6 November 2008
10.1126/science.1166777

Gold-Catalyzed Synthesis of Aromatic Azo Compounds from Anilines and Nitroaromatics

Abdessamad Grirrane, Avelino Corma,* Hermenegildo García*

The selective formation of aromatic azo compounds at preparative or industrial levels requires stoichiometric amounts of environmentally unfriendly transition metals or nitrites. Here, we show that gold nanoparticles supported on titanium dioxide (TiO_2) and nanoparticulated cerium dioxide (CeO_2) catalyze the aerobic oxidation of aromatic anilines to aromatic azo compounds with yields above 98% under mild reaction conditions. Gold on TiO_2 can also act as a reductive catalyst to access the compound directly from nitroaromatics through a two-step, one-pot reaction. The catalytic process shows promise for efficient synthesis of symmetric aromatic azo compounds, and even a range of asymmetric aromatic azo compounds.

Aromatic azo compounds are high-value chemicals widely used in industry as dyes, pigments, food additives, and drugs (*1*–*3*). They are obtained either by reduction of nitroaromatics or by oxidation of anilines. Despite their importance, however, no current catalytic route offers high yields and selectivities. Therefore, the preparation of aromatic azo compounds is carried out today using stoichiometric reagents and, frequently, environmentally unfriendly transition metals (*4*). Examples include oxidation of aromatic amines with lead tetraacetate (*5*) and reduction of nitroaromatics with lead metal (*6*, *7*). An alternative route to asymmetrically substituted aromatic azo compounds entails coupling of diazonium salts with electron-rich aromatic compounds (*8*). This process requires stoichiometric amounts of nitrite salts to form the diazonium salt and generates equivalent amounts of inorganic salt waste. A previous report on the catalytic oxidation of aniline with hydrogen peroxide using microporous crystalline titanosilicate TS-1 shows minimal azobenzene formation, instead noting nitrosobenzene and azoxybenzene products (*9*).

A sustainable chemical process for highly selective synthesis of aromatic azo compounds is thus of great fundamental as well as practical interest. We demonstrate such a process here with an environmentally benign catalyst for oxidation of anilines by oxygen under mild reaction conditions, with yields above 98%.

We recently discovered that gold on TiO_2 (Au/TiO_2) is an excellent catalyst for the chemoselective reduction of nitroaromatics to anilines (*10*). The key to this process is the capacity of the metal to induce H_2 dissociation and the specific conformation of the adsorbed nitroaromatic reactant at the interface between the nanoparticles of gold and the TiO_2 support (*11*). According to Haber's mechanism (*11*), one route for hydrogenation of nitrobenzene to aniline takes place through bimolecular coupling of aniline and nitrosobenzene, forming azo benzene as intermediate, which is subsequently rapidly hydrogenated to two anilines (Scheme 1). The intermediacy of the azo compound in the selective hydrogenation of nitroaromatics, when occuring through the above route, was supported by performing the hydrogenation of azobenzene in the presence of Au/TiO_2 and observing the formation of aniline (*10*). Taking into account the principle of microscopic reversibility and considering that the azo compound is more difficult to oxidize than aniline, we were motivated to explore gold nanoparticles supported on TiO_2 as catalyst for the oxidation of anilines to the corresponding aromatic azo compounds (Scheme 1).

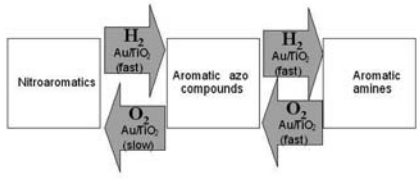

Scheme 1.

On the basis of this hypothesis we exposed aniline to gold nanoparticles on TiO_2 (Au/TiO_2) under mild aerobic oxidation conditions, i.e., 3 to 5 bars of oxygen pressure at 100°C (*12*), and observed selective conversion to the corresponding azobenzenes (Fig. 1 and Table 1).

Control experiments showed that thermal oxidation of aniline does not occur, and the TiO_2 support alone induced significantly lower conversion, indicating that gold plays an important role in the catalytic process (fig. S1). Moreover, to produce active Au/TiO_2 catalysts, the gold must be prepared in the form of nanometer-scale crystallites. When the average size of the gold nanoparticles is increased from 4 to 25 nm, the activity of the catalyst strongly decreases (Table 1).

As observed with other gold-catalyzed processes (*13*), the nature of the support has a strong influence on the activity of the gold nanoparticles. Whereas gold nanoparticles on TiO_2 proved active and selective catalysts for formation of azobenzene, gold with similar crystallite size on carbon or ferric oxide was not active. Gold supported on nanocrystalline ceria is an active and

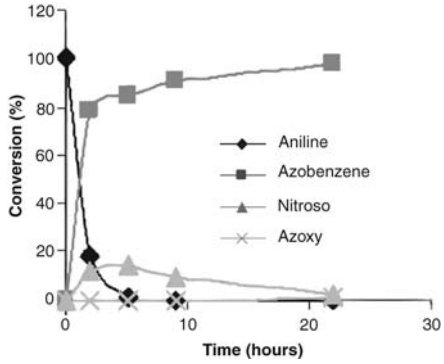

Fig. 1. Time-conversion plot for aniline oxidation, 1.5% Au/TiO_2, 100°C. For reaction conditions, see Table 1.

Instituto de Tecnología Química, Consejo Superior de Investigaciones (CSIC), Universidad Politécnica de Valencia, 46022-Valencia, Spain.

*To whom correspondence should be addressed. E-mail: acorma@itq.upv.es (A.C.); hgarcia@qim.upv.es (H.G.)

selective catalyst for the aerobic oxidation of alcohols (*14*), and it also showed excellent activity and selectivity for formation of azobenzene (Table 1).

We furthermore found that gold is uniquely active for aniline oxidation compared with other noble metals (Table 1 and fig. S1). Our attempts to oxidize aniline to azobenzene with titania- or carbon-supported palladium or platinum nanoparticles under the same reaction conditions were unsuccessful. We also found no catalytic improvement when using, instead of Au/TiO_2 core-shell gold nanoalloys, Au(core)-Pd(shell)/TiO_2 whose preparation and properties have been recently reported (*15*). In addition, Au behaves differently from Pd and Pt (Table 1). These observations can be attributed to the higher affinity of Pd and Pt for amine adsorption, which blocks their activity relative to Au.

Having established that Au/TiO_2 is able to catalyze both the aerobic oxidation of anilines to azobenzenes and the chemoselective hydrogenation of nitroaromatics to anilines (*10*), we explored coupling these two reactions in a single-pot process to transform nitrobenzenes into aromatic azo compounds (Scheme 1). We hydrogenated nitrobenzene to aniline with the Au/TiO_2 catalyst and then, after flushing out the H_2, admitted oxygen at 5 bar into the reaction system (*12*). The results presented in Table 2 show that it is possible to achieve high conversion of nitrobenzene with excellent selectivity to azobenzene through this one-pot procedure.

The general applicability of the catalytic oxidation was tested with a series of substituted anilines (Table 3). The reaction was remarkably selective for azobenzene product regardless of the presence of electron donor or acceptor substituents. The reaction rate depended qualitatively on the Hammett σ constant of the substituent, oxidation being favored by the presence of electron donor substituents. The food additive "butter yellow" can be catalytically synthesized in excellent yield starting from *N,N*-dimethylaniline (Table 3).

Beyond symmetrically substituted azobenzenes, azo dyes composed of two different aromatic rings—one electron-rich and the other electron-poor—constitute an industrially important class of compounds. As noted earlier, these azo dyes are typically synthesized through coupling of the diazonium salt of the electron-poor partner with the electron-rich arene (*8*). Considering the influence of ring substitution on the reaction rate, we thought that the Au catalytic coupling could also be successfully applied to the preparation of these asymmetric aromatic azo dyes by reacting a mixture of the two different anilines directly, provided that one partner proved much more reactive than the other. Our expectation was realized, and we were able to obtain several asymmetrically substituted azobenzenes of industrial interest (Table 4), including methyl orange dye at high selectivity and conversion, using the Au/TiO_2 catalyst.

A reasonable reaction mechanism for the catalytic process would involve as the first step a single-electron oxidation of aniline to the corresponding radical cation, mediated by the TiO_2-supported gold nanoparticles through unsaturated gold sites and/or $Au^{\delta+}$ species formed by interaction with the support (Scheme 2). This mechanism takes into account the higher gold oxidation potential in comparison to palladium or platinum.

We obtained electron paramagnetic resonance data to support the occurrence of this first electron transfer step. Using *N-tert*-butyl-α-phenylnitrone as a trapping agent, we were able to confirm the formation of aniline radical cation when a solution of aniline in toluene is stirred at room temperature in the presence of 1.5 weight percent (wt %) Au/TiO_2 (fig. S2). The measured spectrum matched a simulated spectrum for the trapped anilinium cation structure.

Table 1. Results of the aerobic oxidation of aniline (1a) in the presence of supported metal nanoparticles as catalyst. Reaction conditions: Preheated anilines (93, 13 mg) at 100°C dissolved in toluene (2 ml), stirred magnetically in a reinforced glass vial (3 ml) at an initial O_2 pressure of 5 bar in the presence of the solid catalyst (metal/aniline mol ratio 1%). *, Unidentified product accounts for 10.5%; †, Unidentified product accounts for 11.5%.

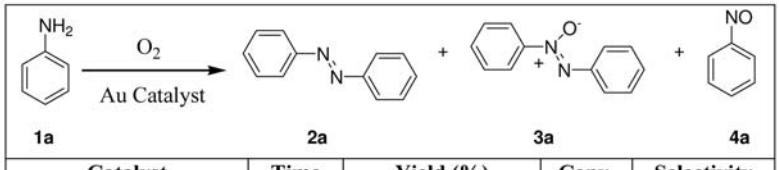

1a 2a 3a 4a

Catalyst	Time (h)	Yield (%) 2a	3a	4a	Conv. (%)	Selectivity (%)
1.5 % Au/TiO_2	9	90	0	10	100	90
	22	98	0.5	1.5	100	98
1.5 % Au/TiO_2 (reused catalyst)	22	99	0	0	100	99
TiO_2	24	52.5	0	0.5	53	99
1.5 % Au/TiO_2 (Particle size 25 nm)	30	4.5	0	0	4,5	99
0.5 % Fe/TiO_2	7	61	0	1	62	98
	24	83.5	0.5	2.5	95	96.5
$Au(1.5\%)Pd(0.8\%)/TiO_2$	34	8.4	0	0	8.4	99
$Au(1.5\%)Pd(1.8\%)/TiO_2$	23	No reaction				
5 % Pd/TiO_2	35	No reaction				
4.4 % Au/Fe_2O_3	47	No reaction				
0.8 % Au/C	69	No reaction				
5 % Pd/C	80	No reaction				
0.2 % Pt/C	40	No reaction				
5 % Pt/TiO_2	70	No reaction				
0.44 % Au/CeO_2	6	91	7	0	98	91
	10	93	7	0	100	93
$Au(0.44\%)Pd(10.15\%)/CeO_2$	20	83	6.5	0*	100	83
CeO_2	42	59	19.5	0†	90	59

Table 2. Synthesis of azobenzene from nitrobenzene through a two-step, one-pot process.

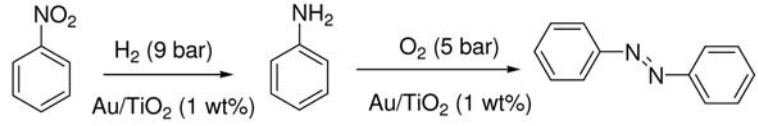

Catalyst	T °C	P (bar)	Time (h)	Yield (%)	Conversion (%)	Selectivity (%)
1.5 % Au/TiO_2	120 °C	H_2 (9 bar)	6	94.6 **Aniline**	98.5	96
	100 °C	O_2 (5 bar)	9	92 **Azobenzene**	100	92

As shown in Scheme 2, the single-electron abstraction would be followed by the coupling of aniline radical cation with neutral aniline to form a three-electron sigma bond. This reaction step is supported by many published precedents for the general tendency of amine radical cations to form N-N bonds that can eventually lead to hydrazines by consecutive losses of two protons and one electron (*16*–*20*).

Once formed, hydrazines should be even more easily oxidized than the parent amine and thus quickly converted to the corresponding azobenzene, following a pathway that again involves alternating transfer of electrons and protons. To support the possibility of this reaction step, we carried out the oxidation of diphenylhydrazine by oxygen in the presence of Au/TiO_2 under the same reaction conditions used for aniline oxidation. We observed that diphenylhydrazine was converted to azobenzene at least 10 times as fast as aniline, as could be expected based on their general relative reactivity. This result explains why we failed to detect hydrazine as an intermediate during aniline oxidation. Under the reaction mechanism proposed in Scheme 2, oxygen serves as the final sink of the electrons, giving rise to the formation of two water molecules.

The mechanism outlined in Scheme 2 could be operating simultaneously with another having nitrosobenzene as a key intermediate. There are precedents for nitrosobenzene reaction with aniline to yield azobenzene as the final product (*21*). The fact that nitrosobenzene 4 has been detected in minor quantities during the course of the initial stages of the reaction lends support to this possibility.

On the basis of the proposed main reaction pathway, we can rationalize that a solid with defect sites or vacancies able to abstract an electron from aniline, as well as to activate oxygen, should catalyze the reaction. In this context, increasing the number of vacancies or defect sites on the TiO_2 surface by doping with iron (*12*, *22*) should enhance the reaction further. Indeed we found that the resulting $Fe\text{-}TiO_2$ material exhibits higher activity than TiO_2 for the formation of azobenzene, whereas Fe_2O_3 is not active (Table 1 and fig. S1).

From the results of the present study and on the basis of the proposed major mechanism, it should be possible to develop a wide array of solid catalysts for the conversion of aromatic amines to azo compounds, provided that enough defect sites are generated on the surface. However, among them, Au/TiO_2 not only gives the highest selectivity of the materials tested here but also should allow the efficient one-pot conversion of a wide range of nitroaromatics into azo compounds.

Table 3. Results of the aerobic oxidation of anilines 1b-f in the presence of supported metal nanoparticles as catalyst. Reaction conditions: Preheated anilines (93, 13 mg) at 100°C dissolved in toluene (2 ml), stirred magnetically in a reinforced glass vial (3 ml) at an initial O_2 pressure of 5 bar in the presence of the solid catalyst (metal/aniline mol ratio 1%). *, 3-bar oxygen pressure.

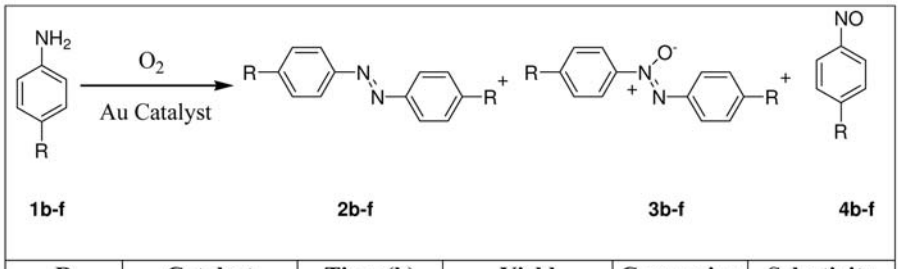

R	Catalyst	Time (h)	Yield			Conversion (%)	Selectivity (%)
			2	3	4		
OCH_3*	1.5 wt% Au/TiO_2	5	89	3	6	99	90
CH_3	1.5 wt% Au/TiO_2	3	98	0	2	99	98
Cl	1.5 wt% Au/TiO_2	23	64	0	0	65	99
$COCH_3$	1.5 wt% Au/TiO_2	31	44	1	0.5	50	96
$N(CH_3)_2$	1.5 wt% Au/TiO_2	16	99	0	0	99	99

Table 4. Results of the aerobic oxidation of an equimolar mixture of substituted aromatic amines in the presence of 1.5 wt % Au/TiO_2 (1 mol %) as catalyst for the formation of asymmetrically substituted azobenzenes. Reaction conditions: Toluene, 100°C, 5 bar O_2. *, Based on p-$R^1C_6H_4NH_2$; †, Mixtures from two products derived from p-$R^1C_6H_4NH_2$ and p-$R^2C_6H_4NH_2$; ‡, Same reaction conditions using a 1:2 stoichiometry for p-toluidin versus 4-aminoacetophenone.

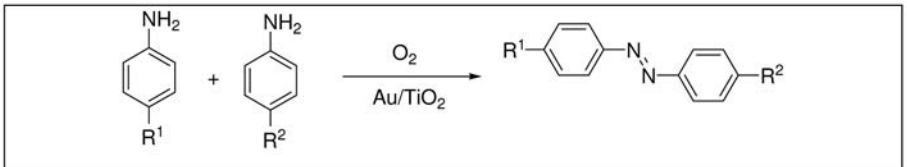

Substrates		Time (h)	Conversion (%)*	Selectivity (%)			
R^1	R^2			Azobenzenes		Nitrosobenzenes†	Azoxybenzenes†
				Asymmetric	Symmetric†		
CH_3	$COCH_3$	44	100	80	9	1	6
CH_3‡	$COCH_3$	43	87	90	5	2	1
$N(CH_3)_2$	SO_3Na	40	99	91			

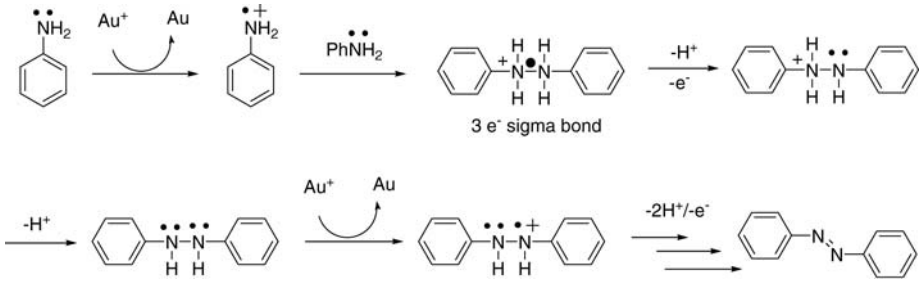

Scheme 2.

References and Notes

1. R. Egli, in *Colour Chemistry: The Design and Synthesis of Organic Dyes and Pigments*, A. P. Peter, H. S. Freeman, Eds. (Elsevier, London, 1991), chap. VII.
2. S. C. Catino, E. Farris, *Concise Encyclopedia of Chemical Technology* (Wiley, New York, 1985).
3. K. Venkataraman, in *The Chemistry of Synthetic Dyes* (Academic Press, London, 1970), chap. VI.
4. J. H. Clark, *Chemistry of Waste Minimization* (Chapman & Hall, London, 1995).
5. H. Firouzabadi, Z. Mostafavippor, *Bull. Chem. Soc. Jpn.* **56**, 914 (1983).
6. K. Ohe, S. Uemura, N. Sugita, H. Masuda, T. Taga, *J. Org. Chem.* **54**, 4169 (1989).
7. A. Osuka, H. Shimizu, H. Suzuki, *Chem. Lett.* **12**, 1373 (1983).
8. H. A. Dabbagh, A. Teimouri, A. N. Chermahini, *Dyes Pigments* **73**, 239 (2007).
9. S. Gontier, A. Tuel, *Appl. Catal. A* **118**, 173 (1994).
10. A. Corma, P. Serna, *Science* **313**, 332 (2006).
11. M. B. Smith, J. March, *Advanced Organic Chemistry*: I (Wiley, New York, ed. 5, 2001).

12. Materials and methods are available as supporting material on *Science* Online.
13. M. Haruta, *Catal. Today* **36**, 153 (1997).
14. A. Abad, P. Concepcion, A. Corma, H. Garcia, *Angew. Chem. Int. Ed.* **44**, 4066 (2005).
15. D. I. Enache *et al*., *Science* **311**, 362 (2006).
16. J. C. Scaiano, S. García, H. García, *Tetrahedron Lett.* **38**, 5929 (1997).
17. O. Brede, A. Maroz, R. Hermann, S. Naumov, *J. Phys. Chem. A* **109**, 8081 (2005).
18. M. Oyama, M. Goto, *Indian J. Chem. Sect. A* **42A**, 733 (2003).
19. W. Hub, S. Schneider, F. Doerr, J. D. Oxman, F. D. Lewis, *J. Am. Chem. Soc.* **106**, 701 (1984).
20. W. Hub, S. Schneider, F. Doerr, J. D. Oxman, F. D. Lewis, *J. Phys. Chem.* **87**, 4351 (1983).
21. E. Lamy-Pitara, B. N' Zemba, J. Barbier, F. Barbot, L. Miginiac, *J. Mol. Catal. Al* **142**, 39 (1999).
22. S. Carrettin *et al*., *Chem. Eur. J.* **13**, 7771 (2007).
23. Financial support by the Spanish DGI (MAT06-14274-C02-01 and CTQ2006-0658) is gratefully acknowledged. A.G. thanks the Spanish CSIC for a JAE research associate contract. A patent covering the use of these catalysts for the aerobic synthesis of azo benzenes has been filed at the Spanish Patent Office.

Supporting Online Material
www.sciencemag.org/cgi/content/full/322/5908/1661/DC1
Materials and Methods
Figs. S1 to S3
Table S1

25 September 2008; accepted 14 November 2008
10.1126/science.1166401

Collective Reactivity of Molecular Chains Self-Assembled on a Surface

Peter Maksymovych,[1,2] Dan C. Sorescu,[3] Kenneth D. Jordan,[1] John T. Yates Jr.[1,4]*

Self-assembly of molecules on surfaces is a route toward not only creating structures, but also engineering chemical reactivity afforded by the intermolecular interactions. Dimethyldisulfide (CH_3SSCH_3) molecules self-assemble into linear chains on single-crystal gold surfaces. Injecting low-energy electrons into individual molecules in the self-assembled structures with the tip of a scanning tunneling microscope led to a propagating chemical reaction along the molecular chain as sulfur–sulfur bonds were broken and then reformed to produce new CH_3SSCH_3 molecules. Theoretical and experimental evidence supports a mechanism involving electron attachment followed by dissociation of a CH_3SSCH_3 molecule and initiation of a chain reaction by one or both of the resulting CH_3S intermediates.

Self-assembled molecular structures on metal and semiconductor surfaces (*1*, *2*) can produce properties that are not observed in isolated adsorbed molecules. For example, the proximity of atoms or molecules can allow their electronic states to delocalize (*3*–*6*), leading to increased electron mobility in the overlayer that can be desirable for potential applications in molecular electronics and organic solar cells (*7*). Other functionalities that are enabled by self assembly include molecular cascades within prearranged molecules (*8*), directional polymerization (*9*), switching of electronic states of surface adatoms in molecular corrals (*10*), and the tunable confinement of electronic surface states in supramolecular gratings (*11*).

Here we report that chemical reactivity can also be induced by self-assembly. A linear chain of molecules (CH_3SSCH_3) adsorbed on a gold surface has been found to respond collectively to electron attachment and undergo a chemical reaction that involves S–S bond dissociation and recombination reactions extending throughout the molecular assembly. The molecular self-alignment reduces the activation energy to break the S–S bond of the CH_3SSCH_3 molecule inside the assembly by at least a factor of 5, allowing for the facile propagation of the chain reaction through as many as 10 neighboring molecules [on the Au(100) surface] before being quenched. The self-assembled molecular structure thus redirects the energy flow toward a chemical chain reaction involving multiple steps, rather than rapid dissipation into the metal bulk.

We have studied electron-induced reactions of CH_3SSCH_3 molecules bonded to Au(111) and Au(100) surfaces using scanning tunneling microscopy (STM) at 5 K to inject electrons and image the reaction products [see supporting online material (SOM)]. Single molecules adsorb on the Au(111) surface with a calculated binding energy of 11.8 kcal/mol in a structural geometry shown in Fig. 1A (*12*). Methyl groups located at the two ends of the S–S bond assume a trans conformation. We observed a total of six equivalent orientations of isolated CH_3SSCH_3 molecules (two mirror images for each of three azimuthal orientations) on the Au(111) surface. At a higher molecular coverage and at adsorption temperatures between 70 and 200 K, "linear" CH_3SSCH_3 chains up to five units in length form on the Au(111) surface. The epitaxial chains run along the $<11\bar{2}>$ crystallographic direction with a periodicity of 0.5 nm (Fig. 1, B and C). Every molecule in the chain has the same orientation of the S–S

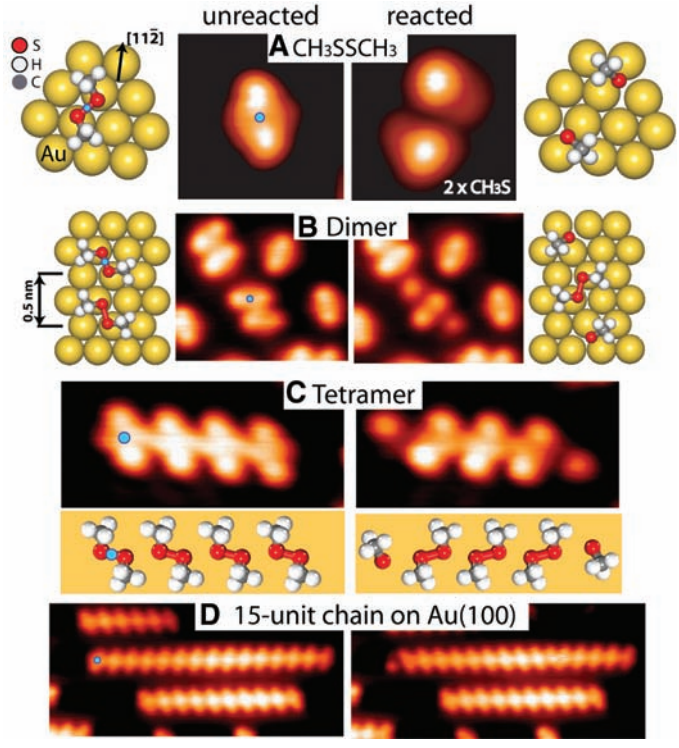

Fig. 1. STM images before and after electron-induced dissociation of a single CH_3SSCH_3 molecule and the self-assembled chains on the Au(111) surface. Schematic ball models of the selected structures are shown aside their STM images. (**A**) Dissociation of CH_3SSCH_3 producing two CH_3S fragments by a pulse of tunneling current at 1.4 V (*12*). (**B** and **C**) Chain reactions in CH_3SSCH_3 dimer and tetramer assemblies on Au(111) induced by a voltage pulse on top of the terminal molecule (blue dot, pulse voltage 0.9 V), leading to the synthesis of CH_3SSCH_3 molecules of opposite conformation. (**D**) A similar chain reaction on the Au(100) surface that involves 10 out of 15 molecules in a row and produces 9 new CH_3SSCH_3 molecules.

[1]Department of Chemistry and Center for Molecular and Materials Simulations, University of Pittsburgh, Pittsburgh, PA 15260, USA. [2]Center for Nanophase Materials Sciences, Oak Ridge National Laboratory, Oak Ridge, TN 37831, USA. [3]U.S. Department of Energy, National Energy Technology Laboratory, Pittsburgh, PA 15236, USA. [4]Department of Chemistry, University of Virginia, Charlottesville, VA 22904, USA.

*To whom correspondence should be addressed. E-mail: johnt@virginia.edu

bond relative to the gold surface, as well as essentially the same trans configuration of the CH_3 groups. Density functional theory (DFT) calculations, described below, predict that the binding energy of the CH_3SSCH_3 molecules to the surface decreases by ~1 kcal/mol upon chain formation, which is consistent with the spontaneous chain growth only at a high molecular coverage.

The effect of electron injection is illustrated in Fig. 1 for the case of a single CH_3SSCH_3 molecule (Fig. 1A), a self-assembled dimer (Fig. 1B), and a tetramer (Fig. 1C) on the Au(111) surface. Electron injection into a single CH_3SSCH_3 molecule (blue circle, pulsed at 0.9 to 1.4 V, 1 to 2 nA, 10 to 100 ms) resulted in its dissociation into equivalent adsorbed CH_3S fragments (*12*), as shown in Fig. 1A. In contrast, similar excitation of the dimer and tetramer created new CH_3SSCH_3 molecules in the interior of the chain and formed one CH_3S entity at each end of the original chain, as seen from a detailed analysis of the electron injection–induced reaction of the tetramer in Fig. 2, A to C. Because we can determine the position of the molecules relative to the underlying surface lattice on the basis of the known crystallographic directions and the adsorption site of the CH_3SSCH_3 molecule (*13*), we infer that the CH_3SSCH_3 molecules produced in the electron-induced chain reactions were translated by ~2.5 Å, relative to the reactant molecules (Fig. 2, D and E).

The production of new CH_3SSCH_3 molecules in the chain's interior, the production of a CH_3S species at each end of the chain, and the 2.5 Å shift of the product species are consistent only with a reaction process where the S–S bonds of a series of CH_3SSCH_3 molecules in the chain are broken and new S–S bonds are formed, as shown schematically in Fig. 1, B and C, for the dimer and tetramer. The chain reaction can be envisioned as a sequence of elementary steps ($CH_3S + CH_3SSCH_3 \rightarrow CH_3SSCH_3 + CH_3S$), each of which is closely reminiscent of the photo-

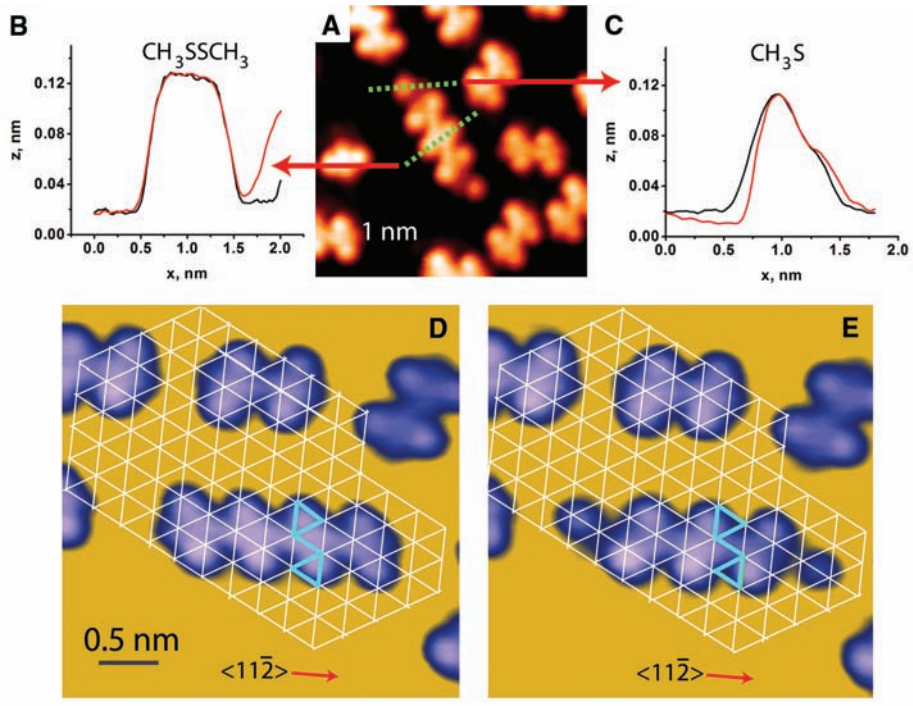

Fig. 2. Topographic analysis of the products of the chain reaction of the CH_3SSCH_3 tetramer on Au(111). (**A**) STM image of the reacted CH_3SSCH_3 tetramer. (**B**) Line profile of isolated CH_3SSCH_3 (black) compared with CH_3SSCH_3 in the middle of the reacted chain (red); the line profiles were taken along the corresponding green dashed lines in (A). (**C**) STM line profile of isolated CH_3S (black) compared with CH_3S at the end of the reacted chain (red). (**D** and **E**) Triangulation of CH_3SSCH_3 tetramer [surface lattice derived from studies of CH_3SSCH_3 adsorption (*13*)]. The product molecules are shifted by 2.5 Å along the <11$\bar{2}$> direction.

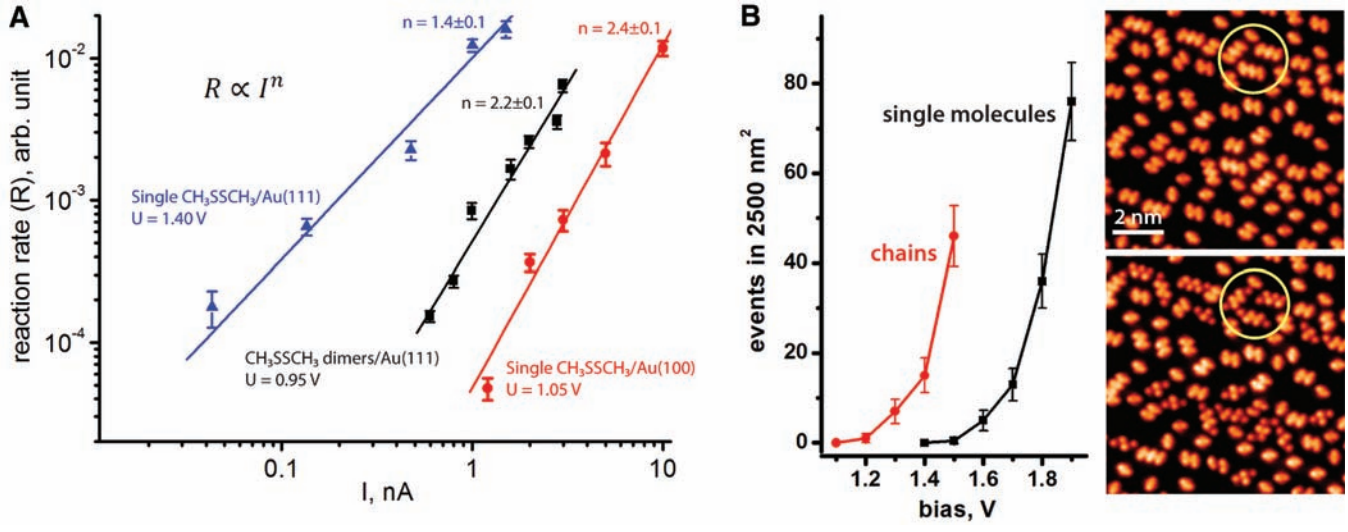

Fig. 3. (**A**) Kinetics of the chain reaction and single-molecule dissociation of CH_3SSCH_3 molecules on Au(111) and Au(100) surfaces obtained from statistical analysis of 100 to 200 single-molecule (chain) excitations. *n* is a slope of the least-squares fit of the reaction rate as a function of tunneling current in the log-log coordinates. Error bars are from fit to Poisson distribution. (**B**) Yield of the long-range reaction (*22*) as a function of the excitation energy for self-assembled chains (red) and single molecules (black) on Au(111). The excitation pulse (I = 20 pA, 1-s duration for both data sets) was applied at an uncovered point near the center of the field of view, and the reaction events were counted in the surrounding area of 2500 nm^2. Each point represents an average of one to three subsequent pulses. (Right) STM images showing the same area before and after several pulses with voltages up to 1.5 V. Many chains are observed to react (e.g., yellow circle with three trimers), whereas single molecules remain intact throughout the image. Error bars are from the square root of the even count, assuming a Gaussian distribution.

induced free-radical substitution reactions in the gas phase involving the thyil radical (RS•) (*14*). Although partial surface bonding of the intermediate CH_3S species (see below) differentiates it from a free radical, we believe that the chain process observed here represents the atomic-level observation of a radical-mediated chain reaction along the lines of the early postulates in the field of gas-phase kinetics (*15*).

As seen in Figs. 1 and 2, the new CH_3SSCH_3 molecules produced in the chain reaction are aligned in a different way relative to the gold lattice, as compared with the original molecules. The realignment can best be visualized as a reflection of the molecule in the mirror plane that runs perpendicular to the chain. A large number of measurements have shown that such realignment does not result from electron injection from the scanning tunneling microscope tip into isolated adsorbed CH_3SSCH_3 molecules; only S–S bond scission or diffusion of the whole molecule occurs (*12*). The chain reaction thus represents a new reaction coordinate for CH_3SSCH_3 molecules dissociating on a surface that appears by virtue of self-assembly. On Au(111), the twofold bonding sites are thermodynamically favorable for the CH_3S species (*13*), which makes them the sole product of single-molecule dissociation. However, the close packing of the CH_3SSCH_3 molecules in the self-assembled chains prevents binding of the nascent CH_3S to the twofold Au sites. Instead, the CH_3S fragment is made to react with a neighboring CH_3SSCH_3 molecule, and a chain reaction occurs in which CH_3S species induce the scission of neighboring S–S bonds. The DFT calculations (see below), predict that after the initial S–S bond-breaking event, subsequent steps proceed with zero or only very small energy barriers, resembling the control of the steric factor in surface processes initiated by electronic excitation on single-crystal templates, such as in surface-aligned photochemistry (*16*, *17*).

A chain reaction can also be induced by pulsing electrons into CH_3SSCH_3 molecules self-assembled on the Au(100) surface, and it is very similar to its analog on Au(111). As seen in Fig. 1D, the reaction of the 15-unit chain of CH_3SSCH_3 molecules on Au(100) produces a terminal CH_3S species, followed by 9 contiguous reoriented CH_3SSCH_3 molecules, and then another CH_3S species embedded in the partially reacted chain, thus involving a total of 10 CH_3SSCH_3 molecules. As on Au(111), the apparent tilt of the CH_3SSCH_3 molecules relative to chain direction is seen to be switched by the reaction, signaling the involvement of the S–S bond dissociation/recombination processes. The most likely cause for the incomplete reaction in the 15-unit chain is energy dissipation to the substrate during the sequence of thermo-neutral steps.

Insight into the process leading to the chain reaction comes from the measurement of the average single-molecule reaction rate as a function of the STM current, as described by W. Ho (*18*). As shown in Fig. 3A, the rate of a single CH_3SSCH_3 dissociation scales as the 1.4 ± 0.1th power of the current at a tunneling bias of 1.40 eV. We therefore interpret single-molecule dissociation to be a one-electron process. The quantum yield for the single-molecule reaction is at least 10^{-7} events per electron, which is several orders of magnitude higher than that found for surface reactions caused by direct vibrational excitation of the molecules by tunneling electrons (*18*–*20*). These observations support a mechanism involving electron capture into the lowest unoccupied molecular orbital (LUMO) of the adsorbed CH_3SSCH_3 molecule (*21*). This orbital is antibonding and localized on the S–S bond (Fig. 4A). The DFT calculations predict the LUMO to be centered at ~1.8 eV above the Fermi level (Fig. 4A), which, considering broadening of the levels and additional image-charge stabilization of the transient anion, is in good agreement with the observed reaction onset at 1.4 eV. After the electron capture, the reaction can proceed by either of two separate routes: (i) dissociation of the anion state, in which case the process is known as dissociative attachment (*21*), or (ii) electron detachment leaving a vibrationally hot CH_3SSCH_3 molecule, which then proceeds to dissociate. At present, we cannot determine which of these two processes is dominant.

One electron–induced dissociation of single CH_3SSCH_3 molecules is independently confirmed by a kinetic study of the long-range dissociation that occurs in a large area around the scanning tunneling microscope tip (up to 50-nm radius at 2.0 eV) if the electron energy exceeds 1.4 eV, as

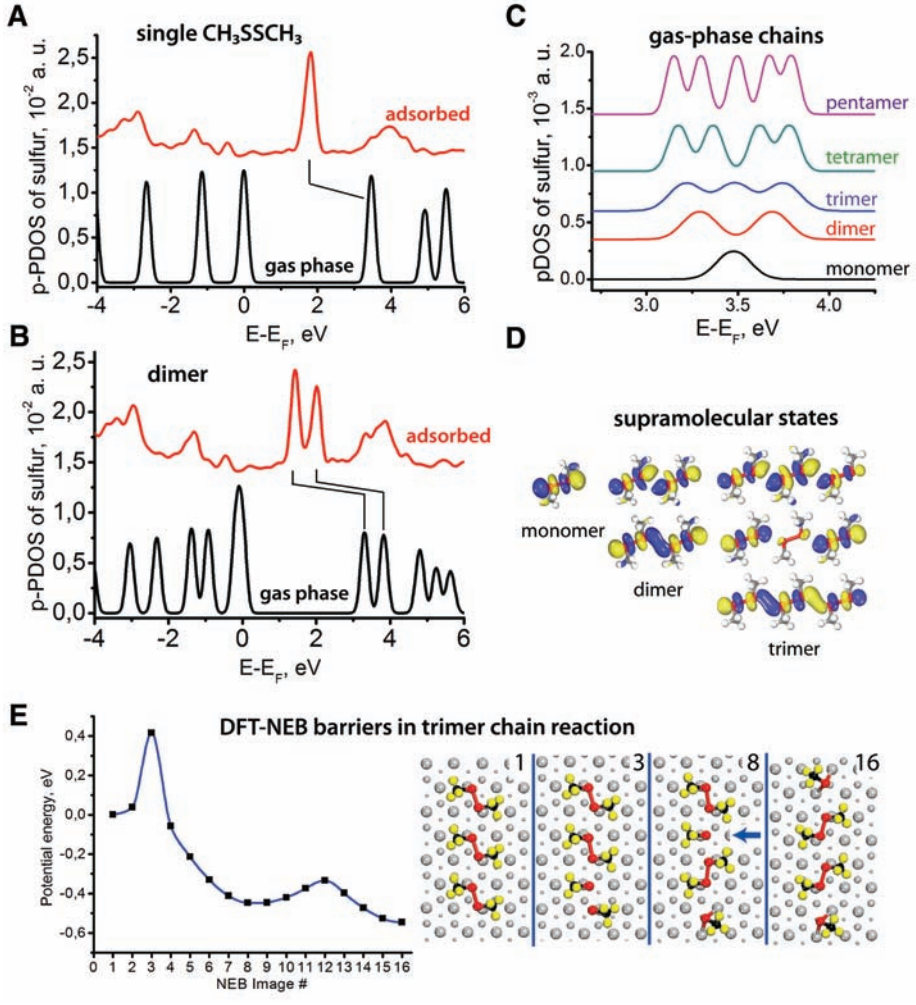

Fig. 4. Density of states projected onto p orbitals of sulfur atoms (p-PDOS) in (**A**) a single CH_3SSCH_3 molecule on Au(111) (red) and in the gas phase (black) and (**B**) a CH_3SSCH_3 dimer on Au(111) (red) and in the gas phase (black). (**C**) p-PDOS of sulfur atoms in the gas-phase assemblies of CH_3SSCH_3 molecules with peaks that correspond to low-lying supramolecular orbitals. The orbitals are shown for the monomer, dimer, and trimer. The structures used in calculations correspond to the equilibrium geometry of the adsorbed chains calculated in the slab models. (**D**) Representative supramolecular orbitals are shown for the dimer and trimer in the order of ascending energy from bottom to top. (**E**) Potential energy diagram calculated for the consecutive chain reaction scenario of the CH_3SSCH_3 trimer on Au(111) using DFT and NEB methods. Four representative NEB images are shown at right. The blue arrow in image 8 indicates the intermediate atop-bonded CH_3S species. a.u., arbitrary units; *E*, electron energy; E_F, Fermi energy.

detailed in (*22*). The long-range reaction is caused by hot electrons transported laterally via a surface resonance of Au(111). The chain reactions are observed to be similarly long-range (Fig. 3B) above a threshold excitation energy, identifying them as one-electron processes under these conditions. An important distinction between the long-range reactions involving single molecules and those involving CH_3SSCH_3 chains on the Au(111) [as well as the Au(100)] surface is a substantially lower (by >0.2 eV) energy threshold for the chain reaction, as determined from a statistical analysis of the long-range reactions (left panel in Fig. 3B). This observation is also confirmed by the STM images shown at the right in Fig. 3B, where several consecutive excitation pulses in the center of the STM image with a maximum energy of 1.5 eV cause multiple chain reactions in the surrounding area (for instance, trimers in the yellow circle), whereas all of the isolated molecules in the field of view remain intact.

Figure 4, A and B, provides the details of the calculated electronic structure of a single CH_3SSCH_3 molecule and the self-assembled dimer (see SOM), both in the gas phase (blue curves) and adsorbed on a four-layer slab of Au(111) (red curves). The purpose of the gas-phase calculations is to estimate the degree of molecular orbital overlap that can exist between CH_3SSCH_3 molecules positioned at a distance and in the orientation closest to their adsorbed state. Therefore the gas-phase species are frozen in their optimized adsorbed configuration. The major changes upon adsorption are: (i) the LUMOs shift downward in energy upon adsorption by ~1.6 eV (single molecule) and ~1.8 eV (dimer), and (ii) the LUMO of the monomer is split into two or more low-lying orbitals in the dimer and longer self-assembled chains (Fig. 4, C and D). In the tetramer chain, the LUMO is calculated to be 0.4 eV closer to the Fermi level than is the LUMO of an isolated CH_3SSCH_3 molecule (Fig. 4, A and B). This result explains the lower threshold energy (by >0.3 eV) (Fig. 3B) for the initiation of the chain reaction in the tetramer, as compared with that for dissociation of the isolated molecule. The LUMO-derived orbitals are considerably less broadened upon adsorption as compared with other molecular orbitals (Fig. 4, A and B), which implies that the former do not mix appreciably with the electronic states of the gold substrate (*23*). Direct imaging by STM of the LUMO of the isolated CH_3SSCH_3 molecules or their chains is not possible on gold surfaces because of the high efficiency of dissociation.

The chain reaction can also be induced by tunneling electrons at a substantially lower energy (i.e., 0.7 to 1.0 eV) than the 1.2-eV threshold reported in Fig. 3B, if the scanning tunneling microscope tip is positioned directly above a molecular unit of the chain, as in Fig. 1. In this case, the reaction is strictly localized to the chain under the scanning tunneling microscope tip, and the reaction rate scales approximately quadratically with tunneling current (Fig. 3A), establishing a two-electron mechanism (*19*). The energy of each electron is substantially higher than any of the fundamental frequencies of the CH_3SSCH_3 molecule [the highest of which is a C–H stretch with an energy of ~360 mV (*24*)], whereas at the same time it is about half as large as the onset energy for single-electron dissociation. Although this could signal a direct vibrational excitation process, the sharp increase of the reaction rate in the energy range between 0.7 and 1.0 eV suggests that the two-electron process may also proceed through an anionic intermediate, with the first electron causing direct vibrational excitation and the second being captured by a vibrationally hot CH_3SSCH_3 molecule.

How does the transient anion formed by electron attachment to a CH_3SSCH_3 chain on a gold surface evolve? In the case of the surface-resonance assisted excitation, the hot electron is captured by a delocalized orbital, as shown in Fig. 4. However, the initially formed delocalized anionic state is likely to become rapidly localized on an individual CH_3SSCH_3 molecule through vibronic coupling. When the tip is positioned directly above the chain, the resulting anion is expected to be initially localized on a single CH_3SSCH_3 molecule, because the molecule directly under the tip will probably be electronically decoupled from the chain by either the electric field of the tip or the vibrational excitation in the two-electron regime. In general, anion states on metal surfaces have very short (subfemtosecond) lifetimes (*25*). However, even with such a short lifetime, a small fraction of the CH_3SSCH_3 anions could dissociate before electron detachment. This possibility is intriguing because this process would be barrierless, whereas the DFT calculations give a barrier of ~0.4 eV for breaking the first S–S bond for the neutral chain. Otherwise, the molecule can dissociate in the ground electronic state if the neutralization of the anion provides enough vibrational excitation to the molecule.

The dissociation of either neutral or anionic CH_3SSCH_3 molecules at the end of a chain produces CH_3S fragments with considerable excess kinetic energy, one of which impinges on a neighboring CH_3SSCH_3 molecule, leading to cleavage of its S–S bond, the formation of a new S–S bond, and the ejection of another CH_3S fragment that can repeat the process. In the event that the initially cleaved CH_3SSCH_3 is in the interior of the chain, both CH_3S fragments induce reactions in the two directions along the chain, as has been observed experimentally after locally pulsing a molecule in the middle of the chain. Gradual dissipation of the kinetic energy to the underlying bulk eventually quenches the chain reaction. We calculated the energy landscape for such a scenario for the neutral trimer assembly (Fig. 4E) and found that the barrier for breaking the first S–S bond is ~0.4 eV [nudged-elastic band (NEB) images 0 to 3)], as mentioned above, and that the S–S bond shifting process (NEB images 4 to 8) then proceeds without barriers. A small second barrier (~0.1 eV) in Fig. 4E is associated with the motion of the terminal CH_3S group toward its bridge-bonded site. The main reason for the nearly activationless interior reaction is the formation of a metastable complex, where an intermediate atop-bonded CH_3S species is stabilized by the neighboring CH_3SSCH_3 molecule.

The discovery of electron-induced chain reactions on surfaces suggests a number of future research directions. In addition to exploring the intriguing reaction dynamics in these systems with the use of ultrafast techniques, one can envision designer molecular assemblies on surfaces where chain reactions yield the desired final product via low-energy and stereospecific pathways. Also, the broad field of photochemistry on surfaces (*26*) will now have to account for chain processes in surface reaction mechanisms and in photocatalyst degradation.

References and Notes

1. J. V. Barth, G. Costantini, K. Kern, *Nature* **437**, 671 (2005).
2. G. M. Whitesides, B. Grzybowski, *Science* **295**, 2418 (2002).
3. L. Scifo *et al*., *Nano Lett.* **6**, 1711 (2006).
4. R. Temirov, S. Soubatch, A. Luican, F. S. Tautz, *Nature* **444**, 350 (2006).
5. M. Akai-Kasaya, K. Shimizu, Y. Watanabe, M. Aono, Y. Kuwahara, *Phys. Rev. Lett.* **91**, 255501 (2003).
6. N. Nilius, T. M. Wallis, W. Ho, *Science* **297**, 1853 (2002); published online 22 August 2002 (10.1126/science.1075242).
7. X.-Y. Zhu, *Surf. Sci. Rep.* **56**, 1 (2004).
8. A. J. Heinrich, C. P. Lutz, J. A. Gupta, D. M. Eigler, *Science* **298**, 1381 (2002); published online 24 October 2002 (10.1126/science.1076768).
9. Y. Okawa, M. Aono, *Nature* **409**, 683 (2001).
10. K. R. Harikumar, J. C. Polanyi, P. A. Sloan, S. Ayissi, W. A. Hofer, *J. Am. Chem. Soc.* **128**, 16791 (2006).
11. Y. Pennec *et al*., *Nat. Nanotechnol.* **2**, 99 (2007).
12. P. Maksymovych, J. T. Yates Jr., *J. Am. Chem. Soc.* **128**, 10642 (2006).
13. P. Maksymovych, D. C. Sorescu, J. T. Yates Jr., *J. Phys. Chem. B* **110**, 21161 (2006).
14. D. D. Carlson, A. R. Knight, *Can. J. Chem.* **51**, 1410 (1973).
15. M. Polanyi, *Atomic Reactions* (Williams and Norgate, London, 1932).
16. J. B. Giorgi, R. Kuhnemuth, J. C. Polanyi, *J. Chem. Phys.* **113**, 807 (2000).
17. C. E. Tripa, J. T. Yates Jr., *Nature* **398**, 591 (1999).
18. W. Ho, *J. Chem. Phys.* **117**, 11033 (2002).
19. H. Ueba, T. Mii, N. Lorente, B. N. J. Persson, *J. Chem. Phys.* **123**, 084707 (2005).
20. Y. Sainoo *et al*., *Phys. Rev. Lett.* **95**, 246102 (2005).
21. C. D. Lindstrom, X.-Y. Zhu, *Chem. Rev.* **106**, 4281 (2006).
22. P. Maksymovych, D. B. Dougherty, X.-Y. Zhu, J. T. Yates Jr., *Phys. Rev. Lett.* **99**, 016101 (2007).
23. K. J. Franke *et al*., *Phys. Rev. Lett.* **100**, 036807 (2008).
24. Y. Sainoo *et al*., *Phys. Rev. Lett.* **95**, 246102 (2005).
25. L. Bartels *et al*., *Phys. Rev. Lett.* **80**, 2004 (1998).
26. J. T. Yates Jr., H. Petek, *Chem. Rev.* **106**, 4113 (2006).

27. We thank D. B. Dougherty for fruitful discussions. P.M. and J.T.Y were supported by the W. M. Keck Foundation and the Army Research Office, and K.D.J acknowledges support from NSF through grant CHE0518253. A grant of computer time at the Pittsburgh Supercomputer Center is gratefully acknowledged. P.M. performed part of this research as a Eugene P. Wigner Fellow and staff member at the Oak Ridge National Laboratory, managed by UT-Battelle, for the U.S. Department of Energy under contract DE-AC05-00OR22725.

Supporting Online Material

www.sciencemag.org/cgi/content/full/322/5908/1664/DC1
SOM Text
References

29 August 2008; accepted 13 November 2008
10.1126/science.1165291

Mechanism of Threading a Polymer Through a Macrocyclic Ring

Alexander B. C. Deutman,[1] Cyrille Monnereau,[1] Johannes A. A. W. Elemans,[1] Gianfranco Ercolani,[2] Roeland J. M. Nolte,[1]* Alan E. Rowan[1]*

The translocation of biopolymers through pores and channels plays a fundamental role in numerous biological processes. We describe here the mechanism of the threading of a series of polymer chains through a synthetic macrocycle, which mimics these natural processes. The threading of polymers involves a kinetically favorable "entron" effect, which is associated with the initial filling of the cavity by the end of the polymer. A preassociation between the outside of the macrocycle and the polymer induces a process in which the polymer end loops back into the cavity of the macrocycle. This looping mechanism results in accelerated threading rates and unidirectional motion and is reminiscent of the protein translocation through membrane pores.

The movement of biopolymer chains through channels and pores in membranes and through toroidal protein assemblies are essential processes in nature. The former process can be observed in DNA and protein transport through membranes (*1*) and during infection of cells by viruses (*2*). The mechanically interlocked rotaxane architecture, present in the latter process, is critical to the high fidelity of DNA replication by polymerases and the degradation of DNA by exonucleases (*3*). Rotaxane architectures have been extensively explored because of their unique dynamic properties, for example, as synthetic molecular motors (*4*) and shuttles (*5*–*8*) and as models of muscles (*9*, *10*). In a previous paper (*11*), we reported on a catalytically active synthetic rotaxane system that operates analogously to the naturally occurring DNA polymerases. In this synthetic analog, the catalytic macrocycle has to first find the open end of a polymer substrate and then thread onto it in a fashion analogous to the natural biopolymers that translocate through pores and channels in membranes. The intriguing question is how, in both systems, this threading of a long polymer through a nanometer-sized pore or macrocycle actually occurs. In natural systems, it is known that interactions between the polymer chain and a recognition site in the vicinity of the pore are essential for efficient and selective translocation of biopolymers across membranes (*12*, *13*). In order to obtain more information about the mechanisms governing the threading, we synthesized a series of oligomer and polymer derivatives containing chains of different lengths that are open at one end and blocked at the other. Close to the blocked end, a trap (a viologen molecule) is incorporated into the chain that can only be reached via the open end of the polymer (*14*, *15*) (Fig. 1). By measuring the threading kinetics of these chains through synthetic macrocycles (**1**-H_2 and derivatives), we found that in this mimetic system, as in its natural counterparts, interactions between the outside of the macrocycle and a recognition site on the polymer chain have a critical influence on the threading process.

We examined the pseudorotaxane complex formation of the macrocycles with oligomers ranging in length from 5 to 22 atoms (**O5** to **O22**) and polymers ranging from 90 to 440 atoms (**P1** to **P7**), as presented in Fig. 1 (*15*). Threading rates (k_{on}) were measured by studying the kinetics of approach to equilibrium at low concentrations ($<10^{-6}$ M) with the help of fluorescence quenching spectroscopy in 1:1 (v/v) mixtures of chloroform and acetonitrile (*14*, *16*). Dilution experiments allowed the determination of the rates of complex dissociation (dethreading, k_{off}). In all cases, the threading-on process followed second-order kinetics and the de-threading process, first-order kinetics. Our ^{1}H nuclear magnetic resonance (NMR) investigations (fig. S5) revealed that only 1:1 complexes are formed between the macrocycles and the polymers, independent of the relative ratios of the two components. The calculated rate constants (k_{on}) for the threading of **1**-H_2 and **1**-Zn over the series of different chains are presented in Table 1 and Fig. 2. The metallated macrocycle **1**-Zn was a substitute for the manganese derivative used in the previous catalytic studies (*11*) because the latter compound is nonfluorescent. The rate constants for the threading of **1**-H_2 over each of the individual chains are higher than those of **1**-Zn (*15*), but the length dependencies are similar. Starting from **O5**, a decrease in threading rate was observed upon lengthening the chain. Once the chain length is larger than eight atoms, the threading-on rates remain constant within experimental error up to a chain length of 22 atoms. This observation is counterintuitive because an approximate threefold increase in length is expected to result in a fivefold decrease in rate in that region, according to the fits with Eq. 4 as will be discussed below. The threading over the polymer chains (with lengths varying from 90 to 440 atoms) is as expected considerably slower, and the log-log plot of rate constant against chain length reveals a linear decrease for both **1**-H_2 and **1**-Zn. In the following, the three different chain length regions (five to eight atoms, 8 to 22 atoms, and 90 to 440 atoms) are treated separately. We start with the last chain length region.

Fluorescence quenching of the porphyrin by the viologen is only observed after the macro-

Table 1. Rate constants (k_{on}) and transition state parameters $\Delta H^{\neq}$ and $\Delta S^{\neq}$ for the threading process. See supporting material (table S1) for the estimated errors in k_{on}. Values for **P3**, **P5**, and **P7** were taken from the literature (*14*).

Guest	Atoms (n)	1-H_2 k_{on} (M^{-1} s^{-1})	1-Zn k_{on} (M^{-1} s^{-1})	2-H_2 k_{on} (M^{-1} s^{-1})	2-Zn k_{on} (M^{-1} s^{-1})	1-H_2 $\Delta H^{\neq}$ (kJ·mole^{-1})	1-H_2 $\Delta S^{\neq}$ (J·mole^{-1} K^{-1})
O5	5	5.0×10^6	8.1×10^5	2.8×10^6	5.3×10^5	15 ± 7	−67 ± 25
O6	6	2.4×10^6	3.2×10^5	1.6×10^6	2.1×10^5	22 ± 4	−50 ± 15
O7	7	1.5×10^6	1.7×10^5	1.2×10^6	1.4×10^5	21 ± 2	−56 ± 10
O8	8	1.3×10^6	1.4×10^5	1.1×10^6	1.2×10^5	19 ± 2	−65 ± 10
O9	9	*	1.4×10^5	*	*	*	*
O10	10	1.5×10^6	1.4×10^5	1.3×10^6	1.3×10^5	19 ± 2	−63 ± 10
O12	12	*	1.5×10^5	1.2×10^6	1.3×10^5	*	*
O13	13	*	1.6×10^5	*	*	*	*
O18	18	1.7×10^6	1.7×10^5	1.2×10^6	1.7×10^5	16 ± 2	−72 ± 10
O20	20	1.6×10^6	1.6×10^5	1.1×10^6	*	*	*
O22	22	*	1.6×10^5	1.1×10^6	1.4×10^5	*	*
P1	90	7.5×10^4	1.0×10^4	1.4×10^5	4.1×10^4	*	*
P2	150	4.0×10^4	5.9×10^3	1.0×10^5	1.4×10^4	*	*
P3	170	3.6×10^4	*	*	*	20 ± 2	−88 ± 10
P4	266	2.1×10^4	3.3×10^3	5.0×10^4	6.0×10^3	*	*
P5	300	1.9×10^4	*	*	*	20 ± 2	−94 ± 10
P6	390	1.3×10^4	2.3×10^3	3.8×10^4	2.4×10^3	*	*
P7	440	1.2×10^4	*	*	*	21 ± 2	−97 ± 10

*Not determined.

[1]Institute for Molecules and Materials, Radboud University Nijmegen, Toernooiveld 1, 6525ED Nijmegen, Netherlands. [2]Dipartimento di Scienze e Tecnologie Chimiche, Università di Roma Tor Vergata, Via della Ricerca Scientifica, 00133 Roma, Italy.

*To whom correspondence should be addressed. E-mail: a.rowan@science.ru.nl (A.E.R.); r.nolte@science.ru.nl (R.J.M.N.)

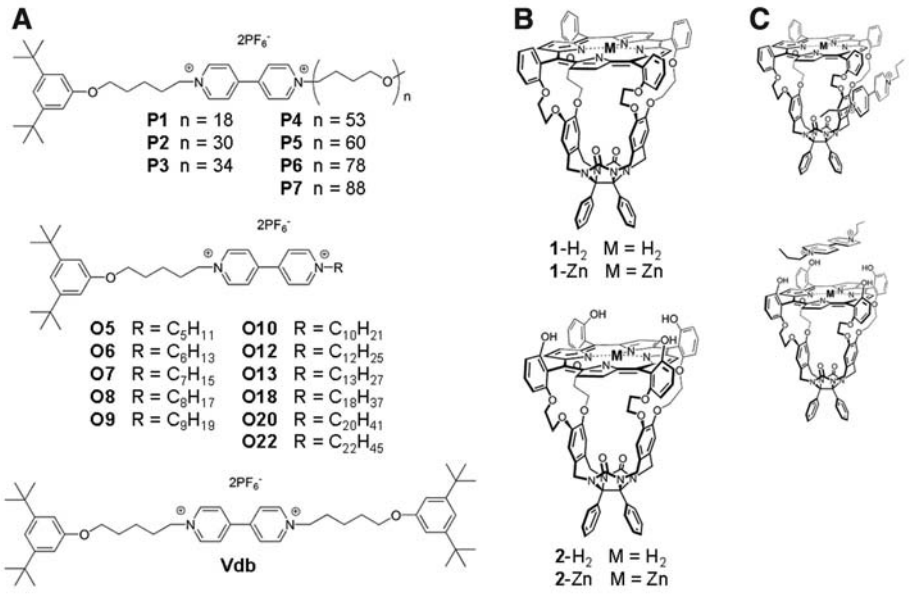

Fig. 1. Structural formulae of the compounds used in this study. (**A**) Threads. (**B**) Macrocycles. (**C**) Binding geometries of the viologen derivatives to the outside of the macrocycles.

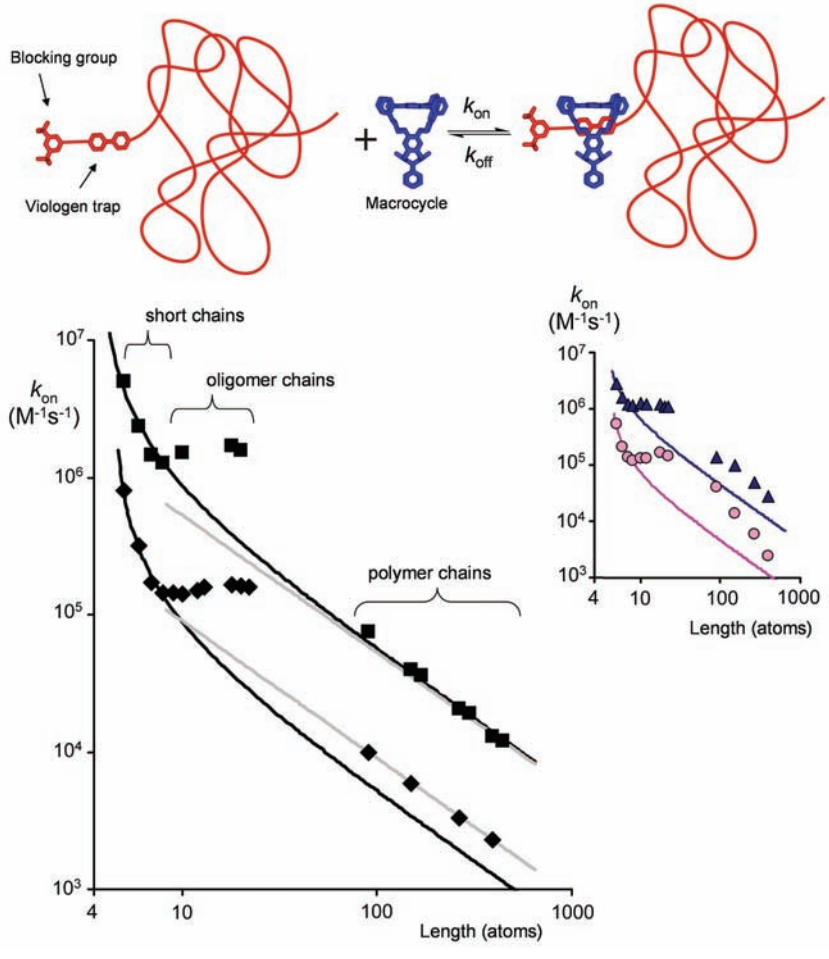

Fig. 2. Binding of the macrocyclic compounds to the viologen derivatives. (**Top**) Cartoon of the binding process. (**Bottom**) Log-log plot of the rate constants (k_{on}) versus chain length for the threading of **1**-H_2 (■) and **1**-Zn (◆). The fit according to Eq. 1 is presented as a gray line and the fit according to Eq. 4 as a black line. (Inset) The log-log plot of the rate constants (k_{on}) versus chain length for **2**-H_2 (▲) and **2**-Zn (●) with the fits according to Eq. 4 in order to illustrate the enhanced threading over the polymer chains via the intramolecular mechanism.

cycle has completely traversed the polymer chain and reached the trap. As a result, it is not possible to directly distinguish between the two important events that take place, that is, the binding to the open end of the polymer chain and the movement of the macrocycle along the chain. The overall threading process can, however, be rationalized by envisaging a consecutive hopping mechanism (*17*, *18*) (Fig. 3A). After the initial binding with rate constant $k_{initial}$ (a second-order process), the movement along the chain consists of first-order hopping steps in which the macrocycle travels randomly from one local energy minimum on the chain to the next. The number of these energy minima (n) depends linearly on the length of the chain. After the complete traversing of the polymer, the macrocycle reaches the trap from which it can dissociate back onto the chain again with a rate constant $k_{V\text{-}off}$. By assuming that the movement along the chain is independent of the position on the chain, we obtained an energy diagram (Fig. 3A) in which all hopping steps have equal rate constant k_{hop}. Assuming that the free energy states of the local energy minima on the chain are higher than those of the initial (M + P) and the end (V) situation, the Bodenstein steady-state approximation (*19*) can be used to derive the overall rate constants of the threading-on ($k_{on\text{-}overall}$) and the dethreading ($k_{off\text{-}overall}$) processes as a function of chain length (Eqs. 1 and 2; see also fig. S12 and accompanying text).

$$k_{on-overall} = \frac{k_{initial}}{n+1} \quad (1)$$

$$k_{off-overall} = \frac{k_{V-off}}{n+1} \quad (2)$$

The observed rates depend solely on the rate of initial binding ($k_{initial}$ and $k_{V\text{-}off}$) and the factor $1/(n+1)$, which describes the probability of fully traversing the chain after the initial binding. The speed of movement (which is directly related to the magnitude of k_{hop}) is simply not expressed in the observed threading rates, and the complicated dynamics of the translocation process can therefore be ignored (*20*). Equation 1 indeed closely describes the experimentally observed length dependencies for the threading over the polymer chains, as can be seen in Fig. 2. From the fit, it can therefore be concluded that the initial binding event ($k_{initial}$) is independent of the length of the polymer, suggesting that entanglements play no substantial role in the studied systems. The above conclusion is further confirmed by the measured values for the enthalpy ($\Delta H^{\neq}$) and entropy ($\Delta S^{\neq}$) of activation, which were extracted from Eyring plots of the threading kinetics measured at different temperatures (fig. S14). Table 1 (rows for **P3**, **P5**, and **P7**) reveals that the activation entropy for the threading of **1**-H_2 becomes more negative upon increasing polymer lengths, whereas the activation enthalpy remains constant. By substituting Eq. 1 into the Eyring equation, the overall enthalpy of activation is expected to remain constant, whereas the entropy of activation will

be chain length–dependent (Eq. 3; see supporting text).

$$\Delta S^{\neq}_{\text{overall}} = \Delta S^{\neq}_{\text{initial}} - R\ln(n+1) \qquad (3)$$

The length dependency of the threading rates over the shortest chains (ranging from five to eight atoms) is clearly different from that of the polymer chains. Instead of a length dependency according to Eq. 1, the decrease in rate constant upon each additional atom in the chain is significantly higher. The observed rate constants for the threading over a chain of six atoms is consistently more than a factor of 2 lower than that for the threading over a chain of five atoms (Table 1 entries **O5** and **O6**). This observation can be rationalized with the help of what we term an "entron effect" involving the filling of the cavity. Both theoretical (*21*) and experimental (*22*) studies have revealed that filling the dimensions of a pore or a channel with a molecular chain is relatively fast compared with the subsequent movement of the chain through the pore. Analogously, the filling of the macrocycles with the initial atoms of the chain can be expected to be kinetically easy. The resulting entron effect can be accommodated into the consecutive hopping model by adding one single energy level for the number (x) of atoms needed to fully fill the cavity of the macrocycle (Fig. 3B) and by defining the second-order rate constant k_{entron} for the binding of the macrocycle onto the entron and the first-order rate constant $k_{\text{entron-off}}$ for the threading-off the entron. The overall threading-on rate equation is now given by Eq. 4.

$$k_{\text{on-overall}} = \frac{k_{\text{entron}}}{\frac{k_{\text{entron-off}}}{k_{\text{hop}}}(n-x)+1} \qquad (4)$$

Equation 4 (n being the number of atoms in the chain) indeed closely describes the observed length dependencies of the short chains for both **1**-H_2 and **1**-Zn (Fig. 2). Iterative fitting provided values for x of 5.1 and 5.4 for **1**-H_2 and **1**-Zn, respectively, which is in good agreement with molecular modeling, confirming that about five chain atoms are needed to fill the cavities. Moreover, Eq. 4 closely describes the observed length dependency for the threading of **1**-H_2 over both the short and the polymer chains. A slight deviation from the fit (and thus in k_{entron}) is observed for the treading of **1**-Zn over the polymer chains, presumably as a result of interactions between the oxygen atoms and the zinc center.

The threading rates remain constant between 8 and 22 atoms (Table 1 and Fig. 2), instead of decreasing by a factor up to 5 as predicted. Apparently, from a chain length of 8 atoms or more, another pathway of threading the chains must be operative. Initially a model was envisaged in which the macrocycle threads on via a fold in the polymer chain (Fig. 3F). However, this model was discarded on the basis of slippage studies that revealed that the cavity of **1**-H_2 is too small to accommodate a folded chain (fig. S6 and accompanying text). A second mechanism was considered in which the threading is initiated and guided by interactions between the outside of the macrocycle and the chain, leading to accelerated rates by means of transition state stabilization. The ^{1}H NMR titrations of **1**-H_2 and **1**-Zn with viologen double-blocked (**Vdb**) (which cannot enter the cavities) indeed revealed weak complex formation (association constant K_a = 44 M^{-1} and K_a = 40 M^{-1} for **1**-H_2 and **1**-Zn, respectively) in which the viologen moiety binds to the outside of the cavity (Fig. 1C). Molecular modeling studies demonstrated that, starting from chain lengths of about eight atoms, the viologen derivatives can form the outside macrocycle-viologen complex and at the same time loop the initial part of the chain inside the cavity, like a dog biting its own tail (Fig. 3E). Consequently, chains longer than eight atoms can thread all but the last eight atoms through the cavity while simultaneously forming the outside macrocycle-viologen complex.

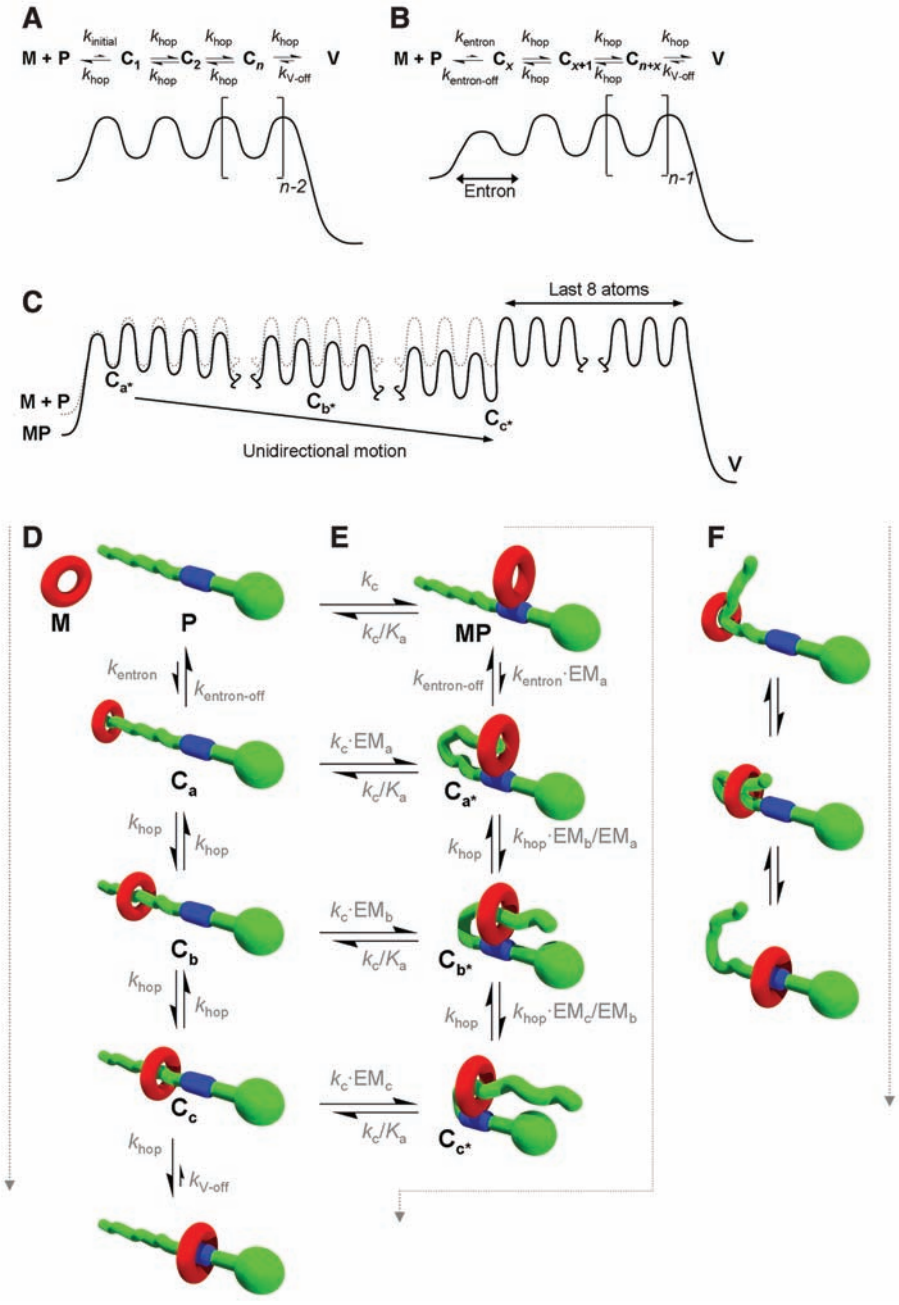

Fig. 3. Schematic representations of the energy landscapes and mechanisms of the threading process. (**A**) Consecutive hopping mechanism. (**B**) Consecutive hopping mechanism with entron effect included. (**C**) Consecutive hopping mechanism for the specific binding model as presented in (D) and (E), revealing the transition state stabilization and unidirectional motion as a result of the outside complex formation (black line compared to gray line). (**D**) Intermolecular threading path. (**E**) Intramolecular looping path. (**F**) Alternative path of binding and subsequent movement of the macrocycle over a folded chain.

This intramolecular looping mechanism resembles that of a ring-closure reaction (MP→C_{a*} in Fig. 3E), and the threading rate will therefore depend on the effective molarity (EM) of the reactive components (the cavity and the open chain end). The EM (*23*) describes the relative ease of ring-closure reactions compared with intermolecular reactions under otherwise identical conditions and has been tabulated in the literature (*24*). EM values contain all the intrinsic parameters of chains relevant for ring closure such as ring strain and torsional entropy. In line with intuition, EM values become smaller when the chains connecting the reactive components become longer. According to the model (Fig. 3E), the intramolecular path will be more favored than the intermolecular path as long as $K_aEM > 1$, in which K_a is the association constant of the outside-viologen complex. At the given values of K_a (≈40 M^{-1}), these conditions are met for chains shorter than 40 atoms (because $EM = 0.025$ M for chains of 40 atoms), which is in line with the observation that the polymer chains (90 to 440 atoms) apparently do not benefit from this looping process. The intramolecular process will not only be lower in transition state energy than the intermolecular process but also energetically downhill in the direction of the viologen trap. In the process of moving along the chain toward the viologen moiety ($C_{a*} \rightarrow C_{b*} \rightarrow C_{c*}$ in Fig. 3E), the chain length between the reactive components (the outside of the macrocycle and the viologen moiety) decreases, and the EM value consequently increases ($EM_a < EM_b < EM_c$), resulting in a downhill reaction coordinate (Fig. 3C). The resulting unidirectional movement continues until the loop becomes too small (C_{c*}, Fig. 3, C and E) and the viologen dissociates from the outside of the macrocycle, after which the last eight atoms are traversed in a nonstabilized fashion and the macrocycle embraces the viologen trap. As a result, the traversing of the last eight atoms becomes rate-limiting, which is in agreement with the experimental results that the observed rates never become significantly higher than the rate of traversing a chain of eight atoms (Fig. 2).

To further support the model, we synthesized two different porphyrin macrocycles (**2**-H_2 and **2**-Zn) (*25*) with -OH functionalities on the outside of the cavity, which form stronger outside complexes with **Vdb** [$K_a = 2 \times 10^4$ M^{-1} and 5×10^4 M^{-1} for **2**-Zn and **2**-H_2, respectively; see figs. S9, S10, and accompanying text (*16*)]. This modification was expected to result in higher threading rates over the polymer chains as well because $K_aEM > 1$ in a larger region of chain lengths. It should be noted that, even at these high association constants, quenching caused by the outside complexes is less than 5% of the total measured quenching at the applied experimental concentrations (fig. S11). The fluorescence threading studies of **2**-H_2 and **2**-Zn revealed that both **2**-H_2 and **2**-Zn traverse the short chains and the oligomer chains in an analogous fashion to **1**-H_2 and **1**-Zn (Fig. 2 inset and Table 1). However, the threading over the polymer chains is significantly faster for both **2**-H_2 (on average 2.2 times) and **2**-Zn (up to a factor of 4). These results thus support the idea that the higher affinity of **2**-H_2 and **2**-Zn for the viologen moiety on the outside of the macrocycle enhances the rates of threading over the polymer chains via the intramolecular looping process.

The experimentally determined length dependencies for the threading process can be described by a modified consecutive hopping model, which includes a kinetically favorable so-called entron effect. The above results highlight that weak supramolecular interactions between the outside of the macrocycle and the chain have a dramatic effect on the overall threading process. It is a classical example of how small interactions can lead to accelerated rates by means of transition state stabilization. In our simple biomimetic model system, these interactions both initiate and guide the threading process, resulting in accelerated rates and mimicking the natural translocation systems in which interactions between the biopolymer and a receptor in the vicinity of the pore are fundamental and essential steps in efficient and selective translocation (*12*, *13*). Given that our studies show that even weak interactions between the macrocyclic exterior and the polymer chains already cause significant increases in the threading rates, it is very likely that such assisted threading mechanisms not only play a role in the specific natural examples but also in a much larger number of natural polymer translocation systems. Another intriguing effect of the mechanism is that unidirectional motion (achieved without the application of an external driving force) is facilitated toward the trapping site. This driving force should allow for the design of novel artificial machines (*26*) and catalysts in which the threading can be finely controlled.

References and Notes

1. W. Wickner, R. Schekman, *Science* **310**, 1452 (2005).
2. E. J. Mancini *et al.*, *Cell* **118**, 743 (2004).
3. A. Johnson, M. O'Donnell, *Annu. Rev. Biochem.* **74**, 283 (2005).
4. E. R. Kay, D. A. Leigh, F. Zerbetto, *Angew. Chem. Int. Ed.* **46**, 72 (2007).
5. R. A. Bissell, E. Cordova, A. E. Kaifer, J. F. Stoddart, *Nature* **369**, 133 (1994).
6. A. M. Brouwer *et al.*, *Science* **291**, 2124 (2001); published online 22 February 2001 (10.1126/science.1057886).
7. J. D. Badjic, V. Balzani, A. Credi, S. Silvi, J. F. Stoddart, *Science* **303**, 1845 (2004).
8. E. R. Kay, D. A. Leigh, *Nature* **440**, 286 (2006).
9. M. C. Jiménez, C. Dietrich-Buchecker, J.-P. Sauvage, *Angew. Chem. Int. Ed.* **39**, 3284 (2000).
10. Y. Liu *et al.*, *J. Am. Chem. Soc.* **127**, 9745 (2005).
11. P. Thordarson, E. J. A. Bijsterveld, A. E. Rowan, R. J. M. Nolte, *Nature* **424**, 915 (2003).
12. G. Blobel, *ChemBioChem* **1**, 86 (2000).
13. T. A. Rapoport, *Nature* **450**, 663 (2007).
14. R. G. E. Coumans, J. A. A. W. Elemans, R. J. M. Nolte, A. E. Rowan, *Proc. Natl. Acad. Sci. U.S.A.* **103**, 19647 (2006).
15. P. Hidalgo Ramos *et al.*, *J. Am. Chem. Soc.* **129**, 5699 (2007).
16. Materials and methods are detailed in supporting online material available at *Science* Online.
17. W. Herrmann, B. Keller, G. Wenz, *Macromolecules* **30**, 4966 (1997).
18. A. Harada, J. Li, M. Kamachi, *Nature* **356**, 325 (1992).
19. L. P. Hammett, *Physical Organic Chemistry* (McGraw-Hill, New York, ed. 2, 1970), p. 112.
20. A. B. Kolomeisky, *Biophys. J.* **94**, 1547 (2008).
21. E. Slonkina, A. B. Kolomeisky, *J. Chem. Phys.* **118**, 7112 (2003).
22. A. Meller, L. Nivon, D. Branton, *Phys. Rev. Lett.* **86**, 3435 (2001).
23. L. Mandolini, *Adv. Phys. Org. Chem.* **22**, 1 (1986).
24. C. Galli, L. Mandolini, *Eur. J. Org. Chem.* 3117 (2000).
25. P. Thordarson *et al.*, *J. Am. Chem. Soc.* **125**, 1186 (2003).
26. W. R. Browne, B. L. Feringa, *Nat. Nanotechnol.* **1**, 25 (2006).

27. This research was supported by a National Research School Combination Catalysis Controlled by Chemical Design grant, Nederlandse Organisatie voor Wetenschappelijk Onderzoek Veni, Vidi and Vici grants (J.A.A.W.E. and A.E.R.), a Koninklijke Nederlandse Akademie van Wetenschappen grant (R.J.M.N.), and a Nanoned grant (A.E.R. and R.J.M.N.).

Supporting Online Material

www.sciencemag.org/cgi/content/full/322/5908/1668/DC1
Materials and Methods
Figs. S1 to S18
Table S1
References

14 August 2008; accepted 14 November 2008
10.1126/science.1164647

A Dynamic Marine Calcium Cycle During the Past 28 Million Years

Elizabeth M. Griffith,[1,2]* Adina Paytan,[2] Ken Caldeira,[3] Thomas D. Bullen,[4] Ellen Thomas[5,6]

Multiple lines of evidence have shown that the isotopic composition and concentration of calcium in seawater have changed over the past 28 million years. A high-resolution, continuous seawater calcium isotope ratio curve from marine (pelagic) barite reveals distinct features in the evolution of the seawater calcium isotopic ratio suggesting changes in seawater calcium concentrations. The most pronounced increase in the $\delta^{44/40}$Ca value of seawater (of 0.3 per mil) occurred over roughly 4 million years following a period of low values around 13 million years ago. The major change in marine calcium corresponds to a climatic transition and global change in the carbon cycle and suggests a reorganization of the global biogeochemical system.

The marine calcium (Ca^{2+}) cycle is related to processes that control oceanic alkalinity and atmospheric CO_2, playing an important role in earth's climate (*1*). Calcium carbonate ($CaCO_3$) sedimentation in the ocean represents the largest carbon sink in the combined atmosphere, biosphere, and ocean system, and thus strongly influences the global carbon cycle (*2*). Fluctuations in $CaCO_3$ sedimentation reflect imbalances in the long-term

carbon cycle and are related to global changes in climate and tectonics (*3*). Such fluctuations may also be reflected in the marine Ca^{2+} cycle and seawater Ca^{2+} concentrations and isotopic ratios (*4*, *5*).

Changes in Ca^{2+} concentration of seawater throughout the Phanerozoic are revealed in brine inclusions (*6*, *7*), elemental ratios in marine skeletal carbonates (*8*), and the changing abundance of carbonate and potash-evaporite minerals (*9*, *10*). Shifts in seawater Ca^{2+} concentration during the past 28 million years (My) are thought to reflect predominantly sedimentological factors (e.g., carbonate deposition and dolomitization) (*11*), although changes in sea-floor generation rates may also play a role (*12*).

The amount of Ca^{2+} in the modern ocean and its isotopic composition [$\delta^{44/40}Ca_{seawater}$ (*13*)] are determined by the balance between riverine and hydrothermal inputs and removal through $CaCO_3$ deposition and alteration of oceanic crust and their respective isotopic compositions (fig. S1). Estimates for the isotopic composition of Ca^{2+} inputs from continental rivers range from $\delta^{44/40}Ca$ = –0.87 to –1.30 per mil (‰) (*5*, *14*–*16*); hydrothermal inputs average –0.96 ± 0.20‰ (*15*). When $CaCO_3$ is precipitated from seawater, its Ca-isotopic composition is 0.7 to 1.6‰ less than that of dissolved Ca^{2+} in seawater, depending on which mineral, calcite or aragonite, is precipitated and on parameters such as temperature and precipitation rate (*17*). Alteration of oceanic crust, estimated to account for less than 10% of the Ca^{2+} sink in the modern ocean, has an average $\delta^{44/40}Ca$ between 0.7 and 1.7‰ less than $\delta^{44/40}Ca_{seawater}$ (*18*). Due to the range of isotopic signatures in the modern ocean and the uncertainty of the representative average values, it is not known precisely whether or over what time scale the marine Ca^{2+} cycle is in isotopic steady state (*5*, *14*, *15*, *19*).

Recent work using Ca-isotopic ratios measured in marine carbonates (*14*, *16*, *19*–*21*) has shown that the isotopic signature recorded in carbonates fluctuated over time. However, there is no consensus as to whether seawater composition or environmental and physiological factors ultimately control the Ca-isotopic composition measured in marine carbonates (*16*, *19*). We present a high-resolution, continuous seawater Ca-isotope curve from marine (pelagic) barite ($BaSO_4$) to help explain factors controlling the cycles of calcium and carbon over the past 28 My.

Marine barite, a minor component of marine sediments, is a useful recorder of changes in seawater chemistry (*22*–*24*). Calcium (Ca^{2+}) substitutes for barium (Ba^{2+}) in the barite crystal lattice, providing an archive of Ca-isotopes in a highly stable sulfate mineral (*25*). Marine barite has advantages over carbonate minerals for studying the seawater Ca-isotopic ratio because of its resistance to diagenesis in oxic pelagic sediments and its uninterrupted record over important climate intervals associated with carbonate dissolution (*22*). In addition, marine barite precipitates inorganically in seawater; thus, no physiological "vital effects" are expected (*22*).

The measured $\delta^{44/40}Ca$ of Holocene marine barite separated from more than 20 core-top deep sea sediment samples in the major ocean basins are indistinguishable from each other, with a $\delta^{44/40}Ca$ of –2.01 ± 0.15‰ (average $2\sigma_{mean}$) (*25*). The offset from seawater (isotopic fractionation) is not strongly related to any measured environmental parameter (*25*) and encompasses the expected range of conditions over the past 28 My at the location of our down-core samples. This offset can therefore be considered constant during the past 28 My (*26*).

The seawater Ca-isotope curve for the past 28 My was reconstructed from marine barite at a resolution better than 1 My from 51 sediment samples collected by the Deep Sea Drilling Project (DSDP) and the Ocean Drilling Program (ODP) at sites 572 to 575, 1218, and 1219 in the east equatorial Pacific (*27*).

The marine barite $\delta^{44/40}Ca_{seawater}$ record (Fig. 1) displays a long-term trend toward more positive values, in general agreement with existing seawater Ca-isotope records from biogenic carbonates (Fig. 1 and table S1). However, our data also reveal features that correspond with shifts in the marine carbon and oxygen isotope records (Fig. 1). The $\delta^{44/40}Ca_{seawater}$ remained fairly stable at around –0.3‰ ± 0.1‰ ($2\sigma_{mean}$, n = 26) from 28 million years ago (Ma) until around 13 Ma. From 13 Ma to 8 Ma, it rose to the modern value, where it remained until the present (0 ± 0.1‰, $2\sigma_{mean}$, n = 23).

We use a numerical model to investigate the implications of this Ca-isotope record for the marine calcium biogeochemical cycle in relation to major climatic events and perturbations in the carbon cycle [following (*14*); for details, see (*27*)]. The state variables in the model are the isotopic composition of seawater Ca^{2+} (model input from the barite data) and its concentration. Model parameters include the isotopic signature of the combined input flux of Ca^{2+} (riverine, hydrothermal, and dolomitization) and the isotopic fractionation during $CaCO_3$ precipitation. The oceanic residence time of Ca^{2+} is taken to be 1.3 My (*21*) and assumed to be constant (*28*). Using a constant sedimentation flux (and changing residence time) did not drastically vary the pattern in calculated Ca^{2+} concentrations (*27*).

An initial condition for 28 Ma is constructed in the model, and the set of equations are solved simultaneously, so the system is allowed to evolve

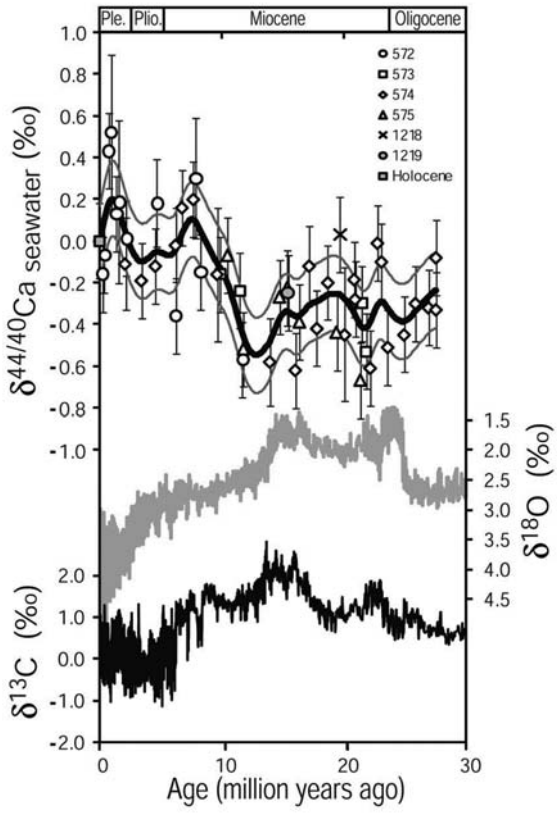

Fig. 1. Ca-isotopic composition of seawater ($\delta^{44/40}Ca_{seawater}$) over the past 28 My. All the Ca-isotopic ratios are reported in per mil relative to seawater and are plotted with respect to the chronology in (*33*) [see (*27*)]. Error bars are the precision of each sample calculated as the $2\sigma_{mean}$ of replicate analyses on the thermal ionization mass spectrometer or the average $2\sigma_{mean}$ if only one analysis was made. The bold solid black curve is the cubic smoothing spline of the data (*34*) with ± 0.18‰ (average $2\sigma_{mean}$) in gray. Two samples with $2\sigma_{mean}$ > 0.4‰ were removed from the trend and figure. Averages of duplicate samples are plotted. Smoothed global $\delta^{18}O$ and $\delta^{13}C$ synthesis of benthic (deep sea) foraminifera reported relative to Pee Dee belemnite in per mil (*35*). Pleistocene, Ple.; Pliocene, Plio.

[1]Department of Geological and Environmental Sciences, Stanford University, Building 320, Room 118, Stanford, CA 94305, USA. [2]Institute of Marine Sciences, University of California, Santa Cruz, CA 95064, USA. [3]Department of Global Ecology, Carnegie Institution of Washington, 260 Panama Street, Stanford, CA 94305, USA. [4]Branch of Regional Research, Water Resources Division, U.S. Geological Survey, MS 420, 345 Middlefield Road, Menlo Park, CA 94025, USA. [5]Department of Geology and Geophysics, Yale University, Post Office Box 208109, New Haven, CT 06520, USA. [6]Department of Earth and Environmental Sciences, Wesleyan University, 265 Church Street, Middletown, CT 06459, USA.

*To whom correspondence should be addressed. E-mail: egriffith@ucsc.edu

toward the present. In the model, the assumption of constant average values estimated for the present-day Ca^{2+} system (sources and sinks) (fig. S1) leads to unacceptable seawater Ca^{2+} fluctuations. Accordingly, the isotopic composition of the input flux of Ca^{2+} ($\delta^{44/40}Ca_{in}$) and/or the isotopic fractionation associated with the sink ($\Delta^{44/40}Ca_{sed}$) must have varied over this time period. First, we varied $\delta^{44/40}Ca_{in}$ with time (Fig. 2A), constrained at points where the Ca^{2+} concentration is known from measurements of brine inclusions (*7*) and linearly extrapolated between these points as described in (*27*).

Because the first approach assumes time-dependent isotopic variation in the input flux (Fig. 2A), the general long-term trend in the Ca-isotopic composition of seawater is directly related to changes in the isotopic signature of this flux. With these assumptions, a shift in $\delta^{44/40}Ca_{in}$ to more positive values likely reflects a shift in the weathered terrain to more continental sourced silicate rocks with a more positive $\delta^{44/40}Ca$ value (*16*). An increase from 6% to 17% in the contribution of silicate weathering to the total weathering flux can explain the data (*27*). The $\delta^{44/40}Ca$ value of carbonates subjected to weathering also changes, contributing about 0.1‰ of the 0.6‰ long-term increase in the modeled $\delta^{44/40}Ca_{in}$ over this time period (*20*).

Dolomitization (a source of Ca^{2+} to the oceans) could have influenced $\delta^{44/40}Ca_{in}$ in the past. Dolomitization releases Ca^{2+} by diffusional exchange with Mg^{2+}, adding Ca^{2+} depleted in ^{44}Ca without affecting the seawater carbonate flux (*19*). The rate of marine dolomite formation has decreased over the Cenozoic to a present minimum (*11*), consistent with the increasing $\delta^{44/40}Ca_{seawater}$ over the past 28 My, but it is unclear how important this process has been as a source of Ca^{2+} during this time interval or over the observed transition about 13 Ma.

In addition, the isotopic fractionation associated with the sink ($\Delta^{44/40}Ca_{sed}$) likely changed. Shifts in the $\Delta^{44/40}Ca_{sed}$ could have been caused by changes in temperature during precipitation, rate of precipitation, or in the mineralogy of the deposited carbonates (aragonite versus calcite), which is controlled by the dominant calcifying organisms (*10*, *20*). In the second approach (Fig. 2B), $\Delta^{44/40}Ca_{sed}$ varies and is calculated as the difference between seawater values in this study and the bulk carbonate (output) record of (*21*). $\delta^{44/40}Ca_{in}$ also varies, as in the first model, and is likewise constrained by the long-term trend in seawater Ca^{2+} concentration from fluid inclusions (*27*). This results in a slightly different $\delta^{44/40}Ca_{in}$ reconstruction due to the differences in $\Delta^{44/40}Ca_{sed}$ histories we used. Changing the $\Delta^{44/40}Ca_{sed}$ in addition to $\delta^{44/40}Ca_{in}$ does not in general change the shape of the modeled seawater Ca^{2+} concentration curve.

In summary, model results indicate that the isotopic composition of the combined input flux of Ca^{2+} and/or isotopic fractionation during carbonate precipitation must have changed over the past 28 My (*21*, *16*), and these results suggest changes in seawater Ca^{2+} concentrations. Specifically, the relatively abrupt (<5 My) changes in the $\delta^{44/40}Ca_{seawater}$ curve indicate large, rapid transient changes in the amount of Ca^{2+} in the ocean, of up to twice the present value (Fig. 2), and/or transient fluctuations in the Ca-isotopic composition of the input or sedimentation fluxes of up to 1‰. However, such large and abrupt changes in the Ca-isotopic compositions of these input or output fluxes is outside the range of measured present-day values (*5*, *14*–*16*) and does not seem to be a likely mechanism for explaining all variation in our seawater Ca-isotope record.

The most prominent change in the oceanic Ca^{2+} concentration corresponds to a major climatic transition at ~13 Ma (middle Miocene), when the earth's climate changed from a period of relative global warmth into a cooler climate, while the Antarctic ice sheet increased in volume (*29*). This increase in Ca^{2+} concentration may be a consequence of an increase in the Ca^{2+} flux to the ocean.

An increase in the Ca^{2+} flux from continental weathering (without an accompanying increase in carbonate deposition) from recently exposed continental shelves, increased weathering, and/or transport of weathered material into the oceans associated with glaciation might have resulted from a drop in sea level as shown by the sharp 0.5‰ increase in the $\delta^{18}O$ of benthic foraminifera (*30*) (Fig. 1). Increased weathering of carbonate sediments (relative to silicate sediments) increases the flux of Ca^{2+} to the ocean relative to the carbon (C) flux providing a potential means for decoupling the Ca^{2+} and C systems (*19*). The rate of change in the Ca^{2+} flux must be decoupled from and higher than the rate of change in the flux of C; otherwise, Ca^{2+} flux variations are quickly (<<1 My) buffered by feedbacks involving terrestrial rock weathering and marine C-$CaCO_3$ deposition/dissolution processes.

The calcium carbonate compensation depth (CCD), the water depth where the calcite rain rate is balanced by its dissolution rate such that all calcite produced in the water column is dissolved, records the balance between $CaCO_3$ deposition/dissolution in deep sea sediments (*31*). Shifts in the CCD occurred during the past 28 My (*31*), resulting from changes in deep ocean chemistry and the supply rate of $CaCO_3$ to the sediments, but long-term changes in the equatorial Pacific CCD (>1 My) do not appear to be solely controlled by oceanic Ca^{2+} concentrations (fig. S7).

A change in the marine carbon cycle occurred during the middle Miocene climatic transition, when the carbon isotopic composition of bulk carbonates ($\delta^{13}C_{carb}$) began to decrease by about 2‰ to modern values (*30*) (Fig. 1). If the total C flux to the ocean had been constant, this would have implied a shift to more continental-sourced

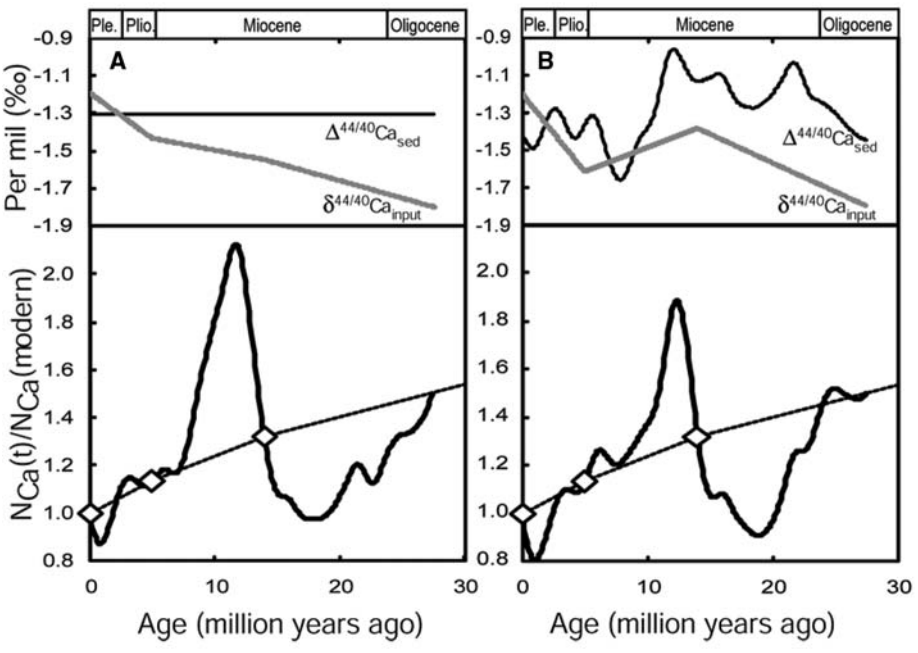

Fig. 2. Time varying isotopic composition of the calcium input flux to the oceans ($\delta^{44/40}Ca_{in}$) and isotopic fractionation during calcium carbonate precipitation before sedimentation ($\Delta^{44/40}Ca_{sed}$) in per mil used in the numerical models (top). Calculated ratio of amount of calcium in the oceans [$N_{Ca}(t)$], relative to the present value [$N_{Ca}(modern)$] constrained using data (open diamonds) from (*7*). Solid black line is $N_{Ca}(t)$ / $N_{Ca}(modern)$; dashed black line is Phanerozoic trend (*7*) (bottom). Numerical model assuming (**A**) constant $\Delta^{44/40}Ca_{sed}$ or (**B**) varying $\Delta^{44/40}Ca_{sed}$ calculated from the difference between seawater $\delta^{44/40}Ca$ (this study) and measured contemporaneous bulk nannofossil ooze carbonates (*14*, *21*).

rocks rich in organic C relative to carbonate weathering over the past ~13 My (*31*). Previous interpretations of $^{87}Sr/^{86}Sr$, $^{187}Os/^{186}Os$, and δ^7Li records agree with a change in the nature of weathered material at this time (*32*).

Many aspects of the biogeochemical Ca^{2+} cycle need to be constrained better by observational and experimental data and paleoceanographic and geologic evidence before a unique interpretation of the causes of the long-term trend and abrupt transitions in $\delta^{44/40}Ca_{seawater}$ is possible. Reconstructions of the global CCD and high-resolution records of seawater Ca^{2+} concentrations (e.g., from fluid inclusions or other proxies) and of the rate of dolomitization and sea-floor generation are all needed.

Our identification of an abrupt middle Miocene change in the $\delta^{44/40}Ca_{seawater}$ record from marine barite attests to the dynamic nature of an element deemed "conservative" in the present ocean and demonstrates that we cannot assume that concentrations of Ca^{2+} in seawater have been stable over the Cenozoic.

References and Notes

1. H. C. Urey, *The Planets, Their Origins and Development* (Yale Univ. Press, New Haven, CT, 1952).
2. A. J. Ridgwell, M. J. Kennedy, K. Caldeira, *Science* **302**, 859 (2003).
3. M. I. Budyko, A. B. Ronov, A. L. Yanshin, *History of the Earth's Atmosphere* (Springer-Verlag, New York, 1987).
4. J. Skulan, D. J. DePaolo, T. L. Owens, *Geochim. Cosmochim. Acta* **61**, 2505 (1997).
5. P. Zhu, J. D. Macdougall, *Geochim. Cosmochim. Acta* **62**, 1691 (1998).
6. T. K. Lowenstein, M. N. Timofeeff, S. T. Brennan, L. A. Hardie, R. V. Demicco, *Science* **294**, 1086 (2001).
7. J. Horita, H. Zimmermann, H. D. Holland, *Geochim. Cosmochim. Acta* **66**, 3733 (2002).
8. J. A. D. Dickson, *Science* **298**, 1222 (2002).
9. P. A. Sandberg, *Nature* **305**, 19 (1983).
10. L. A. Hardie, *Geology* **24**, 279 (1996).
11. H. D. Holland, *Am. J. Sci.* **305**, 220 (2005).
12. C. P. Conrad, C. Lithgow-Bertelloni, *Geology* **35**, 29 (2007).
13. The Ca-isotopic composition of a sample is expressed as the deviation from a standard solution value, using δ-notation in per mil: $\delta^{44/40}Ca = [(^{44}Ca/^{40}Ca_{\ sample} - {}^{44}Ca/^{40}Ca_{\ standard}) / {}^{44}Ca/^{40}Ca_{\ standard}] \times 1000$, where $^{44}Ca/^{40}Ca_{\ standard}$ refers to the $^{44}Ca/^{40}Ca$ isotopic ratio of seawater.
14. C. L. De La Rocha, D. J. DePaolo, *Science* **289**, 1176 (2000).
15. A. D. Schmitt, F. Chabaux, P. Stille, *Earth Planet. Sci. Lett.* **213**, 503 (2003).
16. N. G. Sime *et al.*, *Geochim. Cosmochim. Acta* **71**, 3979 (2007).
17. N. Gussone *et al.*, *Geochim. Cosmochim. Acta* **69**, 4485 (2005).
18. M. Amini *et al.*, *Geochim. Cosmochim. Acta* **72**, 4107 (2008).
19. A. Heuser *et al.*, *Paleoceanography* **20**, 10.1029/2004PA001048 (2005).
20. M. S. Fantle, D. J. DePaolo, *Earth Planet. Sci. Lett.* **237**, 102 (2005).
21. J. Farkaš *et al.*, *Geochim. Cosmochim. Acta* **71**, 5117 (2007).
22. A. Paytan, M. Kastner, E. E. Martin, J. D. Macdougall, T. Herbert, *Nature* **366**, 445 (1993).
23. A. Paytan, M. Kastner, D. Campbell, M. H. Thiemens, *Science* **304**, 1663 (2004).
24. A. V. Turchyn, D. P. Schrag, *Science* **303**, 2004 (2004).
25. E. M. Griffith, E. A. Schauble, T. D. Bullen, A. Paytan, *Geochim. Cosmochim. Acta* **72**, 5641 (2008).
26. Range of parameters measured include conditions relevant to the ranges for the measured samples (DSDP-ODP sites): Holocene core-top sample sites include the average annual temperature in the upper 700 m of the water column, where the majority of marine barite is thought to precipitate, 1 to 14°C; the depth of each core-top location, 3175 to 4431 m; water column barite saturation at sea floor, SI = 0.6 to 0.8 and at 700 m, SI = 0.8 to 1.2; average upper (700 m) water column: salinity (34.2 to 34.9), carbonate concentration (86.65 to 139.56 μmol/kg), and dissolved oxygen concentration (1.1 to 6.2 ml/l); bulk sedimentation rate (1.3 to 2.7 cm/thousand years) and barite accumulation rates (0.7 to 23.4 mg m^{-2} $year^{-1}$).
27. Materials and methods are available as supporting material on *Science* Online.
28. A constant residence time in the model requires that the output flux of Ca^{2+} and the total amount of dissolved Ca^{2+} in the oceans vary together. This is a valid assumption if changes in Ca^{2+} concentration occurred due to changes in the input flux of Ca^{2+} to the ocean that are not accompanied with changes in the C cycle. If a change in Ca^{2+} input flux was associated with and compensated by a change in $CaCO_3$ sedimentation through an increase in alkalinity, no change in Ca^{2+} concentration would result. Increasing or decreasing the residence time by 50% gives similar fluctuations but different magnitudes (peak concentrations range from 180% to 290% of present values) (fig. S5). Modeling the Ca^{2+} system with full carbonate chemistry reveals the sensitivity of the Ca^{2+} cycle to changes in C on long time scales (>10,000 years) (*27*). A mechanism for decoupling the two cycles is required in order to result in changes in Ca^{2+} concentration. These might include changes in the rate of dolomitization or the Ca:bicarbonate ratio in the riverine flux due to shifts in the weathering regime.
29. A. Holbourn, W. Kuhnt, M. Schulz, H. Erlenkeuser, *Nature* **438**, 483 (2005).
30. M. Lyle, *Paleoceanography* **18**, 10.1029/2002PA000777 (2003).
31. D. A. Hodell, P. A. Mueller, J. A. McKenzie, G. A. Mead, *Earth Planet. Sci. Lett.* **92**, 165 (1989).
32. E. C. Hathorne, R. H. James, *Earth Planet. Sci. Lett.* **246**, 393 (2006).
33. L. Lourens, F. Hilgen, N. J. Shackleton, J. Laskar, D. Wilson, in *A Geological Time Scale 2004*, F. Gradstein, J. Ogg, A. G. Smith, Eds. (Cambridge Univ. Press, Cambridge, UK, 2004), pp. 409–440.
34. Generated using a smoothing parameter ($P = 0.80$) and data weighted by its precision in the MATLAB 7.6.0.324 (R2008a) cubic smoothing spline function csaps.
35. J. Zachos, M. Pagani, L. Sloan, E. Thomas, K. Billups, *Science* **292**, 686 (2001).

36. Samples provided by the Integrated Ocean Drilling Program. We thank A. Eisenhauer, J. Fitzpatrick, W. A. Griffith, R. Jones, and G. Li for analytical assistance. Supported by NSF CAREER Grant OCE-0449732 (A.P.) and by a National Defense Science and Engineering Graduate Fellowship and an NSF Graduate Research Fellowship (E.M.G.).

Supporting Online Material

www.sciencemag.org/cgi/content/full/322/5908/1671/DC1
Materials and Methods
Figs. S1 to S7
Table S1
References

22 July 2008; accepted 7 November 2008
10.1126/science.1163614

Earthquake Supercycles Inferred from Sea-Level Changes Recorded in the Corals of West Sumatra

Kerry Sieh,[1]* Danny H. Natawidjaja,[2] Aron J. Meltzner,[1] Chuan-Chou Shen,[3] Hai Cheng,[4] Kuei-Shu Li,[3] Bambang W. Suwargadi,[2] John Galetzka,[1] Belle Philibosian,[1] R. Lawrence Edwards[4]

Records of relative sea-level change extracted from corals of the Mentawai islands, Sumatra, imply that this 700-kilometer-long section of the Sunda megathrust has generated broadly similar sequences of great earthquakes about every two centuries for at least the past 700 years. The moment magnitude 8.4 earthquake of September 2007 represents the first in a series of large partial failures of the Mentawai section that will probably be completed within the next several decades.

Large sections of the great arcuate fault beneath the eastern flank of the Indian Ocean have failed progressively over the past 8 years in an extraordinary sequence of big earthquakes (Fig. 1) (*1–4*). The largest of these failures of the Sunda megathrust, in 2004, caused the most devastating tsunami the world has seen in many generations. One question of great humanitarian and scientific importance is which remaining unruptured sections of the megathrust will fail next.

Until late 2007, the largest remaining unbroken Sumatran section had been the 700-km-long Mentawai patch, dormant since two great earthquakes in 1797 and 1833 (*5*). Modeling of coral and instrumental geodetic data had shown most of the patch to have been highly coupled throughout at least the past half-century (*6*, *7*). That is, overlying and underlying blocks have been locked together, and strains continue to accumulate. These observations had led to concerns that the remainder of the Mentawai patch might rupture soon (*8–11*). In September 2007, rapid-fire failure of portions of the Mentawai patch produced a moment magnitude (M_w) 8.4 earthquake and several large aftershocks (*12*), which served to further elevate anxiety.

[1]Tectonics Observatory, California Institute of Technology, Pasadena, CA 91125, USA. [2]Research Center for Geotechnology, Indonesian Institute of Sciences, Bandung, Indonesia. [3]Department of Geosciences, National Taiwan University, Taipei, Taiwan, ROC. [4]Department of Geology and Geophysics, University of Minnesota, Minneapolis, MN 55455, USA.

*To whom correspondence should be addressed at the Earth Observatory of Singapore, Nanyang Technological University, 639798 Singapore. E-mail: sieh@ntu.edu.sg

This paper shows that the history of the Mentawai section through the past few hundred years implies that the next large failure is likely to occur within the next few decades. We have extracted that history of strain accumulation and relief from corals on the fringing coral reefs directly above locked parts of the Sumatran megathrust.

Corals, growing just below the intertidal zone, record in their upper surfaces a history of local sea level (*5*, *7*, *13*–*15*). Annual lowest tidal levels limit the highest levels to which the coral colonies can grow (*3*), termed the highest level of survival (HLS) (*13*). Flat-topped pancake-like heads record sea-level stability. Heads with HLS surfaces that rise toward colony perimeters reflect rising sea levels during their decades of growth. This morphology inspired the name "microatolls" (*16*), diminutive analogs of Darwin's slowly drowning tropical islands that are ornamented with an outer band of living coral reef (*17*). Changes in sea level recorded in microatoll HLS history reflect the lowering and raising of the islands in the course of elastic strain accumulation and relief. U-Th disequilibrium dating of coral can yield errors for uplift during earthquakes of just a few years (*18*–*20*).

Three paleoseismic sites, spanning 110 km of the Mentawai patch in the source region of the September 2007 earthquakes (Fig. 1 and fig. S1), show that major episodes of emergence (*21*) have occurred four times in the past 700 years.

At Bulasat, the first of the four emergences occurred in 1347 ± 18, the date of death of microatolls living at this and the Saomang site, a few kilometers to the south (Fig. 2A) [supporting online material (SOM), including figs. S1 to S7]. Undisturbed microatolls of this vintage rest at an elevation about 110 to 120 cm above our arbitrary datum, HLS in 2002.

The next emergence event occurred in 1607 ± 4, after decades of rapid submergence. Direct evidence for emergence in 1797 is not preserved in the corals at the Bulasat site. However, two microatolls at nearby Saomang (SOM, including figs. S8 to S10) document relative sea-level rise of about 9 mm/year through part of the 17th and 18th centuries. These time series constrain the magnitude of uplifts in 1797 and 1833. Also, a microatoll at Saomang that died in 1833 yields a record for the early 19th century. This series' lack of colinearity with the records from the early 1700s reveals at least one emergence between about 1730 and 1810 (Fig. 2A). The most plausible date is 1797, the date of a historical large earthquake that is also clear in paleoseismic records at nearby sites (*5*). Extrapolation of these records implies emergence of about 1 m in 1797.

A living microatoll and continuous global positioning system (GPS) station at Bulasat yield comparable modern subsidence rates of ~13 and 15 mm/year. The GPS station recorded uplift of 73 cm during the September 2007 M_w 8.4 and 7.9 earthquakes (table S1B).

The Bulasat time series (Fig. 2A) resembles a saw blade. The tip of each sawtooth is the date of an emergence that presumably relates to a large earthquake, as in 2007. The back of each tooth is a ramp that slopes down to the date of the

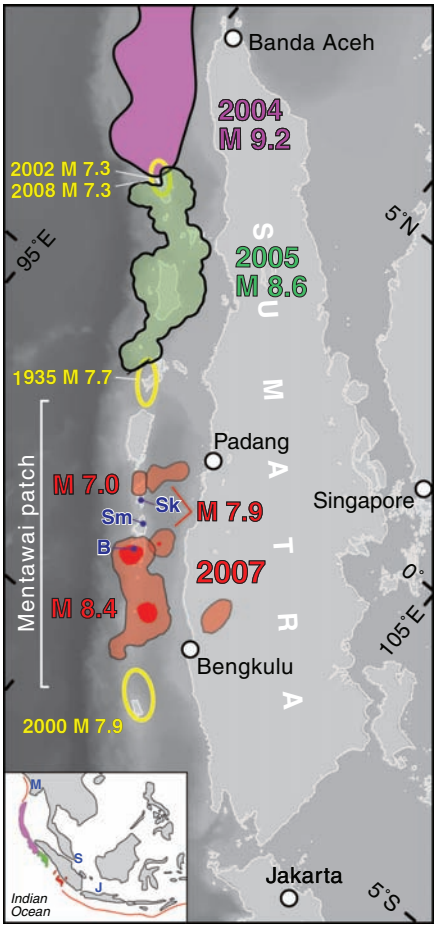

Fig. 1. Recent seismic ruptures of the Sunda megathrust, offshore of Sumatra, delineate highly coupled large (pink, green, and orange) and weakly coupled small (yellow) patches. The September 2007 sequence involved partial rupture of the Mentawai patch, which last broke in 1797 and 1833. B (Bulasat), Sm (Simanganya), and Sk (Sikici) indicate principal paleoseismic sites. Adapted from (*1*, *3*, *5*, *12*, *15*). (**Inset**) M, S, and J are Myanmar, Singapore, and Java. The red line is the Sunda megathrust.

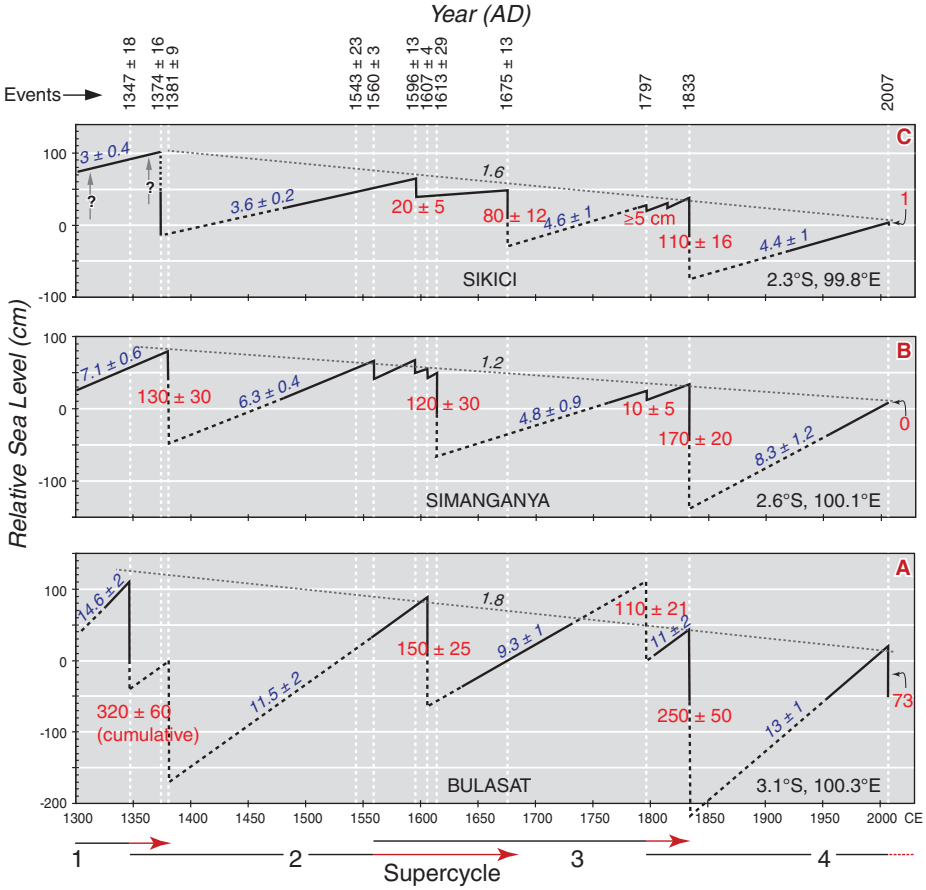

Fig. 2. Histories of interseismic submergence and coseismic emergence through seven centuries at sites (**A**) Bulasat, (**B**) Simanganya, and (**C**) Sikici. Data constrain solid parts of the curves well (fig. S4); dotted portions are inferred. Emergence values (in centimeters ± 2σ) are red. Interseismic submergence rates (in millimeters per year, ± 2σ) are blue. Millennial emergence rates are black. Vertical dashed white lines mark dates of emergences. Red arrows at bottom highlight the timing of the failure sequence for each supercycle.

previous earthquake. For the most part, the microatolls document the sloping part of the tooth for only a few decades before the earthquakes. The lack of data immediately after large earthquakes is a consequence of coseismic elevation of the entire reef flat above low tide levels if emergence is greater than about 1 m (*22*). At an interseismic submergence rate of 10 mm/year, one century is needed to bring each vertical meter of the reef flat back below low tide levels and able once again to support coral growth. Thus, we cannot rule out the possibility that the 3.2-m emergence of Bulasat in the mid- to late 1300s could have occurred in more than one closely timed event.

To estimate the magnitude of the preinstrumental emergences, we extrapolate the interseismic subsidence rates back to the dates of the events (dotted sloping lines in Fig. 2A). Coseismic emergences are probably larger than the values given by linear extrapolation, because transient postseismic vertical deformation is commonly opposite in sign to the coseismic signal (*23*). However, this correction would probably be small; subsidence at GPS stations that rose 1.7 to 3 m during the great Nias-Simeulue megathrust earthquake of 2005 has been only about 1% of the uplift value. And during the 6 months after the 73 cm of uplift in September 2007, only 2 cm of subsidence occurred at Bulasat.

The Simanganya site is about 60 km northwest of Bulasat, on the northeastern coast of North Pagai island (Fig. 1) (SOM, including figs. S11 to S24). The records at Simanganya and Bulasat are strikingly similar but not identical (Fig. 2).

The oldest large field of microatolls at Simanganya died late in the 14th century (Fig. 2B). The weighted mean date of death of five colonies is 1381 ± 9. This emergence appears to have occurred about one to six decades later than emergence at Bulasat.

The record of events around 1600 is complicated. Discordant elevations of 16th-century microatolls hint at significantly variable settling due to seismic shaking at the site. Thus, we use the elevation of the highest microatoll to infer sea level at the time of the first emergence, 1560 ± 3. Two microatolls constrain the magnitude of emergence to ~20 cm. The longest-lived microatoll records a large emergence in 1613 ± 29, preceded by two small emergences of ~10 and >10 cm about 5 and 25 years earlier. Thus, Simanganya experienced three small emergences in the decades before the big event of about 1613.

One of the Simanganya microatolls records emergences that we associate with the 1797 and 1833 earthquakes (*5*). Its internal stratigraphy implies that emergence was about 10 cm in 1797. A modern specimen yields a record of submergence for the latter half of the 20th century. Linear extrapolation of this record back in time yields ~1.7 m of emergence in 1833. During the seismic episode of September 2007, vertical deformation at Simanganya was nil (table S1A).

At Sikici, on the northeast coast of Sipora island, large emergences occurred in the late 14th century, late in the 16th century, late in the 17th century, and in 1833 and 2007 (Fig. 2C) (SOM, including figs. S25 to S41).

Evidence for emergence in ~1374 appears in three microatolls that represent a large population. Although we chose these three colonies because of their relatively high degree of preservation and their nearly flat, untilted upper surfaces, the tops of these microatolls vary by tens of centimeters in elevation. This implies that their substrate

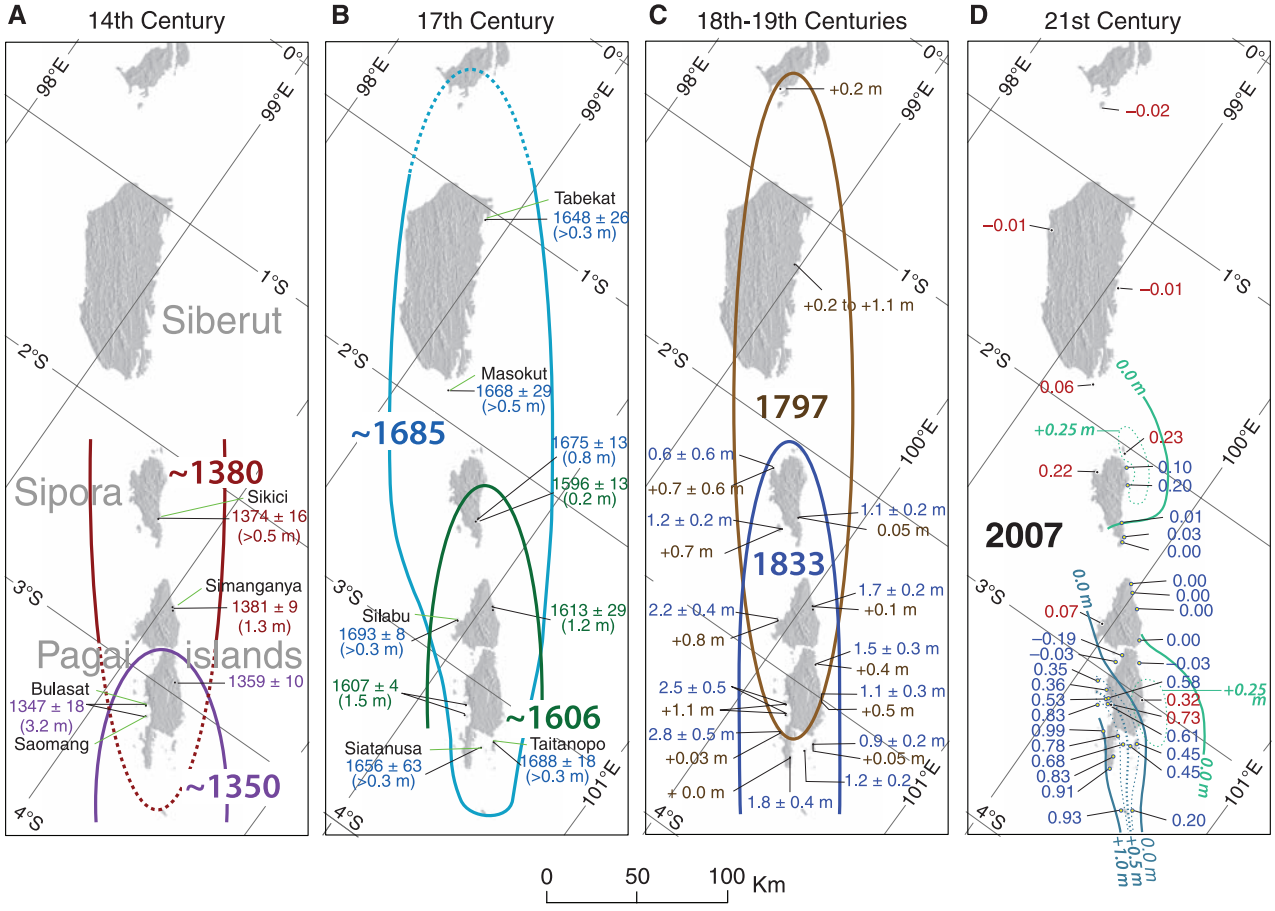

Fig. 3. Four emergence episodes of the past seven centuries. Each episode consists of more than one major event. (**A** and **B**) Emergence amounts are below the year of emergence (±2σ); colors indicate proposed event correlations. (**C**) Emergences attributed to the 1797 and 1833 earthquakes are brown and blue, respectively. (**D**) Uplift values for the 12 to 13 September 2007 sequence are red (GPS) and blue (coral). Contours of uplift in blue and green show the amounts attributable to the M_w 8.4 and M_w 7.9 events, respectively (SOM, including table S1). The 2007 events probably herald the beginning of the next failure sequence.

compacted to different degrees (fig. S4 and arrows in Fig. 2C). Compaction probably occurred during the seismic shaking associated with emergence, because younger microatolls do not display large elevation differences within their populations. The differing elevations of the 14th-century microatolls mean that we can say only that the original elevation of the population relative to modern sea level was at least as high as the highest colony.

Eight sampled Sikici microatolls record events of the 16th and 17th centuries. The best-preserved and dated records show slow sea-level rise from ~1480 to 1590, ~20 cm of emergence in 1596 ± 13, and a subsequent 80 years of sea-level stability, followed by another large emergence in 1675 ± 13. The living outer perimeters of four of the colonies were too thin to survive the 20-cm emergence of ~1596. The best-preserved of these four also show a small (6 cm) emergence 12 to 15 years before death. Such a small emergence could be tectonic, but an oceanographic cause is also plausible.

The 1797 and 1833 events appear in one sample (*5*). A 10-cm emergence 36 years before death appears to represent emergence in 1797. Extrapolation of a 4.4 mm/year rate of submergence from a modern microatoll (*7*) implies about 1.1 m of emergence in 1833. Within error, the magnitude of uplift (1 ± 6 cm) in September 2007 is nil (table S1A).

A few other localities also yielded useful, though shorter and less complete, records. Those that help constrain the 1797 and 1833 events are described in (*5*). Six others assist in piecing together the record before 1797 (SOM, including fig. S1).

The broadly similar sea-level histories of Bulasat, Simanganya, and Sikici imply similar histories of strain accumulation and relief on the underlying megathrust. Throughout the past seven centuries, all three sites have experienced interseismic submergence punctuated by correlated episodes of rapid emergence that are complex in both space and time.

The first emergence episode comprised two events, which occurred first at Bulasat and a decade or so later at the other two sites (Figs. 2 and 3A). The next episode began in ~1560 with a small emergence at Simanganya (Fig. 2B). In about 1600, all three sites rose suddenly (Figs. 2 and 3B). The largest emergence at Sikici was much later, ~1680. Emergence also occurred at about this time at Silabu, Siantanusa, and Taitanopo but could not have been more than about 10 cm at Saomang. Simanganya may also have risen in ~1680, but the reef there might have still been too far out of the water to allow corals to be growing on the reef flat. Two microatolls (figs S42 and S43) suggest that this event extended as far north as Masokut and Tabekat.

Zones of emergence associated with both the great 1797 and 1833 earthquakes span all three major sites (Figs. 2 and 3C), but emergence in 1797 is much less than in 1833. Uplift in 2007 was 73 cm at Bulasat but nil at the other two sites.

Because each of the three past episodes of emergence consists of two or more discrete events, we refer to the broad periods of strain accumulation and relief as supercycles rather than merely cycles (Fig. 2). The corals record only the last few decades of supercycle 1 and only the strain-accumulation phase and initial part of the strain-relief phase of supercycle 4, but they capture all of supercycles 2 and 3.

At each site, emergence over each supercycle varies by no more than 40% (about 1 to 1.2 m at Sikici, 1.2 to 1.8 m at Simanganya, and 1.5 to 3.6 m at Bulasat). Sites with high emergence values are also sites with high rates of interseismic submergence. The largest events at each site are the last events in their failure sequence.

Emergences in 1797, 1833, and 2007 (Figs. 3C and 3D) are well-enough known to model the locations and magnitudes of slip on the megathrust. Tilt of the islands away from the trench implies megathrust ruptures under the islands that extend updip to the west (*5*, *12*). The similarity of emergence values in 1797, 1833, and 2007 to those in earlier centuries suggests that megathrust slip in the earlier episodes was also centered beneath and west of the islands.

At each site, rates of interseismic submergence show little variation from supercycle to supercycle. This implies that the pattern of coupling (locking) on the megathrust defined by 20th-century coral and GPS data (*6*, *7*) has persisted through the interseismic periods of the past several supercycles. The only major exception is Sikici's flat interseismic curve between ~1600 and 1680. This aberration may imply that the megathrust beneath Sikici was largely decoupled during those eight decades.

At least two of the three ancient failure sequences began with events that were smaller than their culminating events. Moreover, the megathrust rupture of September 2007 is far smaller than the amount of potential slip that has accumulated since the 1797-1833 couplet (Fig. 4 and fig. S44).

Failure initiation by smaller ruptures and the emergence of individual sites during both these and culminating large events imply either structural or rheological heterogeneity of the megathrust. As stresses approach failure levels, patches that are slightly more prone to failure yield first. The size of these patches may limit slip to less than the full 10 m or so of accumulated potential slip. Years or decades later, when the stronger patches fail, the remaining potential slip on the weaker patches is relieved in concert with slip on the stronger patches (Fig. 4 and fig. S44A). Thus, the culminating large earthquake has a larger magnitude than the initiating large earthquake. Because smaller earthquakes have also preceded some (*24*, *25*), though not all, large modern ruptures elsewhere, this mechanism may commonly apply.

The 700-year record of Sumatran megathrust supercycles implies that the M_w 8.4 earthquake of 2007 was the beginning of an episode of failure of the Mentawai patch. If previous cycles are indicative of the one now in progress, the earthquakes of 2007 will turn out to be smaller than the culminating earthquake of supercycle 4. In fact, the amount of potential slip that was not relieved in September 2007 is enough to generate a M_w 8.8 earthquake.

This event would generate widely distributed strong seismic shaking in western Sumatra and would undoubtedly produce great damage in Padang and neighboring cities and villages. Moreover, models based on the rupture of rectangular sources under the Mentawais yield tsunami with several meters of overland flow depth along the coast at Padang and Bengkulu and 1 km or so of inundation distance (*26*). These results imply that losses of life and property could equal or exceed those in Aceh province in 2004.

Over the past 700 years, three episodes of emergence lasted variously from a few decades to a little over a century. This past variability precludes a precise empirical forecast of the next great earthquake and tsunami. Nonetheless, to those living in harm's way on the coasts of western Sumatra, it should be useful to know that the next great earthquake and tsunami are likely to occur within the next few decades, well within the lifetimes of children and young adults living there now.

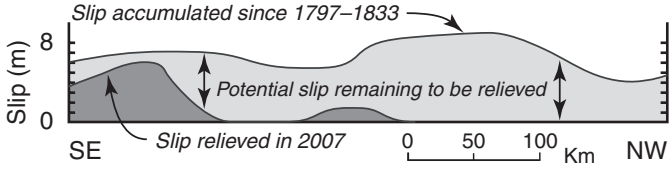

Fig. 4. Comparison of slip during the 2007 events and remaining potential slip on the Mentawai patch. The long axis is parallel to and through the Mentawai island chain. See SOM, fig. S44, and (*12*) for more details.

References and Notes

1. M. Chlieh *et al.*, *Bull. Seismol. Soc. Am.* **97**, S152 (2007).
2. H. R. DeShon, E. R. Engdahl, C. H. Thurber, M. Brudzinski, *Geophys. Res. Lett.* **32**, L24307 (2005).
3. R. W. Briggs *et al.*, *Science* **311**, 1897 (2006).
4. R. E. Abercrombie, M. Antolik, G. Ekström, *J. Geophys. Res.* **108**, 2018 (2003).
5. D. H. Natawidjaja *et al.*, *J. Geophys. Res.* **111**, B06403 (2006).
6. M. Chlieh, J.-P. Avouac, K. Sieh, D. H. Natawidjaja, J. Galetzka, *J. Geophys. Res.* **113**, B05305 (2008).
7. D. H. Natawidjaja *et al.*, *J. Geophys. Res.* **112**, B02404 (2007).
8. K. Sieh, paper presented at the International Workshop on Tectonics of Plate Convergence Zones: Toward the Seamless Understanding from Earthquake Cycles to Geomorphic Evolution, University of Tokyo, Tokyo, Japan, 28 to 29 September 2006.

9. K. Sieh, *Philos. Trans. R. Soc. London Ser. A* **364**, 1947 (2006).
10. K. Sieh, paper presented at the First International Conference of Aceh and Indian Ocean Studies, Banda Aceh, Indonesia, 24 to 26 February 2007.
11. K. Sieh, *J. Earthquake Tsunami* **1**, 1 (2007).
12. O. Konca *et al.*, *Nature* **456**, 631 (2008).
13. J. Zachariasen, K. Sieh, F. W. Taylor, R. L. Edwards, W. S. Hantoro, *J. Geophys. Res.* **104**, 895 (1999).
14. J. Zachariasen, K. Sieh, F. W. Taylor, W. S. Hantoro, *Bull. Seismol. Soc. Am.* **90**, 897 (2000).
15. D. H. Natawidjaja *et al.*, *J. Geophys. Res.* **109**, B04306 (2004).
16. D. R. Stoddart, T. P. Scoffin, *Atoll Res. Bull.* **224**, 1 (1979).
17. C. Darwin, *The Structure and Distribution of Coral Reefs* (Smith, Elder and Co., London, 1842).
18. R. L. Edwards, F. W. Taylor, G. J. Wasserburg, *Earth Planet. Sci. Lett.* **90**, 371 (1988).
19. C.-C. Shen *et al.*, *Geochim. Cosmochim. Acta* **72**, 4201 (2008).
20. C.-C. Shen *et al.*, *Chem. Geol.* **185**, 165 (2002).
21. We use the terms "submergence" and "emergence" throughout to refer to changes with respect to a sea-level datum. We use "subsidence" and "uplift" in reference to other geodetic data and when inferring vertical tectonic motions.
22. K. Sieh, *Nature* **434**, 573 (2005).
23. Y.-J. Hsu *et al.*, *Science* **312**, 1921 (2006).
24. K. Sieh, M. Stuiver, D. Brillinger, *J. Geophys. Res.* **94**, 603 (1989).
25. G. Carver *et al.*, *Bull. Seismol. Soc. Am.* **94**, S58 (2004).
26. J. C. Borrero, K. Sieh, M. Chlieh, C. E. Synolakis, *Proc. Natl. Acad. Sci. U.S.A.* **103**, 19673 (2006).
27. This work has been supported by NSF grants EAR-9628301, 9804732, 9903301, 0208508, 0530899, 0538333, and 0809223 (to K.S.) and EAR-0207686 and 0537973 (to R.L.E.); by National Science Council grants 94-2116-M002-012 and 95&96-2752-M002-012-PAE (to C.-C.S.); by LIPI (Indonesian Institute of Science) and RUTI (International Joint Research Program of the Indonesian Ministry of Research and Technology); and by the Gordon and Betty Moore Foundation. This is Caltech Tectonics Observatory contribution number 86 and Earth Observatory of Singapore contribution number 1.

Supporting Online Material

www.sciencemag.org/cgi/content/full/322/5908/1674/DC1
SOM Text
Figs. S1 to S44
Tables S1 to S4
References

22 July 2008; accepted 8 October 2008
10.1126/science.1163589

Shock Metamorphism of Bosumtwi Impact Crater Rocks, Shock Attenuation, and Uplift Formation

Ludovic Ferrière,[1] Christian Koeberl,[1]* Boris A. Ivanov,[2] Wolf Uwe Reimold[3]

Shock wave attenuation rate and formation of central uplifts are not precisely constrained for moderately sized complex impact structures. The distribution of shock metamorphism in drilled basement rocks from the 10.5-kilometer-diameter Bosumtwi crater, and results of numerical modeling of inelastic rock deformation and modification processes during uplift, constrained with petrographic data, allowed reconstruction of the pre-impact position of the drilled rocks and revealed a shock attenuation by ~5 gigapascals in the uppermost 200 meters of the central uplift. The proportion of shocked quartz grains and the average number of planar deformation feature sets per grain provide a sensitive indication of minor changes in shock pressure. The results further imply that for moderately sized craters the rise of the central uplift is dominated by brittle failure.

During the contact and compression phase of hypervelocity impact, a spherical shock wave is generated, propagates through the target rocks (*1*), and is attenuated rapidly with increasing distance. Consequently, a variety of shock effects are produced in rock-forming minerals, including formation of planar deformation features (PDFs) and high-pressure phases. The relative spatial distribution of these shock transformations and deformations formed at different pressures and temperatures [e.g., (*2*, *3*)] in autochthonous rocks, at the scale of the impact structure, can be used to estimate maximum shock pressures and, consequently, the rate of shock attenuation. However, many parameters—such as rock type as well as lithological contrasts, texture, fabric, grain size, preshock orientation of grains, porosity, and volatile content—influence the shock levels attained locally. Furthermore, and typical in the case of complex impact structures (i.e., craters with diameters ≥2 to 4 km on Earth) (*4*), the original position and distribution of the shocked rocks is modified when, because of gravitational instability of the transient cavity rim, rebound of the crater floor leads to formation of a central uplift. Redistribution of rock is also associated with the collapse of the initially oversteepened central uplift (*5*).

There have been several efforts to estimate shock wave decay, mainly from nuclear and explosion crater studies or by numerical modeling [e.g., (*6*–*8*)]. Few studies have tried to quantify shock pressure distribution in simple (*9*) and complex impact structures (*9*–*16*) [see supporting

[1]Department of Lithospheric Research, University of Vienna, Althanstrasse 14, A-1090 Vienna, Austria. [2]Institute for Dynamics of Geospheres, Russian Academy of Sciences, Leninsky Prospect 38-1, 119334 Moscow, Russia. [3]Museum of Natural History (Mineralogy), Humboldt University, Invalidenstrasse 43, D-10115 Berlin, Germany.

*To whom correspondence should be addressed. E-mail: christian.koeberl@univie.ac.at

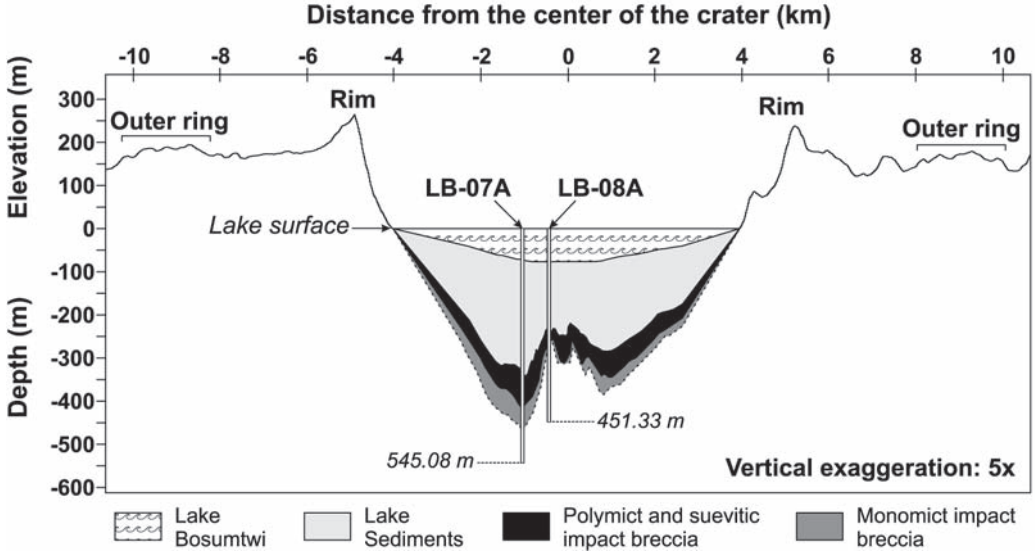

Fig. 1. Cross section of the Bosumtwi impact structure, based on Shuttle Radar Topography Mission (SRTM) data for the regional topography of the exposed portion of the crater (profile from west to east) and on a northwest-southeast seismic reflection profile (*21*) across the central crater. Location of boreholes LB-07A and LB-08A are given. The volume of lake sediments is based on seismic reflection data. The distribution of polymict and suevitic impact breccia and monomict impact breccia is based on observations from cores LB-07A and LB-08A (*19*, *20*), as well as interpretations of seismic reflection data. Depths and elevations are relative to lake level. SRTM data were available online (www2.jpl.nasa.gov/srtm/; accessed 3 March 2008).

online material (SOM text)] by using the frequency of shock-induced deformations in quartz grains from samples taken along profiles across the erosion surface of an impact structure. Only three investigations have explored the relative vertical decay of recorded shock pressure in complex impact structures, two for the ~40-km-diameter Puchezh-Katunki impact structure (*13*, *15*) and another for the ~65-km-diameter Kara crater (*11*).

We characterized the shock wave attenuation in the uppermost part of the central uplift of the Bosumtwi impact structure, a moderately sized (10.5-km diameter) and well-preserved complex impact structure [e.g., (*17*)], and attempted to reconstruct the original position of the sampled section in the target before crater modification. This is possible by combining petrographic investigations (at the microscale) with modeling of inelastic rock deformation (at the mesoscale) and modification processes during uplift (at the megascale). This approach allows us to constrain shock wave attenuation and rock deformation during central uplift formation.

We studied drill core samples from the central part of the structure retrieved in the 2004 International Continental Scientific Drilling Program (ICDP) Bosumtwi drilling project (*18*–*20*) (SOM text). The central uplift extends ~130 m above the crater moat, is ~1.9 km wide (*21*), and is composed of metasedimentary rocks [mostly metagraywacke (MGW) and shale] (*19*). Two cores were retrieved by the ICDP project: core LB-08A from the outer flank of the central uplift and core LB-07A from the deep crater moat (Fig. 1 and SOM text).

To derive the distribution of shock metamorphic effects with depth, we studied 18 MGW samples from 271.4- to 451.2-m depth in core LB-08A (Fig. 1), recording modal analysis and shock deformation properties of 8991 quartz grains (*22*) (tables S1 and S2). We determined 1056 crystallographic orientations of sets of PDFs in 602 quartz grains (table S3) because predominance of specific orientations of PDFs in quartz has long been considered to indicate different shock pressures [e.g., (*23*)].

The abundance of shocked quartz grains (i.e., quartz grains with planar fractures and/or PDFs) decreases with increasing depth (for PDFs, compare with Fig. 2). We interpret this decrease to reflect the variation of shock pressure in the uppermost part of the central uplift. Similarly, the average number of PDF sets per quartz grain (*N*) decreases steadily with depth, from ~2.1 at 271-m depth to ~1.6 at 442 m (Fig. 3). We interpret the decrease of *N* as evidence of the shock pressure attenuation with distance from shock wave origin.

No clear change was evident over this interval in the relative frequencies of the main crystallographic orientations of PDF sets in quartz grains with increasing depth (Fig. 2 and table S3). Most of the poles to the PDF planes correspond to the $\omega\{10\bar{1}3\}$ orientation, and only a few, typically less than 5 relative-percent (rel%) of the orientation data obtained per section, correspond to basal [i.e., parallel to (0001)] planes. Only two samples, KR8-85 and KR8-89, from 390- to 400-m depth, show a higher proportion of basal PDF, at about 27 and 19 rel%, respectively (table S3). These two MGW samples originated just below a 10-m-thick layer of comparatively fine-grained metasedimentary rocks (phyllite and slate; Fig. 2); thus, it is possible that shock wave interference at the transition from metapelite to MGW resulted in the local formation of a larger proportion of basal PDFs [basal PDFs are formed at lower pressures (from 8 to 10 GPa) than $\omega\{10\bar{1}3\}$ orientations (>10 GPa); e.g., (*2*)]. However, about 50% of the basal PDFs measured in these two samples occur in association with $\omega\{10\bar{1}3\}$ PDF (i.e., dual sets of PDFs in the same quartz grain), which indicates relatively high shock pressures. Thus, minor variations of the relative proportions of crystallographic orientations of PDF sets in quartz grains with depth cannot be used to quantify the slight attenuation of the shock pressure along the ~200-m-long bedrock section investigated here. Because the relative proportion of shocked quartz grains, as well as the number of PDF sets per quartz grain, steadily decrease with depth (Figs. 2 and 3), we infer that the shock wave was attenuated but not by much.

On the basis of the relative abundances of quartz grains with PDFs, the presence of multiple sets of PDFs in quartz grains (up to four sets), and the occurrence of various PDF set orientations, we estimate that the studied section experienced peak shock pressures of up to ~25 to 30 GPa [e.g., (*2*, *24*–*25*)]. The upper limit of peak shock pressure (i.e., 30 GPa) is further constrained by the lack of isotropization of the quartz grains, which typically begins at this shock pressure [e.g., (*2*)]. The estimated pressure range is much too low for either

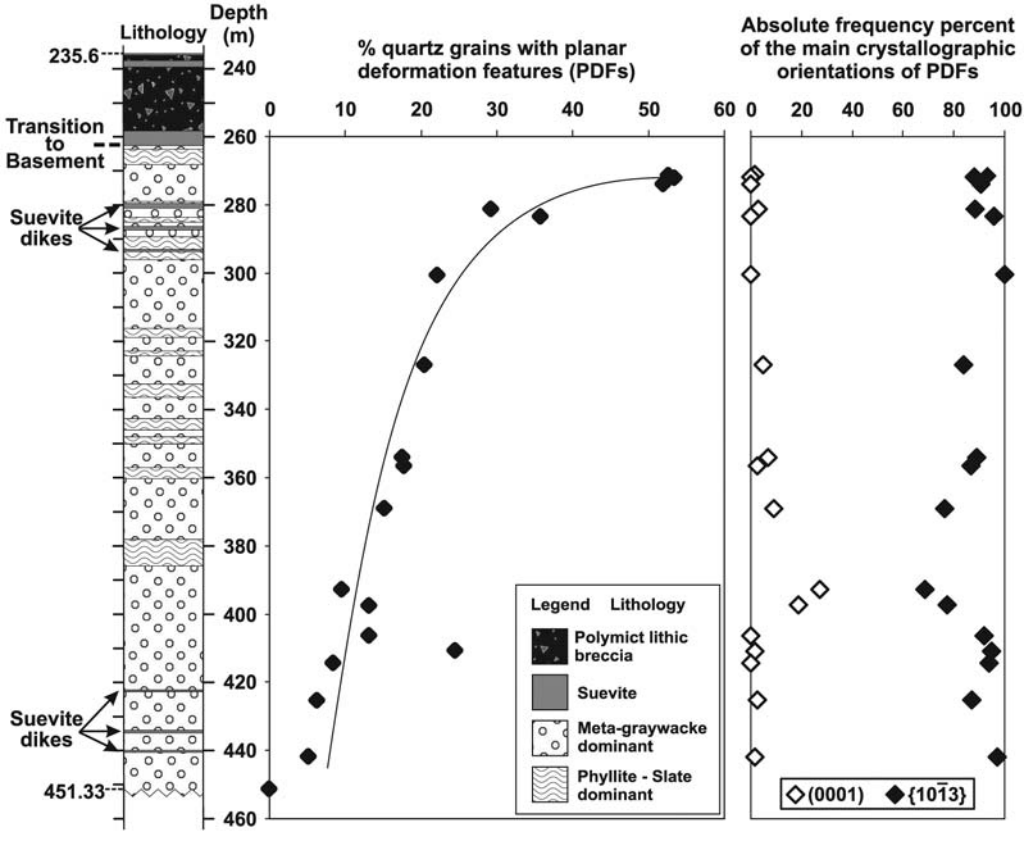

Fig. 2. Simplified lithostratigraphic column for drill core LB-08A [after (*19*)] and PDF data for 18 MGW samples from the basement section. The abundance of quartz grains with PDFs relative to the total number of quartz grains is shown (left, solid diamond) and, on the right, the absolute frequency percent of the two main PDF crystallographic orientations (open diamond symbols for basal PDF and solid diamonds for $\omega\{10\bar{1}3\}$ crystallographic orientation data) in quartz grains, as measured on a universal stage.

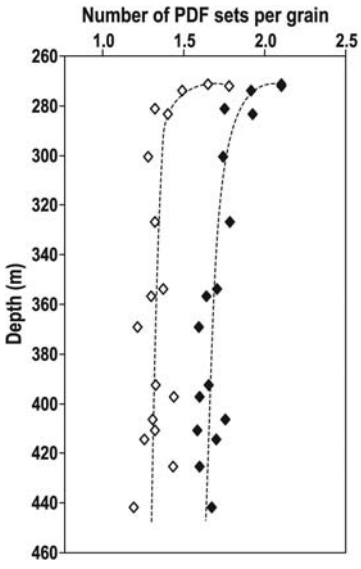

Fig. 3. Average number of PDF sets per host quartz grain (*N*) in MGW samples from the uppermost ~200 m of basement drilled in the central uplift of the Bosumtwi impact structure. For both methods, that is, with use of a petrographic microscope (under horizontal stage examination; open diamonds) and with the U stage (solid diamonds), *N* values follow the same trend of decreasing abundance of PDF sets per grain with increasing depth.

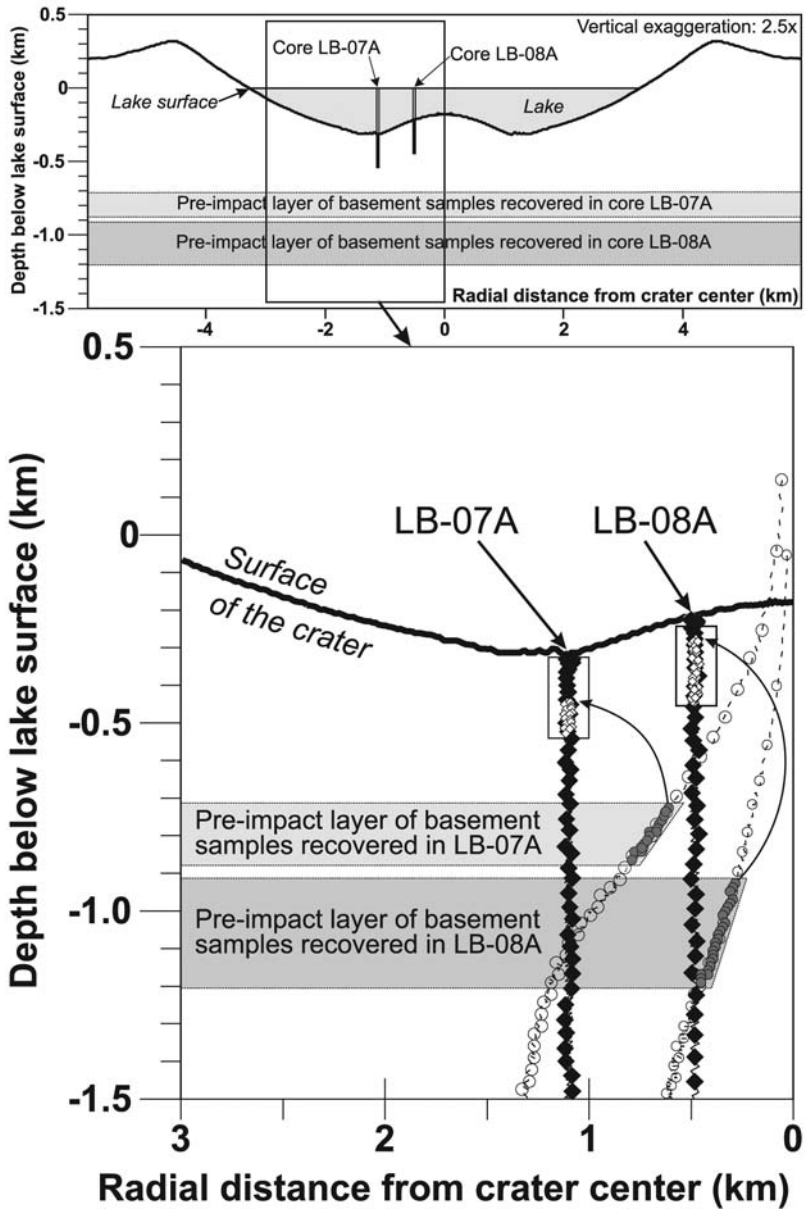

Fig. 4. Calculated crater profile with enlarged inner part showing initial and final positions of rocks recovered in drill cores LB-07A (from the crater moat) and LB-08A (from the outer flank of the central uplift). Solid diamonds show final positions of tracers (0.48- and 1.1-km radial distance from crater center), whereas open circles indicate their initial positions in the preimpact target stratigraphy. Gray dots and open diamonds show, respectively, the initial and the final positions of basement samples (i.e., investigated MGW samples in core LB-08A) recovered in drill cores. Solid diamonds above open diamonds represent the modeled impact breccia. Locations of drill cores are indicated by large open rectangles. Model run with ANEOS (analytical equation of state) granite (*28*), an impact velocity of 20 km^{-1}, and a residual friction (μ) of 0.4. For comparison of the calculated and the actual cross sections of the Bosumtwi crater, see fig. S3.

partial or total shock melting of the whole rock, which is in agreement with macroscopic and microscopic observations on these metasedimentary rocks that have preserved their preimpact texture (*19*) (SOM text). Thus, the rise of the central uplift was not facilitated by shock-induced plasticity, and brittle failure was dominant. This finding is also supported by the presence of abundant faults in the central uplift, as indicated by reflection seismic data (*21*).

To further evaluate the apparent shock attenuation, we calculated the expected shock pressure attenuation and reconstructed the preimpact position of the investigated section of the central uplift by numerical modeling, by using a variant of the SALEB numerical code (*26*) (SOM text). To model the crater and central uplift properly, we did a direct parametric fit of our model to the observed crater geometry without usage of scaling relations for the crater size (SOM text and fig. S3). After modeling, tracers in the vicinity of the exact location of the two drill holes were identified (allowing the tracking of their initial positions), and lastly the position of the top of the "model core" was defined by the maximum recorded shock pressure of 30 GPa (based on our petrographic investigations). Then, the initial position of these tracers was plotted (Fig. 4). Our calculations show that, despite quite similar present-day depths, the initial depth of rocks in the crater moat (core LB-07A) was above that of the rocks in the central uplift corehole (Fig. 4). This specific displacement of the target rocks during crater modification is interesting because it indicates that rocks occurring in the outer flank of the central uplift were originally more deeply buried than the basement rocks drilled below the deep crater moat and, thus, were subjected to somewhat lower shock pressures. Thus, before estimating shock attenuation in complex impact structures, it is important to consider the differential movements of the target rocks, which cause changes in the spherical shock-attenuation scheme. The numerical model (Fig. 4 and SOM text) indicates that the samples investigated in core LB-08A have been uplifted by about 1.2 to 1.5 km. By using the relationship $SU = 0.086D^{1.03}$ (*27*) (where D is the crater diameter), we estimated the amount of structural uplift (*SU*) for the Bosumtwi central uplift at about 1 km, in good agreement with the modeling result.

Taking into account the uplift of target rocks, the calculated apparent shock attenuation along the about-200 m of investigated core is ~5 to 10 GPa (fig. S4). On the basis of the general absence of

changes in the statistics of PDF orientations, a maximum shock attenuation of 5 GPa seems to be the more realistic value.

The percentage of shocked quartz grains and the number of PDF sets per grain are more sensitive indicators of minor changes in shock pressure than pure PDF orientation statistics. The combination of detailed petrographic investigation and numerical modeling indicates that both of these approaches are essential to reconstruct the preimpact position of rocks and to characterize properly the shock pressure distribution at the scale of an impact structure. Our observations suggest that, in the case of the 10.5-km-diameter Bosumtwi impact structure, the uppermost rocks of the central uplift experienced shock pressures below 30 GPa, whereas pressures up to 40 to 45 GPa were recorded for the about-four-times-larger Puchezh-Katunki impact structure (*15*). Shock attenuation in the uppermost part of a central uplift has been, for the first time, constrained by detailed shock degree profiling at the microscale. Numerical modeling of this section of the central uplift has then established where this section of the central uplift was located before uplift formation, which was only possible once the shock regime had been established by micropetrography. The results imply that, for moderately sized impact craters, the rise of the central uplift is dominated by brittle failure, whereas in the case of larger impact structures, and also depending on rock proprieties, the uplifted, relatively stronger shocked rocks may behave in a more ductile manner.

References and Notes

1. D. Stöffler, *Fortschr. Mineral.* **49**, 50 (1972).
2. D. Stöffler, F. Langenhorst, *Meteorit. Planet. Sci.* **29**, 155 (1994).
3. R. A. F. Grieve, F. Langenhorst, D. Stöffler, *Meteorit. Planet. Sci.* **31**, 6 (1996).
4. R. A. F. Grieve, *Annu. Rev. Earth Planet. Sci.* **15**, 245 (1987).
5. H. J. Melosh, *Impact Cratering: A Geological Process* (Oxford Univ. Press, New York, 1989).
6. J. T. Cherry, F. L. Petersen, in *Peaceful Nuclear Explosions* (International Atomic Energy Agency, Vienna, 1970), pp. 241–325.
7. T. J. Ahrens, J. D. O'Keefe, in *Impact and Explosion Cratering*, D. J. Roddy, R. O. Pepin, R. B. Merrill, Eds. (Pergamon, New York, 1977), pp. 639–656.
8. N. K. Mitani, *J. Geophys. Res.* **108**, 5003 (2003).
9. P. B. Robertson, R. A. F. Grieve, in *Impact and Explosion Cratering*, D. J. Roddy, R. O. Pepin, R. B. Merrill, Eds. (Pergamon, New York, 1977), pp. 687–702.
10. R. A. F. Grieve, P. B. Robertson, *Contrib. Mineral. Petrol.* **58**, 37 (1976).
11. L. V. Sazonova, N. N. Karotaeve, G. Y. Ponomarev, A. I. Dabizha, in *Impactites*, A. A. Marakushev, Ed. (Moscow State Univ., Moscow, 1981), pp. 93–133.
12. R. A. F. Grieve, J. M. Coderre, P. B. Robertson, J. Alexopoulos, *Tectonophysics* **171**, 185 (1990).
13. V. I. Fel'dman, L. V. Sazonova, S. I. Kotel'nikov, *Dokl. Akad. Nauk SSSR* **349**, 658 (1996).
14. B. O. Dressler, V. L. Sharpton, B. C. Schuraytz, *Contrib. Mineral. Petrol.* **130**, 275 (1998).
15. V. L. Masaitis, L. A. Pevzner, *Deep Drilling in the Impact Structure: Puchezh-Katunki, Russia* (VSEGEI, St. Petersburg, 1999).
16. R. L. Gibson, W. U. Reimold, *Geol. Soc. Am. Spec. Pap.* **384**, 329 (1996).
17. C. Koeberl, W. U. Reimold, *Yearb. Austrian Geol. Surv.* **145**, 31 (2005).
18. C. Koeberl *et al.*, *Meteorit. Planet. Sci.* **42**, 483 (2007).
19. L. Ferrière, C. Koeberl, W. U. Reimold, *Meteorit. Planet. Sci.* **42**, 611 (2007).
20. L. Coney, R. L. Gibson, W. U. Reimold, C. Koeberl, *Meteorit. Planet. Sci.* **42**, 569 (2007).
21. C. A. Scholz *et al.*, *Geology* **30**, 939 (2002).
22. Materials and methods are available as supporting material on *Science* Online.
23. F. Hörz, in *Shock Metamorphism of Natural Materials*, B. M. French, N. M. Short, Eds. (Mono, Baltimore, 1968), pp. 243–253.
24. A. R. Huffman, W. U. Reimold, *Tectonophysics* **256**, 165 (1996).
25. B. M. French, *Traces of Catastrophe: A Handbook of Shock-Metamorphic Effects in Terrestrial Meteorite Impact Structures* [LPI Contribution No. 954, Lunar and Planetary Institute (LPI), Houston, TX, 1998].
26. B. Ivanov, *Sol. Syst. Res.* **39**, 381 (2005).
27. M. J. Cintala, R. A. F. Grieve, *Meteorit. Planet. Sci.* **33**, 889 (1998).
28. E. Pierazzo, A. M. Vickery, H. J. Melosh, *Icarus* **127**, 408 (1997).

29. Drilling was funded by ICDP, NSF, the Austrian Fonds zur Förderung der wissenschaftlichen Forschung (FWF), the Canadian Natural Sciences and Engineering Research Council, and the Austrian Academy of Sciences. We thank DOSECC (Drilling, Observation and Sampling of the Earth's Continental Crust) for the drilling operations. This work was supported by the Austrian FWF (grants P17194-N10 and P18862-N10) and the Austrian Academy of Sciences. B.A.I. was supported by the Russian Foundation for Basic Science (RFBR grant 08-05-00908-a), and W.U.R.'s research is supported by the German Science Foundation (Deutsche Forschungsgemeinschaft) and Humboldt University of Berlin.

Supporting Online Material

www.sciencemag.org/cgi/content/full/322/5908/1678/DC1
Materials and Methods
SOM Text
Figs. S1 to S4
Tables S1 to S4
References

23 September 2008; accepted 10 November 2008
10.1126/science.1166283

The Spreading of Disorder

Kees Keizer,* Siegwart Lindenberg, Linda Steg

Imagine that the neighborhood you are living in is covered with graffiti, litter, and unreturned shopping carts. Would this reality cause you to litter more, trespass, or even steal? A thesis known as the broken windows theory suggests that signs of disorderly and petty criminal behavior trigger more disorderly and petty criminal behavior, thus causing the behavior to spread. This may cause neighborhoods to decay and the quality of life of its inhabitants to deteriorate. For a city government, this may be a vital policy issue. But does disorder really spread in neighborhoods? So far there has not been strong empirical support, and it is not clear what constitutes disorder and what may make it spread. We generated hypotheses about the spread of disorder and tested them in six field experiments. We found that, when people observe that others violated a certain social norm or legitimate rule, they are more likely to violate other norms or rules, which causes disorder to spread.

In the mid-1990s, the mayor of New York and his police commissioner adopted a "Quality of life campaign." Attention was focused on fighting signs of disorder and petty crime. Graffiti was removed, streets were swept, and signs of vandalism were cleared. This initiative was based on the broken windows theory (BWT) of Wilson and Kelling (*1*). The BWT suggests that signs of disorder like broken windows, litter, and graffiti induce other (types of) disorder and petty crime (*2*). It was thought that removing these signs of disorder would take away an important trigger of disorderly and petty criminal behavior. After the introduction of the campaign, petty crime rates in New York dropped. Since then, approaches based on the BWT have become popular and have been adopted worldwide (e.g., in various cities in the United States, Great Britain, Netherlands, Indonesia, and South Africa).

BWT may be very popular, but it is also highly controversial. So far, it lacks empirical support, and it fails to specify what constitutes disorder. Studies aimed to test the BWT (*3*–*6*) have provided mixed results at best. The National Research Council (NRC) concluded that the research did not provide strong support for the BWT (*7*). There is also little evidence that broken window policing contributed to the sharp decrease in petty crime in New York (*8*–*10*). Moreover, to our knowledge, research on the BWT has so far been correlational, so conclusions about causality are shaky (*6*, *8*). The BWT suggests that a setting with disorder triggers disorderly and petty criminal behavior, but it might be the other way around or both may be caused by a third variable. Furthermore, the BWT gives no insight into what is and what is not a condition of disorder that will spread. Because the BWT forms the backbone of many cities' defense against the growing threat of disorder and petty crime, these shortcomings need to be addressed.

In the present study, we conducted six field experiments that address these issues. Our first step was to conceptualize a disorderly setting in such a way that we can link it to a process of spreading norm violations. Social norms refer either to the perception of common (dis)approval of a particular kind of behavior (injunctive norm) or to a particular behavior common in a setting (descriptive norm) (*11*–*16*). Injunctive norms affect behavior because they provide information about which behavior is most appropriate in a

Faculty of Behavioral and Social Sciences, University of Groningen, 9712 TS Groningen, Netherlands.

*To whom correspondence should be addressed. E-mail: K.E.Keizer@rug.nl

given situation [e.g., (*17*–*19*)]. For example, the antilitter norm is a widely held injunctive norm [e.g., (*20*, *21*)]. The extent to which an injunctive norm affects behavior depends on how much the norm is on people's mind (*22*, *23*). For example, an antilitter norm will be more on people's minds when they see someone picking up a piece of litter (which shows disapprovement of littering) (*12*) or simply see a norm stated on a sign (*24*, *25*). Descriptive norms affect behavior because they provide information about which behavior is most common in a given situation. For example, a littered setting shows that it is common to litter and will therefore enhance littering (*11*, *26*, *27*). Similar to injunctive norms, the more conspicuous the descriptive norm, the more strongly it influences behavior. For example, the probability that a participant litters in a littered setting is enhanced when a lot of litter is present or when the participant watches someone littering (*11*). Injunctive and descriptive norms can be in conflict, as for example in a setting where it is common to litter even though littering is commonly disapproved of. Thus, settings described in BWT as disorderly (e.g., a littered setting) can be conceptualized as settings in which descriptive and injunctive norms are in conflict. The next question then is how behavior is influenced by such a setting.

Injunctive-norm information in a persuasive message is more effective when accompanied by descriptive norm information that is in alignment rather than in conflict with that message (*24*, *28*–*30*). For example, a sign drawing attention to the antilitter norm is more influential in reducing littering when placed in a nonlittered setting than when it is placed in a prelittered setting (*31*). Thus, a setting with graffiti, described by the BWT as a setting showing disorder, can cause the spraying of graffiti because it inhibits the injunctive antigraffiti norm. In honor of the individual who first described this process, we call this the Cialdini effect. The important question for the BWT is whether or not it also causes disorderly (or petty criminal) behavior in general. The question we will address is the following: Do more people litter or even steal in a setting where the antigraffiti norm (injunctive norm) is in conflict with the descriptive norm (setting shows it is common to spray graffiti)?

The Cialdini effect has its basis in people's tendency to reason "if a lot of people are doing this, it's probably a wise thing to do" and to do what they observe others are doing (*32*) However, we believe that there is another, goal-driven mechanism at work as well, which is particularly important for the spread of disorder. Much conformity to injunctive norms is the result of people pursuing the goal to act appropriately. However, people can also pursue a hedonic goal directed at feeling better right now or a gain goal directed at guarding and improving one's resources. All three goals can be in conflict, and the weakening of one is likely to bring another goal to the fore (*33*). In a given situation, the goal to act appropriately is weakened when people observe that others seemingly did (or do) not pursue the goal to act appropriately. In turn, a weakening of this goal strengthens conflicting hedonic and gain goals. For example, when people observe that others have painted graffiti where it should not have been painted, they actually observe inappropriate behavior. This, we predict, weakens their concern for appropriateness and strengthens the goal to do what makes them feel good (for example, by being lazy and throwing paper on the street) or the goal to gain resources (say by stealing). Thus people don't necessarily copy the inappropriate behavior they observe but let concerns other than appropriateness take center stage. In this way, one norm violation fosters violations of other norms, and disorder spreads from one kind of inappropriate behavior to other kinds. We call this the cross-norm inhibition effect. An important implication of this "goal-framing" theory for the BWT is that the effect should not be limited to social norms in the strict sense of the word but would also apply to all sorts of legitimate rules, such as laws, police ordinances, or even legitimate rules established by private companies.

To test this theory, we conducted controlled field experiments in common public spaces (*34*), that is, in locations where ordinary "broken window" kind of disorder could be observed.

Fig. 1.

Participants were people in the public space judged to be 18 years or older. There were no signs in any of the studies that they were aware of being observed by the experimenter. We distinguished between a contextual norm (which the participant witnessed having been violated) and a target norm (a violation committed by the participant).What we manipulated were the indications that the contextual norm was being violated. What we observed as a dependent variable was the relative number of individuals who then violated the target norm, which was inconvenient or costly to follow in this situation. We predicted that disorder (violation of contextual norm) would spread (violation of target norm). To study the robustness of this cross-norm inhibition effect, we conducted six different studies. For ease of description, let us call the situation in which the contextual norm is violated (i.e., inappropriate behavior by others is being displayed) the disorder condition and the one in which it is not violated the order condition. Other factors possibly influencing the results were kept constant between conditions (no signs of other norm or rule violations, same weather conditions, and same period of the day). A confederate posted out of sight observed whether participants did or did not violate the target norm. Gender was coded at first but turned out not to have any impact on the results and was dropped in later experiments. The arrangements in all experiments were such that it was virtually impossible for people not to notice the violations of injunctive norms (such as graffiti, wrongly parked bicycles, and firecrackers).

In study 1, the setting was an alley in Groningen located in a shopping area and commonly used to park bicycles. In the order condition, the walls of the alley were clean (Fig. 1A), whereas in the disorder condition they were covered with graffiti (Fig. 1B). A standard prohibition sign (a round red sign with a round white center) with the text "Graffiti" pointed out the disapproved behavior. The sign was highly noticeable, and every subject entering the setting at least glanced at it. Participants ($N = 77$ in each condition) were all people who came to collect their parked bicycles. In their absence, a flyer with an elastic band had been attached to the handlebar of their bicycle. The flyer was white and thus very noticeable. It read: "We wish everybody happy holidays," signed with the name of a nonexistent sportswear shop. The flyer had to be removed by the participant to easily use the handlebar. Because there were no trash cans in the alley, "not littering" meant taking the flyer with them. We counted throwing the flyer on the ground or hanging it on another bicycle as littering.

The cross-norm inhibition effect of violating the antigraffiti norm on littering was quite substantial. Of the participants in the order condition (nongraffiti), 33% littered compared with 69% of the participants in the disorder condition (graffiti on the walls). The difference is highly significant [$\chi^2(1, 154) = 20.367$, $P < 0.001$]. In Groningen, littering is generally tolerated by the police so that the effect could not be explained by a guess on law enforcement, such as "if people haven't been caught painting graffiti, I will not be caught dropping paper."

We designed the next studies to include a variety of norms in order to address two questions. We wanted to determine whether the cross-norm inhibition effect was restricted to generally accepted social norms or whether, as expected by the goal-framing theory, it also extended to local ordinances by the police or even to normative requests set up by private companies. We also wanted to determine how far the influence would go. In other words, would a norm violation just affect relatively light infractions, such as littering, or would it go so far as to affect the willingness to violate such serious norms as "thou shalt not steal"?

For study 2, we used a police ordinance as a contextual norm and "no trespassing" (as ordered by the police) as the target norm in the setting of a car park. Thus, both contextual and target norms were not general social norms but rules set up by the local police for a particular local situation. A temporary fence (set up by us) closed off the main entrance for people who came to pick up their car, but a gap of about 50 cm was left open in the fence (Fig. 2). We attached two signs to the temporary fence just 60 cm apart and directly next to the gap. The right sign (our contextual norm) indicated that it was prohibited to lock bicycles to the fence. The left sign (our target norm) made clear that it was prohibited to use this entrance and that people had to use an alternative entrance to the car park, which required walking a 200-m detour. In the order condition, four bicycles standing 1 m before the fence were ostensibly not locked to the fence.

In the disorder condition, four bicycles were locked to the fence for everyone to see. The dependent variable was whether pedestrians conformed to the "no throughway" sign (the target

Fig. 2.

Fig. 3.

norm) and walked the 200-m detour to the temporary entrance that was pointed out by the sign. Violating the "no throughway" ordinance meant stepping through the gap in the fence. Subjects (N = 44 in the order condition and N = 49 in the disorder condition) were all people who came to collect their car from the car park. A group of people approaching the fence was counted as one subject.

Again there was a clear cross-norm inhibition effect. Of the participants in the order condition (where bicycles were not locked to the fence), 27% stepped through the gap in the fence, compared with 82% of the participants in the disorder condition (where the bicycles were attached to the fence). The difference is significant [$\chi^2(1, 93) = 27.791$, $P < 0.001$].

Would this also hold for a rule set by a private company that is not enforced with sanctions? In study 3, a parking garage adjacent to a supermarket and health club was used in which the contextual norm established by the private company is to return shopping carts to the supermarket after loading groceries into one's car. A very visible sticker with the text: "please return your shopping carts" attached to the entrance doors of the parking garage focused attention on this normative request (Fig. 3). In the order condition, the garage was clear of shopping carts that were not returned. In the disorder condition, there were four unreturned shopping carts standing around in disarray. The (unreturned) carts used in the disorder condition had no coin deposit system, so people were not financially encouraged to return them. To discourage people who just arrived from using the shopping carts and thus removing the disorder, we smeared the handle bars of the carts with petroleum jelly. Participants (N = 60 in each condition) were visitors of the supermarket and a health club who came to collect their car from the multilevel parking garage. Only people *not* using a shopping cart were included. The target norm was the anti-litter norm, already used in study 1. The dependent variable was whether or not participants who returned to their car littered a flyer (the same flyer as used in study 1) that was placed under the driver's side windshield wiper of their parked car. The results show that even with this private request, a considerable cross-norm inhibition effect could be observed. Of the participants in the condition without shopping carts, 30% littered the flyer, compared with 58% of the participants in the condition for which unreturned shopping carts were present. The difference is significant [$\chi^2(1, 120) = 9.766$, $P = 0.002$].

Is disorder only linked to visual cues of norm violation? Would the cross-norm inhibition effect be of any influence when the contextual norm was merely audible? In our fourth study, we focused on a national law as a contextual norm. In Netherlands it is prohibited by law (with a €60 fine) to set off fireworks in the weeks before New Year's Eve. We wanted to find out, 2 weeks before New Year's Day, whether an offense against this national law would induce people to litter. In contrast to studies 1 to 3, the contextual norm was not made conspicuous (say by a sign stating the law). The law about fireworks is well known, and its violation itself would immediately make the law salient in people's mind. The setting we used was a bicycle shed located near a busy train station. The subjects (N = 50 in the order condition and N = 46 in the disorder condition) were all people who came to collect their parked bicycle. In the order condition, there was no sound of fireworks. In the disorder condition, we set off firecrackers (well within hearing distance of the participants but out of sight to prevent any visual cues). We observed whether participants littered a flyer (the same flyer as used in studies 1 and 3) attached to the handlebar of their bicycle. Of the subjects in the order condition (no fireworks set off), 52% littered the flyer compared with 80% of the subjects that heard fireworks being set off as they entered the bicycle shed. The difference is significant [$\chi^2(1,96) = 8.587$, $P = 0.003$].

For studies 5 and 6, the target norm was stealing, and we examined whether an envelope, visibly containing a €5 note and hanging out of a mailbox, would be stolen more often if a contextual norm was violated. The white (addressed) window envelope sticking out of a mailbox (situated in Groningen) was very noticeable for everyone approaching the mailbox, and it was clearly visible that the envelope contained a €5 note (Fig. 4). The participants were all people who singly passed the mailbox on foot (and the few who actually posted a letter). We conducted a baseline order condition (N = 71) in which the mailbox was not covered with graffiti and the ground around the mailbox was clean. We then conducted two disorder conditions: one in which the mailbox was covered with graffiti without litter on the ground (N = 60, study 5) and one in which there was no graffiti on the mailbox but the space around the mailbox was littered (N = 72, study 6). The circumstances of all three conditions in term of period of the day and weather were held constant. The dependent variable was whether or not people would steal the envelope. Leaving the envelope or pushing it into the mailbox was considered not stealing. Opening the envelope or taking it was considered stealing. Thus, we compared two disorder conditions to the baseline condition.

The study 5 results were quite dramatic. Of the participants in the baseline order condition (no graffiti, no littering), 13% stole the envelope compared with 27% of the subjects in the graffiti disorder condition. The difference is significant [$\chi^2(1, 131) = 4.122$, $P = 0.035$].

The results of study 5 proved to be robust. Compared with the baseline order condition (in which 13% stole the envelope), 25% of the subjects in study 6 stole the envelope in the litter disorder condition. The difference is again significant [$\chi^2(1, 143) = 3.545$, $P = 0.047$]. It is highly unlikely that this effect is due to a guess about the likelihood of law enforcement triggered by littering. People are not likely to infer a low likelihood of law enforcement against stealing from the fact that people littered the street, because in Groningen littering is generally tolerated by the police whereas stealing is not. The most likely interpretation of these results is, as before, that one disorder (graffiti or littering) actually fostered a new disorder (stealing) by weakening the goal of acting appropriately.

Our conclusion is that, as a certain norm-violating behavior becomes more common, it will negatively influence conformity to other norms and rules. The effect was not limited to social norms but also applied to police ordinances and even to legitimate requests established by private companies. The mere presence of graffiti more than doubled the number of people littering and

Fig. 4.

stealing. There is a clear message for policymakers and police officers: Early disorder diagnosis and intervention are of vital importance when fighting the spread of disorder. Signs of inappropriate behavior like graffiti or broken windows lead to other inappropriate behavior (e.g., litter or stealing), which in turn results in the inhibition of other norms (i.e., a general weakening of the goal to act appropriately). So once disorder has spread, merely fixing the broken windows or removing the graffiti may not be sufficient anymore. An effective intervention should now address the goal to act appropriately on all fronts.

References and Notes

1. J. Q. Wilson, G. L. Kelling, "Broken windows," *Atl. Mon.* (March 1982), p. 29.
2. M. Gladwell, *The Tipping Point: How Little Things Can Make a Big Difference* (Little, Brown, Boston, 2000).
3. W. G. Skogan, *Disorder and Decline: Crime and the Spiral of Decay in American Neighborhoods* (Univ. of California Press, Berkeley, 1990).
4. G. Kelling, C. Coles, *Fixing Broken Windows: Restoring Order and Reducing Crime in Our Communities* (Free Press, New York, 1996).
5. G. L. Kelling, W. H. Sousa Jr., *Do Police Matter? An Analysis of the Impact of New York City's Police Reforms* (Manhattan Institute Center for Civic Innovation Civic Report No. 22, New York, 2001).
6. R. J. Sampson, S. W. Raudenbush, *Am. J. Sociol.* **105**, 603 (1999).
7. National Research Council, *Fairness and Effectiveness in Policing: The Evidence*, W. Skogan, K. Frydl, Eds. (National Academies Press, Washington, DC, 2004).
8. B. E. Harcourt, *Mich. Law Rev.* **97**, 291 (1998).
9. J. E. Eck, E. R. Maguire, in *The Crime Drop in America,* A. Blumstein, J. Wallman, Eds. (Cambridge Univ. Press, New York, 2000), pp. 207–265.
10. B. E. Harourt, J. Ludwig, *Univ. Chic. Law Rev.* **73**, 271 (2006).
11. R. B. Cialdini, R. R. Reno, C. A. Kallgren, *J. Pers. Soc. Psychol.* **58**, 1015 (1990).
12. R. B. Cialdini, C. A. Kallgren, R. R. Reno, *Adv. Exp. Soc. Psychol.* **24**, 201 (1991).
13. R. B. Cialdini, *Influence: The Psychology of Persuasion* (Morrow, New York, ed. 2, 1993).
14. J. P. Codol, *Eur. J. Soc. Psychol.* **5**, 457 (1975).
15. J. M. Marques, D. Abrams, D. Páez, C. Martinez-Taboada, *J. Pers. Soc. Psychol.* **75**, 976 (1998).
16. L. S. Shaffer, *J. Mind Behav.* **4**, 275 (1983).
17. S. Chaiken, R. Giner-Sorolla, S. Chen, in *The Psychology of Action: Linking Motivation and Cognition to Behavior*, P. M. Gollwitzer, J. A. Bargh, Eds. (Guilford, New York, 1996), pp. 553–578.
18. R. B. Cialdini, M. R. Trost, in *Handbook of Social Psychology*, D. Gilber, S. Fiske, G. Lindzey, Eds. (McGraw-Hill, Boston, ed. 4, 1998), vol. 2, pp. 151–192.
19. M. Deutsch, H. B. Gerard, *J. Abnorm. Soc. Psychol.* **51**, 629 (1955).
20. L. Berkowitz, *Adv. Exp. Soc. Psychol.* **6**, 63 (1972).
21. L. Bickman, *Soc. Psychol.* **87**, 323 (1972).
22. R. R. Reno, R. B. Cialdini, C. A. Kallgren, *J. Pers. Soc. Psychol.* **64**, 104 (1993).
23. S. H. Schwartz, J. A. Fleishman, *Soc. Psychol.* **41**, 306 (1978).
24. R. B. Cialdini, *Curr. Dir. Psychol. Sci.* **12**, 105 (2003).
25. P. L. Winter, J. S. Brad, K. Rhoads, D. W. Barrett, R. B. Cialdini, *Environ. Manage.* **26**, 589 (2000).
26. R. M. Krauss, J. L. Freedman, M. Whitcup, *J. Exp. Soc. Psychol.* **14**, 109 (1978).
27. W. C. Finnie, *Environ. Behav.* **5**, 123 (1973).
28. R. B. Cialdini *et al.*, *Soc. Influence* **1**, 3 (2006).
29. R. N. Rimal, M. K. Lapinski, R. J. Cook, K. Real, *J. Health Commun.* **10**, 433 (2005).
30. P. W. Schultz, A. M. Khazian, A. Zaleski, *Soc. Influence* **4**, 4 (2008).
31. S. M. Reiter, W. Samuel, *J. Appl. Soc. Psychol.* **10**, 45 (1980).
32. R. B. Cialdini, *Psychometrika* **72**, 263 (2007).
33. S. Lindenberg, L. Steg, *J. Soc. Issues* **63**, 117 (2007).
34. Materials and methods are available as supporting material on *Science* Online.

35. We thank the University of Groningen for providing us the necessary means to complete this project. We also thank J. W. Bolderdijk, T. Postmes, J. A. Rothengatter, J. Thøgersen, and four anonymous reviewers for their helpful comments.

Supporting Online Material

www.sciencemag.org/cgi/content/full/322/5908/1681/DC1
Materials and Methods

5 June 2008; accepted 31 October 2008
10.1126/science.1161405

Germ Cell–Intrinsic and –Extrinsic Factors Govern Meiotic Initiation in Mouse Embryos

Yanfeng Lin,* Mark E. Gill,* Jana Koubova, David C. Page

Retinoic acid (RA) is an essential extrinsic inducer of meiotic initiation in mammalian germ cells. However, RA acts too widely in mammalian development to account, by itself, for the cell-type and temporal specificity of meiotic initiation. We considered parallels to yeast, in which extrinsic and intrinsic factors combine to restrict meiotic initiation. We demonstrate that, in mouse embryos, extrinsic and intrinsic factors together regulate meiotic initiation. The mouse RNA-binding protein DAZL, which is expressed by postmigratory germ cells, is a key intrinsic factor, enabling those cells to initiate meiosis in response to RA. Within a brief developmental window, *Dazl*-expressing germ cells in both XX and XY embryos actively acquire the ability to interpret RA as a meiosis-inducing signal.

Diploid eukaryotes generate haploid cells via meiosis, a program of two successive cell divisions preceded by one round of DNA replication. The onset of this program is referred to as meiotic initiation. In mammals, debate has focused on whether meiotic initiation is promoted by factors extrinsic or intrinsic to germline cells (*1*–*6*). Meiotic initiation in female mice, commencing at embryonic day 12.5 (E12.5) (*7*, *8*), is induced by an extrinsic factor, retinoic acid (RA) (*8*–*10*), but RA alone cannot account for the exquisite temporal and cell-type specificity of meiotic initiation. Although diverse somatic cell types are exposed and respond to RA during mammalian development (*11*), meiotic initiation is limited to the germ line. Indeed, embryonic germ cells do not respond specifically to RA until their migration ends, at the developing gonad. Does meiotic initiation in mammals also require an intrinsic competence factor expressed in germ cells? Consider the yeast *Saccharomyces cereviseae*, in which meiosis is induced by a nutrient-depleted environment (*12*). For an *S. cereviseae* cell to be competent to initiate meiosis in response to this extrinsic cue, the cell must express the a/α mating-type heterodimer (*13*). We wondered whether an analogous interplay of extrinsic and intrinsic factors governs meiotic initiation in mammals.

We considered the possibility that the *Dazl* (*Deleted in azoospermia-like*) gene might be an intrinsic meiotic competence factor, given the location and timing of its expression. In both XX and XY mouse embryos, germ cells begin to express *Dazl* at about the time of their arrival at the gonad, between E10.5 and E11.5 (*14*). No somatic lineage has been shown to express *Dazl* (*15*). Furthermore, *Dazl*-deficient mice are infertile because of germ cell–differentiation defects (*16*–*19*). These defects are more consistent and pronounced in inbred C57BL/6 mice (*19*) than in noninbred mice (*16*–*18*). Accordingly, we analyzed *Dazl* function in inbred C57BL/6 animals.

We began by testing whether germ cells survive in *Dazl*-deficient embryonic ovaries as germ cells of *Dazl*-deficient C57BL/6 embryonic testes undergo apoptosis, beginning by E14.5 (*19*, *20*). We detected two germ cell markers—endogenous alkaline phosphatase (AP) activity (*21*) and mouse *vasa* homolog (MVH) protein (*22*)—in the ovaries of wild-type and *Dazl*-deficient embryos (fig. S1, A and B). We also found MVH protein in wild-type and *Dazl*-deficient neonatal ovaries (fig. S1C), which indicates that *Dazl*-deficient ovarian germ cells survive embryonic development (fig. S1, A and B) and persist through birth (fig. S1C).

We then compared the nuclear morphology of germ cells in wild-type and *Dazl*-deficient ovaries at E15.5. By this stage of development, many germ cell nuclei in wild-type ovaries exhibit the chromosome condensation that characterizes early meiotic prophase (Fig. 1A). By contrast, germ cells in *Dazl*-deficient ovaries do not display such condensation (Fig. 1A), which suggests that *Dazl* function might be required for meiotic prophase to occur. We then examined the expression of *Stra8*, which is required for premeiotic DNA replication and the subsequent events of meiotic prophase in germ cells of embryonic ovaries (*8*). As expected,

Howard Hughes Medical Institute, Whitehead Institute, and Department of Biology, Massachusetts Institute of Technology, 9 Cambridge Center, Cambridge, MA 02142, USA.

*These authors contributed equally to this work.

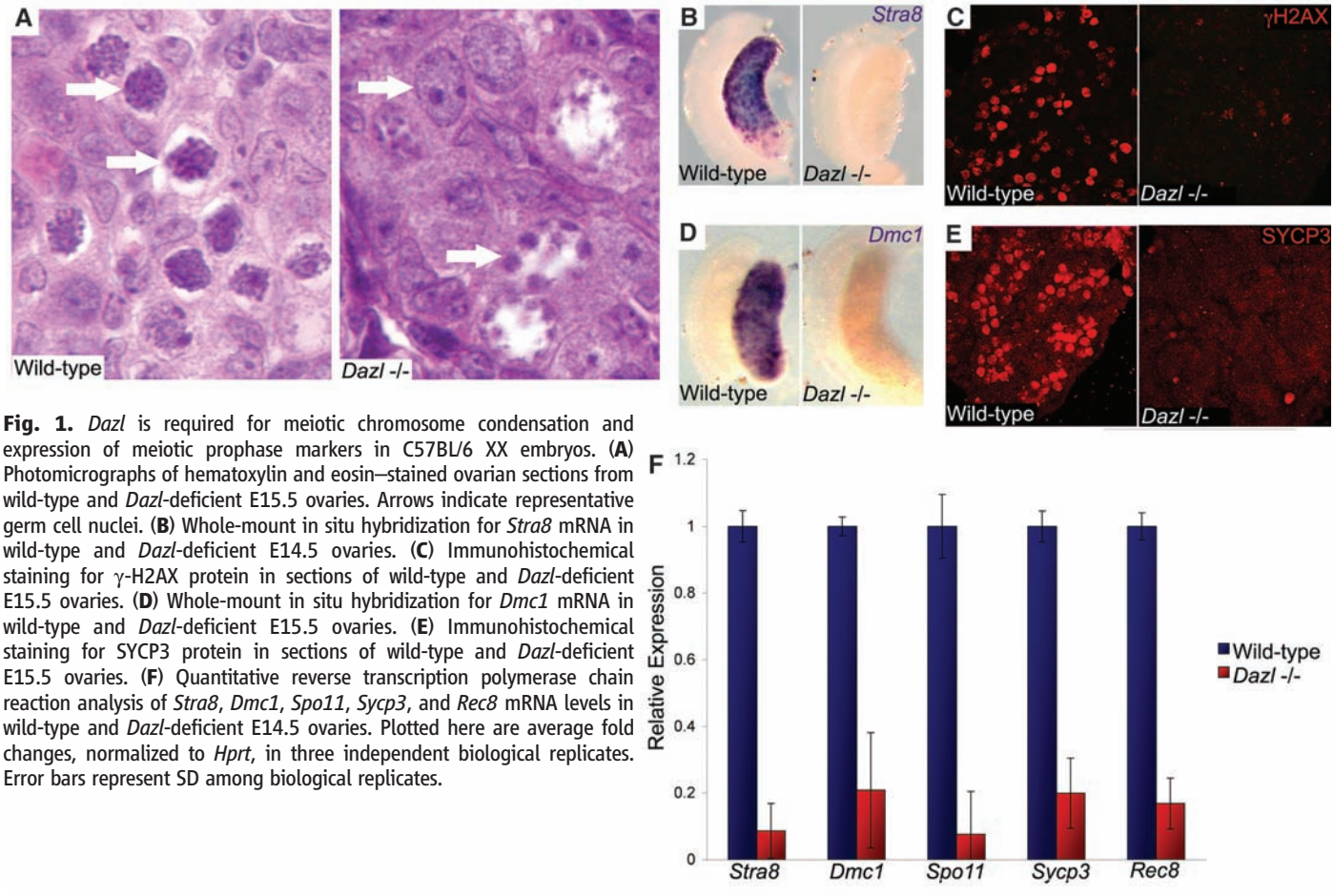

Fig. 1. *Dazl* is required for meiotic chromosome condensation and expression of meiotic prophase markers in C57BL/6 XX embryos. (**A**) Photomicrographs of hematoxylin and eosin–stained ovarian sections from wild-type and *Dazl*-deficient E15.5 ovaries. Arrows indicate representative germ cell nuclei. (**B**) Whole-mount in situ hybridization for *Stra8* mRNA in wild-type and *Dazl*-deficient E14.5 ovaries. (**C**) Immunohistochemical staining for γ-H2AX protein in sections of wild-type and *Dazl*-deficient E15.5 ovaries. (**D**) Whole-mount in situ hybridization for *Dmc1* mRNA in wild-type and *Dazl*-deficient E15.5 ovaries. (**E**) Immunohistochemical staining for SYCP3 protein in sections of wild-type and *Dazl*-deficient E15.5 ovaries. (**F**) Quantitative reverse transcription polymerase chain reaction analysis of *Stra8*, *Dmc1*, *Spo11*, *Sycp3*, and *Rec8* mRNA levels in wild-type and *Dazl*-deficient E14.5 ovaries. Plotted here are average fold changes, normalized to *Hprt*, in three independent biological replicates. Error bars represent SD among biological replicates.

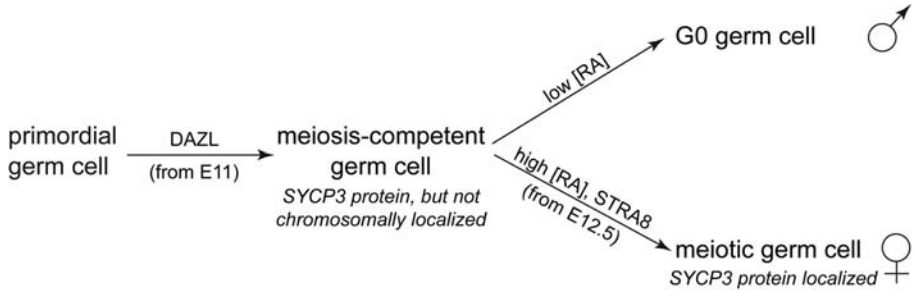

Fig. 2. Embryonic germ cell states: a proposed path by which primordial germ cells acquire meiotic competence (in both XX and XY embryos) and subsequently initiate meiosis (in XX embryos) or undergo G_0 arrest (in XY embryos). "Low [RA]" and "high [RA]" are consequences of differential expression of RA-inactivating enzyme CYP26B1 in embryonic testes and ovaries (*9*, *10*).

Stra8 is expressed abundantly in wild-type ovaries at E14.5 (Fig. 1, B and F). In *Dazl*-deficient ovaries, *Stra8* expression is dramatically reduced if not eliminated (Fig. 1, B and F), which suggests that *Dazl* might have an obligatory function upstream of meiotic initiation; this would account for the absence of meiotic chromosome condensation (Fig. 1A).

If *Dazl* is required for *Stra8* expression and meiotic initiation in embryonic ovaries, then germ cells in *Dazl*-deficient ovaries should not undertake meiotic recombination. We assayed whether *Dazl*-deficient female germ cells form DNA double-strand breaks (DSBs), which initiate meiotic recombination. Cells respond to DNA DSB formation by phosphorylating H2AX, a histone H2A variant, to generate γ-H2AX (*23*). As expected, immunostaining for γ-H2AX revealed the presence of DNA DSBs in many cells of wild-type ovaries at E15.5 (Fig. 1C). In contrast, *Dazl*-deficient ovaries are negative for γ-H2AX, indicating that DNA DSBs have not formed (Fig. 1C). In addition, we asked whether *Dazl*-deficient female germ cells express *Spo11* and *Dmc1*, which encode, respectively, a topoisomerase required to form meiotic DSBs and a recombinase functioning in meiotic DSB repair (*24*). In previous studies, *Stra8* was shown to be required for expression of *Spo11* and *Dmc1* in germ cells of embryonic ovaries (*8*). We found that, in *Dazl*-deficient ovaries, expression of *Dmc1* and *Spo11* is markedly reduced if not eliminated (Fig. 1, D and F). The absence of H2AX phosphorylation and the absence of *Spo11* and *Dmc1* expression indicate that *Dazl*-deficient female germ cells do not engage in meiotic recombination.

These findings are consistent with *Dazl* being required upstream of *Stra8*'s function in meiotic initiation. Does *Dazl* deficiency simply recapitulate the *Stra8* null phenotype (*8*), or does it cause additional abnormalities? We assayed the expression in *Dazl*-deficient embryonic ovaries of the *Sycp3* and *Rec8* genes, which encode, respectively, a component of the synaptonemal complex and a meiosis-specific cohesin (*25*). Both SYCP3 and REC8 proteins function through their loading onto chromosomes. In *Stra8*-deficient female germ cells, as previously reported, *Sycp3* and *Rec8* are transcribed and translated, but the encoded proteins do not load onto chromosomes and therefore do not perform their meiotic functions (*8*). We discovered that, in germ cells of *Dazl*-deficient embryonic ovaries, *Sycp3* function is disrupted at an even earlier step: SYCP3 protein and mRNA levels are markedly reduced as compared with those in wild-type ovaries (Fig.

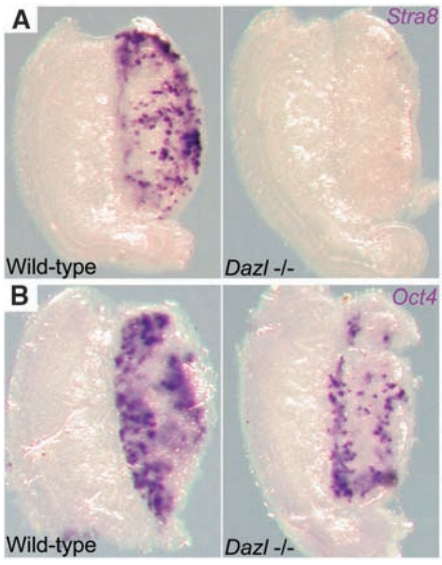

Fig. 3. *Dazl* is required for RA-induced expression of *Stra8* in embryonic testes. Whole-mount in situ hybridization for (**A**) *Stra8* mRNA and (**B**) *Oct4* mRNA in wild-type and *Dazl*-deficient testes dissected at E12.5 and cultured for 48 hours in the presence of 0.7 μM RA is shown.

1, E and F). Similarly, *Rec8* exhibited little or no expression in *Dazl*-deficient ovaries (Fig. 1F). Thus, *Dazl* is required for both *Stra8*-mediated initiation of meiosis in female germ cells and *Stra8*-independent expression of *Sycp3* and *Rec8* there.

We propose a pathway by which embryonic germ cells advance from a primordial state to the initiation of meiosis (Fig. 2). This pathway includes a newly posited cell state, the meiosis-competent gonocyte, whose derivation from a primordial germ cell requires the germ cell–intrinsic factor *Dazl* and whose progression to meiotic initiation and prophase in the female germ line requires the extrinsic meiosis-inducing factor RA and *Stra8*. We propose that this meiosis-competent cell state exists in both male and female embryonic germ lines, despite the fact that meiosis does not initiate in male embryos. The posited meiosis-competent gonocyte contains SYCP3 protein not yet loaded onto chromosomes (Fig. 2), which is consistent with the observation (*6*) that both male and female embryonic germ cells express SYCP3 protein before the sexes take different paths: Female germ cells advance to meiotic prophase, where SYCP3 functions, whereas male germ cells down-regulate SYCP3 and arrest in G_0.

Embryonic testicular germ cells express *Stra8* when exposed to exogenous RA, even though they normally express *Stra8* only after birth (*9*, *10*). Our model predicts that ectopic expression of *Stra8* in RA-treated embryonic testes should require *Dazl* function. We dissected testes from wild-type and *Dazl*-deficient E12.5 embryos, cultured them in the presence of 0.7 μM RA for 48 hours, and assayed *Stra8* expression by whole-mount in situ hybridization. As previously reported (*9*, *10*), RA induced robust expression of *Stra8* in wild-type testes (Fig. 3A). In contrast, in *Dazl*-deficient testes, no induction was observed (Fig. 3A). To confirm that this failure to induce *Stra8* expression in *Dazl*-deficient testes was not due to germ cell apoptosis (*19*), we performed a control in situ hybridization for *Oct4* (Mouse Genome Informatics ID *Pou5f1*), a gene expressed in embryonic germ cells but not in gonadal somatic cells (*26*). We observed abundant *Oct4* expression in RA-cultured testes, both wild-type and *Dazl*-deficient (Fig. 3B). Thus, expression of *Stra8* in response to RA requires *Dazl* in embryonic testis and ovary alike, confirming that *Dazl* is a competence factor for meiotic initiation in embryos of both sexes.

In *S. cereviseae* cells, expression of the a/α mating-type heterodimer is a prerequisite to launching the meiotic initiation program in response to an extrinsic cue. Our findings demonstrate that *Dazl* plays an analogous role in embryonic mice. In both a unicellular eukaryote and a complex animal, meiotic initiation is governed by a cell-intrinsic competence factor and an extrinsic inducing signal.

References and Notes

1. A. G. Byskov, *Nature* **252**, 396 (1974).
2. A. G. Byskov, L. Saxen, *Dev. Biol.* **52**, 193 (1976).
3. S. Upadhyay, L. Zamboni, *Proc. Natl. Acad. Sci. U.S.A.* **79**, 6584 (1982).
4. A. McLaren, *J. Exp. Zool.* **228**, 167 (1983).
5. A. McLaren, D. Southee, *Dev. Biol.* **187**, 107 (1997).
6. A. D. Di Carlo, G. Travia, M. De Felici, *Int. J. Dev. Biol.* **44**, 241 (2000).
7. D. B. Menke, J. Koubova, D. C. Page, *Dev. Biol.* **262**, 303 (2003).
8. A. E. Baltus *et al.*, *Nat. Genet.* **38**, 1430 (2006).
9. J. Bowles *et al.*, *Science* **312**, 596 (2006).
10. J. Koubova *et al.*, *Proc. Natl. Acad. Sci. U.S.A.* **103**, 2474 (2006).
11. M. Mark, N. B. Ghyselinck, P. Chambon, *Annu. Rev. Pharmacol. Toxicol.* **46**, 451 (2006).
12. S. M. Honigberg, K. Purnapatre, *J. Cell Sci.* **116**, 2137 (2003).
13. A. K. Hopper, B. D. Hall, *Genetics* **80**, 41 (1975).
14. J. Seligman, D. C. Page, *Biochem. Biophys. Res. Commun.* **245**, 878 (1998).
15. H. J. Cooke, M. Lee, S. Kerr, M. Ruggiu, *Hum. Mol. Genet.* **5**, 513 (1996).
16. M. Ruggiu *et al.*, *Nature* **389**, 73 (1997).
17. B. H. Schrans-Stassen, P. T. Saunders, H. J. Cooke, D. G. de Rooij, *Biol. Reprod.* **65**, 771 (2001).
18. P. T. Saunders *et al.*, *Reproduction* **126**, 589 (2003).
19. Y. Lin, D. C. Page, *Dev. Biol.* **288**, 309 (2005).
20. Materials and methods are available as supporting material on *Science* Online.
21. M. Ginsburg, M. H. Snow, A. McLaren, *Development* **110**, 521 (1990).
22. Y. Toyooka *et al.*, *Mech. Dev.* **93**, 139 (2000).
23. E. P. Rogakou, D. R. Pilch, A. H. Orr, V. S. Ivanova, W. M. Bonner, *J. Biol. Chem.* **273**, 5858 (1998).
24. L. A. Bannister, J. C. Schimenti, *Cytogenet. Genome Res.* **107**, 191 (2004).
25. H. Scherthan, *Cytogenet. Genome Res.* **103**, 235 (2003).
26. M. Pesce, X. Wang, D. J. Wolgemuth, H. Scholer, *Mech. Dev.* **71**, 89 (1998).

27. We thank H. Cooke for mice carrying the *Dazl*^{Tm1Hgu} allele; C. Heyting for SYCP3 antisera; T. Noce for MVH antisera; and A. Amon, E. Anderson, A. Baltus, A. Bortvin, M. Carmell, G. Fink, A. Hochwagen, Y. Hu, J. Lange, J. Mueller, L. Okumura, and T. Orr-Weaver for advice and comments on the manuscript. Microscopy and image capture were conducted at the W. M. Keck Foundation Biological Imaging Facility at the Whitehead Institute. This work was supported by the Howard Hughes Medical Institute.

Supporting Online Material

www.sciencemag.org/cgi/content/full/322/5908/1685/DC1
Materials and Methods
Fig. S1
References

24 September 2008; accepted 30 October 2008
10.1126/science.1166340

Traction Dynamics of Filopodia on Compliant Substrates

Clarence E. Chan and David J. Odde*

Cells sense the environment's mechanical stiffness to control their own shape, migration, and fate. To better understand stiffness sensing, we constructed a stochastic model of the "motor-clutch" force transmission system, where molecular clutches link F-actin to the substrate and mechanically resist myosin-driven F-actin retrograde flow. The model predicts two distinct regimes: (i) "frictional slippage," with fast retrograde flow and low traction forces on stiff substrates and (ii) oscillatory "load-and-fail" dynamics, with slower retrograde flow and higher traction forces on soft substrates. We experimentally confirmed these model predictions in embryonic chick forebrain neurons by measuring the nanoscale dynamics of single—growth-cone filopodia. Furthermore, we experimentally observed a model-predicted switch in F-actin dynamics around an elastic modulus of 1 kilopascal. Thus, a motor-clutch system inherently senses and responds to the mechanical stiffness of the local environment.

Recent work has demonstrated the importance of substrate stiffness on cell motility, morphology, and fate (*1*). For instance, fibroblasts display a behavior known as durotaxis, preferentially migrating toward regions of higher stiffness (*2*). Softer substrates have been shown to promote branching in primary mouse spinal cord neurons while suppressing the growth of associated glia (*3*, *4*). A recent study has also shown that mesenchymal stem cell fate can be determined by the stiffness of the

Department of Biomedical Engineering, University of Minnesota, Minneapolis, MN 55455, USA.

*To whom correspondence should be addressed. E-mail: oddex002@umn.edu

culture substrate, a phenomenon that requires actomyosin contractility (*5*). Although the importance of actomyosin and substrate adhesions are well appreciated, it is not clear how these components work together to sense and respond to the stiffness of the local environment.

One way cells are thought to probe their environment is through the generation of traction by a "motor-clutch" mechanism where cells utilize molecular clutches to physically link F-actin to the extracellular substrate (*6*). By creating this physical coupling, cells are thought to create a frictional slippage interface that transmits traction forces and slows F-actin retrograde flow, allowing actin polymerization to advance the leading edge (*7*–*9*). If cells use the motor-clutch system to probe their mechanical environment, we wondered how this system would be influenced by substrate stiffness.

To address this question, we first constructed a stochastic physical model of the motor-clutch hypothesis, treating molecular clutches and the substrate as simple, Hookean springs (Fig. 1A). At every time step, n_m myosin motors drive retrograde flow by exerting a force F_M on an F-actin bundle. Next, individual molecular clutches are allowed to reversibly engage the F-actin bundle with rate constants k_{on} and k_{off}. Clutches that successfully engage will build tension with spring constant κ_c, as they are stretched by retrograde motion of F-actin. Tension along engaged clutches increases their off-rate constant, k_{off}*, exponentially according to Bell's Law (*10*), with a characteristic breaking force F_b. Tension in the engaged molecular clutches sums to a traction force that must be balanced by tension and deformation in the compliant substrate with spring constant κ_{sub}. Myosin motors work against this load force, slowing their motor sliding velocity according to a linear force-velocity relation. Finally, actin polymerizes at the plus end of the F-actin bundle with constant velocity to counter retrograde flow and maintain the F-actin bundle. For simplicity, we ignored tension-dependent strengthening of adhesions, as has been reported in some cases (*11*, *12*), as this effect can be added later to increase the model sophistication and complexity if necessary (*13*).

When we simulated the motor-clutch system on compliant substrates, we observed the emergence of two distinct traction force dynamics

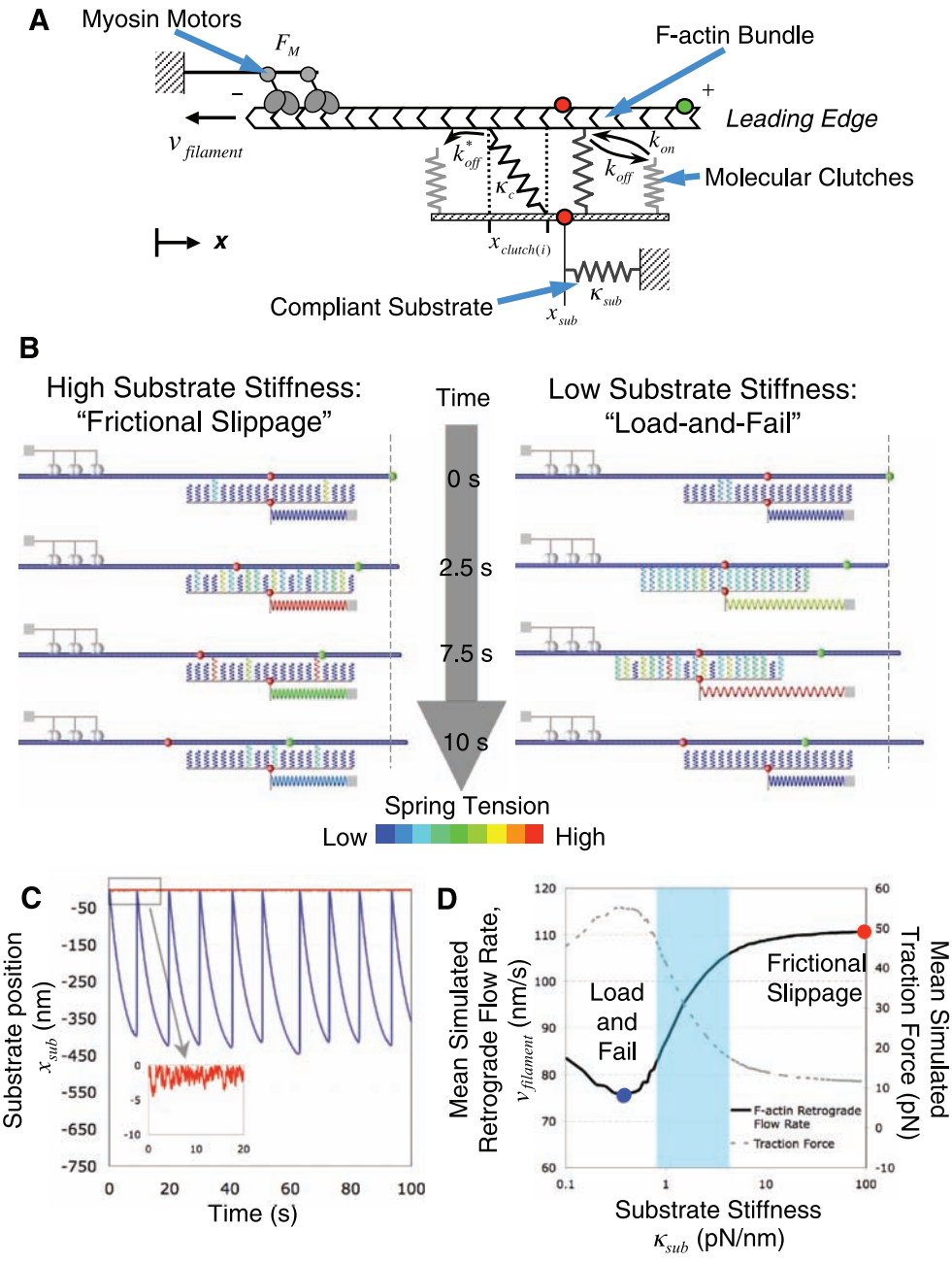

Fig. 1. A model for motor-clutch motility on compliant substrates predicts substrate stiffness-dependent dynamics. (**A**) Schematic representation of a mechano-chemical motor-clutch model. Myosin motors pull an F-actin filament bundle to the left with force, F_M, at velocity, $v_{filament}$. Molecular clutches reversibly engage the F-actin bundle with rates k_{on} and k_{off} to resist retrograde flow. During loading, the clutches are stretched to strains $x_{clutch(i)}$, and they tend to fail with a force-dependent off rate, k_{off}*. Transmitted forces induce a local substrate strain, x_{sub}. The mechanical stiffness of the clutches, κ_c, and of the substrate, κ_{sub}, determine the mechanical resistance to loading. (**B**) Model-predicted substrate stiffness-dependent clutch dynamics. Red markers indicate the initial position of the bundle and substrate and highlight their relative motion. Green markers indicate the initial F-actin bundle position. Stiff substrates exhibit frictional slippage, in which the F-actin bundle constantly slides relative to the substrate (red markers move apart). Soft substrates exhibit load-and-fail dynamics, where the compliant substrate moves with the F-actin bundle until coupling failure. (**C**) Model-predicted substrate position as a function of time highlights load-and-fail on compliant substrates (blue line). Stiff substrates exhibit frictional slippage (red line, also see inset). (**D**) Load-and-fail clutch dynamics are predicted to lead to slower time-averaged F-actin retrograde flow rates and higher traction forces, whereas frictional slippage dynamics lead to increased retrograde flow rates and decreased traction force. The transition zone (light blue area) defines a region of greatest sensitivity to substrate stiffness.

(Fig. 1B and movie S1). On stiff substrates, molecular clutches engage the F-actin bundle but abruptly disengage as lack of compliance in the substrate results in a rapid building of tension within engaged clutches that drastically shortens F-actin/clutch interaction lifetimes. In this case, the F-actin bundle is continuously slipping from the point of contact at a roughly constant velocity. We describe this dynamic as "frictional slippage," a behavior that has previously been observed on stiff glass substrates (*7*, *14*, *15*).

On soft substrates, substrate compliance slows the rate at which tension builds along individually engaged clutches. This prolongs F-actin/clutch interaction times, with most clutches remaining engaged to the F-actin bundle at early times in the cycle (Fig. 1B and movie S1). During this time, there is little relative motion between the F-actin bundle and the substrate as tension slowly develops within the substrate. Because of this lack of resistance, myosin motors work near their unloaded sliding velocity, leading to high rates of F-actin retrograde flow and a slight retraction of the leading edge. As the substrate strains and greater tension builds, clutches largely remain engaged due to sharing of the mechanical load among engaged neighbors. This

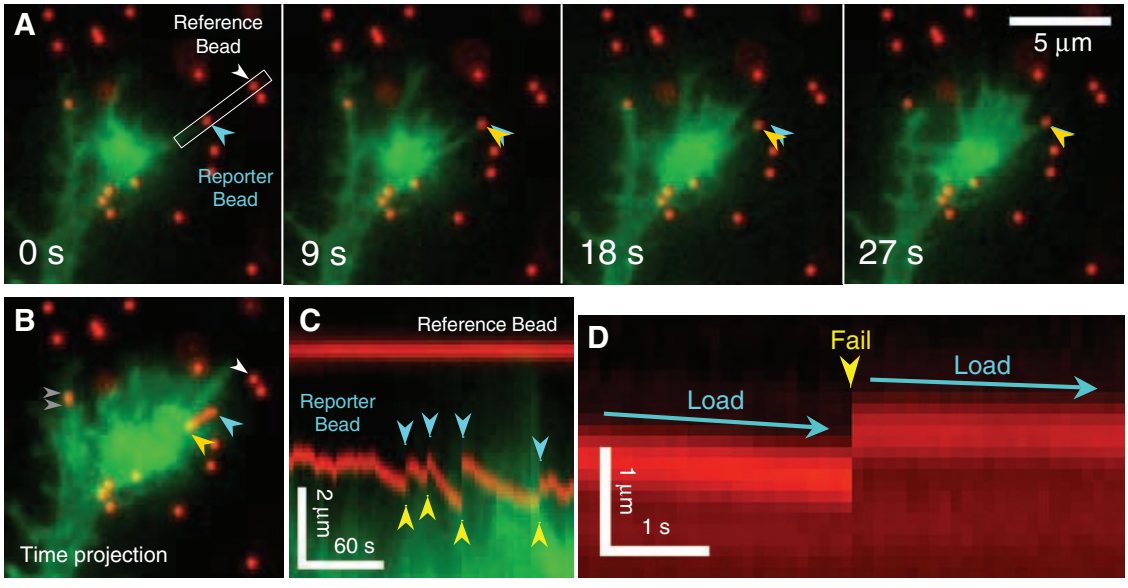

Fig. 2. Growth-cone filopodia on compliant substrates exert traction forces with load-and-fail dynamics. (**A**) Montage of a GFP-actin transected ECFN growth cone on a 730-Pa PAG with embedded fiduciary marker beads acquired at 3-s intervals. A reporter bead underneath a growth-cone filopodium displays periodic motions. Blue arrowheads indicate initial position; yellow arrowheads indicate position at the given time point. The rectangular box indicates a traction-producing filopodium. (**B**) Time projection of the image stack over 5 min. The marker bead in (A) appears as a line (blue and yellow arrowheads). The reference bead (white arrowhead) appears as a single spot. A second marker bead (gray arrowheads) was also pulled retrogradely, as evidenced by the elongated appearance. (**C**) Kymograph of the region indicated in (A). Yellow arrowheads indicate abrupt failure events. (**D**) Marker bead position recorded at 100-ms intervals.

Fig. 3. Growth-cone filopodia F-actin retrograde flow rate abruptly transitions from low to high around an elastic modulus of E = 1 kPa. (**A**) EGFP-actin transfected ECFN growth cone. The rectangular box indicates a filopodium exhibiting retrograde flow. (**B**) Kymograph along region indicated in (A). GFP-actin features create diagonal streaks, allowing the measurement of F-actin retrograde flow. (**C**) Histogram of measured F-actin retrograde flow rates on stiff and soft substrates [stiff substrate (purple): E = 260-Pa PAG, n = 95; soft substrate (red): E = 57-kPa PAG, n = 258; *P < 0.001]. (**D**) Measurements of F-actin retrograde flow over a range of stiffness indicate a narrow region of sensitivity (light blue shaded region) and a trend statistically consistent with model predictions. Very low stiffness (gray region) results in poor cell viability.

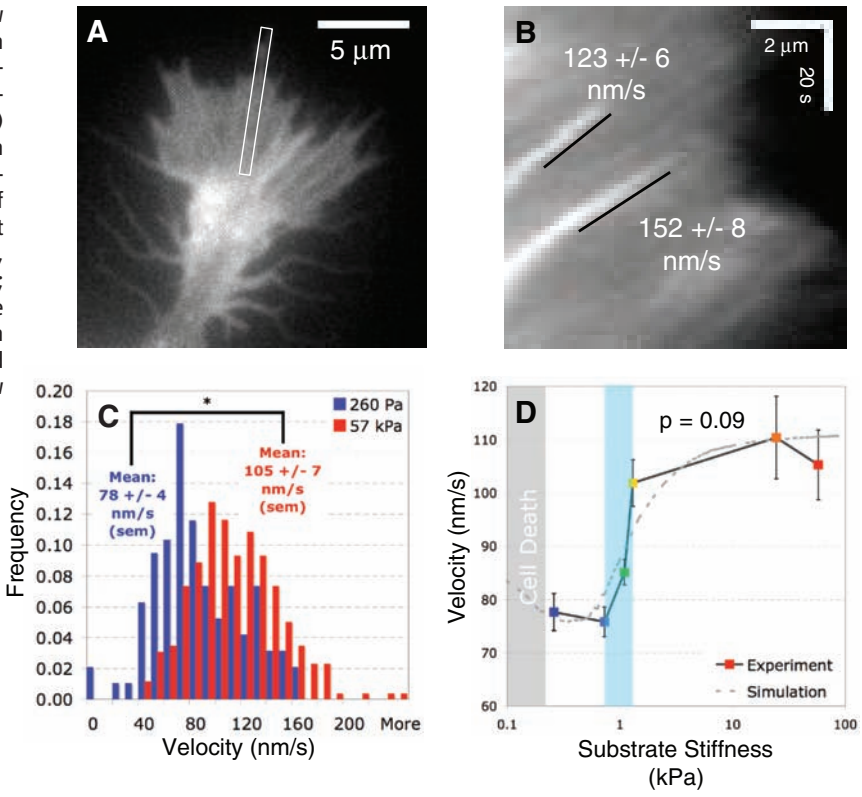

provides considerable resistance to the motor force, substantially slowing retrograde flow. Eventually, the load becomes so great that the stochastic loss of one clutch leads to a cascading failure event, in which the unsupportable load shifts progressively to remaining bonds, further destabilizing the F-actin/clutch interaction. This quickly leads to an abrupt coupling failure where all clutches rapidly disengage, consequently unloading the substrate and causing it to snap back to its initial rest position. Thus, computational modeling of motor-clutch motility on soft substrates predicts the natural emergence of an oscillatory "load-and-fail" traction force dynamic characterized by protracted periods (~10 to 100 s) of increasing tension, followed by an abrupt coupling failure (Fig. 1, B and C).

In addition, simulations predict that these substrate stiffness-dependent changes in clutch dynamics lead to substantial differences in F-actin retrograde flow rates and the mean traction forces exerted on soft versus stiff substrates. On stiff substrates, short-lived F-actin/clutch interactions create a "molecular friction" (*16*), where only a few clutches are engaged at any given time point. Lower average clutch numbers limit the total tension developed along engaged clutches, resulting in lower mean traction forces and higher rates of retrograde flow. On the other hand, load-and-fail dynamics on soft substrates result in higher numbers of engaged clutches on average, increasing the total tension developed along clutches, leading to slower retrograde flow velocity and greater transmission of traction forces (Fig. 1D and fig. S1). As the substrate becomes softer still, modeling predicts a slight increase in retrograde flow rate along with a slight decrease in traction forces (Fig. 1D). This occurs as the system spends a greater fraction of the time weakly loaded, resulting in longer times to generate sufficient tension to substantially resist the myosin motors (movie S1). Thus, a motor-clutch system is predicted to exhibit substrate stiffness-dependent changes in clutch dynamics that result in higher retrograde flow rates with lower traction forces on stiff substrates and lower retrograde flow rates with higher traction forces on soft substrates.

To test these model predictions, we used green fluorescent protein (GFP)–actin transfected embryonic chick forebrain neurons (ECFNs) plated on soft (260 to 730 Pa) or stiff (1.3 to 57 kPa) polyacrylamide gel (PAG) substrates coated with polyethyleneimine as an adhesion promoter. Compliant PAGs embedded with 200-nm-diameter fluorescent fiduciary marker beads allow the visualization of traction forces as deflections of beads from their rest position (*17*–*19*). Using dual-channel epifluorescence imaging in combination with a computational bead-tracking algorithm, we visualized F-actin dynamics in growth-cone filopodia and deflections of underlying marker beads to directly observe traction force transmission dynamics at 1- to 10-Hz frame rates (*13*).

With this system, we find that neurons exhibit a wide variety of region-specific traction force dynamics on compliant PAGs (fig. S2 and movie S2). Whereas axons, neurons, and growth cones exerted randomly directed and fluctuating tractions, growth-cone filopodia frequently displayed large, unidirectional bead deflections several times greater in magnitude than those from other regions of the neuron. Growth-cone motility was dependent on β1-integrin–mediated adhesion (fig. S3 and movie S3), consistent with our earlier studies that made use of magnetic bead force application (*20*).

When we examined the detailed time evolution of filopodial traction forces, we found that substrate-embedded marker beads deflected inwardly toward the growth cone and would occasionally snap back toward their rest position, indicative of the load-and-fail behavior predicted by the motor-clutch model when the substrate is soft (Fig. 2A, fig. S4, and movie S4). A time projection through movie S4 shows that filopodia exert unidirectional tractions along the filopodium axis (Fig. 2B). A kymograph along the axis of the filopodium shows that filopodium exert traction forces with load-and-fail dynamics similar to that predicted by the model, with cycle times on the order of tens of seconds (Fig. 2C). On occasions where more than one filopodium within a growth cone exerted observable tractions, we found substantial variation in both the amplitude and frequency of load-and-fail events (movie S4). This suggests that cells probably have stochastic fluctuations or spatial gradients in one or more motor-clutch parameters, leading to variable dynamics among individual filopodia. When filmed at 100-ms time intervals, we found that failure events occurred very abruptly, with detectable bead relaxations occurring in a single frame (Fig. 2D and fig. S6). Furthermore, loading often occurred immediately (<100 ms) after failure events, demonstrating that failures were attributable to transient clutch disengagement rather than filopodia retracting from the region entirely. We also found that increasing substrate stiffness resulted in an increase in the frequency

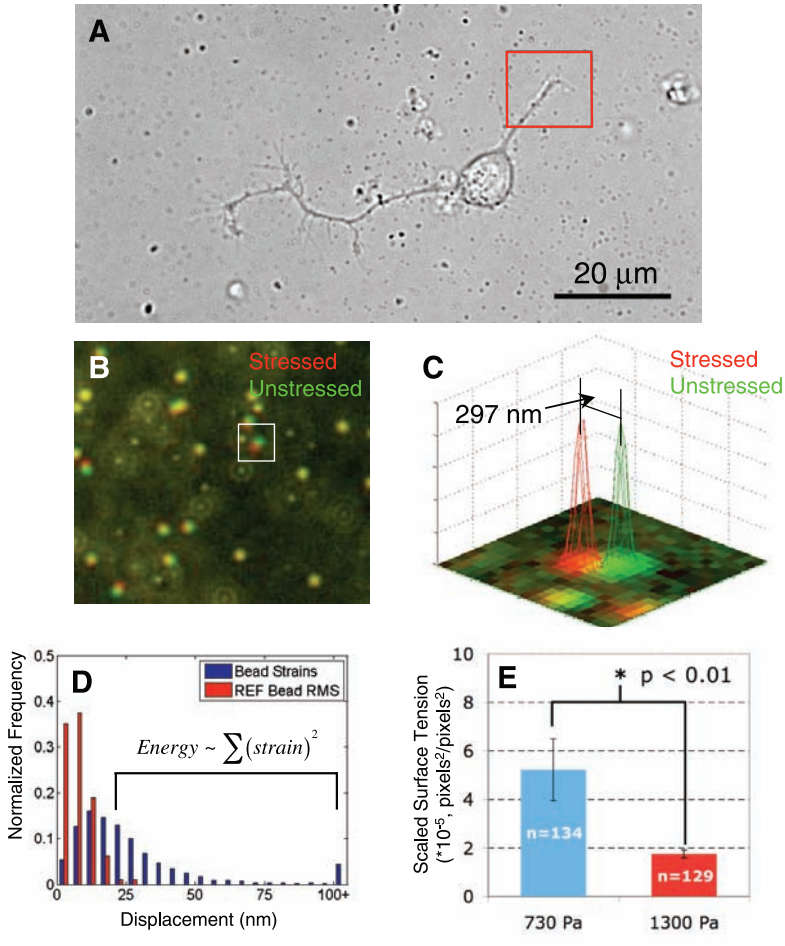

Fig. 4. Surface tension of ECFNs decreases on stiff PAGs. (**A**) Phase image of an ECFN on a PAG substrate. The red box indicates a traction-producing growth cone. (**B**) Stressed/unstressed images of region highlighted in (A) reveal bead strains within the substrate. The white box indicates a region of high stress. (**C**) Image processing of region highlighted in (B) identifies and measures bead strains within the substrate. (**D**) Sum of all bead strains above reference bead noise is used to estimate the relative elastic energy stored within the substrate. (**E**) Surface tension significantly decreases on stiff substrates (mean ± SEM).

of failure events ($P < 0.03$) (fig. S5), which is consistent with the simulation. Together, these data reveal that filopodia exert traction forces with load-and-fail dynamics predicted by a stochastic model for the motor-clutch system on a soft substrate.

To test the model prediction that retrograde flow rate increases with increasing substrate stiffness, we tracked fluorescent GFP-actin features from growth cones of transfected ECFNs on PAG substrates imaged by means of epifluorescence (Fig. 3A). As growth cones crawl, polymerization at the leading edge stochastically gives rise to a fluctuating number of GFP-labeled actin filaments that constitute the filopodial F-actin bundle, creating alternately bright and dark F-actin features that can be quantitatively tracked via digital image analysis (*13*).

As with other motile cell types, the peripheral zone of growth cones exhibits rapid retrograde flow of polymerized actin (Fig. 3B and movie S5). Furthermore, the motion of GFP-actin features was myosin II–dependent (fig. S7) and never observed to move anterogradely (out of $n = 922$ features tracked), demonstrating that the major point of coupling failure lies between the F-actin/substrate interface, rather than between the myosin/F-actin interface. Creating kymographs along filopodia reveals motion of F-actin features that were tracked with a cross-correlation algorithm (*13*). Using this method, we found that retrograde flow was significantly slower on soft substrates ($P < 0.0001$) (Fig. 3C). Untransfected ECFNs also exhibited a similar response to substrate stiffness, suggesting that this effect is independent of GFP-actin (fig. S8). Filopodia on substrates from 730 to 1300 Pa showed high sensitivity to stiffness, abruptly increasing their retrograde flow rates as substrate stiffness increased (Fig. 3D, blue region). Once substrate stiffness exceeded a critical value of ~1300 Pa, retrograde flow rates became insensitive to stiffness, having a mean velocity of ~110 nm/s. On extremely soft substrates (≤ 84 Pa), ECFNs appeared unhealthy, often dying within 1 to 2 days (fig. S9). Thus, measuring the retrograde flow rate over a range of substrate stiffness revealed a trend not significantly different from that predicted by simulation ($P = 0.09$) and suggests that ECFN growth-cone filopodia may transition from load-and-fail dynamics to frictional slippage around 1 kPa (Fig. 3D).

Next, to test the model prediction of increased traction force transmission on softer substrates, we considered the amount of elastic strain energy exerted by ECFNs to displace individual marker beads from their rest position as the cell pulls on the elastic substrate (*13*). To estimate the elastic strain energy stored within the substrate, stressed images of marker beads during ECFN interaction were captured, followed by an unstressed image in which the cell was released from the substrate using trypsin (Fig. 4, A and B). Next, we measured the displacement of every marker bead in the field (Fig. 4C) and estimated the total stored energy by summing the squared displacements of all marker beads above the noise and scaling the result according to the substrate stiffness (Fig. 4D). When normalized to the projected area of the cell, this metric can be considered as a "surface tension" between the cell and the substrate. Using this method, we find that ECFNs on soft PAGs have a threefold higher surface tension as compared with stiffer gels ($P < 0.01$) (Fig. 4E), in agreement with model predictions.

Together, these modeling and experimental results show that a motor-clutch retrograde flow mechanism naturally responds to substrate stiffness, with a very abrupt change around 1 kPa in the specific case of ECFNs grown in vitro. Substrate stiffness-dependent changes in clutch dynamics may serve as a basis for sensing environmental stiffness, providing differential inputs to mechanosensitive elements, ultimately transducing these signals into altered cell motility, cell morphology, and cell fate.

References and Notes

1. T. Yeung *et al.*, *Cell Motil. Cytoskeleton* **60**, 24 (2005).
2. C.-M. Lo, H.-B. Wang, M. Dembo, Y.-L. Wang, *Biophys. J.* **79**, 144 (2000).
3. L. A. Flanagan, Y. E. Ju, B. Marg, M. Osterfield, P. A. Janmey, *Neuroreport* **13**, 2411 (2002).
4. P. C. Georges, W. J. Miller, D. F. Meaney, E. S. Sawyer, P. A. Janmey, *Biophys. J.* **90**, 3012 (2006).
5. A. J. Engler, S. Sen, H. L. Sweeney, D. E. Discher, *Cell* **126**, 677 (2006).
6. T. Mitchison, M. Kirschner, *Neuron* **1**, 761 (1988).
7. K. Hu, L. Ji, K. T. Applegate, G. Danuser, C. M. Waterman-Storer, *Science* **315**, 111 (2007).
8. C. Jurado, J. R. Haserick, J. Lee, *Mol. Biol. Cell* **16**, 507 (2005).
9. L. B. Smilenov, A. Mikhailov, R. J. Pelham Jr., E. E. Marcantonio, G. G. Gundersen, *Science* **286**, 1172 (1999).
10. G. I. Bell, *Science* **200**, 618 (1978).
11. N. Q. Balaban *et al.*, *Nat. Cell Biol.* **3**, 466 (2001).
12. D. Riveline *et al.*, *J. Cell Biol.* **153**, 1175 (2001).
13. Materials and methods are available as supporting material on *Science* Online.
14. A. Mallavarapu, T. Mitchison, *J. Cell Biol.* **146**, 1097 (1999).
15. S. L. Gupton, C. M. Waterman-Storer, *Cell* **125**, 1361 (2006).
16. J. Howard, R. L. Clark, *Appl. Mech. Rev.* **55**, B39 (2002).
17. C. E. Kandow, P. C. Georges, P. A. Janmey, K. A. Beningo, in *Cell Mechanics*, *Methods in Cell Biology*, vol. 83, Y. Wang, D. E. Discher, Eds. (Academic Press, San Diego, CA, 2007), pp. 29–46.
18. R. J. Pelham, Y. Wang, *Proc. Natl. Acad. Sci. U.S.A.* **94**, 13661 (1997).
19. Y. L. Wang, R. J. Pelham, *Methods Enzymol.* **298**, 489 (1998).
20. J. N. Fass, D. J. Odde, *Biophys. J.* **85**, 623 (2003).

21. This research was supported by the Institute for Engineering in Medicine at the University of Minnesota, NSF (grant MCB-0615568), and the National Institute of General Medical Sciences (grant R01-GM-76177). We thank P. Letourneau, D. Bray, and E. Tuzel for stimulating discussions; N. Simha for helpful discussions on gel mechanics; N. Koyano for assistance with in ovo electroporation; and members of the Odde Lab, D. Seetapun, A. Bicek, M. Gardner, and T. Dahl for technical assistance.

Supporting Online Material

www.sciencemag.org/cgi/content/full/322/5908/1687/DC1
Materials and Methods
SOM Text
Figs. S1 to S12
Table S1
References
Movies S1 to S5

22 July 2008; accepted 29 October 2008
10.1126/science.1163595

Structure and Functional Role of Dynein's Microtubule-Binding Domain

Andrew P. Carter,[1]* Joan E. Garbarino,[2]* Elizabeth M. Wilson-Kubalek,[3] Wesley E. Shipley,[2] Carol Cho,[1] Ronald A. Milligan,[3] Ronald D. Vale,[1]† I. R. Gibbons[2]

Dynein motors move various cargos along microtubules within the cytoplasm and power the beating of cilia and flagella. An unusual feature of dynein is that its microtubule-binding domain (MTBD) is separated from its ring-shaped AAA+ adenosine triphosphatase (ATPase) domain by a 15-nanometer coiled-coil stalk. We report the crystal structure of the mouse cytoplasmic dynein MTBD and a portion of the coiled coil, which supports a mechanism by which the ATPase domain and MTBD may communicate through a shift in the heptad registry of the coiled coil. Surprisingly, functional data suggest that the MTBD, and not the ATPase domain, is the main determinant of the direction of dynein motility.

Dyneins are AAA+ adenosine triphosphatases (ATPases) that power minus end–directed movement along microtubules (*1*). The cytoplasmic form of dynein serves many cellular functions including regulation of the mitotic checkpoint (*2*), organization of the Golgi apparatus (*3*), and the transport of vesicles, viruses, and mRNAs (*4*). Several human diseases, such as lissencephaly (*4*), primary ciliary dyskinesia (*5*), neural degeneration (*6*), and male infertility (*7*), result from dynein dysfunction.

The motor region of dynein (Fig. 1A) consists of a ring of AAA+ domains (four of which bind and hydrolyze ATP), a mechanical element (termed the "linker") that is likely involved in driving motility (*8*, *9*), and a ~15-nm "stalk" that has a microtubule-binding domain (MTBD) at its tip. The stalk, which emerges from AAA4 (the fourth nucleotide-binding AAA+ domain in the ring), extends as one α helix of an antiparallel coiled coil (termed CC1), forms the small, globular MTBD, and then returns as the partner helix

of the coiled coil (CC2) and joins AAA5 (a non–nucleotide-binding AAA+ domain) (*10*). The separation of the AAA+ ring from the MTBD by a long and somewhat flexible coiled coil (*8*) distinguishes dynein from kinesin and myosin, where the polymer-binding site and catalytic site are integrated within a single globular motor domain.

The unusual separation of ATPase and MTBD in dynein raises questions about its motility mechanism. First, how might bidirectional communication be relayed through a 15-nm coiled coil such that, in one direction, microtubule binding at the MTBD stimulates ATP turnover in the AAA+ ring, while in the other direction, chemical transitions in the AAA+ ring control the strength of microtubule binding at the MTBD? Second, how does a flexible coiled-coil stalk orient the AAA+ ring such that a force-producing movement of the linker element (with respect to the AAA+ domains) generates a displacement of the cargo toward the minus end of the microtubule?

These questions cannot be addressed without atomic-level structural information about the MTBD and the stalk. Given the large size of the minimal dynein motor domain (>320 kD of the >500-kD heavy-chain polypeptide), we sought to obtain a crystal structure of the MTBD and the distal portion of the coiled-coil stalk of mouse cytoplasmic dynein as a fusion with seryl tRNA-synthetase (SRS) from *Thermus thermophilus*. Previous work showed that such fusion proteins retain the ability to bind to microtubules and that their affinity for microtubules can be varied by changing the register in which the hydrophobic heptad periodicity of the coiled-coil stalk is fused to that of the SRS (*11*). This led to a model in which shifts in registry of the putative coiled coil could control the transition between weak and strong binding states in dynein's motility cycle.

We found that the pattern of two alternate registries (α and β)—having high and low microtubule-binding affinity, respectively—continues along the full length of the stalk (Fig. 1B, fig. S1, and table S1). Although crystals of an SRS-MTBD fusion in a strong microtubule-binding form were not obtained, we succeeded in crystallizing a thermally stable (table S2), weak-binding fusion protein (Fig. 1B, red star). The 2.3 Å structure was phased by molecular replacement, using the SRS as a search model, and refined to an R_{free} of 0.25 (see table S3 for crystallographic statistics). The SRS was present as a dimer, leading to two copies of the MTBD in the asymmetric unit (Fig. 1C, inset).

The coiled coil of the SRS proceeds smoothly into the coiled coil of the dynein stalk, and the distal MTBD consists of a bundle of six α helices (H1 to H6, Fig. 1C). In the basal region of the stalk, CC1 and CC2 form a characteristic antiparallel coiled coil with their registry continuing that of the SRS. After three heptads, the path of the coiled coil is bent by a pair of staggered, highly conserved prolines (Pro^{3285} in CC1 and Pro^{3409} in CC2; fig. S2), with the regular packing of hydrophobic residues in the coiled-coil core being disrupted in the region between the prolines (Fig. 1, C and D). When the heptad registry resumes after the prolines, the registry of CC1 has slipped by one half-heptad relative to that of CC2. The distal portion of CC2 makes extensive hydrophobic interactions with H2, H4, H5, and H6, whereas CC1 makes only a few contacts with H4 (Fig. 1D) before joining directly into H1. This asymmetry suggests that the interface between the stalk and the MTBD serves an important role in the dynein mechanism.

Opposite the point of entry of the coiled coil in the MTBD are three helices (H1, H3, and H6) that contain a high density of conserved, surface-accessible residues (fig. S3, A and B); this surface is largely electropositive (fig. S3C), similar to the microtubule docking site of kinesin (*12*). Mutation of several of these conserved residues to alanine interferes with the binding of *Dictyostelium* cytoplasmic dynein to microtubules (*13*), making this a likely contact site with the microtubule (Fig. 2A and fig. S3, D and E). In support of this model, we obtained a cryo–electron microscopy (cryo-EM) helical reconstruction (Fig. 2B, fig. S4, A to C, and movie S1) of microtubules decorated with a strong microtubule-binding SRS-MTBD

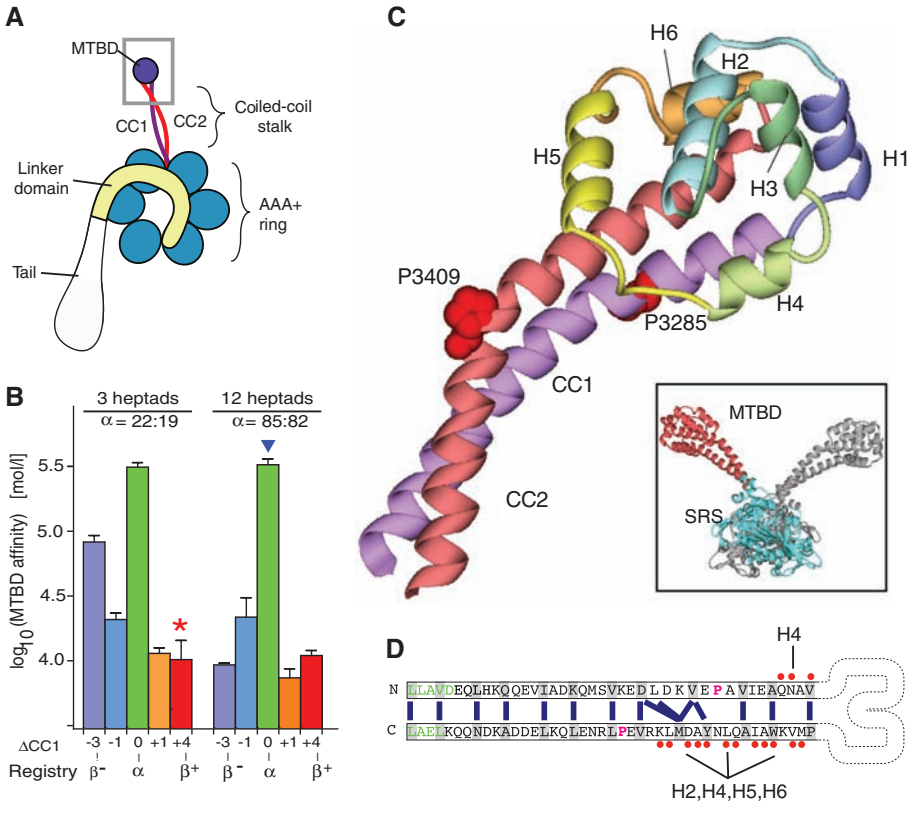

Fig. 1. Crystal structure of the dynein microtubule-binding domain. (**A**) Cartoon of a dynein motor (heavy chain). A gray box highlights the region of the stalk and microtubule-binding domain (MTBD) whose atomic structure is reported. (**B**) Effect of different heptad registries on microtubule-binding affinity of monomeric SRS-MTBD fusions with stalks of one-quarter and full native length. Paired numbers designating each construct (e.g., 22:19) indicate the number of residues between the SRS splice site and the proline marking the stalk-MTBD boundary for CC1 and CC2, respectively. (**C**) Crystal structure of the MTBD, showing the two α helices of the stalk (CC1, purple; CC2, red) that extend out of the SRS coiled coil and connect to the six-helix bundle (H1 to H6) forming the MTBD proper. A staggered pair of conserved prolines (Pro^{3285} and Pro^{3409}) are associated with a kink in the stalk. Inset: dimeric SRS-MTBD fusion protein (chain A, blue SRS with red MTBD; chain B, gray). (**D**) Schematic diagram of the stalk helices (CC1 and CC2) showing the heptad repeat hydrophobic contacts (blue lines) in the core of the coiled coil. The regularity of this repeat is disrupted between the conserved prolines (magenta), resulting in a half-heptad shift in coiled-coil registry. Residues in the SRS are shown in green. Residues in CC1 and CC2 that contact the other helices in MTBD are marked with red dots Abbreviations: A, Ala; C, Cys; D, Asp; E, Glu; F, Phe; G, Gly; H, His; I, Ile; K, Lys; L, Leu; M, Met; N, Asn; P, Pro; Q, Gln; R, Arg; S, Ser; T, Thr; V, Val; W, Trp; Y, Tyr.

[1]Howard Hughes Medical Institute and Department of Cellular and Molecular Pharmacology, University of California, San Francisco, CA 94158, USA. [2]Department of Molecular and Cell Biology, University of California, Berkeley, CA 94720, USA. [3]Department of Cell Biology, Scripps Research Institute, La Jolla, CA 92037, USA.

*These authors contributed equally to this work.
†To whom correspondence should be addressed. E-mail: vale@cmp.ucsf.edu

construct with a 12-heptad stalk (blue triangle in Fig. 1B).

The MTBD and a portion of the stalk were visible in the EM maps, but density was not observed for the distal nine heptads of this construct, most likely because the coiled coil is flexible and not fixed in one conformation. Our EM reconstruction contains more density for the stalk region but otherwise agrees well with a previous cryo-EM study (*14*). Our crystal structure of the MTBD stalk fits well into the cryo-EM density map (Fig. 2B). This docking places the MTBD helices H1 and H3—the candidate microtubule binding helices, according to mutagenesis studies—in a groove at the interface between the α and β tubulin subunits, which is the same location that kinesin motors use for binding to microtubules (fig. S4D) (*14*–*16*). In addition to locating the microtubule-binding interface, these data suggest that the overall shape of our weak-binding crystal structure is similar to that of a strong-binding construct and to native dynein bound to microtubules. However, at finer resolution, we cannot be sure whether our structure corresponds to an exact intermediate in native dynein's motility cycle.

In addition, the proposed microtubule-binding interface shows the greatest root-mean-square (RMS) differences between the two copies of the MTBD attached to the SRS dimer (dark red in Fig. 2C). Although these variations are driven by differences in crystal packing, they likely reflect regions of conformational flexibility in the MTBD that might rearrange in response to different nucleotide states in the catalytic domain (other regions with crystal contacts show little RMS deviation; fig. S5). A possible linchpin for conformational movements in the microtubule-binding helices is a contact between a highly conserved (fig. S2) proline (Pro^{3311}) in H1 and a tryptophan (Trp^{3334}) in H3; this contact is present in one MTBD of the SRS dimer but is disrupted in the other (Fig. 2D).

The direct connectivity of CC1 with H1 (a conformationally flexible helix at a microtubule-binding interface) and CC1's limited contacts with the rest of the MTBD suggest that movement of CC1 is responsible for bidirectional communication along the stalk. We propose that strong microtubule binding changes the conformations of H1, H3, and H4. This results in a movement of CC1 relative to CC2 that propagates to the AAA+ ring and stimulates a rate-limiting chemical transition in the ATPase cycle. A subsequent nucleotide-dependent change in the AAA+ ring then drives the opposite movement of CC1, leading to a reduction in affinity of the MTBD for microtubules.

With respect to the magnitude of sliding, it is possible that communication might occur through a small displacement of the helix similar to that proposed for bacterial chemotaxis receptors (*17*). However, we favor the idea that CC1 is displaced by four residues (fig. S6) relative to a stationary CC2. This model is consistent with biochemical data from SRS fusion proteins (Fig. 1B) (*11*), which show that forcing a change in registry of the stalk at one end can affect the binding affinity of the MTBD, even over a distance of 12 heptad repeats (12 nm). The region between the staggered pair of proline residues (Fig. 1D) may be particularly important for such a conformational change mechanism. This region could facilitate a piston-like movement of CC1 relative to CC2. Alternatively, the slip in heptad register seen in this region of our crystal structure may serve as the starting point for a domino-like movement involving local melting and reformation of the coiled coil that propagates the register change from one end of the stalk to the other.

We next sought to examine the role of the MTBD in determining the direction of dynein motility. The most widely cited model (*8*) for dynein proposes that motility is driven by a minus end–directed swing of the linker domain (Fig. 3B, red arrow). In this model, the MTBD and stalk hold the AAA+ ring in such an orientation that the power stroke is directed along the microtubule axis toward the minus end. To investigate whether the MTBD stalk serves such a role in dynein's mechanism, we engineered an artificially dimerized *Saccharomyces cerevisiae* cytoplasmic dynein (*18*) with its stalk coiled coil

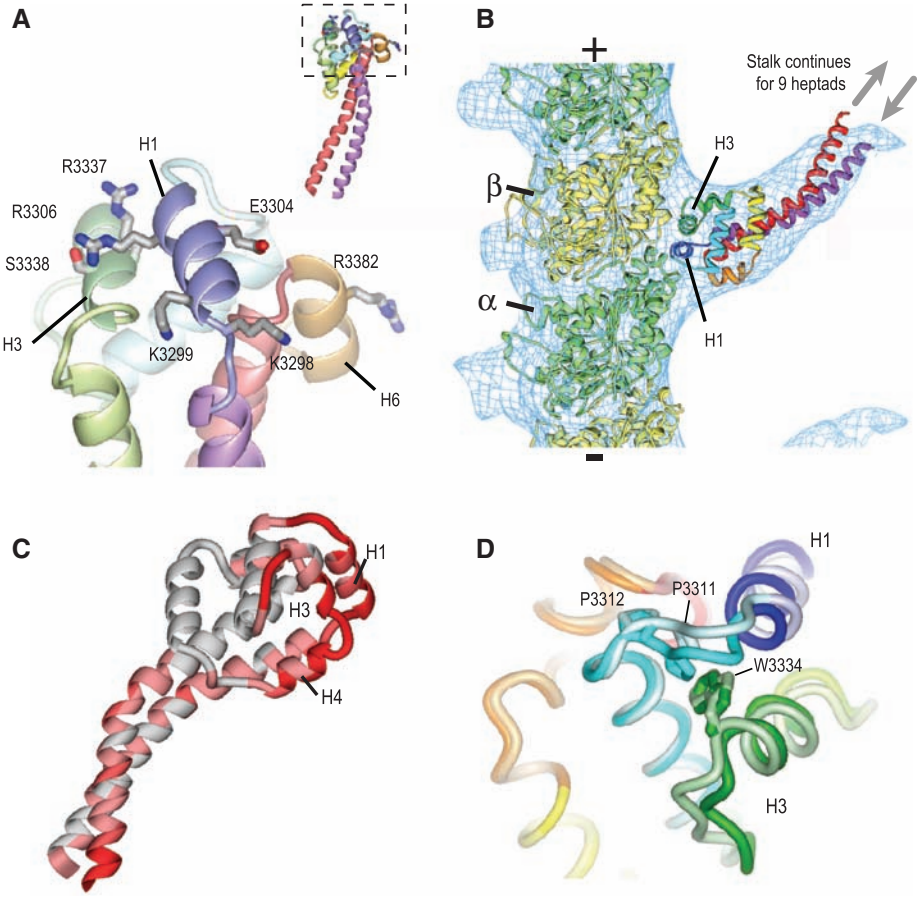

Fig. 2. Microtubule-binding surface of the dynein MTBD. (**A**) Close-up view of the MTBD, showing the putative microtubule-binding helices H1, H3, and H6. Residues that abolish binding when mutated to alanine (*13*) are shown in stick representation. The inset shows this interface (boxed) with respect to the whole MTBD structure. (**B**) A model of the dynein MTBD (crystal structure shown and colored as in Fig. 1C) bound to a tubulin protofilament (α tubulin, green; β tubulin, yellow). Crystal structures were docked into a single protofilament cut from the cryo-EM electron density map of a microtubule decorated with a monomeric, tight-binding (α registry) SRS-MTBD construct containing 12 heptads of dynein stalk (SRS-MTBD-85:82). The plus and minus signs indicate microtubule polarity. The SRS and nine basal heptad repeats of the stalk are not visible in the reconstructed image (gray arrows). (**C**) Conformational differences between the A and B MTBD monomers on an SRS dimer. Regions of high RMS difference are colored dark red. (**D**) Close-up of the H1-H3 interface. Aligned MTBDs are shown in light (chain B) and dark (chain A) coloring. The contact between the highly conserved Pro^{3311} and Trp^{3334} residues is broken in chain B.

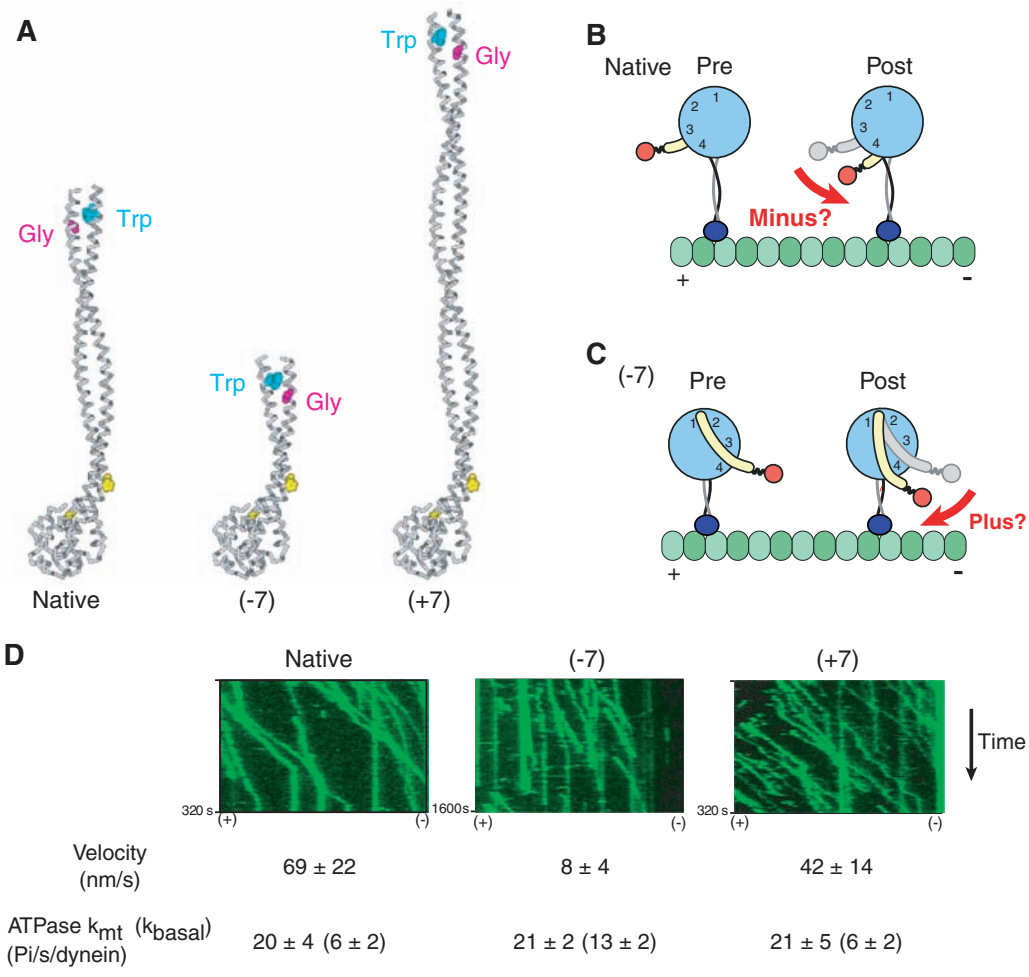

Fig. 3. Rotation of the AAA+ ring by insertion or deletion of stalk sequence does not affect the direction of dynein movement. (**A**) Model of native dynein stalk (at left), showing the pair of conserved prolines (yellow spacefill) marking the MTBD and the conserved Trp-Gly pair that mark the top of the stalk coiled coil. Removal of seven heptads from the middle of the dynein stalk (–7) or insertion of seven heptads from the dynein stalk of *Drosophila* cytoplasmic dynein (+7) rotates the position of the Trp-Gly pair by 180° with respect to the microtubule-binding domain. (**B**) Cartoon of a model for how conformational changes in the AAA+ ring lead to minus end–directed motion [adapted from (*8*)] via rotation of the linker domain (yellow) toward the minus end. (**C**) Cartoon showing how the model in (B) predicts that rotation of the AAA+ ring by 180° due to a change in the length of the stalk should produce a plus end–directed motor. (**D**) Single-molecule fluorescence assay for the directionality of dimeric *S. cerevisiae* dynein constructs [based on GST-$Dyn1_{331kD}$ (*18*)] with different lengths of stalk. Kymographs of tetramethyl rhodamine–labeled dynein constructs from a single axoneme in the assay (green) show that all constructs move unidirectionally toward the minus end of the microtubule. The orientation of the axoneme was determined using fluorescent Cy5-labeled kinesin (see movies S2 to S4). Single-molecule velocities (means ± SD) and ATPase measurements (means ± SD) were determined as described in the supporting online material.

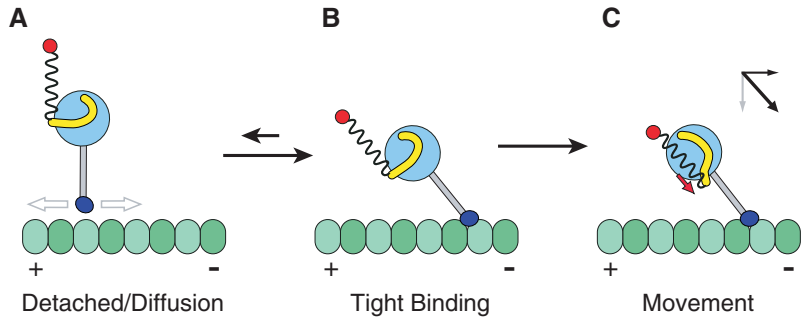

Fig. 4. Model for directional movement of dynein. (**A**) After release from the microtubule, the dynein is in a preconformational change (power stroke) state, with the linker domain (yellow) docked on the AAA+ domain (light blue circle) somewhat removed from the base of the stalk (gray). The rest of the dynein tail domain is represented as a loose spring attached to a cargo (red). The dynein MTBD (dark blue) is diffusing to a new site on the microtubule. (**B**) The MTBD preferentially enters a tightly bound state after binding toward the minus end, with the stalk at an angle. (**C**) An ATP-driven conformational change in the linker domain produces motion whose main vector directional component is parallel to the direction of the stalk (red arrow). The angle of the stalk thus converts this tension generated by the AAA+ domain into a displacement toward the minus end of the microtubule (as shown by the vector diagram), regardless of the orientation of the AAA+ ring.

either lengthened or shortened by seven heptads (fig. S5). On the basis of the coiled-coil nature of the dynein stalk proximal to the proline-associated kink, these stalk length changes would be predicted to rotate the AAA+ ring by 180° (Fig. 3, A and C) and reverse the direction of dynein movement according to the model in Fig. 3B. Even though the native length of the stalk appears to be conserved in all dyneins, we found that dynein constructs with markedly shortened or lengthened stalks could still move processively along microtubules, albeit with reduced velocities. The much slower velocity of the –7 construct may be the result of some degree of uncoupling between the MTBD and AAA+ ring, as reflected by its elevated basal ATPase rate. Remarkably, the movement of both mutants remained minus end–directed (Fig. 3D and movies S2 to S4), which suggests that the orientation of the AAA+ domain does not determine the direction of dynein movement along a microtubule.

To explain the directionality of dynein, we propose that the AAA+ ring does not elicit a lever-like rotation of the linker domain perpendicular to the stalk (as in Fig. 3B); rather, the force vector of the linker domain's conformational change is directed parallel to an angled stalk (compare Fig. 4, B and C). This would explain why a rotation of the head around the stalk axis (Fig. 3) does not affect the direction of movement, because the net force vector would still remain parallel to the tilted stalk.

This model makes the prediction that the stalk is tilted (extending from the AAA+ ring toward the minus end, as in Fig. 4B) at the time when a productive power stroke occurs. The MTBD may preferentially bind to the microtubule at such an angle, as suggested by our cryo-EM map (Fig. 2B) and a recent reconstruction of a whole axonemal dynein in its pre–power stroke state (*19*). Alternatively, the MTBD may rebind to the microtubule at various angles, but respond to a power stroke differently depending on its angle of attachment. A force-producing conformational change would produce a productive, minus end–directed displacement of the cargo if the stalk were pointing toward the minus end (e.g., Fig. 4C), whereas the MTBD would release if the stalk were pointing in the opposite direction (*18*, *20*). Further work will be needed to define the orientation of the stalk at different stages of the motility cycle and to learn how dynein might be able to reverse its direction of motion, as has been reported for a mammalian dynein (*21*).

The model for dynein motility presented here (Fig. 4) differs from the swinging lever arm model developed for myosin and kinesin (*22*). The dynein stalk does not serve as a rigid lever, as proposed elsewhere (*23*), but rather acts as a tether that allows the detached MTBD to explore a range of potential microtubule-binding sites and transmit tension between the AAA+ ring and the MTBD. The large AAA+ ring and its associated linker domain undergo ATP-dependent conformational changes (*8*, *9*) that pull along the stalk axis. This is consistent with the known actions of other AAA+ proteins (*24*) and the previous proposal that dynein acts as a winch (*8*). And it is the MTBD—one of the smallest elements of the large dynein motor protein—that governs the directionality of the motor.

References and Notes

1. I. R. Gibbons, *Cell Motil. Cytoskeleton* **32**, 136 (1995).
2. B. J. Howell *et al.*, *J. Cell Biol.* **155**, 1159 (2001).
3. K. T. Vaughan, *Biochim. Biophys. Acta* **1744**, 316 (2005).
4. R. B. Vallee *et al.*, *J. Neurobiol.* **58**, 189 (2004).
5. M. A. Zariwala *et al.*, *Annu. Rev. Physiol.* **69**, 423 (2007).
6. M. Hafezparast *et al.*, *Science* **300**, 808 (2003).
7. D. Zuccarello *et al.*, *Hum. Reprod.* **23**, 1957 (2008).
8. S. A. Burgess *et al.*, *Nature* **421**, 715 (2003).
9. T. Kon *et al.*, *Nat. Struct. Mol. Biol.* **12**, 513 (2005).
10. M. A. Gee *et al.*, *Nature* **390**, 636 (1997).
11. I. R. Gibbons *et al.*, *J. Biol. Chem.* **280**, 23960 (2005).
12. G. Woehlke *et al.*, *Cell* **90**, 207 (1997).
13. M. P. Koonce, I. Tikhonenko, *Mol. Biol. Cell* **11**, 523 (2000).
14. N. Mizuno *et al.*, *EMBO J.* **23**, 2459 (2004).
15. M. Kikkawa, N. Hirokawa, *EMBO J.* **25**, 4187 (2006).
16. C. V. Sindelar, K. H. Downing, *J. Cell Biol.* **177**, 377 (2007).
17. M. Hulko *et al.*, *Cell* **126**, 929 (2006).
18. S. L. Reck-Peterson *et al.*, *Cell* **126**, 335 (2006).
19. T. Oda *et al.*, *J. Cell Biol.* **177**, 243 (2007).
20. A. Gennerich *et al.*, *Cell* **131**, 952 (2007).
21. J. L. Ross *et al.*, *Nat. Cell Biol.* **8**, 562 (2006).
22. R. D. Vale, R. A. Milligan, *Science* **288**, 88 (2000).
23. N. Mizuno *et al.*, *Proc. Natl. Acad. Sci. U.S.A.* **104**, 20832 (2007).
24. P. A. Tucker, L. Sallai, *Curr. Opin. Struct. Biol.* **17**, 641 (2007).

25. We thank J. Welburn and E. Nogales for advice and equipment; M. Kikkawa for sending his group's electron density map; and N. Bradshaw, J. Kardon, K. Aathavan, A. Dosé, A. Gennerich, A. Roll-Mecak, and S. Reck-Peterson for critically reading the manuscript. Supported by the Jane Coffin Childs Foundation (A.P.C.); NIH grants GM52468-14 (R.A.M.), P01-AR42895 (R.D.V.) and GM30401-29 (I.R.G.)]; the Agouron Institute (A.P.C.); the Leukemia and Lymphoma Society (A.P.C.); and the Howard Hughes Medical Institute. Crystallography data were collected at beamline 8.3.1 of the Advanced Light Source at Lawrence Berkeley National Laboratory. The atomic coordinates and structure factors have been deposited in the Protein Data Bank (code 3ERR). Cryo-EM data were collected in part at the National Resource for Automated Molecular Microscopy at the Scripps Research Institute (NIH P41 RR-17573). Maps were deposited at the EMDataBank (EMD-1581).

Supporting Online Material

www.sciencemag.org/cgi/content/full/322/5908/1691/DC1
Materials and Methods
Tables S1 to S3
Figs. S1 to S7
Movies S1 to S4
References

8 August 2008; accepted 6 November 2008
10.1126/science.1164424

Genomic Loss of microRNA-101 Leads to Overexpression of Histone Methyltransferase EZH2 in Cancer

Sooryanarayana Varambally,[1,2,3]* Qi Cao,[1,2]* Ram-Shankar Mani,[1,2] Sunita Shankar,[1,2] Xiaosong Wang,[1,2] Bushra Ateeq,[1,2] Bharathi Laxman,[1,2] Xuhong Cao,[1,4] Xiaojun Jing,[1,2] Kalpana Ramnarayanan,[5] J. Chad Brenner,[1,2,6] Jindan Yu,[1,2] Jung H. Kim,[1,3] Bo Han,[1,2] Patrick Tan,[5,7] Chandan Kumar-Sinha,[1,2] Robert J. Lonigro,[1,3] Nallasivam Palanisamy,[1,2,5] Christopher A. Maher,[1,2] Arul M. Chinnaiyan[1,2,3,4,6,8]†

Enhancer of zeste homolog 2 (EZH2) is a mammalian histone methyltransferase that contributes to the epigenetic silencing of target genes and regulates the survival and metastasis of cancer cells. EZH2 is overexpressed in aggressive solid tumors by mechanisms that remain unclear. Here we show that the expression and function of EZH2 in cancer cell lines are inhibited by microRNA-101 (miR-101). Analysis of human prostate tumors revealed that miR-101 expression decreases during cancer progression, paralleling an increase in EZH2 expression. One or both of the two genomic loci encoding miR-101 were somatically lost in 37.5% of clinically localized prostate cancer cells (6 of 16) and 66.7% of metastatic disease cells (22 of 33). We propose that the genomic loss of miR-101 in cancer leads to overexpression of EZH2 and concomitant dysregulation of epigenetic pathways, resulting in cancer progression.

Polycomb group proteins, including enhancer of zeste homolog 2 (EZH2), play a master regulatory role in controlling important cellular process such as maintaining stem cell pluripotency (*1*–*3*), cell proliferation (*4*, *5*), early embryogenesis (*6*), and X chromosome inactivation (*7*). EZH2 functions in a multiprotein complex called polycomb repressive complex 2 (PRC2), which includes SUZ12 (suppressor of zeste 12) and EED (embryonic ectoderm development) (*8*, *9*). The primary activity of the EZH2 protein complex is to trimethylate histone H3 lysine 27 (H3K27) at target gene promoters, leading to epigenetic silencing (*10*, *11*). Mounting evidence suggests that EZH2 has properties consistent with those of an oncogene because overexpression promotes cell proliferation, colony formation, and increased invasion of benign cells in vitro (*4*, *5*, *12*) and induces xenograft tumor growth in vivo (*13*). Likewise, knockdown of EZH2 in cancer cells results in growth arrest (*4*, *13*) as well as diminished tumor growth (*10*) and metastasis in vivo (*14*).

EZH2 was initially found to be elevated in a subset of aggressive clinically localized prostate cancers and almost all metastatic prostate cancers (*4*). Subsequently, EZH2 has also been found to be aberrantly overexpressed in breast cancer (*12*), melanoma (*15*), bladder cancer (*16*), gastric cancer (*17*), and other cancers (*5*). Thus, although EZH2 is broadly overexpressed in aggressive solid tumors and has properties of an oncogene, the genetic mechanism of EZH2 elevation in cancer is unclear.

[1]Michigan Center for Translational Pathology, University of Michigan Medical School, Ann Arbor, MI 48109, USA. [2]Department of Pathology, University of Michigan Medical School, Ann Arbor, MI 48109, USA. [3]Comprehensive Cancer Center, University of Michigan Medical School, Ann Arbor, MI 48109, USA. [4]Howard Hughes Medical Institute, University of Michigan Medical School, Ann Arbor, MI 48109, USA. [5]Genome Institute of Singapore, 60 Biopolis Street, 02-01, Genome, Singapore 138672, Singapore. [6]Department of Cellular and Molecular Biology, University of Michigan Medical School, Ann Arbor, MI 48109, USA. [7]National Cancer Centre, 11 Hospital Drive, Singapore 169610, Singapore. [8]Department of Urology, University of Michigan Medical School, Ann Arbor, MI 48109, USA.

*These authors contributed equally to this work.
†To whom correspondence should be addressed. E-mail: arul@umich.edu

Because microRNAs (miRNAs) have gained considerable attention as regulators of gene expression (*18*) and play important roles in cellular differentiation and embryonic stem cell development (*19*), we postulated that they may play a role in modulating EZH2 expression. To test whether miRNAs play a role in controlling EZH2 expression, we computationally nominated those that might contribute to *EZH2* regulation. Because intersecting the results of multiple prediction algorithms can increase specificity at the cost of lower sensitivity (*20*), we integrated the results of the prediction software programs PicTar (*21*), TargetScan (*22*), miRanda (*23*), and miRInspector (*24*). Overall, only 29 miRNAs were found by any program to target *EZH2*, whereas only microRNA-101 (miR-101) and miR-217 were found by all four programs to be predicted to regulate *EZH2* (Fig. 1A and table S1) (*25*). Furthermore, PicTar, miRanda, and TargetScan predicted two miR-101–binding sites within the *EZH2* 3′ untranslated region (3′UTR) (Fig. 1B), whereas PicTar and TargetScan predicted two miR-217 binding sites within the *EZH2* 3′UTR. Of the 34 miRNAs predicted to regulate EZH2 by at least one program (table S1), only miR-101 had a strong negative association with prostate cancer progression from benign to localized disease to metastasis.

To examine whether miR-101 regulates the 3′UTR of *EZH2*, we generated luciferase reporters encoding the normal, antisense, and mutated versions of the EZH2 3′UTR. Overexpression of miR-101, but not miR-217 or control miRNA, decreased the activity of the luciferase reporter encoding the 3′UTR of EZH2 (fig. S1). Similarly, the antisense and mutant EZH2 3′UTR activities were not inhibited by miR-101. To explore whether the 3′UTR binding by miR-101 results in down-regulation of the *EZH2* transcript, we transfected SKBr3 breast cancer cells (which express high levels of endogenous EZH2) with precursors of miR-101, miR-217, and a control miRNA, as well as several other unrelated miRNAs. Quantitative reverse transcription polymerase chain reaction (RT-PCR) demonstrated a reduction in *EZH2* transcript levels by miR-101 (Fig. 1C) but not miR-217 or other control miRs.

To determine whether miR-101 represses EZH2 protein expression, we performed immunoblot analysis using an EZH2-specific antibody as well as antibodies to other PRC2 members, including EED and SUZ12 (Fig. 1D). In addition to miR-101, we included other miRNAs that were predicted to regulate EZH2, including miR-217 and miR-26a. Control miR-495 was predicted by TargetScan to target the PRC1 component BMI-1. Only miR-101 and EZH2 small interfering RNA (siRNA) attenuated EZH2 protein expression. miR-101 overexpression also leads to repression of EZH2's tight binding partners in the PRC2 complex: EED and, to a lesser extent, SUZ12. These proteins are thought to form a coregulated functional complex, and altering the expression of one affects the expression of the others (*5*, *26*, *27*). In this particular case, upon further inspection of the 3′UTRs of the PRC2 components, miR-101 binding sites were found in *EED* (fig. S2) but not in *SUZ12*. Because miRNAs are known to regulate multiple target genes, and in some cases hundreds of genes (*18*), we used the prediction algorithm TargetScan to nominate targets of miR-101. In addition to EZH2 and EED, we tested four predicted targets of miR-101 (table S2) that have been implicated in cancer pathways, including n-Myc, c-Fos, AT-rich interactive domain 1A (also called SWI-like and ARID1A), and fibrillin 2 (FBN2). None of these putative miR-101 targets were affected by overexpression of miR-101 (Fig. 1D). To support the findings from our miR-101–overexpression experiments, we employed antagomiR technology (*28*) to specifically inhibit miR-101 expression in benign immortalized breast epithelial cells (fig. S3). Two independent antagomiRs to miR-101 (i and ii) induced expression of EZH2 protein in benign breast epithelial cells.

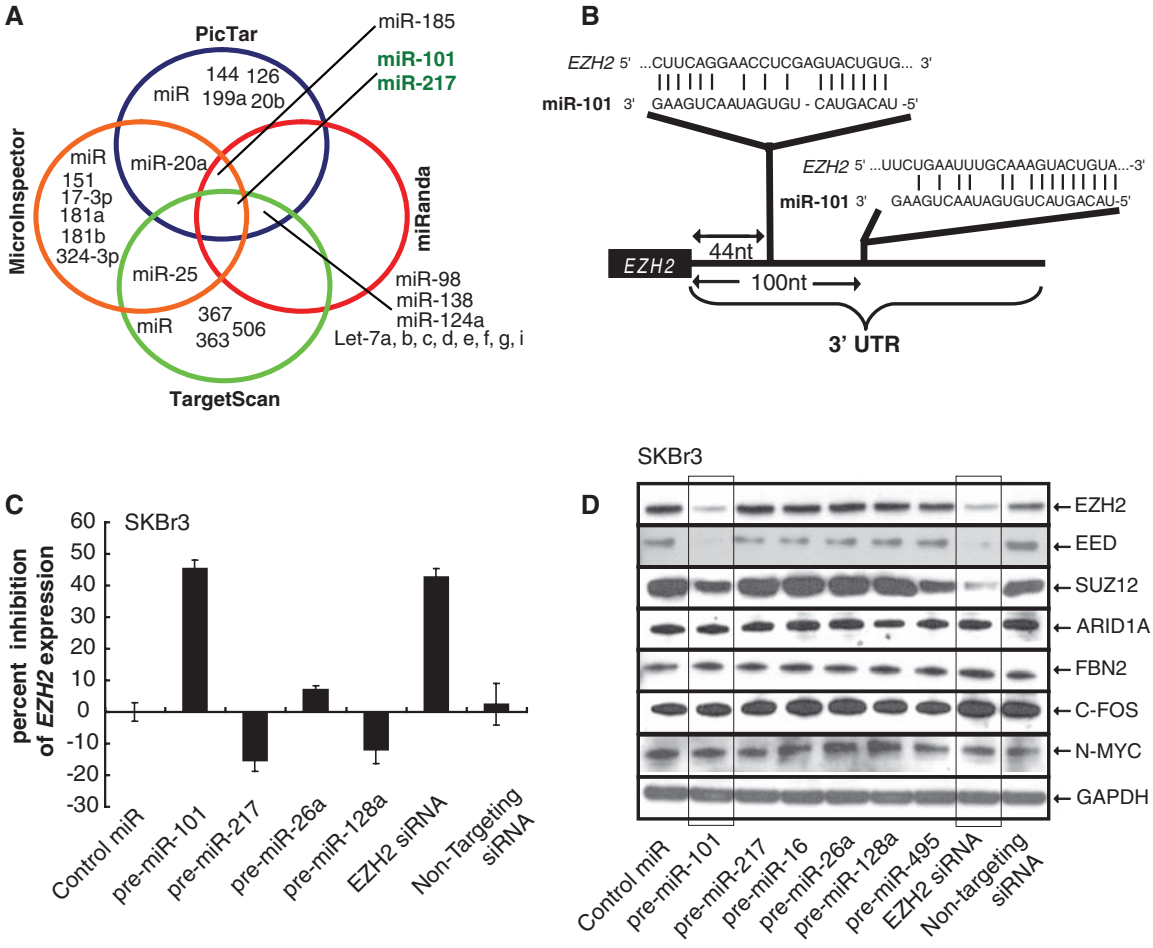

Fig. 1. miR-101 regulates EZH2 transcript and protein expression. (**A**) Venn diagram displaying miRNAs computationally predicted to target EZH2 by PicTar (blue), miRanda (red), TargetScan (green), and MicroInspector (orange). (**B**) Schematic of two predicted miR-101–binding sites in the *EZH2* 3′UTR. (**C**) miR-101 regulates *EZH2* transcript expression. Quantitative RT-PCR of *EZH2* in SKBr3 cells transfected with precursor miR-101 is shown. Control miR and other precursor miRNAs (miR-26a, miR-128a, and miR-217) were also used for transfection. (**D**) miR-101 regulates PRC2 protein expression. miR-101 down-regulates EZH2 protein as well as PRC2 members SUZ12 and EED in SKBr3 cells. Control miRs and EZH2-specific siRNA were also used for transfection. The experiment was performed three independent times and a representative result is displayed. GAPDH, glyceraldehyde-3-phosphate dehydrogenase.

To determine whether miR-101 affects EZH2 and PRC2 function, we evaluated cellular proliferation, a property known to be regulated by EZH2 (*4*, *5*). miR-101 overexpression in SKBr3 and DU145 cells markedly attenuated cell proliferation (Fig. 2A and fig. S4). Overexpression of EZH2 (without an endogenous 3′UTR) rescued the inhibition of cell growth by miR-101, which suggests target specificity.

We previously showed that upon overexpression, EZH2 can induce cell invasion in matrigel-coated basement membrane invasion assays (*12*). Here we show that miR-101 overexpression markedly inhibits the in vitro invasive potential of DU145 prostate-cancer cells (Fig. 2B) and SKBr3 breast cancer cells (fig. S5). Similarly, stable expression of miR-101 in DU145 cells showed a reduction in *EZH2* expression and reduced invasion (fig. S6, A and B). Overexpression of EZH2 rescued the inhibition that was mediated by miR-101. Another in vitro readout for tumorigenic potential, increased cell migration, was also inhibited by miR-101 (fig. S7). Because overexpression of miR-101 attenuates cancer invasion, inhibition of miR-101 should enhance this neoplastic phenotype. Two independent antagomiRs targeting miR-101 (i and ii) induced an invasive phenotype when transfected into benign immortalized breast epithelial cell lines H16N2 or HME (Fig. 2C and fig. S8).

To assess whether miR-101 inhibits anchorage-independent growth, we used a soft-agar assay. DU145 prostate cancer cells stably overexpressing miR-101 exhibited markedly reduced colony formation relative to the parental cells or vector controls (fig. S9). Furthermore, in vivo, DU145 cells expressing miR-101 grew significantly slower than the vector control xenografts (P = 0.0001) (Fig. 2D), demonstrating that miR-101 has properties consistent with that of a tumor suppressor in these particular assays.

Because EZH2 and PRC2 regulate gene expression by trimethylating H3K27, we hypothesized that miR-101 overexpression would result in decreased overall H3K27 trimethylation in cancer cells. SKBr3 breast cancer and DU145 prostate cancer cells transfected with miR-101 or EZH2 siRNA for 7 days displayed a global decrease in trimethyl H3K27 levels (fig. S10A). The effect of miR-101 on H3K27 methylation was negated by overexpression of EZH2 (fig. S10B).

To test the level of promoter occupancy of the H3K27 histone mark, we performed chromatin immunoprecipitation (ChIP) assays in cancer cells overexpressing miR-101. We found significant reduction in the trimethyl H3K27 histone mark at the promoter of known PRC2 target genes

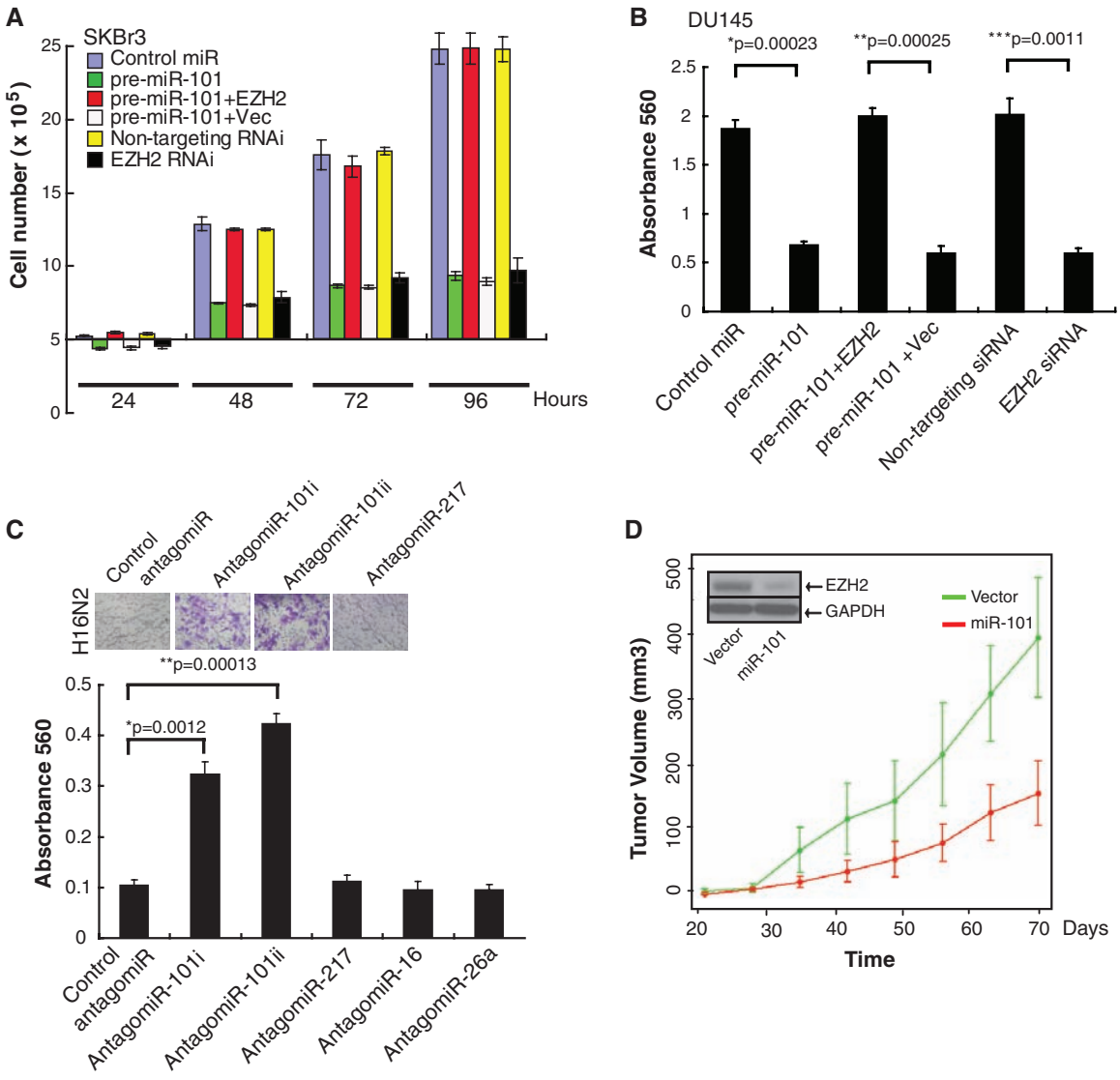

Fig. 2. The role of miR-101 in regulating cell proliferation, invasion, and tumor growth. (**A**) miR-101 overexpression reduces cell proliferation. A cell growth assay of SKBr3 cells treated with either precursor miR-101 or siRNA targeting EZH2 is shown. Cell growth relative to the control miRNA and control siRNA duplex was measured. Rescue experiments were performed by overexpressing EZH2 (minus its endogenous 3′UTR) in miR-101–treated cells. (**B**) miR-101 expression decreases cell invasion of DU145 prostate carcinoma cells. We transfected cells with miR-101, EZH2-specific siRNA, control miR, and nontargeting siRNA. miR-101 was also overexpressed in those cells that overexpressed EZH2 by andenoviral infection. All cells were subjected to a matrigel invasion assay. (**C**) AntagomiRs to miR-101 induce the invasiveness of benign immortalized H16N2 breast epithelial cells. Representative fields of invaded and stained cells are shown in the inset. P values were calculated between control antagomiR, antagomiR-101i, and antagomiR-101ii. (**D**) Overexpression of miR-101 attenuates prostate tumor growth. Overexpression of miR-101 reduces DU145 tumor growth in a mouse xenograft model. Plot of mean tumor-volume trajectories over time for the mice inoculated with (red) miR-101– and (green) vector-expressing DU145 cells. Error bars represent the SE of the mean at each time point. The inset displays the decrease of EZH2 protein levels in miR-101–expressing cell lines.

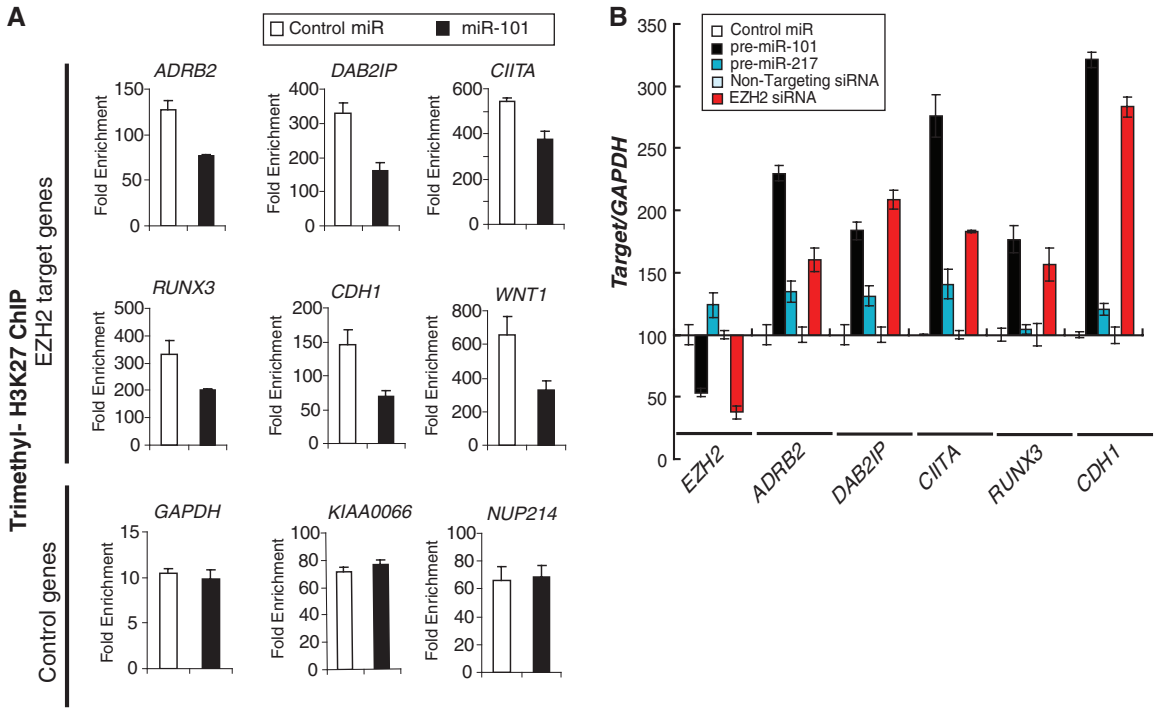

Fig. 3. miR-101 regulation of the cancer epigenome through EZH2 and H3K27 trimethylation. (**A**) ChIP assay of the trimethyl H3K27 histone mark when miR-101 is overexpressed. Known PRC2 repression targets were examined in SKBr3 cells. ChIP was performed to test H3K27 trimethylation at the promoters of *ADRB2*, *DAB2IP*, *CIITA*, *RUNX3*, *CDH1*, and *WNT1*. *GAPDH*, *KIAA0066*, and *NUP214* gene promoters served as controls. (**B**) Quantitative RT-PCR of EZH2 target genes was performed with SKBr3 cells transfected with miR-101. The EZH2 transcript and its known targets, including *ADRB2*, *DAB2IP*, *CIITA*, *RUNX3*, and E-cadherin (*CDH1*) were measured.

such as *ADRB2*, *DAB2IP*, *CIITA*, and *WNT1* in miR-101–overexpressing SKBr3 cells and EZH2 siRNA–treated cells (Fig. 3A and fig. S11). To determine whether the reduced promoter occupancy by H3K27 results in concomitant reduction of gene expression, we performed quantitative RT-PCR on the PRC2 targets tested by ChIP assay. As expected, there was a significant increase in target gene expression in both miR-101– and EZH2 siRNA–treated cells (Fig. 3B). To further explore miR-101 regulation of EZH2 and its possible similarity with EZH2-specific RNA interference (RNAi), we examined whether miR-101 overexpression and *EZH2* knockdown generated similar gene expression profiles. To assess this, we conducted gene-expression array analysis of SKBr3 cells transfected with either miR-101 or EZH2 siRNA duplexes. Genes that were overexpressed at the twofold threshold were significantly overlapping in both the miR-101– and EZH2 siRNA–transfected cells ($P = 6.08 \times 10^{-17}$) (fig. S12). Similarly, those genes that were repressed also had significant overlap ($P = 3.24 \times 10^{-27}$).

We next investigated whether miR-101 expression inversely correlates with EZH2 levels in human tumors. A meta-analysis of a majority of the publicly available miRNA expression data sets suggested that miR-101 is significantly underexpressed in prostate, breast, ovarian, lung, and colon cancers (table S3). Because EZH2 was initially found to be overexpressed in a subset of aggressive clinically localized prostate cancers and almost universally elevated in metastatic disease (*4*), we examined miR-101 in a similar context of prostate cancer progression by doing quantitative PCR analysis (Fig. 4A and fig. S13). As expected, metastatic prostate cancers expressed significantly higher levels of EZH2 as compared with those of clinically localized disease or benign adjacent prostate tissue ($P < 0.0001$). Consistent with a functional connection between miR-101 and EZH2, miR-101 expression was significantly decreased in metastatic prostate cancer relative to that in clinically localized disease or benign adjacent prostate tissue ($P < 0.0001$). miR-217, which like miR-101 was predicted to regulate EZH2, did not exhibit significant differences between metastatic disease and clinically localized prostate cancer or benign prostate tissue ($P = 0.35$ and 0.13, respectively).

To investigate the mechanism for miR-101 transcript loss in prostate cancer progression, we performed quantitative genomic PCR for miR-101. miR-101 has two genomic loci that are on chromosome 1 (miR-101–1) and chromosome 9 (miR-101–2) (fig. S14, A and B). Based on genomic PCR, 2 of 16 clinically localized prostate cancer s and 17 of 33 metastatic prostate cancers exhibited loss of the miR-101–1 locus (Fig. 4B). Similarly, 4 of 16 clinically localized prostate cancers and 8 of 33 metastatic prostate cancers displayed loss of miR-101–2 (Fig. 4B). Figure 4C displays a heat-map representation of matched samples in which miR-101 transcript, *EZH2* transcript, miR-101–1 genomic loci, and miR-101–2 genomic loci were monitored. *EZH2* transcript levels were inversely associated with miR-101 transcript levels across prostate cancer progression to metastasis ($P < 0.0001$). *EZH2* tended to be uniformly elevated in samples in which the miR-101–1 or miR-101–2 genomic loci exhibited a loss in copy number ($P = 0.004$, permutation test).

To formally demonstrate that genomic loss of miR-101 loci was somatic in nature, we identified nine metastatic prostate cancers that exhibited loss of miR-101–1 and obtained DNA from matched normal tissue. As expected, eight of nine cases exhibited a marked decrease in relative levels of miR-101–1 copy number in the cancer as compared with that in matched normal tissue (Fig. 4D). We also explored miR-101 genomic loss in other tumor types. Using a number of experimental platforms, we demonstrated focal loss (~20 kB) of miR-101–1 in a subset of breast, gastric, and prostate cancers (figs. S15 to S17). Furthermore, we explored public-domain high-density array comparative genomic hybridization and single-nucleotide polymorphism array data sets and observed a genomic loss of one or both miR-101 loci in a subset of glioblastoma multiforme, lung adenocarcinoma, and acute lymphocytic leukemia (fig. S18) (*25*).

miR-101, by virtue of its regulation of EZH2, may have profound control over the epigenetic pathways that are active not only in cancer cells but in normal pluripotent embryonic stem cells. Overexpression of miR-101 may configure the histone code of cancer cells to that associated with a more benign cellular phenotype. Because the loss of miR-101 and concomitant elevation of EZH2 are most pronounced in metastatic cancer, we postulate that miR-101 loss may represent a progressive molecular lesion in the development of more aggressive disease. Approaches to reintroduce miR-101 into tumors may have therapeutic benefit by reverting the epigenetic program of tumor cells to a more normal state.

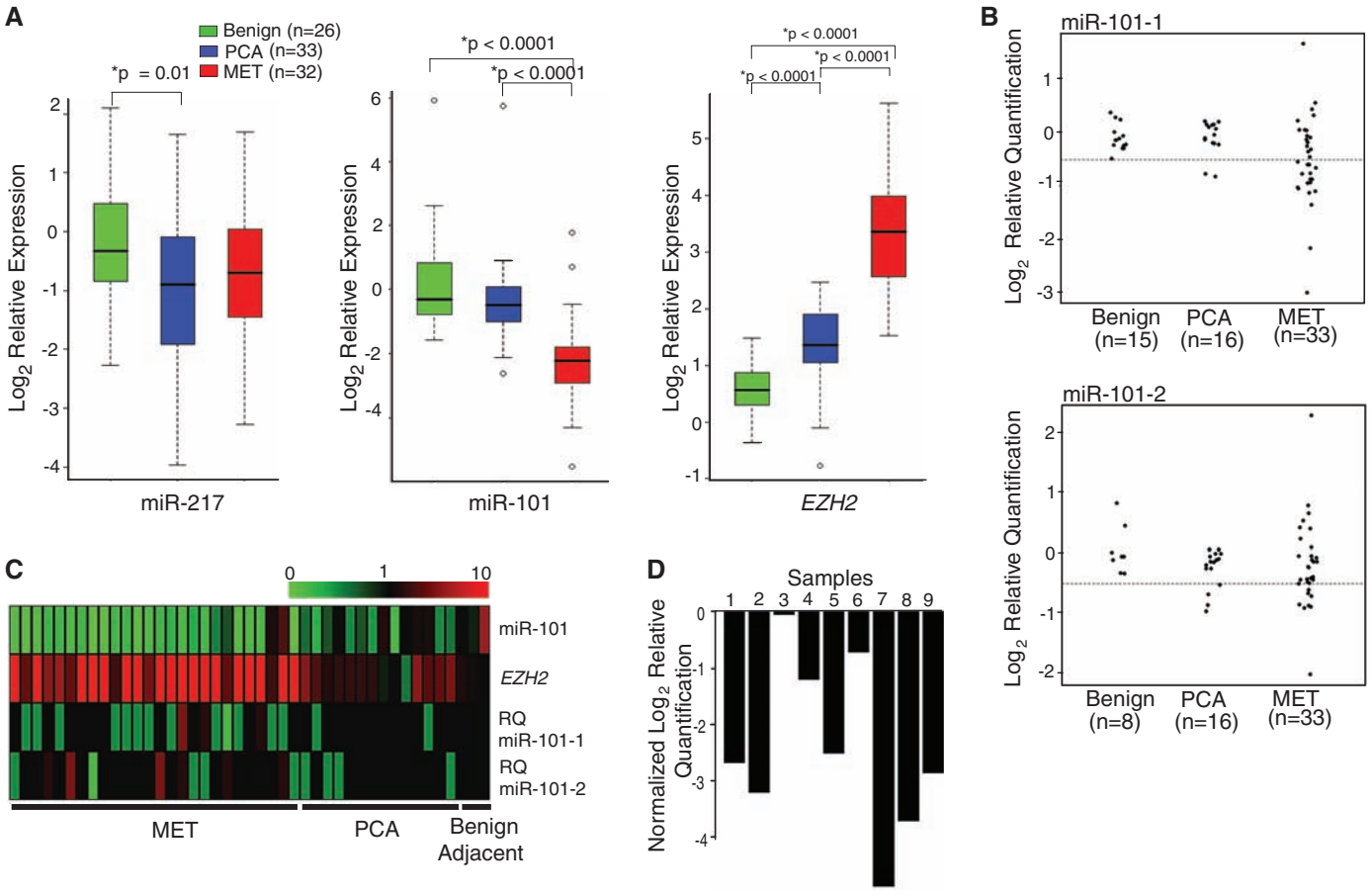

Fig. 4. Genomic loss of the miR-101 locus may explain overexpression of EZH2 in solid tumors. (**A**) miR-101 transcript levels are inversely correlated with EZH2 expression in prostate cancer progression. We performed quantitative PCR for miR-101 and miR-217 by using total RNA from benign adjacent prostate, prostate cancer (PCA), and metastatic (MET) prostate cancer tissue. *EZH2* expression was analyzed from the same RNA samples. (**B**) Genomic PCR of miR-101–1 and miR-101–2 in prostate cancer progression. Vertical axes represent log (base 2) relative quantification values; dashed lines are shown at the deletion threshold of $\log_2(0.7) \approx -0.51$. For clarity, points have been horizontally displaced within each sample class. (**C**) Heat-map representation of matched normal, tumor, and metastatic samples (from right to left) in which miR-101 transcript, *EZH2* transcript, and both miR-101–1 and miR-101–2 relative copy number were assessed. miR-101 and *EZH2* expression is represented by a color scale highlighting down-regulation (green), no alteration (black), and up-regulation (red) of transcripts. miR-101–1 and miR-101–2 relative quantitation (RQ) of copy number are represented as homozygous loss (<0.3; bright green), single-copy loss (<0.7; light green), no copy number change (≥0.7 and ≤1.3; black), single-copy gain (>1.3; light red), and double-copy gain (>1.7; bright red). (**D**) Evidence that the miR-101–1 locus is somatically lost in tumors samples relative to matched normal samples. Nine metastatic prostate cancers were chosen that had copy number loss in the miR-101–1 locus, and matched normal tissue was analyzed for comparison. Bar heights represent differences in $\log_2(RQ)$ values between metastatic and matched normal tissues.

References and Notes

1. L. A. Boyer *et al.*, *Nature* **441**, 349 (2006).
2. T. I. Lee *et al.*, *Cell* **125**, 301 (2006).
3. F. Sher *et al.*, *Stem Cells* **26**, 2875 (2008).
4. S. Varambally *et al.*, *Nature* **419**, 624 (2002).
5. A. P. Bracken *et al.*, *EMBO J.* **22**, 5323 (2003).
6. S. Erhardt *et al.*, *Development* **130**, 4235 (2003).
7. K. Plath *et al.*, *Science* **300**, 131 (2003).
8. R. Cao *et al.*, *Science* **298**, 1039 (2002).
9. A. Kuzmichev, K. Nishioka, H. Erdjument-Bromage, P. Tempst, D. Reinberg, *Genes Dev.* **16**, 2893 (2002).
10. J. Yu *et al.*, *Cancer Cell* **12**, 419 (2007).
11. Q. Cao *et al.*, *Oncogene* 10:1038/onc.2008.333 (2008).
12. C. G. Kleer *et al.*, *Proc. Natl. Acad. Sci. U.S.A.* **100**, 11606 (2003).
13. P. A. Croonquist, B. Van Ness, *Oncogene* **24**, 6269 (2005).
14. F. Takeshita *et al.*, *Proc. Natl. Acad. Sci. U.S.A.* **102**, 12177 (2005).
15. I. M. Bachmann *et al.*, *J. Clin. Oncol.* **24**, 268 (2006).
16. S. Weikert *et al.*, *Int. J. Mol. Med.* **16**, 349 (2005).
17. Y. Matsukawa *et al.*, *Cancer Sci.* **97**, 484 (2006).
18. B. P. Lewis, C. B. Burge, D. P. Bartel, *Cell* **120**, 15 (2005).
19. A. Marson *et al.*, *Cell* **134**, 521 (2008).
20. P. Sethupathy, M. Megraw, A. G. Hatzigeorgiou, *Nat. Methods* **3**, 881 (2006).
21. A. Krek *et al.*, *Nat. Genet.* **37**, 495 (2005).
22. B. P. Lewis, I. H. Shih, M. W. Jones-Rhoades, D. P. Bartel, C. B. Burge, *Cell* **115**, 787 (2003).
23. B. John *et al.*, *PLoS Biol.* **2**, e363 (2004).
24. V. Rusinov, V. Baev, I. N. Minkov, M. Tabler, *Nucleic Acids Res.* **33**, W696 (2005).
25. Materials and methods are available as supporting material on *Science* Online.
26. D. Pasini, A. P. Bracken, M. R. Jensen, E. Lazzerini Denchi, K. Helin, *EMBO J.* **23**, 4061 (2004).
27. W. Fiskus *et al.*, *Mol. Cancer Ther.* **5**, 3096 (2006).
28. J. Krutzfeldt *et al.*, *Nature* **438**, 685 (2005).

29. We thank S. M. Dhanasekaran, S. Tomlins, and J. Yu for helpful discussions; J. Siddiqui and M. Pandhi for technical assistance; and J. Granger and K. Giles for critically reading the manuscript. A.M.C. is supported by a Burroughs Welcome Foundation Award in Clinical Translational Research. This work was supported in part by NIH (Prostate Specialized Program of Reasearch Excellence grant P50CA69568 to A.M.C. and Early Detection Research Network grant UO1 111275 to A.M.C.) and the U.S. Department of Defense (Era of Hope Scholar grant BC075023 to A.M.C., PC051081 to A.M.C. and S.V., and BC083217 to J.C.B.). C.A.M. was supported by an NIH postdoctoral training grant and currently derives support from the American Association of Cancer Research Amgen Fellowship in Clinical/Translational Research and the Canary Foundation and American Cancer Society Early Detection Postdoctoral Fellowship. The microarray data used in this study have been deposited in the National Center for Biotechnology Information Gene Expression Omnibus with the accession number GSE13286.

Supporting Online Material

www.sciencemag.org/cgi/content/full/1165395/DC1
Materials and Methods
Figs. S1 to S18
Tables S1 to S10
References

3 September 2008; accepted 3 November 2008
Published online 13 November 2008;
10.1126/science.1165395
Include this information when citing this paper.

Modafinil Shifts Human Locus Coeruleus to Low-Tonic, High-Phasic Activity During Functional MRI

Michael J. Minzenberg,* Andrew J. Watrous, Jong H. Yoon, Stefan Ursu, Cameron S. Carter

Models of cognitive control posit a key modulatory role for the pontine locus coeruleus–norepinephrine (LC-NE) system. In nonhuman primates, phasic LC-NE activity confers adaptive adjustments in cortical gain in task-relevant brain networks, and in performance, on a trial-by-trial basis. This model has remained untested in humans. We used the pharmacological agent modafinil to promote low-tonic/high-phasic LC-NE activity in healthy humans performing a cognitive control task during event-related functional magnetic resonance imaging (fMRI). Modafanil administration was associated with decreased task-independent, tonic LC activity, increased task-related LC and prefrontal cortex (PFC) activity, and enhanced LC-PFC functional connectivity. These results confirm in humans the role of the LC-NE system in PFC function and cognitive control and suggest a mechanism for therapeutic action of procognitive noradrenergic agents.

Models of prefrontal cortex (PFC) function posit a key modulatory role for the ascending brainstem locus coeruleus-norepinephrine (LC-NE) system (*1*–*5*). These models derive largely from studies of non-human primates, rodents, and computational modeling. LC-NE influence confers the PFC capacity to flexibly regulate goal representations by a "gating" mechanism, by modulating the influence of afferent input to PFC ensembles. This enhances the signal-to-noise ratio in active, task-related cortical ensembles. The phasic mode of LC activity drives these adaptive adjustments in gain that facilitate the dynamic reorganization of target networks (*4*) and serve to optimize performance (*3*) in response to the value of current environmental cues or the ongoing assessment of task-related utility. These adjustments are observable on a trial-to-trial basis during cognitive performance.

In vivo and in vitro studies show that phasic LC activity is promoted by decreases in baseline activity (*6*). In this setting, task-related excitatory LC activity is relatively preserved (*7*). NE transporter (NET) inhibitors elevate NE at LC-NE cell bodies, leading to decreased baseline LC activity, and this NET inhibitor effect also facilitates electrotonic coupling and synchronous activity between LC cells (*8*), which can resonate with PFC neurons (*9*).

Most of the fundamental predictions arising from these models have not been tested in humans. It remains unknown how trial-to-trial variation in LC activity relates to task-related PFC activity during human cognition. We addressed this issue by manipulating synaptic NE levels in healthy subjects with modafinil during event-related functional magnetic resonance imaging (fMRI). Modafinil is a nonamphetamine psychostimulant that inhibits the NET and dopamine transporter (DAT) (*10*), elevating synaptic NE and DA levels in the PFC and elsewhere (*11*). Many of modafinil's cognitive and behavioral effects are mediated by adrenergic receptors (*12*). Modafinil also augments LC-mediated pupillary dilation, consistent with enhanced LC phasic responses to task-relevant events (*13*), indicating the potential to optimize cognitive performance through LC-NE modulation. Modafinil improves PFC-dependent cognition in rodents (*14*), healthy humans (*15*, *16*), and patients with attention-deficit/hyperactivity disorder (*17*) and schizophrenia (*18*).

We reasoned that with systemic administration, NET inhibition by modafinil should increase NE levels at LC cell-body autoreceptors, leading to decreased baseline excitatory drive to LC cells (*19*), manifest as a task-independent pontine deactivation. This has been observed with clonidine infusion during resting-state positron emission tomography (PET) (*20*). This effect should in turn promote phasic LC activity (*3*), manifest as increased task-related activity in the LC. In addition, concurrent NET inhibition at terminal fields in the PFC should augment resulting synaptic NE. These effects together should enhance the coupling of LC-NE system neurotransmission with PFC activity, increasing the strength of the negative correlation of tonic LC activity with PFC activation, measured on a trial-to-trial basis by event-related fMRI.

Twenty-one adults (age 33.3 ± 8 years; 12 male) underwent fMRI on 2 days, with mean test-day interval 5.7 ± 4.1 days, after ingesting either modafinil 200 mg or placebo [see supporting online material (SOM) for details]. During fMRI, subjects performed the Preparing to Overcome Prepotency (POP) Task (*21*). Data analyses focused on the effects of modafinil on (i) cognitive control task performance; (ii) tonic, task-independent LC activity; (iii) task-related activity in LC and the cognitive control network; and (iv) connectivity between the LC and cortical cognitive control regions (see SOM).

No significant effects of modafinil were observed on vital signs or subjective state (see SOM). There were small, nonsignificant effects of drug versus placebo on improved accuracy cost (4.1 ± 7.3% versus 6.5 ± 8.5%; $t = -1.08$, $P = 0.14$ in one-tailed paired t test; Cohen's $d = 0.30$) and reaction time (RT) cost (71 ± 65 msec versus 79 ± 62 msec; $t = -0.56$; $P = 0.29$; Cohen's $d = 0.13$) in the full sample. A substantial percentage of the sample performed near ceiling on placebo, making drug effects more difficult to discern. A subgroup with subceiling performance (accuracy ≤95% on placebo high-control cue trials; $n = 11$) exhibited a significantly improved accuracy cost on drug versus placebo (5.4 ± 9.4% versus 12.2 ± 8.1%; $t = 1.964$, $P = 0.039$ in one-tailed paired t test; Cohen's $d = 0.78$).

Compared to placebo, modafinil treatment was associated with significant tonic, task-independent LC deactivation (Fig. 1 and table S1). Task-related drug effects were observed in the LC (Fig. 2A and table S1) and cognitive control areas (Fig. 2B and table S1) (*22*). In the trial-by-trial analysis of LC-PFC connectivity, the drug increased functional connectivity in a task-independent manner in the cognitive control network (Fig. 3 and table S2).

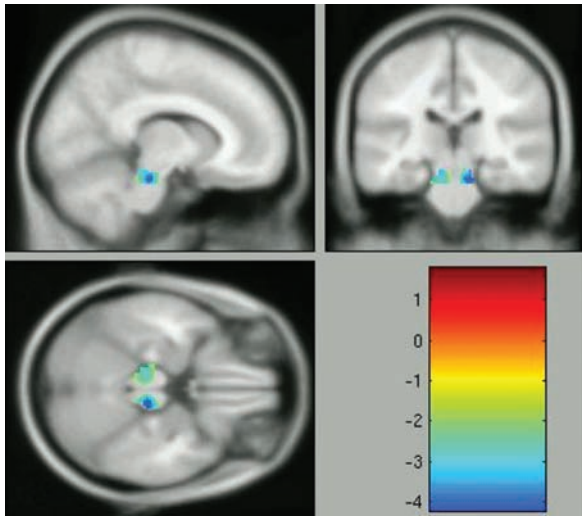

Fig. 1. Statistical parametric maps depict color-coded t statistics at each voxel in the brain, for linear contrast evaluating task-independent effect of modafinil on parameter estimates derived from general linear model (GLM) analysis of BOLD signal change. The bilateral pontine clusters, representing LC deactivation as a task-independent drug effect, are statistically significant at $P < 0.05$, corrected for FDR (see table S1 and other SOM). Maps are overlaid on the MNI T1-152 template brain images and shown in midsaggital, coronal, and axial planes, clockwise from top left.

Department of Psychiatry, University of California, Davis School of Medicine, Sacramento, CA, USA.

*To whom correspondence should be addressed. E-mail: michael.minzenberg@ucdmc.ucdavis.edu

We also evaluated the relationship of performance to modafinil-induced LC deactivation. Subjects with more negative betas by median split (i.e., stronger LC deactivation on drug; n = 10) exhibited a significantly attenuated drug-related RT cost compared to subjects with weaker LC deactivation on drug (n = 11): 36 ± 34 msec versus 104 ± 71 msec (t = 2.748, P = 0.007 in one-tailed independent samples t test; Cohen's d = 1.30). Across subjects with subceiling placebo-day performance (n = 11, defined above in performance results), there was a significant nonlinear relationship of drug-induced LC deactivation with drug-related RT cost (Fig. 4). In these subjects, stronger LC deactivation was strongly associated with attenuated RT cost.

Modafinil administration was associated with task-independent tonic LC deactivation. Inferences regarding the neurochemical basis of this effect are limited with fMRI. However, this pattern of blood oxygen level–dependent (BOLD) signal change is most consistent with the effects of NET inhibition rather than one of several other modafinil effects: activation of orexinergic neurons, elevated extracellular glutamate and serotonin, and decreased extracellular γ-aminobutyric acid (*12*). In each case, the resulting action on LC-NE cells is excitatory, which would be manifest as LC activation rather than deactivation. In addition, the lack of task-independent drug effects at midbrain dopaminergic nuclei, the ventral tegmental area and substantia nigra, suggests that the task-independent drug effect in the pons is noradrenergic rather than dopaminergic. Studies using more selective NET inhibitors (e.g., atomoxetine) will further clarify the neurochemical mechanisms underlying the LC modulation observed here. Measurement of circulating drug levels would also be useful by allowing correlations with neural and cognitive variables.

It is most likely that our pontine activity changes represent actions at LC neurons, although the activation clusters extend outside the LC proper. This is supported by the following: (i) the activation clusters qualitatively extend throughout the three-dimensional (3D) extent of the LC bilaterally, according to human brain atlases (*23*, *24*); (ii) LC-NE dendrites, which are the likely site of membrane potential changes associated with BOLD signal change (*25*), extend in the pons considerably beyond the LC proper in mammals (*26*, *27*), including humans (*28*); (iii) the activation clusters observed here compare favorably, both qualitatively (3D extent) and quantitatively (location of maxima, cluster size), with those reported in several other studies (*20*, *29*–*32*); (iv) although there are other pontine

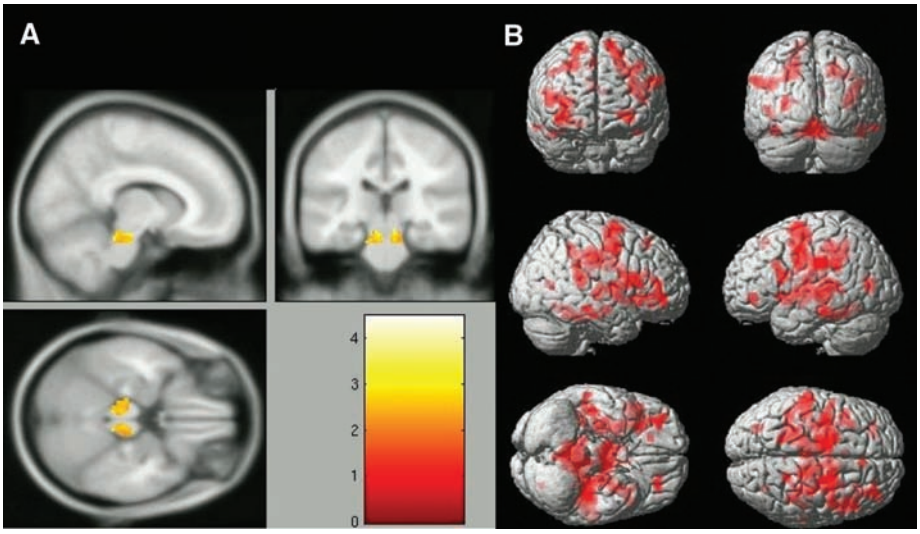

Fig. 2. Statistical parametric maps depict color-coded t statistics at each voxel in the brain, for linear contrast evaluating task-related effect of modafinil on parameter estimates derived from GLM analysis of BOLD signal change. The bilateral pontine clusters in (**A**), representing increased LC activation as a task-related drug effect, are statistically significant at $P < 0.05$, corrected for FDR. The template and spatial coordinates in which the LC clusters are shown are identical to those for the task-independent drug effect shown in Fig. 1. The clusters in the cortex depicted in (**B**) are shown at $P < 0.05$, and the majority are significant at $P < 0.05$ corrected for FDR (table S1).

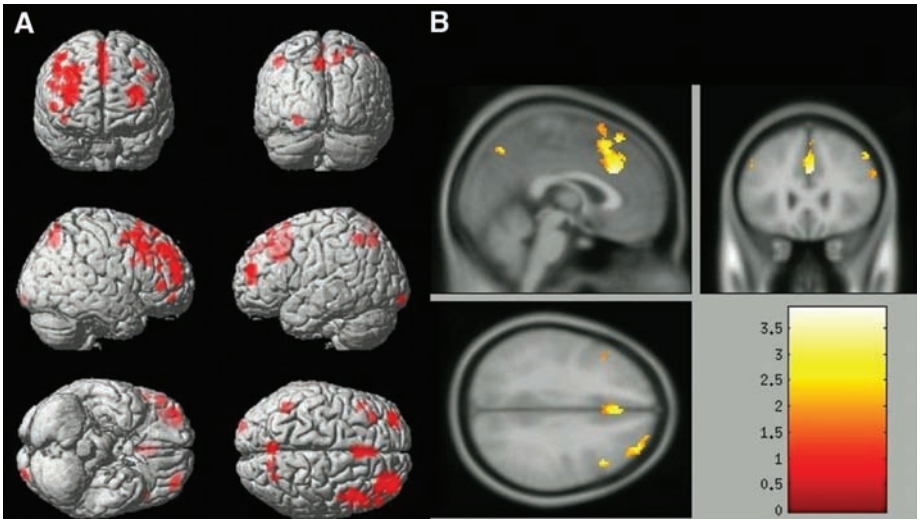

Fig. 3. Statistical parametric maps depicting color-coded t statistics at each voxel in the brain, for linear contrast evaluating task-independent effect of modafinil on the correlation, between the LC seed and all other brain voxels, of trial-by-trial parameter estimates derived from GLM analysis of BOLD signal change. The bilateral pontine clusters observed in Fig. 1, representing significant task-independent LC deactivation, served as the seed in the beta series correlation method. The clusters in the cortex depicted in (**A**) are shown at $P < 0.05$, and the majority are significant at $P < 0.05$ corrected for FDR, as is the large midline anterior cingulate cortex cluster depicted in (**B**) (see table S2 and SOM).

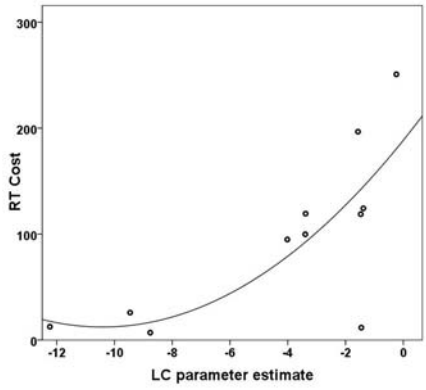

Fig. 4. LC deactivation on modafinil is strongly related to RT cost, across subjects who performed below ceiling (i.e., <95% accuracy) in the high-control (red-cue) condition on placebo (n = 11). For each subject, RT cost is plotted as a function of the mean parameter estimate in the bilateral LC cluster with significant task-independent deactivation on modafinil (see SOM). Quadratic function: R^2 = .56, F = 5.10, df = 2, 8; β (constant) = 188.5, β_1 = 33.8, β_2 = 1.6; P = 0.037.

nuclei containing NE neurons, these do not have ascending projections to the frontal cortex and largely serve autonomic functions. Although the present need for concurrent coverage of the LC and PFC precludes the use of high-resolution fMRI, this method may enhance the localization of pontine nuclei in future studies.

Despite tonic LC deactivation, there was enhancement of task-related activation in the PFC and other terminal fields (*33*). Although this may appear paradoxical, our working model suggests that enhanced task-related phasic LC activity occurs with decreased tonic LC-NE activity. This should be observed during fMRI as a task-independent deactivation, combined with a task-related effect in the opposite direction, which is what we observed. It is possible that the observed PFC effects may be partly mediated by striatal dopamine interactions (*34*), and, because both NET and DAT perform reuptake of extracellular DA in the PFC (*35*), combined NET/DAT inhibition may also increase PFC activity through elevated DA.

Modafinil also increased trial-by-trial LC-PFC coupling. This coupling was negative, consistent with the predicted coincidence of decreased tonic LC activity with positive cortical activation. These results are consistent with evidence that modafinil promotes increased LC-PFC resonance. Because the drug modulated task-independent correlations, tonic LC activity may be the more direct determinant of LC-PFC coupling.

Finally, decreased tonic LC activity in response to modafinil was associated with improved task performance. This relationship is nonlinear, suggesting a particularly sensitive range, at low levels of LC deactivation, where small increments are associated with relatively large adjustments in control. The future use of tasks where subjects perform off-ceiling will facilitate the evaluation of this relationship.

The present results suggest that modafinil shifts the function of the LC-NE system toward a low-tonic/high-phasic pattern of activity to optimize task performance.

References and Notes

1. E. K. Miller, J. D. Cohen, *Annu. Rev. Neurosci.* **24**, 167 (2001).
2. T. W. Robbins, A. C. Roberts, *Cereb. Cortex* **17** (suppl. 1), i151 (2007).
3. G. Aston-Jones, J. D. Cohen, *Annu. Rev. Neurosci.* **28**, 403 (2005).
4. S. Bouret, S. J. Sara, *Trends Neurosci.* **28**, 574 (2005).
5. B. P. Ramos, A. F. Arnsten, *Pharmacol. Ther.* **113**, 523 (2007).
6. E. Brown *et al.*, *J. Comput. Neurosci.* **17**, 13 (2004).
7. G. Aston-Jones, H. Akaoka, P. Charlety, G. Chouvet, *J. Neurosci.* **11**, 760 (1991).
8. V. A. Alvarez, C. C. Chow, E. J. Van Bockstaele, J. T. Williams, *Proc. Natl. Acad. Sci. U.S.A.* **99**, 4032 (2002).
9. R. Lestienne, A. Herve-Minvielle, D. Robinson, L. Briois, S. J. Sara, *J. Physiol. (Paris)* **91**, 273 (1997).
10. B. K. Madras *et al.*, *J. Pharmacol. Exp. Ther.* **319**, 561 (2006).
11. Z. de Saint Hilaire, M. Orosco, C. Rouch, G. Blanc, S. Nicolaidis, *Neuroreport* **12**, 3533 (2001).
12. M. J. Minzenberg, C. S. Carter, *Neuropsychopharmacology* **33**, 1477 (2008).
13. R. H. Hou, C. Freeman, R. W. Langley, E. Szabadi, C. M. Bradshaw, *Psychopharmacology (Berlin)* **181**, 537 (2005).
14. D. M. Eagle, M. R. Tufft, H. L. Goodchild, T. W. Robbins, *Psychopharmacology (Berl.)* **192**, 193 (2007).
15. D. C. Turner *et al.*, *Psychopharmacology (Berl.)* **165**, 260 (2003).
16. U. Muller, N. Steffenhagen, R. Regenthal, P. Bublak, *Psychopharmacology (Berlin)* **177**, 161 (2004).
17. D. C. Turner, L. Clark, J. Dowson, T. W. Robbins, B. J. Sahakian, *Biol. Psychiatry* **55**, 1031 (2004).
18. D. C. Turner *et al.*, *Neuropsychopharmacology* **29**, 1363 (2004).
19. G. K. Aghajanian, C. P. VanderMaelen, *Science* **215**, 1394 (1982).
20. J. T. Coull, C. Buchel, K. J. Friston, C. D. Frith, *Neuroimage* **10**, 705 (1999).
21. A. D. Barber, C. S. Carter, *Cereb. Cortex* **15**, 899 (2005).
22. In contrast, for probe-related BOLD signal change, some drug effects on task-related activity were observed at uncorrected $P < 0.005$; however, none of these effects survived correction for FDR.
23. G. Paxinos, X. Huang, *Atlas of the Human Brainstem* (Academic Press, San Diego, CA, 1995).
24. S. J. DeArmond, M. M. Fusco, M. M. Dewey, *Structure of the Human Brain. A Photographic Atlas* (Oxford Univ. Press, New York, ed. 3, 1989).
25. N. K. Logothetis, B. A. Wandell, *Annu. Rev. Physiol.* **66**, 735 (2004).
26. M. Ishimatsu, J. T. Williams, *J. Neurosci.* **16**, 5196 (1996).
27. A. Ivanov, G. Aston-Jones, *J. Neurophysiol.* **74**, 2427 (1995).
28. K. G. Baker, I. Tork, J. P. Hornung, P. Halasz, *Exp. Brain Res.* **77**, 257 (1989).
29. A. Mohanty, D. R. Gitelman, D. M. Small, M. M. Mesulam, *Cereb. Cortex* **18**, 2604 (2008).
30. V. Sterpenich *et al.*, *J. Neurosci.* **26**, 7416 (2006).
31. B. J. Liddell *et al.*, *Neuroimage* **24**, 235 (2005).
32. S. M. Berman *et al.*, *J. Neurosci.* **28**, 349 (2008).
33. These findings do not appear to represent diffuse effects of a drug-induced change in arousal. First, because tonic LC activity is positively related to arousal, the task-independent decrease in LC activity would be consistent with a decreased arousal, rather than an increase. Second, there were no task-independent cortical activity increases on drug. Third, the Profile of Mood States subscales are generally arousal-dependent, and modafinil effects on these measures were minimal. These findings are consistent with an earlier neuroimaging study of modafinil, which found no significant difference between pretreatment and posttreatment activation levels in visual or auditory cortex in response to sensory stimulation (*36*).
34. T. E. Hazy, M. J. Frank, R. C. O'Reilly, *Philos. Trans. R. Soc. Lond. B Biol. Sci.* **362**, 1601 (2007).
35. E. Carboni, G. L. Tanda, R. Frau, G. Di Chiara, *J. Neurochem.* **55**, 1067 (1990).
36. C. M. Ellis *et al.*, *J. Sleep Res.* **8**, 85 (1999).

37. This work was supported by UL1 RR024146 from the National Center for Research Resources (NCRR) to M.J.M., and MH059883 to C.S.C. The authors have no disclosures to make.

Supporting Online Material

www.sciencemag.org/cgi/content/full/322/5908/1700/DC1
Materials and Methods
SOM Text
Fig. S1
Tables S1 and S2
References

20 August 2008; accepted 4 November 2008
10.1126/science.1164908

A Null Mutation in Human *APOC3* Confers a Favorable Plasma Lipid Profile and Apparent Cardioprotection

Toni I. Pollin,[1] Coleen M. Damcott,[1] Haiqing Shen,[1] Sandra H. Ott,[1] John Shelton,[1] Richard B. Horenstein,[1] Wendy Post,[2] John C. McLenithan,[1,3] Lawrence F. Bielak,[4] Patricia A. Peyser,[4] Braxton D. Mitchell,[1] Michael Miller,[1] Jeffrey R. O'Connell,[1] Alan R. Shuldiner[1,3]

Apolipoprotein C-III (apoC-III) inhibits triglyceride hydrolysis and has been implicated in coronary artery disease. Through a genome-wide association study, we have found that about 5% of the Lancaster Amish are heterozygous carriers of a null mutation (R19X) in the gene encoding apoC-III (*APOC3*) and, as a result, express half the amount of apoC-III present in noncarriers. Mutation carriers compared with noncarriers had lower fasting and postprandial serum triglycerides, higher levels of HDL-cholesterol and lower levels of LDL-cholesterol. Subclinical atherosclerosis, as measured by coronary artery calcification, was less common in carriers than noncarriers, which suggests that lifelong deficiency of apoC-III has a cardioprotective effect.

Elevated plasma levels of low density lipoprotein cholesterol (LDL-C) and triglycerides (TGs) are important contributors to premature coronary heart disease (CHD) (*1*–*3*), and genetic variants causing low LDL-C are associated with reduced risk of CHD (*4*). Recently, nonfasting TG was found to be an independent CHD risk factor (*5*, *6*), showing higher predictive power in one study than fasting TG (FTG), the traditional measure, likely because of the atherogenic remnant lipoproteins generated during absorption and clearance of dietary fat (*5*).

To identify genetic factors contributing to FTG and the postprandial TG (ppTG) dietary response, we performed a single high-fat feeding intervention and genome-wide association study (GWAS) in 809 Old Order Amish individuals as part of the Heredity and Phenotype Intervention (HAPI) Heart Study (*7*). Characteristics of these participants are shown in table S1. These individuals were fed a milkshake containing 782 kcal/m^2 body surface area, with 77.6% of these calories from fat, and had blood drawn for lipid levels 0, 1, 2, 3, 4, and 6 hours after the intervention.

The Affymetrix GeneChip Human Mapping 500K Array Set was used for genotyping leukocyte DNA from these 809 participants. Traits were normalized, and analyses accounting for sex and sex-specific age and age^2; body mass index (BMI) and relatedness among participants were performed as described in the Methods section (*8*).

Results of the GWAS of FTG and ppTG [as estimated by the incremental area under the curve, iAUCTG (*8*)], transformed by their natural logarithm (ln), are shown in table S2 and fig. S1. The strongest evidence for association with both ln-FTG ($P = 3.8 \times 10^{-14}$) and ln-iAUCTG ($P = 2.8 \times 10^{-10}$) occurred on chromosome 11q23 at single-nucleotide polymorphism (SNP) rs10892151, which had a minor allele frequency (MAF) of 0.028 (A allele) (table S2). SNP rs10892151 is located within an intron of the *DSCAML1* (Down syndrome cell adhesion molecule like 1) gene and also lies 823 kb away from the apolipoprotein A and C *APOA1/C3/A4/A5* region, a cluster of more likely candidate genes, given the established key roles of their products in lipid metabolism (*9*). SNP rs681524 (MAF = 0.062), 40 kb from the cluster, showed nominal association with ln-FTG ($P = 1.1 \times 10^{-5}$) and ln-iAUCTG ($P = 0.004$) and was moderately correlated with rs10892151 [standardized linkage disequilibrium coefficient (D') = 0.85, squared correlation coefficient (r^2) = 0.31] (fig. S2).

Rs10892151 A carriers evidenced markedly lower FTGs and ppTGs than noncarriers (table S3), consistent with effects of deleting the *APOC3* gene in mice (*10*), which led to the hypothesis that SNP rs10892151 tagged a loss-of-function mutation in *APOC3*. Sequencing of the coding region of *APOC3* revealed a C → T substitution at the terminal nucleotide of exon 3, the 55th nucleotide from the ATG start codon; this substitution resulted in a premature stop codon for an arginine residue at amino acid position 19 (R19X). This position is located in the signal peptide of the protein, normally cleaved before the secretion of the mature 79–amino acid apoC-III peptide (*11*). Thus, a complete lack of production of apoC-III from alleles containing this mutation would be predicted. Moreover, the location of the premature stop codon in the mRNA transcript of the mutated gene meets the criteria for nonsense-mediated mRNA, in which certain mRNA transcripts with premature stop codons are degraded, rather than translated into protein (*12*, *13*). Indeed, in a sample of 20 study participants [10 carriers of the 19X allele, RX (CT), and 10 noncarriers, RR (CC)] who made up four two-generation families and one pair of siblings, apoC-III protein levels in R19X carriers were approximately half of that in their noncarrier relatives (39% versus 87% of pooled serum control level, $P = 0.0002$) (Fig. 1). ApoC-III levels were highly correlated with ln-FTG levels [partial correlation coefficient (r) = 0.71, $P = 0.0002$] (Fig. 1, nontransformed FTG shown).

The R19X mutation was in strong linkage disequilibrium with (i.e., highly correlated with) the most highly associated GWAS SNP rs10892151 ($D' = 1$, $r^2 = 0.85$) (fig. S2). Pedigree and haplotype analysis were consistent with a single copy of the mutated allele having entered the population before the year 1800 (supporting online text and figs. S3 and S4). Evaluation of the association of this novel R19X mutation with ln-FTG and ln-ppTG in 802 of 809 HAPI Heart GWAS subjects successfully genotyped revealed similar associations to those identified with rs10892151 (Fig. 2 and table S4). R19X heterozygotes had significantly reduced TG levels compared with their RR counterparts at all six time points, with a median FTG (interquartile range) of 31 (25 to 48) versus 57 (42 to 81) mg/dl ($P = 4.1 \times 10^{-13}$) and iAUCTG median of 214 (154 to 338) versus 410 (276 to 608) mg/dl over 6 hours ($P = 2.0 \times 10^{-10}$). Nominal association ($P < 0.05$) of the mutation with ln-TG at 2, 3, and 4 hours, as well as ln-tAUC, ln-iAUC, natural logarithm of maximum TG, and natural logarithm of incremental maximum TG persisted after controlling for ln-FTG. The segregation of the R19X mutation with hypo-TG and blunted ppTG response in a representative family is shown in fig. S5.

R19X carriers had significantly higher HDL-cholesterol (HDL-C) levels (mean ± SD: 67 ± 17 versus 55 ± 14 mg/dl, $P = 9.0 \times 10^{-7}$) and lower total cholesterol (191 ± 35 versus 209 ± 46 mg/dl, $P = 0.02$) and LDL-C (116 ± 32 versus 140 ± 43 mg/dl, $P = 0.001$) levels (Table 1) than noncarriers. There were no differences in BMI ($P = 0.98$) or waist circumference ($P = 0.50$), and fasting glucose and insulin were similar between R19X carriers and noncarriers ($P = 0.53$ and 0.72, respectively). R19X carriers had significantly lower levels of non-HDL ($P = 0.0005$); very low density lipoprotein (VLDL, 1.5×10^{-10}); the most-dense VLDL subfraction, $VLDL_3$ ($P = 2.8 \times 10^{-10}$); intermediate density lipoprotein (IDL, $P = 8.8 \times 10^{-15}$); real LDL ($P = 0.01$); and remnant lipoprotein cholesterol ($P = 3.0 \times 10^{-20}$), as well as higher levels of both HDL_2 ($P = 7.0 \times 10^{-6}$) and HDL_3 ($P = 3.0 \times 10^{-5}$) cholesterol. On the basis of the mutation's effect on TGs, VLDL-C levels increased significantly less in carriers than in noncarriers at 4 hours after the high-fat challenge ($P = 0.0009$) (Table 1).

The hypothesis that a mutation conferring such a favorable lipid profile would be cardioprotective was evaluated in the Amish Family Calcification Study (*14*), which includes 335 of the HAPI Heart fat-challenge participants along with 698 additional Amish individuals, all of

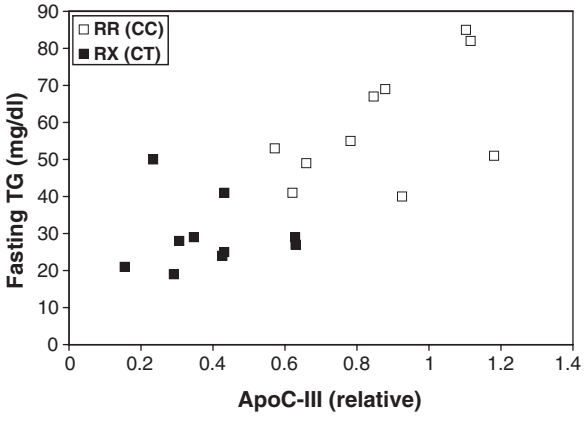

Fig. 1. Triglyceride levels as a function of apoC-III protein levels stratified by *APOC3* R19X genotype in 20 individuals. Filled squares indicate individuals carrying the 19X allele and open squares, noncarriers.

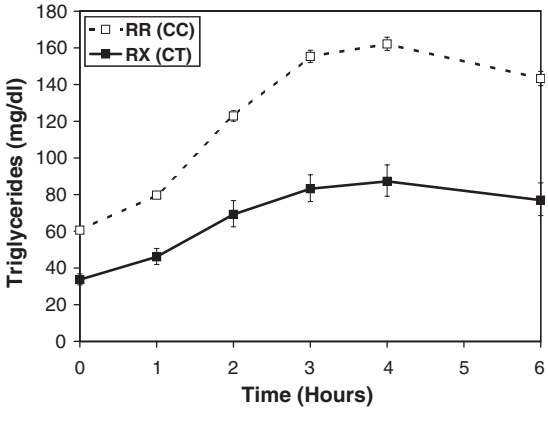

Fig. 2. TG levels before and during the high-fat challenge by R19X *APOC3* genotype. Shown are covariate-adjusted geometric means with 95% confidence intervals. Filled squares indicate individuals carrying the 19X allele and open squares, noncarriers.

[1]Department of Medicine, University of Maryland School of Medicine, Baltimore, MD 21201, USA. [2]Department of Medicine, Johns Hopkins University School of Medicine, Baltimore, MD 21287, USA. [3]Geriatrics Research and Education Clinical Center, Baltimore Veterans Administration Medical Center, Baltimore, MD 21201, USA. [4]Department of Epidemiology, University of Michigan School of Public Health, Ann Arbor, MI 48109, USA.

*To whom correspondence should be addressed. E-mail: tpollin@medicine.umaryland.edu

whom underwent electron beam computed tomography to quantify coronary artery calcification (CAC), a subclinical measure of coronary atherosclerosis. A standard lipid panel was also obtained. The effect of the *APOC3* R19X mutation on decreased FTGs and increased HDL-C levels replicated in the 698 nonoverlapping AFCS participants ($P = 1.9 \times 10^{-22}$ and $P = 1.3 \times 10^{-14}$, respectively; $P = 2.9 \times 10^{-29}$ and 1.3×10^{-17} in the full AFCS). LDL-C levels tended to be lower in R19X carriers than in noncarriers in the nonoverlapping subset, and the difference reached statistical significance in the full AFCS ($P = 0.01$) (table S5).

Among AFCS participants, according to evidence-based clinical guidelines set by the National Cholesterol Education Program Adult Treatment Panel III (ATP-III) (*15*), LDL-C levels, the primary CHD prevention target, were more likely to be optimal (<100 mg/dl) in R19X carriers [odds ratio with 95% confidence limits (OR) = 2.24 (95% CI 1.07 to 4.66)] than in noncarriers (Table 2), although the difference did not quite reach statistical significance ($P = 0.07$). In addition, high HDL-C (≥60 mg/dl), considered by the ATP-III to be cardioprotective enough to cancel out one additional CHD risk factor (*15*), was much more common in R19X carriers than in noncarriers [OR = 7.0 (95% CI: 3.3 to 14.8), $P = 9.1 \times 10^{-6}$]. Notably, ATP-III–defined low HDL-C (<40 mg/dl) was absent in the carriers but present in 13.5% of noncarriers (Fisher's exact test, $P = 4.2 \times 10^{-4}$). All R19X carriers had FTGs in the normal (<150 mg/dl) range (maximum of 77 mg/dl), whereas only 83.6% of noncarriers had normal FTGs (Fisher's exact test, $P = 0.0004$). Among AFCS participants in the baseline age range (30 to 74 years) of the Framingham Heart Study, mutation carriers had significantly lower natural logarithm–transformed 10-year Framingham CHD risk (*16*) than noncarriers [risk ratio = 0.68 (95% CI: 0.58 to 0.79), $P = 3.9 \times 10^{-7}$] (Table 2 and fig. S6).

Consistent with their protective lipid profile, R19X carriers were significantly less likely than noncarriers to have any detectable CAC [OR = 0.35 (95% CI: 0.21 to 0.60), $P = 0.002$] or CAC scores greater than 100 Agatston units [OR = 0.40 (95% CI: 0.18 to 0.85), $P = 0.01$] (fig. S7). CAC scores of 1 to 100 were previously associated with a fourfold and scores greater than 100 with a sevenfold increased risk of major coronary events in comparison with individuals with no detectable calcification in the population-based Multi-Ethnic Study of Atherosclerosis (MESA) after adjustment for standard risk factors (*17*). Among AFCS participants in the age range of the MESA study (45 to 84 years), R19X carriers were significantly less likely to have a score at or above their respective MESA-derived (*18*) ethnicity-, sex-, and age-specific 75th percentile [OR = 0.38 (95% CI: 0.19 to 0.77), $P = 0.003$] (Table 2), a level associated in MESA, after adjustment for traditional risk factors, with an eightfold risk of CHD events in comparison with the lowest two quartiles (*19*). Analysis of the quantitative trait ln(CAC score + 1), which approximated a normal distribution after adjustment for age and sex (fig. S8), yielded a significant negative association between CAC quantity and being a carrier [$\beta_{R19X} = -0.84 \pm 0.30$, e.g., mean ratio = 0.43 (95% CI: 0.24 to 0.78), $P = 0.005$] (table S5).

ApoC-III, secreted from the liver and to a lesser extent by the intestines, is a component of both HDL and apoB-containing lipoprotein particles (*9*, *20*), impairs catabolism and hepatic uptake of apoB-containing lipoproteins (*21*, *22*), appears to enhance the catabolism of HDL particles (*23*), enhances monocyte adhesion to vascular endothelial cells (*24*), and activates inflammatory signaling pathways (*25*). Along with the observed association of elevated apoC-III concentration with increased CHD risk (*26*), the roles of apoC-III in lipoprotein metabolism would predict that apoC-III

Table 1. Morphometric and metabolic characteristics and lipid subfractions by *APOC3* R19X genotype (all analyses except age adjusted for sex and sex-specific age and age^2 and all analyses except age, BMI, and waist adjusted for BMI) in the HAPI Heart Study. Variables analyzed directly are presented as mean ± SD. Variables natural logarithm–transformed for normalization before analysis are presented as median (interquartile range). All values are fasting unless otherwise indicated. SBP, systolic blood pressure; DBP, diastolic blood pressure.

Trait	RR (CC)	RX (CT)	*P* value
n	763	39	–
Age (years)	44 ± 14	42 ± 12	0.66
Sex (%M:%F)	55:45	56:44	–
BMI (kg/m^2)	26.6 ± 4.4	26.6 ± 4.1	0.98
Waist (cm)	87 ± 11	89 ± 12	0.50
SBP (mm Hg)	121 ± 14	119 ± 14	0.67
DBP (mm Hg)	77 ± 9	77 ± 9	0.55
Glucose (mg/dl)	86 ± 9	87 ± 4	0.53
Insulin (μU/ml)	8.1 (6.5–10.2)	8.8 (6.3–12.0)	0.72
Total cholesterol (mg/dl)	209 ± 46	191 ± 35	0.02
Triglycerides (mg/dl)	57 (42–81)	31 (25–48)	4.1×10^{-13}
HDL-C (mg/dl)	55.1 ± 13.9	67.1 ± 17.3	9.0×10^{-7}
HDL_2-C (mg/dl)	13 (10–18)	18 (14–27)	7.0×10^{-6}
HDL_3-C (mg/dl)	41.1 ± 7.4	46.8 ± 9.2	3.0×10^{-5}
NonHDL cholesterol (mg/dl)	159 ± 43	132 ± 29	0.0005
LDL-C (mg/dl)	140 ± 43	116 ± 32	0.001
Real LDL-C (mg/dl)	125 ± 36	109 ± 25	0.01
VLDL-C (mg/dl)	16 (14–20)	12 (12–14)	1.5×10^{-10}
4-hour VLDL-C change (mg/dl)	3.3 ± 2.8	1.8 ± 2.0	0.0009
Remnant lipoprotein-C (mg/dl)	17 (11–26)	6 (4–10)	3.0×10^{-20}
IDL-C (mg/dl)	8 (3–14)	1 (1–2)	8.8×10^{-15}
$VLDL_3$-C (mg/dl)	9 (7–11)	6 (6–7)	2.8×10^{-10}

Table 2. National Cholesterol Education Program ATP-III protective lipid levels, Framingham 10-year CHD risk, and CAC as a function of *APOC3* R19X genotype in the AFCS. Dichotomous traits analyzed by generalized estimating equations (GEE) adjusted for age, sex, and sibship, as described in the methods (*8*), except triglycerides, which contains a zero cell. Framingham 10-year CHD risk analyzed as a natural log-transformed quantitative trait with variance components (adjusted for sex and sex-specific age and age^2) as described in the methods (*8*). Framingham Heart Study comparisons included only individuals age 30 to 74 years to match baseline ages in that study. MESA comparisons included only individuals age 45 to 84 years to match baseline ages in that study.

Parameter	RR (CC)	RX (CT)	OR (95% CI)	*P* value
Optimal LDL-C (< 100 mg/dl)	120/969 (12.4%)	14/59 (23.7%)	2.2 (1.1–4.7)	0.07
High HDL-C (≥ 60 mg/dl)	362/973 (37.2%)	45/59 (76.3%)	7.0 (3.3–14.8)	9.1×10^{-6}
Normal TGs (<150 mg/dl)	840/973 (86.3%)	59/59 (100.0%)	–	0.0004*
Framingham 10-year CHD risk	5.2%†	3.8%†	0.68 (0.58–0.79) ‡	3.9×10^{-7}
Any CAC	526/974 (54.0%)	20/59 (33.9%)	0.35 (0.21–0.60)	0.002
CAC score > 100 Agatston units	283/974 (29.1%)	9/59 (15.3%)	0.40 (0.18–0.85)	0.01
CAC score ≥ 75th MESA percentile	270/753 (35.9%)	10/52 (19.2%)	0.38 (0.19–0.77)	0.003

*By Fisher's exact test. †Median. ‡Risk ratio.

deficiency would decrease atherothrombotic tendency.

Previous reports of apoC-III deficiency in humans were complicated by the prothrombotic effects of accompanying apoA-I and/or apoA-IV deficiency (*27*–*30*), small sample sizes and/or structurally abnormal apoC-III (*31*, *32*). The current report of a favorable lipid profile and reduced subclinical coronary artery atherosclerosis in R19X null mutation carriers provides strong evidence in a relatively large number of individuals that apoC-III deficiency (by ~50% of normal levels) is indeed cardioprotective.

Indirectly lowered *APOC3* expression is one mechanism of the lipid-lowering effect of fibrates (*33*), and the use of several other lipid-lowering agents, including statins, thiazolidinediones, ezetimibe, niacin, fish oil, and weight loss, has also been associated with decreases in apoC-III levels [reviewed in (*20*)]. That a naturally occurring null mutation in *APOC3* confers a favorable lipid profile and apparent cardioprotection and does not result in any obvious detrimental effect raises the possibility that therapies aimed specifically at down-regulating apoC-III expression will be clinically efficacious and safe in reducing the morbidity and mortality associated with CHD.

References and Notes

1. J. L. Goldstein, H. G. Schrott, W. R. Hazzard, E. L. Bierman, A. G. Motulsky, *J. Clin. Invest.* **52**, 1544 (1973).
2. N. Sarwar *et al.*, *Circulation* **115**, 450 (2007).
3. M. Miller *et al.*, *J. Am. Coll. Cardiol.* **51**, 724 (2008).
4. J. C. Cohen, E. Boerwinkle, T. H. Mosley Jr., H. H. Hobbs, *N. Engl. J. Med.* **354**, 1264 (2006).
5. S. Bansal *et al.*, *JAMA* **298**, 309 (2007).
6. B. G. Nordestgaard, M. Benn, P. Schnohr, A. Tybjaerg-Hansen, *JAMA* **298**, 299 (2007).
7. B. D. Mitchell *et al.*, *Am. Heart J.* **155**, 823 (2008).
8. Materials and methods are available as supporting material on *Science* Online.
9. J. P. Kane, R. J. Havel, in *The Online Metabolic and Molecular Bases of Inherited Diseases (OMMBID)* (McGraw-Hill, New York, ed. 8, 2001), chap. 114.
10. N. Maeda *et al.*, *J. Biol. Chem.* **269**, 23610 (1994).
11. A. V. Hospattankar, H. B. Brewer Jr., R. Ronan, T. Fairwell, *FEBS Lett.* **197**, 67 (1986).
12. O. Isken, L. E. Maquat, *Genes Dev.* **21**, 1833 (2007).
13. E. Nagy, L. E. Maquat, *Trends Biochem. Sci.* **23**, 198 (1998).
14. W. Post *et al.*, *Circulation* **115**, 717 (2007).
15. Expert Panel on Detection, Evaluation, and Treatment of High Blood Cholesterol in Adults, *JAMA* **285**, 2486 (2001).
16. P. W. Wilson *et al.*, *Circulation* **97**, 1837 (1998).
17. R. Detrano *et al.*, *N. Engl. J. Med.* **358**, 1336 (2008).
18. R. L. McClelland, H. Chung, R. Detrano, W. Post, R. A. Kronmal, *Circulation* **113**, 30 (2006).
19. A. R. Folsom *et al.*, *Arch. Intern. Med.* **168**, 1333 (2008).
20. E. M. Ooi, P. H. Barrett, D. C. Chan, G. F. Watts, *Clin. Sci. (Lond.)* **114**, 611 (2008).
21. H. N. Ginsberg *et al.*, *J. Clin. Invest.* **78**, 1287 (1986).
22. V. Clavey, S. Lestavel-Delattre, C. Copin, J. M. Bard, J. C. Fruchart, *Arterioscler. Thromb. Vasc. Biol.* **15**, 963 (1995).
23. D. C. Chan, M. N. Nguyen, G. F. Watts, P. H. Barrett, *J. Clin. Endocrinol. Metab.* **93**, 557 (2008).
24. A. Kawakami *et al.*, *Circulation* **113**, 691 (2006).
25. P. Libby, *Circ. Res.* **100**, 299 (2007).
26. F. M. Sacks *et al.*, *Circulation* **102**, 1886 (2000).
27. R. A. Norum *et al.*, *N. Engl. J. Med.* **306**, 1513 (1982).
28. S. K. Karathanasis, R. A. Norum, V. I. Zannis, J. L. Breslow, *Nature* **301**, 718 (1983).
29. S. K. Karathanasis, E. Ferris, I. A. Haddad, *Proc. Natl. Acad. Sci. U.S.A.* **84**, 7198 (1987).
30. J. M. Ordovas, D. K. Cassidy, F. Civeira, C. L. Bisgaier, E. J. Schaefer, *J. Biol. Chem.* **264**, 16339 (1989).
31. A. von Eckardstein *et al.*, *J. Clin. Invest.* **87**, 1724 (1991).
32. H. Liu *et al.*, *J. Lipid Res.* **41**, 1760 (2000).
33. J. Auwerx, K. Schoonjans, J. C. Fruchart, B. Staels, *Atherosclerosis* **124** (suppl.), S29 (1996).

34. We gratefully acknowledge our Amish liaisons, field workers, and clinic staff and the extraordinary cooperation and support of the Amish community, without which these studies would not have been possible. We thank R. Agarwala and A. Schäffer for assistance in pedigree construction and K. Ryan for data management. This work was supported by NIH grants R01 HL088119, R01 AR046838, U01 HL72515, R01 AG18728, and U01 HL084756; General Clinical Research Centers Program, National Center for Research Resources (NCRR), NIH; the University of Maryland General Clinical Research Center, grant M01 RR 16500; University of Maryland Clinical Nutrition Research Unit grant P30 DK072488; the Johns Hopkins University General Clinical Research Center, grant M01 RR 000052; the Baltimore Veterans Administration Geriatric Research and Education Clinical Center (GRECC); and the Paul Beeson Faculty Scholars in Aging Program.

Supporting Online Material

www.sciencemag.org/cgi/content/full/322/5908/1702/DC1
Materials and Methods
SOM Text
Figs. S1 to S8
Tables S1 to S5
References

9 June 2008; accepted 31 October 2008
10.1126/science.1161524

Regulation of Dendritic Cell Migration by CD74, the MHC Class II–Associated Invariant Chain

Gabrielle Faure-André,[1]* Pablo Vargas,[1,2]* Maria-Isabel Yuseff,[1] Mélina Heuzé,[1] Jheimmy Diaz,[1] Danielle Lankar,[1] Veronica Steri,[1] Jeremy Manry,[1] Stéphanie Hugues,[1] Fulvia Vascotto,[1] Jérôme Boulanger,[3] Graça Raposo,[3] Maria-Rosa Bono,[2,4] Mario Rosemblatt,[2,4,5] Matthieu Piel,[3]† Ana-Maria Lennon-Duménil[1]†

Dendritic cells (DCs) sample peripheral tissues of the body in search of antigens to present to T cells. This requires two processes, antigen processing and cell motility, originally thought to occur independently. We found that the major histocompatibility complex II–associated invariant chain (Ii or CD74), a known regulator of antigen processing, negatively regulates DC motility in vivo. By using microfabricated channels to mimic the confined environment of peripheral tissues, we found that wild-type DCs alternate between high and low motility, whereas Ii-deficient cells moved in a faster and more uniform manner. The regulation of cell motility by Ii depended on the actin-based motor protein myosin II. Coupling antigen processing and cell motility may enable DCs to more efficiently detect and process antigens within a defined space.

Dendritic cells (DCs) patrol the body periphery by efficiently moving across tissues while retaining a high capacity for antigen (Ag) internalization. Ags are internalized into endosomes, degraded into peptides that are loaded onto major histocompatibility complex (MHC) molecules, and subsequently exposed at the cell surface of DCs (*1*). If DCs detect an Ag-associated activating signal, they enter into a maturation program that comprises an increase followed by a complete arrest of macropinocytosis and phagocytosis, maximizing uptake and processing of the activating Ag (*2*–*4*), as well as the modification of their migratory properties, enabling them to home to secondary lymphoid organs and present the resulting peptide-MHC complexes to T cells (*5*). Ag uptake and processing and cell migration must therefore be coordinated for DCs to efficiently activate T lymphocytes, suggesting that common regulatory mechanisms are involved. Although little is known about DC locomotion, it was recently shown that DCs move in the interstitial spaces of tissues by using amoeboid-like migration, which requires actomyosin contractility but not integrin-mediated adhesion (*6*).

Several lines of evidence point to the MHCII-associated protein invariant chain (Ii or CD74) as a good candidate to regulate DC migration. Indeed, beyond its key role in MHCII trafficking and peptide loading, Ii was shown to associate with two actin-interacting proteins known to regulate cell locomotion: the motor protein myosin II, which controls actomyosin contractility, and the adhesion molecule CD44 (*7*–*9*). To investigate whether Ii regulates DC migration, we compared the in vivo migratory properties of wild-type (WT) and $Ii^{-/-}$ DCs (fig. S1A). Bone marrow–derived DCs (BM-DCs) were

[1]INSERM U653, Institut Curie, 12 rue Lhomond, 75005, Paris, France. [2]Departamento de Biología, Facultad de Ciencias, Universidad de Chile, Las Palmeras 3425, Santiago, Chile. [3]CNRS UMR144, Institut Curie, 12 rue Lhomond, 75005, Paris, France. [4]Fundación Ciencia para la Vida and Instituto Milenio de Biología Fundamental y Aplicada, Avenida Zañartu 1482, Santiago, Chile. [5]Facultad de Ciencias de la Salud, Universidad Andrés Bello, Avenida Zañartu 1482, Santiago, Chile.

*These authors contributed equally to this work.
†To whom correspondence should be addressed. E-mail: amlennon@curie.fr (A.-M.L.-D.) and mpiel@curie.fr (M.P.)

ERRATUM

Post date 30 January 2009

Reports: "A null mutation in human *APOC3* confers a favorable plasma lipid profile and apparent cardioprotection" by T. I. Pollin *et al.* (12 December 2008, p. 1702). On page 1703, the exon was mischaracterized. The second sentence in the second full paragraph of the first column should read as follows: Sequencing of the coding region of *APOC3* revealed a C → T substitution at the terminal nucleotide of exon 2, the 55th nucleotide from the ATG start codon; this substitution resulted in a premature stop codon for an arginine residue at amino acid position 19 (R19X).

loaded with fluorescent dyes [in the presence of lipopolysaccharide (LPS) to induce CCR7 expression] and transferred into the footpad of C57/BL6 mice, and their arrival at the draining lymph node (DLN) was monitored 48 hours after transfer. Increased numbers of Ii-deficient DCs compared with WT cells were found in the DLN of recipient mice (Fig. 1A and fig. S2A). Fluorescein isothiocyanate (FITC)–painting experiments of the ear also showed that enhanced numbers of endogenous DCs had reached the DLN in $Ii^{-/-}$ mice after 24 hours compared with the numbers in WT mice (Fig. 1B). This difference did not result from passive diffusion of FITC because $Ii^{+/+}$ and $Ii^{-/-}$ mice displayed similar numbers of DCs in LNs at the steady state (fig. S2B). Thus, the absence of Ii facilitates the accumulation in LNs of activated DCs that migrate from the periphery.

Cathepsin S cleaves the cytosolic tail of Ii when MHCII-Ii complexes have reached endolysosomes. This is required for peptide loading onto MHCII and transport of MHCII-peptide complexes to the cell surface (*10*, *11*). In the absence of CatS, MHCII-Ii complexes accumulate in endolysosomes and, to a minor extent, at the plasma membrane (*12*). We analyzed the migratory capacity of $CatS^{-/-}$ DCs, which display enhanced Ii protein levels (fig. S1, A to C) (*10*–*12*). $CatS^{-/-}$ DCs transferred into the footpad of C57/BL6 mice migrated less efficiently from the periphery to LNs than did WT DCs (Fig. 1C). Increased numbers of transferred $CatS^{-/-}$ DCs compared with WT cells were found in the footpad, suggesting that $CatS^{-/-}$ DCs remained at the injection site rather than

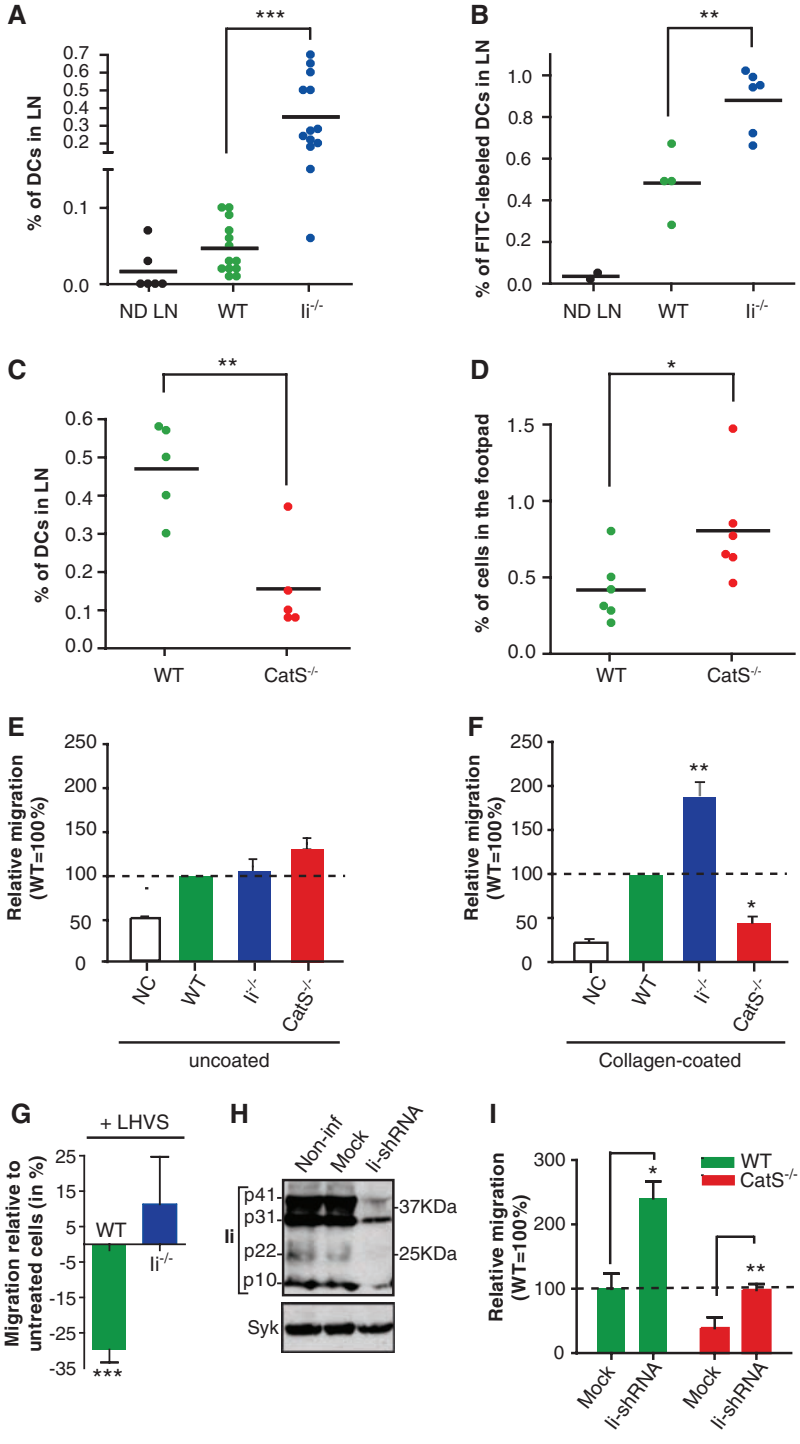

Fig. 1. Ii negatively regulates DC migration in vivo and in collagen-coated transwells. (**A**) Fluorescently labeled WT and $Ii^{-/-}$ DCs were coinjected into the footpad of C57BL/6 recipient mice. Draining and nondraining (ND) LNs were analyzed by flow cytometry after 48 hours. The presence of migrating DCs is displayed as a percentage of total LN cells (each dot represents one mouse, four independent experiments, $***P < 0.0001$). (**B**) Ears from WT or $Ii^{-/-}$ were painted with a FITC-containing irritating solution. Twenty-four hours later, draining LNs were analyzed by flow cytometry (each dot represents one mouse, three independent experiments $**P = 0.004$). (**C**) Migration experiment of transferred WT and $CatS^{-/-}$ BM-DCs performed as described in (A). (**D**) The numbers of fluorescent DCs remaining in the footpad of recipient mice. For (C) and (D), results are from three independent experiments; $**P = 0.0034$; $*P = 0.0445$. (**E** and **F**) Migration of WT, $Ii^{-/-}$, and $CatS^{-/-}$ BM-DCs in uncoated (E) and collagen-coated (F) transwells toward CCL19 and CCL21 (NC, no chemokines). Results are expressed in percentage and normalized to migration of WT DCs (mean ± SD, three independent experiments, $**P = 0.001$, $*P = 0.01$). (**G**) Inhibition of DC migration by the CatS inhibitor LHVS, performed as in (F). The results are represented as the percentage of LHVS-treated DCs that migrated relative to untreated cells (mean ± SD, three independent experiments, $***P = 0.0005$). (**H**) Ii depletion upon infection of day 4 BM-DCs with a lentivirus encoding an Ii shRNA. Infected BM-DCs were collected at day 10, lysed, and analyzed by immunoblotting for Ii and Syk expression. (**I**) Migration experiment of Ii-depleted BM-DCs performed as described in (F). The results are expressed in percentage and normalized to migration of control WT DCs (mean ± SD, two independent experiments, $**P = 0.005$, $*P = 0.05$).

homed to another tissue (Fig. 1D). Thus, enhanced levels of Ii in CatS$^{-/-}$ DCs correlate with reduced in vivo migration.

We next compared the ability of WT, Ii$^{-/-}$, and CatS$^{-/-}$ DCs to migrate toward a CCL19/CCL21 gradient in transwells. Ii-deficient cells migrated more efficiently than WT DCs, and CatS$^{-/-}$ cells showed impaired migration in collagen-coated but not in uncoated transwells (Fig. 1, E and F). Transfer of supernatants between WT, Ii$^{-/-}$ and CatS$^{-/-}$ DCs had no effect on cell migration, and Ii levels did not affect the capacity of DCs to degrade gelatin-FITC (fig. S3, A and B). Thus, down-regulation of DC migration by Ii results neither from altered response to CCL21 and CCL19 chemokines nor from differential secretion of soluble factors.

The specific CatS inhibitor LHVS (N-morpholinurea-homophenylalanyl-leucyl-vinylsulfonemethyl) significantly reduced the migration of WT DCs (Fig. 1G) (*13*). However, incubation of Ii-deficient DCs with LHVS did not compromise their migration (Fig. 1G). This result indicates that decreased migration of CatS$^{-/-}$ DCs resulted from Ii accumulation and not from an Ii-independent action of the protease. This observation was further strengthened by showing that short hairpin-mediated RNA interference (shRNA) depletion of Ii in CatS$^{-/-}$ DCs restored their ability to migrate in collagen-coated transwells (Fig. 1, H and I). Thus, Ii negatively regulates the capacity of DCs to move across a protein matrix in vitro and in vivo.

To unravel the mechanisms by which Ii regulates DC migration, we analyzed DC motility by time-lapse imaging with microfabricated 4-μm-diameter channels (*14*–*16*) (fig. S4). Nonactivated WT BM-DCs displayed an average median instantaneous velocity of 6.5 μm min^{-1} ± 3.4 (median ± SD) (Fig. 2A and movie S1). These values are compatible with the ones recently reported for BM-DC migrating in three-dimensional collagen matrices and in the mouse skin (*6*), validating microchannels as an adequate tool to study DC motility. Strikingly, 71% of Ii$^{-/-}$ DCs migrated at velocities above 6.5 μm min^{-1}, some of them reaching speeds two- to threefold higher (Fig. 2, A to C, and movie S2) ($P = 1.2 \times 10^{-6}$). On the contrary, the velocities of 76% of CatS$^{-/-}$ DCs fell below 6.5 μm min^{-1} (Fig. 2, A to C, and movie S3) ($P = 1.8 \times 10^{-3}$). Hence, Ii levels regulate the speed of DCs that migrate in a confined microenvironment, with Ii-deficiency favoring fast DC migration.

While imaging WT DCs migrating along microchannels, we noticed that most of the cells underwent important speed fluctuations during motion (Fig. 3A and movie S1). Two phases were observed: a motile phase during which pseudopods were extended at the cell front, leading to the formation of big vesicles (most likely macropinosomes), followed by a rather static phase during which these vesicles were transported backward (Fig. 3 and movie S4). Ii$^{-/-}$ DCs showed a more regular, continuous movement, and slow motility phases were rarely observed (Fig. 3A and movie S2). Even when comparing WT and Ii$^{-/-}$ DCs that displayed a similar median velocity, the speed fluctuations undergone by cells during migration were reduced in the absence of Ii (Fig. 3C). These results suggested that Ii regulates DC migration by inducing slowing-down phases during motion. Accordingly, when measuring the local speed variation of individual migrating DCs, we obtained values significantly lower for Ii-deficient cells compared with those of their WT counterpart, verifying that Ii$^{-/-}$ DCs undergo less velocity variation during motion (Fig. 3D) ($P = 7.6 \times 10^{-6}$). Furthermore, 50% of Ii$^{-/-}$ DCs spent most of their time (>80%) migrating faster than 6.5 μm min^{-1} (the WT median speed), whereas only 24% of WT DCs did so (fig. S6). These results indicate that Ii deficiency favors sustained DC migration at high speed. Thus, we conclude that Ii reduces DC migration by transiently slowing down DC velocity.

We next addressed the molecular mechanisms underlying the regulation of DC migration by Ii. Myosin II is required for DCs to migrate in collagen matrices and in vivo (*6*). Accordingly, we found that treatment of WT and Ii-deficient DCs with low concentrations of the myosin II inhibitor blebbistatin impaired their migration in collagen-coated transwells (fig. S7, A and B, and movie S5). In microchannels, the speed of WT DCs significantly decreased when inhibiting myosin II activity, with 76% of the cells migrating at velocities below 6.5 μm min^{-1} (WT median velocity, Fig. 2, A to C) ($P = 2.6 \times 10^{-7}$). Blebbistatin-treated DCs showed a velocity distribution similar to that of CatS$^{-/-}$ cells (Fig. 2, A to C) ($P = 8 \times 10^{-2}$), suggesting that myosin II activity might be compromised in CatS$^{-/-}$ DCs. In view of the ability of myosin II to interact with MHCII-Ii complexes in DCs (*7*), we hypothesized that Ii retention in CatS$^{-/-}$ DCs alters myosin II localization and activity.

To address this hypothesis, we analyzed myosin II and Ii distribution in CatS$^{-/-}$ DCs plated on rectangular fibronectin-coated micropatterns to obtain a spatial intracellular organization close to the one of elongated DCs migrating

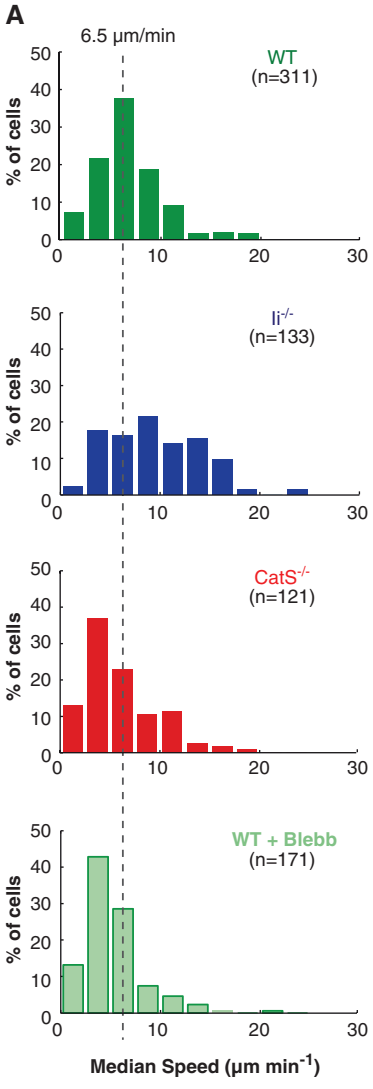

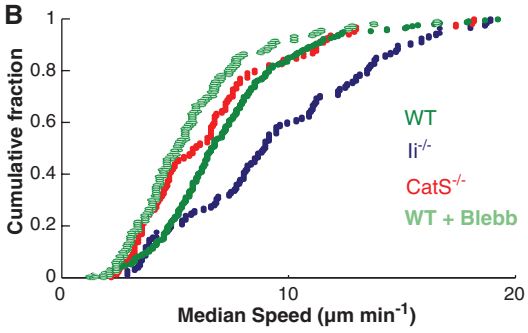

C

	p-value
WT vs Ii$^{-/-}$	1.24×10^{-6}
WT vs CatS$^{-/-}$	1.8×10^{-3}
WT vs WT + Blebb	2.6×10^{-6}
Ii$^{-/-}$ vs CatS$^{-/-}$	1.1×10^{-7}
Ii$^{-/-}$ vs WT + Blebb	8.6×10^{-13}
CatS$^{-/-}$ vs WT + Blebb	8×10^{-2}

Fig. 2. Ii decreases the velocity of DCs migrating in confining microchannels. (**A** and **B**) Distribution of median instantaneous speeds for Ii$^{-/-}$, CatS$^{-/-}$, and WT DCs treated with 20 μM blebbistatin. In (B), speed distribution is represented in a cumulative graph to allow statistical analysis. (**C**) Velocity distributions are significantly different from each other with a 95% confidence interval. Velocity distributions of CatS$^{-/-}$ and blebbistatin-treated DCs are not significantly different.

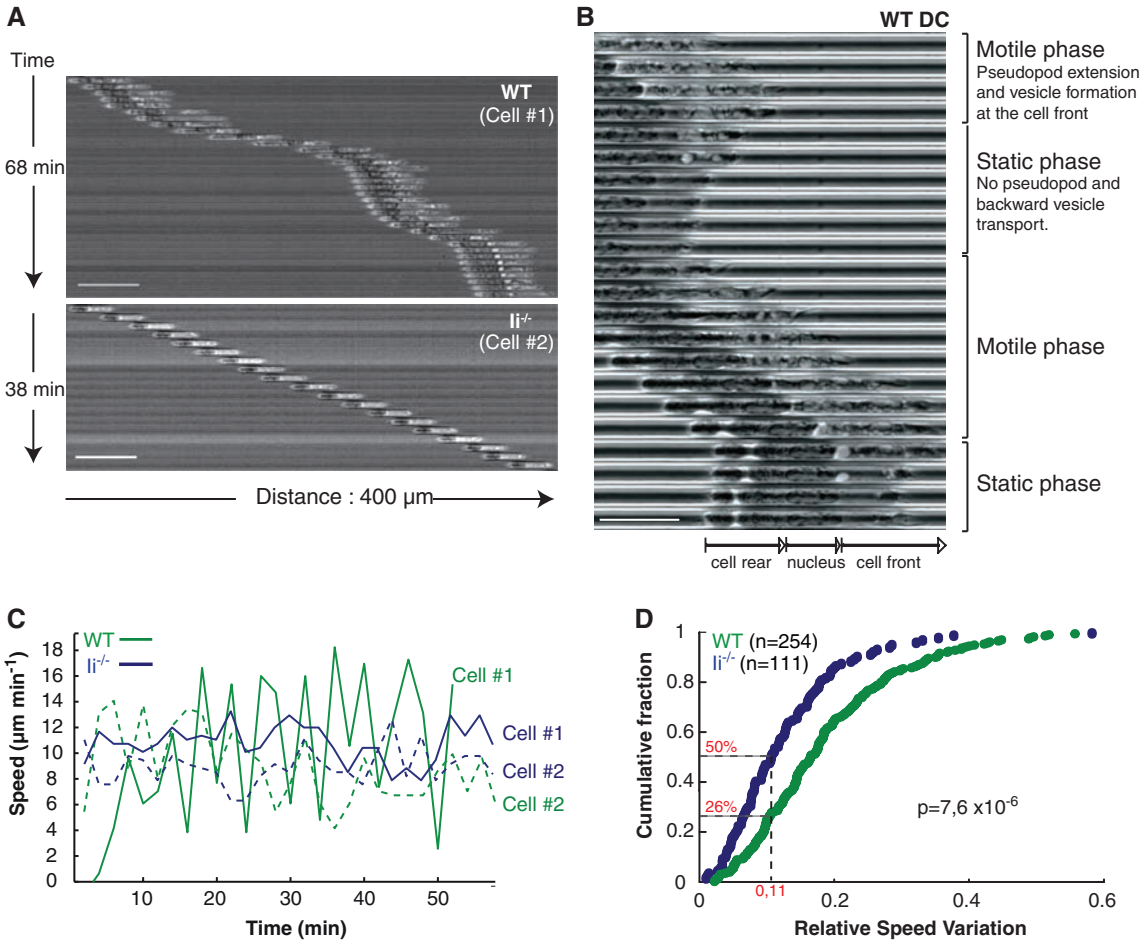

Fig. 3. Ii imposes a discontinuous migration mode to DCs. (**A**) DCs migrating along a 4-µm fibronectin-coated microchannel, covering a distance of 400 µm. Sequential images (10× objective phase) of temporal sequences were placed one below the other (vertical axis). The interval between two images is 2 min. Scale bar indicates 50 µm. (**B**) Sequential high resolution (100×) phase contrast images of a WT cell (movie S1) migrating along a microchannel. The channel part displayed is 88 µm long (vertical axis) with images taken over 14 min (40 s between each image, horizontal axis). Scale bar, 20 µm. (**C**) Representative examples of velocities displayed by individual WT and $Ii^{-/-}$ DCs as a function of time. The data were extracted from movies S1 and S2. WT cell number 1 and $Ii^{-/-}$ cell number 2 correspond to the DCs shown in (A). (**D**) Cumulative distribution of the relative speed variations of WT and $Ii^{-/-}$ DCs, calculated as the average of the local deviation from the local mean (two points before and two points after each time point) divided by the global median velocity.

along microchannels (fig. S8A). Ii-containing structures are known to accumulate in the perinuclear region of $CatS^{-/-}$ DCs (*12*). We observed an enrichment of myosin II heavy chain (MyoIIHC) in these structures (Fig. 4A) compared with a weaker colocalization with the more heterogeneous distribution of Ii in WT DCs, (Fig. 4A and fig. S8B). Equivalent results were obtained in WT cells treated with the CatS inhibitor LHVS (fig. S8B). Cryoimmunoelectron microscopy experiments confirmed the presence of myosin II light chain (MLC) in these enlarged endolysosomal compartments of $CatS^{-/-}$ DCs (Fig. 4B). Because these peculiar compartments form as a result of Ii retention in $CatS^{-/-}$ cells (*17*) and therefore have no structural equivalent to be compared with in WT DCs, it was not possible to provide a rigorous quantification for this qualitative difference. However, we rarely found MLC and Ii colocalizing in endolysosomes of WT DCs (fig. S8C). This result was further verified quantitatively by using biochemistry: The amounts of MyoIIHC and MLC (20 kD) contained in semi-purified endosomal fractions were increased in $CatS^{-/-}$ as compared with WT DCs (fig. S9, A and B). Hence, retention of Ii in endolysosomes of CatS-deficient DCs promotes the association of myosin II to these compartments.

When phosphorylated on Thr^{18} and/or Ser^{19}, MLC binds to and triggers the adenosine triphosphatase (ATPase) activity of the motor, initiating actomyosin contraction (*18*). To assess whether myosin II retention in endolysosomes from $CatS^{-/-}$ DCs decreases its activity, we analyzed the phosphorylation of MLC. Phosphorylation of the full-length 20-kD MLC was considerably decreased in $CatS^{-/-}$ cells compared with WT (Fig. 4, C and D). We consistently observed a 12-kD fragment of MLC that was verified by mass spectrometry in extracts from $CatS^{-/-}$ DCs (Fig. 4C and fig. S9, B and C). However, this MLC fragment did not react with the antiphosphorylated MLC antibody (Ab) (Fig. 4C), suggesting that it is inactive. Inhibition of CatS activity with LHVS triggered the accumulation of this 12-kD MLC fragment in WT but not in $Ii^{-/-}$ DCs (fig. S9D). Hence, retention of Ii in CatS-deficient DCs induces the specific accumulation of a truncated form of MLC. Thus, accumulation of Ii in DCs lacking CatS affects the subcellular localization and the activity of myosin II, providing a possible mechanism for regulation of DC motility by Ii.

We next investigated whether regulation of Ii expression upon DC activation leads to modification of their migratory capacity. Indeed, DCs undergo a transient increase in Ii and MHCII biosynthesis in the first hour after LPS treatment (*4*, *19*). Accordingly, although Ii-myosin II association was observed in nonactivated DCs, it was further increased after 1 hour of LPS treatment (fig. S10, A and B). We found that WT DCs activated with LPS for 2 hours exhibited strong alterations in their ability to migrate along microchannels (movie S6). Early activated WT DCs displayed significantly reduced instantaneous velocities (fig. S10D) and more fluctuant velocities and changed direction more frequently than untreated DCs (Fig. 4, E and F, and fig. S10C). The effect of LPS on motility was less marked in DCs treated with LPS for 12 hours, which moved slightly slower but with a similar persistence than nonactivated DCs (Fig. 4, E and F). LPS had no significant effect on the velocity and directionality of Ii-deficient DCs (Fig. 4, E and F, fig. S10D, and movie S7). Thus, the motility of DCs is regulated upon activation, and such regulation relies at least in part on Ii.

We show that Ii acts as a brake during DC motion by imposing a discontinuous locomotion mode that alternates between high and low motility phases. Down-modulation of cell migration by Ii is likely to result from its direct or

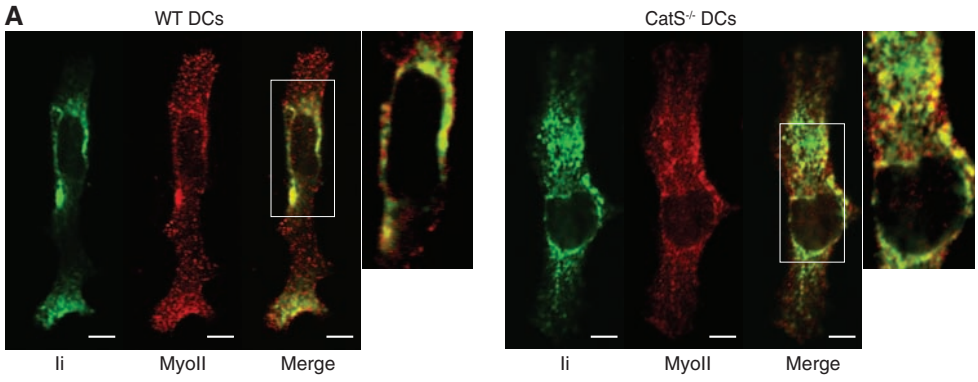

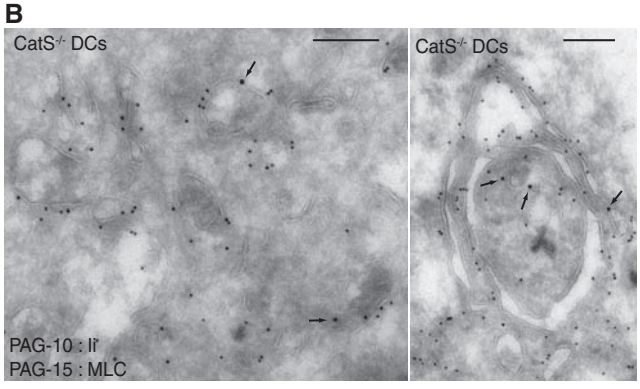

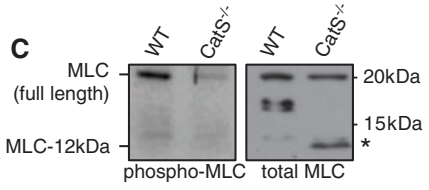

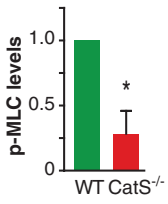

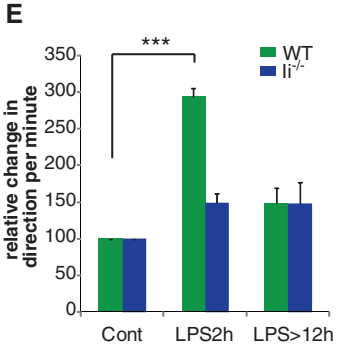

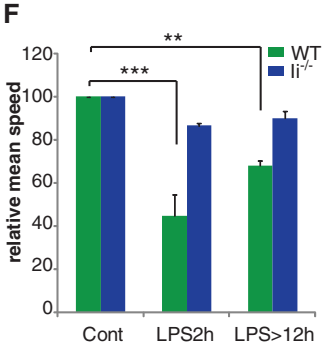

Fig. 4. The levels of Ii modify the localization and phosphorylation of myosin II as well as DC motility. (**A**) Immunofluorescence and confocal microscopy analysis of MyoIIHC and Ii subcellular localization in WT and CatS$^{-/-}$ BM-DCs plated on fibronectin-coated micropatterns. Scale bar, 2 μm. (**B**) Cryoimmunoelectron microscopy of CatS$^{-/-}$ BM-DCs. The colocalization of Ii and MLC was analyzed with secondary Abs coupled to protein A–gold (PAG) of 15-nm and 10-nm diameters, respectively. Scale bar, 200 nm (left) and 500 nm (right). (**C**) WT and CatS$^{-/-}$ DCs were lysed and analyzed by SDS–polyacrylamide gel electrophoresis and immunoblotting using antiphospho-MLC and antitotal MLC Abs sequentially. (**D**) MLC phosphorylation immunoblots were quantified by using Image J software; results were normalized to actin or tubulin expression and expressed as percentage of MLC phosphorylation in WT DCs (mean ± SD, three independent experiments, *P = 0.01). (**E** and **F**) The motility of LPS-pretreated cells along microchannels was analyzed by time-lapse imaging. Data are displayed as (E) the frequency of direction changes per minute and (F) the mean velocities, calculated by averaging instantaneous cell velocity values while taking into account cell directionality. Values are normalized to the ones of untreated cells from the same type (mean ± SD, 100 to 200 cells per condition from two independent experiments, **P < 0.01, ***P < 0.0001).

indirect association with myosin II, which is required for polarized transport of MHCII-Ii complexes to endosomes in B cells (*7*). Ii–myosin II interaction would facilitate the convergence between MHCII and the endocytosed Ag but would temporarily affect the ability of myosin II to promote cell migration, thus leading to a transient decrease in DC velocity. Once in endosomes, Ii–myosin II complexes would dissociate upon Ii cleavage by CatS, restoring high DC motility.

The use of common regulators for Ag processing and cell motility provides a way for DCs to coordinate these two functions in time and space. In immature DCs that patrol peripheral tissues, the periodic low motility phases induced by Ii may enable DCs to efficiently couple Ag uptake and processing to cell migration, facilitating the sampling of the microenvironment. In early-activated DCs, the transient increase in the synthesis and association of Ii with myosin II would reduce the speed and confine the trajectories of the cells by promoting directional changes, enabling DCs to maximize Ag uptake (*2*). The formation of endocytic vesicles at the front of migrating DCs occurred within defined motility phases, suggesting a possible coupling between macropinocytosis and cell locomotion.

The physiological relevance of myosin II–dependent migration in DCs and other leukocytes was recently demonstrated (*6*). The molecular mechanism used by DCs to regulate their migratory capacity via myosin II is likely also used by B lymphocytes, in which myosin II and Ii associate upon B cell receptor engagement (*7*). Indeed, similarly to DCs, activated B cells from Ii$^{-/-}$ mice display enhanced motility ex vivo (fig. S11, A and B). Because myosin II was also shown to respond to Ag receptors in T and natural killer cells (*20*–*22*), we foresee that modulation of myosin II activity might be a general mechanism used by leukocytes to regulate their specific immune function in time and space.

References and Notes

1. J. A. Villadangos, P. Schnorrer, N. S. Wilson, *Immunol. Rev.* **207**, 191 (2005).
2. M. A. West *et al.*, *Science* **305**, 1153 (2004).
3. P. Pierre *et al.*, *Nature* **388**, 787 (1997).
4. M. Cella, A. Engering, V. Pinet, J. Pieters, A. Lanzavecchia, *Nature* **388**, 782 (1997).
5. J. Fink *et al.*, *Lab Chip* **7**, 672 (2007).
6. T. Lammermann *et al.*, *Nature* **453**, 51 (2008).
7. F. Vascotto *et al.*, *J. Cell Biol.* **176**, 1007 (2007).
8. M. F. Naujokas, M. Morin, M. S. Anderson, M. Peterson, J. Miller, *Cell* **74**, 257 (1993).
9. X. Shi *et al.*, *Immunity* **25**, 595 (2006).
10. G. P. Shi *et al.*, *Immunity* **10**, 197 (1999).
11. T. Y. Nakagawa *et al.*, *Immunity* **10**, 207 (1999).
12. C. Driessen *et al.*, *J. Cell Biol.* **147**, 775 (1999).
13. R. J. Riese *et al.*, *J. Clin. Investig.* **101**, 2351 (1998).
14. S. H. Chao, R. Carlson, D. R. Meldrum, *Lab Chip* **7**, 641 (2007).
15. D. Irimia, G. Charras, N. Agrawal, T. Mitchison, M. Toner, *Lab Chip* **7**, 1783 (2007).

16. Microchannels enable cell confinement during motion and therefore mimic the microenvironment encountered by DCs in the constrained interstitial spaces of peripheral tissues and lymphoid organs. They impose a directional migration to cells, which facilitates the extraction of measurable parameters. DCs entered and moved spontaneously and bidirectionally along microchannels, with their cell body being constrained during motion (fig. S4). Time-lapse movies obtained with WT, $Ii^{-/-}$, and $CatS^{-/-}$ DCs were analyzed by drawing kymographs and extracting cell positioning and instantaneous velocity data for individual migrating cells with a specialized computer program (figs. S4 and S5).
17. M. Boes *et al*., *Eur. J. Immunol.* **35**, 2552 (2005).
18. K. Clark, M. Langeslag, C. G. Figdor, F. N. van Leeuwen, *Trends Cell Biol.* **17**, 178 (2007).
19. J. A. Villadangos *et al*., *Immunity* **14**, 739 (2001).
20. J. Jacobelli, S. A. Chmura, D. B. Buxton, M. M. Davis, M. F. Krummel, *Nat. Immunol.* **5**, 531 (2004).
21. M. M. Andzelm, X. Chen, K. Krzewski, J. S. Orange, J. L. Strominger, *J. Exp. Med.* **204**, 2285 (2007).
22. K. Krzewski, X. Chen, J. S. Orange, J. L. Strominger, *J. Cell Biol.* **173**, 121 (2006).
23. The authors thank T. Makushok for setting up the cell migration microchannel system; A. Azicune for cell micropatterning techniques; W. Faigle and D. Lowe for proteomics analysis; C. Recchi for help with gelatin-FITC degradation experiments; H. Overkleeft for synthesizing the LHVS; J. Roger for providing magnetic nanoparticles; M. Leberre, D. Baigl, and Y. Chen for help with microfabrication; and S. Amigorena, M. Sixt, P. Benaroch, V. Soumelis, C. Hivroz, and I. Fernandez for advice on the manuscript. A.-M.L.-D. thanks Y. Bellaïche for help with manuscript redaction. G.F.-A. was supported by a fellowship from the Ministère Français de la Recherche and, together with M.H., from the Association pour la Recherche contre le Cancer (ARC). P.V. and M.-I.Y. benefited from ECOS–Comisíon Nacional de Investigacíon Científica y Technológica, Gobierno de Chile fellowship (CO3S01), Institut Curie and Inserm fellowships, respectively. V.S. was part of the Leonardo Da Vinci project (Unipharma-Graduates, Sapienza University of Rome). This work was funded in part by grants from the ARC, Fondecyt (Chile) to M.-R.B. (1060834) and M.R. (1060253); Agence Nationale pour la Recherche (ANR-06-PCVI-0010) and Human Frontiers Science Program (RGY53/2007) to M.P.

Supporting Online Material

www.sciencemag.org/cgi/content/full/322/5908/1705/DC1
Materials and Methods
Figs. S1 to S11
References
Movies S1 to S7

1 May 2008; accepted 27 October 2008
10.1126/science.1159894

A Role for the ESCRT System in Cell Division in Archaea

Rachel Y. Samson,[1]* Takayuki Obita,[2] Stefan M. Freund,[3] Roger L. Williams,[2] Stephen D. Bell[1]*†

Archaea are prokaryotic organisms that lack endomembrane structures. However, a number of hyperthermophilic members of the Kingdom *Crenarchaea*, including members of the *Sulfolobus* genus, encode homologs of the eukaryotic endosomal sorting system components Vps4 and ESCRT-III (endosomal sorting complex required for transport–III). We found that *Sulfolobus* ESCRT-III and Vps4 homologs underwent regulation of their expression during the cell cycle. The proteins interacted and we established the structural basis of this interaction. Furthermore, these proteins specifically localized to the mid-cell during cell division. Overexpression of a catalytically inactive mutant Vps4 in *Sulfolobus* resulted in the accumulation of enlarged cells, indicative of failed cell division. Thus, the archaeal ESCRT system plays a key role in cell division.

Within the archaeal domain of life, there are two principal Kingdoms, the *Crenarchaea* and the *Euryarchaea*. Studies of microbial diversity have revealed that crenarchaea are one of the most abundant forms of life on Earth (*1*, *2*); however, we know essentially nothing about how cell division occurs in these organisms. This is of particular interest because the sequenced genomes of hyperthermophilic crenarchaeotes lack genes for members of the FtsZ/tubulin and MreB/actin superfamilies of cell division proteins (*3*–*6*). The near-ubiquity of tubulins and actins underscores these proteins' pivotal roles in cell division processes in bacteria, euryarchaea, and eukarya. The absence of orthologs of these proteins in the crenarchaea has prompted us to attempt to identify the crenarchaeal cell division machinery, using species of the genus *Suflolobus* as a model system. In metazoa, the ESCRT (endosomal sorting complex required for transport) system, in addition to its roles in endosomal trafficking and viral egress (*7*–*10*), plays a role in membrane abscission during cytokinesis (*11*–*13*). Most hyperthermophilic crenarchaea encode homologs of ESCRT-III components and the adenosine triphosphatase (ATPase) Vps4 (*14*, *15*) that could potentially be involved in cell division (figs. S1 to S3). *Sulfolobus* encodes four ESCRT-III homologs and a single Vps4 homolog. No homologs of the ESCRT-0, -I, or -II systems are apparent. The Vps4 gene is located within an operon-like structure with an ESCRT-III homolog and a third protein predicted to contain a coiled-coil structure (fig. S1).

First, we profiled the cell-cycle expression of the *Sulfolobus* ESCRT machinery in synchronized cultures of *Sulfolobus acidocaldarius* (*16*, *17*) (Fig. 1, A and B). Transcripts of Saci1372 (Vps4) and ESCRT-III homologs Saci1373, -0451, and -1416 underwent a characteristic modulation, with lowest levels in S phase–enriched populations (at the 30-min time point) and levels peaking between three and four times higher in populations enriched in dividing cells (at 180 min). In agreement with this result, levels of Saci1373 (ESCRT-III) protein were highest in dividing cell populations (Fig. 1C, upper panel). In contrast, Vps4 protein remained nearly constant across the cell cycle (Fig. 1C, middle panel). Immunostaining with antibodies to Saci1373 (ESCRT-III) revealed a distinct subcellular localization of the protein. More specifically, in cells where the two nucleoids had separated, a band or belt of Saci1373 (ESCRT-III) was detected between the two nucleoids, correlating with the site of membrane ingression (Fig. 2, figs. S5 and S6, and movie S1). Similar results were observed for Vps4 localization, although in addition to the strong staining at mid-cell, we generally observed a weaker, diffuse background distributed throughout the cell body (Fig. 2). The highly specific localization of these proteins to the mid-cell in dividing cells suggested a role in cell division–related processes.

In eukaryotes, ESCRT-III family proteins are capable of both homo- and heteromultimeric interactions resulting in the generation of protein lattices. We tested the ability of the four *Sulfolobus* ESCRT-III homologs to interact with one another using yeast two-hybrid assays (Fig. 3A). A series of interactions between these proteins was detected, indicating that the archaeal ESCRT-III proteins have the capacity to form an extended lattice. In eukaryotes, Vps4 plays a pivotal role in disassembling the ESCRT-III lattice and has been shown to interact with ESCRT-III proteins via the MIT domain of Vps4 and the C-terminal tails of ESCRT-IIIs. We tested whether the Saci1373 (ESCRT-III) and Vps4 proteins interact directly. Full-length (residues 1 to 261) Saci1373 (ESCRT-III) and Saci1372 (Vps4) did indeed interact (Fig. 3, B and C). The minimal interaction sites comprised residues 183 to 193 of Saci1373 (ESCRT-III), a notably hydrophobic and proline-rich region (Fig. 3B), and the MIT domain of Saci1372 (Vps4) (Fig. 3C). To better understand the basis of this interaction, we determined the co-crystal structure of the MIT domain of Saci1372 (Vps4) with a peptide corresponding to residues 183 to 193 of Saci1373 (ESCRT-III). The MIT domain forms a three-helix bundle, and the peptide binds in an extended configuration to the groove formed between helices α1 and α3 (Fig. 3D). The residues interacting with the MIT domain constitute part of a 183-(R/K)XLLP(D/E)LPXPP-193 motif (*18*) present in most orthologs of Saci1373. Among the four Saci ESCRT-III–like subunits, only Saci1373

[1]Medical Research Council (MRC) Cancer Cell Unit, Hills Road, Cambridge CB2 0XZ, UK. [2]MRC Laboratory of Molecular Biology, Hills Road, Cambridge, CB2 0QH, UK. [3]MRC Centre for Protein Engineering, Hills Road, Cambridge CB2 0QH, UK.

*Present address: Sir William Dunn School of Pathology, South Parks Road, Oxford, OX1 3RE, UK.

†To whom correspondence should be addressed. E-mail: stephen.bell@path.ox.ac.uk

has this MIT-binding motif (fig. S2). Two other ESCRT-III–like subunits (Saci1416 and Saci0451) bound the Saci1372 (Vps4) MIT domain with lower affinity, whereas Saci1601 does not bind (fig. S7). Pro^{187} of this motif is a *cis*-Pro that forces a sharp kink in the bound peptide so that Leu^{186} and Pro^{187} have only limited contact with the MIT domain. The core residues in contact with the MIT domain (189-LP-190) are essential for maintaining interaction with the MIT domain in solution (figs. S2 and S8). This mode of interaction is distinct from the previously characterized structures of complexes of yeast and human Vps4 MIT domains with interacting peptides [MIMs (MIT-interacting motifs)] derived from ESCRT-III family members Vps2 and human CHMP1A and -2B (*14*, *19*). In those structures, the MIM formed an amphipathic alpha helix that binds between α2 and α3 of the MIT domain (Fig. 3E). However, the MIM in human CHMP6 (termed MIM2) binds in an extended configuration along the groove formed by helices 1 and 3 of the MIT domain (*20*). Although the CHMP6 MIM2 lacks the *cis*-Pro equivalent of Saci1373 Pro^{187} and the corresponding kink of the main chain, the residues interacting with the Vps4 MIT domain and the extended main-chain conformations for these residues are essentially the same as we observe for Saci1373 binding to the Saci1372 (Vps4) (Fig. 3F). Despite the 2- billion-year evolutionary gulf between *Sulfolobus* Saci1373 (ESCRT-III) and human CHMP6, the sequences of the MIT-interacting peptides of these two proteins are clearly conserved at the primary sequence level.

Thus, archaeal ESCRT components are cell-cycle–regulated, interact via an evolutionarily conserved interface, and show specific subcellular localization to the site of membrane ingression during archaeal cell division. To further test the in vivo role of the *Sulfolobus* ESCRT components, we generated an episomal vector to direct arabinose-inducible expression of a target gene in *S. solfataricus* (*21*) (figs. S9 to S11). We transformed *S. solfataricus* with either an empty vector or vector containing wild-type Vps4 or an ATPase-defective [Glu^{206}→Gln^{206} (E206Q), "Walker B"] mutant of Vps4 (Fig. 4, A to C).

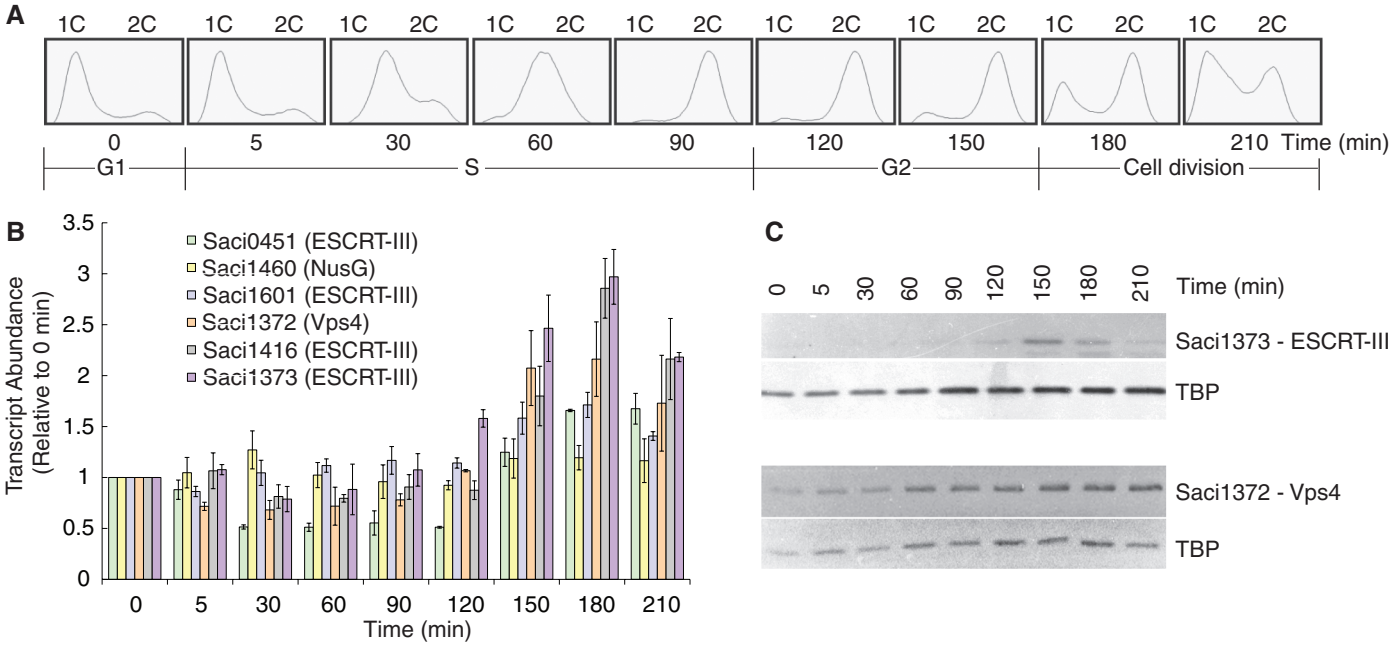

Fig. 1. (**A**) Flow cytometric analysis of samples taken at the indicated time points during the progression of a synchronized culture of *S. acidocaldarius*. The positions of peaks corresponding to one chromosome content (1C) and 2C genome contents are indicated. The cell-cycle stages are indicated at the bottom. (**B**) Real-time polymerase chain reaction measurements of transcript abundance of the indicated ESCRT-III homologs, Vps4, and a housekeeping control (the *nusG* transcription elongation factor). Experiments were performed in triplicate, and the SD is indicated by the error bars. All samples were normalized to the level detected at 0 min. (**C**) Western blot analysis of the levels of Saci1373 (ESCRT-III), Vps4, and the general transcription factor TATA box–binding protein (TBP) proteins across the cell cycle. Samples were taken at the indicated times during the growth of synchronized *S. acidocaldarius* cultures.

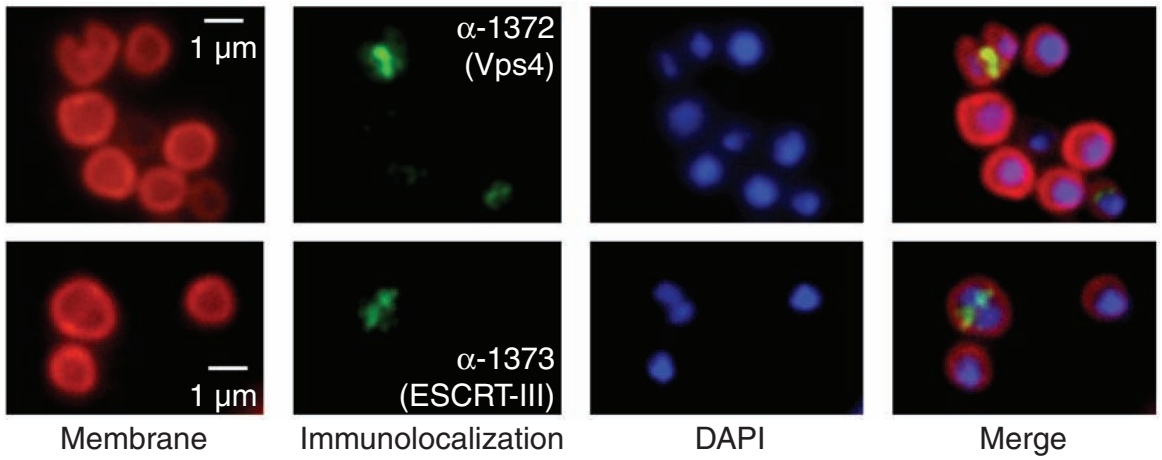

Fig. 2. Localization of (**Top**) Saci1372 (Vps4) and (**bottom**) Saci1373 (ESCRT-III). Representative images are shown. Images show the FM4-64X staining for membrane (red), DAPI staining for DNA (blue), antibody labeling of ESCRT-III or Vps4 (green), and merged images. Scale bar, 1 μm. Additional images are shown in figs. S6 and S7 and movie S1.

Overexpression of wild-type Vps4 results in the appearance of only a small proportion of enlarged cells with elevated DNA content, indicated by red triangles in Fig. 4B. Induction of the mutant Vps4 E206Q results in a far more dramatic phenotype (Fig. 4, C and D). Considerably enlarged cells, up to four times the diameter of wild-type cells, were observed that showed intense 4′,6′-diamidino-2-phenylindole (DAPI) staining, indicative of elevated DNA content. In addition, a large number of "ghost" cells lacking DNA were seen (Fig. 4D). Flow cytometry of the cells containing overexpressed Vps4 (E206Q) revealed an aberrant profile with a significant proportion of the cells containing less than one or more than two genome equivalents. The cells with more than two chromosomes formed a broad continuum with non-integral genome contents, indicating that, in the absence of proper cell division, DNA replication is misregulated.

Here we have shown that *Sulfolobus* ESCRT system homologs play a role in the cell division process. The ESCRT system in human cells is involved in membrane abscission at the final stages of cytokinesis (*12*, *13*). However, there is no evidence of yeast ESCRT proteins being involved in cell division, leading to speculation that this role in human cells may be a recent evolutionary acquisition. Our findings suggest that the role of the ESCRT proteins in cell division may pre-date the divergence of the crenarchaeal and eukaryotic lineages and thus be reflective of the ancestral role of this complex. Just as

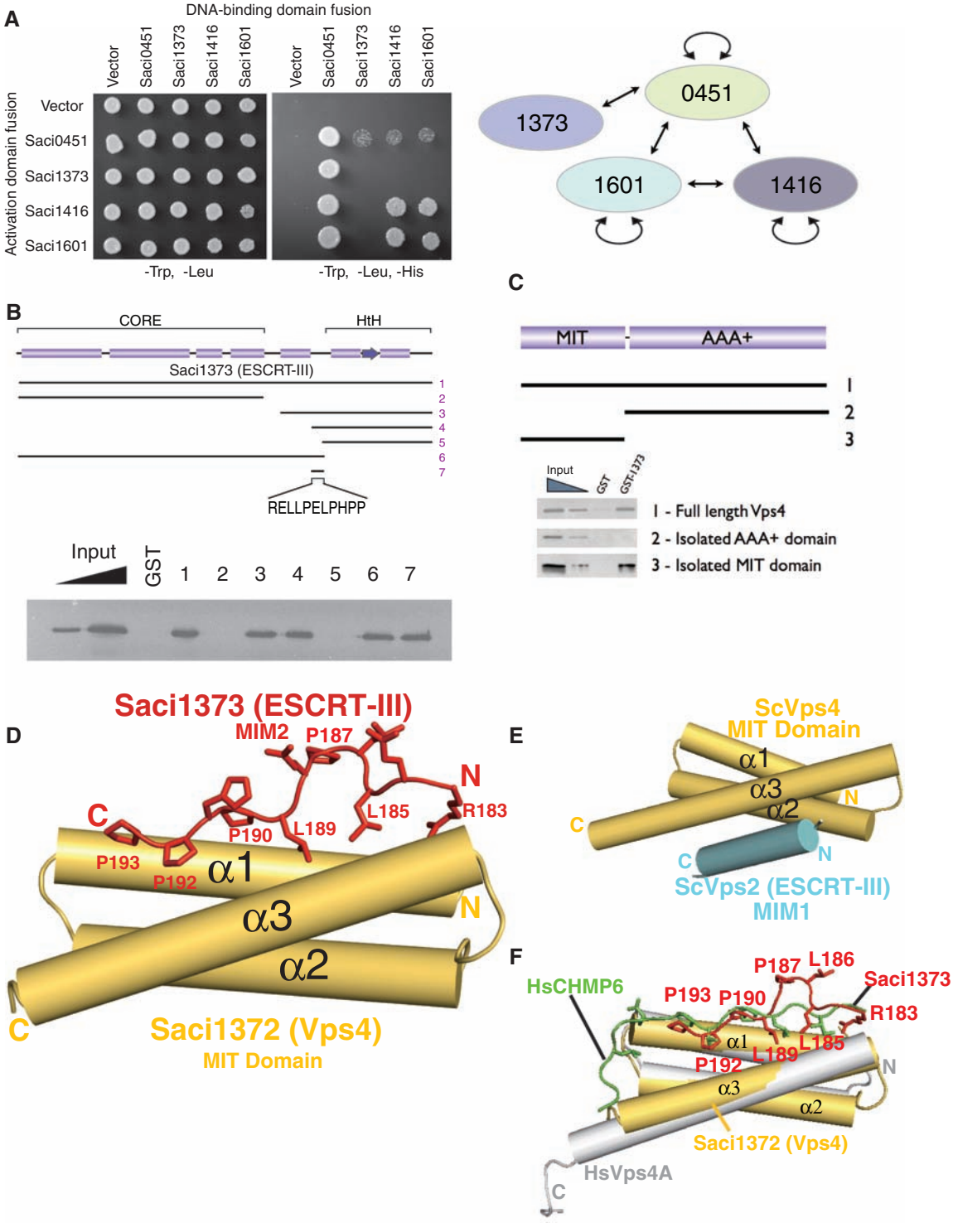

Fig. 3. (**A**) Interactions between ESCRT-III proteins detected by yeast two-hybrid analyses. Yeast cells containing the indicated plasmids were plated in media lacking leucine and tryptophan to select for plasmids and lacking histidine to score for interactions. (**B**) Identification of the minimal interaction site on Saci1373 (ESCRT-III) for binding Vps4. Glutathione *S*-transferase (GST) fusions of ESCRT-III fragments were used in pull-down assays with the full-length Vps4. The results of the pull-downs are shown in the lower panel. The input lanes contain 25 and 5% of input. (**C**) Identification of the interaction domain of Vps4 that binds Saci1373 (ESCRT-III). GST-Saci1373 (ESCRT-III) was used in pull-down assays with the full-length (1), C-terminal AAA+ domain (2), or isolated MIT domain (3) of Vps4. (**D**) A schematic representation of the interaction of Saci1373 (red) with the Saci1372 Vps4 MIT domain (yellow). (**E**) An illustration of the interaction of the yeast Vps4 MIT domain (yellow) with the C-terminal MIM1 motif (blue) of the yeast Vps2 ESCRT-III subunit. The MIM1 motif slots between MIT helices α2 and α3 (*14*). (**F**) The Saci1373 MIM2 (red)/Saci1372 MIT (yellow) interaction is closely related in structure with the CHMP6 MIM2 (green, extended)/VPS4A MIT (gray helices) interaction (*20*).

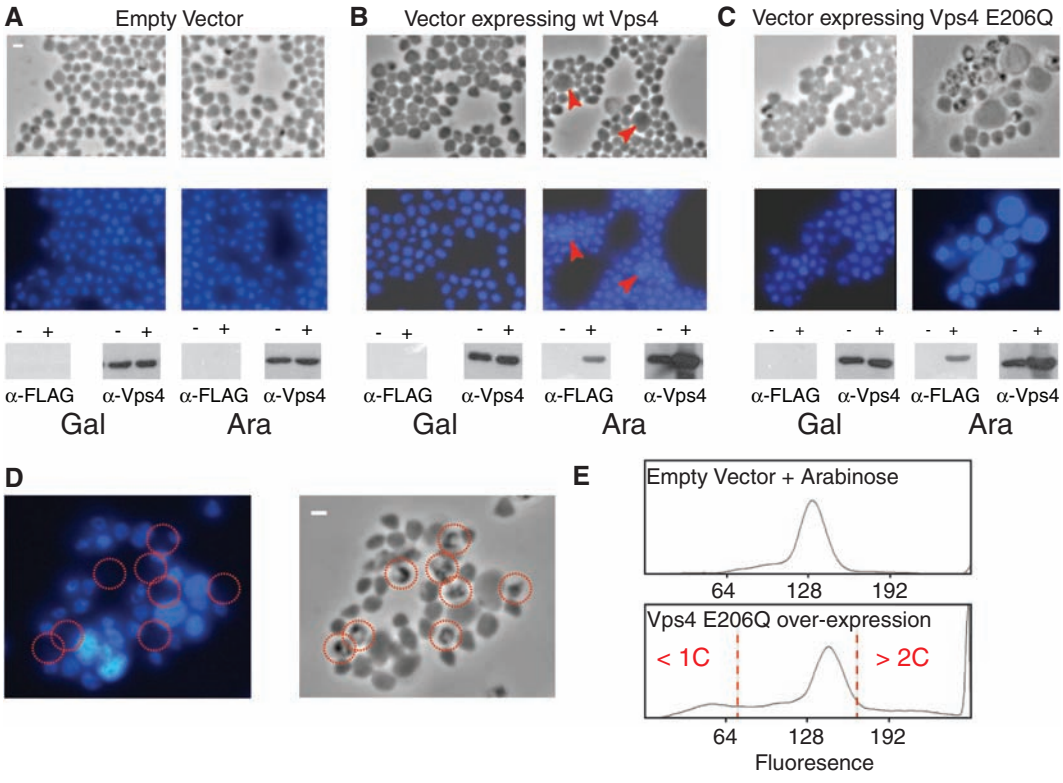

Fig. 4. (**A** to **C**) Phase contrast and fluorescent microscopy of DAPI-stained *S. solfataricus* cells containing either vector pRYS1 (A), pRYS1-wtVps4 (B), or pRYS1-Vps4 E206Q (C). In each panel, the left-hand images show cells grown in the repressing conditions (in the presence of galactose) and the right-hand images show cells in which expression of the plasmid-encoded gene is induced by the addition of arabinose. Red arrowheads in (B) indicate enlarged cells with elevated DNA content. The lower panels show the results of Western blotting with either antiserum to FLAG or antiserum to Vps4. The antiserum to the FLAG tag detects only the plasmid-encoded Vps4; the antiserum to Vps4 detects both plasmid and chromosomally encoded Vps4. The − and + symbols correspond to cells before and after the addition of either galactose (Gal) or arabinose (Ara). (**D**) An enlarged image of cells overexpressing Vps4 E206Q (phase contrast image on the left, fluorescent DAPI image on the right). Cells lacking discernable DAPI staining are circled in red. (**E**) Flow cytometric profile of cells grown in arabinose containing either empty vector or vector overexpressing Walker B (E206Q) Vps4. Cells with less than 1C or more than 2C genome content are indicated.

mammalian ESCRT-III subunits appear to have multiple roles in cell biology, the role of the archaeal ESCRT-III subunits may not be limited to cell division. Dominant-negative mammalian ESCRT-III subunits block HIV-1 budding and release (*10*, *22*). Indeed, a recent report revealed that the *S. solfataricus* ESCRT-III–like subunit Sso0881, the ortholog of Saci1416 (figs. S1 to 3), is associated with viral particles of the *Sulfolobus* turreted icosahedral virus (STIV) (*23*). Finally, the reduced complexity of the archaeal ESCRT apparatus provides a simplified model with which to investigate the core mechanisms of lattice formation and breakdown by this system.

References and Notes

1. M. B. Karner, E. F. DeLong, D. M. Karl, *Nature* **409**, 507 (2001).
2. C. M. Santelli *et al.*, *Nature* **453**, 653 (2008).
3. J. Pogliano, *Curr. Opin. Cell Biol.* **20**, 19 (2008).
4. N. A. Dye, L. Shapiro, *Trends Cell Biol.* **17**, 239 (2007).
5. W. Margolin, *Nat. Rev. Mol. Cell Biol.* **6**, 862 (2005).
6. R. Carballido-Lopez, J. Errington, *Trends Cell Biol.* **13**, 577 (2003).
7. J. Martin-Serrano, *Traffic* **8**, 1297 (2007).
8. R. L. Williams, S. Urbe, *Nat. Rev. Mol. Cell Biol.* **8**, 355 (2007).
9. R. C. Piper, D. J. Katzmann, *Annu. Rev. Cell Dev. Biol.* **23**, 519 (2007).
10. J. H. Hurley, S. D. Emr, *Annu. Rev. Biophys. Biomol. Struct.* **35**, 277 (2006).
11. C. Spitzer *et al.*, *Development* **133**, 4679 (2006).
12. J. G. Carlton, J. Martin-Serrano, *Science* **316**, 1908 (2007).
13. E. Morita *et al.*, *EMBO J.* **26**, 4215 (2007).
14. T. Obita *et al.*, *Nature* **449**, 735 (2007).
15. C. F. V. Hobel, S. V. Albers, A. J. M. Driessen, A. N. Lupas, *Biochem. Soc. Trans.* **36**, 94 (2008).
16. I. G. Duggin, S. McCallum, S. D. Bell, *Proc. Natl. Acad. Sci. U.S.A.* **105**, 16737 (2008).
17. See supplementary methods on *Science* Online.
18. Single-letter abbreviations for the amino acid residues are as follows: D, Asp; E, Glu; H, His; K, Lys; L, Leu; P, Pro; R, Arg; and X, any amino acid.
19. M. D. Stuchell-Brereton *et al.*, *Nature* **449**, 740 (2007).
20. C. Kieffer *et al.*, *Dev. Cell* **15**, 62 (2008).
21. J. M. Lubelska, M. Jonuscheit, C. Schleper, S. V. Albers, A. J. M. Driessen, *Extremophiles* **10**, 383 (2006).
22. K. Fujii, J. H. Hurley, E. O. Freed, *Nat. Rev. Microbiol.* **5**, 912 (2007).
23. W. S. A. Maaty *et al.*, *J. Virol.* **80**, 7625 (2006).

24. We thank O. Perisic and I. Duggin for advice and helpful discussions, C. Mueller-Dieckmann for help with European Synchrotron Radiation Facility beamline ID29, and S. McCallum for flow cytometry. The work was supported by the Wellcome Trust (grant 083639/Z/07/Z to R.L.W.), the Edward Penley Abraham Trust (S.D.B.). and the MRC (R.L.W. and S.D.B.). The coordinates for the structure reported in this work have been deposited in the Protein Data Bank (accession number 2w2u).

Supporting Online Material

www.sciencemag.org/cgi/content/full/1165322/DC1
Materials and Methods
Figs. S1 to S11
Tables S1 to S3
References
Movie S1

2 September 2008; accepted 3 November 2008
Published online 13 November 2008;
10.1126/science.1165322
Include this information when citing this paper.

De Novo Formation of a Subnuclear Body

Trish E. Kaiser,[1] Robert V. Intine,[1,2] Miroslav Dundr[1]*

The mammalian cell nucleus contains structurally stable functional compartments. We show here that one of them, the Cajal body (CB), can be formed de novo. Immobilization on chromatin of both CB structural components, such as coilin, and functional components of the CB, such as the SMN complex, spliceosomal small nuclear ribonucleoproteins (RNPs), small nucleolar RNPs, and small Cajal body–specific RNPs, is sufficient for the formation of a morphologically normal and apparently functional CB. Biogenesis of the CB does not follow a hierarchical assembly pathway and exhibits hallmarks of a self-organizing structure.

Compartmentalization of the nucleus contributes significantly to the regulation of nuclear functions (*1*–*5*). The structure of intranuclear compartments is maintained in the absence of defining membranes and despite a highly dynamic exchange of their components with the surrounding nucleoplasm (*6*, *7*). It has been suggested that nuclear bodies are formed by either an ordered assembly pathway or self-organization (*3*, *5*). To discriminate between these

two alternatives, we used as a model the Cajal body (CB), a major nuclear body involved in the biogenesis and recycling of several classes of small nuclear ribonucleoproteins (snRNPs).

To assess the ability of CB proteins to nucleate the formation of a CB de novo, we immobilized fusion proteins between the *Escherichia coli* Lac Repressor (LacI) and green fluorescent protein (GFP)–tagged CB components on chromatin in a previously characterized HeLa cell line (*8*) in which 256 repeats of the Lac operator (LacO) (*9*) are stably integrated on chromosome 7 (*10*). Several CB fusion proteins, including coilin, SMN (survival of motor neuron gene), and Nopp140, were efficiently targeted to the LacO array, and their accumulation appeared as discrete foci (Fig. 1). LacI stained with red fluorescent protein (Cherry-LacI) was coexpressed to distinguish the position of the LacO array from endogenous CBs. Immobilization of one of the two major structural components of CBs, coilin or SMN, was sufficient to trigger the formation of CBs, as indicated by the presence of endogenous coilin (Fig. 1A) and SMN (Fig. 1B) in the newly formed bodies. CBs formed in 52.1% of cells expressing LacI-coilin and in 50.7% of cells expressing LacI-SMN (Fig. 1F). Tethering of the non–CB protein SR (serine-arginine–rich) splicing factor SC35 (Fig. 1C), the major nucleolar protein B23 (Fig. 1D), or nucleoporin NUP62 (fig. S1A) did not lead to formation of a coilin-positive body. Immobilization of the PML body component PML protein did not lead to the formation of CB (fig. S1B); however, PML protein nucleated a PML body, as indicated by recruitment of the PML component Sp100 (Fig. 1E). We conclude that one of the major nuclear compartments, the CB, can be formed de novo. Furthermore, our results with PML suggest that this type of nucleation may be applicable to other nuclear bodies.

De novo formed CBs were functional by several criteria. They contained components of several functional groups of proteins present in endogenous CBs, including: the SMN protein complex, as indicated by the presence of Gemin2 (Fig. 2A), Gemin5 (fig. S2A); components of spliceosomal snRNPs (SmB/B′ and SmD1 Fig. 2B), the U4-specific protein hPrp31 (fig. S2B); the U5-specific protein hSnu114, and the small nucleolar ribonucleoproteins' (snoRNPs) chaperone Nopp140 (Fig. 2C). In addition, U85 scaRNA, a CB-specific snRNA guide RNA, is present (Fig. 2D). As expected for a functional CB, co-immunoprecipitation experiments demonstrated physical interaction between GFP–LacI-coilin and endogenous coilin, SMN, and Gemin2 (Fig. 2F). Additionally, in the presence of the dominant-negative mutant ΔRG coilin, which lacks the RG domain responsible for the interaction with SMN, de novo CBs display the same physical separation of CB from their twin nuclear gem body as observed for endogenous CBs (Fig. 2E) (*7*). Inverse fluorescence recovery after photobleaching (iFRAP) in de novo CBs, formed by tethering Cherry–LacI-SMN, demonstrated that GFP-coilin has similar dissociation kinetics in de novo formed CBs as in endogenous CBs (Fig. 2G) (*7*). Moreover, the size of de novo formed CB on the LacO array corresponds to the size of endogenous CBs present in cells, which suggests a size criticality in the nuclear body formation.

To establish the kinetics of de novo CB formation, we treated cells with isopropyl-β-D-thiogalactopyranoside (IPTG) for 16 hours, which prevents binding of fusion proteins to the LacO, which, in turn, leads to the disassembly of the de novo formed CB (fig. S3). When IPTG is washed out, LacI-fusion proteins accumulated on the LacO array within 30 min (fig. S3A), with newly forming CBs visible after 2 hours (fig. S3, C, D, and E). No differences in the assembly dynamics of various CB components were detected, which suggested that the components are not recruited in a stepwise manner, but rather, accumulate concurrently.

Coilin and SMN are known to be essential for the structural integrity of CBs (*11*). To test whether coilin and SMN are also required for CB formation, we selectively depleted the cells of coilin or SMN by RNA interference (fig. S4, A and B) and probed for formation of CBs. Depletion (knockdown) of SMN prevented formation of de novo CBs when coilin was tethered (Fig. 3, A and B). Similarly, no CBs formed when coilin was immobilized in primary fibroblasts derived from a spinal muscular atrophy (SMA) patient with severely reduced SMN protein levels (fig. S4C). However, immobilized coilin is still capable of accumulating fibrillarin (Fig. 3C) and Nopp140 on the array, which indicates that, in the absence of SMN, coilin still interacts with snoRNPs. When the dominant-negative ΔRG coilin mutant was tethered, which disrupts interaction between coilin with SMN (*12*), in a wild-type SMN background, CB did not form de novo (fig. S5A). Tethering of SMN to chromatin in cells when coilin was knocked down was still sufficient to nucleate de novo residual gem bodies detected

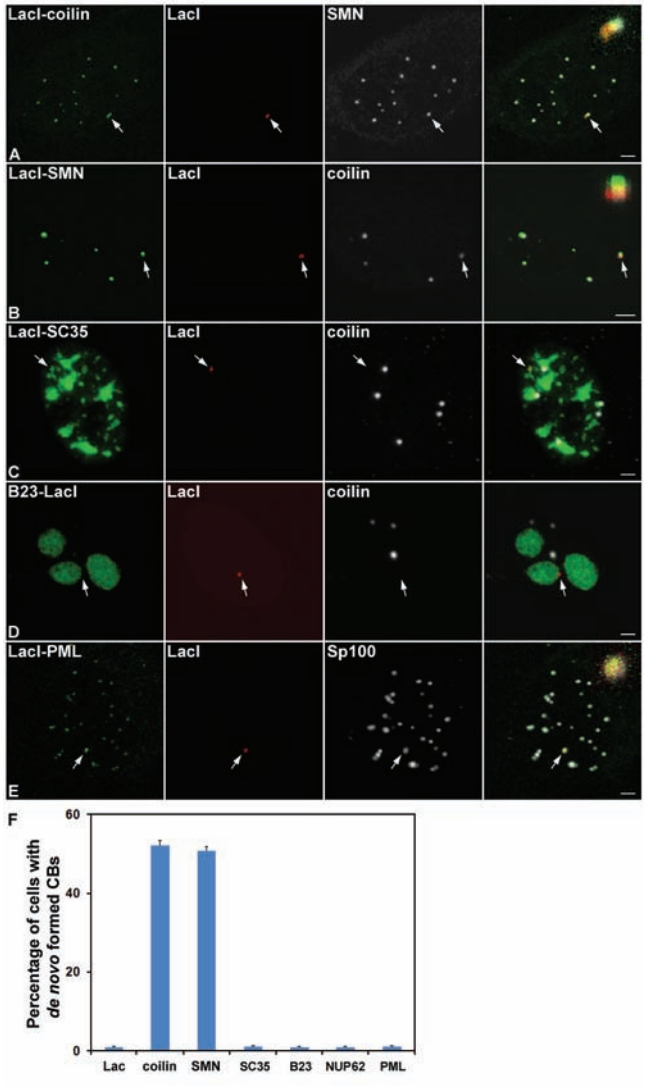

Fig. 1. Immobilization of a single structural component leads to nuclear body formation. Immunofluorescence microscopy on HeLa cells transiently transfected with various GFP-LacI fusion proteins (green), Cherry-LacI (red) and stained with the indicated antibody (**A** to **E**). (Insets) High magnification view of formed CB. Arrows, the location of the tethered fusion proteins. Quantification of de novo CB formation (**F**). Values represent means ± SD (n = 65 to 95 cells) from two independent experiments. Scale bar, 2 μm.

[1]Department of Cell Biology, Rosalind Franklin University of Medicine and Science, North Chicago, IL 60064, USA. [2]Dr. William M. Scholl College of Podiatric Medicine at Rosalind Franklin University of Medicine and Science, North Chicago, IL 60064, USA.

*To whom correspondence should be addressed. E-mail: mirek.dundr@rosalindfranklin.edu

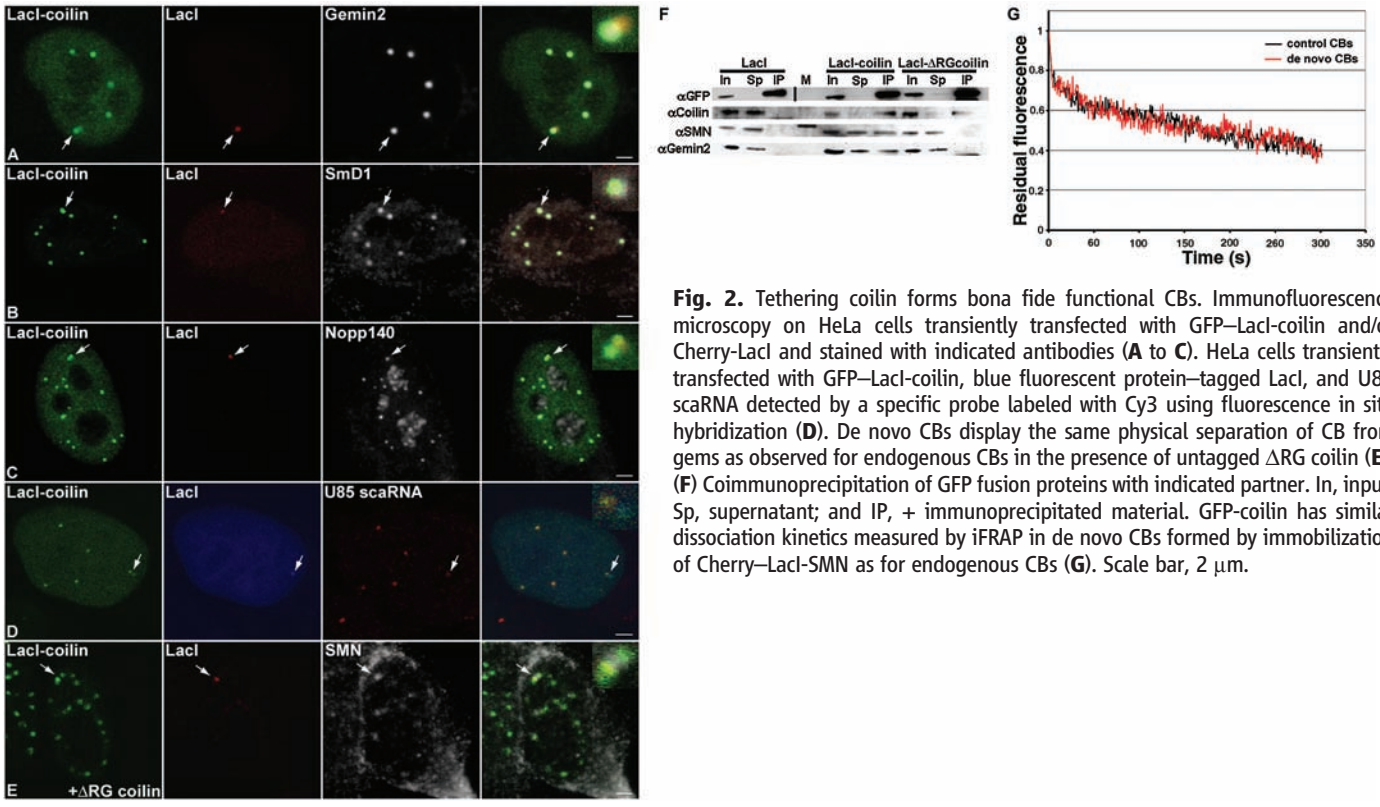

Fig. 2. Tethering coilin forms bona fide functional CBs. Immunofluorescence microscopy on HeLa cells transiently transfected with GFP—LacI-coilin and/or Cherry-LacI and stained with indicated antibodies (**A** to **C**). HeLa cells transiently transfected with GFP—LacI-coilin, blue fluorescent protein—tagged LacI, and U85 scaRNA detected by a specific probe labeled with Cy3 using fluorescence in situ hybridization (**D**). De novo CBs display the same physical separation of CB from gems as observed for endogenous CBs in the presence of untagged ΔRG coilin (**E**). (**F**) Coimmunoprecipitation of GFP fusion proteins with indicated partner. In, input; Sp, supernatant; and IP, + immunoprecipitated material. GFP-coilin has similar dissociation kinetics measured by iFRAP in de novo CBs formed by immobilization of Cherry—LacI-SMN as for endogenous CBs (**G**). Scale bar, 2 μm.

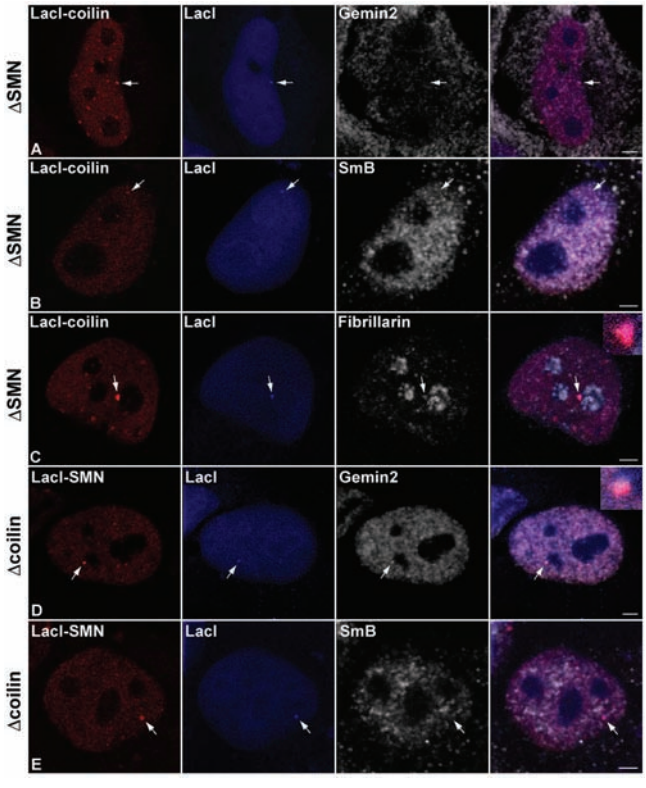

Fig. 3. Coilin and SMN are required for Cajal body formation. Immobilization of coilin on chromatin in HeLa cells lacking SMN did not lead to formation of de novo CBs (**A** and **B**), but lead to accumulation of snoRNPs on the array detected by fibrillarin (**C**). Immobilization of SMN on chromatin in HeLa cells lacking coilin could nucleate de novo gem bodies detected by Gemin2 (**D**), but did not lead to accumulation of snRNPs (**E**). Scale bar, 2 μm.

by Gemin2 (Fig. 3D), but was insufficient to cause accumulatation of snRNPs and snoRNPs (Fig. 3E) (*13*). Dominant-negative SMNΔ2b (fig. S5, B and C) and SMNΔC26 (fig. S5, D and E) mutants, which are unable to homopolymerize SMN (*14*), failed to nucleate CBs (fig. S5, B to E), which suggests that SMN's self interaction is a critical step in CB formation. These data indicate that coilin and SMN are required factors that act cooperatively to facilitate CB formation.

Given the two CB assembly models, the ordered assembly pathway and self-organization, two distinct predictions about the ability of other CB components to nucleate de novo formation can be made. If CBs form in a hierarchical pathway, only upstream components should be able to nucleate formation. In contrast, if CBs form by self-organization, many, if not all, CB components should be sufficient to nucleate CBs. When, Gemin3, a SMN complex component, was tethered to the LacO array, de novo CBs were nucleated with the same efficiency (51.6%) as coilin (52.1%) or SMN (50.7%) (Fig. 4, B and H). Nopp140, a snoRNP chaperone, which directly interacts with the N terminus of coilin (*15*), nucleated CB with even higher efficiency (91%) (Fig. 4, A and H). These CBs contained all the same CB components as the de novo CBs formed by tethering of coilin or SMN (fig. S6), which demonstrates that proteins other than coilin and SMN have the ability to form CB.

Although spliceosomal U snRNPs are major components of the CB, wherein they undergo the final steps of maturation and are recycled after splicing, they are not considered structural CB components (*16*, *17*). Tethering of SmD1, which directly interacts with SMN; SmE and SmG, which interact indirectly with SMN as a part of the Sm ring (*18*); and Tgs1, the trimethylguanosine synthetase, which interacts with Sm proteins (*19*), nucleated CB with high efficiency (81.7 to 93.1%) (Fig. 4H). In contrast, immobilization of Snurportin1, which binds the hypermethylated cap of snRNPs and promotes their import to the nucleus (*20*), nucleated de novo CBs with lower

efficiency (48.3%) (Fig. 3H and fig. S7D) than Sm proteins. To exclude the possibility that these effects were due to the association of these Sm proteins with immature snRNPs, which are still part of the SMN complex, we probed the ability of mature snRNPs to nucleate CB. To this end, we tethered the U2 snRNP–specific A′ protein (fig. S7E), the U4 snRNP–specific hPrp3 (Fig. 4D), the U4/U6 snRNP assembly factor SART3 (fig. S7F), and the U5 snRNP–specific human WD repeat domain 57 (WDR57 or snRNP 40 kD) (fig. S7G) to the LacO array. All these snRNP-specific proteins efficiently form de novo CBs with 88.6 to 93.4% efficiency (Fig. 4H).

CBs also play a significant role in the assembly steps of nucleolar snoRNPs (*21*), and we probed whether snoRNPs are able to nucleate CBs. The snoRNP-specific proteins box C/D U3 snoRNP–specific 55-kD protein (Fig. 4E), box C/D methyltransferase fibrillarin (fig. S7H), and box H/ACA snoRNP–specific protein dyskerin

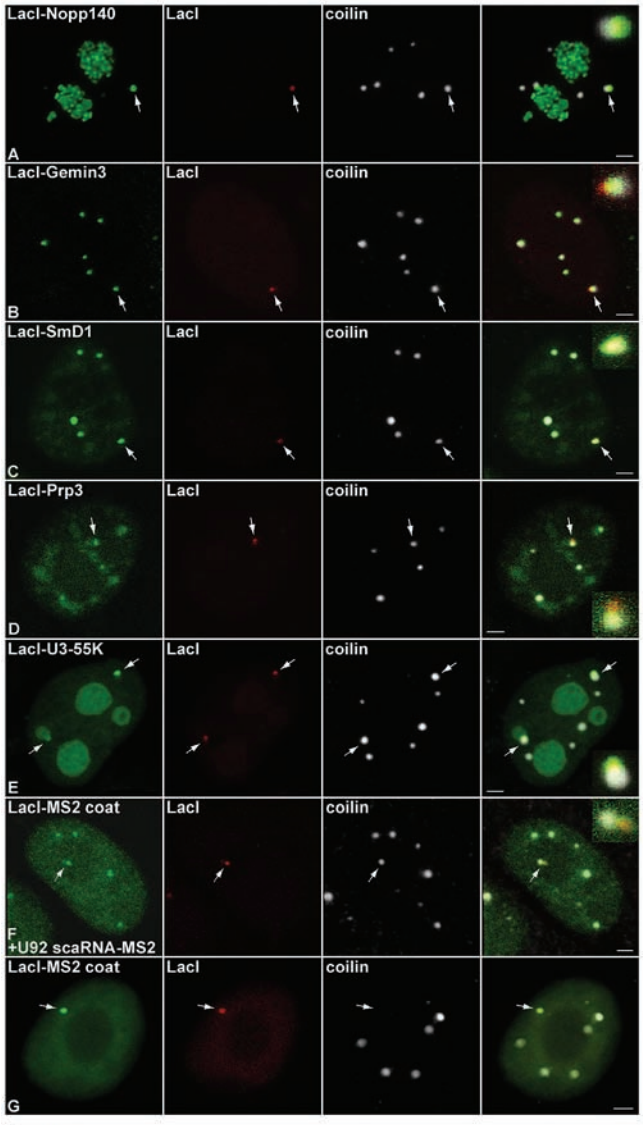

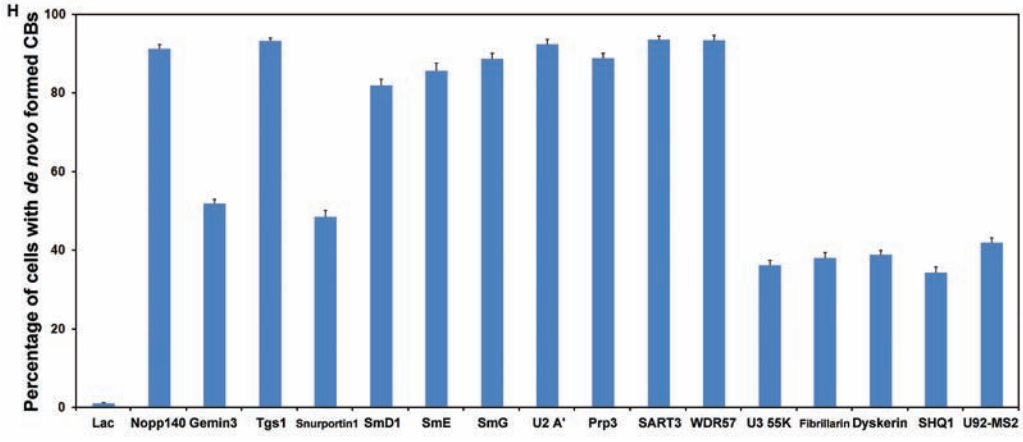

Fig. 4. Other Cajal body components are capable of forming Cajal bodies de novo. Immunofluorescence microscopy on HeLa cells transiently transfected with CB components fused with GFP-LacI, Cherry-lacI, and coilin-specific antibody (**A** to **G**). Arrows indicate the location of de novo formed CB. Immobilization of U92 scaRNA tagged with the MS2 loop by coexpression of GFP—LacI-NLS-MS2 coat protein on chromatin leads to de novo CB formation (F). In contrast, in the absence of the U92-MS2 scaRNA, GFP—LacI-MS2 coat protein is targeted to the LacO array only (G). Quantitative analysis of de novo CB formation efficiency on the LacO array (**H**). Values represent the means ± SD (n = 65 to 95 cells) from two independent experiments (H). Scale bar, 2 μm.

(NAP57) (fig. S7I) were tethered to the LacO array. In all cases, the snoRNP-specific proteins yielded the lowest efficiency of CB formation (from 34.1 to 37.8%) (Fig. 4H). Overall, these data strongly demonstrate that immobilized mature snRNPs have the ability to form CBs, and snRNPs, in general, do so with a significantly higher efficiency than snoRNPs, SMN, or coilin.

Finally, to test whether not only proteins, but also a small CB-associated RNA, could nucleate de novo formation, we tethered the U92scaRNA using the bacteriophage MS2 stem loop–coat protein system (*22*). Tethered U92 scaRNA, indeed, nucleated CB with 41.6% efficiency (Fig. 4, F and G). Overall, these data indicate that snRNPs, snoRNPs, and scaRNAs can nucleate CBs; of these, snRNPs are the most efficient (Fig. 4H). The fact that these functional groups of CB components have the capacity for de novo CB biogenesis (table S1) indicates that CB formation does not follow a strict linear assembly pathway, but can be triggered by a number of functional CB components.

Here, we demonstrate the formation of a nuclear body de novo. We suggest that CB formation occurs by self-organization based on two observations (*3*, *5*, *23*, *24*). First, formation of CBs does not involve a hierarchical assembly pathway, because it can be initiated by a large array of CB components, and second, CB de novo assembly occurs temporally by concomitant, not sequential, association of proteins with the newly forming structure. Specifically, it appears that CBs are formed by protein–ribonucleoprotein interactions among CB components, which then directly or indirectly bind coilin and SMN. The previously reported, self-oligomerization of coilin and SMN might facilitate the stabilization of transient interactions among CB components. Our observation that a body forms when PML protein is tethered further suggests that de novo formation may also apply to other nuclear bodies. It seems that the CB does not require a specific locus for nucleation in contrast to the nucleolus, which is formed around specific ribosomal DNA loci. Our findings that snRNPs are the most efficient CB nucleators suggest that CBs primarily form as result of a local snRNP accumulation associated with snRNP function, such as snRNP assembly or regeneration after splicing (*16*, *17*). We suggest that once a threshold of local snRNP concentration is reached, CB formation is initiated by self-organization. This is consistent with previous observations that Sm protein expression enhances the formation of CBs in cells typically lacking CBs, and CB integrity depends on the cellular level of splicing activity and the absolute concentration of nuclear snRNP (*25*). A concentration of snRNPs could be locally elevated in the proximity of multiple genes at high levels of transcription, when they coalesce to form a transcription center (*3*, *26*).

References and Notes

1. A. I. Lamond, D. L. Spector, *Nat. Rev. Mol. Cell Biol.* **4**, 605 (2003).
2. K. E. Handwerger, J. G. Gall, *Trends Cell Biol.* **16**, 19 (2006).
3. T. Misteli, *Cell* **128**, 787 (2007).
4. R. I. Kumaran, R. Thakar, D. L. Spector, *Cell* **132**, 929 (2008).
5. T. Misteli, *Histochem. Cell Biol.* **129**, 5 (2008).
6. J. E. Sleeman *et al.*, *J. Cell Sci.* **116**, 2039 (2003).
7. M. Dundr *et al.*, *J. Cell Biol.* **164**, 831 (2004).
8. Materials and methods are available as supporting material on *Science* online.
9. A. S. Belmont *et al.*, *Methods Cell Biol.* **58**, 203 (1999).
10. M. Dundr *et al.*, *J. Cell Biol.* **179**, 1095 (2007).
11. K. E. Tucker *et al.*, *J. Cell Biol.* **154**, 293 (2001).
12. M. D. Hebert *et al.*, *Genes Dev.* **15**, 2720 (2001).
13. W. Feng *et al.*, *Hum. Mol. Genet.* **14**, 1605 (2005).
14. R. Morse *et al.*, *Hum. Mol. Genet.* **16**, 2349 (2007).
15. C. Isaac, Y. Yang, U. T. Meier, *J. Cell Biol.* **142**, 319 (1998).
16. A. G. Matera, K. B. Shpargel, *Curr. Opin. Cell Biol.* **18**, 317 (2006).
17. D. Stanek *et al.*, *Mol. Biol. Cell* **19**, 2534 (2008).
18. H. Brahms *et al.*, *RNA* **7**, 1531 (2001).
19. J. Mouaikel *et al.*, *Mol. Cell* **9**, 891 (2002).
20. J. Huber *et al.*, *EMBO J.* **17**, 4114 (1998).
21. S. L. Reichow *et al.*, *Nucleic Acids Res.* **35**, 1452 (2007).
22. E. Querido, P. Chartrand, *Methods Cell Biol.* **85**, 273 (2008).
23. T. Misteli, *J. Cell Biol.* **155**, 181 (2001).
24. G. Carrero, M. J. Hendzel, G. De Vries, *J. Theor. Biol.* **239**, 298 (2006).
25. J. E. Sleeman, P. Ajuh, A. I. Lamond, *J. Cell Sci.* **114**, 4407 (2001).
26. P. Fraser, W. Bickmore, *Nature* **447**, 413 (2007).

27. We thank A. Belmont, E. Bertrand, J. Gall, M. Hastings, P. Hemmerich, T. Kiss, I. Lemm, R. Lührmann, G. Matera, T. Meier, T. Misteli, S. Sharma, E. Soutoglou, C. Verheggen, and P. Young for reagents; S. Shevtsov for technical assistance; and T. Misteli for helpful suggestions and critical reading of the manuscript. This research was supported by Schweppe Career Development Award (the Schweppe Foundation) to M.D. and by startup funds from the Rosalind Franklin University of Medicine and Science to M.D.

Supporting Online Material

www.sciencemag.org/cgi/content/full/1165216/DC1
Materials and Methods
Figs. S1 to S7
Table S1

28 August 2008; accepted 8 October 2008
Published online 23 October 2008;
10.1126/science.1165216
Include this information when citing this paper.

The *Air* Noncoding RNA Epigenetically Silences Transcription by Targeting G9a to Chromatin

Takashi Nagano,[1,2]* Jennifer A. Mitchell,[1] Lionel A. Sanz,[3] Florian M. Pauler,[4] Anne C. Ferguson-Smith,[5] Robert Feil,[3] Peter Fraser[1]*

A number of large noncoding RNAs (ncRNAs) epigenetically silence genes through unknown mechanisms. The *Air* ncRNA is imprinted—monoallelically expressed from the paternal allele. *Air* is required for allele-specific silencing of the cis-linked *Slc22a3*, *Slc22a2*, and *Igf2r* genes in mouse placenta. We show that *Air* interacts with the *Slc22a3* promoter chromatin and the H3K9 histone methyltransferase G9a in placenta. *Air* accumulates at the *Slc22a3* promoter in correlation with localized H3K9 methylation and transcriptional repression. Genetic ablation of G9a results in nonimprinted, biallelic transcription of *Slc22a3*. Truncated *Air* fails to accumulate at the *Slc22a3* promoter, which results in reduced G9a recruitment and biallelic transcription. Our results suggest that *Air*, and potentially other large ncRNAs, target repressive histone-modifying activities through molecular interaction with specific chromatin domains to epigenetically silence transcription.

Large ncRNAs such as *Xist*, *Air*, and *Kcnq1ot1* are required for epigenetic silencing of multiple genes in cis (*1*), whereas the recently described *HOTAIR* ncRNA silences genes in trans (*2*). For *Xist*, evidence suggests that specific interactions between the ncRNA and chromatin are essential for gene silencing; however, molecular details of such interactions are lacking. The *Kcnq1ot1* and *Air* ncRNAs are involved in silencing clusters of multiple imprinted genes in cis on mouse chromosomes 7 and 17, respectively. Deletion of their promoters or truncation of the ncRNA results in biallelic, nonimprinted expression of genes in their respective clusters (*3*–*6*). These results suggest that the ncRNA molecules are involved in allele-specific silencing; however, a role for the process of transcription itself has not been ruled out (*7*).

Air expression is imprinted, driven by an antisense promoter located in intron 2 of *Igf2r*, regulated by DNA methylation specific to the parent of origin (*8*). In cells of the embryo proper, *Air* expression results in silencing of the paternal *Igf2r* gene in cis. However, in placenta, two addi-

[1]Laboratory of Chromatin and Gene Expression, The Babraham Institute, Babraham Research Campus, Cambridge CB22 3AT, UK. [2]Division of Cell Biology and Neuroscience, Department of Morphological and Physiological Sciences, Faculty of Medical Sciences, University of Fukui, Fukui 910-1193, Japan. [3]Institute of Molecular Genetics, CNRS UMR-5535 and University of Montpellier-II, 34293 Montpellier, France. [4]CeMM Research Center for Molecular Medicine of the Austrian Academy of Sciences, c/o Vienna Biocenter, Dr. Bohr-Gasse 9/4, 1030 Vienna, Austria. [5]Department of Physiology, Development, and Neuroscience, University of Cambridge, Cambridge CB2 3EG, UK.

*To whom correspondence should be addressed. E-mail: takashi.nagano@bbsrc.ac.uk (T.N.); peter.fraser@bbsrc.ac.uk (P.F.)

tional distant genes, *Slc22a2* and *Slc22a3*, are silenced in cis by *Air* (*5*). We confirmed parent-of-origin–specific placental expression of *Air*, *Igf2r*, *Slc22a2*, and *Slc22a3* by reverse transcription polymerase chain reaction (RT-PCR) in reciprocally derived heterozygous T^{hp} mice (*9*, *10*) in which a large, naturally occurring deletion removes the entire gene cluster. *Air* is expressed predominantly from the paternal allele, whereas expression of *Igf2r*, *Slc22a2*, and *Slc22a3* is predominantly maternal (fig. S1). *Slc22a3* reverts to biallelic expression by embryonic day 15.5 (E15.5), consistent with previous analyses in mouse (*11*) and human (*12*). We verified that this expression pattern is the result of differential transcriptional regulation by primary transcript RT-PCR in T^{hp} placentas (fig. S1) and by RNA fluorescence in situ hybridization (FISH) on wild-type placentas with *Air* and *Slc22a3* probes (Fig. 1A). At E11.5, *Slc22a3* is transcribed primarily on the maternal allele (Fig. 1A, left), in trans to the paternal *Air* signal, as expected. At E15.5, *Slc22a3* transcription occurs both cis and trans to *Air* (paternal and maternal alleles, respectively) (Fig. 1A, right, and 1B). These results demonstrate that *Slc22a3* escapes imprinted silencing of transcription later in gestation.

Air is largely unspliced and is retained in the nucleus (*13*). *Air* RNA FISH signals are considerably larger than primary transcript signals for protein-coding genes (Fig. 1A and fig. S2). We considered the possibility that *Air* functions to silence genes in cis in a manner, analogous to *Xist* "coating" of the inactive X chromosome. To test this, we performed RNA-DNA FISH to detect *Air* RNA and *Slc22a3* locus DNA in placentas from E11.5 and E15.5 (Fig. 1C). Although the *Air* and *Slc22a3* transcription units are >230 kb apart and oriented in different directions, we found that the *Air* RNA "cloud" frequently enveloped paternal *Slc22a3*. However, the extent to which the *Air* RNA overlapped *Slc22a3* varied markedly between E11.5 and E15.5. To quantify the extent to which *Air* "covered" the *Slc22a3* locus, we captured *z*-stacked confocal images of the signal pair, and determined the "cover index" [see (*10*) for definition of cover index].

At E11.5, most paternal *Slc22a3* alleles are enveloped by *Air* and have a high *Air* cover index (80% > 0.4) (Fig. 1D and table S1). This suggests the possibility that *Air* coats *Slc22a3* chromatin in placenta in conjunction with imprinted silencing, reminiscent of descriptions of *Xist*-mediated X inactivation (*14*). At E15.5, when paternal *Slc22a3* escapes *Air*-directed silencing, we found a significant reduction ($P = 0.016$; Fisher's exact test) in *Slc22a3* loci enveloped by *Air* (Fig. 1D and table S1; 47.5% cover index < 0.4). This cannot be accounted for by reduced expression of *Air* or smaller *Air* clouds at E15.5 compared with E11.5 because *Air* expression is considerably higher at E15.5 (fig. S1) and because *Air* clouds are generally larger (see below). These results show a correlation between high *Air* cover index on the *Slc22a3* locus and gene silencing. To confirm that dissociation from the *Air* cloud correlates with gene activation, we measured the *Air* cover index on the transcriptionally active paternal *Slc22a3* alleles using RNA FISH on E15.5 placental sections. The results show that transcribed *Slc22a3* alleles have an extremely low cover index (90% < 0.4) (Fig. 1E and table S1), which demonstrates that the active *Slc22a3* alleles are those most dissociated from *Air*.

To determine whether there is a molecular interaction between *Air* and the imprinted cluster in placenta, we employed RNA TRAP (tagging and recovery of associated proteins). RNA TRAP is derived from RNA FISH and uses the molecular targeting power of in situ hybridization to covalently tag chromatin in the immediate vicinity of a specific RNA in the nucleus (*15*). As a control, we also performed *Air* RNA TRAP on adult heart tissue, in which *Air* is highly expressed (*16*). *Air* silences paternal *Igf2r* in adult heart, but expression of *Slc22a3* is biallelic (not imprinted), and *Slc22a2* is not expressed (*13*). We noted that *Air* RNA FISH signals in adult heart were smaller than *Air* signals in wild-type placenta (Fig. 2A), which suggested that nuclear accumulation of *Air* in heart is less abundant than in placenta. Mice expressing a truncated *Air* (*Air-T*) (*5*) show greatly reduced accumulation in placental nuclei.

The RNA TRAP results (Fig. 2B) show that enrichment across the imprinted domain varies considerably among the three tissues (see tables S2 and S3). The highest and most significant level of enrichment was observed over the *Slc22a3* promoter in E11.5 placenta when paternal *Slc22a3* is silenced (Fig. 2C, red curve). *Air* enrichment at the *Slc22a3* promoter was significantly reduced at E15.5 [$P < 0.001$; two-way analysis of variance (ANOVA) followed by contrast test] when *Slc22a3* escapes imprinting and is biallelically transcribed. A lower, but still significant, level of enrichment was also seen over the body of the *Slc22a3* gene in E11.5 placenta ($P < 0.001$ versus adult heart; $P = 0.024$ versus 2.3 Mb downstream). These results are wholly

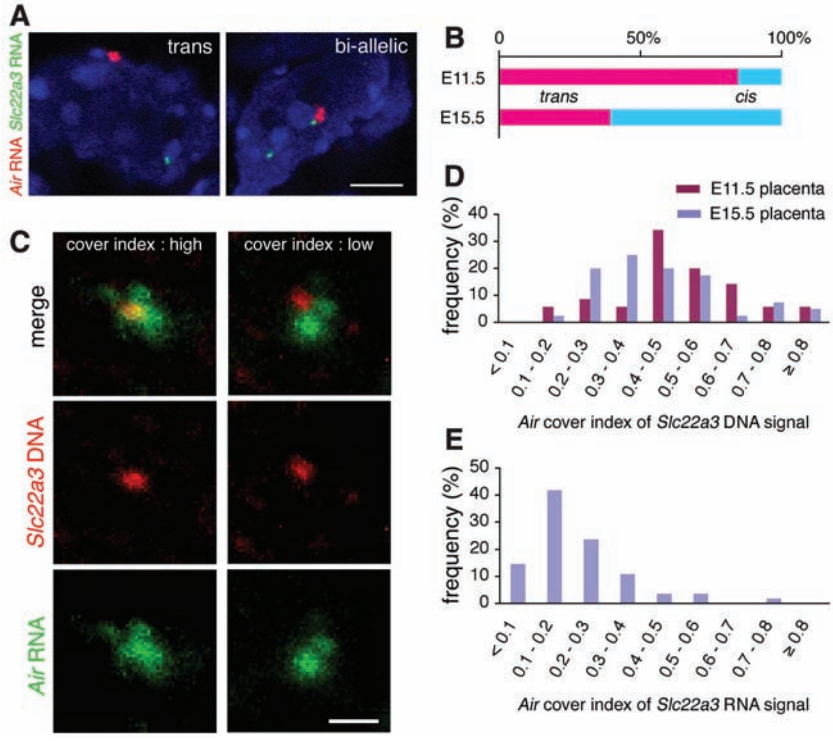

Fig. 1. *Air* ncRNA envelopes the paternal *Slc22a3* locus in correlation with allelic silencing. (**A**) RNA FISH on mouse placental tissue sections with probes for *Air* (red) and *Slc22a3* intron 1 (green) [4′,6′-diamidino-2-phenylindole (DAPI), blue]. Representative cell nuclei with *Slc22a3* signals in trans to *Air* signals (left, maternal *Slc22a3* transcription) and biallelic *Slc22a3* signals (right, maternal and paternal *Slc22a3* transcription). Scale bar, 5 μm. (**B**) The ratio of *Slc22a3* RNA FISH signals in trans (pink, maternal) versus those in cis (blue, paternal) to the *Air* signal in *Air*-positive cells from E11.5 and E15.5 placentas. (**C**) Representative high-magnification RNA-DNA FISH signals on mouse placental sections. (Top) Merged images of *Slc22a3* DNA FISH signals (red) and *Air* RNA FISH signals (green). (Middle and bottom) Separate *Slc22a3* DNA and *Air* RNA images, respectively. Scale bar, 1 μm. (**D**) Distribution of the *Air* RNA cover index on the *Slc22a3* locus in E11.5 and E15.5 placentas. (**E**) Distribution of the *Air* RNA cover index on *Slc22a3* RNA FISH signals in cis with *Air* in E15.5 placentas. Here, the cover index quantifies the extent of overlap between *Slc22a3* RNA FISH signals and *Air* RNA FISH signals.

consistent with the differential *Air* cover index. Rather than uniformly coating the entire imprinted domain, *Air* accumulates specifically at the *Slc22a3* promoter at E11.5, which suggests an interaction between the ncRNA (which probably exists as a ribonucleoprotein complex) and *Slc22a3* promoter chromatin.

We next assessed allele-specific histone modifications throughout the imprinted cluster to test the possibility that accumulation of *Air* on the paternal *Slc22a3* promoter is associated with a specific chromatin signature. We used E11.5 and E15.5 placentas from mice with maternally or paternally derived T^{hp} deletion to assess each chromosome separately. We analyzed histone H3 lysine 4 di- and trimethylation (H3K4me2 and me3) as typical modifications at active promoters, and histone H3 lysine 9 trimethylation (H3K9me3) and histone H3 lysine 27 trimethylation (H3K27me3) as typical modifications at repressed promoters (*17*). We found a higher peak at E11.5 of H3K9me3 enrichment at the paternal *Slc22a3* promoter, three times that at the maternal promoter (Fig. 3), which correlated strongly with the presence of *Air* (see supporting text for results of other modifications and loci). Paternal H3K9me3 at the *Slc22a3* promoter is markedly reduced at E15.5, which correlates with the disappearance of *Air* from the promoter and biallelic transcription. The correlation between the high level of H3K9me3 enrichment at the paternal *Slc22a3* promoter at E11.5 and the accumulation of *Air* suggests that the two may be functionally linked.

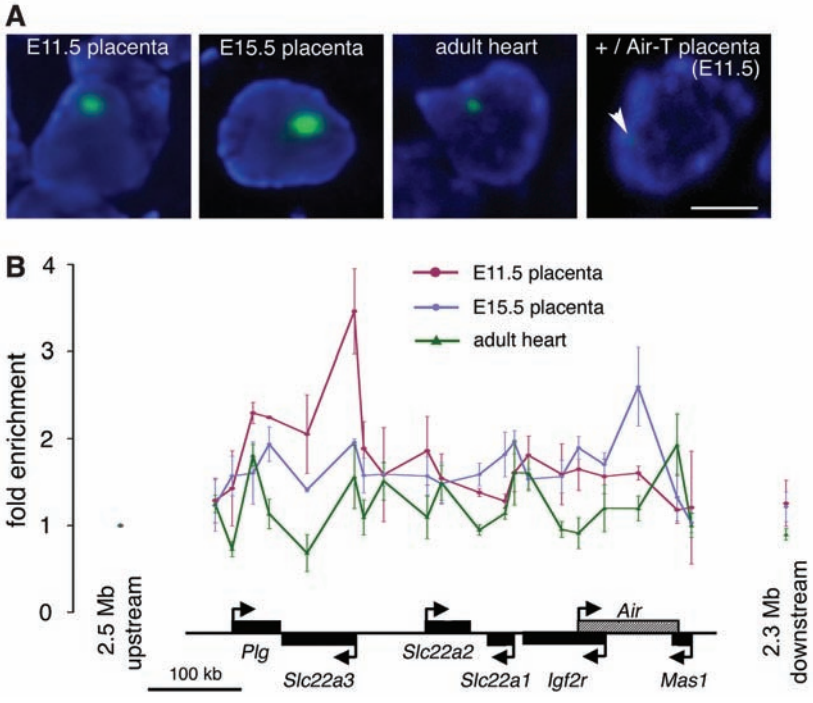

Fig. 2. *Air* accumulates at the *Slc22a3* promoter. (**A**) Detection of biotin deposition in RNA TRAP experiments with identical conditions. *Air* signal in *Air-T* placenta (arrowhead). DAPI, blue. Scale bar, 5 μm. (**B**) *Air* RNA TRAP results on designated tissues. Mean fold enrichment ± SEM in pull down to input [see (*10*) for details] normalized to 2.5 Mb upstream, from three biological replicates.

Fig. 3. H3K9 methylation at the *Slc22a3* promoter correlates with *Air* accumulation. Allele-specific H3K9me3 analyzed by native ChIP using $+/T^{hp}$ placentas (for maternal allele) and $T^{hp}/+$ placentas (for paternal allele) at E11.5 and E15.5. Mean fold enrichment ± SD in pull down to input normalized to 2.5 Mb upstream. A second biological replicate showed similar results.

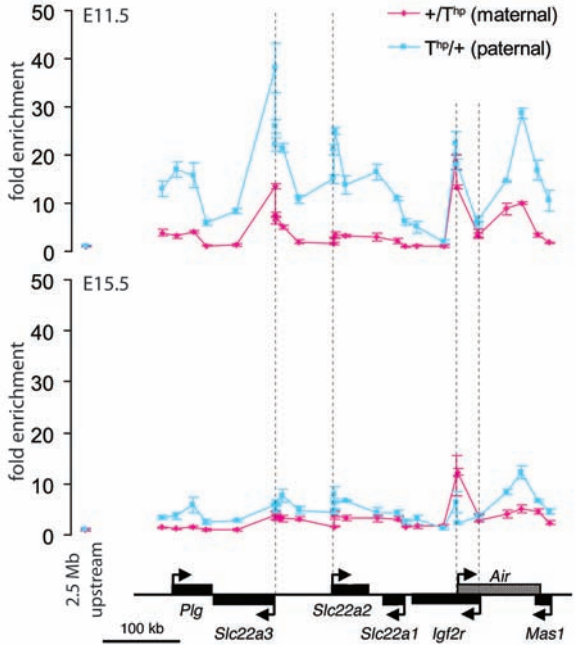

One possibility is that *Air* silences paternal *Slc22a3* transcription by recruiting histone-modifying activities to the *Slc22a3* promoter to methylate chromatin on H3K9. The G9a histone methyltransferase is involved in H3K9 di- and trimethylation and allelic silencing of some genes in the *Kcnq1*-imprinted domain in placenta (*18*). We investigated a potential functional link between G9a and *Air* in placenta by RNA immunoprecipitation (RNA IP) (*19*). RNA IP with antibodies raised against two distinct G9a epitopes bring down *Air* RNA (Fig. 4A and fig. S6). Furthermore, allele-specific chromatin immunoprecipitation (ChIP) with these G9a antibodies shows consistent substantial enrichment only at the paternal *Slc22a3* promoter (Fig. 4B and fig. S7). To examine the possibility that G9a is targeted to the *Slc22a3* promoter through recruitment by *Air*, we assessed G9a association with *Slc22a3* promoter chromatin by ChIP at E11.5 in wild-type and +/*Air-T* placentas. *Air-T* mice express truncated *Air*, which results in biallelic expression of *Slc22a3*, *Slc22a2*, and *Igf2r* in placenta (*5*). *Air-T* RNA FISH signals are weak (Fig. 2A), and *Air* RNA TRAP in E11.5 *Air-T* placenta does not bring down any detectable DNA from the cluster, which suggests that accumulation of truncated *Air* at the *Slc22a3* promoter is greatly reduced. The ChIP results (Fig. 4C) show a significant reduction in G9a enrichment over the *Slc22a3* promoter in +/*Air-T* placentas compared with wild type. Comparison of this finding with the parental allele-specific data from Fig. 4B obtained with the same antibody shows the expected trend in reduction of G9a occupancy at the *Slc22a3* promoter from the respective genotypes. These data show that full-length *Air* is necessary for normal G9a targeting to the paternal *Slc22a3* promoter.

We assessed allelic transcription in wild-type and $G9a^{-/-}$ placentas by RNA FISH at E9.5 [one day before death of $G9a^{-/-}$ embryos (*18*)]. We observed significant shifts toward 50% paternal to maternal *Slc22a3* transcription in $G9a^{-/-}$ placentas compared with wild type ($P = 0.012$; *t* test), which showed that G9a is required for silencing paternal *Slc22a3* (Fig. 4D). Monoallelic transcription of *Igf2r* was maintained in $G9a^{-/-}$ placentas ($P = 0.679$; *t* test), which demonstrated that G9a is not required for imprinted silencing of paternal *Igf2r* (Fig. 4D). We excluded the possibility that these results were

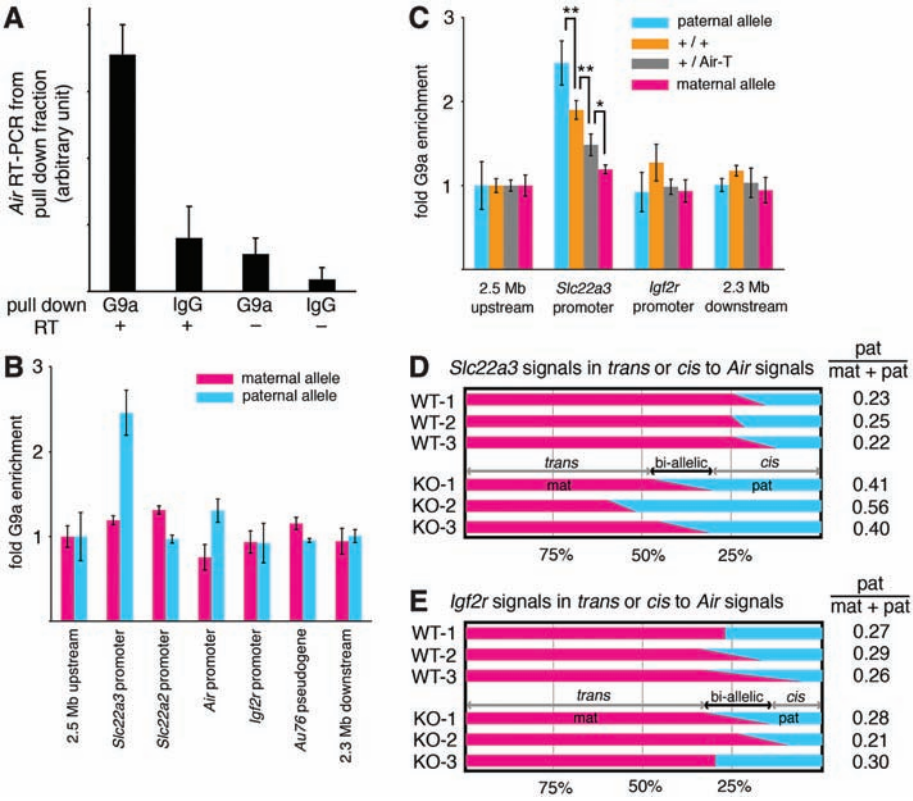

Fig. 4. *Air* recruitment of G9a to the *Slc22a3* promoter is required for gene silencing. (**A**) RNA IP with and without G9a-specific antibody or immunoglobulin G (IgG) in E11.5 placenta. *Air* RNA detected by RT-PCR. Arbitrary units on the *y* axis, mean ± SEM derived from several measurements. (**B**) Allele-specific ChIP with G9a from T^{hp} placentas at E11.5. Mean fold enrichment ± SEM of G9a pull down over IgG pull down, normalized to the pull down at 2.5 Mb upstream is shown. (**C**) G9a ChIP with wild-type and *+/Air-T* E11.5 placentas as described in (B), $*P < 0.05$; $**P < 0.01$; one-way ANOVA and contrast test. (**D**) *Slc22a3* RNA FISH signals in trans to *Air* signal (red bars, maternal), biallelic (pink/blue tapering segments, maternal and paternal), or cis to *Air* (blue bars, paternal) in three E9.5 wild-type (WT) and three $G9a^{-/-}$ gene knockout (KO) placentas. The ratio of paternal *Slc22a3* signal is shown on the right. (**E**) *Igf2r* RNA FISH signals analyzed as in (D).

caused by a developmental delay by showing that *Slc22a3* and *Igf2r* are imprinted in wild-type placenta a day earlier at E8.5 (fig. S8). *Slc22a2* is not expressed on E8.5 or E9.5 (fig. S8), which precludes its analysis in $G9a^{-/-}$ placenta. These results are consistent with our RNA TRAP and ChIP data showing significant enrichment of *Air* and G9a at the *Slc22a3* promoter, but not at the *Igf2r* promoter (see Figs. 2B and 4B). These data show that *Slc22a3* and *Igf2r* are silenced by different mechanisms in the placenta.

We conclude that *Air* silences the imprinted *Slc22a3* and *Igf2r* genes by different mechanisms in placenta. We propose that *Air* silences transcription of the distal paternal *Slc22a3* gene via a specific interaction between the ncRNA and chromatin at the *Slc22a3* promoter. This interaction may be mediated by factor(s) associated with the ncRNA and/or the *Slc22a3* promoter. Accumulated *Air* at the promoter recruits G9a and leads to targeted H3K9 methylation and allelic silencing. Although paternal *Igf2r* silencing is also controlled by *Air*, our RNA TRAP data show that this is not through a ncRNA interaction with the *Igf2r* promoter, and analysis of $G9a^{-/-}$ placentas shows that it does not require G9a. An alternative, although not mutually exclusive, explanation for our data is that *Air* creates a repressive nuclear compartment, similar to that described for *Xist* (*20*) and that the observed interaction between *Slc22a3* and *Air* is the result of the recruitment of *Slc22a3* promoter (and G9a) to the *Air* compartment. In summary, our results show that *Air* (and potentially other large ncRNAs such as *Xist*) can function through specific interaction with chromatin and mediates targeted recruitment of repressive histone-modifying activities to epigenetically silence transcription.

References and Notes

1. D. Umlauf, P. Fraser, T. Nagano, *Biol. Chem.* **389**, 323 (2008).
2. J. L. Rinn *et al.*, *Cell* **129**, 1311 (2007).
3. D. Mancini-Dinardo, S. J. Steele, J. M. Levorse, R. S. Ingram, S. M. Tilghman, *Genes Dev.* **20**, 1268 (2006).
4. J. Y. Shin, G. V. Fitzpatrick, M. J. Higgins, *EMBO J.* **27**, 168 (2008).
5. F. Sleutels, R. Zwart, D. P. Barlow, *Nature* **415**, 810 (2002).
6. A. Wutz *et al.*, *Development* **128**, 1881 (2001).
7. F. M. Pauler, M. V. Koerner, D. P. Barlow, *Trends Genet.* **23**, 284 (2007).
8. R. Lyle *et al.*, *Nat. Genet.* **25**, 19 (2000).
9. D. P. Barlow, R. Stoger, B. G. Herrmann, K. Saito, N. Schweifer, *Nature* **349**, 84 (1991).
10. Materials and methods are available as supporting material on *Science* Online.
11. R. Zwart, F. Sleutels, A. Wutz, A. H. Schinkel, D. P. Barlow, *Genes Dev.* **15**, 2361 (2001).
12. D. Monk *et al.*, *Proc. Natl. Acad. Sci. U.S.A.* **103**, 6623 (2006).
13. C. I. Seidl, S. H. Stricker, D. P. Barlow, *EMBO J.* **25**, 3565 (2006).
14. C. M. Clemson, J. A. McNeil, H. F. Willard, J. B. Lawrence, *J. Cell Biol.* **132**, 259 (1996).
15. D. Carter, L. Chakalova, C. S. Osborne, Y. F. Dai, P. Fraser, *Nat. Genet.* **32**, 623 (2002).
16. F. M. Pauler, S. H. Stricker, K. E. Warczok, D. P. Barlow, *Genome Res.* **15**, 1379 (2005).
17. T. S. Mikkelsen *et al.*, *Nature* **448**, 553 (2007).
18. A. Wagschal *et al.*, *Mol. Cell. Biol.* **28**, 1104 (2008).
19. B. K. Sun, A. M. Deaton, J. T. Lee, *Mol. Cell* **21**, 617 (2006).
20. J. Chaumeil, P. Le Baccon, A. Wutz, E. Heard, *Genes Dev.* **20**, 2223 (2006).

21. We thank A. Segonds-Pichon for statistics, G. Kelsey and W. Reik for critical reading, D. Barlow and members of the Fraser lab for discussions. P.F. is a Senior Fellow of the Medical Research Council, UK. This work was supported by the Biotechnology and Biological Sciences Research Council, UK, and by the Agence National de la Recherche and Institut National de Cancer, France. The authors declare that they have no competing financial interests.

Supporting Online Material

www.sciencemag.org/cgi/content/full/1163802/DC1
Materials and Methods
SOM Text
Figs. S1 to S8
Tables S1 to S5
References

25 July 2008; accepted 28 October 2008
Published online 6 November 2008;
10.1126/science.1163802
Include this information when citing this paper.

Automated Microarray Processing

The Geniom RT Analyzer enables automated processing of microarrays on febit's Geniom biochips. The compact device, which makes use of microfluidics, provides high sample throughput, reproducibility, and sensitivity in a variety of applications. The instrument's programmable, precise temperature control optimizes hybridizations and enables the use of enzymatic reactions directly on the microfluidic array for signal enhancement and primer extension assays.

febit
For information 781-391-4360
www.febit.com

Materials Microscope

The Axio Scope.A1 is a flexible, high-performance modular microscope designed for routine applications in materials microscopy. The flexibility of the microscope is achieved by the availability of five different microscope upper bodies, three different lower bodies, and two Vario columns that can be combined into a customized system. The Axio Scope A.1 offers large scalability of the sample area height, which can be set for sizes up to 380 mm high. Two-position sliders, four-position reflector turrets, and six-position reflector turrets are available. Users can quickly switch between the different contrasting techniques. In addition to traditional contrasting techniques in reflected and transmitted light such as brightfield and darkfield, the instrument also is capable of innovative techniques such as differential interference contrast in circularly polarized light.

Carl Zeiss MicroImaging
For information 800-233-2343
www.zeiss.com/micro

Noninterfering Protein Assay

The NI Protein Assay is a sensitive, colorimetric protein assay that overcomes interference of common laboratory agents present in protein solutions and shows minimal protein-to-protein variation. The assay requires only 0.5 μg to 50 μg protein in a sample. The assay is unaffected by the presence of common laboratory agents, such as reducing agents, chelating agents, detergents, chaotropes, and salts. It can be used to estimate protein during protein purification, electrophoresis, cell biology, molecular biology, and other research applications.

G-Biosciences/Genotech
For information 314-991-6034
www.gbiosciences.com

High-Volume Microplates

A range of sterile, high-volume microplates is optimized for large-scale, high-yield growth of bacteria, yeast, and mammalian or insect cell lines. They are available in a choice of well formats (24-well, 48-well, and 96-well) and well volumes (4 ml to 10 ml). They are fully compatible with automated liquid handling systems and other robotic sample processing equipment. They are manufactured from an ultrapure grade polypropylene that has zero leachates as well as excellent temperature and chemical resistance. The plate wells are rectangular with a "v" bottom to optimize sample concentration and recovery.

Porvair Sciences
For information +44-1372-824290
www.porvair-sciences.com

Sequencing Analysis Software

The latest version of NextGENe sequencing analysis software includes improved single nucleotide polymorphism (SNP) and insertion/deletion (indel) capabilities. It incorporates a unique condensation tool that statistically polishes the data to remove chemistry and instrument-related errors, followed by raw data sorting by a 12-base-pair anchor sequence and sequence shoulders, and assembly by further condensation cycles. The assembled sample data are then compared with a reference data bank, with SNPs and indels automatically displayed. The software can be used for data from the Illumina Genome Analyzer, Roche 454 system, and Applied Biosystems SOLiD system. It runs on low-cost, 64-bit Windows computers.

SoftGenetics
For information 888-791-1270
www.softgenetics.com

Gel Documentation System

The G:BOX EF gel documentation system produces accurate images of gels and blots stained with both visible-light and low-light emitting fluorescent dyes. It features a 16-bit, lightly cooled, charge-coupled device camera inside a light-tight darkroom, integrated to one-click GeneSnap image capture software. This makes generating images of gels and blots labeled with fluorescent dyes emitting faint or slow-developing signals both quick and simple. To visualize common fluorescent and visible dyes, such as ethidium bromide, Coomassie blue, and silver stain, the darkroom comes with Syngene's transilluminator, white epi-illumination overhead lighting, and the NovaGlo visible light converter, which transforms the transilluminator's ultraviolet light into visible light. Researchers can image any commercially available fluorescent dye by attaching Syngene's computer-controlled EPI RGB lighting module and filter wheel.

Syngene
For information 800-686-4407
www.syngene.com

Electronically submit your new product description or product literature information! Go to **www.sciencemag.org/products/newproducts.dtl** for more information.

Newly offered instrumentation, apparatus, and laboratory materials of interest to researchers in all disciplines in academic, industrial, and governmental organizations are featured in this space. Emphasis is given to purpose, chief characteristics, and availabilty of products and materials. Endorsement by *Science* or AAAS of any products or materials mentioned is not implied. Additional information may be obtained from the manufacturer or supplier.

Science Careers
Classified Advertising

For full advertising details, go to **ScienceCareers.org** and click **For Advertisers**, or call one of our representatives.

UNITED STATES & CANADA
E-mail: advertise@sciencecareers.org
Fax: 202-289-6742

Joribah Able
Industry – US & Canada
Phone: 202-326-6572

Alexis Fleming
Northeast Academic
Phone: 202-326-6578

Tina Burks
Southeast Academic
Phone: 202-326-6577

Daryl Anderson
Midwest/Canada Academic
Phone: 202-326-6543

Nicholas Hintibidze
West Academic
Phone: 202-326-6533

EUROPE & INTERNATIONAL
E-mail: ads@science-int.co.uk
Fax: +44 (0) 1223 326532

Tracy Holmes
Associate Director, *Science* Careers
Phone: +44 (0) 1223 326525

Alex Palmer
Phone: +44 (0) 1223 326527

Dan Pennington
Phone: +44 (0) 1223 326517

Susanne Kharraz Tavakol
Phone: +44 (0) 1223 326529

Louise Moore
Phone: +44 (0) 1223 326528

JAPAN
Mashy Yoshikawa
Phone: +81 (0) 3 3235 5961
E-mail: myoshikawa@aaas.org

To subscribe to *Science*:
In US/Canada call 202-326-6417 or 1-800-731-4939.
In the rest of the world call +44 (0) 1223 326515.

Science makes every effort to screen its ads for offensive and/or discriminatory language in accordance with US and non-US law. Since we are an international journal, you may see ads from non-US countries that request applications from specific demographic groups. Since US law does not apply to other countries we try to accommodate recruiting practices of other countries. However, we encourage our readers to alert us to any ads that they feel are discriminatory or offensive.

Science Careers
From the journal *Science* AAAS

POSITIONS OPEN

ASSISTANT PROFESSOR (TENURE TRACK)
Department of Environmental Sciences
School of the Coast and Environment

The Department of Environmental Sciences within the Louisiana State University School of the Coast and Environment is searching for an Assistant Professor (tenure track) with expertise in either environmental economics or environmental chemistry. This position will further the University's Flagship Agenda, and is designed to build on departmental strengths and provide synergy and linkages to existing programs. The Department of Environmental Sciences currently offers a B.S. in coastal and environmental sciences, an M.S. in environmental sciences, and is awaiting approval of a doctoral degree program. The Department and the School are strongly committed to diversity and encourage applications from individuals with varied backgrounds and perspectives. Required qualifications: Ph.D. in environmental economics, environmental chemistry, or related field at the time of appointment; establish strong programs of research and extramural funding; excel in teaching and undergraduate and graduate mentoring; and work collaboratively to address compelling questions in environmental sciences.

We seek applicants from one of the following areas of expertise. Environmental economics: environmental and ecological sustainability; environmental impact assessment; economic effects of environmental policies; valuation of ecological services; environmental decision modeling. Environmental chemistry: chemical and physical properties of environmental chemicals, fates, and effects; chemical hazards and risk assessments; trace detection of environmental pollutants; chemical reactions in the environment.

Additional qualifications desired: expertise in geospatial technology including remote sensing and Geographic Information Systems and quantitative/statistical skills; ability to employ an integrated, system approach in addressing global environmental problems.

An offer of employment is contingent on a satisfactory pre-employment background check. Application deadline is February 16, 2009, or until a candidate is selected. Appointments will begin in August 2009. Applicants should submit a letter describing their research and teaching interests, current curriculum vitae (including e-mail address) and the names and contact information (with e-mail addresses) for three references to: **Chair, Department of Environmental Sciences, 1285 Energy, Coast and Environment Building, Louisiana State University, Reference: Log #2077, Baton Rouge, LA 70803-5705. E-mail: nlam@lsu.edu.** *LSU is an Equal Opportunity/Equal Access Employer.*

ASSISTANT CURATOR, TENURE TRACK
Robert A. Pritzker Center for Meteorites and Polar Studies
The Field Museum

The Department of Geology seeks a broadly interested, productive colleague with an innovative, specimen-based research program in meteoritics. The successful candidate will have a Ph.D. and a record of scientific achievement. In addition to research, the position entails curation of a world-class collection of meteorites, and significant collections of gems and minerals, ores and rocks, requiring a broad knowledge of all classes of meteorites, and of sampling requirements for a wide range of modern analytical techniques. Curators also participate in a variety of public learning programs (including exhibits, mentoring, and informal education), development, and administrative and service activities. Interaction with colleagues and participation in undergraduate and graduate education at area universities also are encouraged.

Consideration of applications begins on February 13, 2009. Please include: curriculum vitae, statement of research objectives, and copies of relevant publications. Also arrange for three references to submit letters of recommendation. Direct applications to: **Search Committee, Department of Geology, The Field Museum, 1400 S. Lake Shore Drive, Chicago, IL 60605-2496.** Electronic submission to **Karsten Lawson, e-mail: klawson@fieldmuseum.org** is encouraged. *The Field Museum is an Equal Opportunity/Affirmative Action Employer; qualified minorities and women are encouraged to apply.*

POSITIONS OPEN

ISENBERG PROFESSORSHIP in INTEGRATED LIFE SCIENCES
University of Massachusetts Amherst

The College of Natural Sciences and Mathematics (NSM) at UMass Amherst seeks candidates at the **ASSOCIATE or FULL PROFESSOR** level for the NSM Isenberg Endowed Professorship. We seek a prominent individual who does integrative work in any area of the life sciences using interdisciplinary approaches that complement existing strengths in systems biology, biomedicine, biomaterials, nanomedicine, bioinformatics, and mathematical or computational biology. The Isenberg Professorship was established with the support of **Ronnie and Eugene M. Isenberg** to catalyze interdisciplinary work in management, engineering, and science by promoting integrative approaches using technology, innovation, and entrepreneurship. The successful candidate will participate in campus initiatives by working collaboratively across NSM disciplinary boundaries and interacting closely with existing Isenberg Professors in the College of Engineering and the Isenberg School of Management.

The Isenberg Professor will benefit from an environment at the UMass Amherst campus that promotes life sciences research and innovation through interdisciplinary collaboration. These efforts are bolstered by the Commonwealth of Massachusetts $1 billion Life Sciences Initiative that includes increased faculty recruitment and capital expansion on the Amherst campus.

The NSM Isenberg Professor will hold an academic appointment in the appropriate participating Department(s) of NSM. These include Biochemistry and Molecular Biology, Biology, Computer Science, Polymer Science and Engineering, Chemistry, Mathematics and Statistics, and Physics. Rank and salary will be commensurate with qualifications and experience.

Evaluation of applications will begin on December 31, 2008, and continue until the position is filled.

Applications should include curriculum vitae, a summary of research interests and accomplishments (five pages), and copies of one to three key publications. Candidates will be contacted by the Search Committee to arrange for at least three letters of recommendation after the initial evaluation of applications is completed. Applications should be mailed to **Ms. Cheryl Daggett, Personnel Manager, Dean of the College of Natural Sciences and Mathematics, Lederle Graduate Research Tower - Room 716, University of Massachusetts, Amherst, MA 01003;** or sent to **e-mail: daggett@nsm.umass.edu.** Please include Isenberg Professorship Search in the subject line.

The University of Massachusetts is an Affirmative Action/Equal Opportunity Employer. Women and members of minority groups are encouraged to apply.

The Department of Biology at Indiana University of Pennsylvania invites applications for two tenure-track positions in biology from the following three areas: (1) **VERTEBRATE BIOLOGIST,** (2) **DEVELOPMENTAL BIOLOGIST,** or (3) **APPLIED/ENVIRONMENTAL MICROBIOLOGIST.**

Appointments will be at the **ASSISTANT PROFESSOR** level and available in August 2009, pending availability of funds. Doctorate required; postdoctoral experience preferred. We seek energetic, innovative individuals to join a department undergoing transition as a number of senior faculty retire. Successful applicants will help build a student-centered learning community, teach introductory as well as specialty-area courses, develop a productive research program that involves both undergraduate and graduate students, and commit themselves to the Teacher-Scholar Model. All applicants must be work eligible. Applications are due by January 19, 2009. For full announcement, including application instructions, see **websites: http://nsm1.nsm.iup.edu/luciano/** or **http://www.iup.edu.employment** or call **telephone: 724-357-2352.** *Indiana University of Pennsylvania is an Equal Opportunity Employer and is a member of the State System of Higher Education. Minorities/Females/Persons with Disabilities/Veterans.*

ÉCOLE POLYTECHNIQUE
FÉDÉRALE DE LAUSANNE

EPFL Center for Neuroprosthetics

Faculty Positions at the interface of Neuroscience and Bioengineering at Ecole Polytechnique Fédérale de Lausanne (EPFL)

The Brain-Mind Institute and the Institute of Bioengineering at EPFL invite applications for faculty positions at all ranks, from **tenure track assistant professor to full professor,** for the newly-launched **Center for Neuroprosthetics.** The Center, situated between the School of Life Sciences and the School of Engineering, seeks outstanding individuals working in the man-machine interface for motor control with invasive and non-invasive sensing and stimulation, in audition, in vision, and in spinal cord repair. The open faculty positions are offered in an environment of both theoretical and experimental research, rich for the development of novel enabling technologies as well as for seeking deeper understanding of fundamental mechanisms underlying the field of neuroprosthetics.

The Brain-Mind Institute offers a broader context of neuroscience, with strengths in cognition, behavior, cellular and molecular neuroscience, computational neuroscience, and neurodegeneration, among others. The School of Engineering and the Institute of Bioengineering offer strength in areas that include bio-MEMS/NEMS, bioelectronics, robotics and learning, integrated systems, biomaterials, biophotonics, molecular and computational systems biology, and stem cell biotechnology.

Excellent experimental infrastructure are available including core facilities in animal physiological and behavioral phenomics, animal and human imaging, quantitative light microscopy, genomics and proteomics, micro- and nano-fabrication, and electron microscopy and surface analysis.

Successful candidates are expected to initiate independent, creative research programs and participate in undergraduate and graduate teaching. Internationally competitive salaries, start-up resources and benefits are offered.

Applications should include a curriculum vitae with a list of publications, a concise statement of research and teaching interests, and the names and addresses (including e-mail) of at least five referees. Applications should be uploaded to:
http://neuroprosthetics-rec.epfl.ch.

The deadline for applications is **28 February 2009.**

Enquiries may be addressed to:
Prof. Jeffrey A. Hubbell,
E-mail: **neuroprosthetics-rec@epfl.ch**

For additional information on EPFL, the Schools of Engineering and Life Sciences, the Institute of Bioengineering, and the Brain-Mind Institute, and Institute of Bioengineering, please consult the web sites: **http://www.epfl.ch, http://sti.epfl.ch, http://sv.epfl.ch, http://bmi.epfl.ch,** and **http://ibi.epfl.ch.**

EPFL aims to increase the presence of women amongst its faculty, and qualified female candidates are strongly encouraged to apply.

ORI

Department of Health and Human Services
Office of Public Health and Science
Office of Research Integrity

Health Scientist Administrator Position

The Division of Investigative Oversight (DIO) within The Office of Research Integrity (ORI) is seeking two experienced scientists or physicians with research/clinical experience to serve under the Director, DIO, as an Investigator/Scientist. DIO's primary task is to conduct oversight reviews of institutional investigations of research misconduct. Applicants should be experienced in running a research program, supervising students and postdoctoral fellows, successfully competing for Federal extramural or intramural funds, and preparing peer reviewing manuscripts and grant applications. Applications with a broad range of experience and scientific interests are preferable because of the wide range of topics that ORI deals with. Good oral and written communication skills are essential.

Please apply online at **http://usajobs.opm.gov/** and go to job announcement **HHS-OS-2009-0034**. Applications must be received by approximately **December 24, 2008**. If you need assistance, contact the **Rockville, MD, HelpDesk at 888-478-4340 (7:30 am - 4:00pm M-F)** or **quickquestions@psc.gov (TTY/TDD: 800-877-8339**). The position is at the GS-13/14 level ($98,033-$127,442), with the actual salary commensurate with experience. You may also reach **John Dahlberg, Director of DIO** at **240-453-8800/John.Dahlberg@hhs.gov** for more information. This position offers full benefits including retirement, health insurance, life and long-term health care insurance, and thrift-saving plan participation (matched up to 5% of your salary).

Selection will be based on merit and without consideration for race, color, religion, sex, national origin, politics, marital status, sexual orientation, physical handicap, or membership or non-membership in an employee organization.

Massachusetts Institute of Technology

FACULTY POSITIONS
in Mechanical Engineering

The Department of Mechanical Engineering seeks outstanding candidates for tenure-track faculty positions in the following fields to begin July 1, 2009 or thereafter:

- Dynamical Systems and Controls
- Energy
- Solid Mechanics
- Broadly in Mechanical Engineering

Applicants should hold an earned Ph.D. in mechanical engineering or a closely related field by the beginning of the appointment. Faculty duties include teaching at the graduate and undergraduate levels, research, and supervision of student research. We seek candidates who will provide inspiration and leadership in research and actively contribute to core mechanical engineering undergraduate and graduate level teaching. New faculty hires are expected to have a research focus in one of the disciplinary fields listed above, or broadly in mechanical engineering. Applicants must have demonstrated: (1) outstanding research strength; (2) a strong disciplinary background; (3) strong experimental and/or theoretical skills; and (4) the potential ability to synthesize new devices and systems by working across disciplinary boundaries. Appointment would be at the assistant or untenured associate professor level. In exceptional cases, a senior faculty appointment may be possible.

Applicants should send a curriculum vitae, a research statement, a teaching statement, and copies of not more than three publications. They should also arrange for four individuals to submit letters of recommendation on their behalf. This information must be entered electronically at the following site: **http://search-meche.mit.edu/**. Submission of applications before **January 31, 2009** is strongly encouraged; full consideration will be given to applications submitted by **February 28, 2009**. Please refer to the web address for detailed description of each position.

MIT is an Equal-Opportunity/Affirmative Action Employer. Women and underrepresented minorities are especially encouraged to apply.

Science Careers online @sciencecareers.org

NIAID
NATIONAL INSTITUTE OF ALLERGY AND INFECTIOUS DISEASES

RESEARCH FELLOW

The National Institute of Allergy and Infectious Diseases (NIAID), a major research component of the National Institutes of Health (NIH) and the Department of Health and Human Services, is recruiting for a Research Fellow. The position will be available in the Molecular Pathology Section of the Laboratory of Immunopathology, and scientists with a M.D., Ph.D., or D.V.M. are eligible. The research activity involves (1) studies of the roles played by CTCF in imprinting, X chromosome inactivation, and the organization of transcriptional domains; and (2) analyses of BORIS expression and function in gametogenesis and stem/progenitor cells, in response to infectious agents, as well as the consequences of aberrant expression in cancers. This full-time research position offers a unique opportunity to work on investigations that range from basic molecular biology to studies of gene-manipulated mice in a collaborative environment, and provides excellent training for scientists who plan a career in molecular biology, infectious disease and cancer research.

Research Fellow applicants should have three or more years of relevant post-doctoral experience; the salary range is $44,180 - $108,319. A full package of benefits (including retirement, health, life and long term care insurance, Thrift Savings Plan participation, etc.) is available. Applicants with an M.D. degree are eligible for the NIH Loan Repayment Program. Applicants should send their curriculum vitae, a letter of interest, and names and addresses of three (3) references to Victor Lobanenkov, Twinbrook I, Room 1417, 5640 Fishers Lane, Rockville, MD 20892, FAX: (301)-402-0077, email: **vlobanenkov@niaid.nih.gov**

For further information about NIAID and available job opportunities, please visit:
http://healthresearch.niaid.nih.gov/dl

NATIONAL INSTITUTE OF MENTAL HEALTH
PROGRAM OFFICER

The National Institute of Mental Health (NIMH), National Institutes of Health (NIH), Department of Health and Human Services, is inviting inquiries from potential candidates for a Program Officer position within the Adult Psychopathology and Psychosocial Intervention Research Branch, Division of Adult Translational Research and Treatment Development (DATR). This Program Officer will provide leadership and direction for a research program of national and international scope in the area of Schizophrenia Spectrum Disorders. The incumbent will be responsible for program leadership and development, project management and administration, and scientific activities. The Branch supports research on the foundations of psychopathology and promotes translational research on the development, onset, and course of adult psychopathology and its fundamental processes, such as emotion, cognition, and motivation. The program encompasses research on modifiable risk and protective factors and modern psychometric techniques, especially via interdisciplinary approaches that integrate biology and psychology. The scientific and technical background appropriate for this position could come from any of a large number of areas, including, but not limited to: psychiatry, psychology, and public health. Candidates must have a relevant doctoral degree and research experience in schizophrenia spectrum disorders. An individual filling this position would work closely with the Branch Chief, Adult Psychopathology and Psychosocial Intervention Research Branch, DATR. The ability to work both independently and collaboratively is required. Strong scientific, analytic, communication, and organizational skills are also required. This is a permanent position. Salary will be commensurate with experience.

To explore interest in potential candidacy for this position, email or fax curriculum vitae to **Michael Kozak, Ph.D., at kozakm@mail.nih.gov or 301-443-4611 (fax)**. Telephone inquires are welcome at **301-443-6471**. With nationwide responsibility for improving the health and well being of all Americans, the Department of Health & Human Services oversees the research programs of the National Institutes of Health. **http://www.os.dhhs.gov**

NATIONAL CANCER INSTITUTE (NCI)

Metabolism Branch
Center for Cancer Research
Tenured or Tenure Track Researcher

The Metabolism Branch, NCI, is searching for a tenure-track or tenured investigator engaged in laboratory-based research in the biology of normal or malignant lymphocytes. The research program should be in any area of basic or patient oriented investigation that complements the existing focus of the Branch on the pathogenesis, diagnosis or treatment of lymphomas and multiple myeloma. The Metabolism Branch is located on the Bethesda campus of the NIH. Current areas of research include the molecular diagnosis of lymphomas, the use of genome-wide RNA interference screens to uncover molecular targets in cancer, the analysis of signal transduction and transcription factor networks in normal and malignant B cells, the biochemistry of transcriptional regulation, the development of monoclonal and cytokine-based therapies for lymphomas, and the clinical evaluation of novel chemotherapeutic strategies and molecularly-targeted therapies for lymphoma. Candidates for the position should have an M.D./Ph.D., Ph.D., or M.D. and strong research credentials. Applicants for this position should submit a curriculum vitae including bibliography, a statement of research interests, a two-page outline of the proposed research program, and three letters of recommendation to **Drs. Thomas A. Waldmann and Louis M. Staudt, Attention: Jean Decker, Bldg 10, Rm 4N115, 10 Center Drive, M.S.C. 1374, Bethesda, MD, 20892-1374**. You may also e-mail your application to: **deckerj@mail.nih.gov**.

WWW.NIH.GOV

Division of Cancer Treatment and Diagnosis
Cancer Diagnosis Program

Announcement Number: NCI-09-303077-DH

Position: Supervisory Medical Officer, GS-602-15
Associate Director, Cancer Diagnosis Program
Division of Cancer Treatment and Diagnosis

The National Cancer Institute (NCI) is responsible for stimulating and supporting scientific discovery and its application to achieve a future when all cancers are uncommon and easily treated. We are seeking a highly energetic and creative individual to head its Cancer Diagnosis Program (CDP) within the Division of Cancer Treatment and Diagnosis (DCTD).

CDP is responsible for planning and coordinating the development of new predictive and prognostic molecular diagnostics, biologic and informatics resources, programs for development of new molecular technologies and investigator-initiated research that forms the basis for new developments in diagnostics research; planning and directing the evaluation of new diagnostic technologies and the applicability of these technologies to clinical decision-making; coordinating technology development activities with other components of the NCI, with academic researchers and with industry; coordinating development of biologic and informatics resources with other programs of the Institute, other Federal agencies, and outside organizations both on a national and international scale; maintaining liaison with the FDA regarding development of new diagnostic devices; coordinating the activities of the branches within the program to assure productive interactions and effective technology transfer; and assessing the activities of the program as a whole. The goals of this position are as follows:

- Planning, developing, directing and managing an extramural program of national and international scope which supports research designed to develop improved ability to make more accurate diagnoses and to guide the choice of therapy, to stage tumors more precisely for prognostic and therapeutic decisions, to detect cancer recurrences at earlier stages, and to monitor more effectively changes during and following therapy
- Establishing program priorities and evaluating program effectiveness
- Providing a broad spectrum of information, advice and consultation to individual scientists and institutional science management officials relative to National Institutes of Health (NIH) and NCI funding and scientific review policies and procedures, preparation of grantt applications and choice of funding instruments
- Providing NCI management with recommendations as to funding needs, priorities and strategies for the support of relevant research areas consistent with the current state of development of individual research activities and the promise of new initiatives
- Planning, developing and managing research resources necessary for the conduct of the coordinated research program
- Planning, organizing and conducting meetings and workshops both nationally and internationally to further program objectives and maintain contact with the relevant scientific community to identify and evaluate new research trends relating to its program responsibilities. The Associate Director is responsible for managing the Program for the Assessment of Clinical Cancer Tests (PACCT), which was launched in 2000, to ensure efficient and effective translation of new technologies and understanding of cancer into clinical tools to guide treatment decisions and improve patient outcomes.

The Cancer Diagnosis Program has approximately 15 employees and contractors and administers a research budget of approximately $3 million, excluding the research grant portfolio which accounts for another $80 million. The program is located in Rockville, Maryland. For more information, the CDP website can be accessed at **http://dctd.cancer.gov/ProgramPages/CDP.htm**.

Qualifications Required: Candidates must have a medical degree (M.D./D.O.) or equivalent and board certification or eligibility in either Medical Oncology/Hematology, Pathology or Surgery is desirable. Candidates should be nationally or international recognized in the field of molecular diagnostics. A broad-based knowledge in molecular diagnostics as well as extensive experience and background in one or more molecular diagnostic specialties for the development of state of the art molecular research programs is required. Understanding of and experience in clinical research, including knowledge and understanding of the science and regulatory issues related to clinical trials is required. Other qualifications include a demonstrated ability to communicate clearly and effectively both in writing and orally, skill in establishing and maintaining effective collaborative relationships with other health care professionals and scientists within and outside the organization and demonstrated experience providing managerial leadership to other professional staff including coordination of work within the Program, Division, NCI and NIH or comparable organizations. Appointments are limited to only U.S. citizens.

Salary and Benefits: Total annual compensation will be commensurate with education and experience. Various incentives may apply in individual circumstances, based on experience and expertise. A recruitment incentive/bonus and relocation expenses may also be available to the selectee. Full Federal benefits including health and life insurance options, retirement, paid holidays, vacation and sick leave will be provided.

How to apply: To obtain the mandatory application requirements and other necessary information, please visit: **http://jobsearch.usajobs.opm.gov/a9nih.asp**, Vacancy Announcement number**, NCI-09-303077-DH**. For more information on applying, please contact **Ms. Mary Lou Weathers at (301) 402-5059, email: weatherm@mail.nih.gov.**

APPLICATIONS MUST BE RECEIVED BY FEBRUARY 13, 2009.

Children's Hospital Boston

HARVARD MEDICAL SCHOOL

Director of Vascular Biology Program
Children's Hospital Boston and Harvard Medical School

Children's Hospital Boston and Harvard Medical School jointly seek an internationally recognized scientist in the field of Vascular Biology to serve as Director of the Vascular Biology Program at Children's Hospital Boston. The Director will be appointed as a chaired Professor in the Department of Surgery at Children's Hospital Boston and Harvard Medical School.

The Director's duties will include leading a multi-disciplinary community of collaborative researchers and clinician-scientists whose areas of expertise extend from fundamental molecular mechanisms to development of clinical diagnostics and therapeutics in the field of vascular biology. The Director will be responsible for developing a scientific vision for the program; mentoring its junior and senior faculty; leading faculty search, recruitment and promotion activities; interfacing with academic and clinical department chairs and hospital leaders; developing intellectual property strategies; overseeing the administrative and financial operations of the Program; and raising philanthropic funds to support key programmatic activities. The Director also will be expected to run his or her own vigorous research program in vascular biology. Candidates should have excellent communication capabilities, demonstrated scientific and administrative leadership skills, and a world-recognized record of research excellence.

Please forward your curriculum vitae and inquiries to:

Mohamed H. Sayegh, M.D.
Director of Transplantation Research Center
Children's Hospital Boston
221 Longwood Ave
Boston, MA 02115
msayegh@rics.bwh.harvard.edu

Children's Hospital Boston is an Equal Opportunity Affirmative Action Employer; women and minorities are encouraged to apply.

UNIVERSITY OF BASEL

The Faculty of Science of the University of Basel announces an opening in the Department of Physics for a

Tenure Track
Assistant Professorship in Theoretical Physics

with a specialisation in **Astro/Particle Physics**. In this broad field we are looking for candidates with a strong research background related e.g. to Hadron Physics and/or General Relativity and applications in Astrophysics who complement, strengthen and expand our activities (www.physik.unibas.ch). Duties will include teaching theoretical physics courses related to the physics and nanophysics bachelor, master and doctoral programs. Tenure track assistant professorships are open for promotion to tenured associate professorships after four to five years.

Applicants should provide a curriculum vitae, a publication list indicating five outstanding papers, a statement of research interests, a statement of teaching interests and experience, together with the names and addresses of five potential referees to: **Prof. Dr. Eberhard Parlow, Dean, Faculty of Science, University of Basel, Klingelbergstrasse 50, 4056 Basel, Switzerland**, and electronically (pdf or zip) to Dekanat-Philnat@unibas.ch.

The deadline for receipt of applications is 15 February 2009, but applications will continue to be considered until the position is filled. The University of Basel is an equal opportunity employer and encourages applications from female candidates. For additional information please contact any of the faculty members in astro/particle physics, http://www.physik.unibas.ch

UNI BASEL

Drexel UNIVERSITY COLLEGE OF MEDICINE

DEPARTMENT OF PHARMACOLOGY & PHYSIOLOGY

FACULTY POSITIONS

The Department of Pharmacology and Physiology at Drexel University College of Medicine is actively seeking applications for full-time tenure-track faculty to fill positions in a number of areas. Applications at the Assistant or Associate Professor level will be considered as part of the first step of an initiative to expand the Department's research activities.

We seek outstanding candidates with demonstrated ability to pursue research in a number of areas including cellular and molecular pharmacology, behavioral pharmacology, integrative/animal model systems, neuropharmacology and epigenetics. Candidates will be expected to demonstrate the capacity to establish or transfer an outstanding and scientifically sound research program, attract and maintain research funding, be committed to training and education at the graduate and medical school levels, and to participate in creating a collegial and collaborative research environment. Competitive start-up packages will be available.

The Department of Pharmacology and Physiology is one of four basic science departments within the College of Medicine. Opportunities for collaborative efforts with these departments as well as with the clinical departments, the School of Biomedical Engineering and College of Engineering are ongoing and strongly encouraged, as are collaborations with other institutions and organizations within the Greater Philadelphia Area.

The Department of Pharmacology and Physiology is in the process of renovating laboratory and support space to accommodate new and existing faculty as part of the overall initiative to enhance the departmental research and educational strengths. There is a newly established program in Drug Discovery and Development within the Department of Pharmacology and Physiology, an intent to develop an emphasis within the department on pain research, along with University-wide strategic initiatives in autism and pain. Candidates with this experience in the above-named areas will be given special consideration during this initial review period.

For more information please consult the following websites for Department of Pharmacology and Physiology (**http://www.drexelmed.edu;**) and on medical education at Drexel University College of Medicine (**http://webcampus.drexelmed.edu/**). Applicants should submit curriculum vitae, a statement summarizing their current research and future research directions, and the names of three references to **Carolann.Imbesi@Drexelmed.edu**. Review of applications will begin immediately with the intent of hiring by the fall of 2009.

Assistant or Associate Professors of Climate Change Science - #10099
Cornell University, College of Agriculture and Life Sciences

Cornell University, located in Ithaca, New York, is an inclusive, dynamic, and innovative Ivy League university and New York's land-grant institution. Its staff, faculty, and students impart an uncommon sense of larger purpose and contribute creative ideas and best practices to further the university's mission of teaching, research, and outreach.

Assistant or Associate Professor – Two tenure-track positions in Climate Change Science: Atmospheric Science or Terrestrial Biogeochemistry. College of Agriculture and Life Sciences, Cornell University, Ithaca, New York. Cornell University has recently established a Climate Change Initiative as part of its Center for a Sustainable Future (CCSF, **sustainablefuture.cornell.edu**). The Center serves to focus and integrate the growing interest across departments in sustainability, as well as to generate real-world impacts. As part of the Climate Change Initiative, the Center seeks to facilitate hire over the next 3 years of several faculty members in the biological and physical sciences, social sciences, engineering, and the humanities. We seek applications for two tenure-track positions at the ASSISTANT or ASSOCIATE PROFESSOR rank in climate change science, one in Atmospheric Science and one in Terrestrial Biogeochemistry. For both, we seek candidates to address regional and global scale issues by employing theoretical and empirical approaches such as modeling, earth-observing system and/or spatial information technologies, data-assimilation, spatial statistics, and time-series analysis. The Atmospheric Science position will address the interactions of the atmosphere with earth surfaces. The Terrestrial Biogeochemistry position will focus on the interaction of terrestrial surface processes with global environmental change. The scope of these positions is intentionally broad and a wide range of research areas will be considered. These "open department" searches seek to place outstanding candidates in departments they best match. Potential home departments are Biological and Environmental Engineering, Crop and Soil Sciences, Earth and Atmospheric Sciences, and Natural Resources. Both positions will involve 50% research and 50% instructional responsibilities and developing an internationally recognized and externally funded research program in Climate Change Science.

Qualifications: Ph.D. in relevant field. Applicants should submit a cover letter indicating why they feel they are a good fit for an interdisciplinary Climate Change Initiative at Cornell, together with a curriculum vitae, a research plan (2-3 pages), and a statement of teaching interests. All materials, including PDF files of selected reprints should be submitted electronically, by emailing a single PDF file to **biogeochemistry-search@cornell.edu** or **atmospheric-search@cornell.edu** (please limit to 15MB). Applicants should also provide names of three individuals who may be contacted to provide letters of recommendation. Applications will be reviewed beginning February 9, 2009; the searches will remain open until qualified applicants are identified.

College of Agriculture and Life Sciences
Developing Leaders – Improving Lives

Cornell University
Cornell University is an Affirmative Action/ Equal Opportunity Employer and Educator.

http://chronicle.com/jobs/profiles/2377.htm

uni.lu
UNIVERSITÉ DU LUXEMBOURG

The University of Luxembourg, established in 2003, invites applications for the position of founding a new interdisciplinary centre being established by the University

Director of the Centre for Systems Biology, Luxembourg (CSBL) (M/F)

The CSBL will be an autonomous, highly interdisciplinary unit within the University of Luxembourg whose Director will develop the vision, participate in the recruitment of key faculty and establish its research programs. The Centre is intended to provide a research focus for the development of the future biological sciences in the University, and its Director will report directly to the Rector of the University.

Candidates must have extensive experience in leading significant academic research units, with experience in building and maturing new units, have an outstanding record of scientific achievement and have a focus on an innovative systems approach to biological research. Substantial experience in recruiting, leading the integration of multiple scientific disciplines into a coherent program and the multidisciplinary (biology, mathematical and computational biology, and new technologies) development of research teams is mandatory. Candidates from related disciplines are welcome to apply. The new Director will lead in the establishment and growth of the CSBL that is expected to achieve prominence among European research institutions over the next decade, and contribute substantially to the application of research to understanding human disease. The candidate may also expect to spend significant time within the institute of our research partner in the United States.

The scientific vision, people skills and the managerial and scientific maturity of the successful candidate are critical. The University of Luxembourg has established a strong collaborative research program with the Institute for Systems Biology, Seattle Washington, USA, and the new Director will have the responsibility to lead this collaborative research effort while building the CSBL and forging this joint international collaborative effort. The successful candidate will have access to resources from the University and from competitive third parties to accomplish the ambitious goals of the establishment and development of a visible centre of true excellence in research related to the systems biology of human disease. Further, a strong interest in translating research into practice would be an important advantage.

Candidates should forward a CV and a statement of vision for the development of the Centre for Systems Biology, Luxembourg to: **Prof. Dr. Eric Tschirhart • University of Luxembourg • 162a, avenue de la Faïencerie • L-1511 Luxembourg**

Applications must be sent **before January 14th, 2009**

The University of Luxembourg is an equal opportunity employer. Applications will be handled in strictest confidence.

Science Careers online @sciencecareers.org

Max-Planck-Institut für demografische Forschung

Max Planck Institute for Demographic Research

www.demogr.mpg.de

The Max Planck Institute for Demographic Research
seeks a path-breaking recent Ph.D.
eager to develop a highly innovative

Independent Junior Research Group

at a frontier of mathematical,
biological, historical, social,
economic or qualitative demography.

The successful candidate will be given ample resources to establish and direct an independent research program. For this purpose, he or she will be guaranteed funding to recruit and lead a team of researchers, for operating expenses, scientific collaborators, and technical and secretarial support.

The successful candidate will start a five-year contract (with the possibility of a prolongation after positive evaluation) between July and October 2009. The payment corresponds to the W2 level on the German university scale, equivalent to an Assistant or Associate Professor.

Applicants should have completed a doctoral degree in the past decade. They should have an outstanding record - or show exceptional promise - as demographic scholars.

The Max Planck Society is committed to employing more handicapped individuals and to increasing the share of women in areas where they are underrepresented, and therefore expressly encourages applications from such qualified individuals.

The applicant should submit a three to five page description of a research program, along with a work plan, a complete CV, and three personal references.

Please send applications by January 31, 2009 to appl_irg@demogr.mpg.de.

MAX-PLANCK-GESELLSCHAFT

Senior Faculty Position
Redox Biology Center and Department of Biochemistry
University of Nebraska-Lincoln (UNL)

The **Redox Biology Center (RBC)** at UNL, funded as a Center of Biomedical Research Excellence by the National Institutes of Health, invites nominations and applications from established investigators for a senior faculty position at the **Full or Associate Professor** level in the **Department of Biochemistry**. The title will be commensurate with experience. The RBC is a major focus group for research in redox biology, incorporating investigators at UNL and the University of Nebraska Medical Center in Omaha. Areas such as thiol-based redox signaling and gene regulation, redox control of neurodegenerative diseases and cancer, roles of redox processes in aging, biochemistry of redox-active trace elements, structural biology, proteomics/metabolomics, microbial pathogenesis and redox homeostasis are all current target areas of investigation. The Center operates mass-spectrometry and imaging/spectroscopy core research facilities and has access to University wide core facilities including microscopy, bioinformatics, flow cytometry and genomics.

The successful applicant will be expected to lead an internationally recognized, federally funded research program and contribute to the development and leadership of the Center. In addition, the incumbent will be expected to contribute to the teaching missions of the Department of Biochemistry. A PhD (or equivalent) in Biochemistry or related field, a minimum of 3 years experience in leading a successful research program in a faculty or equivalent senior position, and a minimum of 3 years experience teaching and/or mentoring students/research staff is required. The position will be housed in the state-of-the-art George W. Beadle Center, and carries with it a 12-month, state-funded appointment. This senior hire is one of several positions that Biochemistry and the RBC will fill during the next four years.

Lincoln, Nebraska is one the Midwest's most beloved cities that has fine culinary and artistic treasures, a budding live music scene, and numerous parks, golf courses and bike trails. To learn more about the Center and the Department, please visit http://www.unl.edu/RedoxBiologyCenter and http://biochem.unl.edu.

Applicants should go to **https://employment.unl.edu**, search for position **#080893** and make application according to the instructions. Complete the faculty academic/administrative information form and attach a letter of application, curriculum vitae, a succinct statement of research interests, and arrange to have three letters of reference sent to: **Search Committee, Redox Biology Center, University of Nebraska, N146 Beadle Center, Lincoln, NE 68588-0662, USA**. Email reference letters will also be accepted at **redox2@unl.edu**. Review of applications will begin on **January 20, 2009** and continue until the position is filled.

The University of Nebraska has an active National Science Foundation ADVANCE gender equity program, and is committed to a pluralistic campus community through Affirmative Action, Equal Opportunity, work-life balance, and dual careers.

UNIVERSITY of LOUISVILLE
dare to be great

The Department of Biology at the University of Louisville, **http://www.louisville.edu/a-s/biology**, invites applications for the following tenure-track positions to begin Fall 2009:

CONSERVATION BIOLOGY
Endowed Chair

The Wallace Endowment fund is supporting a Chair (rank open) in Conservation Biology who will complement existing strengths of the Department in ecosystem, restoration, and organismal ecology. Conservation biologists with interests and expertise in landscape ecology (ecological impacts of fragmentation, disturbance and land-use change), GIS, or simulation modeling are especially encouraged to apply.

BIOCHEMISTRY AND MOLECULAR / CELLULAR BIOLOGY
Assistant Professor

This position is open to individuals using any Eukaryotic model system. Research expertise and interests may include, but are not limited to: metabolism, metabolic regulation, mechanisms of host defense, hormonal regulation and development. Individuals with research programs that target insect, fungal, or plant systems or with research programs with a focus in developmental biology (any system) are strongly encouraged to apply. Primary teaching duties will include contributions to the core undergraduate curriculum in Cellular and Molecular Biology and teaching graduate level material in the applicant's area of specialization.

MICROBIOLOGY / EMERGING PATHOGENS – Rank Open

This position is open to individuals with a Microbiology background with an emphasis on Emerging Pathogens. Rank is open and depends on commensurate experience including an existing extramurally funded research program. Applicants are encouraged to apply that use molecular evolutionary, genetics, ~omics and other approaches to dissect host-emerging pathogen interactions. The new faculty member will become part of a multidisciplinary group at the new U of L Center for Predictive Medicine for Biodefense and Emerging Infectious Diseases, and work with the NIH-NIAID Regional Biocontainment Laboratory (BL3).

Successful candidates are expected to contribute to undergraduate and graduate programs and to maintain an excellent record of research productivity and external funding. Ph.D. and Post-doctoral experience required. Applicants must apply on-line at **www.louisville.edu/jobs**. If you are applying for the Endowed Chair position, choose Job ID # 23480. For the Biochemistry and Molecular position, choose Job ID # 23481, and for the Microbiology position, choose Job ID # 23482. Please attach a curriculum vitae with your on-line application. Send statements of research and teaching interests, representative reprints and contact information for three references directly to, Department of Biology, University of Louisville, Louisville, KY 40292. Review of applications will begin on December 15th and will continue until the positions are filled.

The University of Louisville is an Affirmative Action, Equal Opportunity, Americans with Disabilities Employer, committed to diversity and in that spirit, seeks applications from a broad variety of candidates.

THE OHIO STATE UNIVERSITY Medical Center

POSITION AVAILABLE:

Chair: Department of Biomedical Informatics

We seek a distinguished senior scientist with a vigorous research program, commitment to education and the broad vision, experience and energy to chair the Department of Biomedical Informatics (BMI). BMI is a tenure-initiating unit of the Ohio State University College of Medicine.

The Ohio State University (OSU) is a leading comprehensive teaching and research university with a core responsibility for the advancement and dissemination of knowledge. OSU has some of the finest facilities in the world, including state-of-the-art technology and a library system with one of the largest research and academic collections in North America.

BMI's mission is to be the worldwide leader in transforming, creating and applying cutting-edge biomedical informatics discoveries to improve individuals' lives through personalized healthcare. BMI contributes to OSU's mission via innovative teaching and through high-impact research and publications. Furthermore, BMI and Ohio State's Medical Center's CIO have created a solid and vibrant partnership to leverage IT and informatics across the entire enterprise, thus creating a rare capability to effectively translate research into practice. BMI is a proven catalyst for collaboration leading to increased funding, greater visibility and reputation for the University as a whole.

BMI contains the Division of Anatomy and strong research programs with five foci: Genomics, Systems Biology, Clinical and Translational Informatics, Imaging Informatics and High Performance and Grid Computing.

Applicants should have established research programs with extramural funding, have outstanding administrative experience, be a distinguished researcher with an international reputation, have exceptional communication skills as demonstrated by a track record of publication and be an admirable leader as demonstrated by the ability to mentor junior faculty, scientists and students. The candidate must be a critical, strategic and visionary thinker who can develop and enhance the research enterprise across the five foci of BMI and throughout the University. M.D. and/or Ph.D required.

Candidates with demonstrable interdisciplinary research interests are especially encouraged to apply.

Applicants should e-mail a cover letter, detailed CV, and list of references to:
(single document PDF submissions are preferred)

Dan Dolan, Director
Senior Recruitment & Sourcing
The Ohio State University Medical Center
dan.dolan@osumc.edu

bmi.osu.edu | medicine.osu.edu

The Ohio State University is an equal opportunity and affirmative action employer.

MAX PLANCK INSTITUTE
FOR CHEMICAL ECOLOGY

Outstanding Early-Career Scientist

The Max Planck Society announces an INDEPENDENT JUNIOR RESEARCH GROUP to be hosted at THE MAX PLANCK INSTITUTE FOR CHEMICAL ECOLOGY.

We seek an outstanding early-career scientist to lead an independent junior research group working in the area of chemically-mediated interactions among organisms. Candidates should have a record of internationally recognized research accomplishments. While there is no restriction on the precise area of research, it should complement and interact synergistically with the other groups and departments at the Institute. Current research focuses on the ecology, evolution, chemistry and biochemistry of interactions among plants, insects and microbes, as well as biodiversity-related topics.

The Institute offers a stimulating and interdisciplinary research environment with strong links to the Friedrich Schiller University, Jena, and the Leibniz Institute for Natural Product Research and Infection Biology. Ph.D. studies are coordinated by an International Max Planck Research School. The Institute provides state-of-the-art equipment, greenhouses and insect rearing facilities including laboratories for experimental work with transgenic plants and insects.

Funding for the group leader position (equivalent to an assistant professor) and associated support is guaranteed for five years with the possibility of extension for up to four additional years. The group will be provided with modern laboratory space, funds for positions for a post-doc, Ph.D. student and technical assistant, and an adequate budget for running costs.

To apply please register and upload (1) a CV including a list of publications, (2) one page summary of your scientific achievements and a two pages statement of your future research plans, and (3) up to three of your most important papers at:

http://www.ice.mpg.de

Also please arrange to have two letters of recommendation uploaded directly by your referees at the above webpage. The deadline for receiving applications is **December 31, 2008.** Please note that a symposium (scientific presentation of short listed candidates plus interviews) is planned in conjunction with the recruitment of a similar position at the MPI for Evolutionary Biology in Plön on **January 29/30, 2009.** Location: Max Planck Institute for Chemical Ecology, Jena, Germany.

The Max Planck Society is an equal opportunity employer, and is very interested in raising the proportion of women in areas where they are underrepresented. Thus applications from female scientists are especially encouraged.

Further information can be obtained from:

Prof. Jonathan Gershenzon, Managing Director
E-Mail: gershenzon@ice.mpg.de

Max Planck Institute for Chemical Ecology
Hans-Knöll-Straße 8
D-07745 Jena
Germany

FACULTY POSITION

Department of Molecular Pathology

The Department of Molecular Pathology invites applications for a tenure/tenure-track faculty position at the PROFESSOR level. We are seeking an outstanding investigator with special emphasis on molecular mechanisms of solid tumor stem cell involvement in cancer and application to diagnosis and therapy. Ph.D. or M.D. scientists with appropriate research experience should submit curriculum vitae, a short summary of research interests and three letters of reference to:

Dr. Ralph B. Arlinghaus
c/o Ms. Alice Powell
Department of Molecular Pathology (Unit 951)
The University of Texas M. D. Anderson Cancer Center
P.O. Box 301429
Houston, TX 77230-1429
E-mail: apowell@mdanderson.org

THE UNIVERSITY OF TEXAS
MD ANDERSON
CANCER CENTER
Making Cancer History®

M. D. Anderson Cancer Center is an equal opportunity employer and does not discriminate on the basis of race, color, national origin, gender, sexual orientation, age, religion, disability or veteran status except where such distinction is required by law. All positions at The University of Texas M. D. Anderson Cancer Center are security sensitive and subject to examination of criminal history record information. Smoke-free and drug-free environment.

---

cnrs

IN 2009
CNRS IS RECRUITING FOR 300 TENURED RESEARCHER POSITIONS
IN ALL FIELDS OF SCIENCE

- MATHEMATICS • PHYSICS
- NUCLEAR AND HIGH-ENERGY PHYSICS
- CHEMISTRY
- SCIENCE AND TECHNOLOGY OF INFORMATION AND ENGINEERING
- UNIVERSE AND EARTH SCIENCE
- ENVIRONMENT AND SUSTAINABLE DEVELOPMENT
- LIFE SCIENCES • HUMANITIES AND SOCIAL SCIENCES

CNRS encourages junior and senior scientists from around the world to apply for its tenured researcher positions.

CNRS provides an enriching scientific environment:
- numerous large-scale facilities
- highly skilled technical support
- multiple international and interdisciplinary networks
- access to university research and teaching
- lab-to-lab and international mobility

Application deadline: January 6th, 2009

www.cnrs.fr

The Leibniz Institute of Plant Genetics and Crop Plant Research (IPK: www.ipk-gatersleben.de) invites applications for a **group leader position** in

Plant Taxonomy
(position number 58/11/08)

The IPK campus is home to an international community comprising about 100 scientists and 60 PhD students covering most fields of plant sciences.

The Genebank Department, where the position will be located, hosts a molecular-systematic lab, a herbarium, ample greenhouse facilities, several reference collections, and the Federal *ex situ* genebank, holding c. 150.000 accessions. The IPK provides of an excellent technical infrastructure including the Plant Genome Resources Centre, where state of the art technologies for high throughput sequencing and genotyping are available.

The applicant should hold a PhD in a relevant field of biology, and have an excellent track record of research in taxonomy, systematics or related fields. He or she should be able to establish an internationally visible research program on cultivated plants.

IPK seeks to increase the proportion of female staff members in the faculty and therefore encourages interested female candidates to apply. In case of equal qualifications, preference will be given to disabled applicants.

Applicants should send their CV, master degree, doctorate certificate, the names and contact information of two references, a list of publications and grants received, reprints of their four most-important publications, and a research plan by **January 15th, 2009** as a hard copy and in electronic form to

Leibniz Institute of Plant Genetics
and Crop Plant Research (IPK)
Personalwesen
Corrensstraße 3, D-06466 Gatersleben
Germany
Tel.: +49-39482-5327
Fax: +49-39482-5286
E-Mail: beckerj@ipk-gatersleben.de

IPK GATERSLEBEN

Proteostasis Therapeutics, Inc.

Proteostasis Therapeutics, Inc. is a biotechnology company focused on discovering and developing novel small molecule therapeutics that control the body's Proteostasis Network™. The Proteostasis Network consists of over 500 proteins working through a number of biological pathways to maintain a critical balance among protein synthesis, transcription, translation, folding, aggregation, trafficking and degradation to ensure health. Stress on the Proteostasis Network from aging, genetic or environmental insults can lead to imbalances that result in serious diseases. Advances in our ability to characterize and pharmacologically control the Proteostasis Network create new opportunities to treat a wide range of diseases.

Proteostasis Therapeutics, Inc. is an exciting young company at the forefront of the field of Proteostasis Network research. We are committed to building a high performing cross-disciplinary team where everyone's input is valued and employees are self driven by the pursuit of excellence. We are seeking highly motivated individuals to join our rapidly growing team of dedicated scientists and professionals in developing new therapies for serious diseases.

- Head of Pharmacology (Job Code: WN-HP)
- Proteomics Scientist/Senior Scientist (Job Code: DG-PSS)
- Bioinformatics Scientist (Job Code: HG-BS)
- Cell Biology Scientist (Job Code: DG-CBS)
- Scientist in Mouse Models and Cell Biology (Job Code: DG-MMS)
- Bioinformatics Analyst (Job Code: HG-BA)
- Cell Biology Research Associates(Job Code: DG-CBA)

Full job descriptions and a list of open positions are on our website: **www.proteostasis.com**.

Washington University in St. Louis
School of Medicine

Head of Department of Cell Biology and Physiology

Washington University School of Medicine in St. Louis invites applications for a tenured faculty position to become the head of the Department of Cell Biology and Physiology. We are seeking an academic leader with a Ph.D. and/or M.D. degree and training in cell biology, physiology, and related fields. The successful candidate is expected to have an internationally distinguished record in research and teaching. Experience with administration and program development will be very helpful. Excellent interpersonal skills as well as a strong vision to further departmental development will be critical. The candidate should have demonstrated ability to work cooperatively and collegially within a diverse environment. Additional information about the department is available at: **http://www.cellbio.wustl.edu/** The Department head will be responsible for continued growth of the Department through the recruitment of new faculty.

Contact: Interested candidates should send their curriculum vitae, statement of interest, and three references to: **Adelaide Donnelly, Washington University School of Medicine, 660 S. Euclid Ave, Campus Box 8222, St. Louis, MO 63110, USA**; or via e-mail to: **donnella@wustl.edu**. Applications will be reviewed beginning **January 2009**. The position will remain open until filled.

Washington University is an Equal Opportunity Employer and committed to building diversity. Women and minority candidates are strongly encouraged to apply.

ETH
Eidgenössische Technische Hochschule Zürich
Swiss Federal Institute of Technology Zurich

University of Zurich

Professor of Biogeosciences/Evolution of Life
Assistant Professor (Tenure Track) of Biogeosciences/ Evolution of Life

The Department of Earth Sciences (www.erdw.ethz.ch) at ETH Zurich and the Faculty of Science of the University of Zurich invite applications for a professorship in the area of Biogeoscience/Evolution of Life/Early Life. Applications at senior (full professor) or junior level (assistant professor with tenure track) will be considered. The appointment is a combined ETH Zurich and University of Zurich professorship.

The successful candidate should have a strong earth science background and is expected to develop an internationally recognized research program in the field of Biogeosciences/Evolution of Life. Areas of interest include but are not restricted to molecular palaeontology, micropaleontology and biodiversity, biomarker characterization of organic sediments, isotopic biogeochemistry, biomineralization, environmental geomicrobiology, ecosystems in the earth history, biogeochemistry, origin and evolution of life, biodiversity in earth history. Potential candidates will use multiple analytical approaches in their work. In addition of developing a broad interdisciplinary biogeoscience research program, the future professor will be expected to contribute to ETH Zurich's and the Universitiy's continuing tradition in undergraduate teaching which includes field excursions as well as the participation in the development of new courses at Master level. He or she will be expected to teach undergraduate level courses (German or English) and graduate level courses (English).

Assistant professorships have been established to promote the careers of younger scientists. The initial appointment is for four years with the possibility of renewal for an additional two-year period and promotion to a permanent professorial position.

Please submit your application together with a curriculum vitae, a list of publications, and a statement of your teaching and research interests **to the President of ETH Zurich, Prof. Dr. Ralph Eichler, Raemistrasse 101, 8092 Zurich, Switzerland, no later than February 28, 2009.** With a view toward increasing the number of female professors, ETH Zurich specifically encourages female candidates to apply.

Reginald A. Daly Postdoctoral Fellowship
Harvard University
Department of Earth and Planetary Sciences

The Department of Earth and Planetary Sciences at Harvard University invites applicants for the Reginald A. Daly Postdoctoral Research Fellowship.

The Department seeks outstanding candidates in the broad field of Earth and Planetary Sciences. **We encourage applications of candidates pursuing field observations, lab-based science, and theory, and interested in geology, geochemistry, ocean, atmosphere and climate dynamics and chemistry, seismology, geophysics, planetary sciences, and other related fields.** These honorific postdoctoral fellowships are awarded for a one-year period, with an anticipated extension for a second year. Daly fellows carry out independent research, yet are encouraged to interact with one or more research groups in the department. Applicants are welcome to contact members of the department before applying.

The Daly Fellowship 2009 Application includes a curriculum vitae, names and affiliation of three referees, a one-page statement of the applicant's doctoral research, and a one to two page postdoctoral research proposal. Applications are due **January 15, 2009**.

Please apply online at: http://www.eps.harvard.edu/daly.php

For more information please contact: **Daly Postdoctoral Search Committee, dalypostdoc@eps.harvard.edu, Department of Earth and Planetary Sciences, Harvard University, 20 Oxford Street, Cambridge, MA 02138.**

Applicants are responsible for contacting the referees to have their letters sent directly to the e-mail above by the January 15, 2009 deadline. The annual salary is $54,000 with additional funds of $15,000 available for research support over a two-year period. Applicants should have a recent Ph.D. or should be 2009-degree candidates. Completion of the Ph.D. is required by the time of the appointment.

We particularly encourage applications from women and minorities. Harvard University is an Affirmative Action/Equal Opportunity Employer.

Assistant Professor
The Department of Genetics

The Department of Genetics at the University of Texas M.D. Anderson Cancer Center invites applications from researchers using genetic approaches in model organisms (e.g., C. elegans, Drosophila, yeast, zebra fish, mouse) for a tenure-track Assistant Professor position. The department seeks to complement its existing programs in developmental biology, DNA repair, RNA splicing, cell division, and human and mouse cancer genetics. We offer a very attractive recruitment package, active graduate and post-doctoral training programs, and the unmatched scientific environment of the Texas Medical Center, the world's largest biomedical center. Applicants must hold a Ph.D. and/or M.D. degree, and will be expected to develop an internationally recognized, extramurally funded research program. To apply, please send within a single pdf file: (1) Cover Letter; (2) Curriculum Vitae; (3) Short Research Summary (three page maximum); and (4) Contact Information for three references by December 31, 2008, to: **GeneticModelSearch@mdanderson.org**.

Jill M. Schumacher, Ph.D.
Associate Professor
Department of Genetics
The University of Texas M.D. Anderson Cancer Center
1515 Holcombe Blvd., Unit 1010, Houston, TX 77030

THE UNIVERSITY OF TEXAS
MD ANDERSON
CANCER CENTER
Making Cancer History®

M. D. Anderson Cancer Center is an equal opportunity employer and does not discriminate on the basis of race, color, national origin, gender, sexual orientation, age, religion, disability or veteran status except where such distinction is required by law. All positions at The University of Texas M. D. Anderson Cancer Center are security sensitive and subject to examination of criminal history record information. Smoke-free and drug-free environment.

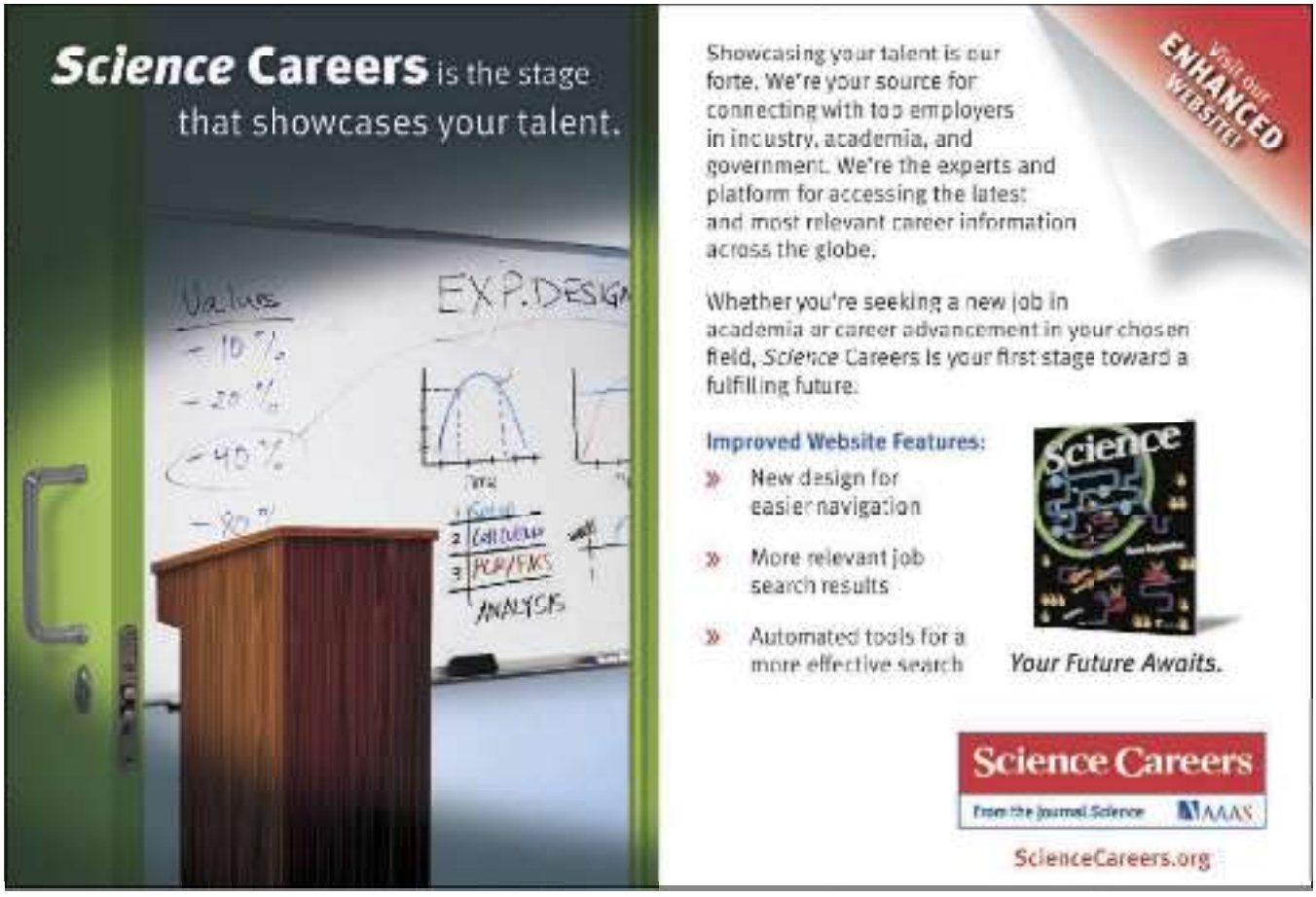

LSU Health Sciences Center

Tenure-track Faculty Positions in Immunology/Vaccine-Related Research

Gene Therapy Program

Applications are invited for open rank tenure track positions in the Gene Therapy Program at the Louisiana State University Health Sciences Center in New Orleans. The positions would particularly suit individuals with interest in gene delivery and/or vaccination for modulation or prophylaxis of infectious or neoplastic disease, and studies of underlying host responses. These are areas of current strength within the Program. We are particularly interested in candidates who have a strong track record in translational research and who will develop first-rate research programs in one or more of these areas. Current external funding held by Program members exceeds $23 million, mostly from the National Institutes of Health, and includes Federal and State Program Grant awards. The Program was founded in 2000 and is a key partner both in the Louisiana Gene Therapy Research Consortium (LGTRC) and the Louisiana Vaccine Center that was recently established with $5.5M of State funding.

The facilities and start-up support provided by the Program are excellent. The Program is located in the Clinical Sciences Research Building at LSUHSC and has developed strong interdisciplinary research programs with the adjacent Stanley Scott Cancer Center and a variety of basic science and clinical Departments. The Program currently funds state of the art core facilities in morphology & imaging, genomics and vector development, and oversees a BSL-3 bio-containment facility. First class immunology and proteomics cores are available. Program members will also have direct access to wet lab space in the New Orleans BioInnovation Center and a Good Manufacturing Practice lab currently under construction that will facilitate the development of clinical trials arising from Program research.

Applicants must hold a PhD and/or an MD degree and should send an email including CV and the names and contact information (email addresses) of three individuals that can serve as references to: **genetherapy@lsuhsc.edu**.

LSUHSC is an Equal Opportunity/Affirmative Action Employer.

R·I·T

Organismal Biologist

The School of Life Sciences at the Rochester Institute of Technology invites applications for one and possibly more (subject to available funding) tenure-track positions in organismal biology. Successful candidates will teach core courses such as Comparative Animal Physiology, contribute to teaching of majors and non-majors introductory biology, and develop discipline-specific elective courses. We seek candidates with a demonstrated commitment to undergraduate teaching and research who will broaden our existing strengths in organismal and evolutionary biology. Candidates who can develop local field and laboratory research programs suitable for undergraduate and MS student participation are particularly encouraged to apply. Candidates are required to hold a Ph.D. and post-doctoral training is preferred.

The School of Life Sciences has more than 30 full-time Faculty and more than 700 full-time students across our undergraduate majors: Biology, Biotechnology, Bioinformatics, Environmental Science, and Biomedical Sciences; and 30+ graduate students in our Masters programs in Bioinformatics and Environmental Science.

Applicants for this position should apply online at **https://mycareer.rit.edu**. Search for **IRC27598**. Please upload your letter of interest; a vita; summaries of teaching and research interests, and a statement of your experience with and commitment to RIT's core values, honor code, and statement of diversity. Please arrange to have 3 letters of reference sent to **science@rit.edu** (preferred) or mailed to: **Dr. Larry Buckley, Associate Head of Life Sciences, Rochester Institute of Technology, 85 Lomb Memorial Drive, Rochester, NY 14623**. Review of applications will begin **January 2009** and will continue until position is filled with a start date of late August, 2009.

The Rochester Institute of Technology is an Equal Opportunity/Affirmative Action Employer. All qualified individuals with the ability to contribute in meaningful ways to the university's continuing commitment to its core values, honor code and diversity statement are encouraged to apply.

UC San Diego

Postdoctoral Position
Signaling and Epithelial Polarity

Position available to carry out research on novel signaling pathways in glomerular epithelial cells (podocytes). Projects involve signaling from cell junctions/slit diaphragms and the interface between G protein signaling and growth factor signaling in both health and disease. For information on specific projects see recent publications. Strong background in molecular cell biology, signaling, protein chemistry, cell fractionation, and immunofluorescence required. Experience with mass spec, live cell imaging, G proteins, and/or computational biology desirable.

To apply send resume and names of three references to:

Dr. Marilyn G. Farquhar
Department of Cellular and Molecular Medicine
University of California San Diego
La Jolla, CA 92093-0651
Email: mfarquhar@ucsd.edu

Equal Opportunity Employer.

Assistant Professor
Redox Biology Center and Department of Veterinary and Biomedical Sciences
University of Nebraska – Lincoln (UNL)

The **Redox Biology Center (RBC)** at UNL, funded as a Center of Biomedical Research Excellence by the National Institutes of Health, invites applications for a **tenure-leading Assistant Professor** position in the Department of Veterinary and Biomedical Sciences in the general area of redox neuroscience and related fields, focusing on neuronal function and disease and role of oxidation-reduction processes. The Center is a focus group for research in redox biology involving investigators at the University of Nebraska – Lincoln and the Eppley Cancer Research Center in Omaha. Areas such as thiol-based redox signaling and gene regulation, redox control of neurodegenerative diseases, cancer and aging, biochemistry of redox-active trace elements, structural biology, proteomics/metabolomics, microbial pathogenesis and redox homeostasis are all current targets of investigation. The Center also operates mass-spectrometry and spectroscopy core research facilities. The successful applicant will be expected to develop an active, independent research program and teach one course per year at the undergraduate or graduate level. The position offers a 12-month, state-funded appointment and a generous start-up package and will be housed in the Veterinary and Biomedical Building. A Ph.D. degree in a related scientific field, experience in teaching at least one course to either graduates or undergraduates, and at least 1 year of postdoctoral experience are required.

This hire is one of several new faculty positions that the RBC will fill in various areas of redox biology during the next three years. To learn more about the Center, please visit **http://www.unl.edu/RedoxBiologyCenter**. To view the complete job details and make application for the position, go to the web site at **https://employment.unl.edu**. Click on **"Search Job Openings"**, enter requisition number **080949** and make application according to the instructions. Complete the faculty academic administrative information form and attach a letter of application, curriculum vitae, succinct statement of research interests and arrange to have three letters of reference sent to: **VBMS Search Committee Chair, c/o Joyce Ore, Administrative Coordinator, Nebraska Redox Biology Center, University of Nebraska – Lincoln, N146 Beadle Center, Lincoln, NE 68588-0662.** Email reference letters will also be accepted at **redox2@unl.edu**. Review of applications will begin on **January 5, 2009** and will continue until a successful candidate has been identified or the recruitment process is closed.

The University of Nebraska has an active National Science Foundation ADVANCE gender equity program, and is committed to a pluralistic campus community through Affirmative Action, Equal Opportunity, work-life balance, and dual careers.

University of California Irvine

Faculty Positions
Environment Institute: Global Change, Energy, and Sustainable Resources

The Environment Institute is recruiting faculty at levels of Assistant (tenure track) to Full (tenured) Professor. These positions represent part of the initial allocation of eight faculty to be affiliated with the Institute and participate in its planning. Faculty will teach and maintain research labs in their primary departments within the School of Biological Sciences, School of Physical Sciences, or Henry Samueli School of Engineering. Future recruitments may involve additional Schools. UC Irvine seeks to build on its strengths in environmental research and develop broad, campus-wide collaborations that relate global change, energy, and sustainable resources to societal needs. This recruitment addresses the areas of interest listed below.

- Global change and human impacts on biological and physical systems: e.g., biodiversity; ecosystem processes and modeling; ecophysiology; ecohydrology; coastal processes; climate change; resource management.
- Energy and changes in utilization of energy: e.g., innovative materials for generation and storage; renewables, including wave and wind; biofuels; nuclear fusion; waste management.
- Sustainable resources for the near future: e.g., water availability; clean air and clean water; green building/city design; transportation; waste systems; industrial ecology; life-cycle analysis.

Applicants must have a Ph.D. plus post-doctoral experience related to this recruitment. UC Irvine faculty teach at undergraduate and graduate levels, maintain an externally funded research program, and direct graduate research. Candidates will present a research seminar in their host department plus a campus-wide forum relating their research to issues at the interfaces of science, technology and/or society.

Applications may be submitted through the UC Irvine recruitment system at **https://recruit.ap.uci.edu/apply/**. More information is available at **http://environment.uci.edu**. Selection process will begin 12 January 2009. Related positions are available in the Henry Samueli School of Engineering, School of Biological Sciences, and School of Physical Sciences. UC is an Equal Opportunity Affirmative Action Employer committed to excellence through diversity. UC Irvine is the recipient of an NSF ADVANCE Award for gender equity, expanded to include racial/ethnic equity.

The University of Wisconsin Madison

FACULTY POSITION

The Department of Medical Microbiology and Immunology, School of Medicine and Public Health at University of Wisconsin-Madison seeking highly qualified applicants for tenure track position in Global Infectious Diseases. Applicants should have PhD, MD, DVM, or equivalent, and qualifications for appointment at rank of Associate or full Professor with tenure. Will consider established investigators with record of accomplishment such that tenure would be achieved within 1-2 years; initial appointment would be Assistant Professor.

Successful candidate has significant research experience in field of global infectious disease and ongoing record of competitive research funding. Scientific expertise in human infectious disease and/or zoonoses preferred. Excellent interpersonal, communication, and administrative skills required. Ideal candidate has track record of integrating science and policy on a global level and/or experience networking with academia, industry, and international scientific community. See **http://www.ohr.wisc.edu/pvl/pv_060624.html**.

To apply, submit cover letter, curriculum vitae, statement of teaching interests, and 2-page statement of current and future research plans related to global infectious diseases. 3 references from persons knowledgeable with applicant's research, leadership and/or teaching abilities must be separately supplied. Application review starts **January 1, 2009**; will continue until position filled. Email application materials to **twiklund@wisc.edu**. Emailed reference letters must be on letterhead and include signatures. Alternatively, application and letters can be mailed to: **GIDI Search Committee, c/o T Wiklund, 1550 Linden Dr, Madison WI 53706-1521.**

Information about Medical Microbiology and Immunology:
http://www.medmicro.wisc.edu/
Information about UW School of Medicine and Public Health:
http://www.med.wisc.edu/
Position sponsored, in part, by Promega Corporation:
http://www.promega.com/

University of Wisconsin is Equal Opportunity Affirmative Action Employer. Women and persons of color especially encouraged to apply. Criminal background check will be conducted prior to hire.

Science Careers online @sciencecareers.org

POSITIONS OPEN

The Department of Anesthesiology at the University of California San Diego **(website: http://anessom.ucsd.edu/),** UCSD, is actively recruiting to fill a research faculty position at the **ASSISTANT PROFESSOR** (tenure track) and early **ASSOCIATE PROFESSOR** (tenured) levels. The qualified candidate will have either an M.D. and/or Ph.D. degree, an international reputation, an outstanding record of research accomplishments with an independent research program, and demonstrated ability to procure extramural federal grant funding.

Ischemia reperfusion injury: the successful candidate will join an ongoing research program on ischemia reperfusion injury in the heart and brain in young and aged animals. Experience in the molecular, cellular, and whole animal models of ischemic preconditioning, with an emphasis on the role of caveolins in cytoprotection and on mitochondrial function, is a requirement.

Neural mechanisms of pain and analgesia: the successful candidate will be a strategic thinker and is expected to significantly enhance ongoing research with visionary leadership. Demonstrated ability to mentor undergraduate and postgraduate students, as well as junior clinical and research faculty, is an asset. Laboratory facilities and initial intramural funding are available to the successful applicant. Applicants should submit curriculum vitae, their research interests and qualifications, a list of at least five references, and a cover letter expressing their interest in the position. Review of applications will begin January 1, 2009, and will continue until positions are filled. Please send letter and curriculum vitae to:

Gerard R. Manecke, Jr., M.D.
Clinical Professor and Chairman
Department of Anesthesiology
University of California San Diego Medical Center
9500 Gilman Drive, MC 0801
La Jolla, CA 92103-0801

UCSD is an Equal Opportunity/Affirmative Action Employer with a strong institutional commitment to excellence through diversity.

RARE DISEASE DIRECTOR
National Disease Research Interchange

Located in Philadelphia, National Disease Research Interchange (NDRI), a nonprofit 501(c)(3) which distributes human biomaterials to scientists, is seeking a Rare Disease Director to administer their National Rare Disease Program funded by NIH. Must have proven administrative skills, record of successful grant applications to NIH, and familiarity with NIH grant requirements. The Director is responsible for recruitment of personnel, interaction with rare disease voluntary health organizations, administration of staff, and interaction with scientists. No bench research involved. Qualified candidates must have advanced science degree; Ph.D.; experience in administration, business, and marketing skills; and ability to write grant proposals. Communications, customer services, and interpersonal skills are required. E-mail resumes to **e-mail: jobs@ndriresource.org.**

Attn.: S. McGovern
1628 John F. Kennedy Boulevard
8th Floor, 8 Penn Center
Philadelphia, PA 19103

POSTDOCTORAL POSITION in IMMUNOBIOCHEMISTRY

The laboratory of **Dr. Pam Fraker** at Michigan State University (MSU) seeks a Postdoctoral student for a series of studies regarding the impact of obesity, diabetes, and other metabolic diseases on immune defense to include hematopoietic processes and generation of inflammatory factors. A team of MSU faculty have begun collaborative studies of both patients and mouse models. This translational research project requires an industrious candidate willing to combine immunology, metabolism and molecular biology. A generous salary with benefits will be provided for this position that is available immediately. If interested, send curriculum vitae and three references to **e-mail: fraker@msu.edu.**

POSITIONS OPEN

FACULTY POSITIONS in BIOINFORMATICS

The University of North Texas (UNT) seeks candidates for two positions in bioinformatics at the rank of tenure-track **ASSISTANT PROFESSOR.** Candidates will be expected to develop an identifiable research program, obtain extramural funding, and support instructional needs at the graduate and undergraduate levels. Two positions are sought, and are anticipated to be joint appointments between biological sciences, computer science and engineering, or mathematics, depending upon the candidate's areas of expertise. The successful candidates will be an integral part of two new research initiatives, plant signaling mechanisms and developmental physiology and genetics. Candidates must have a Ph.D. in bioinformatics, computer science, mathematics, life sciences, or a related discipline, and have postdoctoral experience and evidence of scholarship in bioinformatics. Candidates will interact with current faculty in life sciences, mathematics, and computer sciences. Preference will be given to applicants who have expertise with systems approaches to biological questions and may include expertise in pattern recognition, statistical methods, database development, and user interfaces in the analysis and handling of large genetic and metabolite data sets. Competitive startup funds and salary are available. Send cover letter with qualifications and research interests, curriculum vitae, two to three representative publications, and names/contact information of three references to: **Dr. Rebecca Dickstein, Bioinformatics Search Committee Chair, University of North Texas, 1155 Union Circle #305220, Denton, TX 76203-5017.** In addition, e-mail the curriculum vitae to **e-mail: beccad@unt.edu.** Applications will be reviewed beginning February 2, 2009, and continue until the positions are filled. UNT is the largest and most comprehensive University in the north Texas region with 96 Bachelor's, 111 Master's, and 50 doctoral degree programs. It is the fourth largest University in Texas, with nearly 35,000 students. UNT is located in Denton in the vibrant and rapidly expanding Dallas-Fort Worth metropolitan area with easy access to DFW airport. Candidates will have the opportunity to interact with other scientists at UNT focused on modeling and computational sciences such as those in the Center for Advanced Scientific Computing and Modeling (CASCaM). New research initiatives, several of which include a focus in informatics, were announced in September 2008, by the UNT administration **(website: http://web3.unt.edu/news/story.cfm?story=11146).** For further information, see **website: http://www.unt.edu.**

ADA/Equal Opportunity Employer/Affirmative Action.

FACULTY POSITION, CANCER GENETICS
Northwestern University
Feinberg School of Medicine

Northwestern University Feinberg School of Medicine and the Robert H. Lurie Comprehensive Cancer Center are recruiting an outstanding individual for full-time, tenure-track, faculty position at the level of **ASSOCIATE or FULL PROFESSOR** depending upon prior experience and research accomplishments. This position will be filled by a senior researcher in the broad area of cancer genetics. The successful candidate will be also appointed as the co-leader of the Cancer Genomics Program at Robert H. Lurie Comprehensive Cancer Center.

Candidates should have a Ph.D. and/or M.D. degree and exceptional research potential, with significant prior accomplishments. Applications must include curriculum vitae, and a brief statement of their research interests. To ensure consideration, completed applications must be received by November 30, 2008. Submissions to (e-mail preferred):

Leonidas Platanias, M.D., Ph.D.
Deputy Director
Robert H. Lurie Comprehensive Cancer Center
303 E. Chicago Avenue
Lurie 3-125
Chicago, IL 60611
E-mail: c-alexa@northwestern.edu

Reference faculty position # P-155-04.

Northwestern University is an Affirmative Action/Equal Opportunity Employer; hiring is contingent upon eligibility to work in the United States.

Recruitment of staff scientists in biology and public health at the INSTITUT PASTEUR Paris, France

The Institut Pasteur will recruit up to 10 staff scientists in 2009. The recruitment campaign is aimed at young Ph.D. or M.D/Ph.D. scientists.The Institut Pasteur offers a highly attractive scientific environment with 130 research groups working on basic biological research and biomedical applications. Research fields include developmental biology, neurosciences, genomics, bioinformatics, structural biology, bacteriology, parasitology, virology, mycology, immunology, chemistry, epidemiology, and the physiopathology of infections.

Candidates should select and contact a host laboratory (listed on the Institut Pasteur web site **http://www.pasteur.fr/ip/easysite/go/03b-000010-011/research/scientific-departments**). Applications should include a research project that should fall within the research themes of the host laboratory and should be approved by the laboratory Director. Dossiers should be sent to Dr Isabelle Saint Girons, Direction de l'Evaluation Scientifique, Institut Pasteur, 28 rue du Docteur Roux, 75724 Paris cedex 15, France before 16th February 2009. For further information, mail to **recruit@pasteur.fr**. For details concerning application forms see **http://www.pasteur.fr/ip/easysite/go/03b-00002p-019/institut-pasteur/job-posting-and-tenders/senior-group-leaders-positions/recruitment**

Institut Pasteur

SCIENCE FACULTY
NYU Abu Dhabi

New York University (NYU) is establishing a new comprehensive liberal arts campus in Abu Dhabi, the capital of the United Arab Emirates. New York University Abu Dhabi (NYUAD), a partner campus of New York University New York (NYUNY), will consist of a highly selective liberal arts college (Arts, Humanities, Social Sciences, Sciences and Engineering), distinctive graduate programs, and a world-class Institute for advanced research, scholarship, and creative work. NYUNY and NYUAD will be integrally connected, together forming the foundation of a unique global network university, actively linked as well to NYU's study and research sites on five continents.

The Division of Science, Engineering, Technology and Mathematics at NYUAD is now recruiting faculty of exceptional quality in teaching and in professional accomplishment. The Division is specifically looking for professors of Biology, Chemistry, Computer Science, Neuroscience, Mathematics and Physics. Recruited faculty will start by teaching an innovative, three-semester foundational core, called the Science Foundations series. The Science Foundations series is especially designed to integrate basic concepts from mathematics, physics, chemistry, biology, computer science, and neuroscience and is required for all science majors at NYUAD. Science instruction at NYUAD will start in AY2010; however, applicants could start at NYUNY in September, 2009. Modern science laboratories will be constructed and become available for faculty research within a start-up phase spread over several subsequent years. Faculty may spend time at NYU in New York and at its other global campuses. The terms of employment are competitive compared to U.S. benchmarks and include housing and educational subsidies for children.

*The review of applications will begin in **January 2009** and will continue until the positions are filled.* To apply for this position, please send ONE document only (pdf or word) via email to: **nyuad.science@nyu.edu**. This document should contain a cover letter (please address the letter to NYUAD Science Search Committee), a curriculum vitae, statements of teaching experience and research interests, contact information for references and representative publications. Electronic submissions are preferred, but you may also send a hard copy to: **NYUAD Science Search Committee, New York University, 70 Washington Square South, Rm. 1242, New York, NY 10012**. Information concerning the faculty, programs and facilities of NYU Abu Dhabi, can be obtained at: **http://nyuad.nyu.edu**

NEW YORK UNIVERSITY
ABU DHABI

NYU Abu Dhabi is an Equal Opportunity/Affirmative Action Employer.

CSH 74th Cold Spring Harbor Symposium on Quantitative Biology

evolution
THE MOLECULAR LANDSCAPE

May 27 – June 1, 2009

Abstract Deadline: March 6, 2009

Organizers
David Stewart, Bruce Stillman and Jan Witkowski
Cold Spring Harbor Laboratory

Topics
Evolution of Molecular Functions
Evolution of Molecular Machines
Origins of Cellular Life
Natural Selection and Speciation
Evolution in Action
Sex and Sexual Selection
Diversity of Life
Genome Evolution
Evolution and Development
Development of Biological Systems
Domestication of Animals and Plants
Human Origins
Evolution of Social Behavior
Evolution and Society
Evolution and the Public

Speakers/Chairs
Leif Andersson
Frances Arnold
Nick Barton
Richard Behringer
Janet Browne
Carlos Bustamante
Sean Carroll
Thomas Cech
Brian Charlesworth
Quentin Cronk
Jeff Dangl
Eric Davidson
Bernard Degnan
Daniel Dennett
John Doebley
Russell Doolittle
W. Ford Doolittle
Niall Ferguson
Barbara Forrest
Kevin Foster
Claire Fraser-Liggett
Seth Grant
Volker Hartenstein
Marc Hauser
David Haussler
Paul Hebert
Hopi Hoekstra
Gerald Joyce
Nicole King
David Kingsley
Eugene Koonin
Leonid Kruglyak
Richard Lenski
Michael Levine
Tom Little
Derek Lovley
Robert Martienssen
Kenneth Miller
Armin Moczek
Eric Olson
Svante Pääbo
Kevin Padian
David Page
Nipam Patel
Steven Pinker
Venki Ramakrishnan
Matt Ridley
Gene Robinson
Barbara Schaal
Eugenie Scott
Doug Soltis
Pam Soltis
Jack Szostak
Joe Thornton
Sarah Tishkoff
Paul Turner
Doug Wallace
Tim White
Edward Wilson
Richard Wrangham

Celebrating the 200th birthday of Charles Darwin and the 150th anniversary of the publication of *The Origin of the Species*

©English Heritage Photo Library. By kind permission of Darwin Heirlooms Trust.

http://www.cshl.edu/meetings • e-mail: meetings@cshl.edu
phone: 516.367.8346 • fax: 516.367.8845

Science Careers online @sciencecareers.org

POSITIONS OPEN

TENURE-TRACK POSITION in BIOCHEMISTRY
Specializing in Nuclear Magnetic Resonance Spectroscopy

The Department of Biochemistry at the University of Texas Health Science Center at San Antonio invites applications from Investigators at all levels for a tenure-track position in the area of nuclear magnetic resonance (NMR) studies of biological macromolecules. Applicants are expected to have expertise in developing and/or applying techniques in NMR spectroscopy to gain insights into macromolecular structure, function, and dynamics. The successful candidate will join a faculty with strong research programs in NMR, X-ray crystallography, and other biophysical approaches to structure/function analysis of biological macromolecules (see **website: http://biochem.uthscsa.edu).** Access will be provided to state-of-the-art NMR equipment operated by the Department, including a Bruker AV 500, a Bruker DRX 600 fitted with a TXI cryoprobe, and a Bruker AV 700 megahertz (MHz) fitted with a TCI cryoprobe. Additionally, planning is underway for purchase and installation of a 900 MHz cryoprobe-equipped spectrometer (see **website: http://nmr.uthscsa.edu).**

San Antonio offers a rich multicultural environment, excellent educational and recreational opportunities, a temperate climate, and a very reasonable cost of living. A generous startup package will be provided, along with access to a large array of other shared facilities/centers operated by the Department, including those for X-ray crystallography, analytical ultracentrifugation, mass spectrometry, surface plasmon resonance, microcalorimetry, and others. Candidates will be expected to develop a vigorous, externally funded research program and contribute to teaching in the graduate, medical, or dental curricula. Applicants should send a curriculum vitae, a one-to-two page summary of past and proposed research, and three letters of reference either electronically or in printed form to: **Ms. Esther L. James (e-mail: jamese@uthscsa.edu, Department of Biochemistry, MC 7760, University of Texas Health Science Center at San Antonio, 7703 Floyd Curl Drive, San Antonio, TX 78229-3900).** Questions should be addressed to the **Chair of the Search Committee, Andrew Hinck, Ph.D. (e-mail: hinck@uthscsa.edu).**

All faculty appointments are designated as security-sensitive positions. The University of Texas Health Science Center at San Antonio is an Equal Employment Opportunity/Affirmative Action Employer.

FACULTY POSITION in NEUROSCIENCE

The Department of Cell Biology and Neuroscience at Montana State University (MSU) invites applications for a tenure-track position at the **ASSISTANT and/or ASSOCIATE** level. We are seeking **NEUROSCIENTISTS** who use innovative approaches to investigate problems that complement existing departmental strengths. We are particularly interested in candidates who employ genetic and imaging technologies to manipulate and/or measure neural circuit formation or activity in the nervous system. These technologies could include the development of new sensors, new genetic strategies for temporally or spatially restricted expression, and opto-genetic approaches for imaging or stimulating neural circuits. Successful candidates are expected to initiate and maintain a nationally competitive, vigorous, externally funded research program and teach at both the undergraduate and graduate level. This is a nine-month position with complete salary support that can be augmented in the summer with grant funds. Applicants should send curriculum vitae, a two-page summary of research accomplishments and future plans, and the names and addresses of three references, via e-mail and in PDF format, to **Dr. Frances Lefcort, c/o Lisa Musgrave** at **e-mail: cbn@cns.montana.edu.** The review of applications will begin on January 5, 2009, and continue until the position is filled (see **website: http://www.montana.edu/cbn).**

POSITIONS OPEN

ASSISTANT PROFESSOR
Biological Oceanography

The Department of Biology at the University of Tampa invites applications for a full-time, tenure-track position beginning in August 2009, to teach introduction to oceanography, introductory biology courses, and nonscience majors.

The Department is interested in attracting a broadly trained **BIOLOGICAL OCEANOGRAPHER** to complement the existing faculty in marine science and biology. The candidate is expected to engage in research activities that involve undergraduates. Startup funds are available.

Ph.D. required; prior teaching and research experience with undergraduates desirable.

For additional information about the University, go to **website: http://www.ut.edu.**

For details and to apply, go to **website: https://jobs.ut.edu.**

Review of applications will begin January 1, 2009, and continue until the position is filled.

The University of Tampa is an Equal Opportunity Employer/Affirmative Action Employer.

OPPORTUNITY of EMPLOYEE FACULTY POSITION
University of Puerto Rico

The Department of Biology of the University of Puerto Rico at Río Piedras **(website: http://biology.uprrp.edu)** invites application for a tenure-track position in cellular/molecular biology/biochemistry. Investigators with expertise in celullar mechanisms (e.g., signal transduction, intracellular trafficking, protein metabolism) are particularly encouraged to apply. Candidates must hold a Ph.D. or equivalent and have postdoctoral experience. They are expected to develop active research programs and to teach at the graduate and undergraduate levels. Interested candidates should send resume, a statement of current and future research and teaching goals, representative publications, and three letters of reference to: **Dr. James Ackerman, P.O. Box 23360, UPR Station, San Juan, PR 00931-3360** or **e-mail: ackerman.upr@gmail.com.** Applications will be reviewed from January 16, 2009, until the position is filled. *University of Puerto Rico is an Equal Opportunity Employer.*

OPPORTUNITY of EMPLOYEE FACULTY POSITION
University of Puerto Rico

The Department of Biology of the University of Puerto Rico at Río Piedras **(website: http://biology.uprrp.edu)** invites applications for a tenure-track position in genetics. Candidates must hold a Ph.D. or equivalent and have postdoctoral experience. The position entails participation in the undergraduate program by coordinating and teaching genetics lectures and laboratories, and to conduct research in genetics, or in science education. Interested candidates should send resume, statement of teaching philosophy, current and future research goals, representative publications, and three letters of reference to: **Dr. James Ackerman, P.O. Box 23360, UPR Station, San Juan, PR 00931-3360** or **e-mail: ackerman.upr@gmail.com.** Applications will be reviewed from January 16, 2009, until the position is filled. *University of Puerto Rico is an Equal Opportunity Employer.*

ASSISTANT PROFESSOR of BIOLOGY

The Biology Department at Armstrong Atlantic State University, **website: http://www.biology.armstrong.edu,** seeks applications for a tenure-track position in eukaryotic cell/molecular biology. A Ph.D. is required; postdoctoral experience preferred. A second position is also available for an Assistant Professor (renewable up to three years), both beginning August 2009. Review of completed applications will begin on January 5, 2009, and continue until the position is filled. Please visit **website: http://www.hr.armstrong.edu/jobs.htm** for details.

POSITIONS OPEN

Denison University, a selective liberal arts college, invites applications for two two-year positions for an **ORGANISMAL BIOLOGIST and a MOLECULAR BIOLOGIST,** to begin August 2009. Teaching load for each position is two courses with laboratories each semester; all courses have enrollments of 24 or less. Teaching responsibilities include a sophomore-level course (ecology and evolution or cell and molecular biology, respectively) and a nonmajors course in the candidate's area of interest. In addition, the Organismal Biologist will teach animal behavior and an advanced course on a major taxonomic group; the Molecular Biologist will teach two advanced courses (refer to **website: http://www.denison.edu/biology/** for a list of potential topics for both positions, as well as a detailed description of the Department and its curriculum). Opportunities exist to support research with students. Demonstrated ability in undergraduate teaching is expected and a Ph.D. is preferred (all-but-dissertation acceptable). Please submit electronic application materials (a cover letter clearly indicating the position and advanced course preferences, curriculum vitae, statement of teaching philosophy, undergraduate and graduate transcripts, and three letters of recommendation) online at **website: https://employment.denison.edu.** Review of applications will begin January 23, 2009, and continue until positions are filled. *Denison is an Affirmative Action/Equal Opportunity Employer. Women and minorities are encouraged to apply.*

FACULTY POSITIONS in GENETICS
Department of Genetics
North Carolina State University

The Department of Genetics at North Carolina State University invites applications at the **ASSISTANT PROFESSOR** level for two tenure-track faculty positions. Successful candidates will establish research programs that complement existing departmental research strengths. Preference will be given to applicants with research expertise in population genetics, systems genetics, or epigenetics.

Go to **website: http://jobs.ncsu.edu/applicants/central?quickfind=82501** to apply. Review of applications will begin January 6, 2009, and continue until the positions are filled.

NCSU is an Affirmative Action/Equal Opportunity Employer. NC State welcomes all persons without regard to sexual orientation. Individuals with disabilities desiring accommodations in the application process should call ***telephone: 919-515-5727*** *or* ***fax: 919-515-3355.***

Get your questions answered.
Careers Forum
www.ScienceCareers.org

MARKETPLACE

Oligo Labeling Reagents
- BHQ®/CAL Fluor®/Quasar® Amidites
- Amidites for 5′ & Int. Modifications
- Standard and Specialty Amidites

BIOSEARCH TECHNOLOGIES
Advancing Nucleic Acid Technology™
+1.800.GENOME.1
www.btilabeling.com

For COLLAGEN Detection...
Connect with Cosmo Bio

ELISAs to measure COLLAGENs: Type 1 (hu); Type 2 (hu, ms, rt, +). **ELISAs to measure ANTI-COLLAGEN ANTIBODIES:** Type 1 (hu); Type 2 (hu, ms, rt, +). **SPECIFIC ANTIBODIES:** Types 1, 2, 3, 4, 5, 6, 7, 8, 9, 10, 11, 12, 14.

Research Products from Japan
www.cosmobio.com
Cosmo Bio Co., Ltd.